

**INTERNATIONAL COUNCIL FOR RESEARCH AND INNOVATION
IN BUILDING AND CONSTRUCTION**

WORKING COMMISSION W18 - TIMBER STRUCTURES

CIB - W18

MEETING THIRTY-FOUR

VENICE

ITALY

AUGUST 2001

Lehrstuhl für Ingenieurholzbau und Baukonstruktionen
Universität Karlsruhe
Germany
Compiled by Rainer Görlacher
2001

ISSN 0945-6996

CONTENTS

- 0 List of Participants
- 1 Chairman's Introduction
- 2 Co-operation With Other Organisations
- 3 Timber Columns
- 4 Stress Grading
- 5 Stresses for Solid Timber
- 6 Timber Joints and Fasteners
- 7 Load Sharing
- 8 Laminated Members
- 9 Structural Stability
- 10 Fire
- 11 Glued Joints
- 12 Any Other Business
- 13 Venue and Program for Next Meeting
- 14 Close
- 15 List of CIB W18 Papers/Venice, Italy 2001
- 16 Current List of CIB-W18 Papers

CIB-W18 Papers 34-2-1 up to 34-18-1

0 List of Participants

INTERNATIONAL COUNCIL FOR RESEARCH AND INNOVATION
IN BUILDING AND CONSTRUCTION
WORKING COMMISSION W18 - TIMBER STRUCTURES

MEETING THIRTY-FOUR
VENICE, ITALY 22-24 AUGUST 2001

LIST OF PARTICIPANTS

AUSTRIA

K Frühwald
G Schickhofer

Joanneum Research, Judenburg
Graz University of Technology

BULGARIA

I Totev

University of Architecture, Civil Engineering and Geodesy, Sofia

CANADA

F Lam
I Smith

University of British Columbia
University of New Brunswick, Fredericton

CZECH REPUBLIK

P Kuklik

Czech Technical University

DENMARK

P Ellegaard
H J Larsen
J Nielsen

Aalborg University
BYG.DTU, Lyngby
Aalborg University

FINLAND

M Kairi
J Kangas
J Leskela

Finnforest Oyj, Lohja
VTT Building Technology, Espoo
Finnish Forest Industries Federation, Helsinki

FRANCE

J P Biger
L Daudeville
T Lamadon
P Racher
F Rouger

Bureau Veritas
Laboratoire Sols, Solides, Structures, Grenoble
Bureau Veritas
C.U.S.T. Aubiere Cedex
CTBA, Bordeaux

GERMANY

P Becker
A Bernasconi
H J Blaß
J Ehlbeck
P Glos
R Görlacher

Bauhaus University, Weimar
Federal Research Centre for Forestry and Forest Products, Hamburg
University of Karlsruhe
University of Karlsruhe
München University of Technology
University of Karlsruhe

| | |
|-----------------|----------------------------------|
| M Grosse | Bauhaus University, Weimar |
| P Haller | University of Dresden |
| V Krämer | University of Karlsruhe |
| H Kreuzinger | München University of Technology |
| K Rautenstrauch | Bauhaus University, Weimar |
| M Romani | University of Karlsruhe |

ITALY

| | |
|-------------|-------------------------------------|
| M Ballerini | University of Trento |
| A Ceccotti | Universities of Florence and Venice |

JAPAN

| | |
|------------|--------------------------------------|
| S Nakajima | Building Research Institute, Tsukuba |
| M Yasumura | Shizuoka University |

THE NETHERLANDS

| | |
|------------|--|
| W Bakens | CIB, Rotterdam |
| A Jorissen | SHR-Timber Research and ABT Consulting Engineers |

NORWAY

| | |
|---------|--|
| K Solli | Norwegian Institute of Wood Technology, Oslo |
|---------|--|

SLOVENIA

| | |
|---------|-------------------------|
| B Dujic | University of Ljubljana |
|---------|-------------------------|

SWEDEN

| | |
|-----------------|---|
| C Bengtsson | Swedish National Testing and Research Institute, Borås |
| M Hansson | Lund University |
| T Isaksson | Lund University |
| J Jönsson | Lund University |
| B Källsner | Swedish Institute for Wood Technology Research, Stockholm |
| J König | Swedish Institute for Wood Technology Research, Stockholm |
| S Ohlsson | Dynalyse AB, Partille |
| S Thelandersson | Lund University |

SWITZERLAND

| | |
|------------|---|
| A Mischler | Swiss Federal Institute of Technology, Zurich |
|------------|---|

UK

| | |
|--------------|---|
| R Bainbridge | TRADA Technology LTD, Buckinghamshire |
| R F Marsh | Consultant, London |
| V Enjily | British Research Establishment, Garston |

USA

| | |
|-------|--------------------------------------|
| B Yeh | American Plywood Association, Tacoma |
|-------|--------------------------------------|

- 1. Chairman's Introduction**
- 2. Co-operation With Other Organisations**
- 3. Timber Columns**
- 4. Stress Grading**
- 5. Stresses for Solid Timber**
- 6. Timber Joints and Fasteners**
- 7. Load Sharing**
- 8. Laminated Members**
- 9. Structural Stability**
- 10. Fire**
- 11. Glued Joints**
- 12. Any Other Business**
- 13. Venue and Program for Next Meeting**
- 14. Close**

**INTERNATIONAL COUNCIL FOR RESEARCH AND INNOVATION
IN BUILDING AND CONSTRUCTION**

WORKING COMMISSION W18 - TIMBER STRUCTURES

MEETING THIRTY FOUR

VENICE, ITALY 22 - 24 AUGUST 2001

MINUTES

(F Lam)

1. CHAIRMAN'S INTRODUCTION

HJ Blass opened the meeting and welcomed the participants to the 34th meeting of CIB W18, working commission 18 "Timber Structures of the International Council for Research and Innovation in Building and Construction". The chairman thanked A Ceccotti, Istituto Universitario di Architettura di Venezia, for hosting the meeting. He mentioned that the very successful 19th CIB W18 meeting in Florence Italy was also hosted by A Ceccotti.

The chairman asked the participants to rise in commemoration of a long time CIB W18 participant George Stern who passed away on March 19, 2001.

Papers brought directly to the meeting would not be accepted for presentation, discussions, or publication. Papers presented by non-authors or non-coauthors are not recommended except in exception situations because the discussion process might be compromised. For this meeting there were several cases where the abstracts were submitted but not the final paper. The numbering will be updated for the final proceedings.

In total there were 32 papers. The presentations should be limited to 20 minutes with 10 minutes discussion period. Presenters were reminded that they should conclude the presentation with a general proposal or statements concerning impact of the research results on existing or future codes and standards. One of the main targets of this group is the translation of research results into design rules in codes or the development and harmonisation of existing and new standards.

There were 9 topics covered in this meetings: timber columns (2 papers), stress grading (1 paper), stresses for solid timber (1 paper), timber joints and fasteners (15 papers), load sharing (1 paper), laminated members (6 papers), structural stability (3 papers), fire (2 papers), and glued joints (1 paper). The program showed that the area of timber joints and fasteners has the largest research interest.

Questions on meeting proceedings should be directed at R Görlacher. The participants were asked to check the participant address list under circulation for accuracy.

2. CO-OPERATION WITH OTHER ORGANISATIONS

(a) RILEM

A RILEM meeting on Timber Fasteners will be held in September 2001. J Ehlbeck reported on activities of RILEM TC 169 "Test methods for load transferring metal works for use in timber structures". There was no meeting last year. Main work had already been completed. Contact with European Organisation for Technical Approval EOTA was initiated to establish guidelines/rules for calibration and verification of models. R Görlacher has been active in support of the work.

(b) CEN

HJ Larsen reported as chair of TC124 which deals with material for timber structures with the exception of wood based panels. In the past TC124 had close contact with activities of CIB W18. The nature of work of TC124 has changed. Some examples of current activities included: acceptance of grading rules for timber; standardisation of production requirements of glulam; joints; and glued structures. These activities will come to an end soon and will refocus more on research activities.

J König reported on TC 250 Subcommittee 5 activities. Eurocode 5 is involved in conversion of European pre-standards (ENV) to European standards (EN). Timetable for the various activities is as follows:

General and Buildings Part 1-1: Project team finalised their work. In Mid September final draft will be sent to SC5 for agreement and will be sent to CEN later for formal vote.

Fire, Part 1-2: Project team will submit new draft in October.

Bridges, Part 2: Project team will submit first draft in October.

Next SC5 meeting has been scheduled for Nov 15/16 2001 aiming to have agreement on Part 1-1 to go to CEN for formal vote and to discuss Part 1-2 and Part 2.

(c) IABSE

Report was not available.

(d) IUFRO S5.02

F Rouger reported that he has stepped down as chair of IUFRO S5.02 because of heavy workload. There were no activities. New Chairman is needed.

(e) COST

F Rouger: COST E24, a COST action on Probabilistic Design, has been set up. Eligible and interested persons are welcome to participate. Data to support statistical properties for connections are needed by A J M Leijten.

3. TIMBER COLUMNS

Paper 34-2-1 Long-Term Experiments with Columns: Results and Possible Consequences on Column Design – W Moorkamp, W Schelling, P Becker, K Rautenstrauch

Presented by: P Becker

- H J Blass received clarification that series 5 and 6 had the same cross-section and loaded to 100% of the service load. He questioned that a lower service load would be more appropriate for the wet case.
- P Becker agreed that the service load may be too high for the wet group
- H J Blass stated that the mechano sorptive effect should be higher for the smaller specimens.
- P Becker answered that for the relatively small difference in cross sectional sizes considered in this study, this would not be serious.

Paper 34-2-2 Proposal for Compressive Member Design Based on Long-Term Simulation Studies – P Becker, K Rautenstrauch

Presented by: P Becker

- S Thelandersson asked why several points were chosen for the mean and characteristic value.
- P Becker answered that only 10 columns were simulated for their long term behaviour out of 1000 simulated members. These 10 points were chosen near the mean and the characteristic value.
- H J Blass commented that cross sectional dimensions were recorded at the mid span yet the moisture changed over the entire column length.
- P Becker responded that in the non-linear cases, the mid span was most critical although this approach may be conservative. This is not an issue for the compact column case.
- H Kreuzinger asked for clarification of the proposed code format.
- P Becker provided a brief review of the proposal.
- H J Larsen clarified that the slender column case has been covered in this study but the non-slender column case where strength criteria is needed has not been resolved. He commented that the statement in the design proposal as per restricted to 50% of design values can be better formulated.
- P Becker agreed with the first comment and responded that the permanent load should be restricted to 50% of design values for the creep case.

4. STRESS GRADING

Paper 34 - 5 - 1 Influence of Proof Loading on the Reliability of Members – F Lam, S Abayakoon, S Svensson, C Gyamfi

Presented by: F Lam

- V Enjily asked whether species effect was considered? He commented that higher proof load level of up to 10% would lead to larger damage. He asked also about reversal of load direction.
- F Lam responded that this study focused on Hem-fir only. Other species can be considered with the same procedures but different load duration model would be needed. He agreed that one would see more damage in the weak specimens when higher proof load level was used. This was confirmed in the simulation study at higher proof load (not presented). Reversal of load direction was not considered in the study.
- P Glos commented that the increase in benefits seemed to be very limited.
- F Lam briefly reviewed the potential benefits.
- H J Larsen stated that the gain of 10 to 15% was significant considering only 1% of the material would be destroyed via proof loading. He asked whether it is possible to build such a machine for mills. Are there plans to do so?
- F Lam responded that on-line proof-loader exist in finger joint operations in North America and Japan. Some applications include flanges for I-Beams and laminates for Glulam Beams.
- S Thelandersson asked about the target beta level of 3.5. Is this level an official code value. Also were there any assumptions on the load side of the equation tied to the target beta.
- F Lam responded that beta of 3.5 was not a target value in the code but was chosen in this study for illustration only. The target beta value in the Canadian code was approximately 2.8 which was set at similar level as steel and concrete. Gumbel distribution for snow load, and normal distribution for dead load was assumed on the load side of the equation. These were consistent over all material considered.
- I Smith asked whether there was a real threshold level. He commented that B Leicester did double pass proof loading in the past and a lot of damage was observed.
- F Lam answered that in this study the mean threshold level was approximately 0.5 with a rather large COV of 30%. This was based on past DOL study. The existence of threshold level is a complicated debate that is beyond the scope of the study. Double pass proof loading was not considered in the study.

5. STRESSES FOR SOLID TIMBER

Paper 34 - 6 - 1 Material Strength Properties for Canadian Species Used in Japanese Post and Beam Construction - J D Barrett, F Lam, S Nakajima

Presented by: F Lam

- H J Blass asked whether density values were measured. He also asked whether the bending strength was defined as the stress at the worst defect.
- F Lam answered that density value was obtained from each specimen and the bending strength was calculated from the highest stress zone.
- S Thelandersson asked which distribution was assumed for the COV of the lower tail.
- F Lam responded that he would check with D. Barrett about this. (2P Weibull distribution was assumed)

- R Marsh asked whether the Japanese would accept different test methods on the basis of models rather than on tests.
- F Lam responded that the Japanese Ministry officers usually considered these request on a case-by-case basis. If validated model were available, they would consider it.
- M Yasumura stated that joints are important for seismic issues. What was the motivation for the study. He also asked whether long-term issues were considered.
- F Lam agreed that connection information would be important and a second study has been planned to consider the seismic design issues. The values obtained in the current study would still be important for general member design. Long-term issues have not been considered.
- P Glos stated that the ASTM standards still differed from ISO.
- F Lam stated that ISO and ASTM standards are similar.
- H J Larsen explained that with the ISO standard there is no stipulation about the location of worst defect. The researcher would decide and document the location in the study.

6. TIMBER JOINTS AND FASTENERS

Paper 34 - 7 - 1 Splitting Strength of Beams Loaded by Connections Perpendicular to Grain, Model Validation – A J M Leijten, A Jorissen

Presented by: A Jorissen

- H J Larsen discussed and presented results of a model (34-7-16) and compared the model predictions with the current paper. He concluded that the simpler model of (34-7-16) was shown to be more robust because after calibration it could predict the results from different experiments with reasonable accuracy. The G and G_c terms in the model have physical meaning unlike the blackbox approach followed by the current paper. A copy of his discussion was made available to the participants.
- M Ballerini asked about the $\sqrt{GG_c}$ values in Table 1 which were approximately 18.5 and 12 for Type A and B respectively.
- A Jorissen answered that in the proposal lower bound was chosen if the designer were not able to distinguish between the connector types. He stated that the $\sqrt{GG_c}$ values were not purely a black box approach although some inconsistencies were observed in some cases.
- V Enjily asked whether the referred UK tests were done at BRE. If so they were metal plated members and would not be appropriate for the bolted connections.
- A Jorissen confirmed that the UK tests were done at BRE and clarified point 3 in the conclusion. He stated that some of the data could still be used for model verification if the connection zone was not too large compared to the test span.
- J P Biger asked whether the conclusions could be extended to big beams. He stated that dictating rules would be important to guide designers to design connection with tensile stress perpendicular to grain.
- H J Larsen commented that if splitting mode governed then the approach should be valid for big beams. He stated that design rules for multiple fasteners would be more important as the current rules for connector spacing in the parallel and perpendicular to grain direction do not work.

- H J Blass stated that one should not encourage engineer to design connections that would be subjected to such failure mode. Zipper type failures should be avoided.
- I Smith commented that the validations were conducted with tests where stable crack growth occurred. Validations with test situations with unstable crack growth would be more convincing.

Paper 34 - 7 - 2 Numerical LEFM analyses for the evaluation of failure loads of beams loaded perpendicular-to-grain by single-dowel connections – M Ballerini, R Bezzi

Presented by: M Ballerini

- P Becker asked whether one or more than one connectors were used.
- M Ballerini answered only one connector was modelled because wanted to focus on a_r . He stated that connection geometry would also have an impact.
- L Daudeville asked whether crack length was measured.
- M Ballerini answered critical crack length would be difficult to measure and second mode was not important. He also agreed that other failure criteria could be tried later.
- I Smith stated that the experiments were displacement control and velocity of crack growth is very important in fracture. Load control would yield a different crack growth rate.
- M Ballerini agreed.

Paper 34 - 7 - 3 Dowel joints loaded perpendicular to grain - H J Larsen, P J Gustafsson

Presented by: H J Larsen

- A Jorissen asked why the F_{ult} values predicted for 1x1 and 2x1 cases from Equation 1 shown in Table 2 Page 8 were the same.
- H Larsen answered that although real material properties were used by the theory, it would not be able distinguish the different between the 1x1 and 2x1 cases.
- S Thelandersson asked whether it would be possible to use FEM to refine the approach.
- H J Larsen answered that it might be possible to calculate more accurately the work done. The idea was to try to obtain a simpler form and calibrate it.
- J Ehlbeck clarified the variables used in Equation 5 and the test results fitted the equation predictions.
- L Daudeville commented that the use of LEFM would be enough for this problem and questioned why such a large specimen (1 m) was used.
- H Larsen answered that there was a past RILEM report that considered the chosen specimen size in the experiment was a stable one.

Paper 34 - 7 - 4 Quality Control of Connections based on in V-shape glued-in Steel Rods – J Kangas, A Kevarinmäki

Presented by: J Kangas

- H J Blass asked about quality control issue.
- J Kangas answered that it was not an issue as drilling machines were very accurate.

Paper 34 - 7 - 5 Testing Connector Types for Laminated-Timber-Concrete Composite Elements – M Grosse, S Lehmann, K Rautenstrauch

Presented by: M Grosse

- H J Blass commented that the load slip curves were shown up to 4 mm of displacement and questioned how did the joints behave after 4 mm.
- M Grosse stated that tests were performed up to 15 mm and the information shown up to 4 mm was representative.
- A Ceccotti asked about the difference of the two types of shear tests.
- M Grosse answered that the single shear joint test method was found to be better especially for the log and recommended the single shear joint test.

Paper 34 - 7 - 6 Behaviour of Axially Loaded Glued-in Rods - Requirements and Resistance, Especially for Spruce Timber Perpendicular to the Grain Direction – A Bernasconi

Presented by: A Bernasconi

- H J Blass commented on the density influence.
- A Bernasconi answered that he was surprised also about the slight density effect only which is difficult to isolate.
- F Lam asked about the conclusion that capacity for the perpendicular to grain case was penetration depth independent.
- A Bernasconi answered that it was valid within a certain applicable distance. He also commented that from literature the screw driven case seemed to have higher capacity.
- L Daudeville stated that the stress distribution might not be constant.
- A Bernasconi answered that gluing parallel to grain depends on material and would not have constant stress distribution while in the gluing perpendicular to grain cases the difference in MOE was so high that a constant stress distribution could be assumed.
- J König commented that the influence of hole direction could be attributed to size effect.
- A Bernasconi clarified it with respect to the size effects of strength of timber.
- H J Larsen stated that fracture mechanics type problem always have a square root of size term.
- J Kangas commented that shear distribution could be checked with strain gauges.

- S Thelandersson commented about the plastic behaviour in the length direction where the glue was loaded and questioned about the long term stability and sensitivity to moisture effects.
- A Bernasconi clarified that epoxy glue was used and didn't have data on the long-term and moisture issues. Also he stated that the epoxy glue was brittle and it would be possible to verify with gluing in the parallel to grain direction although constant shear stress was not present. He stated that the glue did not fail; the timber did.
- A Jorissen asked whether 3D model was used and whether it was possible to calculate the stresses in the perpendicular to loading direction.
- A Bernasconi answered only 2D model was used and it was possible to estimate the stresses in the perpendicular to loading direction.

Paper 34 - 7 - 7 Embedding characteristics on fibre reinforcement and densified timber joints - P Haller, J Wehsener, T Birk

Presented by: P Haller

- H J Larsen questioned whether the difference in performance in the connection using different type of fibre glass versus aramid was a result of different fibre type or different volume of fibre.
- P Haller stated that the same weight of fibre was used; therefore, it was a fibre type effect.
- A Jorissen questioned about the improvements to tension perpendicular strength.
- P Haller responded that it would be even more efficient to reinforce for tension perpendicular strength; however, he did not have the numbers at hand.
- V Enjily asked about the cost.
- P Haller responded that with the machine shown large quantity of fibre could be produced at relatively low cost. Although Aramid would be expensive, this research aimed to optimise the connection. Densified wood was done in a hot press. Company doing such densification usually worked in electrical industry and wood can be densified also relatively cheaply.

Paper 34 - 7 - 8 GIROD – Glued-in Rods for Timber Structures – C Bengtsson, C-J Johansson

Presented by: C Bengtsson

- H J Larsen questioned the timing for providing information for Eurocode 5. He also questioned the “scientific” ways to consider fatigue test for modelling both the parallel and perpendicular directions.
- C Bengtsson answered that this is an overview paper and the model could be used in both directions.
- J Kangas questioned the 0 to 90 degree interpolation shown on page 3 as it seemed to contradict Hankinson.
- J König and H.J. Larsen had further discussions on the provision of information for Eurocode 5.

Paper 34 - 7 - 9 Criteria for Damage and Failure of Dowel-Type Joints Subjected to Force Perpendicular to the Grain – M Yasumura

Presented by: M Yasumura

- V Enjily commented that the reversal loading should be considered as this is possible in some load cases.
- Smith asked why crack initiation prediction was not considered rather than cracked specimens.
- M Yasumura agreed from scientific perspective and maintained from practical/technical perspective the approach in this paper is correct.
- H J Blass commented that small cracks would always occur anyway.
- H J Larsen agreed.

Paper 34 - 7 - 10 Interaction Between Splitting and Block Shear Failure of Joints – A J M Leijten, A Jorissen, J Kuipers

Presented by: A Jorissen

- H J Blass commented that the load configuration reported here was different from previous papers.
- A Jorissen agreed and the results could not be compared.
- H J Blass stated that the splitting load perpendicular and block shear failures occurred at different planes; therefore, it was not surprising that there would be no interaction.
- I Smith asked how do you pick the points fitted on the line on figure 10 on the load parallel to grain axis.
- A Jorissen clarified that the data for different types of tests were plotted.

Paper 34 - 7 - 11 Limit states design of dowel-fastener joints – Placement of modification factors and partial factors, and calculation of variability in resistance – I Smith, G Foliente

Presented by: I Smith

- H J Blass commented that the use of the expression of $F_y d^3/6$ assumed large strains in the fastener that might approach 45 degree. This would be true for thin fasteners not bolts.
- I Smith agreed and stated tests of actual fasteners such as bolts would be performed to calibrate the expression.

Paper 34 - 7 - 12 Design and Modelling of Knee Joints - J Nielsen, P Ellegaard

Presented by: J Nielsen

- H J Blass asked what spans were intended for these structures and how would one deal with different roof angles.
- J Nielsen answered 8 m to 10 or 11 m and most roof angles were 44 to 45 degrees.

- V Enjily asked what were the production problems with the double plates.
- J Nielsen answered the first plate was pushed in and then the second plate was slightly offset and pushed in. Alignment and wood compression problems were observed.
- H J Blass asked why thicker 2 mm plates were not used.
- J Nielsen answered such plates were not available.
- S Olsson commented that it seemed the timber structures had similar behaviour as steel structure (no cracking); however, by increasing the plate thickness the structure had brittle failure mode again. Was this desirable?
- J Nielsen answered that it was a problem identified by the truss manufacturer. It was a good solution to move the failure to the timber to obtain more ultimate use of the timber.
- J Kangas commented that the title promised too much and asked why existing models were not considered.
- J Nielsen agreed and stated that additional work would be needed to address the compression failure parallel to grain and crack failures. Rotational stiffness of plate was already included in the model and it could predict the deflections and forces. Refinements have been initiated to improve predictions.
- V Enjily commented that usually 4 small plates were used as a solution and bigger plates would be a good idea if manufacturing issues were resolved.
- J Nielsen agreed.
- F Lam commented that moving the failure mode to the wood would increase variability in the load capacity which would not be good from reliability perspective.
- B Källsner asked about the potential damage in the timber at the boundaries of the two-plate system.
- J Nielsen agreed and stated that same size plates were used to ensure second plate would not cause problem at the boundaries.

Paper 34 - 7 - 13 Timber-Steel Shot Fired Nail Connections at Ultimate Limit States - R J Bainbridge, P Larsen, C J Mettem, P Alam, M P Ansell

Presented by: R J Bainbridge

- H J Blass asked why use the average values for the penetration depth of the head and point side nail.
- R J Bainbridge answered that it was a simplification as the penetration depth was governed by the explosive charge delivery and there would be fluctuation.
- H J Blass suggested that the minimum penetration depth should be considered for design.
- R J Bainbridge agreed.
- H J Larsen commented that the stated objective seemed to promise too much. He asked would anyone take up this connection method commercially. Also he questioned how much was the gain by using finch beams rather than timber in terms of economy and performance.
- R J Bainbridge answered the commercial aspect is a separate issue from this paper. The industry was encouraged by the potential use of lower grade timber.
- H J Blass stated that in Germany 3.2 mm nails driven with airgun have been available.
- H J Larsen commented that these systems have not been frequently used either.

- H J Blass asked what was the final angle of the failed nails.
- R J Bainbridge answered the angles were not measured and the information was not available at hand.
- H J Blass commented corrosion might be a problem as zinc coating could be damaged during installation.
- R J Bainbridge answered the manufacturer did not think it would be a problem.
- V Enjily commented that the distortion of timber after installation from moisture effects might be an issue.
- I Smith commented that the friction between timber and steel plate might change after installation thus influencing the performance.
- R J Bainbridge answered this was not considered in the initial study.
- J Ehlbeck asked which equation was used to predict the characteristic load R_k , with reference to information on Page 7. This is an issue related to characteristic versus design loads.
- R J Bainbridge clarified that there was a misprint in Pg 7. The correct term should be characteristic values not design values (Fig 10).

7. LOAD SHARING

Paper 34 - 8 - 1 System Effect in Sheathed Parallel Timber Beam Structures – M Hansson, T Isaksson

Presented by: M Hansson

- H J Blass asked about the first slide and how was the composite action taken into account.
- M Hansson explained that McCutcheon model took composite action into consideration.
- V Enjily asked about T&G floors and commented that it would be nice if the model could consider I-beam.
- M Hansson answered they were not considered in this study.
- H J Blass commented that uniformly distributed load was considered here and concentrated loads would be more important for the I-Beam case. He also questioned the term “Weakest” beam in the paragraph above Fig 8.
- M Hansson agreed that wording needed to be refined.
- F Rouger questioned why mean strength rather than minimum value was used in the single T-beam model stated in paragraph 3 on Page 10.
- P Glos commented that system effect is a function of the timber quality and only high quality of timber was considered in this study. One would get lower system factors compared to those obtained by Foschi.
- M Hansson agreed.
- A Jorissen asked would DOL also affect system behaviour.
- M Hansson answered that it was not considered.

8. LAMINATED MEMBERS

Paper 34 - 12 - 1 High-Strength I-Joist Compatible Glulam Manufactured with LVL Tension Laminations – B Yeh, T G Williamson

Presented by: B Yeh

- G Schickhofer asked about the definition of beam and commented that with the LVL reinforcement the member behaved more like an I-beam. He also asked what were the volume factors used for the LVL and Glulam.
- B Yeh responded that different volume factors for the LVL and Glulam were used. The idea was to provide design values for designers.
- P Glos questioned the last conclusion in the paper on the relationship between beam bending strength and laminate strength.
- B Yeh stated that joint type would affect tensile strength of LVL because load transfer from lumber to LVL would not be the same as lumber to lumber; therefore, the relationship between beam bending strength and laminate tensile strength would be manufacturer dependent.
- M Yasumura asked about the size effect of the product.
- B Yeh stated that volume effect with exponent of 1/10 was used which would be appropriate for Douglas fir.
- G Schickhofer restated that the member behaved more like an I beam
- B Yeh stated that all beam failures were in the LVL (tension). This member had no failure in the finger joints.

Paper 34 - 12 - 2 Evaluation of Glulam Shear Strength Using A Full-Size Four-Point Test Method – B Yeh, T G Williamson

Presented by: B Yeh

- I Smith asked about the nature of the failure mode.
- B Yeh answered that the failure was typically in the late and early wood band. The flat or quarter sawn lumber will have an influence however this was not controlled in the production.
- F Lam asked would deeper beams be also considered.
- B Yeh stated that there were no plans to consider deeper beams as they would typically span long distances and bending would govern.

Paper 34 - 12 - 3 Design Model for FRP Reinforced Glulam Beams – M Romani, H J Bläß

Presented by: M Romani

- V Enjily asked about the manufacturing issues.
- M Romani answered that it would be similar to normal glulam manufacturing and no problem for the manufacturer.
- A Jorissen asked about the improvement of stiffness.

- M Romani answered that the stiffness improvements (15%) were less than strength improvements (34%). It would be similar to normal glulam manufacturing and no problem for the manufacturer.
- B Yeh commented that there have been much activities in the US in this area.
- H J Blass commented that they were aware of the US groups but information exchange was only in one direction.
- B Yeh asked about volume effect.
- H J Blass answered that it was not considered in this study.
- I Smith commented that one of the US patents dealt with the process of “hairing-up”. In this study and in the University of Maine study, it seemed that this was not required.
- F Lam asked whether pre-pregnated fibre glass could be considered.
- M Romani answered no but thicker glass may be needed.
- G Schickhofer asked whether shear failure would become an issue.
- M Romani answered no shear failures were observed.

Paper 34 - 12 - 4 Moisture induced stresses in glulam cross sections – J Jönsson

Presented by: J Jönsson

- A Jorissen commented about the MOE difference between the outside and inside of the specimen.
- J Jönsson clarified that it was the annual ring direction effect.

Paper 34 - 12 - 5 Load Carrying Capacity of Nail-Laminated Timber under Concentrated Loads – V Krämer, H J Blass

Presented by: V Krämer

- S Thelandersson commented that there was agreement with displacement but what about strength.
- V Krämer answered that the exact bending capacity was not known and linear elastic behaviour was assumed. In the second step realistic load-slip behaviour of the nails would be needed.
- I Smith commented the in service nail might loosen and gaps might occur. He asked how could these moisture related effect be taken into consideration.
- V Krämer answered that work has been initiated to test nail connections.
- H J Blass added that this would only be a limited study as the system was intended to be used in building not bridges.
- I Smith added that empirical rules were available for bridges.
- G Schickhofer commented that nail laminated deck is in EC5 therefore study with regard to gaps would be important.
- V Krämer agreed.
- V Enjily commented that he saw the benefits and asked whether such system would be intended for low quality timber.
- H J Blass explained that in effect high quality timber would be used.

Paper 34 - 12 - 6 Determination of Shear Strength Values for GLT Using Visual and Machine Graded Spruce Laminations – G Schickhofer

Presented by: G Schickhofer

- H J Larsen commented that standard test methods for shear strength were available and asked whether such test have been performed with the point that the standard test would be more cost effective.
- G Schickhofer answered that EN408 test configuration was not tried.
- H J Larsen commented that one should not standardise complicated beam test methods if cheaper tests were available.
- G Schickhofer agreed but stated that real glulam behaviour would also be important.
- P Glos commented that he agreed with the results in general; however, there appeared to be some contradiction of results between the visually graded and the machine stress rated timber of the same strength class with reference to the general conclusion in the paper.
- G Schickhofer agreed and explained only a limited sample size of 15 specimens were available.
- P Glos commented that the conclusions should be qualified with limited sample size.
- B Yeh commented that he agreed with the concept that shear strength should be tensile strength independent. He questioned the use of overhang in the test which could increase the measured shear strength.
- G Schickhofer answered that only a small overhang was used and it was chosen via the optimisation step to reduce the compression perpendicular to grain stresses in the wood near the support. Tests comparing 50 mm and 500 mm of overhang did not show increases.
- B Yeh asked how the I-section was made with the web centered.
- G Schickhofer answered that there was no manufacturing problem.

Paper 34 - 12 - 7 Mechanically Jointed Beams: Possibilities of Analysis and some special Problems – H Kreuzinger

Presented by: H Kreuzinger

- A Jorissen questioned why a zero shear zone existed in Figures 13 and 14 in the paper.
- H Kreuzinger stated that this was a beam with two parts and the zone of zero shear corresponded to the area where there was no shear connector between the two parts.

9. STRUCTURAL STABILITY

Paper 34 - 15 - 1 A simplified plastic model for design of partially anchored wood-framed shear walls – B Källsner, U A Girhammar, Liping Wu

Presented by: B Källsner

- V Enjily asked how was the shear wall fixed to the foundation.
- B Källsner said that the practice in Sweden was not clear.
- V Enjily commented that the assumptions in the model were not realistic with respect to the directions of the nail forces as the walls are subject to both racking and overturning.
- B Källsner agreed that the model did not fully describe the real case; however, equilibrium conditions were met and the model worked well.
- V Enjily commented that ring shank nails were used which might not be realistic as the failure mode would be biased towards pull through failure.
- B Källsner answered that the fasteners showed plastic behaviour. Failure in the nails were nail withdrawal and sometimes pull through were observed.
- S Thelandersson commented that in Sweden one or two stories to med rise houses wind loads would be important. In the one to two stories houses simple metal plate anchorages were used. For the higher houses the calculations would become a problem. He also commented that the model presented was elegant; however, one must be careful with the assumptions as the assumed force distribution might be different from reality.

Paper 34 - 15 - 2 The Effect of the Moisture Content on the Performance of the Shear Walls – S Nakajima

Presented by: S Nakajima

- H J Blass asked what types of nails were used and whether they had corrosion protection.
- S Nakajima stated that smooth shank nails were used and small amount of rust was observed as they did not have any corrosion protection. He agreed that this might lead to increase in capacity in the nail tests.
- V Enjily commented that the test method for panel shear will be changed in CEN and received clarification that the service class order referred to the Japanese case.
- S Nakajima agreed that international harmonisation of service class order should be considered in the future.

Paper 34 - 15 - 3 Evaluation of Damping Capacity of Timber Structures for Seismic Design – M Yasumura

Presented by: M Yasumura

- A Ceccotti commented that that the 2% damping is only for the test specimens. For structural design of real structures, 5% damping would be appropriate because other energy dissipation components might not be considered in the test specimens.
- M Yasumura agreed.
- B Dujic commented that the suggested 2% damping should be model dependent. A sophisticated hysteretic model can use this.
- M Yasumura agreed and suggested that for the simpler model higher damping level should be used.
- P Glos questioned the loading rate effect on nail joints.

- M Yasumura stated that the nail joints test showed higher loading rate effects compared to shear wall tests. This can be explained because the speed of each nail in a wall test and the displacement of each nail in a wall tests were not always the same as those in the individual nail test. In the wall test the speed referred to the movement between the top of the wall and the support.
- L Daudeville asked and received clarification on the relationship between energy dissipation versus the loading rate.

10. FIRE

Paper 34 - 16 – 1 Influence of the Strength Determining Factors on the Fire Resistance Capability of Timber Structural Members – I Totev, D Dakov

Presented by: I Totev

- H J Blass asked how were the beams graded for the thickness.
- I Totev answered that they were cut.
- J König stated that the knots on the edge should be positive effect.
- I Totev agreed but stated that if the knots had been located originally away from the edge, the burnt member might have knots nearer to the edge.
- J König asked about the load level in relation to the code.
- I Totev clarified that the load level was related to Bulgaria standard.
- A Jorissen commented on the low Coefficient of Determination <0.5 in Figures 8 and 9.
- I Totev agreed and stated only 15 specimens were used.
- J König commented that the charring depth was found to be greater on the tension side in this paper; this meant state of stress had some influence on the charring rate. However, the Swedish tests (7 years ago) showed state of stress did not have influence on charring rates.
- I Totev stated that the tension side might have caused some of the char to fall of and might expose more wood to the fire.

Paper 34 - 16 - 2 Cross section properties of fire exposed rectangular timber members - J König, B Källsner

Presented by: J König

- H J Blass asked whether EC 5 part 5 will have only one simplified method.
- J König answered no. The project team made a proposal but it was rejected.
- R Marsh asked why not apply an adjustment factor to the current method.
- J König answered keeping the reduced properties method would be more logical and accurate. More importantly accurate values to be used in the method would be critical.
- A Jorissen questioned about structures exposed to real fire.
- J König answered that standard fire scenario was used as real fire would be too complicated.

- R Marsh agreed that this was only an indicative method and could not be used to deal with real fire situations.

Paper 34 - 16 – 3 Pull-Out Tests on Glued-in Rods at High Temperatures – A Mischler, A Frangi

Presented by: A Mischler

- H J Blass asked why the behaviour of the glued-in rod at 80°C and 100°C did not coincide with data from the manufacturer.
- A Mischler agreed with the observation. He stated that steel plates might have been used on the manufacturer tests as compared to the wood-adhesive-steel interaction of the glue-in rod connections. He commented that the manufacturer test results could not be relied upon.
- S Olsson commented on the Kollmann diagram and asked whether residual stresses in wood be a means to explain the observations.
- A Mischler responded that this was a moisture effect according to Kollmann
- V Enjily stated that he agreed with S. Olsson comment
- J König commented on the effect of moisture and temperature on MOE. He stated that oven tests were under steady state condition. Kollmann was able to keep the specimens moist although there was some surface drying in the specimens. In fire situation one would experience transient conditions with movement of moisture front and it would be more complicated. He also stated that temperature and shear strength relationships are available in the Euro Code.
- S Thelandersson commented about more test with ISO fire and asked how much wood would be needed to protect the glued-in rod for ISO fire test.
- A Mischler responded that models in the Euro Code could be used to estimate the amount of wood needed and then ISO fire test could be conducted to confirm.
- J Kangas commented that in the Finnish V-connections brittle behaviour was not observed. With angle across the grain type fasteners used in the Finnish V-connections, it was not possible to obtain the cylindrical failures.

11. GLUED JOINTS

Paper 34 - 18 - 1 Performance Based Classification of Adhesives for Structural Timber Applications - R J Bainbridge, C J Mettem, J G Broughton, A R Hutchinson

Presented by: R J Bainbridge

- W Bakens stated that in development of performance based concepts in other communities different terminologies were used with different groups and asked if there was linkage with some of these groups.
- R J Bainbridge responded that links have been established through CEN mandates.

12. ANY OTHER BUSINESS

Dr. Bakens, Secretary General of CIB, discussed issues related to the scope and objectives, work program and planned output of CIB. He also addresses the internal structure, future meetings, publication, and membership issues. He mentioned the following thematic areas that would be supported by CIB: Sustainable construction, performance based building, and construction reengineering. He also suggested the CIBW18 to meet in Toronto Canada in 2004 to coincide with the CIB general meeting. He also reminded that the delegates should be CIB members and invited candidates not yet members to apply for CIB memberships. Developing countries funds for CIB members from developing countries is available from CIB.

R Gutkowsky, University of Colorado Fort Collins, presented an invitation for the 2003 36th CIBW18 meeting to be held in Colorado USA.

13. VENUE AND PROGRAM FOR NEXT MEETING

Kyoto Japan will be the venue for the 35th CIBW18 meeting during September 16, 2002 to September 19, 2002 with a one-day excursion. H J Blass thanked the Japanese delegate for the invitation and asked R. Marsh to share his positive experience about visiting Japan from the European perspective.

With feedback from the meeting participants, H J Blass stated that the venue 36th CIBW18 meeting will be Colorado USA. Also the venue for the 37th CIBW18 meeting should be in Europe and it could be in Germany.

14. CLOSE

H J Blass: The paper number given in the green handout will be renumbered. The correct paper number will be available from our website next week. Master copy of the paper, should be sent to R Görlacher before October 1, 2001. The proceedings will be available by the end of 2001. A list of participants for 34th CIB W18 will also be available from the website.

H J Blass again thanked the Italian host A Ceccotti and A Mattarucco for successfully hosting the 34th CIBW18 meeting. He also thanked the participants for attending the meeting.

The 34th CIBW18 meeting was closed.

**15. List of CIB-W18 Papers,
Venice, Italy 2001**

List of CIB-W18 Papers, Venice, Italy 2001

- 34 - 2 - 1 Long-Term Experiments with Columns: Results and Possible Consequences on Column Design – **W Moorkamp, W Schelling, P Becker, K Rautenstrauch**
- 34 - 2 - 2 Proposal for Compressive Member Design Based on Long-Term Simulation Studies – **P Becker, K Rautenstrauch**
- 34 - 5 - 1 Influence of Proof Loading on the Reliability of Members – **F Lam, S Abayakoon, S Svensson, C Gyamfi**
- 34 - 6 - 1 Material Strength Properties for Canadian Species Used in Japanese Post and Beam Construction - **J D Barrett, F Lam, S Nakajima**
- 34 - 7 - 1 Splitting Strength of Beams Loaded by Connections Perpendicular to Grain, Model Validation – **A J M Leijten, A J M Jorissen**
- 34 - 7 - 2 Numerical LEFM Analyses for the Evaluation of Failure Loads of Beams Loaded Perpendicular-to-Grain by Single-Dowel Connections – **M Ballerini, R Bezzi**
- 34 - 7 - 3 Dowel Joints Loaded Perpendicular to Grain - **H J Larsen, P J Gustafsson**
- 34 - 7 - 4 Quality Control of Connections based on in V-shape glued-in Steel Rods – **J Kangas, A Kevarinmäki**
- 34 - 7 - 5 Testing Connector Types for Laminated Timber-Concrete Composite Elements – **M Grosse, S Lehmann, K Rautenstrauch**
- 34 - 7 - 6 Behaviour of Axially Loaded Glued-in Rods - Requirements and Resistance, Especially for Spruce Timber Perpendicular to the Grain Direction – **A Bernasconi**
- 34 - 7 - 7 Embedding Characteristics on Fibre Reinforcement and densified Timber Joints - **P Haller, J Wehsener, T Birk**
- 34 - 7 - 8 GIROD – Glued-in Rods for Timber Structures – **C Bengtsson, C-J Johansson**
- 34 - 7 - 9 Criteria for Damage and Failure of Dowel-Type Joints Subjected to Force Perpendicular to the Grain – **M Yasumura**
- 34 - 7 - 10 Interaction Between Splitting and Block Shear Failure of Joints – **A J M Leijten, J Kuipers, A J M Jorissen**
- 34 - 7 - 11 Limit States Design of Dowel-Fastener Joints – Placement of Modification Factors and Partial Factors, and Calculation of Variability in Resistance – **I Smith, G Foliente**
- 34 - 7 - 12 Design and Modelling of Knee Joints - **J Nielsen, P Ellegaard**

- 34 - 7 - 13 Timber-Steel Shot Fired Nail Connections at Ultimate Limit States -
R J Bainbridge, P Larsen, C J Mettem, P Alam, M P Ansell
- 34 - 8 - 1 System Effect in Sheathed Parallel Timber Beam Structures – **M Hansson, T Isaksson**
- 34 - 12 - 1 High-Strength I-Joist Compatible Glulam Manufactured with LVL Tension Laminations – **B Yeh, T G Williamson**
- 34 - 12 - 2 Evaluation of Glulam Shear Strength Using A Full-Size Four-Point Test Method – **B Yeh, T G Williamson**
- 34 - 12 - 3 Design Model for FRP Reinforced Glulam Beams – **M Romani, H J Blaß**
- 34 - 12 - 4 Moisture Induced Stresses in Glulam Cross Sections – **J Jönsson**
- 34 - 12 - 5 Load Carrying Capacity of Nail-Laminated Timber under Concentrated Loads – **V Krämer, H J Blaß**
- 34 - 12 - 6 Determination of Shear Strength Values for GLT Using Visual and Machine Graded Spruce Laminations – **G Schickhofer**
- 34 - 12 - 7 Mechanically Jointed Beams: Possibilities of Analysis and some special Problems – **H Kreuzinger**
- 34 - 15 - 1 A Simplified Plastic Model for Design of Partially Anchored Wood-Framed Shear Walls – **B Källsner, U A Girhammar, Liping Wu**
- 34 - 15 - 2 The Effect of the Moisture Content on the Performance of the Shear Walls – **S Nakajima**
- 34 - 15 - 3 Evaluation of Damping Capacity of Timber Structures for Seismic Design – **M Yasumura**
- 34 - 16 - 1 Influence of the Strength Determining Factors on the Fire Resistance Capability of Timber Structural Members – **I Totev, D Dakov**
- 34 - 16 - 2 Cross Section Properties of Fire Exposed Rectangular Timber Members - **J König, B Källsner**
- 34 - 16 - 3 Pull-Out Tests on Glued-in Rods at High Temperatures – **A Mischler, A Frangi**
- 34 - 18 - 1 Performance Based Classification of Adhesives for Structural Timber Applications - **R J Bainbridge, C J Mettem, J G Broughton, A R Hutchinson**

16. Current List of CIB-W18(A) Papers

CURRENT LIST OF CIB-W18(A) PAPERS

Technical papers presented to CIB-W18(A) are identified by a code CIB-W18(A)/a-b-c, where:

- a denotes the meeting at which the paper was presented.
Meetings are classified in chronological order:

- 1 Princes Risborough, England; March 1973
- 2 Copenhagen, Denmark; October 1973
- 3 Delft, Netherlands; June 1974
- 4 Paris, France; February 1975
- 5 Karlsruhe, Federal Republic of Germany; October 1975
- 6 Aalborg, Denmark; June 1976
- 7 Stockholm, Sweden; February/March 1977
- 8 Brussels, Belgium; October 1977
- 9 Perth, Scotland; June 1978
- 10 Vancouver, Canada; August 1978
- 11 Vienna, Austria; March 1979
- 12 Bordeaux, France; October 1979
- 13 Otaniemi, Finland; June 1980
- 14 Warsaw, Poland; May 1981
- 15 Karlsruhe, Federal Republic of Germany; June 1982
- 16 Lillehammer, Norway; May/June 1983
- 17 Rapperswil, Switzerland; May 1984
- 18 Beit Oren, Israel; June 1985
- 19 Florence, Italy; September 1986
- 20 Dublin, Ireland; September 1987
- 21 Parksville, Canada; September 1988
- 22 Berlin, German Democratic Republic; September 1989
- 23 Lisbon, Portugal; September 1990
- 24 Oxford, United Kingdom; September 1991
- 25 Åhus, Sweden; August 1992
- 26 Athens, USA; August 1993
- 27 Sydney, Australia; July 1994
- 28 Copenhagen, Denmark, April 1995
- 29 Bordeaux, France, August 1996
- 30 Vancouver, Canada, August 1997
- 31 Savonlinna, Finland, August 1998
- 32 Graz, Austria, August 1999
- 33 Delft, The Netherlands, August 2000
- 34 Venice, Italy, August 2001

b denotes the subject:

- 1 Limit State Design
- 2 Timber Columns
- 3 Symbols
- 4 Plywood
- 5 Stress Grading
- 6 Stresses for Solid Timber
- 7 Timber Joints and Fasteners
- 8 Load Sharing
- 9 Duration of Load
- 10 Timber Beams
- 11 Environmental Conditions
- 12 Laminated Members
- 13 Particle and Fibre Building Boards
- 14 Trussed Rafters
- 15 Structural Stability
- 16 Fire
- 17 Statistics and Data Analysis
- 18 Glued Joints
- 19 Fracture Mechanics
- 20 Serviceability
- 21 Test Methods
- 100 CIB Timber Code
- 101 Loading Codes
- 102 Structural Design Codes
- 103 International Standards Organisation
- 104 Joint Committee on Structural Safety
- 105 CIB Programme, Policy and Meetings
- 106 International Union of Forestry Research Organisations

c is simply a number given to the papers in the order in which they appear:

Example: CIB-W18/4-102-5 refers to paper 5 on subject 102 presented at the fourth meeting of W18.

Listed below, by subjects, are all papers that have to date been presented to W18. When appropriate some papers are listed under more than one subject heading.

LIMIT STATE DESIGN

- 1-1-1 Limit State Design - H J Larsen
- 1-1-2 The Use of Partial Safety Factors in the New Norwegian Design Code for Timber Structures - O Brynildsen
- 1-1-3 Swedish Code Revision Concerning Timber Structures - B Noren
- 1-1-4 Working Stresses Report to British Standards Institution Committee BLC/17/2
- 6-1-1 On the Application of the Uncertainty Theoretical Methods for the Definition of the Fundamental Concepts of Structural Safety - K Skov and O Ditlevsen
- 11-1-1 Safety Design of Timber Structures - H J Larsen
- 18-1-1 Notes on the Development of a UK Limit States Design Code for Timber - A R Fewell and C B Pierce
- 18-1-2 Eurocode 5, Timber Structures - H J Larsen
- 19-1-1 Duration of Load Effects and Reliability Based Design (Single Member) - R O Foschi and Z C Yao
- 21-102-1 Research Activities Towards a New GDR Timber Design Code Based on Limit States Design - W Rug and M Badstube
- 22-1-1 Reliability-Theoretical Investigation into Timber Components Proposal for a Supplement of the Design Concept - M Badstube, W Rug and R Plessow
- 23-1-1 Some Remarks about the Safety of Timber Structures - J Kuipers
- 23-1-2 Reliability of Wood Structural Elements: A Probabilistic Method to Eurocode 5 Calibration - F Rouger, N Lheritier, P Racher and M Fogli
- 31-1-1 A Limit States Design Approach to Timber Framed Walls - C J Mettem, R Bainbridge and J A Gordon
- 32 -1-1 Determination of Partial Coefficients and Modification Factors- H J Larsen, S Svensson and S Thelandersson
- 32 -1-2 Design by Testing of Structural Timber Components - V Enjily and L Whale
- 33-1-1 Aspects on Reliability Calibration of Safety Factors for Timber Structures – S Svensson and S Thelandersson
- 33-1-2 Sensitivity studies on the reliability of timber structures – A Ranta-Maunus, M Fonselius, J Kurkela and T Toratti

TIMBER COLUMNS

- 2-2-1 The Design of Solid Timber Columns - H J Larsen
- 3-2-1 The Design of Built-Up Timber Columns - H J Larsen
- 4-2-1 Tests with Centrally Loaded Timber Columns - H J Larsen and S S Pedersen
- 4-2-2 Lateral-Torsional Buckling of Eccentrically Loaded Timber Columns- B Johansson
- 5-9-1 Strength of a Wood Column in Combined Compression and Bending with Respect to Creep - B Källsner and B Norén
- 5-100-1 Design of Solid Timber Columns (First Draft) - H J Larsen
- 6-100-1 Comments on Document 5-100-1, Design of Solid Timber Columns - H J Larsen and E Theilgaard
- 6-2-1 Lattice Columns - H J Larsen
- 6-2-2 A Mathematical Basis for Design Aids for Timber Columns - H J Burgess

- 6-2-3 Comparison of Larsen and Perry Formulas for Solid Timber Columns-
H J Burgess
- 7-2-1 Lateral Bracing of Timber Struts - J A Simon
- 8-15-1 Laterally Loaded Timber Columns: Tests and Theory - H J Larsen
- 17-2-1 Model for Timber Strength under Axial Load and Moment - T Poutanen
- 18-2-1 Column Design Methods for Timber Engineering - A H Buchanan, K C Johns,
B Madsen
- 19-2-1 Creep Buckling Strength of Timber Beams and Columns - R H Leicester
- 19-12-2 Strength Model for Glulam Columns - H J Blaß
- 20-2-1 Lateral Buckling Theory for Rectangular Section Deep Beam-Columns-
H J Burgess
- 20-2-2 Design of Timber Columns - H J Blaß
- 21-2-1 Format for Buckling Strength - R H Leicester
- 21-2-2 Beam-Column Formulae for Design Codes - R H Leicester
- 21-15-1 Rectangular Section Deep Beam - Columns with Continuous Lateral Restraint -
H J Burgess
- 21-15-2 Buckling Modes and Permissible Axial Loads for Continuously Braced Columns -
H J Burgess
- 21-15-3 Simple Approaches for Column Bracing Calculations - H J Burgess
- 21-15-4 Calculations for Discrete Column Restraints - H J Burgess
- 22-2-1 Buckling and Reliability Checking of Timber Columns - S Huang, P M Yu and
J Y Hong
- 22-2-2 Proposal for the Design of Compressed Timber Members by Adopting the
Second-Order Stress Theory - P Kaiser
- 30-2-1 Beam-Column Formula for Specific Truss Applications - W Lau, F Lam and J D
Barrett
- 31-2-1 Deformation and Stability of Columns of Viscoelastic Material Wood - P Becker
and K Rautenstrauch
- 34-2-1 Long-Term Experiments with Columns: Results and Possible Consequences on
Column Design – W Moorkamp, W Schelling, P Becker, K Rautenstrauch
- 34-2-2 Proposal for Compressive Member Design Based on Long-Term Simulation
Studies – P Becker, K Rautenstrauch

SYMBOLS

- 3-3-1 Symbols for Structural Timber Design - J Kuipers and B Norén
- 4-3-1 Symbols for Timber Structure Design - J Kuipers and B Norén
- 28-3-1 Symbols for Timber and Wood-Based Materials - J Kuipers and B Noren
- 1 Symbols for Use in Structural Timber Design

PLYWOOD

- 2-4-1 The Presentation of Structural Design Data for Plywood - L G Booth
- 3-4-1 Standard Methods of Testing for the Determination of Mechanical Properties of
Plywood - J Kuipers
- 3-4-2 Bending Strength and Stiffness of Multiple Species Plywood - C K A Stieda

- 4-4-4 Standard Methods of Testing for the Determination of Mechanical Properties of Plywood - Council of Forest Industries, B.C.
- 5-4-1 The Determination of Design Stresses for Plywood in the Revision of CP 112 - L G Booth
- 5-4-2 Veneer Plywood for Construction - Quality Specifications - ISO/TC 139. Plywood, Working Group 6
- 6-4-1 The Determination of the Mechanical Properties of Plywood Containing Defects - L G Booth
- 6-4-2 Comparison of the Size and Type of Specimen and Type of Test on Plywood Bending Strength and Stiffness - C R Wilson and P Eng
- 6-4-3 Buckling Strength of Plywood: Results of Tests and Recommendations for Calculations - J Kuipers and H Ploos van Amstel
- 7-4-1 Methods of Test for the Determination of Mechanical Properties of Plywood - L G Booth, J Kuipers, B Norén, C R Wilson
- 7-4-2 Comments Received on Paper 7-4-1
- 7-4-3 The Effect of Rate of Testing Speed on the Ultimate Tensile Stress of Plywood - C R Wilson and A V Parasin
- 7-4-4 Comparison of the Effect of Specimen Size on the Flexural Properties of Plywood Using the Pure Moment Test - C R Wilson and A V Parasin
- 8-4-1 Sampling Plywood and the Evaluation of Test Results - B Norén
- 9-4-1 Shear and Torsional Rigidity of Plywood - H J Larsen
- 9-4-2 The Evaluation of Test Data on the Strength Properties of Plywood - L G Booth
- 9-4-3 The Sampling of Plywood and the Derivation of Strength Values (Second Draft) - B Norén
- 9-4-4 On the Use of the CIB/RILEM Plywood Plate Twisting Test: a progress report - L G Booth
- 10-4-1 Buckling Strength of Plywood - J Dekker, J Kuipers and H Ploos van Amstel
- 11-4-1 Analysis of Plywood Stressed Skin Panels with Rigid or Semi-Rigid Connections- I Smith
- 11-4-2 A Comparison of Plywood Modulus of Rigidity Determined by the ASTM and RILEM CIB/3-TT Test Methods - C R Wilson and A V Parasin
- 11-4-3 Sampling of Plywood for Testing Strength - B Norén
- 12-4-1 Procedures for Analysis of Plywood Test Data and Determination of Characteristic Values Suitable for Code Presentation - C R Wilson
- 14-4-1 An Introduction to Performance Standards for Wood-base Panel Products - D H Brown
- 14-4-2 Proposal for Presenting Data on the Properties of Structural Panels - T Schmidt
- 16-4-1 Planar Shear Capacity of Plywood in Bending - C K A Stieda
- 17-4-1 Determination of Panel Shear Strength and Panel Shear Modulus of Beech-Plywood in Structural Sizes - J Ehlbeck and F Colling
- 17-4-2 Ultimate Strength of Plywood Webs - R H Leicester and L Pham
- 20-4-1 Considerations of Reliability - Based Design for Structural Composite Products - M R O'Halloran, J A Johnson, E G Elias and T P Cunningham
- 21-4-1 Modelling for Prediction of Strength of Veneer Having Knots - Y Hirashima
- 22-4-1 Scientific Research into Plywood and Plywood Building Constructions the Results and Findings of which are Incorporated into Construction Standard Specifications of the USSR - I M Guskov

- 22-4-2 Evaluation of Characteristic values for Wood-Based Sheet Materials - E G Elias
 24-4-1 APA Structural-Use Design Values: An Update to Panel Design Capacities -
 A L Kuchar, E G Elias, B Yeh and M R O'Halloran

STRESS GRADING

- 1-5-1 Quality Specifications for Sawn Timber and Precision Timber - Norwegian
 Standard NS 3080
- 1-5-2 Specification for Timber Grades for Structural Use - British Standard BS 4978
- 4-5-1 Draft Proposal for an International Standard for Stress Grading Coniferous Sawn
 Softwood - ECE Timber Committee
- 16-5-1 Grading Errors in Practice - B Thunell
- 16-5-2 On the Effect of Measurement Errors when Grading Structural Timber-
 L Nordberg and B Thunell
- 19-5-1 Stress-Grading by ECE Standards of Italian-Grown Douglas-Fir Dimension
 Lumber from Young Thinnings - L Uzielli
- 19-5-2 Structural Softwood from Afforestation Regions in Western Norway - R Lackner
- 21-5-1 Non-Destructive Test by Frequency of Full Size Timber for Grading - T Nakai
- 22-5-1 Fundamental Vibration Frequency as a Parameter for Grading Sawn Timber -
 T Nakai, T Tanaka and H Nagao
- 24-5-1 Influence of Stress Grading System on Length Effect Factors for Lumber Loaded
 in Compression - A Campos and I Smith
- 26-5-1 Structural Properties of French Grown Timber According to Various Grading
 Methods - F Rouger, C De Lafond and A El Quadrani
- 28-5-1 Grading Methods for Structural Timber - Principles for Approval - S Ohlsson
- 28-5-2 Relationship of Moduli of Elasticity in Tension and in Bending of Solid Timber -
 N Burger and P Glos
- 29-5-1 The Effect of Edge Knots on the Strength of SPF MSR Lumber - T Courchene,
 F Lam and J D Barrett
- 29-5-2 Determination of Moment Configuration Factors using Grading Machine
 Readings - T D G Canisius and T Isaksson
- 31-5-1 Influence of Varying Growth Characteristics on Stiffness Grading of Structural
 Timber - S Ormarsson, H Petersson, O Dahlblom and K Persson
- 31-5-2 A Comparison of In-Grade Test Procedures - R H Leicester, H Breitingner and H
 Fordham
- 32-5-1 Actual Possibilities of the Machine Grading of Timber - K Frühwald and
 A Bernasconi
- 32-5-2 Detection of Severe Timber Defects by Machine Grading - A Bernasconi,
 L Boström and B Schacht
- 34-5-1 Influence of Proof Loading on the Reliability of Members – F Lam, S Abayakoon,
 S Svensson, C Gyamfi

STRESSES FOR SOLID TIMBER

- 4-6-1 Derivation of Grade Stresses for Timber in the UK - W T Curry
- 5-6-1 Standard Methods of Test for Determining some Physical and Mechanical
 Properties of Timber in Structural Sizes - W T Curry
- 5-6-2 The Description of Timber Strength Data - J R Tory

- 5-6-3 Stresses for EC1 and EC2 Stress Grades - J R Tory
- 6-6-1 Standard Methods of Test for the Determination of some Physical and Mechanical Properties of Timber in Structural Sizes (third draft) - W T Curry
- 7-6-1 Strength and Long-term Behaviour of Lumber and Glued Laminated Timber under Torsion Loads - K Möhler
- 9-6-1 Classification of Structural Timber - H J Larsen
- 9-6-2 Code Rules for Tension Perpendicular to Grain - H J Larsen
- 9-6-3 Tension at an Angle to the Grain - K Möhler
- 9-6-4 Consideration of Combined Stresses for Lumber and Glued Laminated Timber - K Möhler
- 11-6-1 Evaluation of Lumber Properties in the United States - W L Galligan and J H Haskell
- 11-6-2 Stresses Perpendicular to Grain - K Möhler
- 11-6-3 Consideration of Combined Stresses for Lumber and Glued Laminated Timber (addition to Paper CIB-W18/9-6-4) - K Möhler
- 12-6-1 Strength Classifications for Timber Engineering Codes - R H Leicester and W G Keating
- 12-6-2 Strength Classes for British Standard BS 5268 - J R Tory
- 13-6-1 Strength Classes for the CIB Code - J R Tory
- 13-6-2 Consideration of Size Effects and Longitudinal Shear Strength for Uncracked Beams - R O Foschi and J D Barrett
- 13-6-3 Consideration of Shear Strength on End-Cracked Beams - J D Barrett and R O Foschi
- 15-6-1 Characteristic Strength Values for the ECE Standard for Timber - J G Sunley
- 16-6-1 Size Factors for Timber Bending and Tension Stresses - A R Fewell
- 16-6-2 Strength Classes for International Codes - A R Fewell and J G Sunley
- 17-6-1 The Determination of Grade Stresses from Characteristic Stresses for BS 5268: Part 2 - A R Fewell
- 17-6-2 The Determination of Softwood Strength Properties for Grades, Strength Classes and Laminated Timber for BS 5268: Part 2 - A R Fewell
- 18-6-1 Comment on Papers: 18-6-2 and 18-6-3 - R H Leicester
- 18-6-2 Configuration Factors for the Bending Strength of Timber - R H Leicester
- 18-6-3 Notes on Sampling Factors for Characteristic Values - R H Leicester
- 18-6-4 Size Effects in Timber Explained by a Modified Weakest Link Theory- B Madsen and A H Buchanan
- 18-6-5 Placement and Selection of Growth Defects in Test Specimens - H Riberholt
- 18-6-6 Partial Safety-Coefficients for the Load-Carrying Capacity of Timber Structures - B Norén and J-O Nylander
- 19-6-1 Effect of Age and/or Load on Timber Strength - J Kuipers
- 19-6-2 Confidence in Estimates of Characteristic Values - R H Leicester
- 19-6-3 Fracture Toughness of Wood - Mode I - K Wright and M Fonselius
- 19-6-4 Fracture Toughness of Pine - Mode II - K Wright
- 19-6-5 Drying Stresses in Round Timber - A Ranta-Maunus
- 19-6-6 A Dynamic Method for Determining Elastic Properties of Wood - R Görlacher

- 20-6-1 A Comparative Investigation of the Engineering Properties of "Whitewoods" Imported to Israel from Various Origins - U Korin
- 20-6-2 Effects of Yield Class, Tree Section, Forest and Size on Strength of Home Grown Sitka Spruce - V Picardo
- 20-6-3 Determination of Shear Strength and Strength Perpendicular to Grain - H J Larsen
- 21-6-1 Draft Australian Standard: Methods for Evaluation of Strength and Stiffness of Graded Timber - R H Leicester
- 21-6-2 The Determination of Characteristic Strength Values for Stress Grades of Structural Timber. Part 1 - A R Fewell and P Glos
- 21-6-3 Shear Strength in Bending of Timber - U Korin
- 22-6-1 Size Effects and Property Relationships for Canadian 2-inch Dimension Lumber - J D Barrett and H Griffin
- 22-6-2 Moisture Content Adjustments for In-Grade Data - J D Barrett and W Lau
- 22-6-3 A Discussion of Lumber Property Relationships in Eurocode 5 - D W Green and D E Kretschmann
- 22-6-4 Effect of Wood Preservatives on the Strength Properties of Wood - F Ronai
- 23-6-1 Timber in Compression Perpendicular to Grain - U Korin
- 24-6-1 Discussion of the Failure Criterion for Combined Bending and Compression - T A C M van der Put
- 24-6-3 Effect of Within Member Variability on Bending Strength of Structural Timber - I Czmocho, S Thelandersson and H J Larsen
- 24-6-4 Protection of Structural Timber Against Fungal Attack Requirements and Testing- K Jaworska, M Rylko and W Nozynski
- 24-6-5 Derivation of the Characteristic Bending Strength of Solid Timber According to CEN-Documents prEN 384 - A J M Leijten
- 25-6-1 Moment Configuration Factors for Simple Beams- T D G Canisius
- 25-6-3 Bearing Capacity of Timber - U Korin
- 25-6-4 On Design Criteria for Tension Perpendicular to Grain - H Petersson
- 25-6-5 Size Effects in Visually Graded Softwood Structural Lumber - J D Barrett, F Lam and W Lau
- 26-6-1 Discussion and Proposal of a General Failure Criterion for Wood - T A C M van der Put
- 27-6-1 Development of the "Critical Bearing": Design Clause in CSA-086.1 - C Lum and E Karacabeyli
- 27-6-2 Size Effects in Timber: Novelty Never Ends - F Rouger and T Fewell
- 27-6-3 Comparison of Full-Size Sugi (*Cryptomeria japonica* D. Don) Structural Performance in Bending of Round Timber, Two Surfaces Sawn Timber and Square Sawn Timber - T Nakai, H Nagao and T Tanaka
- 28-6-1 Shear Strength of Canadian Softwood Structural Lumber - F Lam, H Yee and J D Barrett
- 28-6-2 Shear Strength of Douglas Fir Timbers - B Madsen
- 28-6-3 On the Influence of the Loading Head Profiles on Determined Bending Strength - L Muszyński and R Szukala
- 28-6-4 Effect of Test Standard, Length and Load Configuration on Bending Strength of Structural Timber- T Isaksson and S Thelandersson
- 28-6-5 Grading Machine Readings and their Use in the Calculation of Moment Configuration Factors - T Canisius, T Isaksson and S Thelandersson

- 28-6-6 End Conditions for Tension Testing of Solid Timber Perpendicular to Grain - T Canisius
- 29-6-1 Effect of Size on Tensile Strength of Timber - N Burger and P Glos
- 29-6-2 Equivalence of In-Grade Testing Standards - R H Leicester, H O Breitingner and H F Fordham
- 30-6-1 Strength Relationships in Structural Timber Subjected to Bending and Tension - N Burger and P Glos
- 30-6-2 Characteristic Design Stresses in Tension for Radiata Pine Grown in Canterbury - A Tsehaye, J C F Walker and A H Buchanan
- 30-6-3 Timber as a Natural Composite: Explanation of Some Peculiarities in the Mechanical Behaviour - E Gehri
- 31-6-1 Length and Moment Configuration Factors - T Isaksson
- 31-6-2 Tensile Strength Perpendicular to Grain According to EN 1193 - H J Blaß and M Schmid
- 31-6-3 Strength of Small Diameter Round Timber - A Ranta-Maunus, U Saarelainen and H Boren
- 31-6-4 Compression Strength Perpendicular to Grain of Structural Timber and Glulam - L Damkilde, P Hoffmeyer and T N Pedersen
- 31-6-5 Bearing Strength of Timber Beams - R H Leicester, H Fordham and H Breitingner
- 32-6-1 Development of High-Resistance Glued Robinia Products and an Attempt to Assign Such Products to the European System of Strength Classes - G Schickhofer and B Obermayr
- 32-6-2 Length and Load Configuration Effects in the Code Format - T Isaksson
- 32-6-3 Length Effect on the Tensile Strength of Truss Chord Members - F Lam
- 32-6-4 Tensile Strength Perpendicular to Grain of Glued Laminated Timber - H J Blaß and M Schmid
- 32-6-5 On the Reliability-based Strength Adjustment Factors for Timber Design - T D G Canisius
- 34-6-1 Material Strength Properties for Canadian Species Used in Japanese Post and Beam Construction - J D Barrett, F Lam, S Nakajima

TIMBER JOINTS AND FASTENERS

- 1-7-1 Mechanical Fasteners and Fastenings in Timber Structures - E G Stern
- 4-7-1 Proposal for a Basic Test Method for the Evaluation of Structural Timber Joints with Mechanical Fasteners and Connectors - RILEM 3TT Committee
- 4-7-2 Test Methods for Wood Fasteners - K Möhler
- 5-7-1 Influence of Loading Procedure on Strength and Slip-Behaviour in Testing Timber Joints - K Möhler
- 5-7-2 Recommendations for Testing Methods for Joints with Mechanical Fasteners and Connectors in Load-Bearing Timber Structures - RILEM 3 TT Committee
- 5-7-3 CIB-Recommendations for the Evaluation of Results of Tests on Joints with Mechanical Fasteners and Connectors used in Load-Bearing Timber Structures - J Kuipers
- 6-7-1 Recommendations for Testing Methods for Joints with Mechanical Fasteners and Connectors in Load-Bearing Timber Structures (seventh draft) - RILEM 3 TT Committee
- 6-7-2 Proposal for Testing Integral Nail Plates as Timber Joints - K Möhler

- 6-7-3 Rules for Evaluation of Values of Strength and Deformation from Test Results - Mechanical Timber Joints - M Johansen, J Kuipers, B Norén
- 6-7-4 Comments to Rules for Testing Timber Joints and Derivation of Characteristic Values for Rigidity and Strength - B Norén
- 7-7-1 Testing of Integral Nail Plates as Timber Joints - K Möhler
- 7-7-2 Long Duration Tests on Timber Joints - J Kuipers
- 7-7-3 Tests with Mechanically Jointed Beams with a Varying Spacing of Fasteners - K Möhler
- 7-100-1 CIB-Timber Code Chapter 5.3 Mechanical Fasteners;CIB-Timber Standard 06 and 07 - H J Larsen
- 9-7-1 Design of Truss Plate Joints - F J Keenan
- 9-7-2 Staples - K Möhler
- 11-7-1 A Draft Proposal for International Standard: ISO Document ISO/TC 165N 38E
- 12-7-1 Load-Carrying Capacity and Deformation Characteristics of Nailed Joints - J Ehlbeck
- 12-7-2 Design of Bolted Joints - H J Larsen
- 12-7-3 Design of Joints with Nail Plates - B Norén
- 13-7-1 Polish Standard BN-80/7159-04: Parts 00-01-02-03-04-05. "Structures from Wood and Wood-based Materials. Methods of Test and Strength Criteria for Joints with Mechanical Fasteners"
- 13-7-2 Investigation of the Effect of Number of Nails in a Joint on its Load Carrying Ability - W Nozynski
- 13-7-3 International Acceptance of Manufacture, Marking and Control of Finger-jointed Structural Timber - B Norén
- 13-7-4 Design of Joints with Nail Plates - Calculation of Slip - B Norén
- 13-7-5 Design of Joints with Nail Plates - The Heel Joint - B Källsner
- 13-7-6 Nail Deflection Data for Design - H J Burgess
- 13-7-7 Test on Bolted Joints - P Vermeyden
- 13-7-8 Comments to paper CIB-W18/12-7-3 "Design of Joints with Nail Plates"- B Norén
- 13-7-9 Strength of Finger Joints - H J Larsen
- 13-100-4 CIB Structural Timber Design Code. Proposal for Section 6.1.5 Nail Plates - N I Bovim
- 14-7-1 Design of Joints with Nail Plates (second edition) - B Norén
- 14-7-2 Method of Testing Nails in Wood (second draft, August 1980) - B Norén
- 14-7-3 Load-Slip Relationship of Nailed Joints - J Ehlbeck and H J Larsen
- 14-7-4 Wood Failure in Joints with Nail Plates - B Norén
- 14-7-5 The Effect of Support Eccentricity on the Design of W- and WW-Trussed with Nail Plate Connectors - B Källsner
- 14-7-6 Derivation of the Allowable Load in Case of Nail Plate Joints Perpendicular to Grain - K Möhler
- 14-7-7 Comments on CIB-W18/14-7-1 - T A C M van der Put
- 15-7-1 Final Recommendation TT-1A: Testing Methods for Joints with Mechanical Fasteners in Load-Bearing Timber Structures. Annex A Punched Metal Plate Fasteners - Joint Committee RILEM/CIB-3TT

- 16-7-1 Load Carrying Capacity of Dowels - E Gehri
- 16-7-2 Bolted Timber Joints: A Literature Survey - N Harding
- 16-7-3 Bolted Timber Joints: Practical Aspects of Construction and Design; a Survey - N Harding
- 16-7-4 Bolted Timber Joints: Draft Experimental Work Plan - Building Research Association of New Zealand
- 17-7-1 Mechanical Properties of Nails and their Influence on Mechanical Properties of Nailed Timber Joints Subjected to Lateral Loads - I Smith, L R J Whale, C Anderson and L Held
- 17-7-2 Notes on the Effective Number of Dowels and Nails in Timber Joints - G Steck
- 18-7-1 Model Specification for Driven Fasteners for Assembly of Pallets and Related Structures - E G Stern and W B Wallin
- 18-7-2 The Influence of the Orientation of Mechanical Joints on their Mechanical Properties - I Smith and L R J Whale
- 18-7-3 Influence of Number of Rows of Fasteners or Connectors upon the Ultimate Capacity of Axially Loaded Timber Joints - I Smith and G Steck
- 18-7-4 A Detailed Testing Method for Nailplate Joints - J Kangas
- 18-7-5 Principles for Design Values of Nailplates in Finland - J Kangas
- 18-7-6 The Strength of Nailplates - N I Bovim and E Aasheim
- 19-7-1 Behaviour of Nailed and Bolted Joints under Short-Term Lateral Load - Conclusions from Some Recent Research - L R J Whale, I Smith and B O Hilson
- 19-7-2 Glued Bolts in Glulam - H Riberholt
- 19-7-3 Effectiveness of Multiple Fastener Joints According to National Codes and Eurocode 5 (Draft) - G Steck
- 19-7-4 The Prediction of the Long-Term Load Carrying Capacity of Joints in Wood Structures - Y M Ivanov and Y Y Slavic
- 19-7-5 Slip in Joints under Long-Term Loading - T Feldborg and M Johansen
- 19-7-6 The Derivation of Design Clauses for Nailed and Bolted Joints in Eurocode 5 - L R J Whale and I Smith
- 19-7-7 Design of Joints with Nail Plates - Principles - B Norén
- 19-7-8 Shear Tests for Nail Plates - B Norén
- 19-7-9 Advances in Technology of Joints for Laminated Timber - Analyses of the Structural Behaviour - M Piazza and G Turrini
- 19-15-1 Connections Deformability in Timber Structures: A Theoretical Evaluation of its Influence on Seismic Effects - A Ceccotti and A Vignoli
- 20-7-1 Design of Nailed and Bolted Joints-Proposals for the Revision of Existing Formulae in Draft Eurocode 5 and the CIB Code - L R J Whale, I Smith and H J Larsen
- 20-7-2 Slip in Joints under Long Term Loading - T Feldborg and M Johansen
- 20-7-3 Ultimate Properties of Bolted Joints in Glued-Laminated Timber - M Yasumura, T Murota and H Sakai
- 20-7-4 Modelling the Load-Deformation Behaviour of Connections with Pin-Type Fasteners under Combined Moment, Thrust and Shear Forces - I Smith
- 21-7-1 Nails under Long-Term Withdrawal Loading - T Feldborg and M Johansen
- 21-7-2 Glued Bolts in Glulam-Proposals for CIB Code - H Riberholt
- 21-7-3 Nail Plate Joint Behaviour under Shear Loading - T Poutanen

- 21-7-4 Design of Joints with Laterally Loaded Dowels. Proposals for Improving the Design Rules in the CIB Code and the Draft Eurocode 5 - J Ehlbeck and H Werner
- 21-7-5 Axially Loaded Nails: Proposals for a Supplement to the CIB Code - J Ehlbeck and W Siebert
- 22-7-1 End Grain Connections with Laterally Loaded Steel Bolts A draft proposal for design rules in the CIB Code - J Ehlbeck and M Gerold
- 22-7-2 Determination of Perpendicular-to-Grain Tensile Stresses in Joints with Dowel-Type Fasteners - A draft proposal for design rules - J Ehlbeck, R Görlacher and H Werner
- 22-7-3 Design of Double-Shear Joints with Non-Metallic Dowels A proposal for a supplement of the design concept - J Ehlbeck and O Eberhart
- 22-7-4 The Effect of Load on Strength of Timber Joints at high Working Load Level - A J M Leijten
- 22-7-5 Plasticity Requirements for Portal Frame Corners - R Gunnewijk and A J M Leijten
- 22-7-6 Background Information on Design of Glulam Rivet Connections in CSA/CAN3-086.1-M89 - A proposal for a supplement of the design concept - E Karacabeyli and D P Janssens
- 22-7-7 Mechanical Properties of Joints in Glued-Laminated Beams under Reversed Cyclic Loading - M Yasumura
- 22-7-8 Strength of Glued Lap Timber Joints - P Glos and H Horstmann
- 22-7-9 Toothed Rings Type Bistyp 075 at the Joints of Fir Wood - J Kerste
- 22-7-10 Calculation of Joints and Fastenings as Compared with the International State - K Zimmer and K Lissner
- 22-7-11 Joints on Glued-in Steel Bars Present Relatively New and Progressive Solution in Terms of Timber Structure Design - G N Zubarev, F A Boitemirov and V M Golovina
- 22-7-12 The Development of Design Codes for Timber Structures made of Compositive Bars with Plate Joints based on Cylindrical Nails - Y V Piskunov
- 22-7-13 Designing of Glued Wood Structures Joints on Glued-in Bars - S B Turkovsky
- 23-7-1 Proposal for a Design Code for Nail Plates - E Aasheim and K H Solli
- 23-7-2 Load Distribution in Nailed Joints - H J Blass
- 24-7-1 Theoretical and Experimental Tension and Shear Capacity of Nail Plate Connections - B Källsner and J Kangas
- 24-7-2 Testing Method and Determination of Basic Working Loads for Timber Joints with Mechanical Fasteners - Y Hirashima and F Kamiya
- 24-7-3 Anchorage Capacity of Nail Plate - J Kangas
- 25-7-2 Softwood and Hardwood Embedding Strength for Dowel type Fasteners - J Ehlbeck and H Werner
- 25-7-4 A Guide for Application of Quality Indexes for Driven Fasteners Used in Connections in Wood Structures - E G Stern
- 25-7-5 35 Years of Experience with Certain Types of Connectors and Connector Plates Used for the Assembly of Wood Structures and their Components- E G Stern
- 25-7-6 Characteristic Strength of Split-ring and Shear-plate Connections - H J Blass, J Ehlbeck and M Schlager
- 25-7-7 Characteristic Strength of Tooth-plate Connector Joints - H J Blass, J Ehlbeck and M Schlager

- 25-7-8 Extending Yield Theory to Screw Connections - T E McLain
- 25-7-9 Determination of k_{def} for Nailed Joints - J W G van de Kuilen
- 25-7-10 Characteristic Strength of UK Timber Connectors - A V Page and C J Mettem
- 25-7-11 Multiple-fastener Dowel-type Joints, a Selected Review of Research and Codes - C J Mettem and A V Page
- 25-7-12 Load Distributions in Multiple-fastener Bolted Joints in European Whitewood Glulam, with Steel Side Plates - C J Mettem and A V Page
- 26-7-1 Proposed Test Method for Dynamic Properties of Connections Assembled with Mechanical Fasteners - J D Dolan
- 26-7-2 Validatory Tests and Proposed Design Formulae for the Load-Carrying Capacity of Toothed-Plate Connected Joints - C J Mettem, A V Page and G Davis
- 26-7-3 Definitions of Terms and Multi-Language Terminology Pertaining to Metal Connector Plates - E G Stern
- 26-7-4 Design of Joints Based on in V-Shape Glued-in Rods - J Kangas
- 26-7-5 Tests on Timber Concrete Composite Structural Elements (TCCs) - A U Meierhofer
- 27-7-1 Glulam Arch Bridge and Design of it's Moment-Resisting Joints - K Komatsu and S Usuku
- 27-7-2 Characteristic Load - Carrying Capacity of Joints with Dowel - type Fasteners in Regard to the System Properties - H Werner
- 27-7-3 Steel Failure Design in Truss Plate Joints - T Poutanen
- 28-7-1 Expanded Tube Joint in Locally DP Reinforced Timber - A J M Leijten, P Ragupathy and K S Virdi
- 28-7-2 A Strength and Stiffness Model for the Expanded Tube Joint - A J M Leijten
- 28-7-3 Load-carrying Capacity of Steel-to Timber Joints with Annular Ring Shanked Nails. A Comparison with the EC5 Design Method - R Görlacher
- 28-7-4 Dynamic Effects on Metal-Plate Connected Wood Truss Joints - S Kent, R Gupta and T Miller
- 28-7-5 Failure of the Timber Bolted Joints Subjected to Lateral Load Perpendicular to Grain - M Yasumura and L Daudeville
- 28-7-6 Design Procedure for Locally Reinforced Joints with Dowel-type Fasteners - H Werner
- 28-7-7 Variability and Effects of Moisture Content on the Withdrawal Characteristics for Lumber as Opposed to Clear Wood - J D Dolan and J W Stelmokas
- 28-7-8 Nail Plate Capacity in Joint Line - A Kevarinmäki and J Kangas
- 28-7-9 Axial Strength of Glued-In Bolts - Calculation Model Based on Non-Linear Fracture Mechanics - A Preliminary Study - C J Johansson, E Serrano, P J Gustafsson and B Enquist
- 28-7-10 Cyclic Lateral Dowel Connection Tests for seismic and Wind Evaluation - J D Dolan
- 29-7-1 A Simple Method for Lateral Load-Carrying Capacity of Dowel-Type Fasteners - J Kangas and J Kurkela
- 29-7-2 Nail Plate Joint Behaviour at Low Versus High Load Level - T Poutanen
- 29-7-3 The Moment Resistance of Tee and Butt - Joint Nail Plate Test Specimens - A Comparison with Current Design Methods - A Reffold, L R J Whale and B S Choo

- 29-7-4 A Critical Review of the Moment Rotation Test Method Proposed in prEN 1075 - M Bettison, B S Choo and L R J Whale
- 29-7-5 Explanation of the Translation and Rotation Behaviour of Prestressed Moment Timber Joints - A J M Leijten
- 29-7-6 Design of Joints and Frame Corners using Dowel-Type Fasteners - E Gehri
- 29-7-7 Quasi-Static Reversed-Cyclic Testing of Nailed Joints - E Karacabeyli and A Ceccotti
- 29-7-8 Failure of Bolted Joints Loaded Parallel to the Grain: Experiment and Simulation - L Davenne, L Daudeville and M Yasumura
- 30-7-1 Flexural Behaviour of GLT Beams End-Jointed by Glued-in Hardwood Dowels - K Komatsu, A Koizumi, J Jensen, T Sasaki and Y Iijima
- 30-7-2 Modelling of the Block Tearing Failure in Nailed Steel-to-Timber Joints - J Kangas, K Aalto and A Kevarinmäki
- 30-7-3 Cyclic Testing of Joints with Dowels and Slotted-in Steel Plates - E Aasheim
- 30-7-4 A Steel-to-Timber Dowelled Joint of High Performance in Combination with a High Strength Wood Composite (Parallam) - E Gehri
- 30-7-5 Multiple Fastener Timber Connections with Dowel Type Fasteners - A Jorissen
- 30-7-6 Influence of Ductility on Load-Carrying Capacity of Joints with Dowel-Type Fasteners - A Mischler
- 31-7-1 Mechanical Properties of Dowel Type Joints under Reversed Cyclic Lateral Loading - M Yasumura
- 31-7-2 Design of Joints with Laterally Loaded Dowels - A Mischler
- 31-7-3 Flexural Behaviour of Glulam Beams Edge-Jointed by Lagscrews with Steel Splice Plates - K Komatsu
- 31-7-4 Design on Timber Capacity in Nailed Steel-to-Timber Joints - J Kangas and J Vesa
- 31-7-5 Timber Contact in Chord Splices of Nail Plate Structures - A Kevarinmäki
- 31-7-6 The Fastener Yield Strength in Bending - A Jorissen and H J Blaß
- 31-7-7 A Proposal for Simplification of Johansen's Formulae, Dealing With the Design of Dowelled-Type Fasteners - F Rouger
- 31-7-8 Simplified Design of Connections with Dowel-type fasteners - H J Blaß and J Ehlbeck
- 32-7-1 Behaviour of Wood-Steel-Wood Bolted Glulam Connections - M Mohammad and J H P Quenneville
- 32-7-2 A new set of experimental tests on beams loaded perpendicular-to-grain by dowel-type joints- M Ballerini
- 32-7-3 Design and Analysis of Bolted Timber Joints under Lateral Force Perpendicular to Grain - M Yasumura and L Daudeville
- 32-7-4 Predicting Capacities of Joints with Laterally Loaded Nails - I Smith and P Quenneville
- 32-7-5 Strength Reduction Rules for Multiple Fastener Joints - A Mischler and E Gehri
- 32-7-6 The Stiffness of Multiple Bolted Connections - A Jorissen
- 32-7-7 Concentric Loading Tests on Girder Truss Components - T N Reynolds, A Reffold, V Enjily and L Whale
- 32-7-8 Dowel Type Connections with Slotted-In Steel Plates - M U Pedersen, C O Clorius, L Damkilde, P Hoffmeyer and L Esklidsen
- 32-7-9 Creep of Nail Plate Reinforced Bolt Joints - J Vesa and A Kevarinmäki

- 32-7-10 The Behaviour of Timber Joints with Ring Connectors - E Gehri and A Mischler
- 32-7-11 Non-Metallic, Adhesiveless Joints for Timber Structures - R D Drake, M P Ansell, C J Mettem and R Bainbridge
- 32-7-12 Effect of Spacing and Edge Distance on the Axial Strength of Glued-in Rods - H J Blaß and B Laskewitz
- 32-7-13 Evaluation of Material Combinations for Bonded in Rods to Achieve Improved Timber Connections - C J Mettem, R J Bainbridge, K Harvey, M P Ansell, J G Broughton and A R Hutchinson
- 33-7-1 Determination of Yield Strength and Ultimate Strength of Dowel-Type Timber Joints – M Yasumura and K Sawata
- 33-7-2 Lateral Shear Capacity of Nailed Joints – U Korin
- 33-7-3 Height-Adjustable Connector for Composite Beams – Y V Piskunov and E G Stern
- 33-7-4 Engineering Ductility Assessment for a Nailed Slotted-In Steel Connection in Glulam– L Stehn and H Johansson
- 33-7-5 Effective Bending Capacity of Dowel-Type Fasteners - H J Blaß, A Bienhaus and V Krämer
- 33-7-6 Load-Carrying Capacity of Joints with Dowel-Type Fasteners and Interlayers - H J Blaß and B Laskewitz
- 33-7-7 Evaluation of Perpendicular to Grain Failure of Beams caused by Concentrated Loads of Joints – A J M Leijten and T A C M van der Put
- 33-7-8 Test Methods for Glued-In Rods for Timber Structures – C Bengtsson and C J Johansson
- 33-7-9 Stiffness Analysis of Nail Plates – P Ellegaard
- 33-7-10 Capacity, Fire Resistance and Gluing Pattern of the Rods in V-Connections – J Kangas
- 33-7-11 Bonded-In Pultrusions for Moment-Resisting Timber Connections – K Harvey, M P Ansell, C J Mettem, R J Bainbridge and N Alexandre
- 33-7-12 Fatigue Performance of Bonded-In Rods in Glulam, Using Three Adhesive Types - R J Bainbridge, K Harvey, C J Mettem and M P Ansell
- 34-7-1 Splitting Strength of Beams Loaded by Connections Perpendicular to Grain, Model Validation – A J M Leijten, A Jorissen
- 34-7-2 Numerical LEFM analyses for the evaluation of failure loads of beams loaded perpendicular-to-grain by single-dowel connections – M Ballerini, R Bezzi
- 34-7-3 Dowel joints loaded perpendicular to grain - H J Larsen, P J Gustafsson
- 34-7-4 Quality Control of Connections based on in V-shape glued-in Steel Rods – J Kangas, A Kevarinmäki
- 34-7-5 Testing Connector Types for Laminated-Timber-Concrete Composite Elements – M Grosse, S Lehmann, K Rautenstrauch
- 34-7-6 Behaviour of Axially Loaded Glued-in Rods - Requirements and Resistance, Especially for Spruce Timber Perpendicular to the Grain Direction – A Bernasconi
- 34-7-7 Embedding characteristics on fibre reinforcement and densified timber joints - P Haller, J Wehsener, T Birk
- 34-7-8 GIROD – Glued-in Rods for Timber Structures – C Bengtsson, C-J Johansson
- 34-7-9 Criteria for Damage and Failure of Dowel-Type Joints Subjected to Force Perpendicular to the Grain – M Yasumura
- 34-7-10 Interaction Between Splitting and Block Shear Failure of Joints – A J M Leijten, A Jorissen, J Kuipers

- 34-7-11 Limit states design of dowel-fastener joints – Placement of modification factors and partial factors, and calculation of variability in resistance – I Smith, G Foliente
- 34-7-12 Design and Modelling of Knee Joints - J Nielsen, P Ellegaard
- 34-7-13 Timber-Steel Shot Fired Nail Connections at Ultimate Limit States - R J Bainbridge, P Larsen, C J Mettem, P Alam, M P Ansell

LOAD SHARING

- 3-8-1 Load Sharing - An Investigation on the State of Research and Development of Design Criteria - E Levin
- 4-8-1 A Review of Load-Sharing in Theory and Practice - E Levin
- 4-8-2 Load Sharing - B Norén
- 19-8-1 Predicting the Natural Frequencies of Light-Weight Wooden Floors - I Smith and Y H Chui
- 20-8-1 Proposed Code Requirements for Vibrational Serviceability of Timber Floors - Y H Chui and I Smith
- 21-8-1 An Addendum to Paper 20-8-1 - Proposed Code Requirements for Vibrational Serviceability of Timber Floors - Y H Chui and I Smith
- 21-8-2 Floor Vibrational Serviceability and the CIB Model Code - S Ohlsson
- 22-8-1 Reliability Analysis of Viscoelastic Floors - F Rouger, J D Barrett and R O Foschi
- 24-8-1 On the Possibility of Applying Neutral Vibrational Serviceability Criteria to Joisted Wood Floors - I Smith and Y H Chui
- 25-8-1 Analysis of Glulam Semi-rigid Portal Frames under Long-term Load - K Komatsu and N Kawamoto
- 34-8-1 System Effect in Sheathed Parallel Timber Beam Structures – M Hansson, T Isaksson

DURATION OF LOAD

- 3-9-1 Definitions of Long Term Loading for the Code of Practice - B Norén
- 4-9-1 Long Term Loading of Trussed Rafters with Different Connection Systems - T Feldborg and M Johansen
- 5-9-1 Strength of a Wood Column in Combined Compression and Bending with Respect to Creep - B Källsner and B Norén
- 6-9-1 Long Term Loading for the Code of Practice (Part 2) - B Norén
- 6-9-2 Long Term Loading - K Möhler
- 6-9-3 Deflection of Trussed Rafters under Alternating Loading during a Year - T Feldborg and M Johansen
- 7-6-1 Strength and Long Term Behaviour of Lumber and Glued-Laminated Timber under Torsion Loads - K Möhler
- 7-9-1 Code Rules Concerning Strength and Loading Time - H J Larsen and E Theilgaard
- 17-9-1 On the Long-Term Carrying Capacity of Wood Structures - Y M Ivanov and Y Y Slavic
- 18-9-1 Prediction of Creep Deformations of Joints - J Kuipers
- 19-9-1 Another Look at Three Duration of Load Models - R O Foschi and Z C Yao

- 19-9-2 Duration of Load Effects for Spruce Timber with Special Reference to Moisture Influence - A Status Report - P Hoffmeyer
- 19-9-3 A Model of Deformation and Damage Processes Based on the Reaction Kinetics of Bond Exchange - T A C M van der Put
- 19-9-4 Non-Linear Creep Superposition - U Korin
- 19-9-5 Determination of Creep Data for the Component Parts of Stressed-Skin Panels - R Kliger
- 19-9-6 Creep an Lifetime of Timber Loaded in Tension and Compression - P Glos
- 19-1-1 Duration of Load Effects and Reliability Based Design (Single Member) - R O Foschi and Z C Yao
- 19-6-1 Effect of Age and/or Load on Timber Strength - J Kuipers
- 19-7-4 The Prediction of the Long-Term Load Carrying Capacity of Joints in Wood Structures - Y M Ivanov and Y Y Slavic
- 19-7-5 Slip in Joints under Long-Term Loading - T Feldborg and M Johansen
- 20-7-2 Slip in Joints under Long-Term Loading - T Feldborg and M Johansen
- 22-9-1 Long-Term Tests with Glued Laminated Timber Girders - M Badstube, W Rug and W Schöne
- 22-9-2 Strength of One-Layer solid and Lengthways Glued Elements of Wood Structures and its Alteration from Sustained Load - L M Kovaltchuk, I N Boitemirova and G B Uspenskaya
- 24-9-1 Long Term Bending Creep of Wood - T Toratti
- 24-9-2 Collection of Creep Data of Timber - A Ranta-Maunus
- 24-9-3 Deformation Modification Factors for Calculating Built-up Wood-Based Structures - I R Kliger
- 25-9-2 DVM Analysis of Wood. Lifetime, Residual Strength and Quality - L F Nielsen
- 26-9-1 Long Term Deformations in Wood Based Panels under Natural Climate Conditions. A Comparative Study - S Thelandersson, J Nordh, T Nordh and S Sandahl
- 28-9-1 Evaluation of Creep Behavior of Structural Lumber in Natural Environment - R Gupta and R Shen
- 30-9-1 DOL Effect in Tension Perpendicular to the Grain of Glulam Depending on Service Classes and Volume - S Aicher and G Dill-Langer
- 30-9-2 Damage Modelling of Glulam in Tension Perpendicular to Grain in Variable Climate - G Dill-Langer and S Aicher
- 31-9-1 Duration of Load Effect in Tension Perpendicular to Grain in Curved Glulam - A Ranta-Maunus
- 32-9-1 Bending-Stress-Redistribution Caused by Different Creep in Tension and Compression and Resulting DOL-Effect - P Becker and K Rautenstrauch
- 32-9-2 The Long Term Performance of Ply-Web Beams - R Grantham and V Enjily

TIMBER BEAMS

- 4-10-1 The Design of Simple Beams - H J Burgess
- 4-10-2 Calculation of Timber Beams Subjected to Bending and Normal Force - H J Larsen
- 5-10-1 The Design of Timber Beams - H J Larsen
- 9-10-1 The Distribution of Shear Stresses in Timber Beams - F J Keenan

- 9-10-2 Beams Notched at the Ends - K Möhler
- 11-10-1 Tapered Timber Beams - H Riberholt
- 13-6-2 Consideration of Size Effects in Longitudinal Shear Strength for Uncracked Beams - R O Foschi and J D Barrett
- 13-6-3 Consideration of Shear Strength on End-Cracked Beams - J D Barrett and R O Foschi
- 18-10-1 Submission to the CIB-W18 Committee on the Design of Ply Web Beams by Consideration of the Type of Stress in the Flanges - J A Baird
- 18-10-2 Longitudinal Shear Design of Glued Laminated Beams - R O Foschi
- 19-10-1 Possible Code Approaches to Lateral Buckling in Beams - H J Burgess
- 19-2-1 Creep Buckling Strength of Timber Beams and Columns - R H Leicester
- 20-2-1 Lateral Buckling Theory for Rectangular Section Deep Beam-Columns - H J Burgess
- 20-10-1 Draft Clause for CIB Code for Beams with Initial Imperfections - H J Burgess
- 20-10-2 Space Joists in Irish Timber - W J Robinson
- 20-10-3 Composite Structure of Timber Joists and Concrete Slab - T Poutanen
- 21-10-1 A Study of Strength of Notched Beams - P J Gustafsson
- 22-10-1 Design of Endnotched Beams - H J Larsen and P J Gustafsson
- 22-10-2 Dimensions of Wooden Flexural Members under Constant Loads - A Pozgai
- 22-10-3 Thin-Walled Wood-Based Flanges in Composite Beams - J König
- 22-10-4 The Calculation of Wooden Bars with flexible Joints in Accordance with the Polish Standart Code and Strict Theoretical Methods - Z Mielczarek
- 23-10-1 Tension Perpendicular to the Grain at Notches and Joints - T A C M van der Put
- 23-10-2 Dimensioning of Beams with Cracks, Notches and Holes. An Application of Fracture Mechanics - K Riipola
- 23-10-3 Size Factors for the Bending and Tension Strength of Structural Timber - J D Barret and A R Fewell
- 23-12-1 Bending Strength of Glulam Beams, a Design Proposal - J Ehlbeck and F Colling
- 23-12-3 Glulam Beams, Bending Strength in Relation to the Bending Strength of the Finger Joints - H Riberholt
- 24-10-1 Shear Strength of Continuous Beams - R H Leicester and F G Young
- 25-10-1 The Strength of Norwegian Glued Laminated Beams - K Solli, E Aasheim and R H Falk
- 25-10-2 The Influence of the Elastic Modulus on the Simulated Bending Strength of Hyperstatic Timber Beams - T D G Canisius
- 27-10-1 Determination of Shear Modulus - R Görlacher and J Kürth
- 29-10-1 Time Dependent Lateral Buckling of Timber Beams - F Rouger
- 29-10-2 Determination of Modulus of Elasticity in Bending According to EN 408 - K H Solli
- 29-10-3 On Determination of Modulus of Elasticity in Bending - L Boström, S Ormarsson and O Dahlblom
- 29-10-4 Relation of Moduli of Elasticity in Flatwise and Edgewise Bending of Solid Timber - C J Johansson, A Steffen and E W Wormuth
- 30-10-1 Nondestructive Evaluation of Wood-based Members and Structures with the Help of Modal Analysis - P Kuklik

- 30-10-2 Measurement of Modulus of Elasticity in Bending - L Boström
- 30-10-3 A Weak Zone Model for Timber in Bending - B Källsner, K Salmela and O Ditlevsen
- 30-10-4 Load Carrying Capacity of Timber Beams with Narrow Moment Peaks - T Isaksson and J Freysoldt

ENVIRONMENTAL CONDITIONS

- 5-11-1 Climate Grading for the Code of Practice - B Norén
- 6-11-1 Climate Grading (2) - B Norén
- 9-11-1 Climate Classes for Timber Design - F J Keenan
- 19-11-1 Experimental Analysis on Ancient Downgraded Timber Structures - B Leggeri and L Paolini
- 19-6-5 Drying Stresses in Round Timber - A Ranta-Maunus
- 22-11-1 Corrosion and Adaptation Factors for Chemically Aggressive Media with Timber Structures - K Erler
- 29-11-1 Load Duration Effect on Structural Beams under Varying Climate Influence of Size and Shape - P Galimard and P Morlier
- 30-11-1 Probabilistic Design Models for the Durability of Timber Constructions - R H Leicester

LAMINATED MEMBERS

- 6-12-1 Directives for the Fabrication of Load-Bearing Structures of Glued Timber - A van der Velden and J Kuipers
- 8-12-1 Testing of Big Glulam Timber Beams - H Kolb and P Frech
- 8-12-2 Instruction for the Reinforcement of Apertures in Glulam Beams - H Kolb and P Frech
- 8-12-3 Glulam Standard Part 1: Glued Timber Structures; Requirements for Timber (Second Draft)
- 9-12-1 Experiments to Provide for Elevated Forces at the Supports of Wooden Beams with Particular Regard to Shearing Stresses and Long-Term Loadings - F Wassipaul and R Lackner
- 9-12-2 Two Laminated Timber Arch Railway Bridges Built in Perth in 1849 - L G Booth
- 9-6-4 Consideration of Combined Stresses for Lumber and Glued Laminated Timber - K Möhler
- 11-6-3 Consideration of Combined Stresses for Lumber and Glued Laminated Timber (addition to Paper CIB-W18/9-6-4) - K Möhler
- 12-12-1 Glulam Standard Part 2: Glued Timber Structures; Rating (3rd draft)
- 12-12-2 Glulam Standard Part 3: Glued Timber Structures; Performance (3 rd draft)
- 13-12-1 Glulam Standard Part 3: Glued Timber Structures; Performance (4th draft)
- 14-12-1 Proposals for CEI-Bois/CIB-W18 Glulam Standards - H J Larsen
- 14-12-2 Guidelines for the Manufacturing of Glued Load-Bearing Timber Structures - Stevin Laboratory
- 14-12-3 Double Tapered Curved Glulam Beams - H Riberholt
- 14-12-4 Comment on CIB-W18/14-12-3 - E Gehri
- 18-12-1 Report on European Glulam Control and Production Standard - H Riberholt

- 18-10-2 Longitudinal Shear Design of Glued Laminated Beams - R O Foschi
- 19-12-1 Strength of Glued Laminated Timber - J Ehlbeck and F Colling
- 19-12-2 Strength Model for Glulam Columns - H J Blaß
- 19-12-3 Influence of Volume and Stress Distribution on the Shear Strength and Tensile Strength Perpendicular to Grain - F Colling
- 19-12-4 Time-Dependent Behaviour of Glued-Laminated Beams - F Zaupa
- 21-12-1 Modulus of Rupture of Glulam Beam Composed of Arbitrary Laminae - K Komatsu and N Kawamoto
- 21-12-2 An Appraisal of the Young's Modulus Values Specified for Glulam in Eurocode 5- L R J Whale, B O Hilson and P D Rodd
- 21-12-3 The Strength of Glued Laminated Timber (Glulam): Influence of Lamination Qualities and Strength of Finger Joints - J Ehlbeck and F Colling
- 21-12-4 Comparison of a Shear Strength Design Method in Eurocode 5 and a More Traditional One - H Riberholt
- 22-12-1 The Dependence of the Bending Strength on the Glued Laminated Timber Girder Depth - M Badstube, W Rug and W Schöne
- 22-12-2 Acid Deterioration of Glulam Beams in Buildings from the Early Half of the 1960s - Preliminary summary of the research project; Overhead pictures - B A Hedlund
- 22-12-3 Experimental Investigation of normal Stress Distribution in Glue Laminated Wooden Arches - Z Mielczarek and W Chanaj
- 22-12-4 Ultimate Strength of Wooden Beams with Tension Reinforcement as a Function of Random Material Properties - R Candowicz and T Dziuba
- 23-12-1 Bending Strength of Glulam Beams, a Design Proposal - J Ehlbeck and F Colling
- 23-12-2 Probability Based Design Method for Glued Laminated Timber - M F Stone
- 23-12-3 Glulam Beams, Bending Strength in Relation to the Bending Strength of the Finger Joints - H Riberholt
- 23-12-4 Glued Laminated Timber - Strength Classes and Determination of Characteristic Properties - H Riberholt, J Ehlbeck and A Fewell
- 24-12-1 Contribution to the Determination of the Bending Strength of Glulam Beams - F Colling, J Ehlbeck and R Görlacher
- 24-12-2 Influence of Perpendicular-to-Grain Stressed Volume on the Load-Carrying Capacity of Curved and Tapered Glulam Beams - J Ehlbeck and J Kürth
- 25-12-1 Determination of Characteristic Bending Values of Glued Laminated Timber. EN-Approach and Reality - E Gehri
- 26-12-1 Norwegian Bending Tests with Glued Laminated Beams-Comparative Calculations with the "Karlsruhe Calculation Model" - E Aasheim, K Solli, F Colling, R H Falk, J Ehlbeck and R Görlacher
- 26-12-2 Simulation Analysis of Norwegian Spruce Glued-Laminated Timber - R Hernandez and R H Falk
- 26-12-3 Investigation of Laminating Effects in Glued-Laminated Timber - F Colling and R H Falk
- 26-12-4 Comparing Design Results for Glulam Beams According to Eurocode 5 and to the French Working Stress Design Code (CB71) - F Rouger
- 27-12-1 State of the Art Report: Glulam Timber Bridge Design in the U.S. - M A Ritter and T G Williamson
- 27-12-2 Common Design Practice for Timber Bridges in the United Kingdom - C J Mettem, J P Marcroft and G Davis

- 27-12-3 Influence of Weak Zones on Stress Distribution in Glulam Beams - E Serrano and H J Larsen
- 28-12-1 Determination of Characteristic Bending Strength of Glued Laminated Timber - E Gehri
- 28-12-2 Size Factor of Norwegian Glued Laminated Beams - E Aasheim and K H Solli
- 28-12-3 Design of Glulam Beams with Holes - K Riipola
- 28-12-4 Compression Resistance of Glued Laminated Timber Short Columns- U Korin
- 29-12-1 Development of Efficient Glued Laminated Timber - G Schickhofer
- 30-12-1 Experimental Investigation and Analysis of Reinforced Glulam Beams - K Oiger
- 31-12-1 Depth Factor for Glued Laminated Timber-Discussion of the Eurocode 5 Approach - B Källsner, O Carling and C J Johansson
- 32-12-1 The bending stiffness of nail-laminated timber elements in transverse direction- T Wolf and O Schäfer
- 33-12-1 Internal Stresses in the Cross-Grain Direction of Wood Induced by Climate Variation – J Jönsson and S Svensson
- 34-12-1 High-Strength I-Joist Compatible Glulam Manufactured with LVL Tension Laminations – B Yeh, T G Williamson
- 34-12-2 Evaluation of Glulam Shear Strength Using A Full-Size Four-Point Test Method – B Yeh, T G Williamson
- 34-12-3 Design Model for FRP Reinforced Glulam Beams – M Romani, H J Blaß
- 34-12-4 Moisture induced stresses in glulam cross sections – J Jönsson
- 34-12-5 Load Carrying Capacity of Nail-Laminated Timber under Concentrated Loads -- V Krämer, H J Blaß
- 34-12-6 Determination of Shear Strength Values for GLT Using Visual and Machine Graded Spruce Laminations – G Schickhofer
- 34-12-7 Mechanically Jointed Beams: Possibilities of Analysis and some special Problems – H Kreuzinger

PARTICLE AND FIBRE BUILDING BOARDS

- 7-13-1 Fibre Building Boards for CIB Timber Code (First Draft)- O Brynildsen
- 9-13-1 Determination of the Bearing Strength and the Load-Deformation Characteristics of Particleboard - K Möhler, T Budianto and J Ehlbeck
- 9-13-2 The Structural Use of Tempered Hardboard - W W L Chan
- 11-13-1 Tests on Laminated Beams from Hardboard under Short- and Longterm Load - W Nozynski
- 11-13-2 Determination of Deformation of Special Densified Hardboard under Long-term Load and Varying Temperature and Humidity Conditions - W Halfar
- 11-13-3 Determination of Deformation of Hardboard under Long-term Load in Changing Climate - W Halfar
- 14-4-1 An Introduction to Performance Standards for Wood-Base Panel Products - D H Brown
- 14-4-2 Proposal for Presenting Data on the Properties of Structural Panels - T Schmidt
- 16-13-1 Effect of Test Piece Size on Panel Bending Properties - P W Post
- 20-4-1 Considerations of Reliability - Based Design for Structural Composite Products - M R O'Halloran, J A Johnson, E G Elias and T P Cunningham

- 20-13-1 Classification Systems for Structural Wood-Based Sheet Materials - V C Kearley and A R Abbott
- 21-13-1 Design Values for Nailed Chipboard - Timber Joints - A R Abbott
- 25-13-1 Bending Strength and Stiffness of Izopanel Plates - Z Mielczarek
- 28-13-1 Background Information for "Design Rated Oriented Strand Board (OSB)" in CSA Standards - Summary of Short-term Test Results - E Karacabeyli, P Lau, C R Henderson, F V Meakes and W Deacon
- 28-13-2 Torsional Stiffness of Wood-Hardboard Composed I-Beam - P Olejniczak

TRUSSED RAFTERS

- 4-9-1 Long-term Loading of Trussed Rafters with Different Connection Systems - T Feldborg and M Johansen
- 6-9-3 Deflection of Trussed Rafters under Alternating Loading During a Year - T Feldborg and M Johansen
- 7-2-1 Lateral Bracing of Timber Struts - J A Simon
- 9-14-1 Timber Trusses - Code Related Problems - T F Williams
- 9-7-1 Design of Truss Plate Joints - F J Keenan
- 10-14-1 Design of Roof Bracing - The State of the Art in South Africa - P A V Bryant and J A Simon
- 11-14-1 Design of Metal Plate Connected Wood Trusses - A R Egerup
- 12-14-1 A Simple Design Method for Standard Trusses - A R Egerup
- 13-14-1 Truss Design Method for CIB Timber Code - A R Egerup
- 13-14-2 Trussed Rafters, Static Models - H Riberholt
- 13-14-3 Comparison of 3 Truss Models Designed by Different Assumptions for Slip and E-Modulus - K Möhler
- 14-14-1 Wood Trussed Rafter Design - T Feldborg and M Johansen
- 14-14-2 Truss-Plate Modelling in the Analysis of Trusses - R O Foschi
- 14-14-3 Cantilevered Timber Trusses - A R Egerup
- 14-7-5 The Effect of Support Eccentricity on the Design of W- and WW-Trusses with Nail Plate Connectors - B Källsner
- 15-14-1 Guidelines for Static Models of Trussed Rafters - H Riberholt
- 15-14-2 The Influence of Various Factors on the Accuracy of the Structural Analysis of Timber Roof Trusses - F R P Pienaar
- 15-14-3 Bracing Calculations for Trussed Rafter Roofs - H J Burgess
- 15-14-4 The Design of Continuous Members in Timber Trussed Rafters with Punched Metal Connector Plates - P O Reece
- 15-14-5 A Rafter Design Method Matching U.K. Test Results for Trussed Rafters - H J Burgess
- 16-14-1 Full-Scale Tests on Timber Fink Trusses Made from Irish Grown Sitka Spruce - V Picardo
- 17-14-1 Data from Full Scale Tests on Prefabricated Trussed Rafters - V Picardo
- 17-14-2 Simplified Static Analysis and Dimensioning of Trussed Rafters - H Riberholt
- 17-14-3 Simplified Calculation Method for W-Trusses - B Källsner
- 18-14-1 Simplified Calculation Method for W-Trusses (Part 2) - B Källsner

- 18-14-2 Model for Trussed Rafter Design - T Poutanen
- 19-14-1 Annex on Simplified Design of W-Trusses - H J Larsen
- 19-14-2 Simplified Static Analysis and Dimensioning of Trussed Rafters - Part 2 - H Riberholt
- 19-14-3 Joint Eccentricity in Trussed Rafters - T Poutanen
- 20-14-1 Some Notes about Testing Nail Plates Subjected to Moment Load - T Poutanen
- 20-14-2 Moment Distribution in Trussed Rafters - T Poutanen
- 20-14-3 Practical Design Methods for Trussed Rafters - A R Egerup
- 22-14-1 Guidelines for Design of Timber Trussed Rafters - H Riberholt
- 23-14-1 Analyses of Timber Trussed Rafters of the W-Type - H Riberholt
- 23-14-2 Proposal for Eurocode 5 Text on Timber Trussed Rafters - H Riberholt
- 24-14-1 Capacity of Support Areas Reinforced with Nail Plates in Trussed Rafters - A Kevarinmäki
- 25-14-1 Moment Anchorage Capacity of Nail Plates in Shear Tests - A Kevarinmaki and J. Kangas
- 25-14-2 Design Values of Anchorage Strength of Nail Plate Joints by 2-curve Method and Interpolation - J Kangas and A Kevarinmaki
- 26-14-1 Test of Nail Plates Subjected to Moment - E Aasheim
- 26-14-2 Moment Anchorage Capacity of Nail Plates - A Kevarinmäki and J Kangas
- 26-14-3 Rotational Stiffness of Nail Plates in Moment Anchorage - A Kevarinmäki and J Kangas
- 26-14-4 Solution of Plastic Moment Anchorage Stress in Nail Plates - A Kevarinmäki
- 26-14-5 Testing of Metal-Plate-Connected Wood-Truss Joints - R Gupta
- 26-14-6 Simulated Accidental Events on a Trussed Rafter Roofed Building - C J Mettem and J P Marcroft
- 30-14-1 The Stability Behaviour of Timber Trussed Rafter Roofs - Studies Based on Eurocode 5 and Full Scale Testing - R J Bainbridge, C J Mettem, A Reffold and T Studer
- 32-14-1 Analysis of Timber Reinforced with Punched Metal Plate Fasteners- J Nielsen
- 33-14-1 Moment Capacity of Timber Beams Loaded in Four-Point Bending and Reinforced with Punched Metal Plate Fasteners – J Nielsen

STRUCTURAL STABILITY

- 8-15-1 Laterally Loaded Timber Columns: Tests and Theory - H J Larsen
- 13-15-1 Timber and Wood-Based Products Structures. Panels for Roof Coverings. Methods of Testing and Strength Assessment Criteria. Polish Standard BN-78/7159-03
- 16-15-1 Determination of Bracing Structures for Compression Members and Beams - H Brüninghoff
- 17-15-1 Proposal for Chapter 7.4 Bracing - H Brüninghoff
- 17-15-2 Seismic Design of Small Wood Framed Houses - K F Hansen
- 18-15-1 Full-Scale Structures in Glued Laminated Timber, Dynamic Tests: Theoretical and Experimental Studies - A Ceccotti and A Vignoli
- 18-15-2 Stabilizing Bracings - H Brüninghoff

- 19-15-1 Connections Deformability in Timber Structures: a Theoretical Evaluation of its Influence on Seismic Effects - A Ceccotti and A Vignoli
- 19-15-2 The Bracing of Trussed Beams - M H Kessel and J Natterer
- 19-15-3 Racking Resistance of Wooden Frame Walls with Various Openings - M Yasumura
- 19-15-4 Some Experiences of Restoration of Timber Structures for Country Buildings - G Cardinale and P Spinelli
- 19-15-5 Non-Destructive Vibration Tests on Existing Wooden Dwellings - Y Hirashima
- 20-15-1 Behaviour Factor of Timber Structures in Seismic Zones. - A Ceccotti and A Vignoli
- 21-15-1 Rectangular Section Deep Beam - Columns with Continuous Lateral Restraint - H J Burgess
- 21-15-2 Buckling Modes and Permissible Axial Loads for Continuously Braced Columns- H J Burgess
- 21-15-3 Simple Approaches for Column Bracing Calculations - H J Burgess
- 21-15-4 Calculations for Discrete Column Restraints - H J Burgess
- 21-15-5 Behaviour Factor of Timber Structures in Seismic Zones (Part Two) - A Ceccotti and A Vignoli
- 22-15-1 Suggested Changes in Code Bracing Recommendations for Beams and Columns - H J Burgess
- 22-15-2 Research and Development of Timber Frame Structures for Agriculture in Poland- S Kus and J Kerste
- 22-15-3 Ensuring of Three-Dimensional Stiffness of Buildings with Wood Structures - A K Shenghelia
- 22-15-5 Seismic Behavior of Arched Frames in Timber Construction - M Yasumura
- 22-15-6 The Robustness of Timber Structures - C J Mettem and J P Marcroft
- 22-15-7 Influence of Geometrical and Structural Imperfections on the Limit Load of Wood Columns - P Dutko
- 23-15-1 Calculation of a Wind Girder Loaded also by Discretely Spaced Braces for Roof Members - H J Burgess
- 23-15-2 Stability Design and Code Rules for Straight Timber Beams - T A C M van der Put
- 23-15-3 A Brief Description of Formula of Beam-Columns in China Code - S Y Huang
- 23-15-4 Seismic Behavior of Braced Frames in Timber Construction - M Yasumura
- 23-15-5 On a Better Evaluation of the Seismic Behavior Factor of Low-Dissipative Timber Structures - A Ceccotti and A Vignoli
- 23-15-6 Disproportionate Collapse of Timber Structures - C J Mettem and J P Marcroft
- 23-15-7 Performance of Timber Frame Structures During the Loma Prieta California Earthquake - M R O'Halloran and E G Elias
- 24-15-2 Discussion About the Description of Timber Beam-Column Formula - S Y Huang
- 24-15-3 Seismic Behavior of Wood-Framed Shear Walls - M Yasumura
- 25-15-1 Structural Assessment of Timber Framed Building Systems - U Korin
- 25-15-3 Mechanical Properties of Wood-framed Shear Walls Subjected to Reversed Cyclic Lateral Loading - M Yasumura

- 26-15-1 Bracing Requirements to Prevent Lateral Buckling in Trussed Rafters - C J Mettem and P J Moss
- 26-15-2 Eurocode 8 - Part 1.3 - Chapter 5 - Specific Rules for Timber Buildings in Seismic Regions - K Becker, A Ceccotti, H Charlier, E Katsaragakis, H J Larsen and H Zeitter
- 26-15-3 Hurricane Andrew - Structural Performance of Buildings in South Florida - M R O'Halloran, E L Keith, J D Rose and T P Cunningham
- 29-15-1 Lateral Resistance of Wood Based Shear Walls with Oversized Sheathing Panels - F Lam, H G L Prion and M He
- 29-15-2 Damage of Wooden Buildings Caused by the 1995 Hyogo-Ken Nanbu Earthquake - M Yasumura, N Kawai, N Yamaguchi and S Nakajima
- 29-15-3 The Racking Resistance of Timber Frame Walls: Design by Test and Calculation - D R Griffiths, C J Mettem, V Enjily, P J Steer
- 29-15-4 Current Developments in Medium-Rise Timber Frame Buildings in the UK - C J Mettem, G C Pitts, P J Steer, V Enjily
- 29-15-5 Natural Frequency Prediction for Timber Floors - R J Bainbridge, and C J Mettem
- 30-15-1 Cyclic Performance of Perforated Wood Shear Walls with Oversize Oriented Strand Board Panels - Ming He, H Magnusson, F Lam, and H G L Prion
- 30-15-2 A Numerical Analysis of Shear Walls Structural Performances - L Davenne, L Daudeville, N Kawai and M Yasumura
- 30-15-3 Seismic Force Modification Factors for the Design of Multi-Storey Wood-Frame Platform Construction - E Karacabeyli and A Ceccotti
- 30-15-4 Evaluation of Wood Framed Shear Walls Subjected to Lateral Load - M Yasumura and N Kawai
- 31-15-1 Seismic Performance Testing On Wood-Framed Shear Wall - N Kawai
- 31-15-2 Robustness Principles in the Design of Medium-Rise Timber-Framed Buildings - C J Mettem, M W Milner, R J Bainbridge and V. Enjily
- 31-15-3 Numerical Simulation of Pseudo-Dynamic Tests Performed to Shear Walls - L Daudeville, L Davenne, N Richard, N Kawai and M Yasumura
- 31-15-4 Force Modification Factors for Braced Timber Frames - H G L Prion, M Popovski and E Karacabeyli
- 32-15-1 Three-Dimensional Interaction in Stabilisation of Multi-Storey Timber Frame Buildings - S Andreasson
- 32-15-2 Application of Capacity Spectrum Method to Timber Houses - N Kawai
- 32-15-3 Design Methods for Shear Walls with Openings - C Ni, E Karacabeyli and A Ceccotti
- 32-15-4 Static Cyclic Lateral Loading Tests on Nailed Plywood Shear Walls - K Komatsu, K H Hwang and Y Itou
- 33-15-1 Lateral Load Capacities of Horizontally Sheathed Unblocked Shear Walls – C Ni, E Karacabeyli and A Ceccotti
- 33-15-2 Prediction of Earthquake Response of Timber Houses Considering Shear Deformation of Horizontal Frames – N Kawai
- 33-15-3 Eurocode 5 Rules for Bracing – H J Larsen
- 34-15-1 A simplified plastic model for design of partially anchored wood-framed shear walls – B Källsner, U A Girhammar, Liping Wu
- 34-15-2 The Effect of the Moisture Content on the Performance of the Shear Walls – S Nakajima

34-15-3 Evaluation of Damping Capacity of Timber Structures for Seismic Design –
M Yasumura

FIRE

- 12-16-1 British Standard BS 5268 the Structural Use of Timber: Part 4 Fire Resistance of
Timber Structures
- 13-100-2 CIB Structural Timber Design Code. Chapter 9. Performance in Fire
- 19-16-1 Simulation of Fire in Tests of Axially Loaded Wood Wall Studs - J König
- 24-16-1 Modelling the Effective Cross Section of Timber Frame Members Exposed to Fire
- J König
- 25-16-1 The Effect of Density on Charring and Loss of Bending Strength in Fire - J König
- 25-16-2 Tests on Glued-Laminated Beams in Bending Exposed to Natural Fires -
F Bolonius Olesen and J König
- 26-16-1 Structural Fire Design According to Eurocode 5, Part 1.2 - J König
- 31-16-1 Revision of ENV 1995-1-2: Charring and Degradation of Strength and Stiffness -
J König
- 33-16-1 A Design Model for Load-carrying Timber Frame Members in Walls and Floors
Exposed to Fire - J König
- 33-16-2 A Review of Component Additive Methods Used for the Determination of Fire
Resistance of Separating Light Timber Frame Construction - J König, T Oksanen
and K Towler
- 33-16-3 Thermal and Mechanical Properties of Timber and Some Other Materials Used in
Light Timber Frame Construction - B Källsner and J König
- 34-16-1 Influence of the Strength Determining Factors on the Fire Resistance Capability of
Timber Structural Members – I Totev, D Dakov
- 34-16-2 Cross section properties of fire exposed rectangular timber members - J König,
B Källsner
- 34-16-3 Pull-Out Tests on Glued-in Rods at High Temperatures – A Mischler,
A Frangi

STATISTICS AND DATA ANALYSIS

- 13-17-1 On Testing Whether a Prescribed Exclusion Limit is Attained - W G Warren
- 16-17-1 Notes on Sampling and Strength Prediction of Stress Graded Structural Timber -
P Glos
- 16-17-2 Sampling to Predict by Testing the Capacity of Joints, Components and Structures
- B Norén
- 16-17-3 Discussion of Sampling and Analysis Procedures - P W Post
- 17-17-1 Sampling of Wood for Joint Tests on the Basis of Density - I Smith, L R J Whale
- 17-17-2 Sampling Strategy for Physical and Mechanical Properties of Irish Grown Sitka
Spruce - V Picardo
- 18-17-1 Sampling of Timber in Structural Sizes - P Glos
- 18-6-3 Notes on Sampling Factors for Characteristic Values - R H Leicester
- 19-17-1 Load Factors for Proof and Prototype Testing - R H Leicester
- 19-6-2 Confidence in Estimates of Characteristic Values - R H Leicester
- 21-6-1 Draft Australian Standard: Methods for Evaluation of Strength and Stiffness of
Graded Timber - R H Leicester

- 21-6-2 The Determination of Characteristic Strength Values for Stress Grades of Structural Timber. Part 1 - A R Fewell and P Glos
- 22-17-1 Comment on the Strength Classes in Eurocode 5 by an Analysis of a Stochastic Model of Grading - A proposal for a supplement of the design concept - M Kiesel
- 24-17-1 Use of Small Samples for In-Service Strength Measurement - R H Leicester and F G Young
- 24-17-2 Equivalence of Characteristic Values - R H Leicester and F G Young
- 24-17-3 Effect of Sampling Size on Accuracy of Characteristic Values of Machine Grades - Y H Chui, R Turner and I Smith
- 24-17-4 Harmonisation of LSD Codes - R H Leicester
- 25-17-2 A Body for Confirming the Declaration of Characteristic Values - J Sunley
- 25-17-3 Moisture Content Adjustment Procedures for Engineering Standards - D W Green and J W Evans
- 27-17-1 Statistical Control of Timber Strength - R H Leicester and H O Breitingner
- 30-17-1 A New Statistical Method for the Establishment of Machine Settings - F Rouger

GLUED JOINTS

- 20-18-1 Wood Materials under Combined Mechanical and Hygral Loading - A Martensson and S Thelandersson
- 20-18-2 Analysis of Generalized Volkersen - Joints in Terms of Linear Fracture Mechanics - P J Gustafsson
- 20-18-3 The Complete Stress-Slip Curve of Wood-Adhesives in Pure Shear - H Wernersson and P J Gustafsson
- 22-18-1 Perspective Adhesives and Protective Coatings for Wood Structures - A S Freidin
- 34-18-1 Performance Based Classification of Adhesives for Structural Timber Applications - R J Bainbridge, C J Mettem, J G Broughton, A R Hutchinson

FRACTURE MECHANICS

- 21-10-1 A Study of Strength of Notched Beams - P J Gustafsson
- 22-10-1 Design of Endnotched Beams - H J Larsen and P J Gustafsson
- 23-10-1 Tension Perpendicular to the Grain at Notches and Joints - T A C M van der Put
- 23-10-2 Dimensioning of Beams with Cracks, Notches and Holes. An Application of Fracture Mechanics - K Riipola
- 23-19-1 Determination of the Fracture Energie of Wood for Tension Perpendicular to the Grain - W Rug, M Badstube and W Schöne
- 23-19-2 The Fracture Energy of Wood in Tension Perpendicular to the Grain. Results from a Joint Testing Project - H J Larsen and P J Gustafsson
- 23-19-3 Application of Fracture Mechanics to Timber Structures - A Ranta-Maunus
- 24-19-1 The Fracture Energy of Wood in Tension Perpendicular to the Grain - H J Larsen and P J Gustafsson
- 28-19-1 Fracture of Wood in Tension Perpendicular to the Grain: Experiment and Numerical Simulation by Damage Mechanics - L Daudeville, M Yasumura and J D Lanvin
- 28-19-2 A New Method of Determining Fracture Energy in Forward Shear along the Grain - H D Mansfield-Williams

- 28-19-3 Fracture Design Analysis of Wooden Beams with Holes and Notches. Finite Element Analysis based on Energy Release Rate Approach - H Petersson
- 28-19-4 Design of Timber Beams with Holes by Means of Fracture Mechanics - S Aicher, J Schmidt and S Brunold
- 30-19-1 Failure Analysis of Single-Bolt Joints - L Daudeville, L Davenne and M Yasumura

SERVICEABILITY

- 27-20-1 Codification of Serviceability Criteria - R H Leicester
- 27-20-2 On the Experimental Determination of Factor k_{def} and Slip Modulus k_{ser} from Short- and Long-Term Tests on a Timber-Concrete Composite (TCC) Beam - S Capretti and A Ceccotti
- 27-20-3 Serviceability Limit States: A Proposal for Updating Eurocode 5 with Respect to Eurocode 1 - P Racher and F Rouger
- 27-20-4 Creep Behavior of Timber under External Conditions - C Le Govic, F Rouger, T Toratti and P Morlier
- 30-20-1 Design Principles for Timber in Compression Perpendicular to Grain - S Thelandersson and A Mårtensson
- 30-20-2 Serviceability Performance of Timber Floors - Eurocode 5 and Full Scale Testing - R J Bainbridge and C J Mettem
- 32-20-1 Floor Vibrations - B Mohr

TEST METHODS

- 31-21-1 Development of an Optimised Test Configuration to Determine Shear Strength of Glued Laminated Timber - G Schickhofer and B Obermayr
- 31-21-2 An Impact Strength Test Method for Structural Timber. The Theory and a Preliminary Study - T D G Canisius

CIB TIMBER CODE

- 2-100-1 A Framework for the Production of an International Code of Practice for the Structural Use of Timber - W T Curry
- 5-100-1 Design of Solid Timber Columns (First Draft) - H J Larsen
- 5-100-2 A Draft Outline of a Code for Timber Structures - L G Booth
- 6-100-1 Comments on Document 5-100-1; Design of Solid Timber Columns - H J Larsen and E Theilgaard
- 6-100-2 CIB Timber Code: CIB Timber Standards - H J Larsen and E Theilgaard
- 7-100-1 CIB Timber Code Chapter 5.3 Mechanical Fasteners; CIB Timber Standard 06 and 07 - H J Larsen
- 8-100-1 CIB Timber Code - List of Contents (Second Draft) - H J Larsen
- 9-100-1 The CIB Timber Code (Second Draft)
- 11-100-1 CIB Structural Timber Design Code (Third Draft)
- 11-100-2 Comments Received on the CIB Code
 - a U Saarelainen
 - b Y M Ivanov
 - c R H Leicester
 - d W Nozynski
 - e W R A Meyer

f P Beckmann; R Marsh
g W R A Meyer
h W R A Meyer

- 11-100-3 CIB Structural Timber Design Code; Chapter 3 - H J Larsen
- 12-100-1 Comment on the CIB Code - Sous-Commission Glulam
- 12-100-2 Comment on the CIB Code - R H Leicester
- 12-100-3 CIB Structural Timber Design Code (Fourth Draft)
- 13-100-1 Agreed Changes to CIB Structural Timber Design Code
- 13-100-2 CIB Structural Timber Design Code. Chapter 9: Performance in Fire
- 13-100-3a Comments on CIB Structural Timber Design Code
- 13-100-3b Comments on CIB Structural Timber Design Code - W R A Meyer
- 13-100-3c Comments on CIB Structural Timber Design Code - British Standards Institution
- 13-100-4 CIB Structural Timber Design Code. Proposal for Section 6.1.5 Nail Plates - N I Bovim
- 14-103-2 Comments on the CIB Structural Timber Design Code - R H Leicester
- 15-103-1 Resolutions of TC 165-meeting in Athens 1981-10-12/13
- 21-100-1 CIB Structural Timber Design Code. Proposed Changes of Sections on Lateral Instability, Columns and Nails - H J Larsen
- 22-100-1 Proposal for Including an Updated Design Method for Bearing Stresses in CIB W18 - Structural Timber Design Code - B Madsen
- 22-100-2 Proposal for Including Size Effects in CIB W18A Timber Design Code - B Madsen
- 22-100-3 CIB Structural Timber Design Code - Proposed Changes of Section on Thin-Flanged Beams - J König
- 22-100-4 Modification Factor for "Aggressive Media" - a Proposal for a Supplement to the CIB Model Code - K Erler and W Rug
- 22-100-5 Timber Design Code in Czechoslovakia and Comparison with CIB Model Code - P Dutko and B Kozelouh

LOADING CODES

- 4-101-1 Loading Regulations - Nordic Committee for Building Regulations
- 4-101-2 Comments on the Loading Regulations - Nordic Committee for Building Regulations

STRUCTURAL DESIGN CODES

- 1-102-1 Survey of Status of Building Codes, Specifications etc., in USA - E G Stern
- 1-102-2 Australian Codes for Use of Timber in Structures - R H Leicester
- 1-102-3 Contemporary Concepts for Structural Timber Codes - R H Leicester
- 1-102-4 Revision of CP 112 - First Draft, July 1972 - British Standards Institution
- 4-102-1 Comparison of Codes and Safety Requirements for Timber Structures in EEC Countries - Timber Research and Development Association
- 4-102-2 Nordic Proposals for Safety Code for Structures and Loading Code for Design of Structures - O A Brynildsen
- 4-102-3 Proposal for Safety Codes for Load-Carrying Structures - Nordic Committee for Building Regulations

- 4-102-4 Comments to Proposal for Safety Codes for Load-Carrying Structures - Nordic Committee for Building Regulations
- 4-102-5 Extract from Norwegian Standard NS 3470 "Timber Structures"
- 4-102-6 Draft for Revision of CP 112 "The Structural Use of Timber" - W T Curry
- 8-102-1 Polish Standard PN-73/B-03150: Timber Structures; Statistical Calculations and Designing
- 8-102-2 The Russian Timber Code: Summary of Contents
- 9-102-1 Svensk Byggnorm 1975 (2nd Edition); Chapter 27: Timber Construction
- 11-102-1 Eurocodes - H J Larsen
- 13-102-1 Program of Standardisation Work Involving Timber Structures and Wood-Based Products in Poland
- 17-102-1 Safety Principles - H J Larsen and H Riberholt
- 17-102-2 Partial Coefficients Limit States Design Codes for Structural Timberwork - I Smith
- 18-102-1 Antiseismic Rules for Timber Structures: an Italian Proposal - G Augusti and A Ceccotti
- 18-1-2 Eurocode 5, Timber Structures - H J Larsen
- 19-102-1 Eurocode 5 - Requirements to Timber - Drafting Panel Eurocode 5
- 19-102-2 Eurocode 5 and CIB Structural Timber Design Code - H J Larsen
- 19-102-3 Comments on the Format of Eurocode 5 - A R Fewell
- 19-102-4 New Developments of Limit States Design for the New GDR Timber Design Code - W Rug and M Badstube
- 19-7-3 Effectiveness of Multiple Fastener Joints According to National Codes and Eurocode 5 (Draft) - G Steck
- 19-7-6 The Derivation of Design Clauses for Nailed and Bolted Joints in Eurocode5 - L R J Whale and I Smith
- 19-14-1 Annex on Simplified Design of W-Trusses - H J Larsen
- 20-102-1 Development of a GDR Limit States Design Code for Timber Structures - W Rug and M Badstube
- 21-102-1 Research Activities Towards a New GDR Timber Design Code Based on Limit States Design - W Rug and M Badstube
- 22-102-1 New GDR Timber Design Code, State and Development - W Rug, M Badstube and W Kofent
- 22-102-2 Timber Strength Parameters for the New USSR Design Code and its Comparison with International Code - Y Y Slavik, N D Denesh and E B Ryumina
- 22-102-3 Norwegian Timber Design Code - Extract from a New Version - E Aasheim and K H Solli
- 23-7-1 Proposal for a Design Code for Nail Plates - E Aasheim and K H Solli
- 24-102-2 Timber Footbridges: A Comparison Between Static and Dynamic Design Criteria - A Ceccotti and N de Robertis
- 25-102-1 Latest Development of Eurocode 5 - H J Larsen
- 25-102-1A Annex to Paper CIB-W18/25-102-1. Eurocode 5 - Design of Notched Beams - H J Larsen, H Riberholt and P J Gustafsson
- 25-102-2 Control of Deflections in Timber Structures with Reference to Eurocode 5 - A Martensson and S Thelandersson

- 28-102-1 Eurocode 5 - Design of Timber Structures - Part 2: Bridges - D Bajolet, E Gehri, J König, H Kreuzinger, H J Larsen, R Mäkipuro and C Mettem
- 28-102-2 Racking Strength of Wall Diaphragms - Discussion of the Eurocode 5 Approach - B Källsner
- 29-102-1 Model Code for the Probabilistic Design of Timber Structures - H J Larsen, T Isaksson and S Thelandersson
- 30-102-1 Concepts for Drafting International Codes and Standards for Timber Constructions - R H Leicester
- 33-102-1 International Standards for Bamboo – J J A Janssen

INTERNATIONAL STANDARDS ORGANISATION

- 3-103-1 Method for the Preparation of Standards Concerning the Safety of Structures (ISO/DIS 3250) - International Standards Organisation ISO/TC98
- 4-103-1 A Proposal for Undertaking the Preparation of an International Standard on Timber Structures - International Standards Organisation
- 5-103-1 Comments on the Report of the Consultation with Member Bodies Concerning ISO/TC/P129 - Timber Structures - Dansk Ingeniorforening
- 7-103-1 ISO Technical Committees and Membership of ISO/TC 165
- 8-103-1 Draft Resolutions of ISO/TC 165
- 12-103-1 ISO/TC 165 Ottawa, September 1979
- 13-103-1 Report from ISO/TC 165 - A Sorensen
- 14-103-1 Comments on ISO/TC 165 N52 "Timber Structures; Solid Timber in Structural Sizes; Determination of Some Physical and Mechanical Properties"
- 14-103-2 Comments on the CIB Structural Timber Design Code - R H Leicester
- 21-103-1 Concept of a Complete Set of Standards - R H Leicester

JOINT COMMITTEE ON STRUCTURAL SAFETY

- 3-104-1 International System on Unified Standard Codes of Practice for Structures - Comité Européen du Béton (CEB)
- 7-104-1 Volume 1: Common Unified Rules for Different Types of Construction and Material - CEB

CIB PROGRAMME, POLICY AND MEETINGS

- 1-105-1 A Note on International Organisations Active in the Field of Utilisation of Timber - P Sonnemans
- 5-105-1 The Work and Objectives of CIB-W18-Timber Structures - J G Sunley
- 10-105-1 The Work of CIB-W18 Timber Structures - J G Sunley
- 15-105-1 Terms of Reference for Timber - Framed Housing Sub-Group of CIB-W18
- 19-105-1 Tropical and Hardwood Timbers Structures - R H Leicester
- 21-105-1 First Conference of CIB-W18B, Tropical and Hardwood Timber Structures Singapore, 26 - 28 October 1987 - R H Leicester

INTERNATIONAL UNION OF FORESTRY RESEARCH ORGANISATIONS

- 7-106-1 Time and Moisture Effects - CIB W18/IUFRO 55.02-03 Working Party

**INTERNATIONAL COUNCIL FOR RESEARCH AND INNOVATION
IN BUILDING AND CONSTRUCTION**

WORKING COMMISSION W18 - TIMBER STRUCTURES

**LONG-TERM EXPERIMENTS WITH COLUMNS:
RESULTS AND POSSIBLE CONSEQUENCES ON COLUMN DESIGN**

W Moorkamp

W Schelling

Institute of Building Technology and Timber Construction

University of Hannover

P Becker

K Rautenstrauch

Institute of Structural Engineering

Bauhaus University Weimar

GERMANY

Presented by: P Becker

- H J Blass received clarification that series 5 and 6 had the same cross-section and loaded to 100% of the service load. He questioned that a lower service load would be more appropriate for the wet case.
- P Becker agreed that the service load may be too high for the wet group
- H J Blass stated that the mechano sorptive effect should be higher for the smaller specimens.
- P Becker answered that for the relatively small difference in cross sectional sizes considered in this study, this would not be serious.

Long-term experiments with columns: Results and possible consequences on column design

W. Moorkamp*, P. Becker**, W. Schelling*, K. Rautenstrauch**

* Institute of Building Technology and Timber Construction, University of Hannover, Germany

** Institute of Structural Engineering, Bauhaus-University Weimar, Germany

1 Introduction

Although the importance of finding out about consequences of time-dependent effects to compressive members has been repeatedly emphasized, not many creep experiments have yet been performed with columns observing the time-dependent lateral deflection behaviour under axial load. Humphries/Schniewind (1982) and Cheng/Schniewind (1985) reported about tests with small clear slender ($\lambda=173$) Douglas-fir specimens under varying climatic conditions. Their intention was the evaluation of time-to-failure of columns under high axial loads. The loads corresponded to the 1,4 to 1,8-multiple of the valid service load according to a former American code. The authors registered high failure rates during a maximum test duration of 53 days. Itani & al (1986) performed tests with structural-size slender columns ($\lambda=121/156$) in constant climate also using Douglas-fir specimens. 70% of the individually determined Eulerload proved to be too much for the columns. None of the 60 test specimens survived the duration time of 2000 hours, most of them failed within 200 hours. Itani & al (1986) stated, that the use of a former design formula might lead to unacceptable large errors in column design. Fromhold/Fridley (1998) reported about experiments under combined beam-column loading in constant climate. They concluded, that considering the creep behaviour leads to a much better evaluation of carrying performance of a wooden structural member. Some further tests have been conducted by Härtel (2000). Härtel studied the behaviour of structural-size columns under defined variable climate. He applied the limit load in service range (German code DIN 1052) to his columns and concluded, that time effects are not adequately considered in column design. Some of his measured lateral deflections exceeded the tolerable deflections by multiples.

It seems important, that for creep experiments, which are performed under variable environmental conditions, structural-size specimens are taken. Results of small clear specimens can't be simply transferred to structural-size members. In addition to a much more delayed reaction to humidity changes the inhomogeneity of the natural grown material wood (varying knot density, annual ring width, etc.) becomes more significant. Structural-size specimens were therefore selected for creep tests with columns reported in this paper.

2 Experimental program

2.1 Materials and methods

For experimental tests solid spruce specimens of medium strength class (C 24) with relatively large cross-section were selected. The test material was received from a conventional timber trade without indicating the intended application, so in this respect conditions

corresponded to practical use. Column length was chosen to 1,75 m for all tests. Four different cross-sections were selected (95/95, 95/85, 95/75, 80/60 mm), leading to four different slenderness degrees ($\lambda \cong 64/71/81/101$), defined here by quotient of length and radius of inertia. All specimens were preconditioned in dry climate (20°C/ca. 50% RH). Moisture content at the beginning of the tests varied between 9 and 12%.

It was carefully controlled, that only quartered timber was taken to avoid cracks caused by shrinking, which might lead to inaccurate results.

For the experimental procedure a steel frame was constructed, which allowed a vertical arrangement of the specimens. The load was applied by a lever arm system as shown in figure 1, using a water-barrel with a volume of 200 liters (figure 2). The different loads for columns of different slenderness degree were regulated by the quantity of water in the barrels.

With the existing testing facility four compressive members could be tested simultaneously.

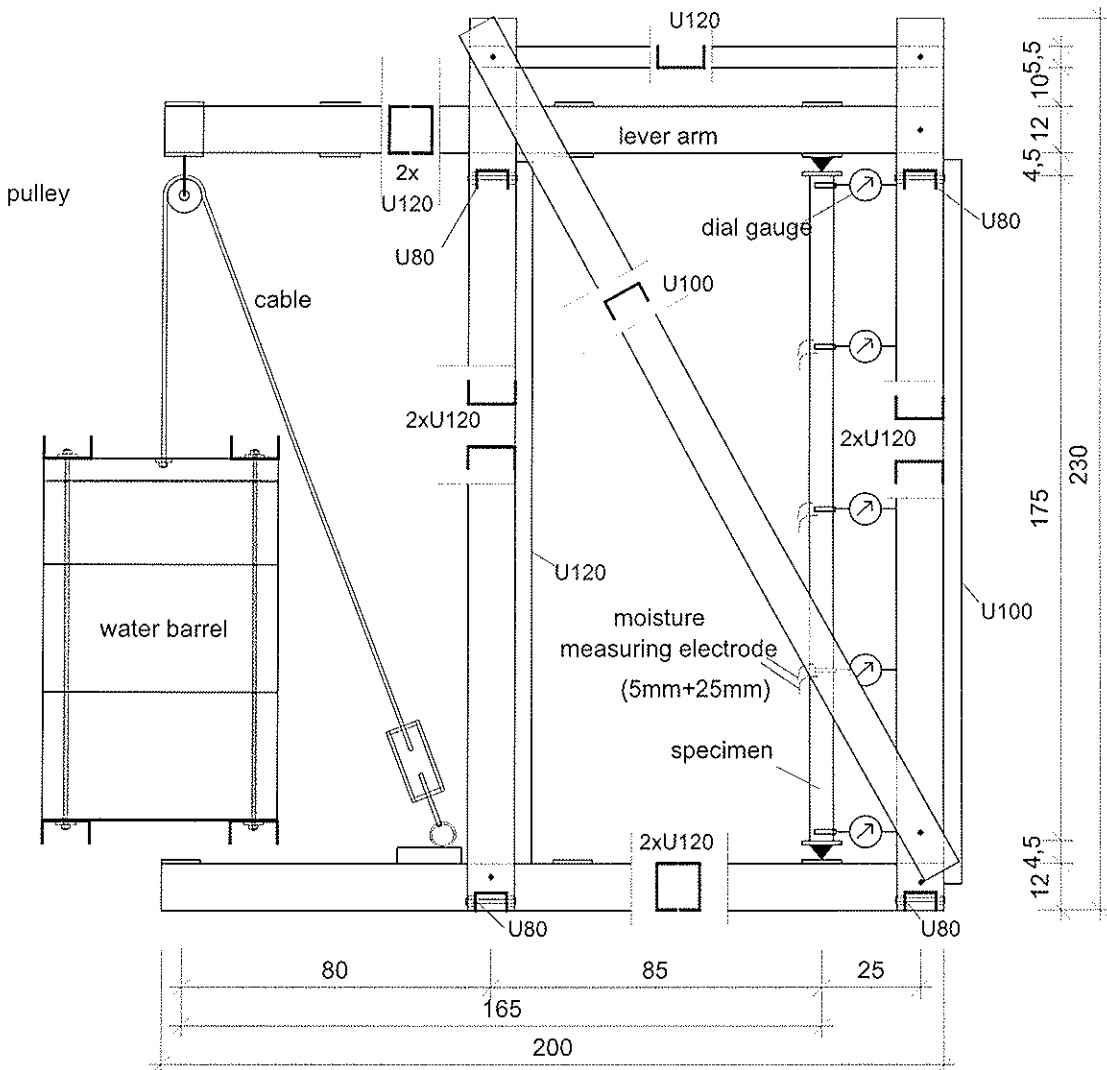


Figure 1: Side view of test frame



Figure 2: Test frame

2.2 Test procedure

The axial load was applied eccentrically to enforce a deflection in direction of the dial gauges. The eccentric load application was necessary, because the stressless predeflection of the specimens was too low (usually less than 1 mm) to predict the direction of deflection. Load eccentricity was chosen to 10 mm for all tested columns.

Sapwood was always positioned in the area of highest expected compressive stresses to create most possibly identical test conditions for the different specimens.

The applied loads were chosen according to the model column method based on German code DIN 1052 (1988) and can be taken from table 1. The combined edge stresses of bending and compressive loading corresponded to the maximum applicable stress-state of the structural member according to the code. So the applied load represents the limit of service range.

The lateral deflection of the column was measured at midspan and quarterpoints using dial gauges with accuracy of 1/100 mm. Deflection was measured on both sides of the cross-section respectively and the mean value was taken to account for possible rotations of the cross-section.

The moisture content of the specimens was electronically taken for depths of 5 mm and 25 mm in mid and quarterpoints respectively.

After completion of tests E-modulus was determined by a four-point bending arrangement. Dry density was also evaluated.

Experiments took place at the University of Hannover/Germany. The test duration was limited to half a year. Tests were performed in variable cyclic climate under laboratory conditions. The relative humidity changed between dry (40 – 50% RH) and wet (80 – 90% RH) phases, which is assumed to cover the natural changes of relative humidity. Two weeks were taken as cycle length, some cycles were extended for comparative reasons. Also some tests were performed in constant dry and constant wet climate to get information about basic creep behaviour of compressive members without changing humidity. Temperature was held constant to approximately 20°C during all tests.

The tested series are listed in table 1. The creep experiments have been conducted as a continuation of the creep tests performed by Härtel (2000). Härtel tested 4 series with solid timber, so numbering goes from Fi-V to Fi-VIII here. Two further (Fi-IX and Fi-X) series have been conducted. The results are not yet finally analysed and will be reported in a later publication.

| Test-Series | cross-section b/h [mm] | slenderness λ [-] | axial load F [kN] | conditions |
|-------------|---------------------------|------------------------------|----------------------|-----------------------------------|
| Fi-V | 80/60 | 101,0 | 9,3 | constant RH (\approx 43%) |
| Fi-VI | 80/60 | 101,0 | 9,3 | constant RH (\approx 90%) |
| Fi-VII | 95/95 | 63,8 | 34,0 | cyclic RH (\approx 45% to 90%) |
| Fi-VIII | 95/85 | 71,3 | 27,3 | cyclic RH (\approx 35% to 90%) |

Table 1: Test series

3 Modeling time-dependent material behaviour of timber

For simulation purposes an extensive material model for timber has been developed. The model contains time and moisture dependent material behaviour. The time-dependent moisture distribution over the members cross-section is covered by a diffusion analysis based on Ficks law of mass transfer. The diffusion coefficient is taken moisture dependent, so the differential equation becomes nonlinear and has to be solved numerically. The cross-section is therefore discretised and the problem is solved with finite difference method for each time increment. For all discrete points a stress-strain analysis is performed. Bernoulli hypothesis is adopted, the deformed cross-section remains plane. From the deformation state at midspan and the present load configuration the deflection state of the whole member is concluded. Describing the time-dependent material behaviour, it is distinguished between viscoelastic, mechano-sorptive, non-linear and hygrorelated deformations. Creep deformation in constant climate – viscoelastic creep – is modeled by a Kelvin chain consisting of four consecutive Kelvin elements. A further Kelvin element is taken for modeling mechano-sorptive creep, parameters depending on maximum moisture change. Nonlinear creep, which only occurs if a defined proportional limit is exceeded, is described in a way corresponding to an additional damper with stress-dependent parameter. Hygrorelated deformation (swelling/shrinkage) is also considered taking the coefficient strain-dependent resulting in the typically cyclic deformation curve as observed in many experiments. Good results are obtained by an additive approach of the different portions as shown in figure 3. The complete model is given in the annex of a related paper (Becker/Rautenstrauch 2001).

In addition to the mechanical behaviour the spreading of mechanical properties in dependence of specific material characteristics (dry density, knot density) is considered, which

enables extensive simulation studies and the determination of characteristic values of long-term capacities. Again this is reported in Becker/Rautenstrauch (2001).

The model was applied in resimulating creep experiments with compressive members and it will be shown, that it is able to cover time and moisture dependent effects in timber structures.

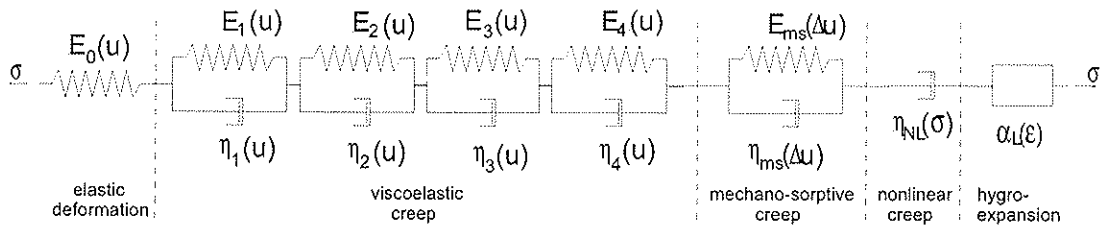


Figure 3: Material model for stress-strain analysis (Becker/Rautenstrauch 2001)

4 Results and Discussion

Experimental results are illustrated in figures 4 to 7. The creep test under constant dry climate (figure 4) resulted in relative deflections between 1,27 and 1,65. The highest relative deflection is obtained for the specimen of lowest quality is would be expected. The simulation of the test, assuming average material properties fits quite well to the mean of the four curves.

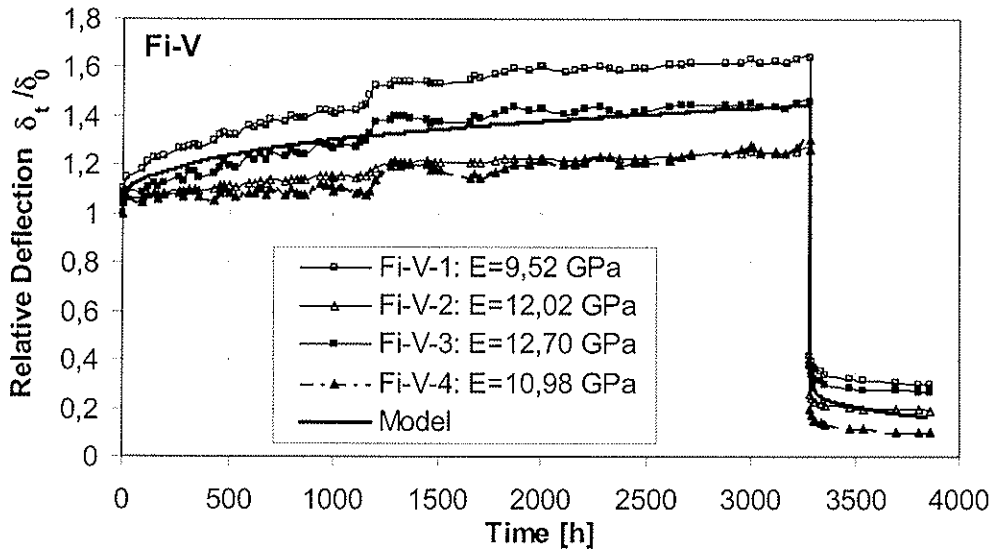


Figure 4: Results of test series Fi-V

The tests under constant moist condition (series Fi-VI, figure 5) exhibited much higher creep than in the Fi-V-series. This can be explained by a strong mechano-sorptive effect: The specimens were built in in dry state and wettened while loaded, which resulted in much larger deformation. Additionally some problems occurred with regulation of climate,

which is the cause of further deformation increase after approximately 2000 hours. Without these problems it seems like the relative deformation would have reached values between 1,8 and 3,0 after half a year. It is surprising, that the specimen of lowest quality (Fi-VI-3) showed the lowest relative deflection. This indicates, that material quality seems not decisive for sensitivity to mechano-sorption rather than the mechano-sorptive characteristics of the material itself. The simulation model underestimated the mechano-sorptive effect and produced a curve, which corresponded to the lower range of series Fi-VI.

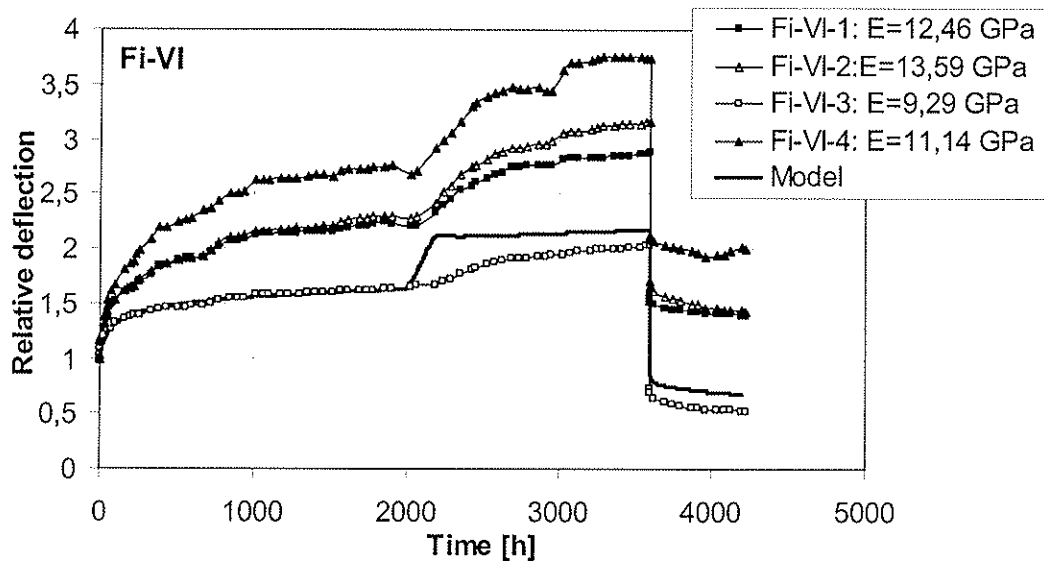


Figure 5: Results of test series Fi-VI

The two series under variable climate (Fi-VII, Fi-VIII) produced results, which are quite confusing compared to former publications about creep behaviour of timber in variable climate. It has been reported for example, that deformation usually increases in dry and decreases in wet phases during climatic cycles, which can be only partly confirmed here. For the majority of the specimen increasing deflection was observed during wet phases. The cyclic deformation behaviour of bending elements has been explained by a stress-dependency of shrinkage/swelling-coefficients, becoming larger under compression and reducing under tension (Hunt/Shelton 1988). Columns might behave a little different, because the complete cross-section usually is under compressive stress. The spread of the series Fi-VII and VIII is larger compared to the series in constant climate. Deflections of series Fi-VIII are a little more pronounced in average, because of more severe relative humidity cycles. Largest deformation is always exhibited by specimens of lowest quality, which indicates, that additional to mechano-sorptive deformation nonlinear creep effects might be involved. If the simulation model assumes a low quality specimen and disproportional deformations occur under lower stresses respectively, a very similar time-deflection curve is obtained (figure 7). Taking average material properties the curves are within the range of mean experimental test progressions. The only difference is, that the simulated curves exhibit the expected cycle of increasing deformation in dry and decreasing deformation in moist phases in contrast to some of the test curves.

The results of the creep experiments with columns indicate, that climatic conditions are quite influential to the long-term performance of compressive members. If the moisture content is kept below 12%, the deformation behaviour doesn't seem to become problematic. Deflections can grow quite large during relatively short durations, if moisture content

changes under load though. Especially under high proportions of permanent load column design methods without considering time-dependent behaviour then have to be seen critically for climatic conditions, which reflect service class 2 or 3 according to Eurocode. The serviceability of compressive members will often not be kept also. Absolute deflections of creep tests exceeded allowable deflections according to codes partly by multiples, which was also the case in the experiments performed by Härtel (2000) with specimens of solid timber and glulam.

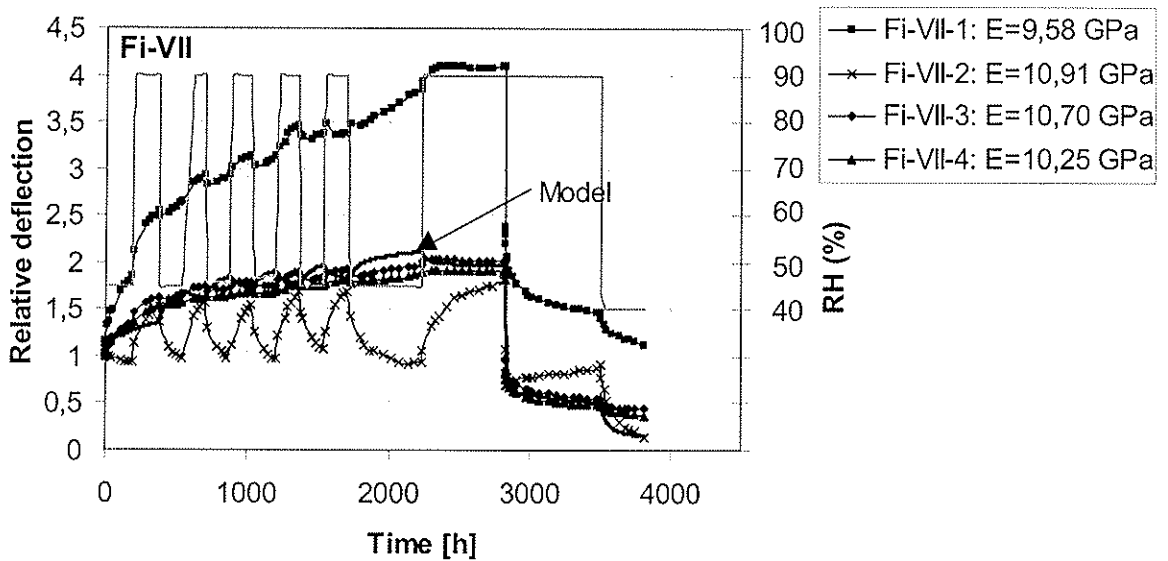


Figure 6: Results of Fi-VII-series

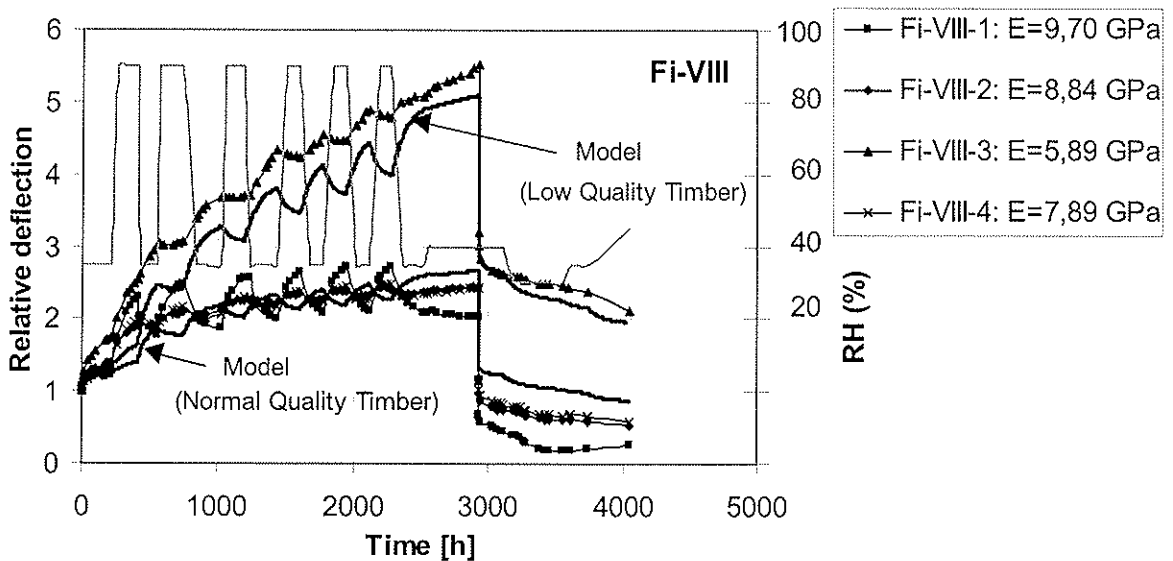


Figure 7: Results of Fi-VIII-series

More insight to the problem could be obtained by applying long-term simulations to columns. It was shown, that an extensive material model, as it is introduced in the article, is able to cover time-dependent effects for compressive members and the spread of observed material behaviour also.

References

- Becker, P., Rautenstrauch, K. (2001) – Proposal for compressive member design based on long-term simulation studies. CIB-W18-Proceedings, Paper 34-2-2, Venice, Italy.
- Cheng, J., Schniewind, A.P. (1985) - Creep buckling of small slender wood columns under cyclic environment. *Wood and Fiber Science* 17(2), 159-169.
- Fromhold, K.L., Fridley, K.J. (1998) - Creep-induced secondary moments in timber beam-columns. *Proceedings of the 5th World Conference on Timber Engineering*, Vol. 2, 356-360, Montreux, Switzerland.
- Härtel, J. (2000) - Experimentelle und theoretische Untersuchungen zum Kriechverhalten hölzerner Druckstäbe unter baupraktischen Bedingungen (Experimental and theoretical investigations to creep behaviour of wooden compressive members under real conditions, in German). PhD-Thesis, University of Hannover, Germany.
- Humphries, M., Schniewind, A.P. (1982) – Behaviour of wood columns under cyclic relative humidity. *Wood Science* 15, 44-48.
- Hunt, D.G., Shelton, C.F. (1988) – Longitudinal moisture-shrinkage coefficients of softwood at the mechano-sorptive creep limit. *Wood Science and Technology* 22, 199-210.
- Itani, R.Y., Griffith, M.C., Hoyle, R.J. (1986) - The effect of creep on long wood column design and performance. *Journal of Structural Engineering* 112(5), 1097-1115.

**INTERNATIONAL COUNCIL FOR RESEARCH AND INNOVATION
IN BUILDING AND CONSTRUCTION**

WORKING COMMISSION W18 - TIMBER STRUCTURES

**PROPOSAL FOR COMPRESSIVE MEMBER DESIGN
BASED ON LONG-TERM SIMULATION STUDIES**

P Becker
K Rautenstrauch
Institute of Structural Engineering
Bauhaus University Weimar

GERMANY

Presented by: P Becker

- S Thelandersson asked why several points were chosen for the mean and characteristic value.
- P Becker answered that only 10 columns were simulated for their long term behaviour out of 1000 simulated members. These 10 points were chosen near the mean and the characteristic value.
- H J Blass commented that cross sectional dimensions were recorded at the mid span yet the moisture changed over the entire column length.
- P Becker responded that in the non-linear cases, the mid span was most critical although this approach may be conservative. This is not an issue for the compact column case.
- H Kreuzinger asked for clarification of the proposed code format.
- P Becker provided a brief review of the proposal.
- H J Larsen clarified that the slender column case has been covered in this study but the non-slender column case where strength criteria is needed has not been resolved. He commented that the statement in the design proposal as per restricted to 50% of design values can be better formulated.
- P Becker agreed with the first comment and responded that the permanent load should be restricted to 50% of design values for the creep case.

Proposal for compressive member design based on long-term simulation studies

Peter Becker, Karl Rautenstrauch
Bauhaus-University Weimar, Germany

1 Introduction

Results of long-term experimental studies with compressive members indicate, that the influence of time-dependent deformation effects to the safety of a structure is more severe than would be expected according to design rules. This especially is the case, if the portion of permanent load is high, resulting into creep deformation. Researchers repeatedly emphasized this.

Creep experiments are extremely time- and money-consuming, which turns out to be problematic. There aren't any creep-tests with columns, that have been conducted for more than half a year, simply too short of duration to draw any conclusion about long-term reliability under service loads. Considering this, long-term simulation studies appear as an appropriate method to observe the long-term behaviour and find out more about time-dependent effects to compressive members. Long-term simulation studies require a model, which reflects long-term material behaviour in a most possibly realistic way. As a consequence especially moist and time-dependent effects have to be covered.

2 Strategy of evaluating long-term capacities of compressive members by long-term simulation studies

2.1 Modeling long-term behaviour of the material

In the present model a diffusion analysis is performed for each time-increment, always providing the current moisture distribution over the cross-section. This is done by applying Ficks law, taking the diffusion coefficient moisture dependent, and solving it by the finite difference method. The effect of surface resistance is considered.

All mechanical properties are taken moisture dependent, decreasing for increasing moisture contents. Compression strength is assumed to be much stronger affected than tension strength.

For time-dependent deformation behaviour it is distinguished between viscoelastic creep, mechano-sorptive creep and hygroexpansion. Good results are obtained by applying an additive approach (figure 1). The creep in constant environmental conditions – so called viscoelastic creep – is modeled by 4 consecutive Kelvin-elements, with a creep limit of 60% of elastic deformation. Kelvin parameters are subjected to the same moisture dependency as the elastic reaction. Therefore relative viscoelastic creep is taken as moisture-independent. Nonlinear creep is assumed to occur, if a proportional stress limit is exceeded depending on moisture content. The nonlinearity refers to an additional additive damper with stress-dependent parameter. The nonlinear creep deformation is therefore assumed as irreversible. Mechano-sorptive creep is modeled by applying one further Kelvin-element with parameters in dependence of maximum moisture content change. Intensity of hygro-

expansion in grain direction is influenced by strain, increasing under compressive strain and decreasing under tension strain. The typically cyclic deformation curve under varying climate is obtained this way.

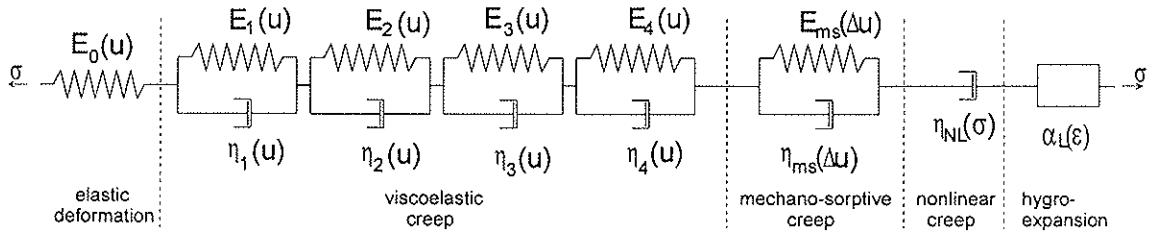


Figure 1: Material model for stress-strain analysis

The stress-strain analysis as described above and in the annex is performed for the midspan cross-section of structural elements simply supported at both ends. From the deformation state at midheight of a member it is concluded to the deflection of the whole element by assuming proportionality of bending moment and second derivative of member deflection. Shear deformation is neglected. This procedure allows the renunciation of member axis discretisation. It leads to slight errors though, if the proportional limit is exceeded.

The model also enables the determination of short-term strength by an incremental load rising procedure. Plasticating ability of the material under compression is considered. The member is discretised in axial direction this time. For including a possible duration-of-load effect, a strain-energy-density-criterion is invented to get a consistent definition of material failure independent to load duration.

The complete model is given in the annex. It works quite well, which is shown by resimulating various creep and duration-of-load tests (Becker 2001, Moorkamp & al 2001).

2.2 Estimation of safety after long-term loading

In most theoretical studies, which dealt with the long-term behaviour of compressive members, the following strategy has been applied: A column with previously defined characteristics has been long-term loaded, which led to additional creep deformation according to an applied creep law. The member in deformed state was then subjected to a load increase until a defined failure criterion was exceeded. The obtained failure load has been compared to design load to get an idea about the safety level. It will be shown in this section, that this procedure is not an appropriate method to estimate the long-term capacity of compressive members.

Curve (1) in figure 2 shows a typical simulated time-deflection curve of a slender column with initial predeflection, which is loaded by the highest possible characteristic permanent axial load (1,02 MPa) according to Eurocode 5. It can be clearly observed, that the lateral deflection has reached an equilibrium state after twenty years of loading, where only climatic changes cause the noticeable annual deformation cycles. If the load in this equilibrium state is raised, column strength turns out to be only slightly lower than the initial value, mainly because of the additional deflection causing a larger moment according to theory of second order. The difference in figure 2 is only 8,3% and will usually not be more than 10%. So it looks like the strength drop is low and safety is quite high. But if the column is loaded by much less (1,70 MPa) than the obvious capacity it fails after a couple of years as illustrated in curve (2). So the long-term capacity is obviously much lower than the short-term strength after long-term use.

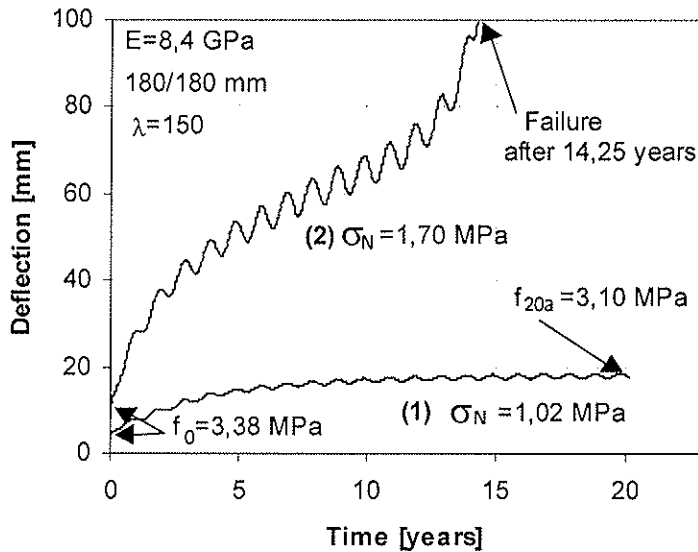


Figure 2: Time-deflection curves of slender column under two different loads

The long-term capacity specifies the load, which the structural element can resist in the long run. This load will be much lower than the short-term strength after long-term service. In which way safeties have to be applied to long-term capacities will be a point of discussion later.

2.3 Determination of long-term capacities

It is not quite guaranteed, if a critical long-term capacity does really exist. This only applies, if the creep law is assumed to contain a creep limit, which is a basic assumption for linear creep in this study.

A precise determination of long-term capacities under the defined conditions is difficult. It has to be done by an iterative and therefore very time-consuming procedure. The results have to be understood as approximations. The iterative process consists of an incremental increase of long-term load, until failure is obtained within a defined time duration. The load increments should be small to guarantee a result of appropriate accuracy.

For estimation of long-term capacity the following criterion has been defined: “If the creep curve after a defined load duration is clearly in the secondary or tertiary creep phase, the critical long-term capacity is exceeded“. This definition and the procedure of estimating long-term capacities is clarified in figure 3. Time-deflection curves of long-term axially loaded columns of different slenderness degrees are illustrated there.

Figure 3a ($\lambda=50$) shows, that under an axial load of 5,7 MPa the long-term capacity is obviously exceeded. Although the column survives the simulated duration the creep curve clearly corresponds to tertiary stage, which indicates failure sometime in future. The same applies to a nominal stress of 5,4 MPa, where the tertiary creep phase has also established. Under smaller axial loads a equilibrium deformation state seems to establish. A closer look shows though, that at least under 5,1 MPa the creep rate still features an increasing character after 40 years of loading. According to the definition the critical long-term capacity is still not achieved. Under an axial load of 4,8 MPa no tertiary creep phase can be observed for the duration time of 40 years, so the long-term capacity should be somewhere like 4,9 or 5,0 MPa.

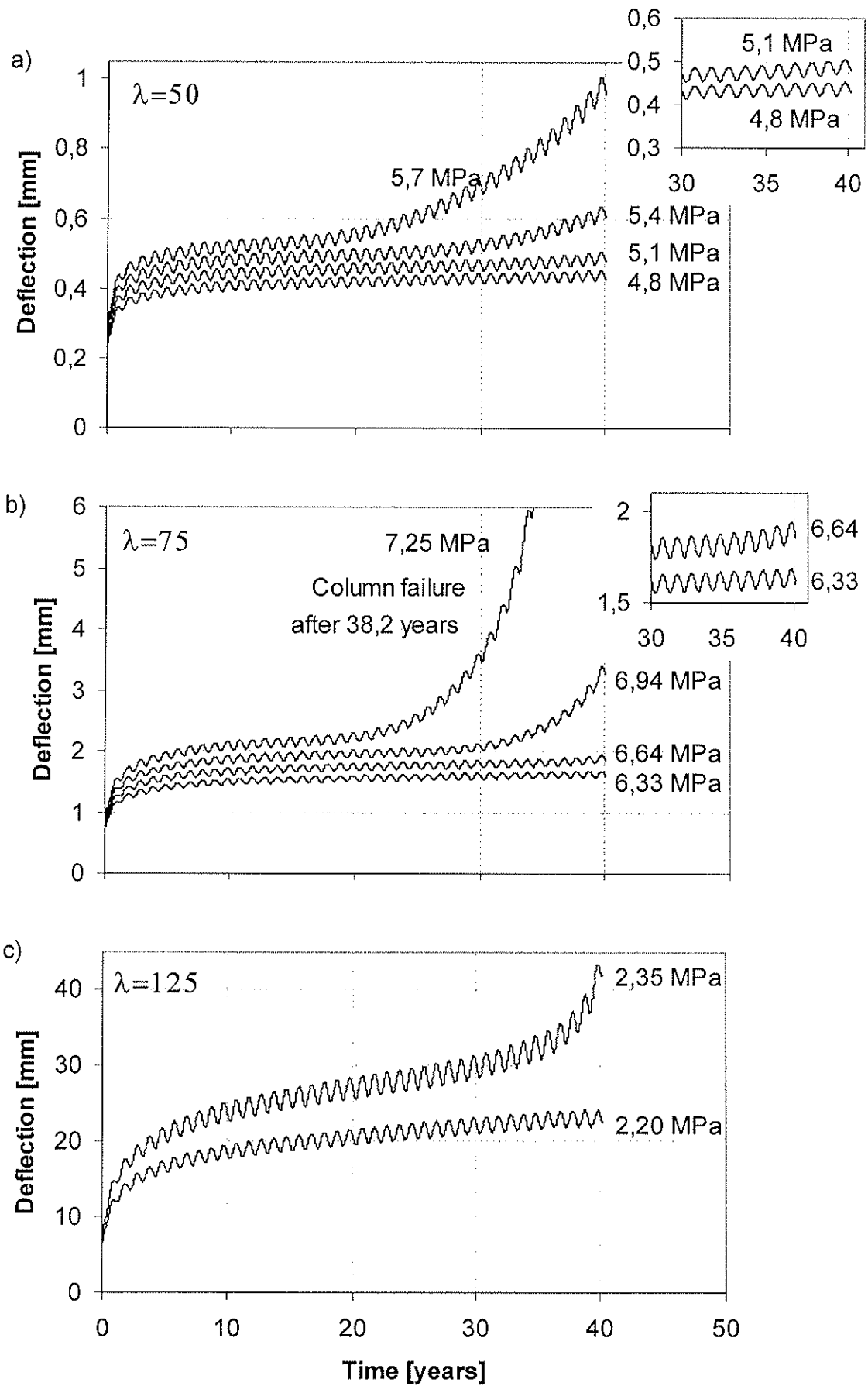


Figure 3: Time-deflection curves for 40-year-load-duration

Fig. 3b shows the time-deflection curves of a medium slender column. It might cause irritations, that capacity seems to be higher than in the first example. This is due to better material quality of the sample. It can be easily observed, that the long-term capacity is exceeded for 7,25, 6,94 and 6,64 MPa (small diagram). In the first case the column fails after a little more than 38 years, in the others the tertiary creep phase is clearly initiated. No failure seems to occur for 6,33 MPa, so long-term capacity should be around 6,4 or 6,5 MPa.

For the slender column ($\lambda=125$) in figure 3c the creep progression is stabilizing under 2,2 MPa, while 2,35 MPa will obviously cause failure probably within the next one or two years. The long-term capacity should be somewhere between 2,2 and 2,3 MPa.

Looking at figure 3 indicates, that the behaviour of compact and slender columns is different. The tertiary creep phase is much more pronounced for columns of low slenderness. The column in figure 3a will probably survive another 40 years under 5,4 MPa before it will fail, although tertiary creep phase and therefore the process of failure has long started. Slender columns tend to fail much faster, if tertiary creep occurs (fig. 3c).

2.4 Specification of characteristic and mean values

It is well known, that material properties of timber are characterized by a wide variability. Therefore it would be very interesting to determine characteristic and mean values for long-term capacities. This would require many simulations with varying material characteristics to get somekind of resulting deviation. It was already mentioned though, that the evaluation of long-term capacities is an iterative and therefore time-consuming process, so the number of simulations should be restricted. For determination of characteristic and mean values considering deviations of material properties the following strategy was therefore applied:

As basic material properties of solid timber, raw density and knot area ratio are randomly determined. With simultaneous consideration of moisture content, which is covered by moisture analysis as described earlier, these parameters explain most of material variability. Stationary mechanical characteristics are computed by using correlation equations of Colling (1990) and further random methods as illustrated in the annex. Plasticating ability of the material under compression is considered by applying the slightly modified material law of Glos (1978). Additionally a stressless predeflection at column midheight is randomly determined according to a recorded deviation of Ehlbeck/Blass (1987). The knowledge of stationary material behaviour enables the evaluation of short-term strength. For each slenderness degree and strength class the short-term strength of 1000 columns with randomly determined characteristics is evaluated to get a deviation of short-term strength. Strength values are sorted in ascending order. Rank 48 to 52 and rank 498 to 502 are selected as being representative for characteristic respectively mean values of carrying capacity of compressive members. Such elements are taken for long-term simulation studies and determination of long-term capacity.

3 Results of simulation studies

In figure 4 quotients of determined long-term capacity and possible characteristic dead load according to the new draft of the German code DIN 1052, which is very similar to EC 5, is given. The values have to be interpreted as simulation results of the chosen material model. It is obvious, that the safeties in particular for compressive members of charac-

teristic capacity are low. Especially for non-slender elements the long-term capacities are even partly lower than allowable long-term loadings. Strength classes C24 and C30 are similarly affected. Effects causing long-term failure of compressive members are quite different depending on slenderness.

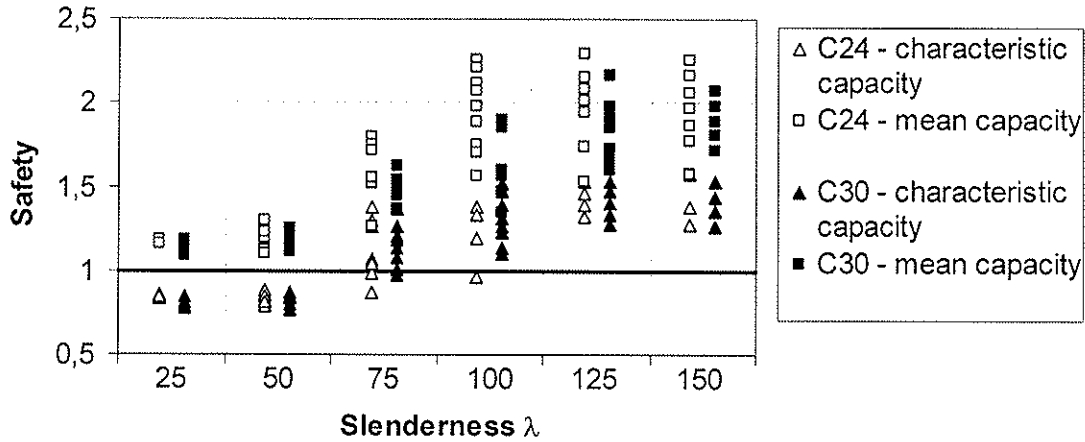


Figure 4: Quotient of axial long-term capacities and characteristic permanent load

3.1 Slender compressive members

The short-term strength of slender compressive members is almost entirely affected by stability behaviour depending on material stiffness (E-modulus). Stressless predeflection is of little additional influence. A reliable estimation of short-term strength is possible by using the following expression.

$$f_0 = \frac{E\pi^2}{\lambda^2} - \frac{(\delta_0/L)^2}{\lambda} \cdot 2000 \cdot E \quad (1)$$

λ represents the members slenderness, defined by the quotient of member length and radius of inertia. δ_0 denotes the stressless predeflection.

In a very similar manner the long-term capacity of a compressive member is exclusively affected by the long-term stability behaviour, which is characterized by de- or increasing deflection rate, affected by time-dependent stiffness of the material. Because of the relatively low stressing of slender elements, nonlinear creep does not occur, so behaviour can be covered by linear viscoelastic theory. A formula derived by Becker/Rautenstrauch (1998) yields excellent agreement with simulation results and can be considered as suitable for estimating long-term capacity of compressive members:

$$f_\infty = \frac{P_E}{1 + k_{\text{def}}} \quad (2)$$

Here P_E stands for the Eulerload, k_{def} denotes the creep factor, which can be taken from codes. With this expression an evaluation of long-term behaviour is easily possible.

3.2 Compact compressive members

The initial capacity of compact columns is almost entirely affected by the compression strength of the material. So compressive strengths of analysed columns in characteristic and mean range are very similar respectively.

The long-term capacity of compact columns turns out to be clearly lower than expected. This can solely attributed to nonlinear creep as it was defined in the material model. If a bending element is exposed to nonlinear creep, harmless stress redistributions will be the consequence. For a compressive member nonlinear creep is followed by a deflection increase, which causes higher internal forces again followed by additional creep. It can be therefore assumed, that an axial dead load, which in combination with moisture content causes nonlinear creep will lead to failure in the long run. According to the material model chosen in the simulation study, nonlinear creep initiates under a defined portion of compressive strength. So the members of characteristic and mean capacity are affected in the same manner respectively, which explains the low spread of results for compact members in figure 4.

It is of course questionable, if the simulation results reflect long-term capacities of compact elements in an appropriate manner. An accurate description of nonlinear creep is probably the most difficult part of time-dependent modeling of timber. A small change in defining the proportional limit or an additional discretisation of the member axis will influence the result. Additionally nonlinear creep was assumed irreversible in the model, which is probably too conservative. Further research in this area is definitely required. As a consequence of the performed simulation study it is out of question though, that the long-term behaviour of compact elements has to be considered critically also. Permanent loads, which exceed the proportional limit should be avoided.

If nonlinear creep actually occurs, the computational coverage of long-term behaviour becomes difficult. Expressions based on linear elastic and viscoelastic theory cannot be applied anymore.

Medium slender compressive members might be affected by the one or the other long-term failure mechanism. That's the reason why such elements show the largest spread of long-term capacities in figure 4.

4 Consequences on compressive member design

Bringing the results of the simulation study in mind it becomes clear, that the present design situation of compressive members contains deficits. This is especially true for elements, which are loaded by a high proportion of permanent or long acting load.

To obtain the intended reliability for compression loading time effects have to be included into the design process. This should not lead to a more complicated design. If equivalent reliabilities have to be applied to long-term capacities is a point of further discussion in coding committees. Long-term failure is a process, which usually extends over years or even decades and is therefore observable far in advance. In contrast to short-term strength, which is characterized by sudden failure, it can be controlled much better. Maybe smaller safeties are acceptable considering this aspect.

4.1 k_c -method

Characteristic capacities determined by the k_c -method can be considered quite conservative concerning short-term strength. So loads of short-term duration give no cause of concern. This conclusion is not valid for long-term loading. To obtain a consistent level of reliability a modification of the method is unavoidable.

Compressive members are especially endangered in service class 2 and 3, where the most creep deformation has to be expected. In service class 1 the average moisture content over

the cross-section will usually not exceed a value of 12%, so there's no danger of occurring nonlinear creep even for highly stressed compact columns. A simple rule to guarantee safety in service classes 2 and 3 would be a restriction of permanent and long-term loads. Compressive stress resulting from permanent and long-term action should not be more than 50% of the design value of compression strength reduced by k_c . This proposal could be easily implemented by a short supplement in the code.

For slender columns ($\lambda \geq 100$), which are not influenced by nonlinear material behaviour, it could be referred to a formula derived by Becker/Rautenstrauch (2001) to obtain a more accurate design. Under dead load the formula offers a very useful estimation of long-term capacity, as was shown by simulations. The expression also covers variable loading. If probabilistic design concept is applied, the prove of long-term stability would then be the following.

$$\left[\frac{(1 + k_{\text{def,G}}) \cdot P_{G,d}}{P_{E,d}} \right]^m + \sum \left[\frac{(1 + k_{\text{def,Q}}) \cdot P_{Q,d}}{P_{E,d}} \right]^m \leq 1 \quad (3)$$

$$m = 1,3 \quad , \quad P_{E,d} = \frac{E_{05} \cdot A \cdot \pi^2}{\gamma_M \cdot \lambda^2}$$

This prove could be offered optionally, if a structural engineer wants to load a compressive member by a greater portion of permanent or long-term load.

4.2 Prove according to theory of second order

The prove according to stress-theory of second order, which is optionally offered in EC 5, turns out to be conservative compared to the k_c -method. Although it has been shown in many studies, that the E-modulus doesn't change under permanent load in contrast to material strength, the code still demands reduction of the characteristic value by the modifying factor. Additionally the given stressless predeflection ($L/333$) seems unrealistic large. Concerning this the draft to the new German code DIN 1052 contains improvements: the modification of the characteristic E-Modulus is abandoned, the stressless predeflection is reduced to $L/400$. According to a distribution of imperfections, published by Ehlbeck/Blass (1987), this value corresponds to the 2%-fractile and is therefore still conservative.

The prove according to theory of second order can be applied to slender columns without any problems. Creep deflections, which should be considered, may be easily calculated with formulas of Becker/Rautenstrauch (2001). The nonlinear M-N-interaction seems appropriate.

Applying theory of second order to compact columns might cause problems for service classes 2 and 3, where nonlinear creep has to be expected. The theory is based on linear elasticity, for consideration of creep on linear viscoelasticity respectively, so nonlinear effects are not covered. The only possibility would be the definition of a proportional limit depending on service class, which must not be exceeded by edge stresses. Otherwise the prove according to theory of second order is not suitable for compact columns and it has to be referred to the k_c -method.

5 Conclusions

Long-term simulation studies with compressive members have indicated, that intended reliability is not reflected by design rules. This especially applies to service classes 2 and 3, where time-dependent deformations should be considered in design process. It has been shown, that there is a difference between long-term capacity and the capacity after long-term use.

Long-term failure of compressive members is caused by different mechanisms depending on slenderness degree:

- For slender columns long-term stability behaviour is characteristic. Because of linearity of deformations of the low-loaded slender members, long-term stability behaviour can be easily covered.
- The long-term capacity of compact columns is exclusively affected by nonlinear creep behaviour. More research is necessary to account for the exact influence.

The k_c -design-concept seems generally suitable for service class 1. For service classes 2 and 3 it is recommended not to exceed 50% of the k_c -reduced design value of compression strength by design values of permanent and long-term acting loads.

The prove according to theory of second order is too conservative concerning initial predeflection and required reduction of E-modulus as given in the present code. Proposals for a more realistic coverage have been submitted. The application of the prove should contain the consideration of creep deformations. For service classes 2 and 3 the prove is not suitable in the present form because of possible nonlinear material behaviour. The k_c -method should then be taken instead.

References

- Becker, P., Rautenstrauch, K. (1998) – Deformation and stability of columns of viscoelastic material wood. CIB-W18-Proceedings, Paper 31-2-1, Savonlinna, Finland.
- Becker, P., Rautenstrauch, K. (2001) – Time-dependent material behaviour applied to timber columns under combined loading. Accepted by „Holz als Roh- und Werkstoff“.
- Becker, P. (2001) – Modellierung des zeit- und feuchteabhängigen Materialverhaltens zur Untersuchung des Langzeittragverhaltens von Druckstäben aus Holz (in German). Research paper, Bauhaus-University Weimar, not yet published.
- Colling, F. (1990) – Biegefestigkeit von BSH-Trägern in Abhängigkeit von festigkeitsrelevanten Einflußgrößen (in German). PhD-Thesis, University of Karlsruhe, Germany.
- Ehlbeck, J., Blass, H.-J. (1987) – Imperfektionsannahmen für Holzdruckstäbe (in German). Holz als Roh- und Werkstoff 45, 231-235.
- Glos, P. (1978) – Zur Bestimmung des Festigkeitsverhaltens von Brettschichtholz bei Druckbeanspruchung aus Werkstoff- und Einwirkungskenngrößen (in German). PhD-Thesis, Technical University München, Germany.
- Moorkamp, W., Becker, P., Schelling, W., Rautenstrauch, K. (2001) – Long-term experiments with columns: Results and possible consequences on column design. CIB-W18-Proceedings, Paper 34-2-1, Venice, Italy.

Annex – Material model

Basic material properties

| | | | |
|--------------|------|--|-------------------------|
| Dry density | C 24 | $\rho_0 = 420 \pm 45$ [kg/m ³] | normally distributed |
| | C 30 | $\rho_0 = 435 \pm 45$ [kg/m ³] | normally distributed |
| Knot density | C 24 | KAR = -2,11 ± 0,25 | lognormally distributed |
| | C 30 | KAR = -2,33 ± 0,25 | lognormally distributed |

Moisture content

Equilibrium MC $u_{RH} = 0,113 RH^{0,54} + 0,192 e^{-0,5(2,7(RH-1)-1)^2} + 0,09 e^{-0,5(20,5(RH-1)-1)^2}$ [-]

Moisture distribution $\frac{\partial u}{\partial t} = \nabla(D \cdot \nabla u)$

Diffusion coefficient $D = 0,5 \cdot \left(1 - \frac{\rho_0 - 420}{420} \cdot 2\right) \cdot e^{4,0 \cdot u}$ [mm² / h]

Surface resistance $u_{sur} = u_{sur} + (u_{RH} - u_{sur}) \cdot (1 - e^{-\beta t})$

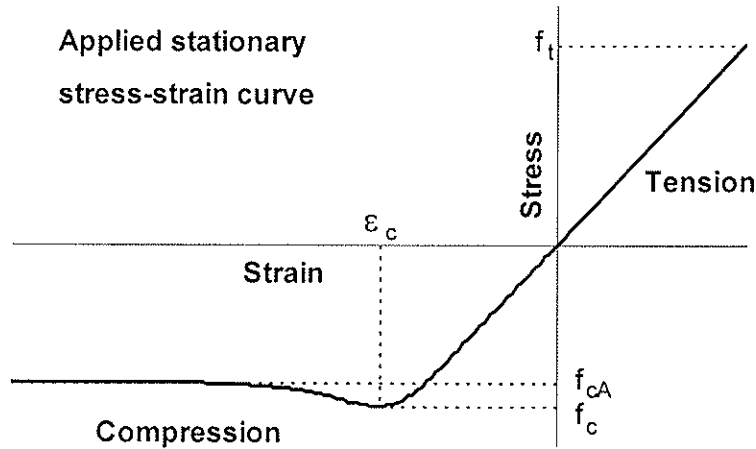
Mechanical properties (u=0,12)

E-modulus (compression) $\ln(\hat{E}_c) = 8,22 + 2,994 \cdot 10^{-3} \cdot \rho_0 - 0,76 \cdot KAR$
 $E_c = \hat{E}_c \pm 0,133 \cdot \hat{E}_c$ [MPa] normally distributed

E-modulus (tension) $\ln(\hat{E}_t) = 8,20 + 3,13 \cdot 10^{-3} \cdot \rho_0 - 1,17 \cdot KAR$
 $\hat{E}_{t,new} = \left(0,15 + 0,85 \frac{E_c}{\hat{E}_c}\right) \cdot \hat{E}_{t,old}$
 $E_t = \hat{E}_t \pm 0,104 \cdot \hat{E}_t$ [MPa] normally distributed

Compression strength $\ln(\hat{f}_c) = 2,586 + 2,8 \cdot 10^{-3} \cdot \rho_0 - 0,825 \cdot KAR$
 $\hat{f}_{c,new} = \left(0,2 + 0,8 \frac{E_c}{\hat{E}_c}\right) \cdot \hat{f}_{c,old}$
 $f_c = \hat{f}_c \pm 0,12 \cdot \hat{f}_c$ [MPa] normally distributed

Tension strength $\ln(\hat{f}_t) = -4,22 + \ln(E_t) \cdot (0,876 - 0,093 \cdot KAR)$
 $\hat{f}_{t,new} = \left(0,2 + 0,8 \frac{E_c}{\hat{E}_c}\right) \left(0,2 + 0,8 \frac{f_c}{\hat{f}_c}\right) \cdot \hat{f}_{t,old}$
 $f_t = \hat{f}_t \pm 0,12 \cdot \hat{f}_t$ [MPa] normally distributed



Moisture dependence of mechanical parameters

E-modulus $E(u) = E_{12} \cdot (1 - 1,5 \cdot (u - 0,12))$

Tens./Compr. strength $f_{t,c}(u) = f_{t,c}(u = 0,12) \cdot \Phi \cdot e^{-\Psi \cdot u}$

Tension $\Phi = \frac{1}{e^{-0,12 \cdot \Psi}}$, $\Psi = 1,51 \cdot \frac{f_t}{f_{t,mean}}$

Compression $\Phi = \frac{1}{e^{-0,12 \cdot \Psi}}$, $\Psi = 4,21 \cdot \frac{f_c}{f_{c,mean}}$

Length effect $\frac{f_2}{f_1} = \left(\frac{L_1}{L_2} \right)^{S_L}$, $S_{Lc} = 0,06$ (Compr.) , $S_{Lt} = 0,17$ (Tension)

with $L_1 = 150$ mm

L_2 : Length of section, with at least 85% of max. stress in midspan

Time-dependent material law

VE plus nonlinear def. $\sigma(t) = E(t)\varepsilon(t) - \int_0^t \frac{\partial Y}{\partial \tau}(t, \tau)\varepsilon(\tau) d\tau - \eta_{NL} \cdot t$

Relaxation function $Y(t, \tau) = E(\tau) \left[\phi_0 + \sum_{i=1}^k \phi_i e^{-(t-\tau)/T_i} \right]$

from $\int_0^t Y(t-\tau)J(\tau) d\tau = t$

Creep function $J(t) = \frac{1}{E_0} \left[1 + \sum_{i=1}^4 \varphi_i (1 - e^{-t/\theta_i}) \right]$

Parameters of creep function

| Kelvin-Element | Retardation Time θ [h] | Creep Factor ϕ [-] |
|----------------|----------------------------------|----------------------------|
| 1 | 15 | 0,08 |
| 2 | 400 | 0,08 |
| 3 | 4000 | 0,22 |
| 4 | 28000 | 0,22 |

Nonlinear parameter

$$\eta_{NL} = \pm \alpha_{NL} \cdot |\sigma - \sigma_{VP}|^{\beta_{NL}}$$

with $\alpha_{NL} = 0,0014$ und $\beta_{NL} = 2$

Proportional limit

$$\frac{\sigma_{VP}(u)}{f(u=0,12)} = A \cdot e^{-B \cdot u^C}$$

with

| | Compression | Tension |
|---|-------------|---------|
| A | 0,0406 | 2,6661 |
| B | -0,6872 | 5,8433 |
| C | -0,5672 | 0,6561 |

Mechano-sorptive creep

$$\frac{d\epsilon_{ms}}{du} = \frac{\sigma - E_{ms}\epsilon_{ms}}{\eta_{ms}}$$

with $\eta_{ms} = \frac{E}{\alpha_L} \cdot 1,25 \cdot 10^{-5}$ [MPa] , $E_{ms} = \frac{\eta_{ms}}{\Delta u}$,

$$\Delta u = u_{max} - u_{min} [-]$$

Swelling/Shrinkage

$$\frac{d\epsilon_{qs}}{du} = \bar{\alpha}_L$$

with $\bar{\alpha}_L = \begin{cases} \alpha_L (1 - b_\alpha \epsilon) & , \epsilon \leq 0 \\ \alpha_L \cdot \exp(-b_\alpha \epsilon) & , \epsilon > 0 \end{cases}$

$$b_\alpha = 180 [-], \alpha_L = 0,008 \pm 0,002 [-] \quad (\text{normally distr.})$$

DOL-modeling

Strain energy density

$$U = \int_0^t \sigma d\epsilon$$

Critical strain energy density $U_{crit,t} = \frac{1}{2} \cdot \frac{f_t^2(u)}{E(u)}$ (Tension)

$$U_{crit,c} = 4 \cdot \frac{f_c(u)^2}{E(u)} \quad (\text{Compression})$$

**INTERNATIONAL COUNCIL FOR RESEARCH AND INNOVATION
IN BUILDING AND CONSTRUCTION**

WORKING COMMISSION W18 - TIMBER STRUCTURES

INFLUENCE OF PROOF LOADING ON THE RELIABILITY OF MEMBERS

F Lam

S Abayakoon

S Svensson

C Gyamfi

Department of Wood Science

University of British Columbia, Vancouver, B. C.

CANADA

Presented by: F Lam

- V Enjily asked whether species effect was considered? He commented that higher proof load level of up to 10% would lead to larger damage. He asked also about reversal of load direction.
- F Lam responded that this study focused on Hem-fir only. Other species can be considered with the same procedures but different load duration model would be needed. He agreed that one would see more damage in the weak specimens when higher proof load level was used. This was confirmed in the simulation study at higher proof load (not presented). Reversal of load direction was not considered in the study.
- P Glos commented that the increase in benefits seemed to be very limited.
- F Lam briefly reviewed the potential benefits.
- H J Larsen stated that the gain of 10 to 15% was significant considering only 1% of the material would be destroyed via proof loading. He asked whether it is possible to build such a machine for mills. Are there plans to do so?
- F Lam responded that on-line proof-loader exist in finger joint operations in North America and Japan. Some applications include flanges for I-Beams and laminates for Glulam Beams.
- S Thelandersson asked about the target beta level of 3.5. Is this level an official code value. Also were there any assumptions on the load side of the equation tied to the target beta.
- F Lam responded that beta of 3.5 was not a target value in the code but was chosen in this study for illustration only. The target beta value in the Canadian code was approximately 2.8 which was set at similar level as steel and concrete. Gumbel distribution for snow load, and normal distribution for dead load was assumed on the load side of the equation. These were consistent over all material considered.
- I Smith asked whether there was a real threshold level. He commented that B Leicester did double pass proof loading in the past and a lot of damage was observed.
- F Lam answered that in this study the mean threshold level was approximately 0.5 with a rather large COV of 30%. This was based on past DOL study. The existence of threshold level is a complicated debate that is beyond the scope of the study. Double pass proof loading was not considered in the study.

Influence of Proof Loading on the Reliability of Members

by

Frank Lam, Sarath Abayakoon, Staffan Svensson and Charles Gyamfi

Department of Wood Science
University of British Columbia, Vancouver, B. C.
Canada

Abstract

Proof loading concept is a recognized quality control technique to improve the characteristics of the lower tail of strength distributions of structural timber products. Very few comprehensive studies are available to quantify the effectiveness on the use of proof loading relating to the choice of proof load level, the potential damage on the members resulting from the application of proof load, and the improvement of performance in the context of reliability based design methods. One of the difficulties is the need of a rather large sample size for an experimental-based study to develop statistically meaningful solutions. This paper illustrates the use of damage accumulation model and reliability based design analyses to quantify the effectiveness of proof loading.

The performance of No. 2 and better Western Hemlock 38 x 140 mm dimension lumber in bending is considered. Damage accumulation laws are established to consider the residual strength of members that survived a proof load. Reliability analyses are conducted to compare the performance of proof-loaded and non-proof loaded members subject to snow load conditions in two locations in Canada. For a given reliability index (β), the improvement of performance can be quantified as characteristic strength adjustment factors for proof loading in terms of the ratio of the performance factors (ϕ) between the original and proof load material. Conversely the gain in reliability, β , for a given ϕ value is also apparent. The adjustment factors depend on the proof load level, the β level, and the distribution selected for fitting the strength data after proof loading.

1 Introduction

Proof loading subjects members up to a small load level and releases the load. During proof loading some members may fail. It is a recognized quality control technique to improve the characteristics of the lower tail of strength distributions of structural timber products. Examples of commercial applications of this technique include proof loading of finger-joined material for use in glue-laminated beams and wood I beams.

Research findings on proof loading of lumber suggest damage due to a moderate level of proof loading is not significant (Woeste *et al.* 1987, Leicester 1988). Woeste *et al.* (1987) did not detect any damage to tension specimens proof loaded in single and reverse bending. Leicester (1988) tested specimens in tension to failure in low cycle fatigue with increasing loads and found that only 10% of the specimens were damaged. The damage was, on the average, 4% of the apparent strength during proof loading. The qualification of the impact of proof loading using an empirical approach is a difficult problem because it would require a large sample size to estimate this relatively small effect. Furthermore, the impact of proof loading from reliability perspective needs to be investigated to quantify the relation between the performance of proof-loaded and original members.

In this paper, the performance of No. 2 and better Western Hemlock 38 mm x 140 mm dimension lumber in bending are considered. A damage accumulation model was used as a tool to estimate the level of damage experienced by members that have undergone proof loading. The residual strengths of the survivors were determined analytically and fitted to different distributions. Reliability analyses were conducted to establish the improvement of performance of proof-loaded members.

2 Damage Model

Several models have been developed for the accumulation of damage in wood members. Equation 1 presents the model proposed by Foschi *et al.* in 1989.

$$\frac{d\alpha}{dt} = a[\tau(t) - \sigma_o \tau_s]^b + c[\tau(t) - \sigma_o \tau_s]^n \alpha \quad [1]$$

The damage parameter, α , equals to 0 when there is no damage and equals to 1 at the time of failure. The five model parameters a , b , c , n and σ_o are assumed to be constants for a given member but varies randomly across members. In equation [1], τ_s is the standard short term strength of the member which can be determined in a ramp load test of short duration with a constant rate of loading. σ_o is the threshold stress ratio. The product $\sigma_o \tau_s$ defines a threshold that must be exceeded for damage to accumulate; *i.e.*, there will be no damage accumulation when $\tau(t)$ does not exceed $\sigma_o \tau_s$.

The parameter a is not independent of the variables τ_s , b , c , n and σ_o . For the case of using a ramp load with a rate of loading K_s to determine the short-term strength, a can be expressed as Equation [2]:

$$a = \frac{K_s (b+1)}{\{\tau_s - \sigma_o \tau_s\}^{b+1}} \quad [2]$$

Each of the four independent parameters b , c , n , and σ_o are modeled as lognormal variables. In the process of damage accumulation calculations, the short-term strength τ_s is also assumed to be lognormally distributed.

The model has been calibrated to experimental results for Western Hemlock 38 mm x 140 mm (nominal 2" x 6"), visually graded, No. 2 and better lumber (Foschi *et al.* 1989). The distribution parameters of the variables in the damage model are shown in Table 1. The parameters in Table 1 are shown for stresses expressed in MPa and psi.

Table 1. Distribution parameters of the variables in the damage model

| | b | | c | | N | | σ_o | |
|---------------|--------|-------|------------------------|-------|-------|-------|------------|-------|
| | Mean | COV | Mean | COV | Mean | COV | Mean | COV |
| Stress in MPa | 37.161 | 0.281 | 1.623×10^{-4} | 0.574 | 1.290 | 0.075 | 0.533 | 0.298 |
| Stress in psi | 37.161 | 0.281 | 2.465×10^{-7} | 0.336 | 1.290 | 0.075 | 0.533 | 0.298 |

Mean and standard deviation of the short-term strength (τ_s) were taken as 47.82 MPa (6936.46 psi) and 19.46 MPa (2822.34 psi) respectively. The ramp rate, K_s , was assumed to be 2678.48 MPa/hr (388500 psi/hr).

3 Proof Loading

The residual strength of a member subjected to a proof load level τ_c can be established by considering the loading scheme shown in Figure 1. The accumulation of damage can be calculated by integrating equation 1 with the appropriate description of $\tau(t)$. Note that damage will accumulate only if $\tau(t) > \sigma_o \tau_s$.

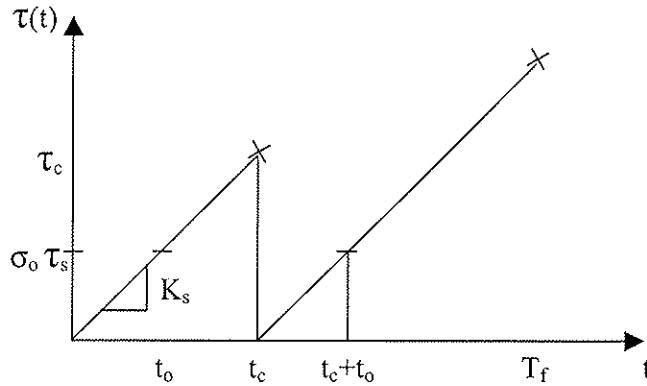


Figure 1- Proof Loading Scheme

The loading rate K_s is the same during the two phases of uploading. Damage at time t_c can be expressed as:

$$\alpha(t_c) = \frac{a}{(b+1)K_s} (K_s t_c - \sigma_o \tau_s)^{b+1} \quad [3]$$

During the second phase of loading, there will be no damage accumulation until $t > t_c + t_o$, and the time to failure is given by:

$$T_f = \left\{ \left[(\tau_s - \sigma_o \tau_s)^{b+1} - (K_s t_c - \sigma_o \tau_s)^{b+1} \right]^{\frac{1}{b+1}} + \sigma_o \tau_s + K_s t_c \right\} \frac{1}{K_s} \quad [4]$$

Once the time to failure is calculated, the residual strength of each member can be determined as:

$$f_R = \left[(\tau_s - \sigma_o \tau_s)^{b+1} - (K_s t_c - \sigma_o \tau_s)^{b+1} \right]^{\frac{1}{b+1}} + \sigma_o \tau_s \quad [5]$$

for $\tau_s > K_s t_c$

Three proof load levels, τ_c , were considered in Monte Carlo simulation studies with 2000 replicates. They are taken as the 1st, 3rd, and 5th percentile of the short-term strength of the members as 17.82 Mpa(2585 psi), 21.22 Mpa(3077 psi), and 23.27 Mpa(3374 psi), respectively. Figures 2 to 4 show the cumulative probability distributions of bending strength for the original and the proof loaded specimens, respectively. The lognormal and the 3-parameter Weibull probability distributions were fitted to the residual strengths of the proof loaded specimens. In addition, the 2-parameter Weibull distribution was fitted to the lower 15 percent of the residual strengths of the proof loaded specimens. Information on the distribution parameters for the various fits is shown in Table 2.

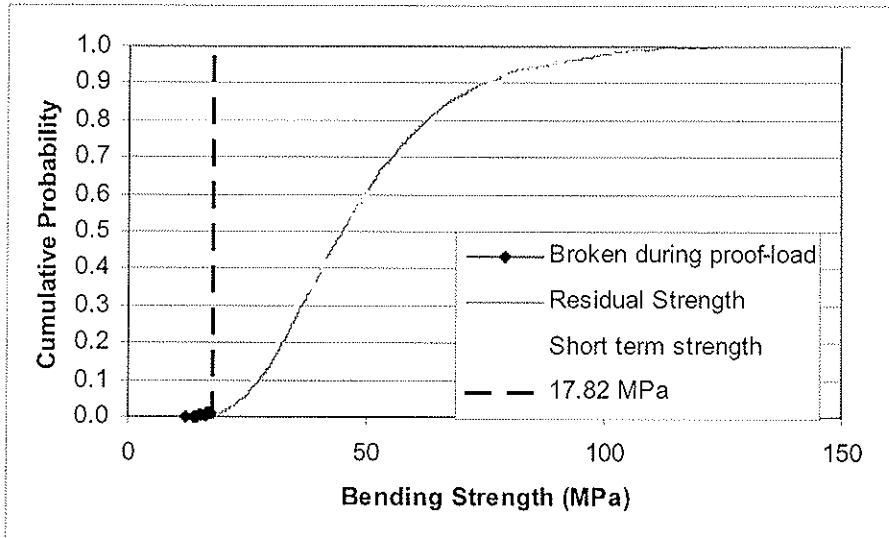


Figure 2 - Cumulative probability distributions of bending strength for the original and the specimens proof loaded to 1% of the short-term strength

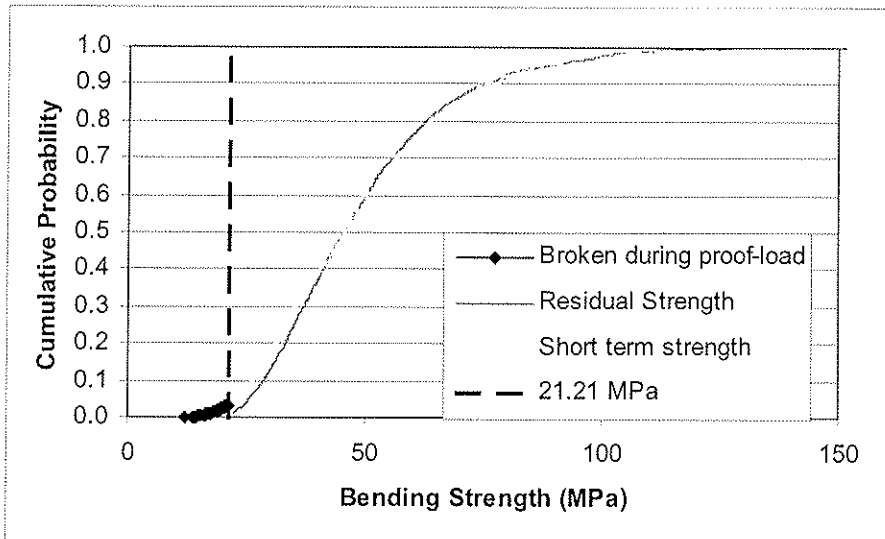


Figure 3 - Cumulative probability distributions of bending strength for the original and the specimens proof loaded to 3% of the short-term strength

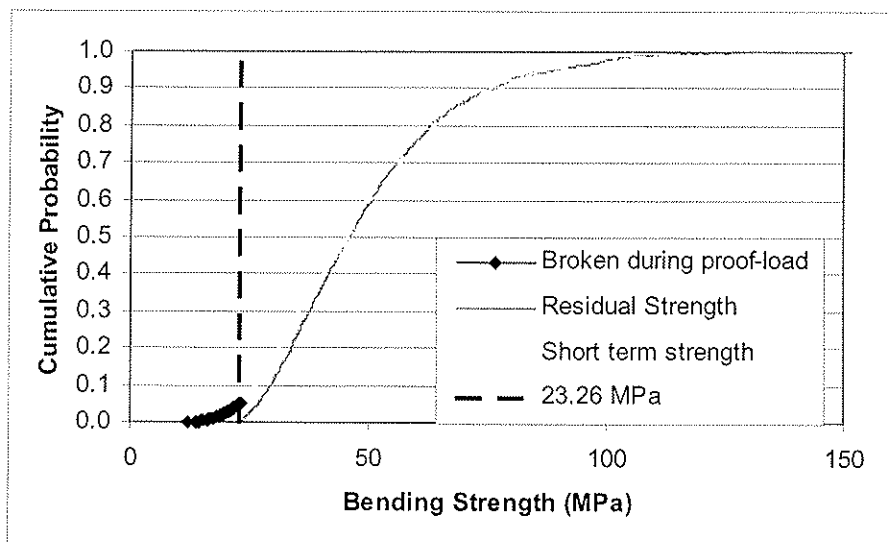


Figure 4 - Cumulative probability distributions of bending strength for the original and the specimens proof loaded to 5% of the short-term strength

Table 2. Distribution parameters for the residual strengths

| Proof load level | lognormal | | 3-parameter Weibull | | | 2-parameter Weibull truncated at 15% | |
|----------------------------|------------|-------|---------------------|---------|------|--------------------------------------|------|
| | Mean (MPa) | COV | Loc (MPa) | m (MPa) | k | m (MPa) | k |
| 1 st Percentile | 48.57 | 0.396 | 17.34 | 35.03 | 1.67 | 41.78 | 5.65 |
| 3 rd Percentile | 49.17 | 0.377 | 20.73 | 31.72 | 1.54 | 40.45 | 6.96 |
| 5 th Percentile | 49.66 | 0.037 | 22.74 | 29.87 | 1.47 | 39.50 | 8.26 |

4 Reliability Analysis

Reliability analyses were performed for the members under dead and snow load conditions for two Canadian cities (Quebec City and Vancouver) following the procedures outlined by Foschi *et al.* (1989).

The limit state design equation for design of bending members can be expressed as:

$$\alpha_D G_D D_N + \alpha_L G_L L_N = \phi F_b \quad [6]$$

where

α_D and α_L are the load factors for dead (1.25) and live (1.5) loads, respectively;
 G_D and G_L are the dead and live load geometric factors that convert the applied loads to bending stresses;
 D_N and L_N are the nominal design dead load and nominal design total roof snow and rain load, respectively;
 F_b is the characteristic bending strength; and
 ϕ is the performance factor.

Equation 6 is the form of the limit state design equation in the Canadian Code on Engineering Design in Wood (Canadian Standards Association, 1994). The failure function developed to relate the bending resistance and the effect of loads for first-order second-moment reliability analyses is as follows:

$$G = R - (G_D D + G_L L) \quad [7]$$

$$G = 0 \quad \Rightarrow \text{Limit State}$$

$$G > 0 \quad \Rightarrow \text{Safe}$$

$$G < 0 \quad \Rightarrow \text{Failure}$$

where R , D , and L are random variables representing the bending strength, dead load, and live snow load, respectively. Statistical distributions and parameters for the snow load for the two Canadian cities, Quebec City and Vancouver, were described in detail in past studies (Foschi *et al.* 1989) where the snow loads are considered on a 30-year return period.

The failure function can be rewritten as:

$$G = R - \frac{(\varepsilon \delta \gamma + \iota) \phi F_b}{\alpha_D \varepsilon \gamma + \alpha_L} \quad [8]$$

where $\gamma = D_N/L_N$; $\delta = D/D_N$; $\iota = L/L_N$; and $\varepsilon = G_D/G_L$. The variables ε and γ were assumed to equal 1.0 and 0.25, respectively. The random variable δ was assumed to be normal with mean of 1.0 and standard deviation of 0.1.

The reliability method can be used to estimate the probability of failure, P_f , by calculating a reliability index β . These two are related by:

$$P_f = \Phi(-\beta) \quad [9]$$

where Φ is the standard normal probability distribution function.

The value of F_b was taken as the 5th percentile strength of the original material as 23.27 MPa. This is equivalent to keeping the same characteristic strength for the material irrespectively of whether they have been proof loaded or not. The improvement in performance for a given β level, is then reflected by the ratio of ϕ between the proof loaded and the original material.

Figures 5 and 6 show example plots of β versus ϕ relationships for Quebec City and Vancouver based on the 2-parameter Weibull distributions censored at the 15% strength level. Figures 7 and 8 show similar relationships for Quebec City based on the lognormal and the 3-parameter Weibull distributions. Table 3 shows the results of the reliability analysis for all the cases in the form of β and ϕ values.

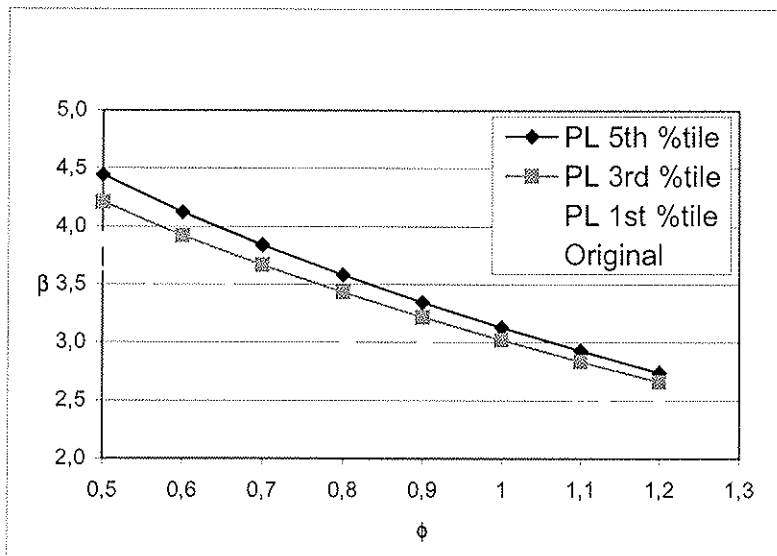


Figure 5 - β versus ϕ relationships for Quebec City based on the 2-parameter Weibull distribution censored at the 15% strength level.

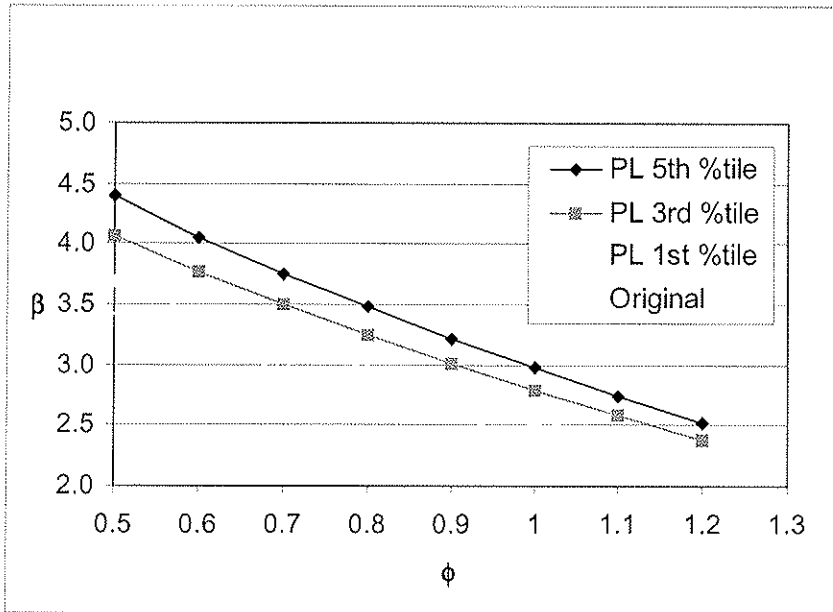


Figure 6 - β versus ϕ relationships for Vancouver based on the 2-parameter Weibull distribution censored at the 15% strength level.

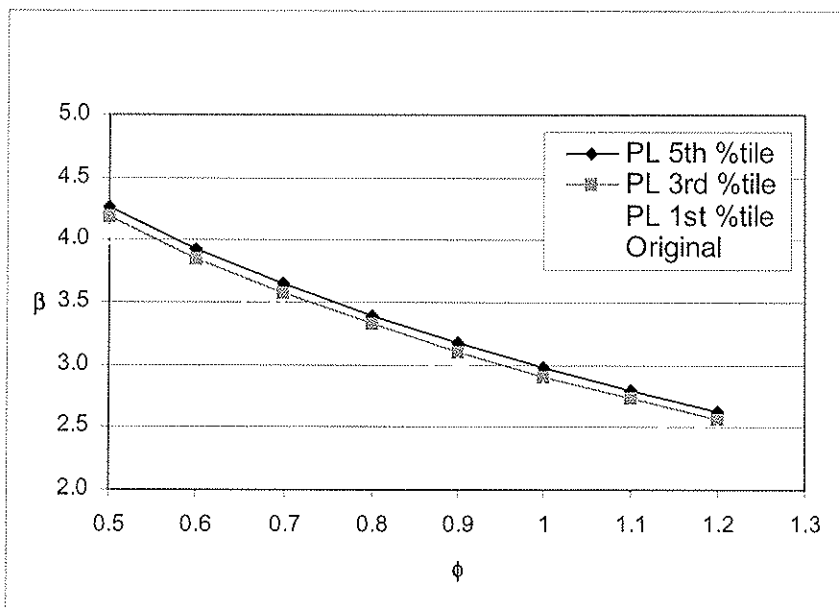


Figure 7 - β versus ϕ relationships Quebec City based on the lognormal distribution

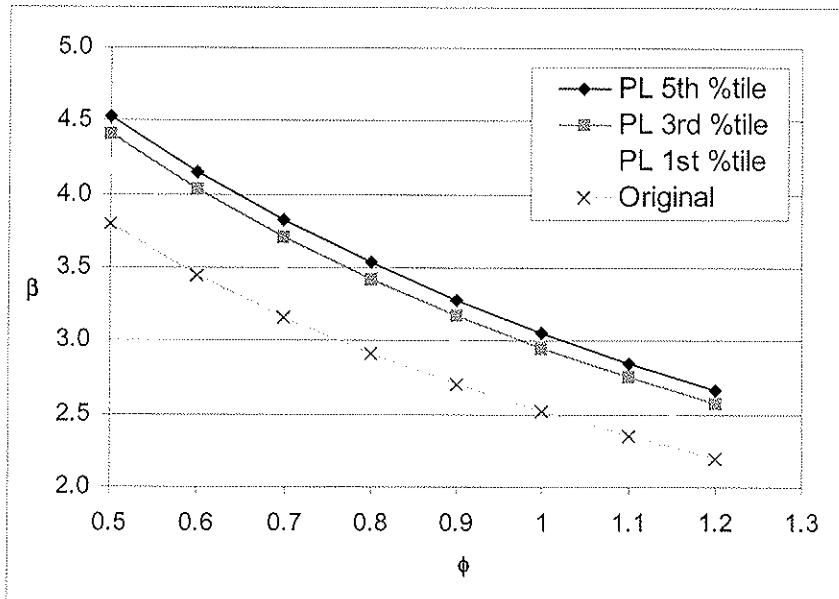


Figure 8 - β versus ϕ relationships Quebec City based on 3-parameter Weibull distribution

From Figures 5 to 8, it is apparent that there are differences in the results depending on the choice of the strength distribution. For the original material, the use of a lognormal distribution to represent the bending strength tends to give a slightly higher β - ϕ relationship compared to the 2-parameter Weibull distributions censored at the 15% strength level. This is because of the sensitivity of the analysis to the tail of the strength distributions.

Similarly, the use of a 3-parameter Weibull distribution to represent the strength distribution is sensitive to location distribution parameter (ϵ) which represents the lower bound of the strength. The determination of the 3-parameter Weibull location parameter in the process of fitting can therefore influence the results of the reliability analyses.

For a given β level, the increase of the ϕ values between the proof-loaded and the original material can be estimated. The results at β value of 3.5 are shown in Table 4. These adjustment factors can be applied to the characteristic strength F_b to account for the impact of proof loading while maintaining a uniform β of 3.5.

In the Canadian Code on Engineering Design in Wood (Canadian Standards Association, 1994), a ϕ value of 0.9 is used in bending member designs. Consider a ϕ of 0.9 for the original material, a corresponding β level can be established. Using this β level, the ratio of the ϕ values between the proof-loaded and the original material can also be estimated as shown in Table 5. Again these adjustment factors can be applied to the characteristic strength F_b to account for the impact of proof loading while maintaining the target β intended in the code.

Table 4 – Characteristic strength adjustment factor for proof loading at $\beta = 3.5$

| City | Quebec City | | | Vancouver | | |
|-----------------------------|-------------------------------|-------------------------------|-------------------------------|-------------------------------|-------------------------------|-------------------------------|
| | 1 st percentile | 3 rd percentile | 5 th percentile | 1 st percentile | 3 rd percentile | 5 th percentile |
| Lognormal | 1.047 | 1.112 | 1.156 | 1.058 | 1.129 | 1.179 |
| 3P Weibull | 1.178 | 1.380 | 1.493 | 1.225 | 1.501 | 1.699 |
| 2P Weibull truncated at 15% | 1.196 | 1.321 | 1.391 | 1.239 | 1.391 | 1.478 |

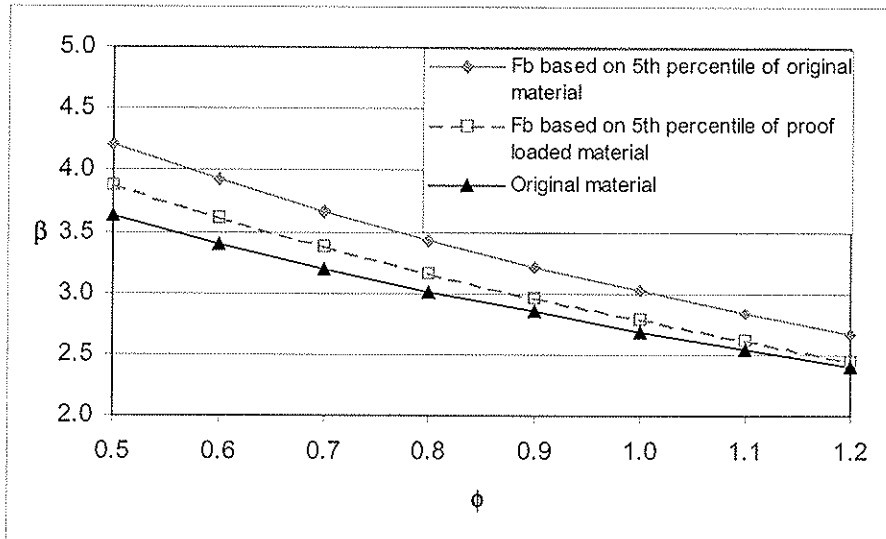
Table 5 - Characteristic strength adjustment factor for proof loading that correspond to a $\phi = 0.9$ for the original material

| City | Quebec City | | | Vancouver | | |
|-----------------------------|-------------------------------|-------------------------------|-------------------------------|-------------------------------|-------------------------------|-------------------------------|
| | 1 st percentile | 3 rd percentile | 5 th percentile | 1 st percentile | 3 rd percentile | 5 th percentile |
| Lognormal | 1.045 | 1.101 | 1.138 | 1.047 | 1.106 | 1.148 |
| 3P Weibull | 1.105 | 1.214 | 1.270 | 1.107 | 1.232 | 1.308 |
| 2P Weibull truncated at 15% | 1.152 | 1.251 | 1.309 | 1.166 | 1.277 | 1.340 |

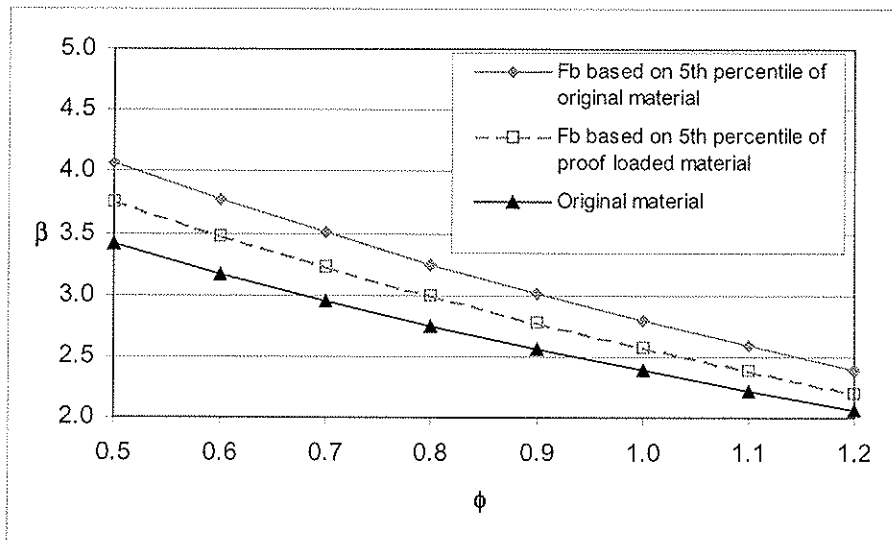
It can be observed that the adjustment factors for proof loading is dependent on: 1) the proof load level; 2) the β level; and 3) the choice of probability distribution to represent the residual and the original strengths. As expected, higher proof load levels lead to higher proof loading adjustment factors. The selection of proof load, however, is an economic and logistic decision that is not within the scope of this paper. Similarly, higher β levels lead to higher proof loading adjustment factors. This is because the member strengths associated with the design points at the higher β levels would be weaker than those at a lower β level. Therefore, the effectiveness of the proof loading process to reduce the very weak specimens for the higher β levels is appropriately recognized by the reliability analysis procedures. Finally the choice of probability distribution to represent the residual and the original strengths has a strong influence on the adjustment factors. In this study, the types of probability strength distributions are kept consistent within each case. As previously discussed, the 2-parameter Weibull distributions censored at the 15% strength level should be used because they represent the lower tails of the strength distributions well and does not rely on the determination of the location parameters ϵ .

The above analyses can be repeated with the values of F_b taken as the 5th percentile strengths of the respective material. Therefore, in such cases, any observed improvements in performance for a given β level, can be attributed to the modifications of the variability of the tails of the distribution as a result of proof loading. As an example, Figures 9(a) and 9(b) illustrate the $\beta - \phi$ relationships of

Quebec City and Vancouver, respectively at a proof load level of the 3rd percentile using the F_b values from the respective strength distributions.



(a) Quebec City



(b) Vancouver

Figure 9 - β - ϕ relationships:-

Lower curve - original

Upper two curves - proof loaded to 3rd percentile with characteristic strength value as the 5th percentile of, (i) short-term strength (continuous curve) and (ii) residual strength (dashed curve)

5 Conclusions

In this study a damage accumulation model is used to assess the damage caused by proof loading in Monte Carlo simulations. The bending strength distribution and residual strength distributions were evaluated in reliability analysis against dead loads and snow load conditions for two Canadian cities.

The $\phi - \beta$ relationships of the proof loaded members show a shift to the right in comparison with the original set. For a given reliability index, the improvement of performance can be quantified as characteristic strength adjustment factors for proof loading in terms of the ratio of ϕ values between the original and proof load material. Conversely the gain in reliability for a given ϕ value is also apparent. The percentage increase depends on the proof load level, the β level, and the distribution selected for fitting the strength data after proof loading.

6 References

- Foschi, R.O., Folz, B.R., and Yao, F.Z., 1989. Reliability-based Design of Wood Structures. Structural Research Series, Report No. 34, Department of Civil Engineering, University of British Columbia, Vancouver, British Columbia, Canada.
- Woeste, F. E., Green, D. W., Tarbell, K. A., Marin, L. A., 1987. Proof loading to assure lumber strength. *Wood and Fiber Science*. 19:283-297.
- Leicester, R. H., 1988. Rogue factors in proof grading. In *Proceedings 1988 International Conference on Timber Engineering*, Seattle, Washington. 1: 345-350.

**INTERNATIONAL COUNCIL FOR RESEARCH AND INNOVATION
IN BUILDING AND CONSTRUCTION**

WORKING COMMISSION W18 - TIMBER STRUCTURES

**MATERIAL STRENGTH PROPERTIES FOR CANADIAN SPECIES
USED IN JAPANESE POST AND BEAM CONSTRUCTION**

J D Barrett

F Lam

Department of Wood Science, The University of British Columbia
CANADA

Shiro Nakajima

Building Research Institute, Tsukuba
JAPAN

Presented by: F Lam

- H J Blass asked whether density values were measured. He also asked whether the bending strength was defined as the stress at the worst defect.
- F Lam answered that density value was obtained from each specimen and the bending strength was calculated from the highest stress zone.
- S Thelandersson asked which distribution was assumed for the COV of the lower tail.
- F Lam responded that he would check with D Barrett about this. (2P Weibull distribution was assumed)
- R Marsh asked whether the Japanese would accept different test methods on the basis of models rather than on tests.
- F Lam responded that the Japanese Ministry officers usually considered these request on a case-by-case basis. If validated model were available, they would consider it.
- M Yasumura stated that joints are important for seismic issues. What was the motivation for the study. He also asked whether long-term issues were considered.
- F Lam agreed that connection information would be important and a second study has been planned to consider the seismic design issues. The values obtained in the current study would still be important for general member design. Long-term issues have not been considered.
- P Glos stated that the ASTM standards still differed from ISO.
- F Lam stated that ISO and ASTM standards are similar.
- H J Larsen explained that with the ISO standard there is no stipulation about the location of worst defect. The researcher would decide and document the location in the study.

Material Strength Properties for Canadian Species Used in Japanese Post and Beam construction

1.0 Introduction

The traditional post and beam system house and the 2x4 platform frame system are widely used in Japanese residential construction. The post and beam house evolved over many centuries to become the preferred method for wooden housing construction in Japan. In the 1970's, the North American 2x4 building system was introduced to the Japanese consumers. Canada is a major supplier of structural wood products for both the traditional and 2x4 housing construction.

Post and Beam housing is built according to the Building Standard Law (BSL). Traditionally post and beam houses have been built with ungraded lumber and requirements for the performance of connectors were stipulated in only general terms. In contrast, 2x4 houses are more "engineered". Lumber is grade stamped and member sizes were determined by engineering calculations based on allowable stresses approved by the Japanese government.

The Kobe earthquake had a major impact on consumer perceptions of wooden housing construction in Japan. Extensive investigations showed that many of the structural problems in Post and Beam construction could be traced to poor maintenance and the quality of the older building built in the late 1940's. The Japanese government has responded by introducing new performance oriented building codes, new housing quality assurance laws and housing performance labeling systems to increase protection for consumers and improve the quality of wooden housing construction.

Procedures for deriving allowable stresses for post and beam and 2x4 construction have been clarified in the new BSL. Requirements for design of post and beam and 2x4 houses have been reformed to include strength and deformation limits that place more emphasis on demonstration of the actual performance of the building components and full-size houses.

The introduction of labeling systems and emphasis on structural integrity and durability have forced lumber suppliers to respond to customer demands for strong, stable and durable building products. Japanese agencies such as the Forestry Agency and the Forest and Forest products Research Institute have collected full-size test data on the structural properties of species used in building construction in Japan. This paper provides information on comprehensive in-grade tests program conducted on Canadian species used in Post and Beam construction and compares results obtained according to different grading rules.

2.0 Lumber Grading Standards

The Japanese BSL does not require the use of grade stamped lumber in housing construction. Article 41 of the BSL states that: “Timber to be used in principal parts necessary for strength shall be free from defects such as knots, rot, slope of grain, wane, etc if they interfere with structural strength”. The BSL provided allowable stresses for selected species as shown in Table 1 with a safety factor of 3. Recently these allowable strength values were converted to “Material Strength Values” intended to represent a 5th percentile of the short term strength as adopted in many international standards. These material strength values now apply to **ungraded lumber**.¹

| Kinds of Timber | Old BSL Allowable Stress | New material Strength Property |
|--|----------------------------------|--------------------------------------|
| | Bending (kgfcm ²) | Bending (MPa) |
| Douglas fir , Japanese Red Pine | 95 | 28.2 |
| Japanese Larch, Cypress | 90 | 27.6 |
| Japanese Hemlock, western Hemlock | 87 | 25.2 |
| Japanese Fir, Japanese Cedar (Sugi) | 75 | 22.2 |

2.1 JAS 143 Structural Softwood Lumber

The Japanese Agricultural Standard provides grading rules for lumber used in post and beam construction. The Japanese Ministry of Lands, Infrastructure and Transport(MLIT)² has provided allowable stress (except modulus of elasticity for three JAS 143 grades. The lumber is categorized for particular end uses as follows:

Type A Structural Lumber; Lumber graded for use in high bending applications

- Structural Lumber I Type A with a cross section less than 36 mm on the short side or those with ends not less than 36 mm and less than 90 mm on the long side
- Structural Lumber II Type A with ends not less than 36 mm on the short side and not less than 90 mm on the long side

Type B structural lumber is graded mainly for compression applications

However, the JAS 143 grading rule is not widely used in commercial practice. Consequently most lumber is supplied in the ungraded condition. Canadian experience has

¹ The MLIT does not provide modulus of elasticity values. Designers rely on MOE values provided by the Architectural Institute of Japan or the individual product manufacturers

² MLIT, formerly the Ministry of Construction.

shown that the JAS 143 rule is restrictive not practical because of the low yields obtained when applied to the many large knotted species growing in British Columbia.

2.2 Proprietary Grading Rules

Canadian lumber producers have developed company specific proprietary “in-house” grading rules matched to individual customer requirements. Until recently, there has been no basis for assigning allowable stresses to these proprietary grades because the proprietary grading rules have not been approved in Japan. However the MLIT material strength values for ungraded lumber could be applicable to the proprietary grades.

2.3 CFLA Grading Rules

The Coast Forest and Lumber Association (CFLA) developed a new visual grading rule for Hem-Fir (N) structural lumber products intended for the Japanese post and beam housing market. The grading rule is titled **CFLA Japanese Product Standard 1 “Structural lumber – Visual grading – Requirements for E 120 Canadian coastal Hem-Fir (N) lumber products used in traditional Japanese post and Beam building construction”**. The evaluation criteria specify a characteristic value of modulus of elasticity of 12000 N/mm². The characteristic value of bending strength shall equal or exceed the bending material strength value for “ungraded” Hemlock³ established by the MLIT.

The CFLA has undertaken a major in-grade lumber testing program on Hem-Fir (N) and Douglas fir (N) lumber to provide the engineering property data to gain acceptance of material strength values for these species in Japan. Sampling, testing and data analysis have been conducted in accordance with the methods recommended by the Japanese Ministry of Lands, Infrastructure and Transport. This paper describes the sampling, testing and data analysis procedures used to derive the characteristic values for Hem-Fir (N) and Douglas-fir (N).

3.0 Sampling

Douglas fir (N) and Hem-Fir (N) lumber was sampled from normal production of mills in the coastal region of British Columbia. Hem-Fir (N) sampling was conducted for five (5) cross-section dimensions⁴ -- 30 x 105, 45 x 90, 45 x 105, 90 x 90 and 105 x 105. Douglas fir (N) was sampled in two sizes 105 x 105 and 45 x 105. Samples were selected from surfaced dry production whenever possible. Alternatively, green lumber was sampled and dried using a conventional commercial kiln schedule. After drying the lumber was surfaced to the final dimensions.

The dry surfaced lumber samples were graded in accordance with the structural requirements of **JPS 1** and the **JAS 143** grade rule. All lumber evaluated in the in-grade

³ Material strength property for ungraded Hemlock in bending is 25.2 N/mm²

⁴ All dimensions in millimeters

testing program was determined to be on-grade by the grading supervisor of the Canadian Mill Services Association.

4.0 Test Methods

This section describes the test matrix and test methods adopted in the Hem-Fir (N) and Douglas-fir (N) in-grade test program.

4.1 Sample Sizes

A minimum of 300 pieces⁵ were selected randomly in each cross-sectional sizes. The sampling matrix for Hem-Fir (N) and Douglas fir (N) are shown in Table 1.

Table 1. Douglas fir (N) and Hem-Fir (N) test matrix.

| Specimen Size (mm) | Sample Size (n) | |
|--------------------|-----------------|-----------------|
| | Hem-Fir (N) | Douglas fir (N) |
| 105 x 105 | 1904 | 932 |
| 90 x 90 | 367 | |
| 30 x 105 | 637 | |
| 45 x 90 | 360 | |
| 45 x 105 | 1351 | 913 |

All test specimens were received in the kiln-dried condition. Following delivery to the University of British Columbia Timber Engineering and Applied Mechanics Laboratory, the material was further air conditioned to an equilibrium moisture content of approximately 15%.

The maximum strength-reducing defect (MSRD)⁶ was identified for each piece. The location of the MSRD was measured and recorded with respect to the numbered end of each piece. The characteristics determining the grade and the MSRD were recorded. The physical dimensions of each piece were also measured and recorded.

⁵ The MLIT test protocol requires a minimum samples size of $0.1537 (CV)^2$. For Hem-Fir (N) and Hem-Fir (N), a minimum **required sample size** ($n = 188$) was estimated using an assumed $CV = 35\%$.

⁶ The MSRD is the defect that was estimated to provide the lowest strength if tested in bending.

4.2 Bending Test Methods

Bending tests used for evaluating modulus of elasticity (MOE) and bending strength (MOR) were conducted in accordance with the requirements of the MLIT test protocol:⁷

- 1/3 point loading conditions
- 18 to 1 span to depth ratio
- Tension edge of the bending specimen was selected at random
- MSRD located randomly within the total test span at a span
- Tests conducted at a loading rate to cause failure in 1 to 5 minutes⁸

The test configuration for the 105-mm deep bending test specimens is shown schematically in Figure 1. The total neutral axis deflection was measured using a full-span yoke located as shown in Figure 1. The total applied load⁹ and mid-span beam deflection were monitored and recorded. The maximum total load was determined from the load vs. deflection data. The modulus of rupture (MOR) and long-span MOE (E_L) were calculated for each specimen based on the actual dimensions recorded at the time of test.

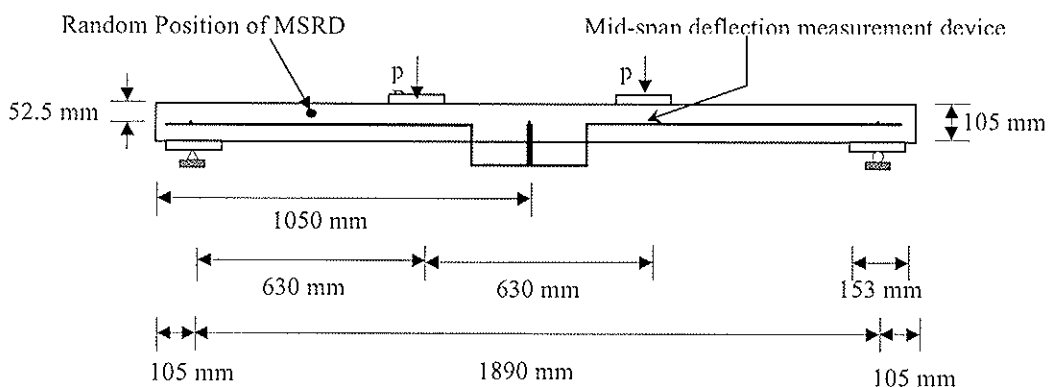


Figure 1. Long span MOE (E_L) test configuration (beam depth $d = 105$ mm)

4.3 Specific Gravity and Moisture Content

Specific gravity and moisture content test blocks were cut from each specimen at the time of test. Moisture content and specific gravity were evaluated using the methods recommended in JIS Z2102-1957 "Method of measuring average width of annual rings, moisture content, and specific gravity of wood"¹⁰.

⁷ The MLIT Test Protocol is consistent with the methods recommended in ASTM D 4761 Standard Methods for Testing Mechanical Properties of Lumber and Wood-base Structural Material (ASTM, 1999).

⁸ Machine cross-head displacement rates were 18.2 mm /minute for the 90 mm x 90 mm material and 21.2 mm /minute for all other sizes.

⁹ In Figure 1, the load p = the total load divided by 2.

¹⁰ ASTM methods ASTM D 4442 "Standard Test Methods for Direct Moisture Content Measurement of Wood and Wood-base Materials" and ASTM D 2395. "Standard Test Methods for Specific Gravity of Wood and Wood Based Materials" (ASTM (1999)) were used as they are equivalent to the JIS Z2102 standard.

5.0 Evaluation of Test Results

This section describes the procedures used to convert test data to characteristic properties for the individual test cells. Subsequently, the characteristic values for the **CFLA JPS 1** grade and **JAS 143** grades are derived by sample size weighting the characteristic properties obtained for the individual test cells.

5.1 Moisture Content Adjustments

The MLIT protocol specifies that the test specimens shall be at 15% moisture content at the time of testing. When an actual moisture content differed from 15%, the E_L and MOR data were adjusted to 15% moisture content. The long-span test MOE values E_L , were adjusted to a standard moisture content of 15% according to procedures specified in ASTM D 2915, "Standard Practice for Evaluating Allowable Properties for Grades of Structural Lumber" (ASTM, 1999). MOR data was adjusted to 15% using the linear surface model adjustment procedure (Barrett and Lau, 1994).

5.2 MOR Data

All the bending tests were conducted at an 18 to 1 span to depth ratio. Therefore, no MOR adjustment is required for loading conditions or span to depth ratio effects.

5.3 E_{true} Calculation

The MOC Protocol specifies the modulus of elasticity E_L must be adjusted to a shear free basis herein denoted as E_{true} . In this study, E_{true} has been calculated using the procedures recommended in ASTM D 198 "Standard Test Methods of Static Tests of Lumber in Structural Sizes" (ASTM, 1999). E_{true} is given by:

$$E_{true} = E_L (1 + 0.939 (d/L)^2 (E/G))$$

where:

| | |
|------------------|---|
| E_L | long-span MOE equals $23 PL^3 / (1296 I \delta_{total})$ |
| P | total load applied to the beam, N |
| L | test span, mm |
| d/L | depth to span ratio (1 to 18) |
| E/G | ratio of the modulus of elasticity to the shear modulus ¹¹ |
| I | moment of inertia of the cross section ($bd^3/12$), mm ⁴ , and |
| δ_{total} | total neutral axis beam deflection, mm |

¹¹ E/G = 16 was adopted for calculations in this paper.

5.4 Test Cell Characteristic Properties

The characteristic modulus of elasticity is taken to be the lower 95 percent confidence limit for the mean (average) value of E_{true} . The lower 95 percent confidence limit for E_{true} -- denoted as $E_{true, mean, 0.95}$ was calculated according to the procedures recommended in ASTM D 2915 "Standard Practice for Evaluating Allowable Properties for Grades of Structural Lumber" (ASTM, 1999).

$$E_{true, mean, 0.95} = E_{true, mean} - (1.96 \text{ (standard deviation of } E_{true})) / n^{0.5}$$

where:

n the sample size for the test cell

The characteristics value for the bending strength is taken to be the lower 5% Non-Parametric Tolerance Limit. The property, denoted as $MOR_{data, 0.05, NTL}$, was calculated in accordance with "The Standard Practice for Establishing Allowable Properties for Visually-Graded Dimension Lumber from In-grade Tests of Full-Size Specimens" (ASTM, 1999)

6.0 Results

This section includes summary statistics and the characteristic properties derived from the in-grade data for Hem-Fir (N) and Douglas fir (N) graded to the **CFLA JPS 1**.

6.1 Summary Statistics -- CFLA Grade Rule

All data has been adjusted to 15% moisture content.

Summary statistics derived from the in-grade tests of Hem-Fir (N) graded to the **CFLA JPS 1** grading rule are provided for MOE and MOR by size in Tables 2 to 3. Results for Douglas fir are shown in Tables 4 and 5. MLIT assigns an MOR material strength of 28.2 MPa for ungraded Douglas fir.

Table 2. MOR summary statistics for Hem-Fir (N) (units - MPa).

| | 105 x 105 mm | 90 x 90 mm | 45 x 105 mm | 30 x 105 mm | 45 x 90 mm |
|--------------------------|-----------------|---------------|----------------|----------------|---------------|
| Count | 1903 | 357 | 1209 | 568 | 360 |
| Average | 50.75 | 52.15 | 55.98 | 54.53 | 56.28 |
| Minimum | 8.53 | 16.12 | 9.22 | 9.23 | 9.95 |
| Maximum | 108.13 | 107.94 | 102.57 | 102.94 | 102.57 |
| Std. Deviation | 16.38 | 17.37 | 16.17 | 17.59 | 17.77 |
| COV | 32.27% | 33.30% | 28.89% | 32.26% | 31.58% |
| MOR _{0.05} | 24.20 | 26.03 | 28.62 | 23.84 | 26.14 |
| MOR _{0.05, NTL} | 23.97 | 25.25 | 27.52 | 22.93 | 25.01 |

Table 3. E_{true} summary statistics for Hem-Fir (N) (units - GPa).

| | 105 x 105 mm | 90 x 90 mm | 45 x 105 mm | 30 x 105 mm | 45 x 90 mm |
|--------------------------|-----------------|---------------|----------------|----------------|---------------|
| Count | 1901 | 357 | 1209 | 568 | 360 |
| Average | 12.41 | 12.53 | 12.72 | 12.63 | 12.32 |
| Minimum | 4.74 | 6.29 | 4.62 | 4.98 | 6.52 |
| Maximum | 26.04 | 18.30 | 20.53 | 20.08 | 21.46 |
| Std. Deviation | 2.44 | 2.17 | 2.34 | 2.65 | 2.54 |
| COV | 19.69% | 17.30% | 18.39% | 20.97% | 20.64% |
| MOE _{0.05, NTL} | 8.54 | 9.21 | 9.03 | 8.50 | 8.27 |
| $E_{true, mean, 0.95}$ | 12.30 | 12.30 | 12.58 | 12.41 | 12.06 |

Table 4. MOR summary statistics for Douglas fir (units – MPa).

| | 105 x 105 mm | 45 x 105 mm |
|--------------------------|-----------------|----------------|
| Count | 932 | 913 |
| Average | 61.11 | 66.46 |
| Minimum | 15.05 | 17.18 |
| Maximum | 102.54 | 114.75 |
| Std. Deviation | 16.37 | 18.95 |
| COV | 26.78% | 28.52% |
| MOR _{0.05} | 33.57 | 32.93 |
| MOR _{0.05, NTL} | 32.82 | 32.37 |

Table 5. E_{true} summary statistics for Douglas fir (units – GPa).

| | 105 x 105 mm | 45 x 105 mm |
|--------------------------|-----------------|----------------|
| Count | 932 | 909 |
| Average | 14.57 | 16.11 |
| Minimum | 8.17 | 6.47 |
| Maximum | 26.64 | 26.50 |
| Std. Deviation | 2.62 | 3.13 |
| COV | 17.98% | 19.43% |
| MOE _{0.05, NTL} | 10.42 | 10.80 |
| $E_{true, mean, 0.95}$ | 14.40 | 15.90 |

Cumulative distribution functions for the moisture content adjusted MOR and E_L are given in Figures 2 and 3 by size for Hem-Fir (N).

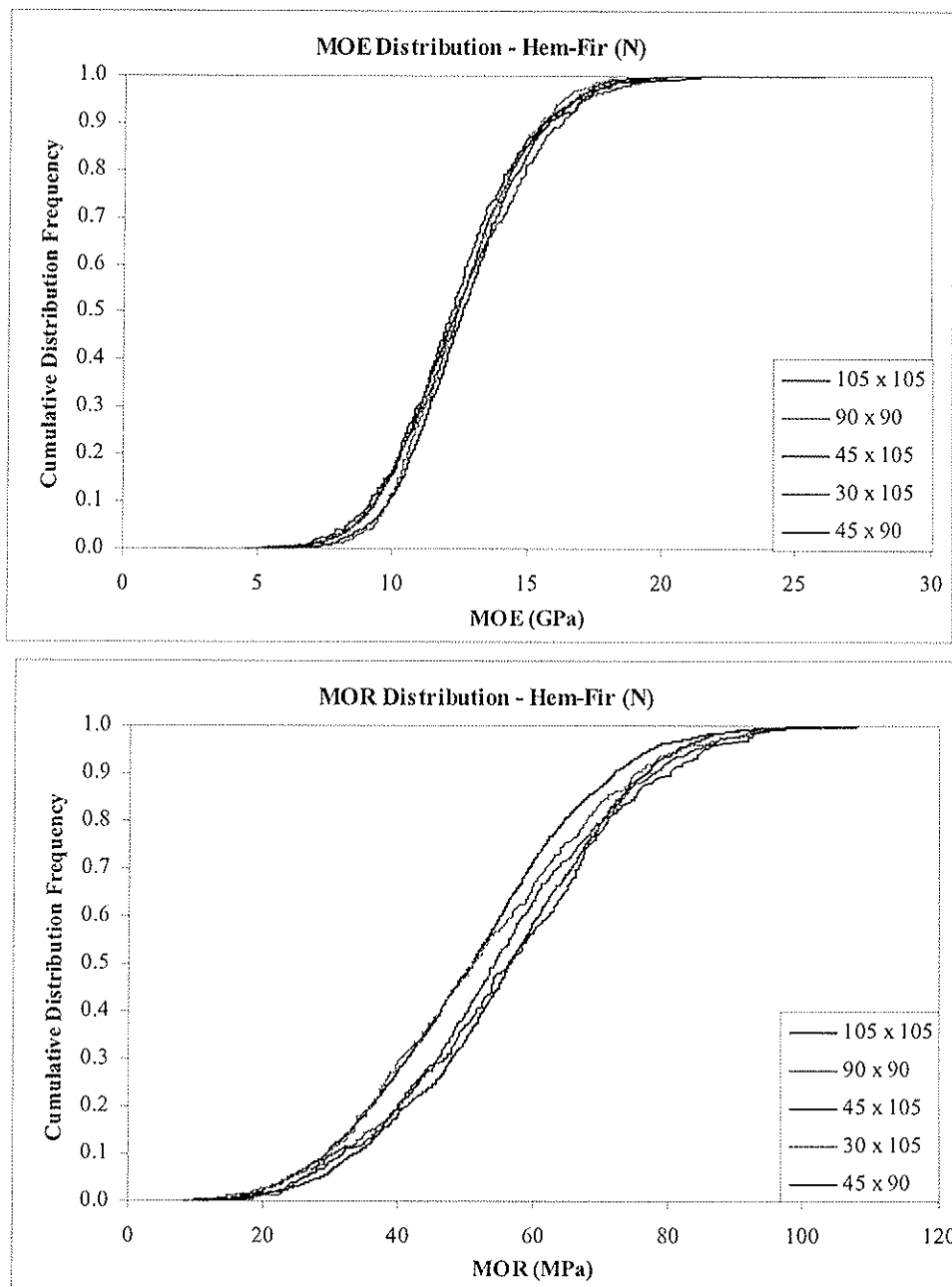


Figure 2. MOR CDF's for Hem-Fir (N) JPS 1 grade

Figure 3. E_{true} CDF's for Hem-Fir (N) JPS 1 grade

Figures 4 and 5 shown the relations between the MOR and MOE CDF's for 105 x 105 mm and 45 x 105 mm Hem-Fir (N) and Douglas fir (N),

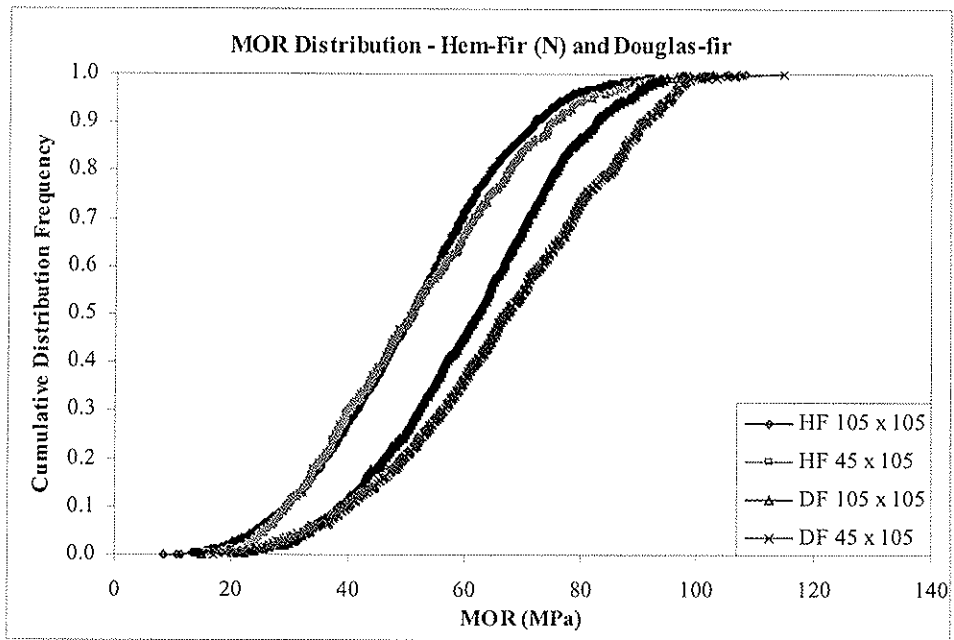


Figure 4. MOR CDF's for H-F (N) and Douglas fir JPS 1 grade

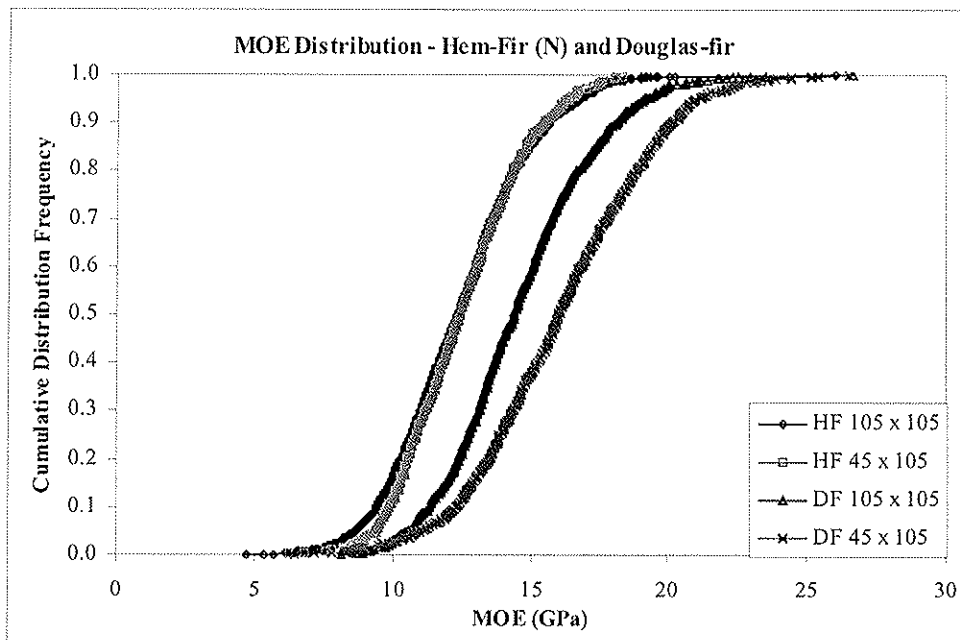


Figure 4. MOE CDF's for H-F (N) and Douglas fir (N) JPS 1 grade

6.2 Summary Statistics for JAS 143 Grades

Summary statistics derived from the in-grade tests of Hem-Fir (N) and Canadian Douglas fir (N) graded to the JAS 143 Structural Softwood Lumber grading rule are provided for MOE and MOR by size in Appendix I and II. The sample size weighted properties are also provided for both the Douglas fir (N) and Hem fir (N) samples.

6.3 Characteristic Properties for the Japanese Building Standard Law

6.3.1 CFLA Grade

The sample size weighted $E_{\text{true, mean, 0.95}}$ and $MOR_{0.05, \text{NTL}}$ were calculated in accordance with procedures prescribed in the Japanese building regulations and **JPS 1**. The test cell characteristic property data and sample sizes are given in Tables 2 and 3. The unrounded characteristic properties for Hem-Fir (N) graded to the **CFLA JPS 1** grading rule are:

$$\begin{aligned} E_{\text{true, mean, 0.95}} &= 12.37 \text{ GPa} \\ MOR_{0.05, \text{NTL}} &= 25.00 \text{ MPa} \end{aligned}$$

Following Japanese practices, the rounded characteristic bending properties and modulus of elasticity are as follows¹².

$$\begin{aligned} E_{\text{true, mean, 0.95}} &= 12.6 \text{ GPa} \\ MOR_{0.05, \text{NTL}} &= 25.2 \text{ MPa} \end{aligned}$$

The Japanese Building Standard Law specifies the compression material strength and tension material strength properties for ungraded Hemlock as follows:

$$\begin{aligned} UCS &= 19.2 \text{ MPa} \\ UTS &= 14.7 \text{ MPa} \end{aligned}$$

6.3.2 JAS 143 Grades

Test results for the individual sizes are shown in Appendix I and II. Estimated material strength properties derived for Hem-Fir (N) and Douglas fir (N) based on the in-grade test results obtained in this study are shown in Tables 6 and 7. The estimated material strength properties are compared with the material strength properties currently published for JAS 143 grades.

In all cases the estimated MOR material strength properties based on the in-grade test results (Table 6) meet or exceed the material strength values currently published for JAS 143 graded lumber.

¹² MLIT rounding rule adopted for converting old BSL allowable stresses to material strengths for ungraded lumber was to round to the nearest larger integer multiple of 0.3.

Similarly the mean MOE values (Table 7) significantly exceed the MOE values that are currently being considered for Hemlock and Douglas fir by the Architectural Institute of Japan.

Table 6 Material strength values for JAS 143 grades (MPa)

| Grade | Hem-Fir (N) In-Grade | JAS 143 Hemlock | Douglas fir(N) In-grade | JAS 143 Douglas-fir |
|--------|-------------------------|--------------------|----------------------------|------------------------|
| JAS A1 | 38.98 | 26.4 | 41.49 | 34.2 |
| JAS A2 | 27.84 | 26.4 | 32.74 | 22.8 |
| JAS A3 | 21.60 | 21.6 | 25.77 | 17.4 |
| JAS B1 | 33.68 | 21.0 | 35.57 | 27.0 |
| JAS B2 | 26.47 | 21.0 | 30.43 | 18.0 |
| JAS B3 | 22.45 | 17.4 | 26.80 | 13.8 |

Table 7. MOE for JAS 143 grades¹³, Hem-Fir (N) and Douglas fir (N) (GPa)

| Grade | Hem-Fir (N) In-Grade | JAS 143 Hemlock | Douglas fir(N) In-grade | JAS 143 Douglas-fir |
|----------------------|-------------------------|--------------------|----------------------------|------------------------|
| JAS A1 | 12.50 | | 16.42 | |
| JAS A2 | 12.91 | | 15.48 | |
| JAS A3 | 12.11 | | 14.10 | |
| JAS B1 | 13.15 | | 15.90 | |
| JAS B2 | 12.55 | | 14.91 | |
| JAS B3 | 11.89 | | 14.24 | |
| Sample Size Weighted | 12.6 | 9.4 | 15.3 | 12 |

6.2 Specified Strengths for the Canadian Building Code

The characteristics properties and specified strengths used in the Canadian code for Engineering Design In Wood (CSA O86) were calculated according to the "Standard Practice Relating Specified Strengths of Structural Members to Characteristic Structural Properties"(4).

The reliability normalization factor for bending members B, is calculated as follows:

$$B = 1.58 - 2.18 V/100$$

where B the reliability normalization factor, and
V the lower tail coefficient of variation (%)¹⁴

The characteristic property for a data cell is given by:

$$R_n = B R_{0.05}$$

¹³ Draft under review by the Architectural Institute of Japan

¹⁴ The coefficient of variation calculated based on the lower 15 percent of the test data.

where R_n the nominal or characteristic strength
 $R_{0.05}$ data cell fifth percentile

The lower tail coefficients of variation, test cell 5th percentiles, reliability normalization factors and corresponding nominal bending strengths are summarized given in Table 4 for the sizes of Hem-Fir (N) presented in this report.

Table 4. Nominal Strength Properties for Hem-Fir (N)

| Size | N | COV (Lower Tail, %) | $R_{0.05}$ MPa | B | R_n |
|-----------|------|------------------------|-------------------|-------|-------|
| 105 x 105 | 1903 | 26.0 | 24.20 | 1.012 | 24.5 |
| 90 x 90 | 357 | 19.5 | 26.03 | 1.155 | 30.1 |
| 45 x 105 | 1209 | 28.4 | 28.62 | 0.961 | 27.5 |
| 30 x 105 | 568 | 32.6 | 23.84 | 0.868 | 20.7 |
| 45 x 90 | 360 | 29.1 | 26.14 | 0.946 | 24.7 |

The sample size weighted average R_n was calculated for strength for Hem-Fir (N) products graded to the **CFLA JPS 1** grading rule and tested at an 18 to 1 span to depth ratio is given by:

$$R_{n, 18} = 25.31 \text{ MPa.}$$

The specified strength is computed by adjusting the nominal bending strength to the “Standard Term” duration of load as follows:

$$R_s = 0.8 R_n = 20.25 \text{ MPa.}$$

The specified strengths for tension and compression can be computed based on known relations to bending strength when tension and compression test data are not available. Therefore the specified tension and compression strengths were calculated from bending strength according to ASTM D 1990 procedures.

The specified tension strength is taken to be 45% of the specified bending strength¹⁵:

$$R_{s, \text{tension}} = 0.45 \times 25.31 \times 0.8 = 9.1 \text{ MPa}$$

The specified compression strength is given by:

$$R_{s, \text{compression}} = 0.67 \times 25.31 \times 0.8 = 13.6 \text{ MPa.}$$

The modulus of elasticity test data (E_L) was adjusted to a 21:1 span to depth ratio and a uniformly distributed load according to procedures of ASTM D 2915. The sample size weighted mean modulus of elasticity for use in the Canadian Building Code is given by:

¹⁵ ASTM D 1990 Establishing Allowable Properties for Visually Graded Dimension Lumber from In-grade Tests of Full-Size Specimens. ASTM (1999)

$$E_{\text{mean, UDL, 21}} = 12.18 \text{ GPa}$$

7.0 CONCLUSIONS

This paper presents the results of the first comprehensive evaluation of the bending strength and modulus of elasticity of Hem-Fir (N) and Douglas Fir (N) lumber produced in the sizes and grades used in Japanese post and beam housing systems. This data base provides the technical information on Canadian Hem-Fir and Douglas fir needed to improve the engineering design of post and beam housing in Japan by providing accurate information on material strength properties of Canadian species imported into Japan

Bending strength and modulus of elasticity data have been developed for lumber graded to CFLA JPS-1 "*Structural lumber – Visual grading – Requirements for E 120 Canadian coastal Hem-Fir (N) lumber products used in traditional Japanese post and Beam building construction*". The material strength properties for Hem-Fir (N) graded to the CFLA JPS 1 grade meet or exceed the material strength values current assigned to ungraded Hemlock in the Japanese building standards. Material strength properties for Douglas fir (N) graded to the CFLA JPS 1 rule substantially exceeds the material strength value assigned for ungraded "Douglas fir" by the MLIT.

Similarly, the material strength properties estimated for Hem-Fir (N) and Douglas fir (N) substantially exceed the values consistently exceed the values currently published for the JAS 143 graded lumber. Therefore there appears to be an opportunity to explore the acceptance of new higher design properties for Hem-Fir (N) and Douglas- fir (N) traditional post and beam lumber products in Japan.

The specified bending strengths have been calculated for use in the National Building Code of Canada (NBCC) following the procedures established by the Code for Engineering Design on Wood CSA O86. The specified tension and compression strengths have been calculated in accordance with procedures ASTM D 1990.

LITERATURE CITED

1. American Society of Testing and Materials ASTM. (1999). Annual Book of ASTM Standards. Section 4 Construction Volume 04.10 Wood. West Conshohocken, PA. U.S.A.
2. Barrett J. D. and Lau, W. (1994). Canadian Lumber Properties. Edited by E.D. Jones Canadian Wood Council. Ottawa, Canada.
3. Iwasaki K.M. (1998). In-grade test sampling program for Canadian Hem-fir. Report prepared for the Council of Forest Industries of BC. Vancouver, Canada.
4. Anon. Standard Practice Relating Specified Strengths of Structural Members to Characteristics Structural Properties. CSA O86.
5. Circular Notice 132 "Evaluation of the material strength of lumber", issued by the Ministry of Construction, March 29, 1996.
6. Ministry of Agriculture, Forestry and Fisheries Notification No. 1627 of November 30, 1994. Japanese Agricultural Standard for Structural Softwood Lumber (JAS 143)

Appendix I: CDF's for Hem-Fir (N) JAS 143 Grades

| | Grade | MOE _{true} (GPa) | MOE _{UDL, 21} (GPa) | N | MOR _{0.05} (MPa) | MOR _{NLT} (MPa) | N |
|---|--------|------------------------------|---------------------------------|------|------------------------------|-----------------------------|------|
| 105 x 105 | JAS A1 | 10.92 | 10.62 | 352 | 38.55 | 38.06 | 352 |
| | JAS A2 | 12.85 | 12.50 | 443 | 28.28 | 26.38 | 445 |
| | JAS A3 | 12.18 | 11.85 | 552 | 24.10 | 21.07 | 552 |
| | JAS B1 | 13.16 | 12.80 | 593 | 34.34 | 33.71 | 593 |
| | JAS B2 | 12.36 | 12.02 | 512 | 24.90 | 25.11 | 514 |
| | JAS B3 | 11.84 | 11.52 | 582 | 21.99 | 21.62 | 582 |
| 90 x 90 | JAS A1 | 13.83 | 13.46 | 40 | 37.87 | 33.60 | 40 |
| | JAS A2 | 13.21 | 12.85 | 73 | 33.23 | 28.39 | 73 |
| | JAS A3 | 12.26 | 11.93 | 121 | 26.07 | 18.97 | 121 |
| | JAS B1 | 13.38 | 13.02 | 84 | 33.94 | 32.50 | 84 |
| | JAS B2 | 12.42 | 12.08 | 101 | 27.33 | 25.76 | 101 |
| | JAS B3 | 12.16 | 11.83 | 144 | 24.63 | 20.11 | 144 |
| 45 x 105 | JAS A1 | 13.58 | 13.21 | 358 | 41.71 | 41.51 | 358 |
| | JAS A2 | 13.05 | 12.69 | 356 | 32.44 | 31.10 | 356 |
| | JAS A3 | 12.13 | 11.80 | 330 | 28.89 | 25.47 | 330 |
| | JAS B1 | 13.34 | 12.97 | 504 | 37.26 | 36.45 | 504 |
| | JAS B2 | 12.68 | 12.33 | 327 | 28.87 | 31.10 | 327 |
| | JAS B3 | 11.92 | 11.59 | 341 | 24.61 | 25.53 | 341 |
| 30 x 105 | JAS A1 | 13.52 | 13.16 | 77 | 40.20 | 37.14 | 77 |
| | JAS A2 | 12.75 | 12.41 | 360 | 29.54 | 23.73 | 360 |
| | JAS A3 | 12.06 | 11.73 | 71 | 17.55 | 16.86 | 71 |
| | JAS B1 | 12.79 | 12.44 | 249 | 29.68 | 27.96 | 249 |
| | JAS B2 | 12.74 | 12.40 | 243 | 25.76 | 24.18 | 243 |
| | JAS B3 | 11.84 | 11.52 | 53 | 14.08 | 21.64 | 53 |
| 45 x 90 | JAS A1 | 13.23 | 12.87 | 56 | 36.22 | 34.94 | 56 |
| | JAS A2 | 12.99 | 12.64 | 110 | 38.52 | 36.32 | 110 |
| | JAS A3 | 11.60 | 11.28 | 118 | 23.69 | 18.82 | 118 |
| | JAS B1 | 12.76 | 12.41 | 86 | 37.12 | 34.94 | 86 |
| | JAS B2 | 12.74 | 12.39 | 124 | 30.20 | 25.01 | 124 |
| | JAS B3 | 11.73 | 11.41 | 113 | 23.88 | 20.77 | 113 |
| Combined (Sampled Size Weighted) | JAS A1 | 12.50 | 12.16 | 883 | 39.80 | 38.98 | 883 |
| | JAS A2 | 12.91 | 12.56 | 1342 | 30.83 | 27.84 | 1344 |
| | JAS A3 | 12.11 | 11.78 | 1192 | 24.37 | 21.60 | 1192 |
| | JAS B1 | 13.15 | 12.79 | 1516 | 34.68 | 33.68 | 1516 |
| | JAS B2 | 12.55 | 12.21 | 1307 | 26.74 | 26.47 | 1309 |
| | JAS B3 | 11.89 | 11.57 | 1233 | 22.86 | 22.45 | 1233 |

Appendix II: CDF's for Douglas fir JAS 143 Grades

| | Grade | MOE _{trise} (GPa) | MOE _{UDL, 21} (GPa) | N | MOR _{0.05} (MPa) | MOR _{NL} (MPa) | N |
|---|--------|-------------------------------|---------------------------------|------|------------------------------|----------------------------|------|
| 105 x 105 | JAS A1 | 15.54 | 15.12 | 309 | 46.94 | 39.57 | 309 |
| | JAS A2 | 14.81 | 14.41 | 311 | 36.96 | 32.18 | 311 |
| | JAS A3 | 13.36 | 13.00 | 312 | 29.06 | 25.08 | 312 |
| | JAS B1 | 15.20 | 14.79 | 546 | 38.95 | 37.72 | 546 |
| | JAS B2 | 14.05 | 13.67 | 218 | 32.17 | 31.10 | 218 |
| | JAS B3 | 13.18 | 12.83 | 168 | 27.06 | 23.97 | 168 |
| 45 x 105 | JAS A1 | 17.32 | 16.85 | 301 | 44.57 | 43.45 | 304 |
| | JAS A2 | 16.17 | 15.73 | 304 | 36.72 | 33.31 | 304 |
| | JAS A3 | 14.85 | 14.45 | 303 | 27.37 | 26.48 | 304 |
| | JAS B1 | 16.68 | 16.23 | 495 | 33.62 | 33.22 | 498 |
| | JAS B2 | 15.90 | 15.47 | 188 | 33.06 | 29.66 | 188 |
| | JAS B3 | 15.03 | 14.62 | 225 | 29.20 | 28.89 | 226 |
| Combined (Sampled Size Weighted) | JAS A1 | 16.42 | 15.97 | 610 | 45.76 | 41.49 | 613 |
| | JAS A2 | 15.48 | 15.06 | 615 | 36.84 | 32.74 | 615 |
| | JAS A3 | 14.10 | 13.71 | 615 | 28.23 | 25.77 | 616 |
| | JAS B1 | 15.90 | 15.47 | 1041 | 36.40 | 35.57 | 1044 |
| | JAS B2 | 14.91 | 14.50 | 406 | 32.58 | 30.43 | 406 |
| | JAS B3 | 14.24 | 13.85 | 393 | 28.29 | 26.80 | 394 |

INTERNATIONAL COUNCIL FOR RESEARCH AND INNOVATION
IN BUILDING AND CONSTRUCTION

WORKING COMMISSION W18 - TIMBER STRUCTURES

SPLITTING STRENGTH OF BEAMS LOADED BY CONNECTIONS
PERPENDICULAR TO GRAIN, MODEL VALIDATION

A J M Leijten

Delft University of Technology

A J M Jorissen

SHR-Timber Research and ABT Consulting Engineers

THE NETHERLANDS

Presented by: A Jorissen

- H J Larsen discussed and presented results of a model (34-7-16) and compared the model predictions with the current paper. He concluded that the simpler model of (34-7-16) was shown to be more robust because after calibration it could predict the results from different experiments with reasonable accuracy. The G and G_c terms in the model have physical meaning unlike the blackbox approach followed by the current paper. A copy of his discussion was made available to the participants.
- M Ballerini asked about the $\sqrt{GG_c}$ values in Table 1 which were approximately 18.5 and 12 for Type A and B respectively.
- A Jorissen answered that in the proposal lower bound was chosen if the designer were not able to distinguish between the connector types. He stated that the $\sqrt{GG_c}$ values were not purely a black box approach although some inconsistencies were observed in some cases.
- V Enjily asked whether the referred UK tests were done at BRE. If so they were metal plated members and would not be appropriate for the bolted connections.
- A Jorissen confirmed that the UK tests were done at BRE and clarified point 3 in the conclusion. He stated that some of the data could still be used for model verification if the connection zone was not too large compared to the test span.
- J P Biger asked whether the conclusions could be extended to big beams. He stated that dictating rules would be important to guide designers to design connection with tensile stress perpendicular to grain.
- H J Larsen commented that if splitting mode governed then the approach should be valid for big beams. He stated that design rules for multiple fasteners would be more important as the current rules for connector spacing in the parallel and perpendicular to grain direction do not work.
- H J Blass stated that one should not encourage engineer to design connections that would be subjected to such failure mode. Zipper type failures should be avoided.
- I Smith commented that the validations were conducted with tests where stable crack growth occurred. Validations with test situations with unstable crack growth would be more convincing.

SPLITTING STRENGTH OF BEAMS LOADED BY CONNECTIONS PERPENDICULAR TO GRAIN, MODEL VALIDATION

A.J.M. Leijten,
Delft University of Technology, the Netherlands
A.J.M. Jorissen,
SHR- Timber Research and ABT Consulting Engineers, the Netherlands

Introduction

At the previous CIB/W18 meeting a fracture mechanical model was presented for splitting of beams when loaded by connections perpendicular to grain Van der Put et al.[1]. The model was validated using experimental test results of Ehlbeck et al. [3]. To react on the comments received at the CIB/W18 meeting and to increase the validity of the model, experimental results of other sources are evaluated.

Summary

Splitting of beams loaded perpendicular to the grain by connections is explained by fracture mechanics, Van der Put et al. [1][2]. The model is validated and calibrated using tests on Spruce beams reported by Ehlbeck et al.[3], Ballerini [4], Reske et al. [5] and Reffolds et al. [6]. A key influence is the ratio between the strength of the connection and the splitting strength of the beam. The model is sufficiently accurate in representing the data irrespective of the type of fasteners. Finally, a design proposal for Eurocode 5 is given.

Splitting failure

This paper deals with the evaluation of test data using the model given in [1]. The splitting caused by connections has much resemblance with the splitting of notched beams, Figure 1. In both cases unstable crack growth which will mainly propagate in grain direction will cause failure.

Initially, the model derived in [2] was meant for notched beams. Afterwards the model was also proposed for connections. The starting point of the model is given in Figure 2 where a static scheme is given of the cracked state. Obviously, the schematisation is a simplification of reality.

As shown in [1] and [2] a model can be derived as given in Equation (1).

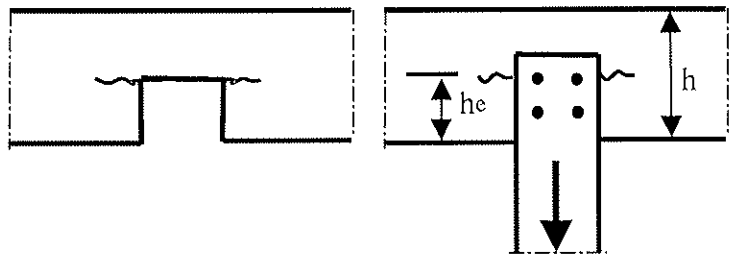


Figure 1 : Splitting of notched beams and joints.

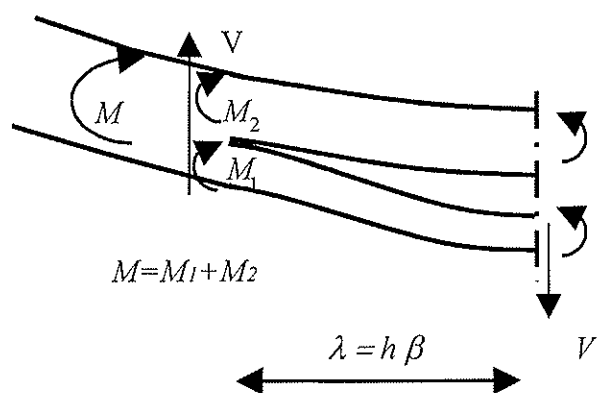


Figure 2: Static scheme of the splitted beam.

$$\frac{V_f}{b\sqrt{h}} = \sqrt{GG_c} \sqrt{\frac{\alpha}{0.6(1-\alpha)}} \sqrt{\frac{n}{n_{cr}}} \quad (1)$$

Where V_f is the critical shear force on either side of the crack, $\alpha = h_c/h$, see Figure 1, b member thickness and $\sqrt{GG_c}$ is the apparent fracture parameter. The last parameter $\sqrt{n/n_{cr}}$ takes into account the number of fasteners divided by the critical number. If $n < n_{cr}$ than $\sqrt{n/n_{cr}} = 1$, see [1]. In case of the span to depth ratio of the beam exceeds about 5, the governing failure mode will in many cases not be splitting caused by the connection but bending or shear of the loaded member itself. It was shown in [1] that the only unknown, the apparent fracture parameter $\sqrt{GG_c}$, could be determined by calibration.

Types of connections

Test results published by Ehlbeck et al., [3], Ballerini [4], Reske et al. [5] and Reffolds et al. [6] are evaluated. It will be shown that most tests support the model. Before going into detail, connections are divided in three groups, depending on the ratio between the splitting strength and connection strength.

- Type A – this connection is over-designed. The connection is much stronger than the splitting strength of the beam (ratio >1) An indication for this type is the relative low embedment stress at splitting. The load slip curve of this connection type is nearly linear up to failure.
- Type B – the load slip curve shows the onset of yielding. The embedment stresses are higher than for type A. In fact this type of connection is a transition between type A and C. A more clear definition is not needed.
- Type C – the connection is under-designed. The splitting strength of the beam connection is much higher than the connection strength (ratio <1). The connection shows high embedment stresses and/or yielding of the fasteners some combined with hardening. Fastener yielding (dowel types) is not always necessary. A plastic behaviour can also occur in the case of rigid (stocky) dowels where the embedment stresses have reached the maximum value resulting in plastic deformation of the dowel through the wood. The original circular holes of the dowels become very elongated. This Type of connection shows considerable plastic deformation. As a secondary failure mode splitting occurs.

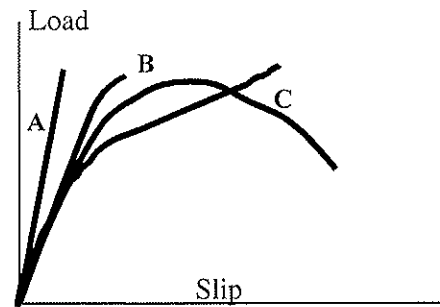


Figure 3: Connection Types

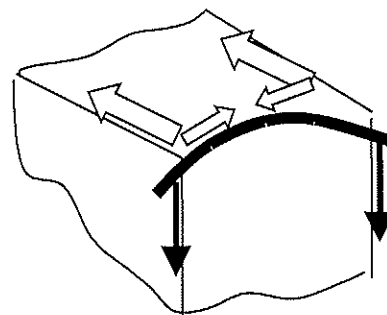


Figure 4: Crack growth when slender fasteners are used

Validation of the model

Connections with nails and dowels

The first data set evaluated deal with connections of dowel type fasteners. It is well known that the failure mode of dowel type fasteners depend, among other variables, of the

slenderness ratio. When a Type C connection has slender fasteners, plastic hinges will occur. At the shear plane of the connection the holes become elongated. When cracks exceed their critical length, these cracks becomes unstable; these cracks grow in the direction of the fastener axes as well as perpendicular to this direction, both in grain direction as shown in Figure 4. For rigid or stocky dowels the embedment stresses are more uniform along the fastener axes and cracks only propagate in one direction along the grain. Both cases can lead to the same or different values of the apparent fracture parameter depending on the ability to deform plastically.

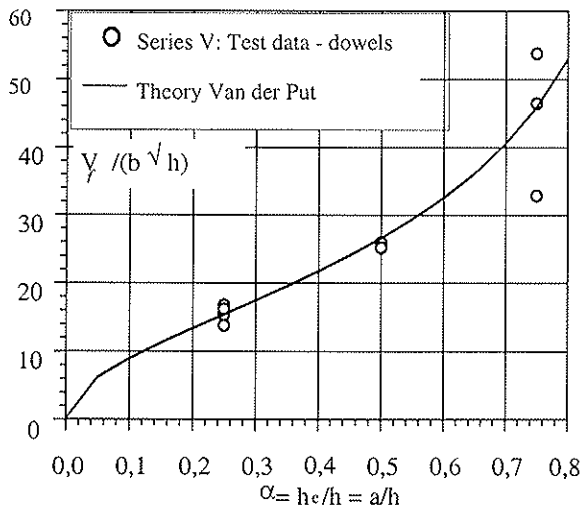


Figure 5: Model evaluation for dowels, eq.(1)

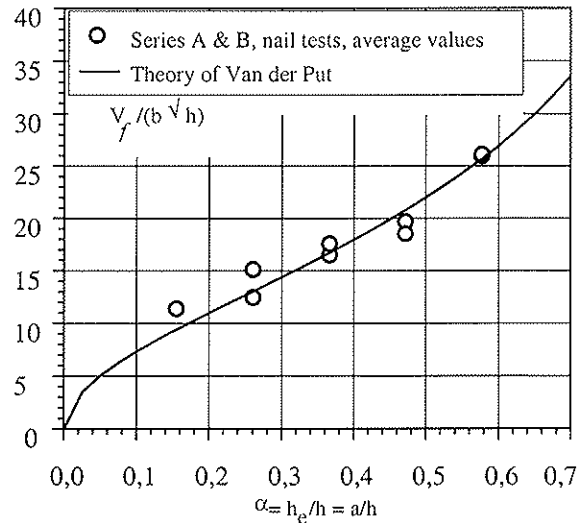


Figure 6: Model evaluation for nails, eq.(1)

In Figures 5 and 6 some of the data by Ehlbeck et al.[2] is presented together with the model calibration from [2]. Summarising the results of the evaluation and accounting for the type of connection it follows:

| | | | |
|--------|------------------------|--------|---|
| Type A | Series B2 to B4, | n = 9 | $\sqrt{GG_c} = 17,1 \text{ N/mm}^{1.5}$ |
| | Series V3, V11/12, V9, | n = 3 | $\sqrt{GG_c} = 20.5 \text{ N/mm}^{1.5}$ |
| Type C | Series remaining V, | n = 12 | $\sqrt{GG_c} = 12.6 \text{ N/mm}^{1.5}$ |
| | Series G, C and A, | n = 53 | $\sqrt{GG_c} = 12.0 \text{ N/mm}^{1.5}$ |

Connections with dowels

Tests reported by Ballerini [4] are now evaluated. The span of the beams was 3400 mm and the beam dimensions were 40x196 and 40x397 mm. The span to height ratio is considerable 17.3 for the smallest beams and 8.6 for the largest beams. The connection consisted of one and two 10 mm diameter dowels in line with the force direction. The dowels fitted in thick metal plates that didn't allow any rotation. These dowels can therefore be considered are rigid or stocky (slenderness ratio 1:4) The slip of the connections was measured. The author reports that except for the connections where the dowels were very close to the loaded edge the mode of failure was more or less plastic. In

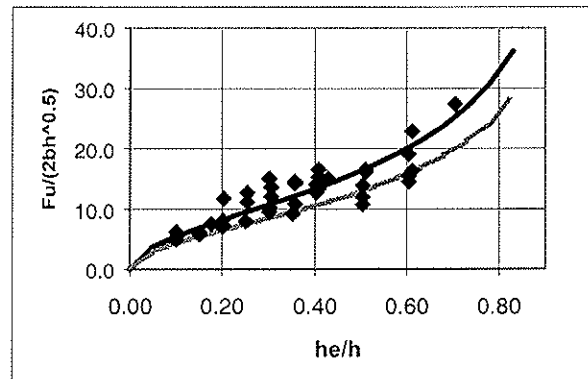


Figure 7: Test results by Ballerini [4]
Top line equation (1) with $\sqrt{GG_c} \approx 9.3 \text{ N/mm}^{1.5}$,
bottom line equation (2)

[4] two load-slip diagrams are presented which show plastic deformations of 4 and 12 mm. In Figure 7 the test results are presented together with the model calibration based on a mean apparent fracture parameter $\sqrt{GG_c} \approx 9.3 \text{ N/mm}^{1.5}$ substituted in Equation (1).

Connections with bolts and steelplates

Similar tests as reported by Ehlbeck et al. [2] were carried out and reported by Reske et al. [5]. In addition to the free supported single span beams loaded in the middle Reske added cantilevered beams loaded at the free end. The steelplates in the steel-timber-steel connection were 9.5 mm thick and fastened with 19 and 12.7 mm diameter bolts. The glued laminated beams were 130x190 mm and 80x190 mm. Except the maximum load also the slip of the connection was reported. The slip taken ranged from 0.9 mm for connections with 6 bolts to 18 mm for connections with one bolt. The model (1) was correlated to fit the test data. However, calibration is only valid if the boundary conditions of the test agree to some extent with the model assumptions. Tests by Reske et al. [5] do not comply with some basic starting points. One of them is the span to beam depth ratio. In case the span is small in relation to the beam depth, part of the load will be transferred directly to the supports. In Reske's tests the span to depth ratio was about 3 over 1. As the number of bolts increase and due to the spacing requirements the jointed area becomes larger, part of the load will be taken directly by the supports leaving a smaller portion to force splitting. This will result in higher value for the apparent fracture parameter as the analyses show. In Figure 8 the effect of the number of bolts on the apparent fracture parameter is given. There appears to be a critical number of bolts of about three beyond which number the apparent fracture parameter, doesn't increase; $\sqrt{GG_c} \approx 34 \text{ N/mm}^{1.5}$. It will therefore be assumed that the tests with more than one bolt belong to the category Type A and B connections. An indication for this is the maximum slip. The maximum slip for these test series ranged from 0.97 mm for connections with 6 bolts to 3,46 mm for joints with 2 bolts. For the tests with only one 19 mm diameter bolt the mean slip is 7.8 mm and the mean apparent fracture parameter $\sqrt{GG_c} = 14.1 \text{ N/mm}^{1.5}$. Within these Series with one bolt there actually was one Series of ten specimens with an average slip of 17.9 mm leading to an apparent fracture parameter as low as $\sqrt{GG_c} = 11.3 \text{ N/mm}^{1.5}$. It is assumed in contrast to the other tests with more than one bolt these belong to Type C.

Connections with punched metal plates

To test the general applicability of the model, test data by

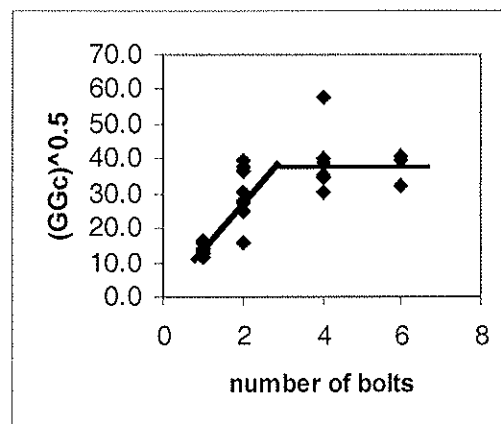


Figure 8: The number of bolts related to the fracture parameter; Reske [5]

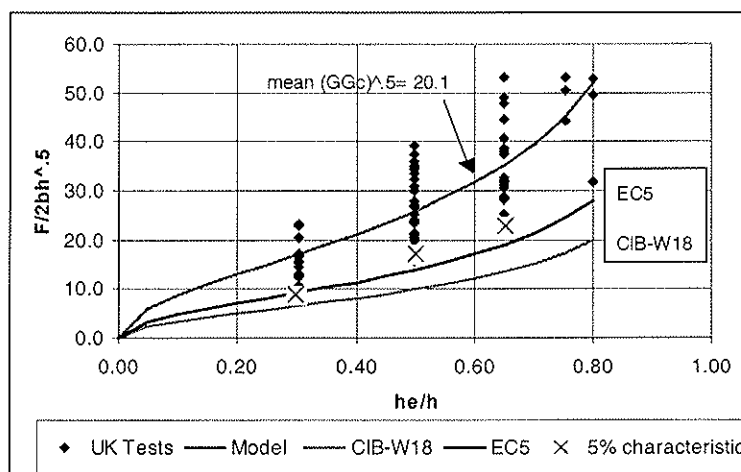


Figure 9: Tests with punched metal plates by Reffolds [6] Top line equation (1), $\sqrt{GG_c} \approx 20.1 \text{ N/mm}^{1.5}$

Reffolds et al. [6] are now being evaluated. The difference with the previous tests is the use of punched metal plate fasteners. As reported the free span of the single supported beams was 600 mm while the beams tested were of two dimensions 35x145 mm and 45x145 mm. It is reported that tests where anchorage failure or premature bending failure occurred were omitted. Anchorage failure indicates under-designed connections compared to the splitting strength, which exhibit considerable plastic deformation. It is therefore assumed that the slip of the remaining tests was very small and all belong to Type A connections. Because the researchers wanted to investigate the effect of punched metal plate length along the grain, a number of plate sizes were tested, ranging from 63, 120, 200 to 401 mm length. Obviously, tests with 200 or even 401 mm wide plates in a span of 600 mm deviate considerably from the model assumption of a point load. In fact using plates of 401 mm length the beam is strengthened over 2/3 of its span leaving the un-reinforced part loaded mainly in shear. It is the author's opinion that these results can better be omitted from the evaluation. For this reason the data as shown in Figure 9 is restricted up to tests with the 200 mm wide plates. For the data belonging to the same h_e/h value, a cross indicates the lower 5% value. The top line running through the mean of the data points is the model prediction based on the mean value of the fracture parameter of $\sqrt{GG_c} \approx 20.1 \text{ N/mm}^{1.5}$. The lower line is the proposed design guideline presented in [1]. The line in between is the proposal presently adopted in the draft Eurocode 5. It can be concluded that the model is able to follow the test data very well while the design proposals can be considered as safe.

Design proposal for Eurocode 5

The results of the data evaluated using equation (1) are summarised in Table 1:

Table 1: Summary of evaluation with Equation (1)

| Connection Type | Test Series | Number of tests | Mean $\sqrt{GG_c}$ [N/mm ^{1.5}] | Tests by |
|-----------------|-----------------------------|-----------------|---|-----------|
| A | B2 to B4 | 9 | 17.1 | Ehlbeck |
| | V3, V11/12, V9 | 4 | 20.5 | Ehlbeck |
| | all tests | 105 | 20.1 | Reffolds |
| | tests with more than 1 bolt | 170 | 34 | Reske |
| C | remaining V | 12 | 12.6 | Ehlbeck |
| | G, C and A | 53 | 12.0 | Ehlbeck |
| | All tests | 44 | 9.3 | Ballerini |
| | tests with 1 bolt | 60 | 11.3 | Reske |

From Table 1 it is clear that for Type A connections the apparent fracture parameter is higher than for Type C connections. Applying Equation (1) as the splitting criterion one would be able to make use of this higher value if the behaviour of the connection is known beforehand. The designer of a connection with dowel type fasteners who aims at a plastic behaviour of the connection before splitting might choose slender or rigid fasteners. The appropriate connection strength for either connection should be lower than the splitting strength. For both a plastic failure mode is than assured. For the slender fasteners by yielding of the steel (Johansen mode II and III) for the rigid fasteners by embedment failure (the fastener cuts through the timber); typical examples of Type C connections. If the connection strength is much higher than the splitting strength he might use values for $\sqrt{GG_c}$ associated with Type A connections. As there is a tendency in the design to stimulate connections with a plastic

behaviour the lower bound of the apparent fracture parameter $\sqrt{GG_c} = 12 \text{ N/mm}^{1.5}$ can be taken as starting point for a design code proposal. Substituted in Equation (1) it follows $\sqrt{(GG_c / 0.6)} = 15.5 \text{ N/mm}^{1.5}$. In order to obtain the characteristic value, the mean value of the apparent fracture parameter can be reduced to $15.5 * 2/3 = 10.3 \text{ N/mm}^{1.5} \approx 10 \text{ N/mm}^{1.5}$, which results in the design proposal given in (2).

$$V_u = b \sqrt{\frac{GG_c}{0.6}} \sqrt{\frac{h_e}{1 - \frac{h_e}{h}}} = 10b \sqrt{\frac{h_e}{1 - \frac{h_e}{h}}} \quad (2)$$

Where V_u is the maximum design shear force on either side of the connection, Figure 10. In Figure 9 a line representing the draft EC5 proposal is added. There the value of 10 in Equation (2) is changed to 14.

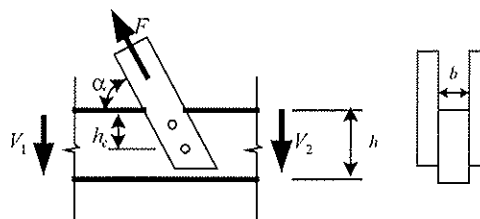


Figure 10: Eurocode 5

Conclusions

After having analysed and evaluated the test results of Ehlbeck et al.[3], Ballerini [4], Reske et al. [5], Reffolds et al. [6], it can be concluded that the model is able to describe the splitting capacity of the timber beams well and irrespective of the type of fastener. The arguments to make a distinction between Type A and C connections, as the apparent fracture parameter is lower for the latter, appears to be correct. For practical application, where the designer aims at equal splitting and connection strength, insuring plastic deformation behaviour of the connection, a safe lower value of the apparent fracture parameter of Type C connections need to be considered. Calibration of the model for Spruce, as shown above, leads to the adoption of a lower bound for $\sqrt{GG_c} \approx 12 \text{ N/mm}^{1.5}$. This finally results in a proposal for design standards as given in Equation (2).

References:

- [1] Van der Put, T.C.A.M., Leijten A.J.M, Proceedings of CIB/W18, paper 33-7-7, Delft, August 2000.
- [2] van de Put, T.C.A.M, 1990: Tension perpendicular to grain at notches and connections , CIB/W18/23-10-1, Lisboa, Portugal
- [3] Ehlbeck, J.,Görlacher,R.,Werner,H., Proceedings of CIB/W18, paper 22-7-2, August 1989.
- [4] Ballerini, M., A new set of experimental tests on beams loaded perpendicular-to-grain by dowel type joints, Proceedings of CIB/W18, paper 32-7-2, August 1999.
- [5] Reske, R.G., Mohammad, M., Quenville, J.H.P., Influence of joint configuration parameters on strength of perpendicular-to-grain bolted timber connections, Proceedings of the World Timber Engineering Conference, Whistler, BC, Canada, July 31 – August 3, 2000.
- [6] Reffold, A., Reynolds, T.N., Choo, B.S., An investigation into the tension strength of nail plate timber joints loaded perpendicular to the grain, Journal of the Institute of Wood Science, Vol. 15, No.1, 1999.

INTERNATIONAL COUNCIL FOR RESEARCH AND INNOVATION
IN BUILDING AND CONSTRUCTION

WORKING COMMISSION W18 - TIMBER STRUCTURES

NUMERICAL LEFM ANALYSES FOR THE EVALUATION OF FAILURE LOADS
OF BEAMS LOADED PERPENDICULAR-TO-GRAIN
BY SINGLE-DOWEL CONNECTIONS

M Ballerini

R Bezzi

University of Trento, Department of Mechanics & Structural Engineering

ITALY

Presented by: M Ballerini

- P Becker asked whether one or more than one connectors were used.
- M Ballerini answered only one connector was modelled because wanted to focus on a_r . He stated that connection geometry would also have an impact.
- L Daudeville asked whether crack length was measured.
- M Ballerini answered critical crack length would be difficult to measure and second mode was not important. He also agreed that other failure criteria could be tried later.
- I Smith stated that the experiments were displacement control and velocity of crack growth is very important in fracture. Load control would yield a different crack growth rate.
- M Ballerini agreed.

Numerical LEFM analyses for the evaluation of failure loads of beams loaded perpendicular-to-grain by single-dowel connections

Marco Ballerini, Roberto Bezzi

University of Trento, Department of Mechanics & Structural Engineering, Italy

Abstract: The paper presents the results of a numerical study performed to evaluate the splitting strength of beams loaded perpendicular-to-grain by single-dowel connections. The investigation, carried out in the framework of LEFM theory, has allowed the derivation of the stress intensity factors (SIF) of beams loaded at mid-span, for different crack lengths and for different distances of the dowel from the loaded edge of beams. The stress intensity factors are computed by means of the virtual crack closure integral method and by means of the displacement extrapolation technique. On the basis of the computed SIFs the splitting failure loads of the beams are derived through the classical Wu's fracture criterion. Finally, comparisons between the results of the two SIF computational approaches and between the numerical failure loads and the experimental ones are reported and discussed.

1 Introduction

The design of dowel-type connections that transfer perpendicular-to-grain forces to timber elements is actually performed with respect mainly to the strength of the connections and with little emphasis to the splitting resistance of the beams. In spite of this, it is well known that frequently it is the formation and the propagation of a crack along the grain of the timber elements that limits the resistance of the whole system.

The prediction of the splitting strength of beams loaded by dowel-type connections is a difficult task since it is affected by the influence of many parameters. The main ones are the distance of the furthest row of fasteners from the loaded edge of the timber elements (a_r) and the connection geometry, summarized in number, size and spacing (horizontal and vertical) of connectors. Although it is well recognised the fundamental contribution of a_r , its role is not completely understood due to above-mentioned not negligible influence of the connection geometry, which masks and makes difficult the analysis of the experimental data. This can be easily detected from the published experimental results on connections with multiple fasteners: [1]+[3], [5] and [6].

On the other side, the investigation of the a_r role by means of single-dowel connections is not easy to perform due to the limited embedding strength of timber perpendicular-to-grain. This can be noticed mainly for high values of a_r , and consequently higher splitting strengths of the beams, as outlined by the research of Ballerini [4].

For what concerns the theoretical prediction of the splitting strength of the beams, two different approaches are available. The first one, due to Ehlbeck, Görlacher and Werner [7], is based on the best fitting of the experimental results reported in [1]+[3] and on theoretical considerations related to the Weibull theory and to the distributions of the tensile stresses perpendicular-to-grain. The latter one, due to TACM van der Put [8-9], is

derived on the basis of an energetic approach in the framework of the Linear Elastic Fracture Mechanics. Although both approaches give reasonable predictions with respect to the experimental data, the structures of prediction formulae are completely different highlighting distinct evaluations of the contributions of the various parameters.

To overcome the above-mentioned limits of experimental investigations, numerical FE analyses can be profitably used to obtain the right contribution of the various parameters affecting the splitting strength of beams loaded by perpendicular-to-grain joints. Particularly, for the nature of the problem into consideration, numerical analyses in the framework of the Linear Elastic Fracture Mechanics (LEFM) seem the most effective ones. Different researchers have already applied LEFM for the study of the strength of timber elements when crack propagation occurs, by the others: Aicher *et al.* [10] for the investigation of the strength of timber beams with holes, and Yasumura *et al.* [11] for the analysis of perpendicular-to-grain bolted joints.

In the following the results of a numerical survey devoted to the evaluation of the influence of a_r on the strength of beams loaded by single-dowel connections are illustrated. Synthetically, the approach consists in the numerical derivation of the stress intensity factors at the crack tip for different crack lengths (L_c), different dowel positions (a_r) and two beam heights (200 and 400 mm); in an evaluation of the failure loads of the timber beams by means of the application of the Wu's fracture criterion with appropriate values of the fracture toughness (K_{Ic}); in a comparison and a discussion of the results with regard to the experimental failure loads of corresponding beams reported in [4].

2 Numerical evaluation of the stress intensity factors in mixed mode problems

The values of stress intensity factors are fundamental for the subsequent derivation of the splitting failure loads of timber beams. Due to this reason, two different methodologies for the SIF evaluation have been followed with the aim of testing the reliability of the different approaches.

The two methodologies are:

- the displacement extrapolation technique;
- the virtual crack closure integral method.

In the following the two methods are shortly illustrated.

2.1 The displacement extrapolation technique

The K_I and K_{II} values are computed starting from the displacements (horizontal and vertical) of the finite elements nearest to the crack tip by means of an extrapolation technique proposed by Chen *et al.* [12].

The method is based on the work of Sih, Paris & Irwin [13] who have shown that if the material is orthotropic with a crack aligned with one of the main directions, at the crack tip the stress and the displacement fields are similar to those of an isotropic material, and can be expressed as the sum of three independent modes.

On the basis of this result and by means of formulae for the stress and the deformations fields in a small region surrounding the crack tip, it is possible to derive the following relations between the horizontal and vertical displacements $u(r, \theta = 180^\circ)$ and $v(r, \theta = 180^\circ)$

along the propagation direction and the SIF in mode II and I:

$$u(r, \theta = 180^\circ) = \frac{K_{II}}{E_I} \sqrt{\frac{2r}{\pi}} \sqrt{2(\chi + \lambda)}$$

$$v(r, \theta = 180^\circ) = \frac{K_I}{E_I} \sqrt{\frac{2r}{\pi}} \lambda \sqrt{2(\chi + \lambda)}$$

In the previous formulae, valid only in plane stress, r is the distance from the crack tip, while λ and χ are:

$$\lambda = \sqrt{\frac{a_{22}}{a_{11}}} \quad , \quad \chi = \frac{2a_{12} + a_{66}}{2a_{11}} \quad \text{with:} \quad a_{ii} = \frac{1}{E_i} \quad , \quad a_{ij} = \frac{-\nu_{ji}}{E_j} .$$

Consequently, the SIF in mode II and I can be expressed as follows:

$$K_{II} = u(r, \theta = 180^\circ) E_I \sqrt{\frac{\pi}{2r}} \frac{1}{\sqrt{2(\chi + \lambda)}} = \Delta u(r, \theta = 180^\circ) \frac{\sqrt{\pi}}{4\sqrt{2r}} E_{II}^*$$

$$K_I = v(r, \theta = 180^\circ) E_I \sqrt{\frac{\pi}{2r}} \frac{1}{\lambda \sqrt{2(\chi + \lambda)}} = \Delta v(r, \theta = 180^\circ) \frac{\sqrt{\pi}}{4\sqrt{2r}} E_I^*$$

where

$$E_I^* = \frac{\sqrt{2} E_I}{\lambda \sqrt{(\lambda + \chi)}} \quad , \quad E_{II}^* = \frac{\sqrt{2} E_I}{\sqrt{(\lambda + \chi)}}$$

and

$$\Delta u = 2u \quad , \quad \Delta v = 2v .$$

From the above expressions is then possible to compute the values of K_I and K_{II} in the nodes (the furthest one - C, and the intermediate one - B) of the finite element nearest to the crack tip. With these SIFs it is then possible to derive the values of K_I and K_{II} at the crack tip by means of the following extrapolation formula proposed by Chen *et al.* in [12]:

$$K_i = \frac{4}{3} K_{iB} - \frac{1}{3} K_{iC} \quad \text{where} \quad i = I, II$$

It is well known that energetic approaches are better than displacement based approaches for the evaluation of the stress intensity factors at the crack tip. However, recent literature results (Guinea *et al.* [14]), have highlighted how it is possible to derive good estimations of SIFs with the displacement extrapolation technique if the FE mesh satisfies some requisites around the crack tip. They are essentially linked to the number and to the types of used elements more than to their size. Particularly, the use of triangular elements, derived by collapsed rectangular 8-nodes quarter point elements, is strongly suggested and a minimum number of 12 elements is recommended around the crack tip.

2.2 The virtual crack closure integral method

This method computes the values of the energy release rates in mode I and II, G_I and G_{II} , from the nodal forces and the displacements at the crack tip. The values of K_I and K_{II} are consequently derived making use, in the case of isotropic linear elastic materials in plane

stress, of the following relations:

$$K_I = \sqrt{E_I G_I}$$

$$K_{II} = \sqrt{E_{II} G_{II}}$$

For rectilinearly anisotropic linear elastic materials, the previous relations are still valid replacing E_I and E_{II} with E_I^* and E_{II}^* , whose expressions have been already defined in the previous chapter.

The method takes origin from the Irwin's virtual crack closure integral which represents the work necessary to close a crack tip from $a+\Delta$ to a .

In case of linear elastic materials, this work is equal to the strain energy release rate when Δ vanishes. Consequently, for unit thickness, the energy release rates for modes I and II can be expressed as:

$$G_I = \lim_{\Delta \rightarrow 0} \frac{W_I}{\Delta} = \lim_{\Delta \rightarrow 0} \frac{1}{2\Delta} \int_0^{\Delta} v(r, 180^\circ) \sigma_y(\Delta - r, 0^\circ) dr$$

$$G_{II} = \lim_{\Delta \rightarrow 0} \frac{W_{II}}{\Delta} = \lim_{\Delta \rightarrow 0} \frac{1}{2\Delta} \int_0^{\Delta} u(r, 180^\circ) \tau_{xy}(\Delta - r, 0^\circ) dr$$

where $v(r, 180^\circ)$ and $u(r, 180^\circ)$ are respectively the opening and slip displacements at a distance r behind the crack tip at $a+\Delta$, while $\sigma_y(\Delta - r, 0^\circ)$ and $\tau_{xy}(\Delta - r, 0^\circ)$ are respectively the normal and tangential stresses ahead of the crack tip along the crack propagation direction.

Rybicki and Kanninen [15] have applied this result to obtain a formula for the strain energy release rates of isotropic materials modelled with 4-noded non-singular quadrilateral elements.

Recently, Raju [16] has extended this approach to the case of non-singular and singular elements of higher order. The extension is valid also for triangular elements obtained by the collapse of rectangular quarter point elements.

In the case of mixed mode conditions and collapsed quarter point elements, type of elements frequently used in LEFM, the expressions of G_I and G_{II} are very complicated and the author itself suggests the use of the following approximate simpler formulae:

$$G_I = -\frac{1}{2\Delta} \left[F_{yi} \{ t_{11}(v_m - v_{m'}) + t_{12}(v_l - v_{l'}) \} + F_{yj} \{ t_{21}(v_m - v_{m'}) + t_{22}(v_l - v_{l'}) \} \right]$$

$$G_{II} = -\frac{1}{2\Delta} \left[F_{xi} \{ t_{11}(u_m - u_{m'}) + t_{12}(u_l - u_{l'}) \} + F_{xj} \{ t_{21}(u_m - u_{m'}) + t_{22}(u_l - u_{l'}) \} \right]$$

In the previous formulae F_{xi} , F_{yi} , F_{xj} and F_{yj} are the nodal forces (along crack propagation direction – x, and perpendicular to it – y) of the element ahead the crack tip in the node at the tip (i) and in the one at the quarter edge length (j). The terms u_m , v_m , u_l and v_l are the slip (u) and opening (v) displacements of the elements behind the tip in the furthest node from the crack tip (m) and in the one at the quarter edge length (l). The apex indicates nodes which belong to the element behind and down under the crack tip.

Finally, the t terms are constants with the following values:

$$t_{11} = 6 - \frac{3\pi}{2} \quad , \quad t_{12} = 6\pi - 20 \quad , \quad t_{21} = \frac{1}{2} \quad , \quad t_{22} = 1$$

The reported formulae have been derived on the basic assumption that the mesh at the crack tip must be symmetric with respect to crack propagation direction and its perpendicular direction.

Raju [16] has shown the effectiveness of the formulae for mixed mode problems particularly when collapsed quarter point elements are used.

The previous formulae for G_I and G_{II} have been derived for isotropic materials. Taking into consideration the energetic approach for their derivation, they have been used for the derivation of the SIFs of orthotropic materials with the formulae reported at the beginning of this chapter.

3 The numerical models

The numerical models refer to the beams with single-dowel connections tested by Ballerini in [4]. The parametric study has considered two beams heights ($h = 200$ and 400 mm), eight dowel distances from the loaded edge of beams ($\alpha = a_r/h = 0.1 \div 0.8$), and twenty half-crack lengths ($\frac{1}{2} L_c = 20 \div 750$ mm). A total amount of 320 models have been realised for this study.

The general layout and the details of the mesh are summarised in figure 1. Due to the symmetry, only half specimen has been modelled.

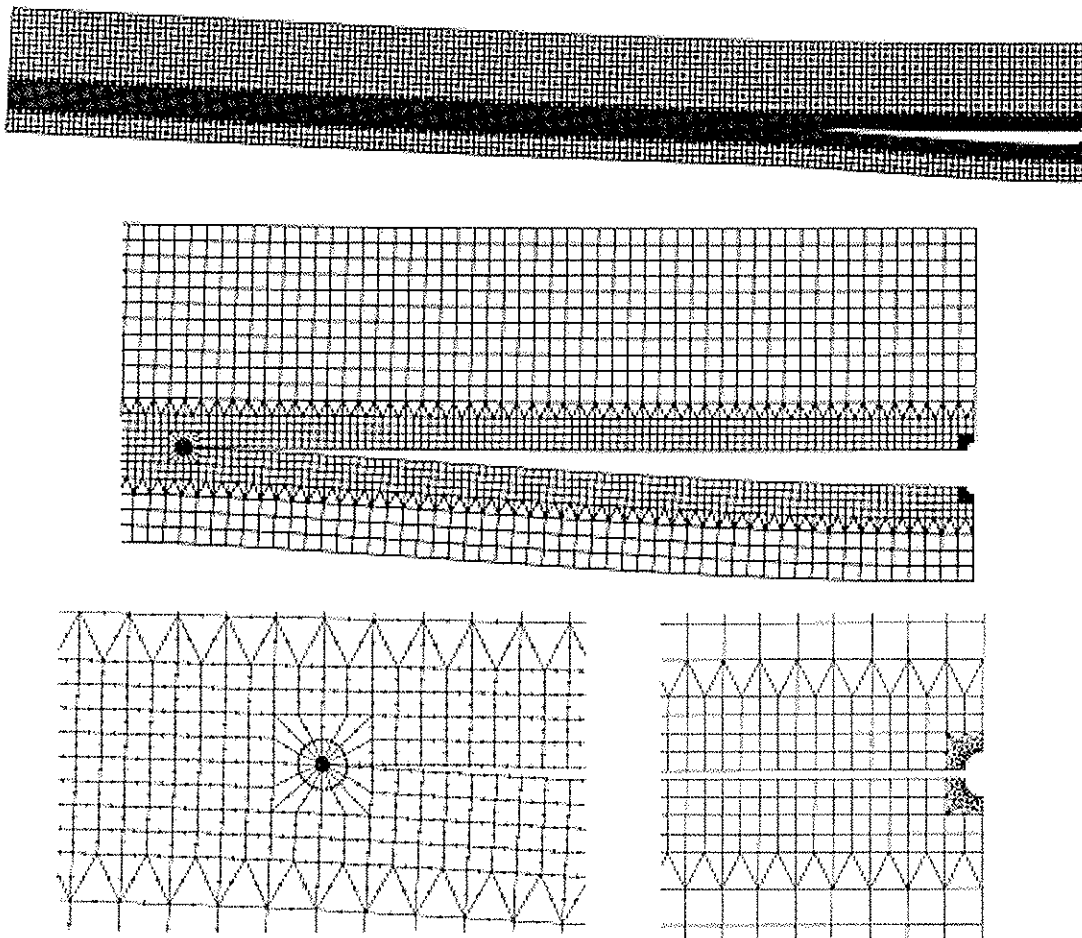


Figure 1 – The mesh and its details at the crack tip and at the connection (specimen S1-2030 with a crack length of 1000 mm).

The analyses have been performed with the commercial FE program ABAQUS-6.1 considering plane stress conditions. The elements used far away from the crack tip are rectangular CPS8 (continuous plane stress 8-nodes element) and triangular CPS6 elements of different sizes. The crack tip has been modelled with 16 collapsed CPS8 quarter point elements. At the connection, contact surfaces have been used between the beam elements and the dowel ones with a friction coefficient of 0.1. A 0.5 kN load (corresponding to 1 kN on the whole beam) has been applied at the dowel.

The wood has been considered linear elastic with the following orthotropic parameters:

$$\begin{aligned} E_x &= 11000 \text{ MPa} \\ E_y &= 890 \text{ MPa} \\ G_{xy} &= 760 \text{ MPa} \\ \nu_{xy} &= 0.37 \end{aligned}$$

4 The numerical results

The numerical results in term of stress intensity factors are reported in figures 2 and 3. Particularly, figure 2 shows the SIFs computed on the basis of the two approaches vs. half-crack length for the two beam sizes and for two very different α values (0.2 and 0.7). For what concern the two computational methodologies, from the graphs it is evident the good agreement between them. Nevertheless, the K_I values obtained from the displacement extrapolation technique show a noticeable scatter particularly evident in the smallest beams.

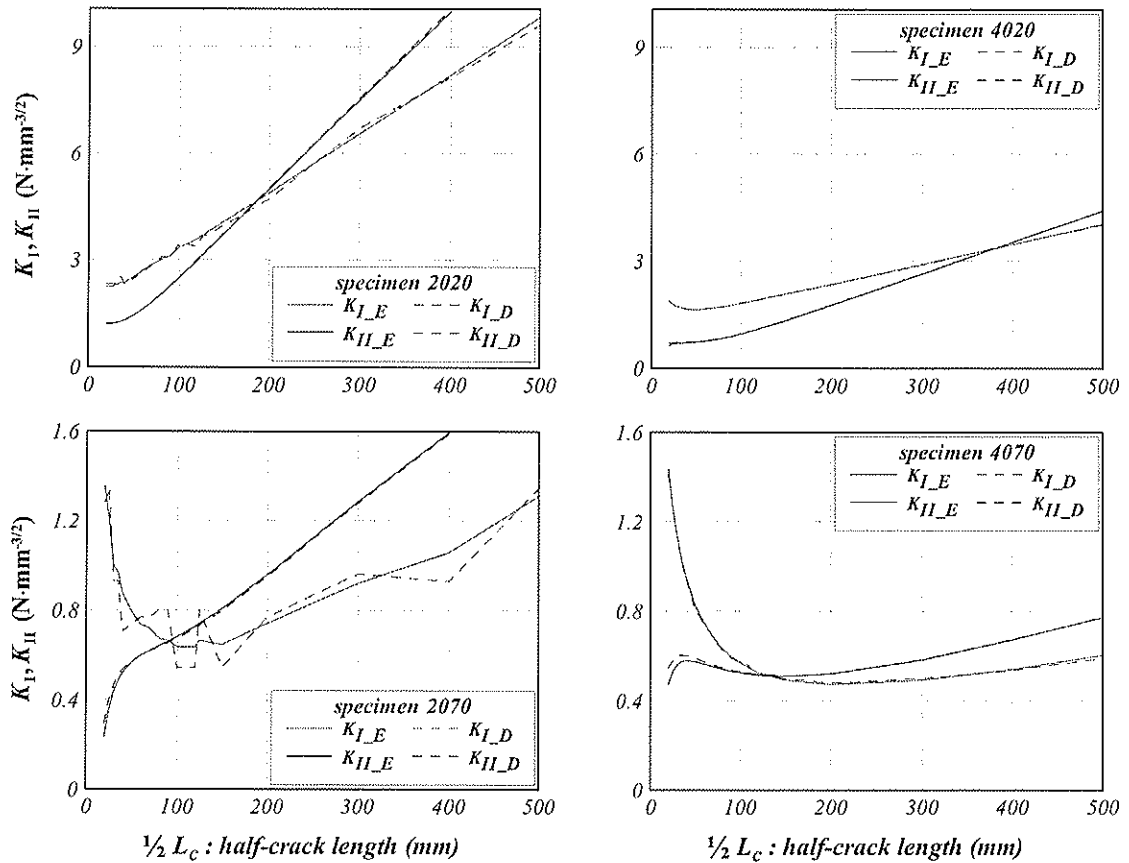


Figure 2 – K_I and K_{II} values obtained by the different approaches vs. half-crack length for some specimens.

The figure 3 reports the SIFs derived by means of the crack closure integral approach for all the numerical models.

From the graphs, it is evident that K_I and K_{II} values decrease significantly when the parameter α or the height of beams increase. However, if the attention is focused on the influence of the parameter a_r , it is possible to notice how specimens characterised by the same distance of the dowel from the loaded edge of the beams have similar SIF values.

Analysing the data with respect to the crack length, the curves representing the K_I values show a minimum that moves toward higher values of L_c when α increases. The mentioned minimum seems to be not present in the curve characterized by an α value of 0.1 and a beam height of 200 mm. This is probably due to the fact that the minimum of this curve is very close to the minimum numerical half-crack length ($\frac{1}{2} L_c$) investigated, which is equal to 20 mm (due to the selected elements size at the crack tip and at the connection) as it is possible to detect from figure 1.

The observed trend of K_I curves is less evident for the K_{II} curves that show minimums only for specimens characterized by higher a_r values ($h = 400$ mm and $\alpha > 0.3 \div 0.4$).

For what concerns the mutual ratio between K_I and K_{II} , from the graphs of both figures it can be noticed the higher values of K_I with respect to K_{II} for small crack lengths. On the contrary, when crack length increases K_{II} grows faster with respect to K_I stressing out how mode II becomes more important. In spite of this, the failure of this specimens seems to be governed prevalently by mode I.

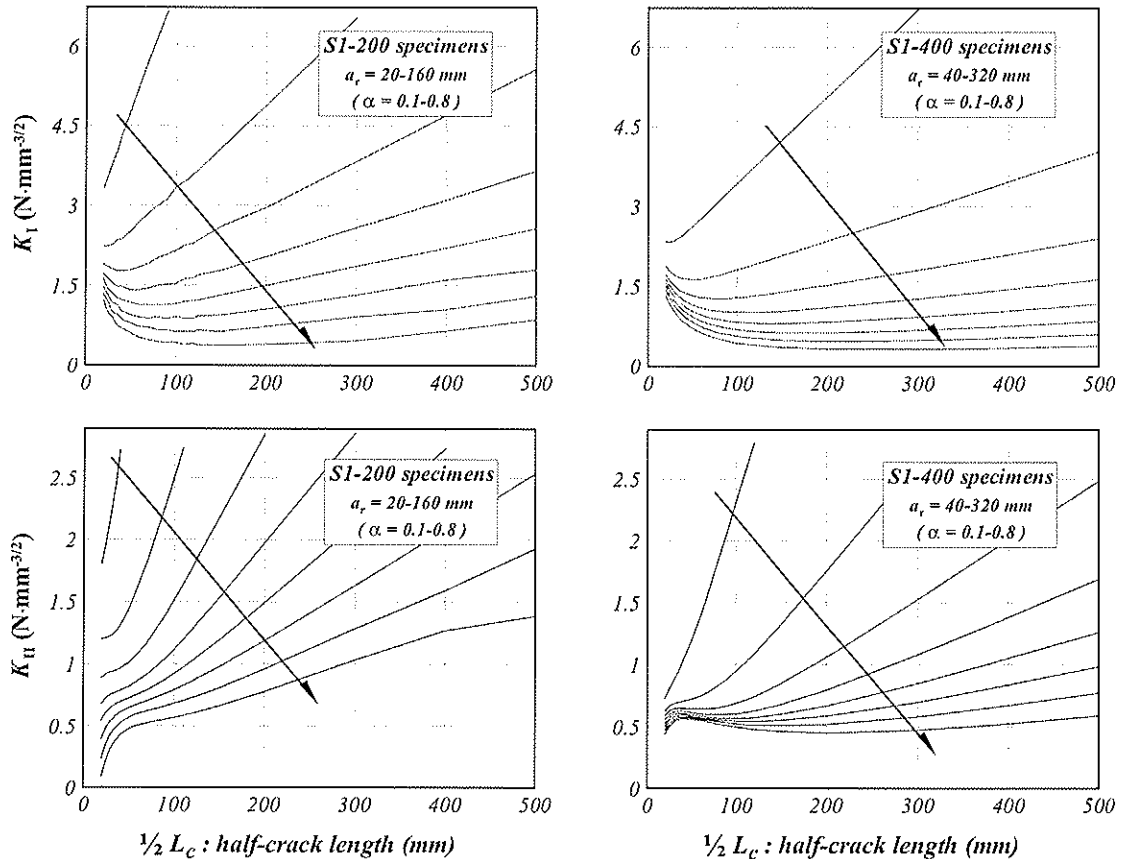


Figure 3 – K_I and K_{II} values of the energetic approach vs. half-crack length for specimens with different heights and different connection positions.

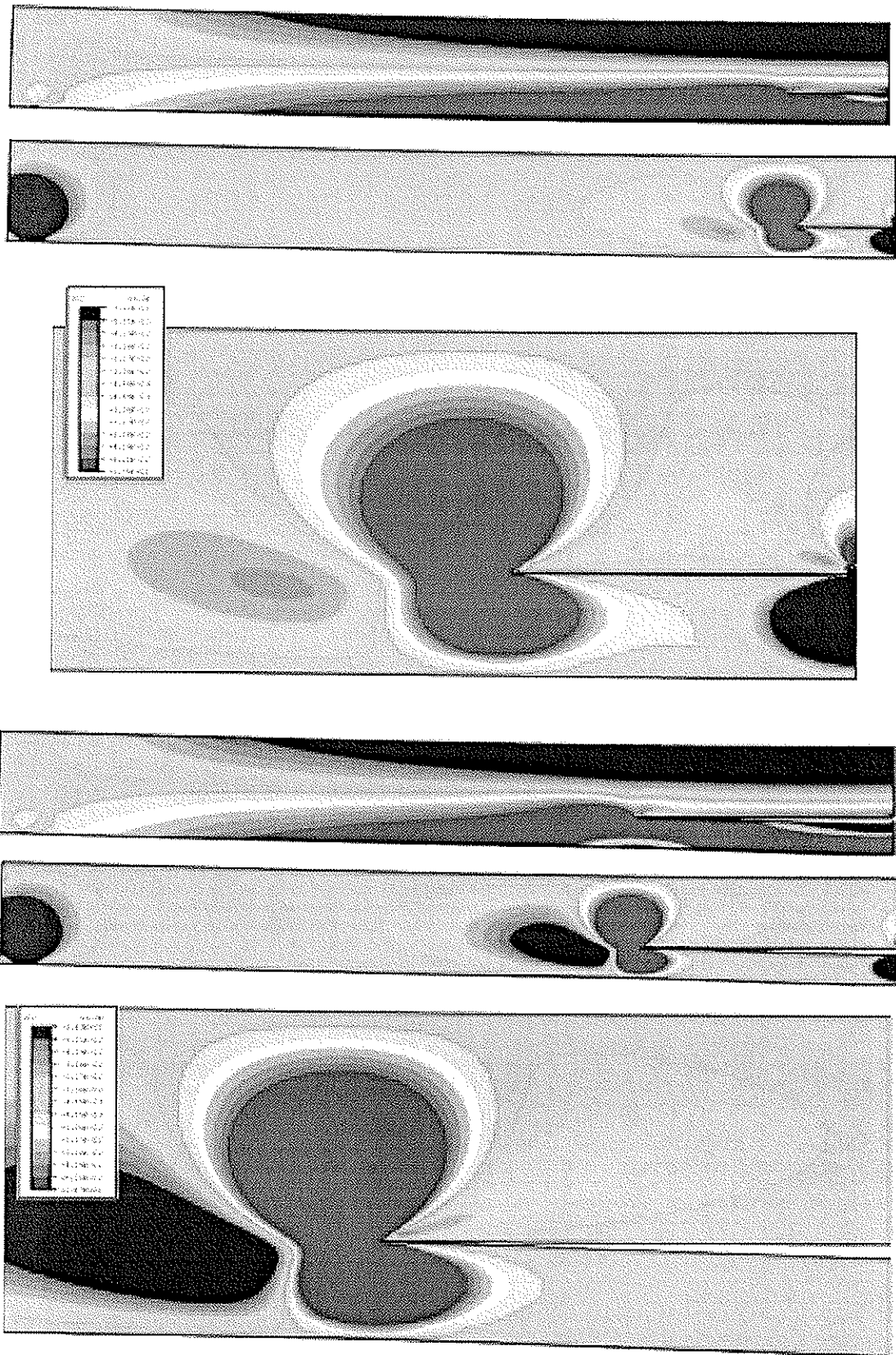


Figure 4 – σ_{11} and σ_{22} stress contours for specimen 2030 with half-crack lengths respectively of 200 and 500 mm.

Finally, figure 4 illustrates the σ_{11} and σ_{22} stress contours for the same specimen and two different crack lengths. Although the stress distribution analysis is not an aim of the research, from the pictures it is possible to detect the more severe situation of specimen with the higher crack length. For what concern σ_{22} , this is evident from the comparison of the detailed pictures at the crack tip, which show a zone of high tension perpendicular-to-grain ahead the crack tip immediately followed by a zone of high compressions which are both more severe for the beam with longer crack length.

With regards to the σ_{11} stress distribution, it is clear the more severe situation of the part of the beam beneath the crack belonging to the model with higher L_c . Indeed, it seems to experience a grater bending moment at mid-span and a sagging moment at the section of the crack tip.

5 Derivation of numerical failure loads and comparison with experimental data

The derivation of the failure load from the computed stress intensity factors has been carried out taking into consideration different crack propagation criteria [17]÷[20]. In this paper however, only the calculations based on the fracture criterion of Wu will be presented. The Wu fracture criterion is:

$$\frac{K_I}{K_{IC}} + \frac{K_{II}}{K_{IIC}}^2 = 1$$

Taking in mind the assumed linear elastic behaviour of the material, it can be written as follows:

$$\frac{k_I}{K_{IC}} F_u + \frac{k_{II}}{K_{IIC}} F_u^2 = 1$$

where the terms k_I and k_{II} are the stress intensity factors for a unit load already computed and reported in figure 3.

For what concerns the critical toughness, values ranging from 0.3 to 0.6 MPa·m^½ and from 1.5 to 2.3 MPa·m^½ for modes I and II (K_{IC} , K_{IIC}) respectively, have been found in literature for spruce with a mean density of 430 kg/m³ [10], [21]÷[23]; the ratio K_{IIC}/K_{IC} usually is between 3÷4.5.

In this work the ratio K_{IIC}/K_{IC} has been set equal to 3. For K_{IC} two values have been assumed: They have been obtained on the basis of two different best fittings of the experimental data: the first one on the whole data set, the second one on the data characterized by lower scattering ($\alpha \leq 0.5$) only.

The graphs reported in figure 5 show the failure loads of the numerical models as a function of the half-crack length. They have been derived with K_{IC} equal to 0.432 MPa·m^½. The figure shows very clearly how the failure loads increase with a_r and α . Indeed, considering the curves with equal α values, it is evident how an increase of a_r produces an increment of the failure load which is however less than linear. Moreover, considering the curves with equal a_r values, it can be noticed how the curves corresponding to the higher values of α show larger failure loads. Also in this case, the growing with α is less than linear.

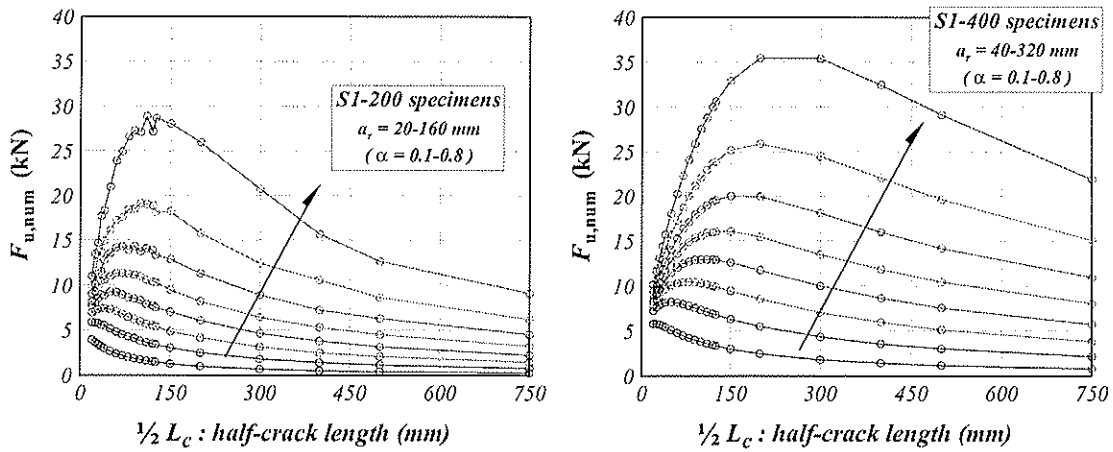


Figure 5 – Numerical failure loads based on Wu fracture criterion vs. crack length.

In figure 6 are reported the critical half-crack lengths as a function of a_r .

The critical crack length is defined as the length at which instable crack propagation occurs. In the graphs of figure 5, it corresponds to the value at which each curve shows the maximum.

As it is possible to see from figure 6, the critical half-crack length shows a linear relationship with a_r . This relationship is equal to $0.67 \cdot a_r$ for both beam heights.

The numerical failure loads at the critical crack lengths have been compared with the experimental failure loads reported in [4]. The comparison, for the K_{IC} value derived by the best fitting of the whole set of data, is reported in figure 7.

From the graph it is evident how the numerical curves are able to catch with a well agreement the general course of the experimental data. However, an underestimation of the failure loads of both S1-200 and S1-400 data with a_r less than 100÷140 mm is noticeable. This is due to the higher scatter of the experimental data for α greater than 0.5, consequence of the influence of the wood embedding strength.

Different numerical failure loads have been obtained considering for the best fitting only the more reliable data. The comparison is reported in figure 8.

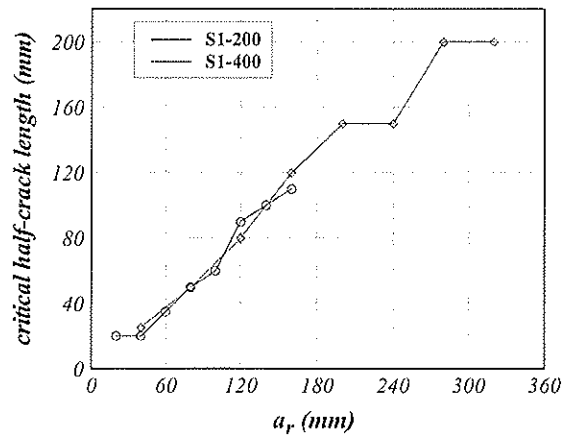


Figure 6 – Numerical critical half-crack length vs. a_r and α .

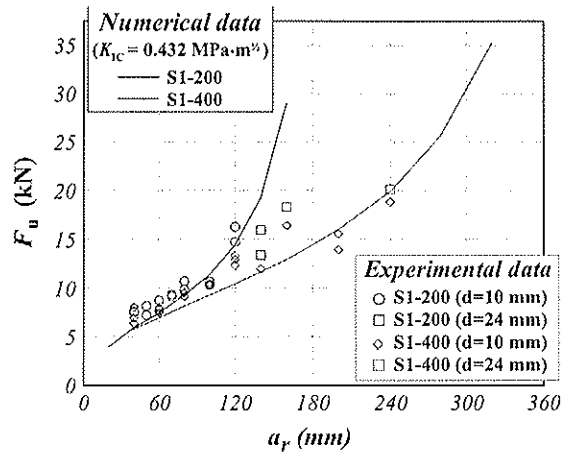


Figure 7 – Experimental and numerical failure loads vs. a_r .

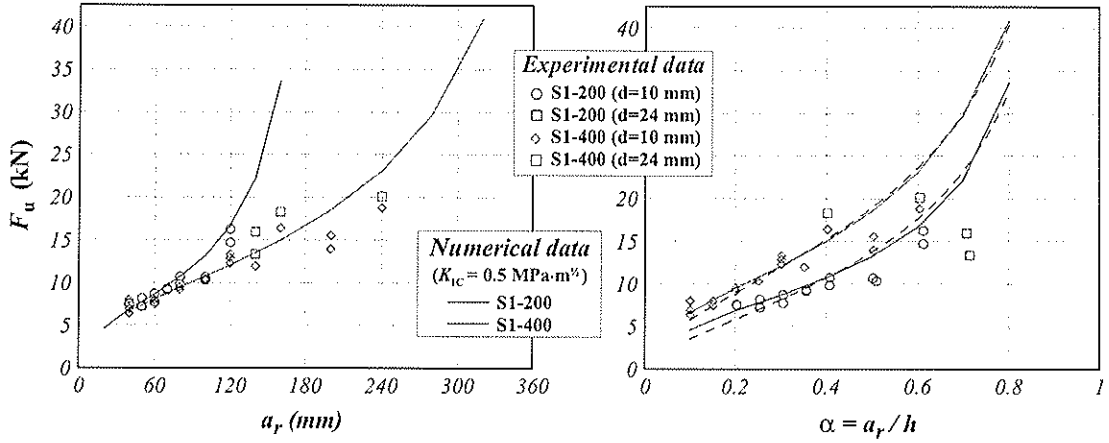


Figure 8 – Experimental and numerical failure loads vs. a_r and α .

From the graphs it is now evident the very good agreement with the experimental data characterized by α values less than 0.5.

In the right graph the dashed lines represent the following two best fitting of the numerical data:

- S1-200

$$F_u = 13.77(\alpha/(1-\alpha))^{0.62} \quad R^2 = 0.99$$
- S1-400

$$F_u = 19(\alpha/(1-\alpha))^{0.54} \quad R^2 = 0.99$$

These fitting are quite in accord with the theoretical formula proposed by Van der Put in [8].

Finally in figure 9, a further comparison between the experimental and the numerical failure loads is reported.

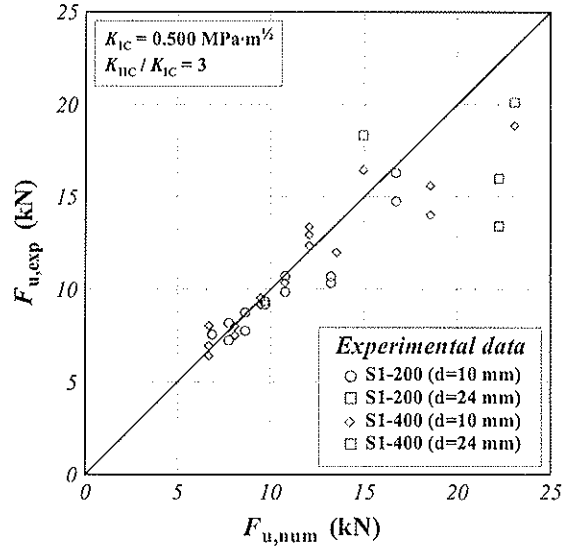


Figure 9 – Comparison $F_{u,exp}$ vs. $F_{u,num}$.

6 Conclusions

The presented parametric numerical work is characterized by a considerable amount of analyses performed to catch the influence of the fundamental parameters a_r and α on the strength of beams with single-dowel connections. Moreover, two different SIF computational approaches have been used for comparison and validation purposes.

The results of the research has allow to derive the following outcomes:

- the results given by the two SIF computational approaches are in good accord, however the ones of the crack closure integral method are more reliable;
- the analysis of the course of computed SIFs has allow to highlight the influence of parameters a_r and α ;
- the numerical failure loads derived on the basis of Wu fracture criterion are in a good agreement with the results of the experimental data;

- the course of these numerical failure loads has allow to highlight the influence of main parameters (a_r and α) on the splitting strength of beams also for those cases where testing is problematic because of the high embedding stresses;
- the fittings made on the course of the numerical failure loads show how the structure of the prediction formula of Van der Put is in a quite good agreement, the parameters of the power fitting however are different for the two beam sizes;
- lastly, a relationship between the numerical critical crack lengths and a_r has been derived.

Acknowledgements

The authors wish to thank the Ministry of the University and Scientific Research whose grants have allowed the development of the research.

References

- [1] **Möhler K., Lautenschläger R., 1978:** *Großflächige Queranschlüsse bei Brettschichtholz*. Forschungsbericht des Lehrstuhls für Ingenieurholzbau und Baukonstruktionen, Universität Karlsruhe.
- [2] **Möhler K., Siebert W., 1980:** *Ausbildung von Queranschlüssen bei angehängten Lasten an Brettschichtholzträger*. Forschungsbericht des Lehrstuhls für Ingenieurholzbau und Baukonstruktionen, Universität Karlsruhe.
- [3] **Ehlbeck J., Görlacher R., 1983:** *Tragverhalten von Queranschlüssen mittels Stahlblechformteilen, insbesondere Balkenschuhe, im Holzbau*. Forschungsbericht der Versuchsanstalt für Stahl, Holz und Steine, Abt. Ingenieurholzbau, Universität Karlsruhe.
- [4] **Ballerini M., 1999:** *A new set of experimental tests on beam loaded perpendicular-to-grain by dowel-type joints*. CIB-W18, paper 32-7-2, Graz, Austria.
- [5] **Reffold A., Reynolds T.N., Choo B.S., 1999:** *An investigation into the tension strength of nail plate timber joints loaded perpendicular to the grain*. Journal of the Institute of Wood Science, Vol. 15, No. 1.
- [6] **Reske R.G., Mohammad M., Quenville J.H.P., 2000:** *Influence of joint configuration parameters on strength of perpendicular-to-grain bolted timber connections*. Proceedings of 6th World Timber Engineering Conference, Whistler, B.C., Canada.
- [7] **Ehlbeck J., Görlacher R., Werner H., 1989:** *Determination of perpendicular-to-grain tensile stresses in joints with dowel-type fasteners: a draft proposal for design rules*. CIB-W18, paper 22-7-2, Berlin, German Democratic Republic.
- [8] **TACM van der Put, 1990:** *Tension perpendicular to the grain at notches and joints*. CIB-W18, paper 23-10-1, Lisbon, Portugal.
- [9] **TACM van der Put, 1992:** *Energy approach for fracture of joints loaded perpendicular to the grain*. COST 508, Workshop on fracture mechanics in wooden structures, Bordeaux, France.
- [10] **Aicher S., Schmidt J., Brunold S., 1995:** *Design of timber beams with holes by means of fracture mechanics*. CIB-W18, paper 28-19-4, Copenhagen, Denmark.
- [11] **Yasumura M., Daudeville L., 1999:** *Design and analysis of bolted timber joints under lateral force perpendicular-to-grain*. CIB-W18, paper 32-7-3, Graz, Austria.

- [12] **Chen L.S., Kuang J.H.**, 1993: *A displacement extrapolation method for two-dimensional mixed-mode crack problems*. Engineering Fracture Mechanics, Vol. 46, No. 5, pp. 735-741.
- [13] **Sih G.C., Paris P.C., Irwin G.R.**, 1965: *On cracks in rectilinearly anisotropic bodies*. International Journal of Fracture Mechanics, Vol. 1, pp. 189-203.
- [14] **Guinea G.V., Planas J., Elices M.**, 2000: *K_I evaluation by the displacement extrapolation technique*. Engineering Fracture Mechanics, Vol. 66, pp. 243-255.
- [15] **Rybicki E.F., Kanninen M.F.**, 1977: *A finite element calculation of stress –intensity factors by a modified crack closure integral*. Engineering Fracture Mechanics, Vol. 9, pp. 931-938.
- [16] **Raju I.S.**, 1987: *Calculation of strain-energy release rate with higher order and singular finite elements*. Engineering Fracture Mechanics, Vol. 28, No. 3, pp. 251-274.
- [17] **Wu E.M.**, 1967: *Application of fracture mechanics to anisotropic plates*. ASME Journal of Applied Mechanics, Series E, Vol. 34, No. 4, pp. 967-974.
- [18] **Jernkvist L.O.**, 2001: *Fracture of wood under mixed mode loading. I. Derivation of fracture criteria*. Engineering Fracture Mechanics, Vol. 68, pp. 549-563.
- [19] **Jernkvist L.O.**, 2001: *Fracture of wood under mixed mode loading. II. Experimental investigation of picea abies*. Engineering Fracture Mechanics, Vol. 68, pp. 565-576.
- [20] **Hunt D.G., Croager W.P.**, 1982: *Mode II fracture toughness of wood measured by a mixed mode test method*. Journal of Material Science Letters 1, 1, pp. 77-79.
- [21] **Valentin G.H., Boström L., Gustafsson P.J., Ranta-Maunus A., Gowda S.**, 1991: *Application of fracture mechanics to timber structures*. RILEM state-of-the-art-report.
- [22] **Tan D.M., Stanzl-Tschegg S.E., Tschegg E.K.**, 1995: *Models of wood fracture in mode I and mode II*. Holz als Roh-und Werkstoff, Vol. 53, No. 3, pp. 159-164.
- [23] **Larsen H.J., Gustafsson P.J.**, 1990: *The fracture energy of wood in tension perpendicular to the grain*. CIB-W18, paper 23-19-2, Lisbon, Portugal.

INTERNATIONAL COUNCIL FOR RESEARCH AND INNOVATION
IN BUILDING AND CONSTRUCTION

WORKING COMMISSION W18 - TIMBER STRUCTURES

DOWEL JOINTS LOADED PERPENDICULAR TO GRAIN

H J Larsen

P J Gustafsson

Division of Structural Mechanics, Lund University

SWEDEN

Presented by: H J Larsen

- A Jorissen asked why the F_{ult} values predicted for 1x1 and 2x1 cases from Equation 1 shown in Table 2 Page 8 were the same.
- H Larsen answered that although real material properties were used by the theory, it would not be able distinguish the different between the 1x1 and 2x1 cases.
- S Thelandersson asked whether it would be possible to use FEM to refine the approach.
- H J Larsen answered that it might be possible to calculate more accurately the work done. The idea was to try to obtain a simpler form and calibrate it.
- J Ehlbeck clarified the variables used in Equation 5 and the test results fitted the equation predictions.
- L Daudeville commented that the use of LEFM would be enough for this problem and questioned why such a large specimen (1 m) was used.
- H Larsen answered that there was a past RILEM report that considered the chosen specimen size in the experiment was a stable one.

Dowel joints loaded perpendicular to grain

H. J. LARSEN

BYG•DTU: Department of Structural Engineering, Technical University of Denmark
and

Division of Structural Mechanics, Lund University, Sweden

P. J. GUSTAFSSON

Division of Structural Mechanics, Lund University, Sweden

1 Abstract

The results of tests with doweled joints in LVL loaded perpendicular to grain are reported. Four joint configurations were tested: 1, 2 and 3 dowels in line and 2 dowels side by side. Further tension and splitting properties perpendicular to grain were determined. Some of the specimens were stored and tested in standard climate (23 °C/65 % RH) but most were stored in an open barn in Southern Sweden. The specimens were long-term loaded in the barn with target load levels relative to the short-term strength of 65% and 80%. Load was applied winter, spring, summer, autumn 2000 and winter 2001 to determine the influence of different climatic conditions. The main results are: The short-term strength is not influenced by the seasons. The short-term strength of the joints can be predicted by a simple equation based on linear fracture mechanics. The load-carrying capacity of two dowels side by side and a single dowel are identical. The effect of loading time for joints loaded perpendicular to grain is much more severe than for timber: the time to failure under a load level of 60 per cent is only 180 days. A safe load level is only about 30 percent of the short-term strength. The drying distortions of the specimens used to determine the tensile strength (40x70x280 mm) have a great influence on the results, the mean value is only 0.67 MPa, the minimum value only 0.25 MPa. Tests are still going on.

1 Introduction

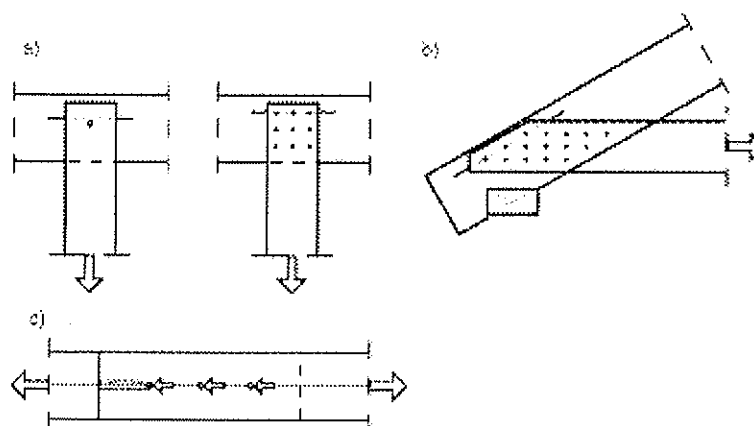


Figure 1. Examples of tension and shear failure of joints. a) and b) Load applied perpendicular (at an angle) to the grain. c) Splitting due to wedge action.

To design timber structures effectively it is necessary to have methods that can correctly predict the load-carrying capacity of overlap joints with dowel type fasteners for both ductile and brittle failures, taking into account the influence of loading and moisture history. Brittle failure may be caused by shear and tension perpendicular to grain (splitting), see figure 1. These phenomena are of course most common when the load has a component perpendicular to the grain, but can also be experienced for load parallel to the grain even with spacing etc. in accordance with normal design practice. As an example may be mentioned the case with several fasteners (especially non-slender fasteners) in line in the force direction.

For ductile failure many researchers have proved that the so-called European Yield Model – first proposed in [Johansen, 1949] – gives an excellent prediction of the load-carrying capacity. For brittle failures only rather crude theoretical expressions exist, and only for very special cases. Design is, therefore, often based on simple empirical or semi empirical rules, e.g. those of [Draft Eurocode 5, 2001], or the load-carrying capacity found from the yield model is reduced rather arbitrarily.

3 Strength analysis

In [Yasumura and Daudeville, 1998] bolted timber joints loaded perpendicular to the grain have been analysed using a finite element method to calculate the stresses around the boltholes and to follow the crack propagation. They conclude that a linear elastic finite element method is an appropriate tool.

Another method for strength analysis is non-linear fracture mechanics, see e.g. [Gustafsson, 1985] and [Broström, 1992]. A very simple expression for the load-carrying capacity for a dowel joint loaded perpendicular to the grain has been proposed by Gustafsson, see below. It is based on a fracture energy balance equation and a chosen displacement field – fulfilling the conditions of geometrical compatibility – for the deformation of the wood during crack propagation.

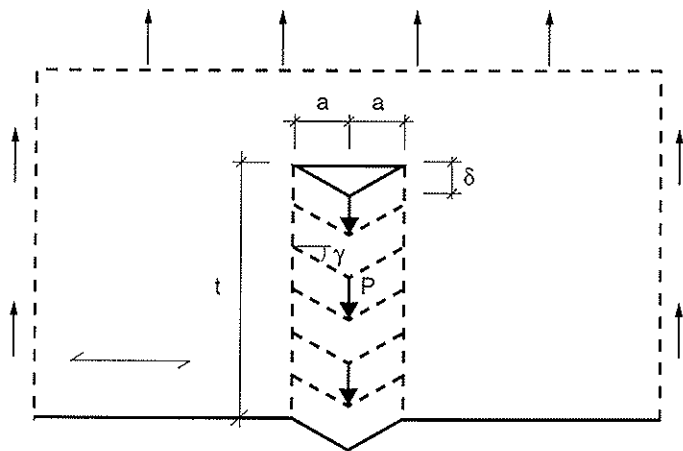


Figure 2. Specimen for which a simple strength equation is derived. The total load is P .

A load P is transferred through one or more dowels placed in line, see figure 2. The distance to the innermost dowel hole is l . The holes are formally regarded as pre-existing cracks located along the grain and having a length $2a$ equal to the diameter of the dowel hole. The strains in the load-carrying region are assumed to be dominated by shear strains, γ , and the assumed deformation pattern is as shown in the figure 2. The displacement of the load P is:

$$\delta = a\gamma = a\tau/G = 0.5aP/(lbG) \quad (1)$$

where b is the thickness of the specimen and G is the shear modulus of the wood, assumed to be linear elastic. The potential energy of the system, W , is the sum of the strain energy in the wood and the potential energy of the load. Since the material is regarded as linear elastic:

$$W = -P\delta/2 = -P^2a/(4lbG) \quad (2)$$

At the limit load where the crack starts to propagate, there is balance between the decrease in the potential energy, $-dW$, and the fracture energy required for propagation of the crack. The energy required for increasing the crack length by $2da$, i.e, increasing a by da , is $G_f b(2da)$, where G_f is the perpendicular to grain fracture energy of the wood. The energy balance:

$$-dW = 2G_f bda \quad (3)$$

together with equation (2) gives the failure load:

$$P_{ult} = 2b\sqrt{2lGG_f} \quad (4)$$

It is noteworthy that the predicted P_{ult} is not affected by the diameter of the hole or by the tensile strength of the wood. Instead, the decisive material parameters are shear stiffness and fracture energy, and the decisive geometrical parameter is the edge distance, l , for the innermost dowel. It must, however, be recalled that the derivation of equation (4) is based on a simplified assumption in terms of a constrained displacement field. Since the chosen displacement field fulfils the compatibility conditions, the stiffness is overestimated and the strain energy for a given load P accordingly underestimated. This means that equation (4) can generally be expected to overestimate the absolute value of the failure load. This can be expressed by means of an efficiency factor, η , for the displacement field, giving

$$P_{ult} = 2b\eta\sqrt{2lGG_f} \quad (5)$$

where $\eta \leq 1.0$.

4 Tests

4.1 Specimens

Six types of specimens were tested, see figure 3. The specimens were double symmetrical. The dowel specimens are named after the number of dowel lines and the number of dowels in the line. The distances $4d$ are the minimum values according to [Draft Eurocode 5, 2001]. DCB stands for Double Cantilevered Beam specimen. T denotes tension specimen.

The specimens were made from 40 mm thick Laminated Veneer Lumber (LVL) from Malarply, Sweden. LVL was chosen to get a uniform material and because of the size of the specimens. The dry density was about 450 kg/m^3 with a coefficient of variation of 2.4 per cent. The dowel diameter was 14 mm and the steel quality ensured that the stresses in the dowels were in the elastic range.

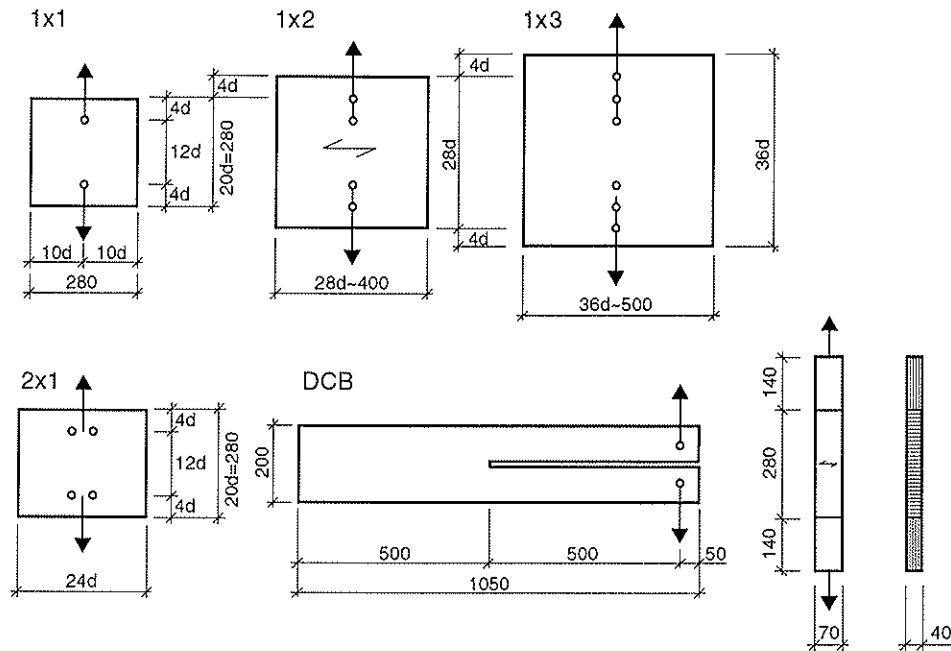


Figure 3. Test specimens. The T-tests were made by gluing LVL with the grain parallel to the axis to the ends of the test section that is loaded perpendicular to the grain.

4.2 Conditioning

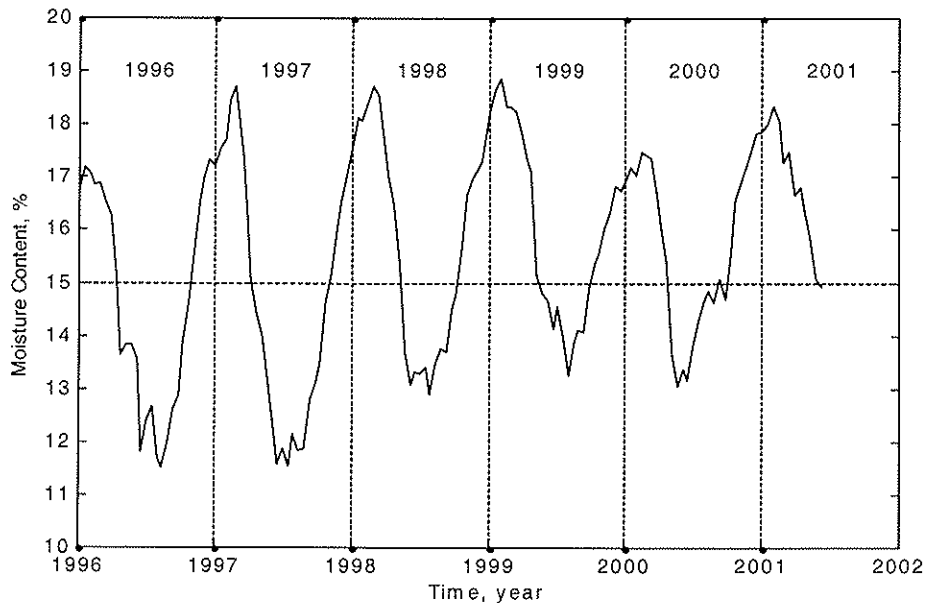


Figure 4. Moisture variations in wood in the test barn.

The specimens for the main series were stored in an open barn in Southern Sweden. To have a realistic moisture variation in the specimens the end grains were sealed with an asphalt tape. The

moisture content of the specimens was controlled. The air temperature and the relative humidity were recorded. The typical variation of the moisture content is shown in figure 4.

4.3 Test set-up

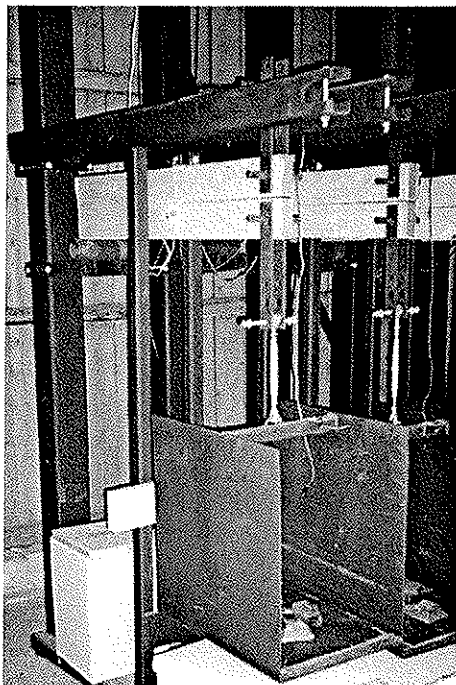


Figure 5. Testing of DCB specimens.

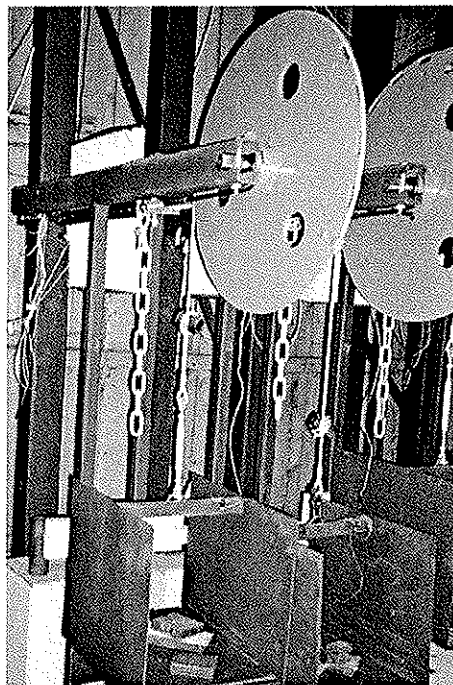


Figure 6. Testing of 1x3 specimens.

The load was transferred by two 4 mm thick steel gusset plates to a 16 mm dowel. The 17 mm hole for the dowel was predrilled in both plates as were the 15 mm holes for the 14 mm dowels in one of the steel plates. This plate was placed on top of the joint and used as lead when drilling 15 mm holes through the LVL and the bottom steel in one operation, thus ensuring a perfect fit. The specimens were loaded with dead load through chains and/or shackles.

The DCB (Double Cantilever Beam) specimens were loaded directly as shown in figure 5. The other five types were tested in rigs as shown in figure 6. A detailed description of the test rigs, which have been used for several EU-projects, can be found in [Gustafsson, 1988] and [Gustafsson, 1997].

4.4 Tests

The main element is the test packages described below tested February 2000 (winter), May 2000 (spring), August 2000 (summer), November 2000 (autumn) and February 2001 (winter).

A test package consists of the following:

- short-term ramp-loading (time to failure about 3 minutes) of 6 specimens of each type, 36 specimens in all
- long-term loading of 5 specimens of each type, 30 specimens in all, under constant load with a load level of about 80 per cent

- long-term load of 5 specimens of each type, 30 specimens in all, under constant loading with a load level of about 65 per cent
- Determination of the moisture profile for two specimens.

The load level is estimated from the short-term results from the same package, which may vary as a result of the varying moisture content (maximum in winter, minimum in summer, and with maximum variations in spring and autumn).

Further, the test programme consists of determination of the following properties after conditioning in standard climate (65 per cent relative moisture content and 23 °C):

- short-term ramp-loading of 10 specimens of each type, 60 specimens in all
- long-term loading of 5 specimens of types 1×1, T and DCB , 15 specimens in all, under constant load with a load level of about 80 per cent
- long-term loading of 5 specimens of types 1×1, T and DCB, 15 specimens in all, under constant load with a load level of about 65 per cent.
- determination of the compression strength and the embedding strength perpendicular and parallel to the grain for 20 specimens, 80 specimens in all.

The short-term strength was also determined for specimens 1×1, 1×2 and 1×3 after conditioning in 35, 65 and 85 per cent relative humidity and 23°C. Each series consisted of 18 specimens, 54 in all.

5 Test results

5.1 Moisture variations

The moisture variations in the wood were followed by weighing 40 mm thick samples. The samples were sealed along their edges. The result is shown in figure 7. The MC indicated by circles and straight lines were obtained by manual weighing every second week and the curve by continuous recording of the weight. The absolute value of the MC was obtained by drying a set of matched specimens. The initial MC December 23 1999 was 9.0 %.

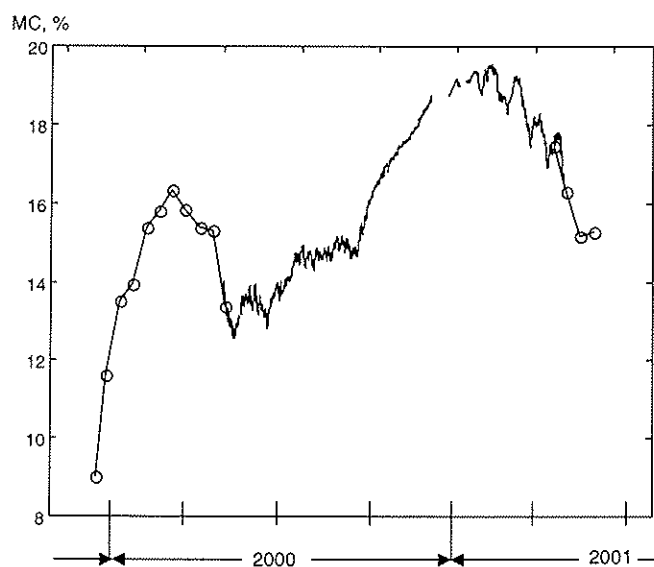


Figure 7. Moisture content

5.2 Short-term strength

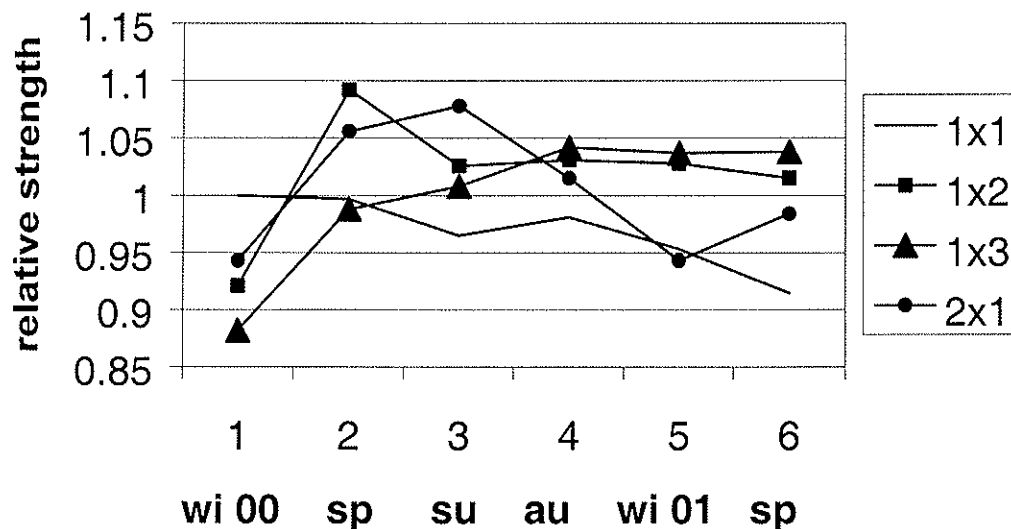


Figure 7. Strength variation over the year

The results from the short-term ramp loading are given in table 1 (at the end of the paper). The variation with the seasons is shown in figure 7.

There are no clear trends, except that the values for winter 2000 are slightly inferior. This may be the result of insufficient conditioning: the LVL was delivered in the beginning of December with a moisture content of about 9 per cent and was tested in the beginning of February after a period with a rapid moisture uptake. In the following all short-term values are treated as one population with properties as shown in table 2.

TABLE 2. Mean short-term strength values compared to the theoretical values according to (4). The coefficient of variation is given in (%). η is the efficiency factor, see (5).

| | | 1x1 | 1x2 | 1x3 | 2x1 | T | DCB |
|-------------------|----|---------------|----------------|----------------|---------------|----------------|----------------|
| $F_{ult, test}$ | kN | 7.43 (5 %) | 11.31 (6 %) | 14.52 (8 %) | 7.64 (7 %) | 1.86 (14 %) | 1.34 (13 %) |
| $F_{ult, theory}$ | kN | 11.97 | 16.93 | 20.73 | 11.97 | | |
| η | | 0.62 | 0.67 | 0.70 | 0.64 | | |

The theoretical failure load $F_{ult, theory}$ is calculated from (4) with the following values: $G_f = 0.40$ N/mm corresponding to the results from the DCB tests, see [Gustafsson and Larsen, 2001] and $G = 500$ MPa. On average the efficiency factor is estimated at $\eta = 0.66$.

The tensile strength found from the T specimens is 0.67 MPa, but with very great variations: the minimum value is 0.25 MPa, the maximum value 1.25 MPa. The specimens with low strength values were generally heavily distorted (curved perpendicular to the panel direction), probably due to release of prestresses from the production.

5.3 Long-term strength

In [Gustafsson and Larsen, 2001] the results of the duration of load testing are analysed for the different seasons. There is a clear influence of the fluctuations of the absolute moisture levels. The time effect is much higher for loading during summer and less pronounced for loading during winter.

In the following the general load duration effect is analysed. To estimate the load level the n test results for a specimen type (e.g. all 1x1) are ranked. It is assumed that the strength of the weakest specimen in a group (with 5 specimens) corresponds to the median of the $0.2n$ weakest specimens, i.e. to the strength of the specimen with rank $0.1n$ (interpolation). The following specimens are assumed to have the same strength as the specimens with rank $0.3n$, $0.5n$, $0.7n$ and $0.9n$. The strength level is calculated as the ratio between the strength and the mean value given in table 2 and it is assumed that the ranking according to time to failure corresponds to the ranking according to strength.

The time effect for the 4 joint configurations was the same and is shown in figure 8. Only specimens that survived more than 1 day are included (for shorter time to failure the estimation of the load level is unreliable). Included are also specimens where the testing was stopped before failure and specimens that are still loaded. For DCB half of the tests were stopped after about 6 months or are still loaded. This means that the estimated time effect is on the safe side (for DCB rather much on the safe side). The best linear fit (correlation coefficient -0.76) is:

$$y = 88.5 - 12.6 x \tag{6}$$

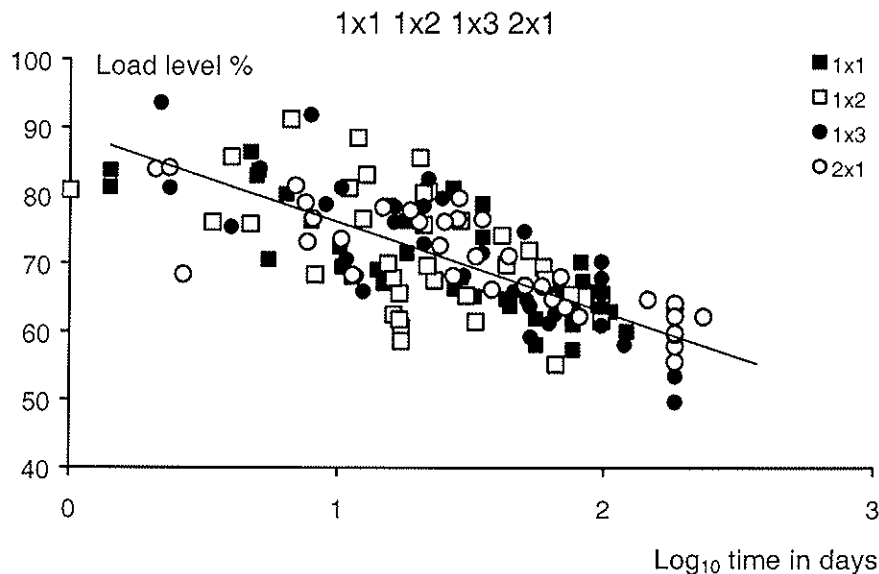


Figure 8. Time to failure as a function of the load level.

where y is the load level in per cent and x is \log_{10} (time to failure in days). A load level of 60 per cent – the long-term strength value often given in codes – corresponds to a loading time of only 180 days. To be safe in 100 years the load level should not exceed about 0.3.

The best linear fit (correlation coefficient 0.59) for DCB is:

$$y = 127 - 22.5 x \quad (6)$$

A load level of 60 per cent corresponds to a loading time of 3 years. The 100 years safe load level value is 0.25.

The scatter of the T-results is so big that it is not possible to give a reasonable estimate of the time effect.

6 References

- Boström, L (1992). Method for determination of the softening behaviour of wood and the applicability of a non-linear fracture mechanics model. *Diss. TUBM-1012, Division of Building Materials, Lund University, Sweden.*
- Draft Eurocode 5 (2001). European Committee for standardisation: prEN 1995-1-1, Design of timber structures, Part 1-1, General rules and rules for buildings.
- Gustafsson, P. J. (1988). A study of the strength of notched beam. Paper CIB-W18A/21-10-1 in *Proceedings of Meeting 21 in CIB Working Commission W18.*
- Gustafsson, P. J. (1995). Fracture mechanics studies of non-yielding materials like concrete. *Diss. TUBM-1012, Division of Building Materials, Lund University, Sweden.*
- Gustafsson, P. J. (1997). Report of Lab 5 in *Consolidated Progress Report of Project AIR2-CT94-1057.*
- Gustafsson, P. J. and Larsen, H. J. (2001). Dowel joints loaded perpendicular to grain. *Symposium on Joints in Timber Structures. 55th RILEM Annual Week. September 2001, Stuttgart, Germany.*
- Johansen, K. W. (1949). Theory of timber connectors. *Publication 9, International Association of Bridge and Structural Engineering, Basel.*
- Yasumura, M and Daudeville, L (1999). Design and analysis of bolted timber joints under lateral force perpendicular to grain. Paper CIB-W18/32-7-3 in *Proceedings of Meeting 32 in CIB Working Commission W18.*

TABLE 1. Test results. Short-term strength (kN).
 minimum – mean – maximum
 strength relative to mean
 (coefficient of variation in per cent)

| | 1x1 | 1x2 | 1x3 | 2x1 | T | DCB |
|---|------------------------------------|--------------------------------------|---------------------------------------|------------------------------------|---|------------------------------------|
| Standard, SBI 25 °C/65 % RF | 7.24-8.12-8.73 1.093 (6.7%) | | | | | 1.33-1.44-1.54 1.075 (5.5%) |
| Standard, ASA 23 °C/65 % RF 10 specimens in each series | 7.23-7.55-8.34 1.016 (5.1%) | 9.49-11.05-11.90 0.977 (6.1%) | 12.71-14.53-16.35 1.001 (7.9%) | 6.56-7.50-8.34 (7.1%) | 1.85-2.49-3.02 1.34 (14.2%) | 0.80-1.05-1.26 0.784 (12.7%) |
| Store 85 % RF – Test 65 % RF | 7.3-7.78-8.3 1.047 (5.3%) | 10.0-11.07-12.7 0.979 (8.8%) | 13.3-15.47-17.8 1.066 (10.8%) | | | |
| Store 30 % RF – Test 65 % RF | 7.2-7.47-7.8 1.005 (2.9%) | 9.7-10.52-11.6 0.930 (6.9%) | 12.5-13.62-14.4 0.938 (5.7%) | | | |
| Winter 2000 moisture: 14.4 % | 7.29-7.64-7.91 1.028 (3.4%) | 9.72-10.42-11.17 0.921 (4.7%) | 10.67-12.81-14.22 0.882 (9.7%) | 6.54-7.20-8.45 0.943 (10.1%) | 0.63-1.12-1.49 ¹ 0.60 (35%) | 1.10-1.22-1.27 0.911 (5.1%) |
| Spring 2000 moisture | 6.84-7.41-7.94 0.997 (5.2%) | 11.47-12.35-13.53 1.092 (7.1%) | 11.62-14.35-15.59 0.988 (10.2%) | 7.52-8.06-8.50 1.056 (4.2%) | 1.02-1.43-2.62 0.77 (43%) | 0.97-1.12-1.26 0.836 (8.8%) |
| Summer 2000 moisture | 6.88-7.17-7.59 0.965 (4.5%) | 10.74-11.60-12.44 1.026 (5.5%) | 11.27-14.63-16.84 1.008 (12.8%) | 7.96-8.23-8.69 1.078 (2.9%) | 1.05-2.05-3.55 1.10 (50%) | 1.00-1.22-1.36 0.911 (11.4%) |
| Autumn 2000 moisture | 6.88-7.29-8.21 0.981 (6.3%) | 11.37-11.66-12.44 1.031 (3.5%) | 14.30-15.13-16.62 1.042 (6.2%) | 6.90-7.75-8.08 1.015 (5.6%) | 2.09-2.46-2.85 1.32 (11%) | 1.25-1.36-1.63 1.015 (10.1%) |
| Winter 2001 moisture | 6.59-7.08-7.40 0.953 (4.6%) | 10.86-11.62-12.86 1.028 (6.5%) | 14.34-15.06-15.97 1.037 (4.3%) | 6.54-7.20-8.45 0.943 (10.1%) | 1.12 ² -1.63-2.09 0.88 (21%) | 1.11-1.34-1.52 1.000 (12.3%) |
| Spring 2001 moisture For 1x2, 1x3 and 2x1 only 5, for DCB only 3 specimens | 6.51-6.80-7.40 0.915 (5.56%) | 11.15-11.48-11.75 1.015 (3.5%) | 13.70-15.07-15.55 1.038 (5.8%) | 7.33-7.51-7.92 0.984 (10.1%) | | 1.11-1.36-1.54 1.015 (12.1%) |

¹ One value (3.19) is disregarded. If this value is included the mean becomes 1.25

² One value (0.80) is disregarded. If this value is included the mean becomes 1.50.

**INTERNATIONAL COUNCIL FOR RESEARCH AND INNOVATION
IN BUILDING AND CONSTRUCTION**

WORKING COMMISSION W18 - TIMBER STRUCTURES

**QUALITY CONTROL OF CONNECTIONS BASED ON
IN V-SHAPE GLUED-IN STEEL RODS**

J Kangas
A Kevarinmäki
VTT Building Technology

FINLAND

Presented by: J Kangas

- H J Blass asked about quality control issue.
- J Kangas answered that it was not an issue as drilling machines were very accurate.

Quality Control of Connections based on in V-shape glued-in Steel Rods

Jorma Kangas, Ari Kevarinmäki

VTT Building Technology

Finland

1 Introduction

Design method of connections based on glued-in rods forming V-shape has been presented in CIB meeting in Delft [1]. It is based on large test series of high capacity connections with numerous rods during the past ten years. In Finland standardised steel elements for these connections and a special apparatus for manufacturing the connections have been developed. They were also used in making the connections for the latest test series. The quality control method is developed for the manufacturer who is specialised in fabricating structures with these apparatuses. The purpose is to prevent or at least to minimise the effect of the possible production errors. Already thirty years glued in screws have been used in Finland in the heel connections of glulam columns. They have their own quality control method.

This paper presents a method for the quality control of manufacturing the V-connections. The steel elements have their own production control. The adhesive has its control method with testing of small joints. The gluing apparatus has its regular checking procedure with small samples taken in short intervals during the production. The length, size, direction and location of the drilled holes have continuous checking with the assembling of the steel elements without the adhesive. Regular bookkeeping of the quality control operations is demanded and checked by exterior quality control organisation.

These guidelines based on the assumption that for glued-in steel rods it will be required the same system of attestation of conformity as for other glued wood constructions. The requirement will be the system of attestation of confirmation ACI. That includes

- 1) Type testing of product by Testing body
- 2) Initial inspection of the factory and of the quality control by Inspection body
- 3) Internal quality control by Manufacturer
- 4) Testing of samples by Manufacturer (no extern testing is required)
- 5) Continuous surveillance, assessment and approval of the production control by Certification body

Quality control procedure contains:

- demands for production conditions and handling of the materials and the products,
- methods for checking the proper sizes and properties of the materials and components used in manufacturing the connections,
- methods for production control and proof loading

2 Certification

In Finland the Producer needs a certificate from VTT (Inspection and Certification body) for the independent manufacturing the V-connections with glued-in rods. The facilities, the skills of the personnel and other conditions for good production will be checked in the certification and the required quality control measures will be set. An exterior supervisor will be needed until the certificate becomes valid.

3 Requisites

3.1 Production conditions

Production hall shall have proper climate during the production. Its temperature and moisture shall be in the required limits: temperature at least 18 °C and relative moisture content 70% at the most. Means are required for glulam elements to be moved safely. Separate room are needed for storing the adhesives.

3.2 Rules for actions

Separate phases of the production shall be written guidelines like the use of the drilling and gluing apparatus, handling of the glulam, activities in quality control and they shall be followed. There shall be ability for rapid reactions in the case of accidents. Protective supplies shall be used in gluing.

4 Materials

4.1 Glulam

Glulam production is under official quality control. The client shall only check that the beams are made to order and design concerning the dimensions, strength class and moisture content and that shall properly be registered. Mean moisture content in the connection area shall not be more than three %-units higher than the lowest designed moisture of the glulam structure. Moisture content shall be measured on each four sides of at least one beam at the distance of 0,5 meter from the end. The glulam beams shall be stored before gluing the rods at least two days under conditions of temperature at least 18 °C and relative moisture content 70% at the most.

4.2 Steel elements

The fabrication of the steel elements shall also be under official quality control concerning the material properties and the quality of welding. Engineering works, which is manufacturing the steel elements shall have a quality control agreement with a notified certification body. Some standardised steel elements used for the heel connections are shown in figure 1. They shall be sand blasted at least in the anchorage area and coated elsewhere with epoxy paint. Coatings approved by testing are allowed also on the rods. The rods in the steel elements shall have the given angles and dimensions. The connection manufacturer shall only check and register those properties. The design of the steel elements shall be based on the yield of the steel instead of timber failure in the connection.

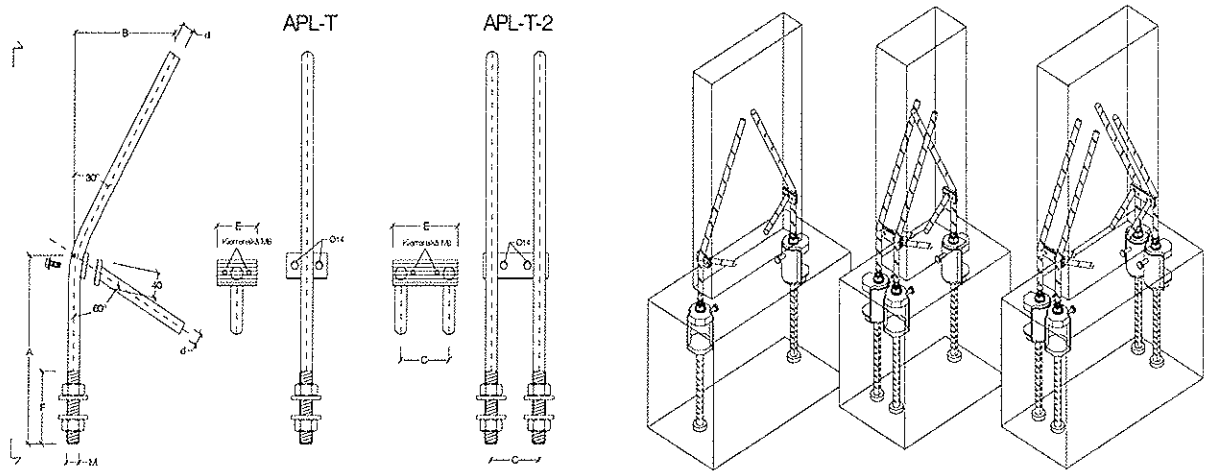


Figure 1. Standardised steel elements and their use for the heel connections.

4.3 Adhesive

In VTT's test series three different Epoxy adhesives have been used and they all behaved very well [2]. The yield limit of the rod material was without exception exceeded with shorter anchorage lengths than are used in steel elements. These adhesives are allowed to be used in gluing the steel rods. When receiving a new portion of adhesive its use shall be checked by making compression test specimens with five rods of slenderness ratio $\lambda=10$ for the proof-loading (Type testing).

Documents about the properties and the guidelines for the use and storing of each adhesive given by the fabricator shall be available and they shall be followed and registered. Those can be e.g. the date of receiving the adhesive, description of the adhesive, shelf life of its components, exact proportions of the components in the adhesive and storing conditions (Internal quality control).

For each workday and at least for every delivery a joint of one rod similar to that of proof-loading shall be made and stored in the same circumstances as the glulam components. Each test joint shall be marked and the test results documented so that its connection to the produced glulam structures can be followed (Testing of samples).

5 Production methods and control

This quality control method is made mainly for the fabricator, who has precision drilling machinery and a computer guided gluing apparatus. They will simplify the quality control and will make it possible to use rather complicated prefabricated steel components with many rods.

5.1 Drilling the holes

The precision drilling machinery has proved to be reliable to make accurate drillings. At first the locations of all holes for the rods or the rod pattern shall be checked and marked on the surface. Then the direction and the depth of the first drilling is set and the hole made and the result is checked. After that all similar holes are made and the same procedure is repeated for the other drillings. The following drillings are then easier, but they will need checking from time to time. In figures 2 and 3 the drilling machine is in action. Finally the whole connection will be assembled for checking, see figure 4. The type of connection, the rod pattern, the thickness of the rods, the anchorage length and the size of drillings shall be registered.

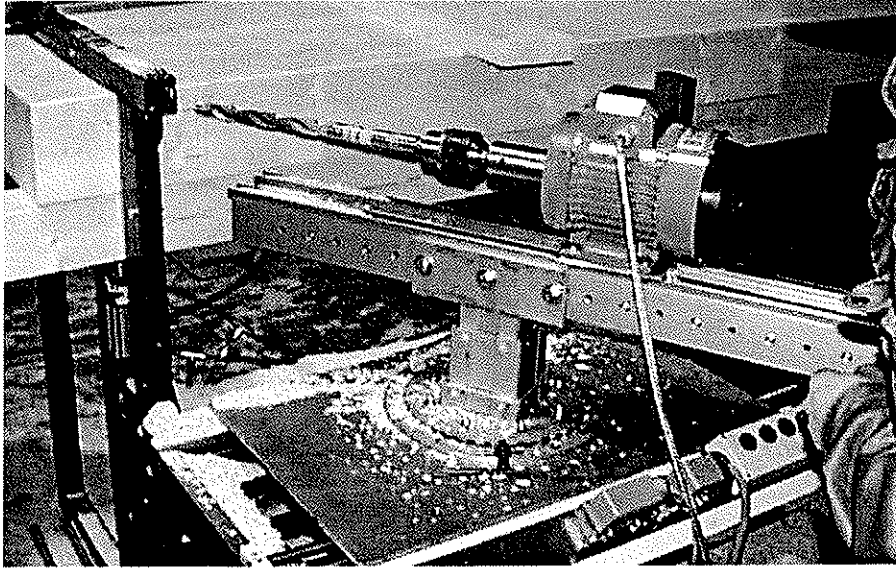


Figure 2. A prototype drilling machine

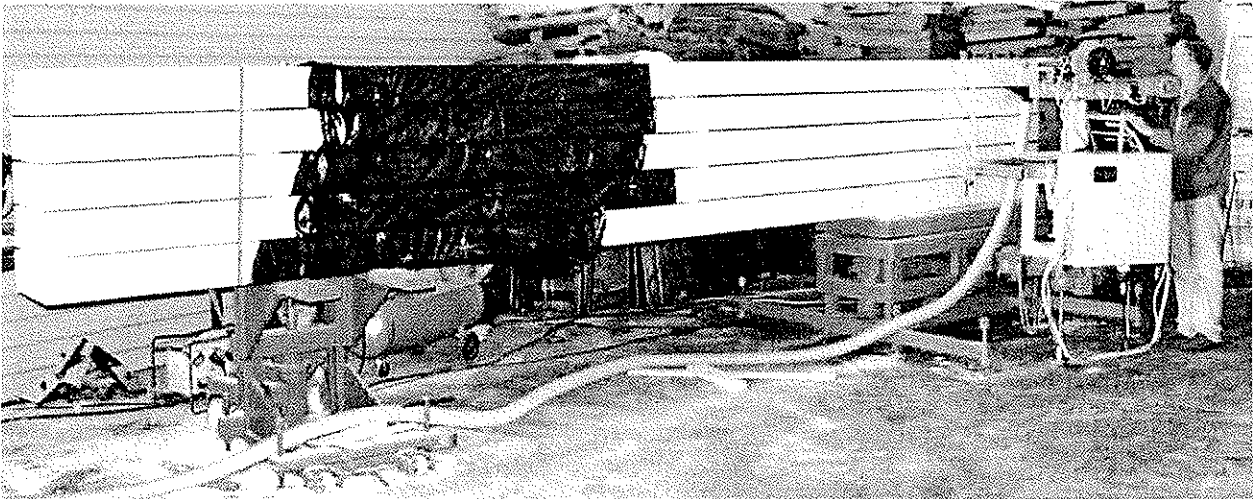


Figure 3. A more advanced drilling machine.

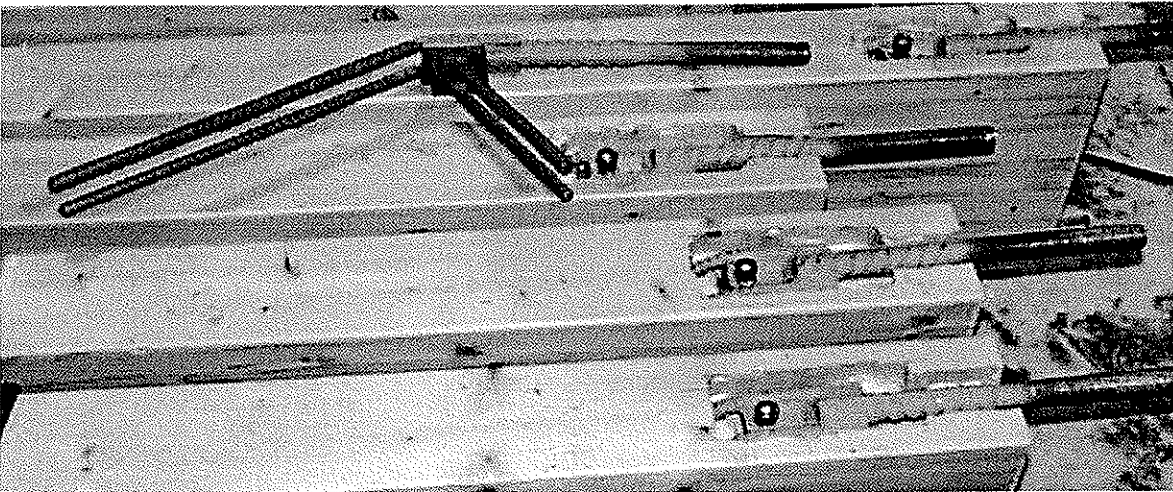


Figure 4. Mortised V-connections for tension members assembled without adhesive for checking.

5.2 Use of the adhesive

The gluing apparatus will make the handling of otherwise difficult Epoxy adhesive very easy. Both components are in separate containers, from which they will be portioned out in chosen ratio guided by computer. By heating the viscosity of the adhesive can be increased to make portioning much easier. Mixing of the components will happen efficiently and safely in a small spiral tube, where the components will flow through separate nozzles. The amount of the adhesive needed for each joint can be calculated and that amount will be delivered and controlled by computer. Due to high viscosity the rods are easy to push into the holes and adhesive can be added onto the joint if necessary. Another method is to inject the adhesive through the holes. The gluing apparatus and the columns after gluing the heel joints can be seen in figure 5.

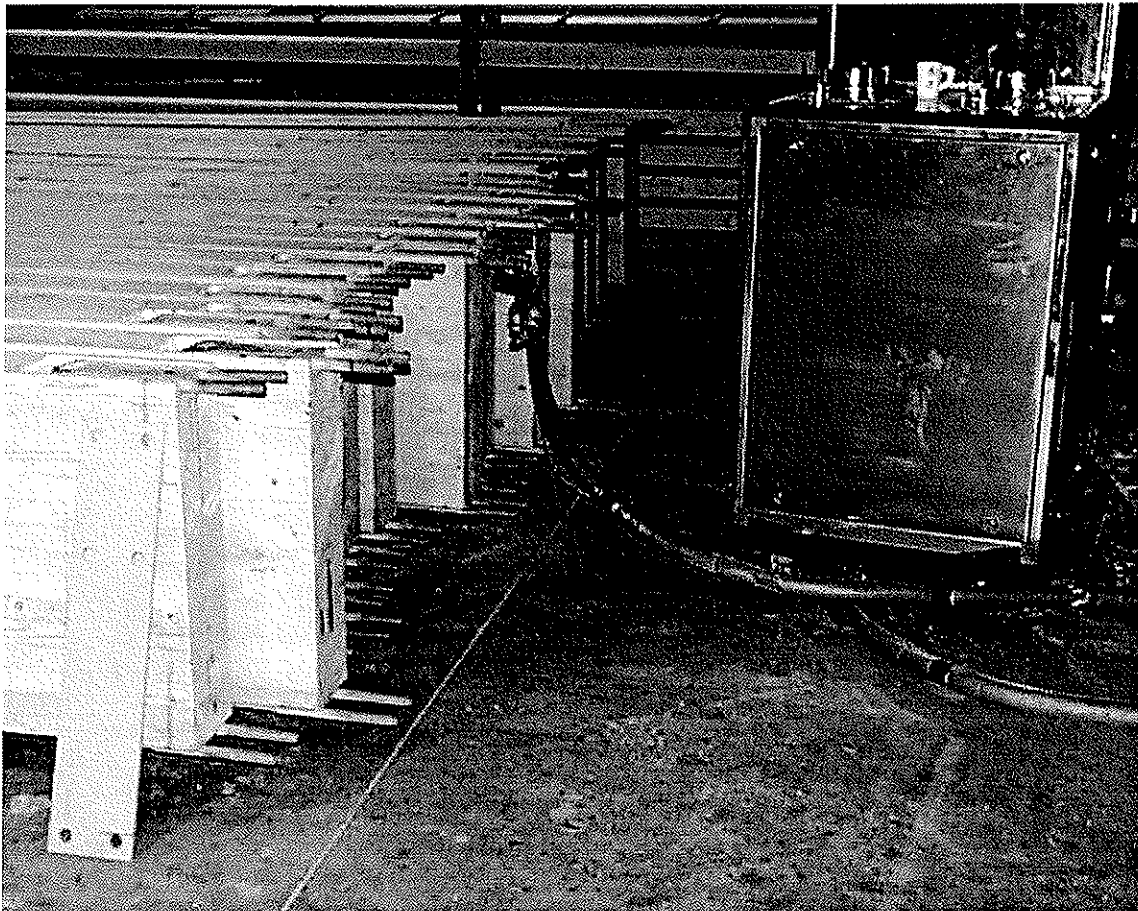


Figure 5. The gluing apparatus and the columns after gluing the heel joints

The duties in quality control are quite clear. Demands for a sufficient amount of adhesive and a good contact to the surfaces are easy to fulfil and to notice. Almost the only task is to take care of the proper proportioning of the components. It is important that the gluing apparatus will work well. Therefore its maintenance shall be regular according to the instructions. In the beginning of each working period the samples of each component delivered from the nozzles shall be measured and their proper ratio shall be checked. During the gluing shall the right colour of the adhesive be observed and small separate samples taken regularly. These activities shall be registered.

5.3 Post handling

The glulam beams can be turned over next day after gluing for preparing the connection on the other edge. The prepared glulam elements shall be stored at least two days on the production conditions before their delivery. They shall be labelled so that its production time can be identified afterwards. The ends of the beams shall be coated to reduce the variation of their moisture content in connection area. The connections shall be protected against damages during the transportation.

6 Proof-loading by manufacturer

Proof-loading in quality control procedure will be used, when receiving a new portion of beforehand accepted adhesive. Its use shall be checked by compression test specimens with five rods of slenderness ratio $\lambda=10$ and the protrusion of 10 mm, see figure 6. The most common rod thickness 20 mm will be used, so its total length is 210 mm and the diameter of the drilled hole 25 mm.

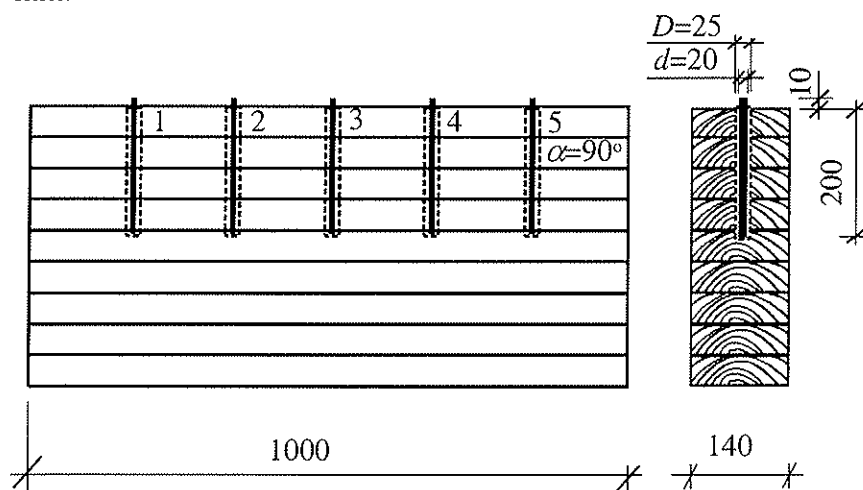


Figure 6. Compression test specimen for checking of adhesive.

The joints will be loaded after about three days with the constant rate of 20 kN/min compressive load. The portion will be acceptable, if the mean capacity of five rods is at least 90 kN. If that limit is not achieved and the failure is obviously not due to adhesive itself (timber failures, buckling of the beam etc.), the test will be repeated with better arrangements. The portion will be rejected, if the repeating will not give better results. During a week for each workday and at least for every delivery made joints of one rod shall be loaded before the delivery of the corresponding structures with the acceptance criterion of 86 kN ($f_{a,k}$). If that limit is not achieved and the failure is obviously not due to adhesive itself, the corresponding connections shall be reinforced.

7 Reporting

The manufacturer shall continuously keep a dated diary about the quality control activities. There shall be written the checking, measuring and testing results and other activities, which are mentioned in the quality control agreement. The names of those, who have carried out the tasks and who are responsible of the quality control shall be written in the diary. The diary shall also contain the signs of those glulam elements, which the quality control will concern. The diaries shall be kept at least five years.

8 Exterior quality control

The exterior quality controller (Certification body) will visit twice a year and that will be renewed unexpectedly if necessary. During the visit the manufacturers own quality control and its book-keeping will be checked thoroughly and the tests and measuring duties will be supervised. The properties of the products also will be checked randomly. The certification body will summarise the reports of the quality control visits and the summary will be delivered to the manufacturer.

9 Acknowledgements

The authors thank Engineering works Anstar Oy and Lamicon Ltd, which allowed us to use their figures from steel elements and apparatuses. They also have given financial support for the preparation of this paper, which is gratefully acknowledged.

10 References

- [1] Kangas J. (2000), "Capacity, Fire resistance and gluing pattern of the rods in V-connections", Proceedings of the meeting 33 of CIB-W18, international council for building research, studies and documentation. Working commission W18A on timber structures, in Delft, The Netherlands, paper 33-7-10, 13p
- [2] Kangas, J., (1994), "Joints of glulam structures based on glued-in ribbed steel rods", VTT Publications 196, Espoo, Finland. 61 p. + app. 20 p.

INTERNATIONAL COUNCIL FOR RESEARCH AND INNOVATION
IN BUILDING AND CONSTRUCTION

WORKING COMMISSION W18 - TIMBER STRUCTURES

TESTING CONNECTOR TYPES FOR
LAMINATED-TIMBER-CONCRETE COMPOSITE ELEMENTS

M Grosse

S Lehmann

K Rautenstrauch

Institute of Structural Engineering

Bauhaus University Weimar

GERMANY

Presented by: M Grosse

- H J Blass commented that the load slip curves were shown up to 4 mm of displacement and questioned how did the joints behave after 4 mm.
- M Grosse stated that tests were performed up to 15 mm and the information shown up to 4 mm was representative.
- A Ceccotti asked about the difference of the two types of shear tests.
- M Grosse answered that the single shear joint test method was found to be better especially for the log and recommended the single shear joint test.

Testing connector types for laminated timber-concrete composite elements

M. Grosse, S. Lehmann, K. Rautenstrauch
Institute of Structural Engineering
Bauhaus- University Weimar, Germany

1. Introduction

The idea of combining the constructionally favourable characteristics of concrete and timber is not new. The thereby mainly tension-stressed timber and compression-stressed concrete offer good carrying behaviour. A good overview of possibilities and state of research of shear connections in timber concrete composite elements is given by Blaß & al. (1996), Kreuzinger (1999), Meierhofer (1994) and Ruske (1998).

The connection between timber and concrete is of fundamental importance for stiffness and carrying performance. Since these systems have usually been realised as timber-concrete composite beams which are mainly taken for bridges or revitalisation of timber beam floors, dowel type connectors were normally studied and taken for the transfer of shear forces.

At the Bauhaus-University Weimar a research program was initiated to develop new connectors for transferring shear forces in laminated timber-concrete-composite plates. In the context of this paper the joints with flat-steel-locks, punched steel sheets and concrete cams are introduced.

An overview of shear tests, performed to examine the load-slip characteristics and bending tests of full sized composite floor elements is also given. Test data and picture material are presented.

2. Constructions of shear connection

2.1 Flat-steel-locks

So called “flat-steel-locks“ are zinc-coated flat steels with a cross-section of 5/40mm, which are driven into sawing cuts in transverse direction of the nail-laminates with a 5°-angle to the vertical. The locks must be arranged only at few points in the compound-joint of a composite element (figure 5). If the compressive force in the concrete layer is not sufficient, an additional reinforcement right above the locks is necessary to cover the tension force, which results from the lever effect by the lock.

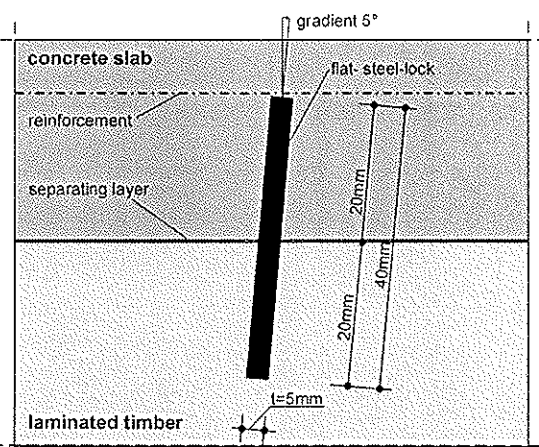


Figure 1: Construction of the flat-steel-lock

2.2 Punched steel sheets

25mm-holes are punched in zinc-coated steel sheets (thickness $t=0,75\text{mm}$) in 50mm-distance (figure 2b). The sheets are placed between two laminates and lengthwise turned down to enable automatic machine-nailing (figure 2a). Before pouring concrete sheets have to be straighten up again and reinforcing steel is placed through the holes in transverse direction.

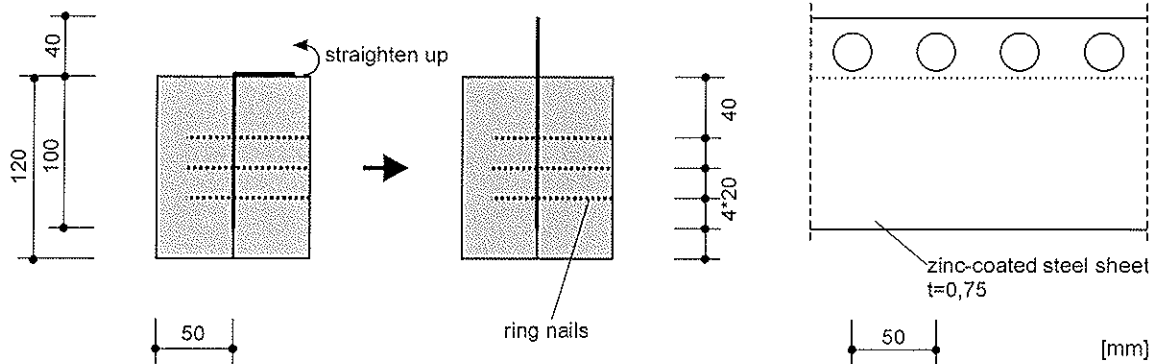


Figure 2: a) Prefabricated lamella for shear connection

b) Zinc-coated punched sheet

2.3 Concrete cams

30mm-diameter-holes are equidistantly drilled into the vertically arranged out-sticking timber laminates (figure 3). The holes can be easily filled out with concrete. These “concrete-cams“ can transfer shear forces between timber and concrete in bending stressed composite elements. In this construction the cams are double-shear stressed. Additionally it can be assumed, that the concrete slab will wedge if transverse stiffness of the laminated timber element is sufficient. Differing to other test configurations the concrete was this time reinforced by steel fibres and a filter line of 0/8 mm was applied.

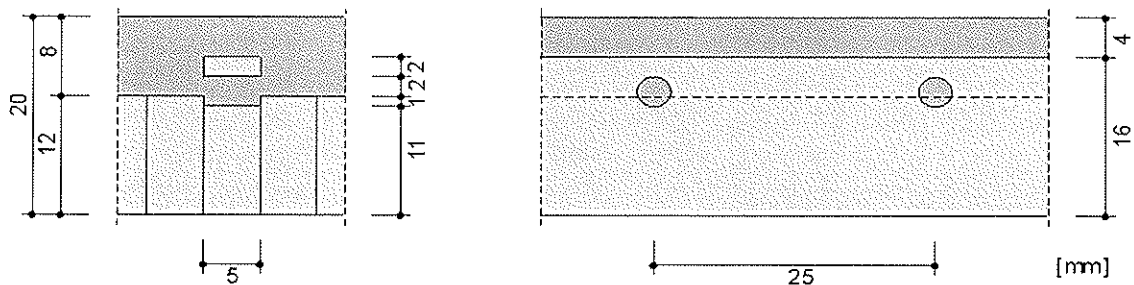


Figure 3: Concrete cam construction

3. Shear tests

The behaviour of the shear connector in the composite joint between timber and concrete is extremely important for the carrying and deformation performance of composite structures with compliant connections. To enable a structural model the load-slip-characteristics, failure load and failure mechanism of each connection type was determined by experimental tests. Shear tests using specimens with only one shear joint have been conducted as illustrated in figure 4. Table 1 shows five different tested variations of specimens. To get meaningful results a sufficient number of short-term shear tests have

been conducted. Experimental procedure and applied load history were taken according to DIN ENV 26891. Test setup with dial indicators and load cells are illustrated in figure 4. The versions HVS/F and HVS/FL have been additionally tested by symmetric shear test with two shear joints, also known as "Push-out"-arrangements.

| Type | connector | Sketch of structure |
|--------|---|---------------------|
| HVS/F | Flat-steel-locks | |
| HVS/FL | Flat-steel-locks with out-sticking boards | |
| HVS/FR | Flat-steel-locks using round timber | |
| HVS/LB | Punched steel sheets | |
| HVS/BN | Concrete cams | |

Table 1: Specimens for shear tests

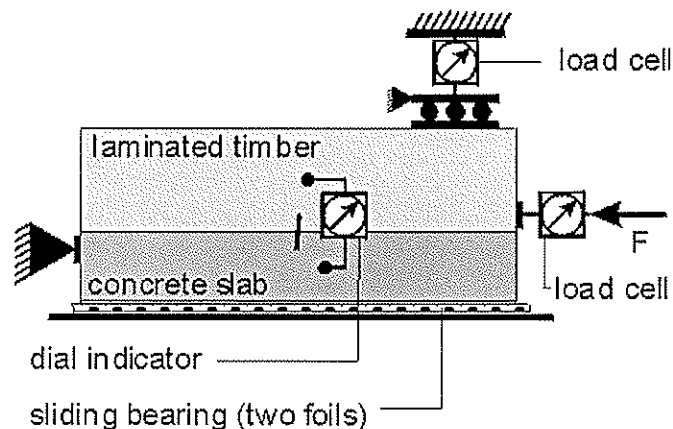


Figure 4: Experimental setup of shear tests

4. Bending tests

Structural size 4-point bending tests with complete composite members were performed to verify the results of shear tests and the structural model. The span of the elements was 4,80 meters. Cross-sections were taken according to table 2. The thickness' of timber and concrete layer were chosen in a way, which gave the nail-laminated timber a higher bending stiffness than the concrete layer ($EI_{concrete} < EI_{timber}$).

| | |
|-------------|--|
| Type HVB/F | |
| Type HVB/FL | |
| Type HVB/FR | |
| Type HVB/LB | |
| Type HVB/BN | |

Table 2: Cross-sections of bending tests

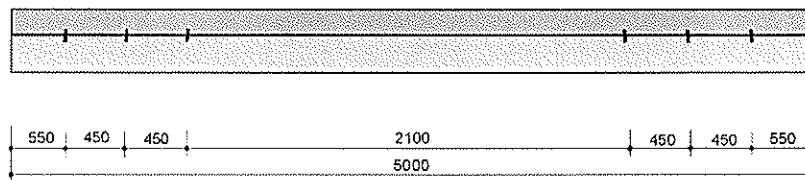


Figure 5: Configuration of the flat-steel-locks for specimens HVB/F HVB/FL and HVB/FR

At least 5 composite elements were tested for each type. Figures 6 and 7 show the experimental setup with dial indicators according to DIN EN 408. Applied loads were taken at the points “f”. Deflections “d”, lift-offs “a” and relative displacements “v” along the shear joint and at the front edges were registered.

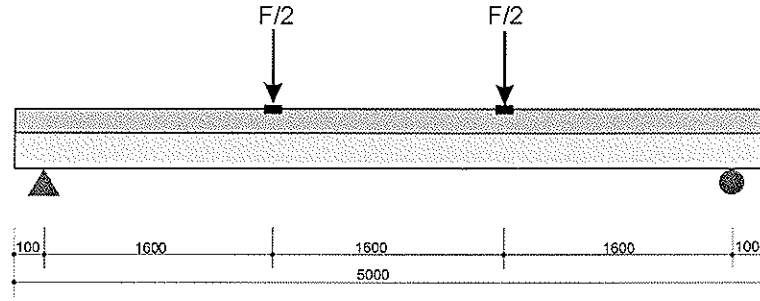


Figure 6: Test system

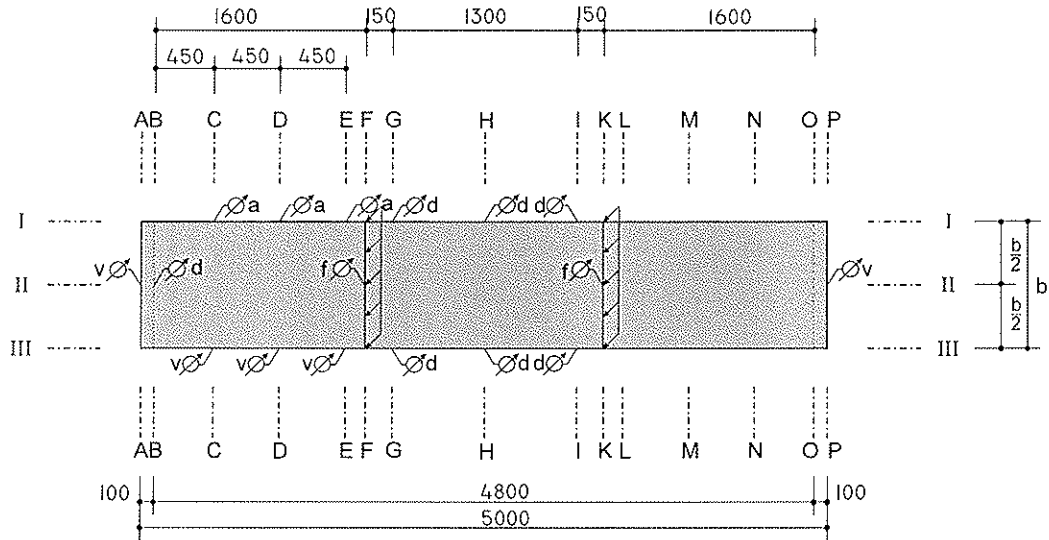


Figure 7: Locations of measuring points

5. Results and conclusions

5.1 Results of the shear-tests

Respectively to DIN ENV 26891 the maximum load F_{max} has been determined and the modulus of displacement k_s has been computed. Mean values are given in table 3. Typical load-displacement-curves, determined in the tests, are presented in the following diagrams (figure 8 to 9). Such diagrams were chosen, where test compliance's corresponded best to mean values of the series. Comments concerning failure mechanisms will be given in chapter 5.2.

| Connector type | Number of specimens | Mean value respectively | | based |
|---|---------------------|-------------------------|---------------|-----------------|
| | | F_{max} [kN] | k_s [kN/mm] | |
| <i>Shear tests</i> | | | | |
| HVSI/F | 10 | 272,7 | 468,6 | per meter width |
| HVSI/FL | 10 | 295,7 | 607,5 | per meter width |
| HVSI/FR | 10 | 302,8 | 455,8 | per meter width |
| HVSI/LB | 3 | 63,6 | 139,1 | per steel sheet |
| HVSI/BN | 10 | 27,9 | 105,8 | per cam |
| <i>Push-out-tests</i> | | | | |
| <i>referring to one flat-steel-lock</i> | | | | |
| HVSI/F | 5 | 326,7 | 539,3 | per meter width |
| HVSI/FL | 5 | 303,3 | 325,3 | per meter width |

Table 3: Results of shear tests

- **Single-point connections using flat-steel-locks**

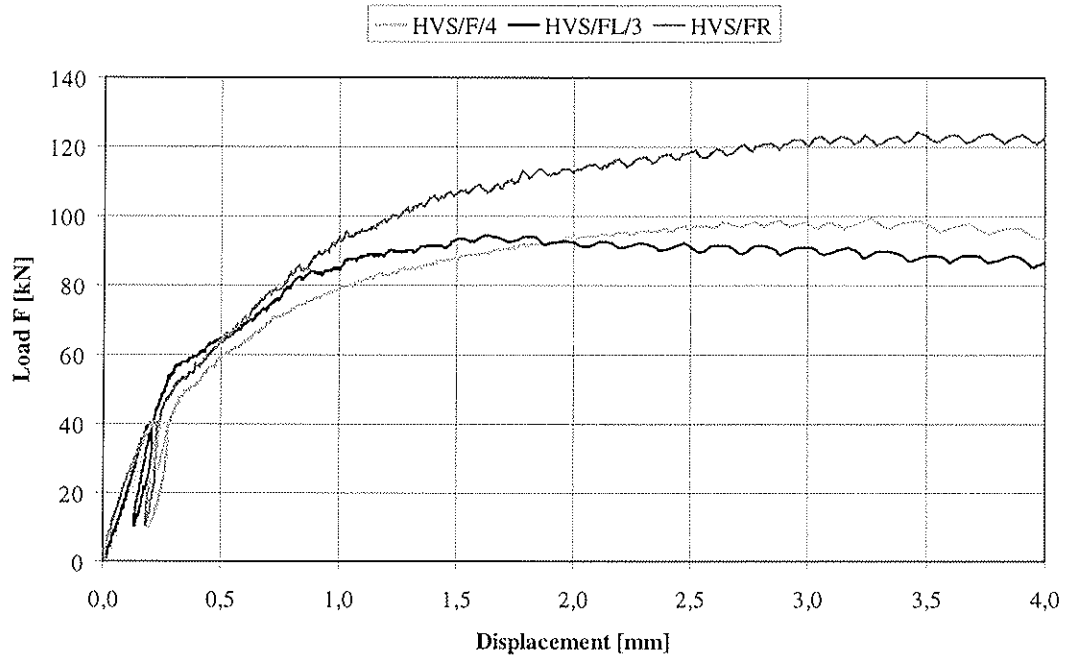


Figure 8: Load-displacement-curves of shear tests, single-point connections using flat-steel-locks

- **Continuous shear connection with punched steel sheets resp. concrete cams**

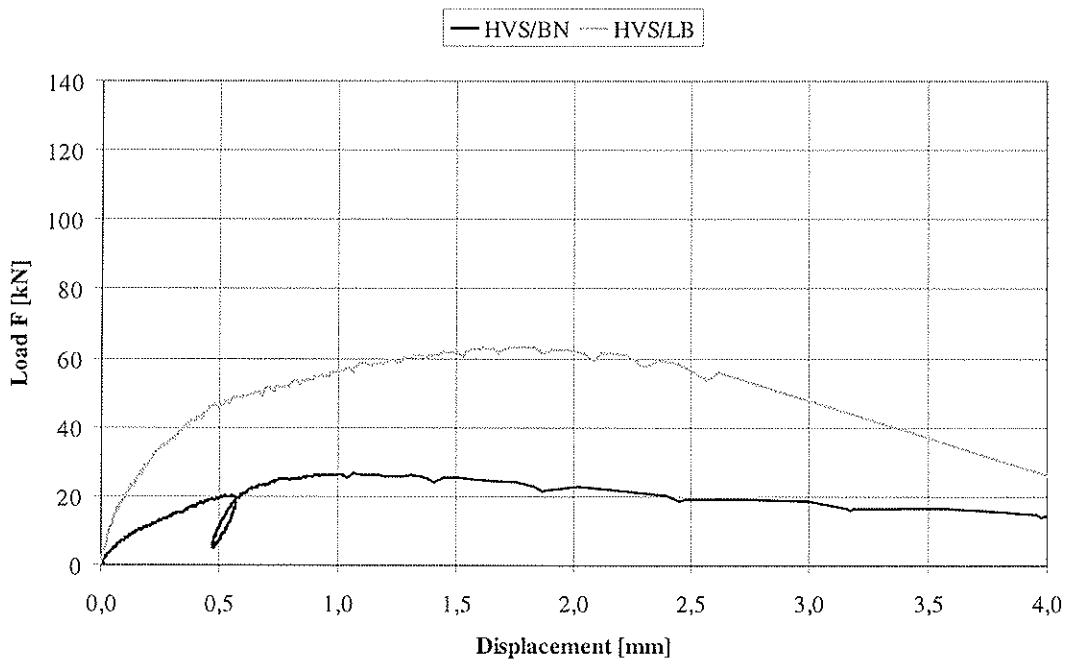


Figure 9: Load-displacement-curves of HVS/BN and HVS/LB series

5.2 Results of bending tests

- **Specimen HVB/F**

The load-deflection-curves (figure 10) show, that midspan-deflection exhibits an approximately linear progression after load application. In the upper load-bearing range deflection starts to increase disproportionately indicating some kind of plasticating behaviour. At the front edges no relative displacement between nail-laminate and concrete

cover was observed in the 0 to 3,5kN range. In the range of 3,5 to approximately 65kN linear behaviour can be assumed.

As expected the horizontal relative displacements alongside of the element within the area of the three flat steel locks showed an increase from midspan to the supports under same load. The cracks in the concrete each occurred at the three flat-steel-locks, symmetrically arranged to load axis. The first crack developed at the outermost connection in a load range of 35 to 45kN. Up to maximum load no unusual relative displacement was observed in perpendicular direction to compound joint (take-off of concrete cover) before and during the test. Only after passing the maximum load and therefore after failure of the shear connection the concrete cover started coming off at locations of the connectors and the compound joint started opening.

The structural-size bending tests showed, that failure of the composite structure initiates in the failure behaviour of the shear connection. As primary cause of failure is the local destruction of concrete in the area of shear transfer at the flat steel locks for all specimens, which was also registered during shear-tests. A pull-out of the flat steel from the sawing cut was not observed before concrete failure. As expected concrete failure first occurred in the area of the flat-steel-lock, which was closest to the support (axes C and N, figure 7). For the timber only hardly observable plastifications occurred in the area of flat steel connector.

- **Specimen HVB/FL**

For these specimens a constant increase of deflection was also observed (figure 10). The curve shows an approximately linear progression at first, followed by a plasticating run. No relative displacements at front edges between timber and concrete were registered under low load level. Only after further load increase relative displacement linearly grew up to loads of approximately 85kN. Afterwards displacements continued growing under decreasing load.

Horizontal and vertical displacements and crack development in the area of flat steel locks behaved as already described for the series HVB/F.

Interpreting the diagrams it has to be kept in mind, that the nailed laminates of the FL-series feature a higher bending stiffness because of varying lamella height. This explains the higher slope of the load-deflection curve of the composite element. The computational model of the tests did not result in a substantially higher rigidity of the connection, which was determined to approximately 540kN/mm per meter. This value acknowledges the results of shear-tests for flat steel locks with constant lamella height (series HVS/F). The additional support of the locks by out-sticking lamellas in series HFB/FL did not result in an improvement of connection compliance also.

- **Specimen HVB/FR**

In this series the shear connection failed early. The concrete slab joined almost loose on the laminated timber. This can be seen in the progression of the load-deflection-curve (figure 10). Compared to series HVB/F and HVB/FL there was only a small contact area of lock and round timber for transferring shear forces. This resulted in a heavy compression of fibres causing some kind of embedding failure. The bending strength could not be exceeded for maximum piston stroke, so fracture did not occur for specimens HVB/FR.

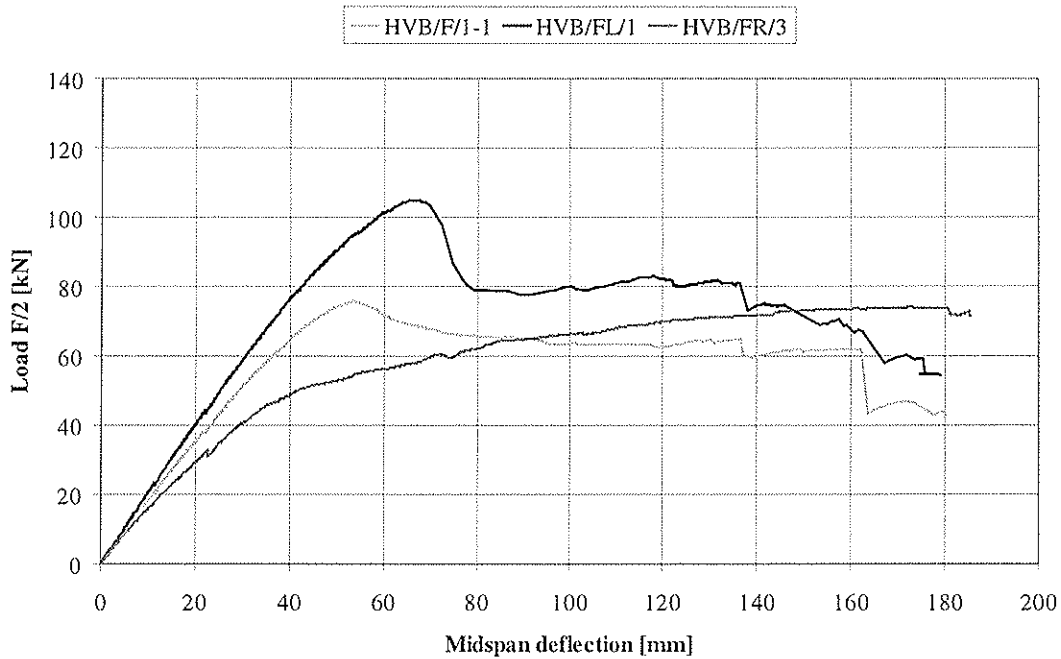


Figure 10: Load-deflection-curve of bending tests, single-point connections using flat-steel-locks

- **Specimen HVB/BN**

Up to 20kN per press no relative displacement between nail-laminate and concrete cover was observed. For a load ($F/2$) up to 60kN a linear elastic load-displacement progression can be assumed. Failure of the shear connection occurred beyond that point, caused by rupture of the concrete cams. So interaction of concrete slab and nail-laminated timber was not possible anymore. After failure of shear connection an observable lift-off of the concrete slab was registered. On approximately 85kN per press rupture of timber occurred.

- **Specimen HVB/LB**

Looking at the load-deflection-curves (figure 11) it can be observed, that midspan-deflection exhibits an approximately linear progression after load application. In the upper load-bearing range deflection starts to increase disproportionately indicating a plasticating behaviour of the test specimen. The rupture of the composite element finally occurred because of failure at the tension edge of the lamellas followed by compressive failure of concrete.

At the front edges no relative displacement between nail-laminate and concrete cover was observed in the 0 to 60,0kN range. The take-off of the concrete was not characterised by unusual failure appearances before and during the test. Because of the continuous connection of nailed laminated timber and concrete slab a take-off was registered relatively late during test procedure.

Damage of the shear connection is mainly caused by a pull-out of punched steel sheets from timber and concrete layer respectively. The thickness of steel sheets is therefore crucial for load-bearing capacity and compliance of the connection, but for practical use it is limited to ensure nailing without predrilling.

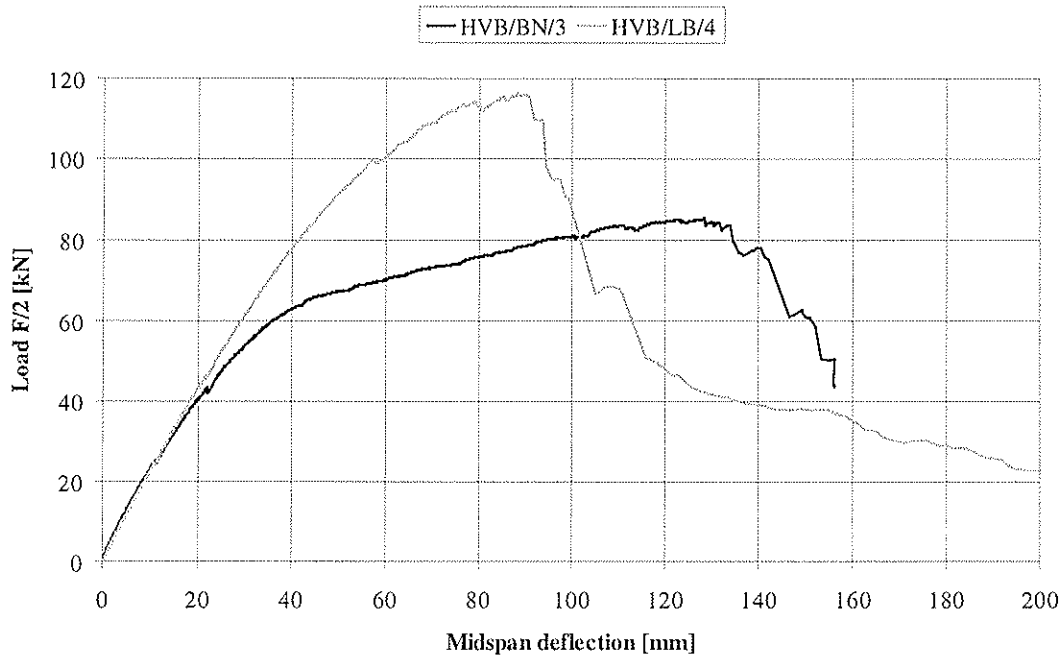


Figure 11: Load-deflection-curve of bending tests, continuous shear connection using punched steel sheets and concrete cams

6. Conclusion

The application of dowel-type connectors in continuously connected timber-concrete composite elements causes constructive, technical and economical problems, which can be hardly solved. It is especially difficult to keep the least edge distance of the connector perpendicular to the grain to the narrow edges of a nail-laminated element, which would require thick members. In addition dowel-type connectors have to be applied in large quantities. The studied connecting methods should enable an easy and economical use in laminated timber-concrete- composite plates.

The series HVB/FR and HVB/BN fell short of expectations, because shear connections failed quite early. For all other joints the results of the shear-test could be verified.

Although only three connectors were taken in the series HVB/F and HVB/FL in the outer third of the members, an increase of bending stiffness was obtained. The same applied on the use of continuous connections with punched steel sheets.

An substantial increase of the load-bearing capacity compared to the pure nail-laminated timber element was not possible with the chosen arrangement of the flat-steel-locks. The shear connections fail first, after a further deflection increase a bending fracture occurs at the lamellae. To prevent failure of the locks and achieve an increased load bearing capacity more connectors could be attached.

Only for the specimens with punched steel sheets a failure of the shear connection was not registered. Bending failure firstly occurred at the tension edges of the lamellae. This was followed by very high deflections leading to failure of the concrete pressure zone in the area of load application.

The application of flat-steel-locks and punched steel sheets for the shear connection yielded good results. Practical use seems easily possible. The increased stiffness leads to smaller deflections of the composite element. This can already be obtained by applying only few flat-steel-locks For most applications the prove of serviceability becomes decisive so design load could be increased considerably.

Code reference

DIN 1052; Holzbauwerke; Teil1- Berechnung und Ausführung (04/88); Teil 1/A1- Änderungen 1(10/96); Teil 2- Mechanische Verbindungen (04/88); Teil 2/A1- Änderungen 1 (10/96)

DIN EN 408:1995; Bauholz für tragende Zwecke und Brettschichtholz- Bestimmung einiger physikalischer und mechanischer Eigenschaften (04/96)

DIN EN 26891:1991; Holzbauwerke – Verbindungen mit mechanischen Verbindungsmitteln, Allgemeine Grundsätze für die Ermittlung der Tragfähigkeit

Publications

Blaß, H. J.;Ehlbeck, J., Schlager, M. 1996: Trag- und Verformungsverhalten von Holz- Beton- Verbundkonstruktionen; Bauen mit Holz; Teil 1 (05/96) S.392-398; Teil 2 (06/96) S. 472-477

Kreuzinger, H. 1999: Die Holz-Beton-Verbundbauweise. Leinfelden-Echterdingen, 25.11.99. In: Informationsdienst Holz. Fachtagungen 1999_2000, Arbeitsgemeinschaft Holz e.V.

Meierhofer, U.A. 1994: Anwendung von Holz- Beton- Verbund im Hochbau; Schweizer Ingenieur und Architekt Nr. 37 (09/94)

Ruske, W. 1998: Holz- Beton- Verbund bei Geschoßdecken; Deutsche Bauzeitschrift (07/98) S. 75-80

**INTERNATIONAL COUNCIL FOR RESEARCH AND INNOVATION
IN BUILDING AND CONSTRUCTION**

WORKING COMMISSION W18 - TIMBER STRUCTURES

**BEHAVIOUR OF AXIALLY LOADED GLUED-IN RODS
- REQUIREMENTS AND RESISTANCE, ESPECIALLY FOR SPRUCE TIMBER
PERPENDICULAR TO THE GRAIN DIRECTION**

A Bernasconi

Institute for Wood Physics, Federal Research Centre for Forestry and
Forest Products, Hamburg

GERMANY

Presented by: A Bernasconi

- H J Blass commented on the density influence.
- A Bernasconi answered that he was surprised also about the slight density effect only which is difficult to isolate.
- F Lam asked about the conclusion that capacity for the perpendicular to grain case was penetration depth independent.
- A Bernasconi answered that it was valid within a certain applicable distance. He also commented that from literature the screw driven case seemed to have higher capacity.
- L Daudeville stated that the stress distribution might not be constant.
- A Bernasconi answered that gluing parallel to grain depends on material and would not have constant stress distribution while in the gluing perpendicular to grain cases the difference in MOE was so high that a constant stress distribution could be assumed.
- J König commented that the influence of hole direction could be attributed to size effect.
- A Bernasconi clarified it with respect to the size effects of strength of timber.
- H J Larsen stated that fracture mechanics type problem always have a square root of size term.
- J Kangas commented that shear distribution could be checked with strain gauges.
- S Thelandersson commented about the plastic behaviour in the length direction where the glue was loaded and questioned about the long term stability and sensitivity to moisture effects.
- A Bernasconi clarified that epoxy glue was used and didn't have data on the long-term and moisture issues. Also he stated that the epoxy glue was brittle and it would be possible to verify with gluing in the parallel to grain direction although constant shear stress was not present. He stated that the glue did not fail; the timber did.
- A Jorissen asked whether 3D model was used and whether it was possible to calculate the stresses in the perpendicular to loading direction.
- A Bernasconi answered only 2D model was used and it was possible to estimate the stresses in the perpendicular to loading direction.

Behaviour of axially loaded glued-in rods - Requirements and resistance, especially for spruce timber perpendicular to the grain direction

Dr. Andrea Bernasconi

Institute for Wood Physics, Federal Research Centre for Forestry and
Forest Products, Hamburg, Germany

1 Introduction

Glued-in rods allow the introduction of high forces in timber elements. The bond between rods and timber is given by an adequate bond system with sufficient ultimate strength and rigidity, in order to assure a strong bond between the rod material and the timber. To describe the behaviour of glued-in rods and to give a basis for the design, it is necessary to determine the influence of different parameters on the strength of the bond system.

Under normal timber building conditions the gluing of steel is complex. The profile of the steel rods - in form of thread or ribs - is an interesting possibility to avoid the gluing of steel. The mechanical connection given by the ribs assure the load transfer from the steel to the glue-line. In the case of a sufficient resistance of the glue system a shear failure of the timber adjacent to the hole occurs. That way the best capacity of the bond is reached.

The shear strength of the timber depends on several parameters. The description of the influence of the different influence factors and the description of the stress distribution in the bond line is the starting point for the experimental analysis of the timber strength with use of pull-out tests.

Following the analysis of the results from several experimental pull-out tests on glued-in rods perpendicular to the grain direction with spruce timber, it shows that the strength depends principally on the hole diameter. The other factors of influence have a smaller influence on the strength. These results allow to give a proposal for the design of glued-in rods perpendicular to the grain with spruce timber.

The described pull-out tests and the results are parts of different projects and were carried out at the ETH in Zurich and at the Institute of Wood Technology of the University of Hamburg.

2 Bond between steel rods and timber

2.1 Principle

The force on the axis of a glued-in rod is introduced into the timber. The rod is glued into a drill-hole. The force transfer takes place through the glue line. Due to the thickness of the steel rod profile the glue line can have a thickness of several millimetres. Special epoxid

glue systems were developed and tested for glued-in rods with spruce, oak and beech timber. Glue-lines up to 8 mm thickness were proved to be effective.

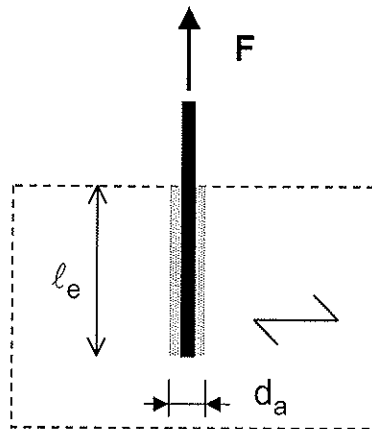


Figure 2.1: Axial loaded glued-in rod

Due to the great thickness the glue line is not just the adhesion line between the steel and the timber, but it should be considered as an element of the bond system. The ribs of the steel rod assure a mechanical connection between the rod and the glue, so that a glue-adhesion on the steel rod is not needed. The load transfer takes place as a local compression of the steel and the glue.

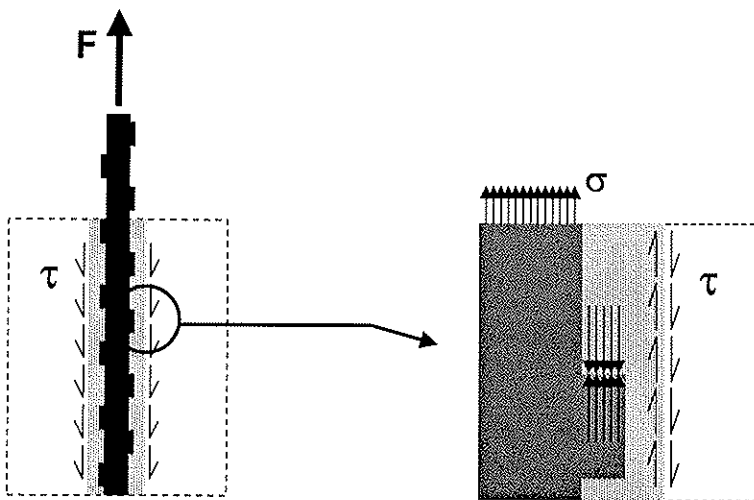


Figure 2.2:
Load transfer in the bond

The functions of the glue are the distribution of the force along the rod axis between the ribs and the load transfer to the timber. The result is a shear stress in the glue line. The load transfer to the timber takes place trough adhesion, as a usual glue-connection.

2.2 Failure modes

2.2.1 Failure of the bond

There exist several kinds of bond failure between the steel rods and the timber as described in the following and shown in figure 2.3:

- Failure of the basis of the steel ribs: shear failure in the steel.

- Failure of the glue on the steel ribs: local compression failure of the glue.
- Failure in the glue line: shear failure of the glue.
- Failure of the adhesion between steel and timber: not sufficient adhesion force or simply incorrect gluing.
- Failure of the timber adjacent to the glue line: shear strength of the timber around the hole.

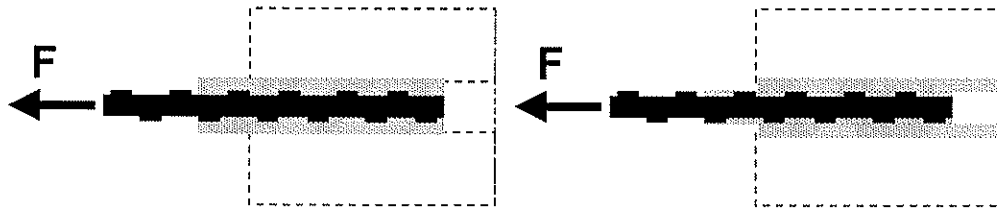


Figure 2.1: Failure in the timber adjacent to the glue-line and failure in the glue-line

The optimal capacity of the bond is reached when the shear failure of the timber occurs. Due to that fact the timber should be the weakest element in the bond or a higher resistance of the other bond elements should prevent all other possibilities of failure.

2.2.2 Other possibilities of failure

Other failure modes for example are the steel failure caused by tension strength in the steel rod or the timber failure outside of the bond. In both cases the bond is not the reason for the failure.

These kinds of failures are important for the correct design of the joints and for the safety of the constructions and therefore must receive attention for design rules. But the resistance of the bond principally does not depend on the possible failure outside of the bond.

In this study only the failure of the bond - as a shear failure of the timber in the hole - is considered. This should give the basic knowledge of the behaviour and the design of joints with glued-in rods. Of course the design of joints or building elements with glued-in rods should consider the possibility of failure outside of the bond.

2.3 Requirement on the bond

The optimal capacity of the bond is reached when a shear failure of the timber occurs. For this a higher resistance should prevent all the other possibility of failure. This can be verified with pull-out tests. When the rod with the layer of glue is pulled out and there are wood fibres on the broken surface, a clear timber failure can be identified. That way the timber resistance specifies the resistance of the bond and the shear strength for the timber in the hole can be described. This is a mechanical property of timber.

The simple requirement, that the failure occurs as a timber failure permits to verify the optimal capacity of the bond. This requirement can be fulfilled with a correct choice of the combination of wood species, rod profile and glue material.

The glue system should assure a strong bond between the steel rod and the timber in order to prevent deformations due to the glue stiffness. This is the case when the stiffness of the glue-line is higher than the timber-stiffness. The glue system should fulfil this requirement.

For the experimental tests different kinds of steel rods (threaded rods and concrete reinforcements steel bars with different ribs) and epoxid-glue-systems were used. The combinations of steel rods and the glue-systems used for the main tests produce always timber failures. Therefore only timber strength outcomes were evaluated. That way the analysis of the timber shear strength is possible.

2.3 Load transfer

2.3.1 Static system and stress distribution

The static system of the introduction of a force trough glued-in rods is the basis for the calculation of the stress in the bond. The distribution of the shear stress in the glue line depends on the size and on the ratio of the stiffness (MOE) and can be analysed with numerical methods. The analysis shows that different shear stress distributions result in case of glued-in rods perpendicular to the grain direction or gluing-in parallel to the grain direction (figure 2.4).

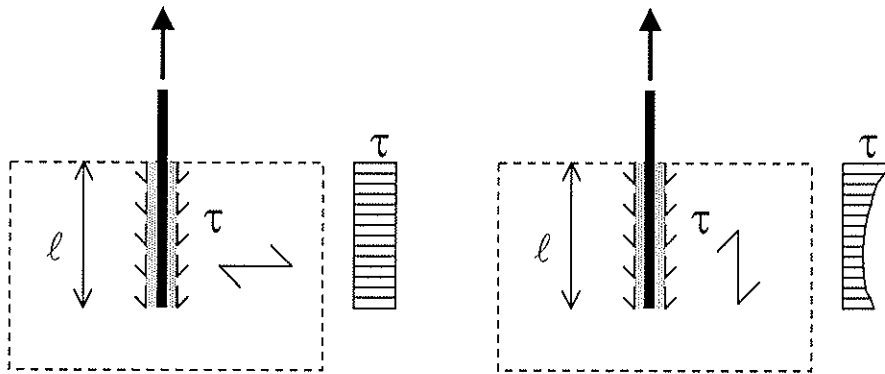


Figure 2.4: Approximation of the stress distribution by gluing perpendicular and parallel to the grain direction

In case of gluing perpendicular to the grain direction a constant stress distribution along the glue-line can be assumed. In case of gluing parallel to the grain direction this assumption is not correct.

2.3.2 Determination of the strength

The shear stress in the glue-line will be calculated under the assumption of a constant distribution by the formula

$$\tau = \frac{F}{\pi \cdot d_a \cdot \ell_e} \quad (2.1)$$

Where: F = axial force on the rod

d_a = hole diameter

ℓ_e = length of the glue-line or anchorage length.

The calculated shear stress refers to the hole surface. In case of a timber failure in the contact surface between the glue and the timber the calculated stress gives the timber strength. In case of gluing perpendicular to the grain direction, the formula exactly gives the strength in the failure surface. Therefore the determined strength is a mechanical property of the timber.

3 Experimental tests and results

3.1 Tests configuration

The pull-out resistance of glued-in rods was tested experimentally. The test configuration is shown in figure 3.1. The height of the specimen varied depending on the anchorage length. The width of the specimens varied between 140 mm and 160 mm.

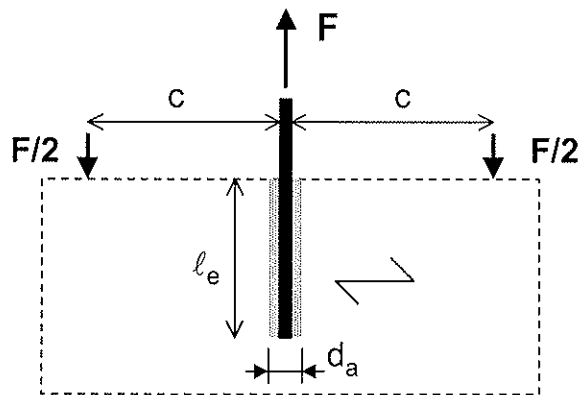


Figure 3.1: Test configuration
 $c = 125 \dots 250$ mm, depending on the equipment

The load was applied at a constant rate of movement and adjusted so that the maximal load was reached within (300 ± 120) seconds.

3.2 Test Material

Glued laminated timber from a normal production was used for the test specimens. For special requirements (for example density) lamellae with specific characteristics were picked out and used for the production of the test specimens. The moisture content of the timber was 12 % at the time of gluing-in of the rods. The density of the specimens was determined before the drilling of the holes.

Most of the tests were carried out with spruce timber. Small series were carried out with beech plywood, beech and oak glue-lam.

For the rods threaded bars and concrete reinforcement steel bars were used. For the gluing different - especially for glued-in rods developed - epoxid-glue-systems were used. Several tests series on glued-in rods perpendicular and parallel to the grain direction were carried out.

3.3 Determination of the timber strength

In this paper only the results of gluing-in perpendicular to the grain direction are presented and discussed. In this case the requirement, that the failure occurs as a timber failure is very simple and permits to verify the optimal capacity of the bond. Preliminary tests have shown, that this requirement can be fulfilled with a correct choice of the combination of wood species, glue material and rod profile. Therefore the results describe the shear

strength of the timber as a mechanical property of the timber. The strength values are calculated according to 2.3.2.

The timber strength varies depending on several factors. The presented tests were carried out and evaluated in order to determine the influence on the strength of the following factors: wood species, length of the glue line (anchorage length), diameter of the hole and density of the timber.

3.4 Results

About 200 experimental tests of glued-in rods perpendicular to the grain direction with spruce timber and 42 tests with beech timber were evaluated.

3.4.1 Influence of the anchorage length

The influence of the anchorage length is shown in figure 3.2 and 3.3. The results in figure 3.2 refer to tests with steel-rods with a 16 mm diameter and a hole diameter of 20 mm. The anchorage lengths vary from 50 up to 250 mm. Therefore the length to hole diameter ratio varies between 2.5 and 12.5. A variation of the strength depending on the anchorage length is not given.

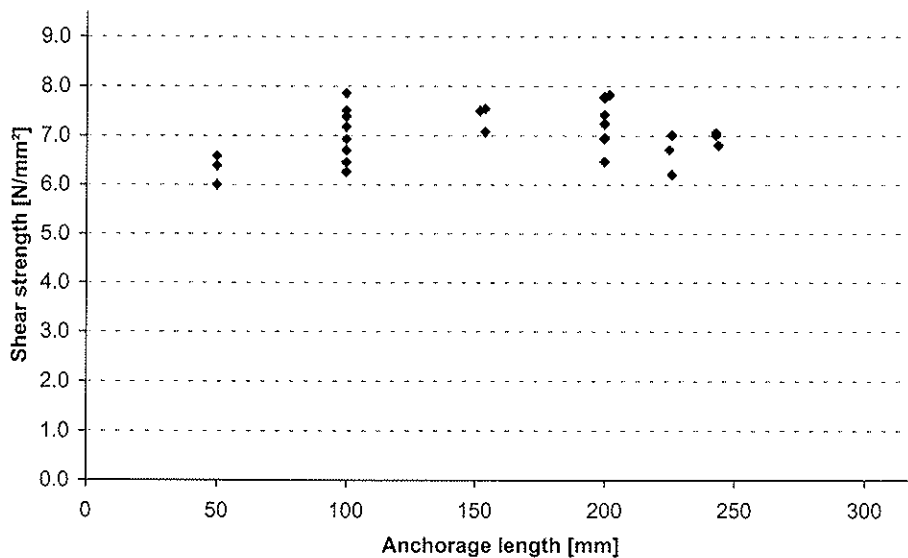


Figure 3.2: Relation between shear strength and anchorage length.
Hole diameter $d_a = 20$ mm, $n = 30$

The results of pull-out tests with the hole diameter 24 mm and anchorage lengths 100 to 350 mm (anchorage length to hole diameter ratio 4.2 to 14.6) are shown in figure 3.3. The influence of the anchorage length is not given.

It was not possible to test glued-in rods with higher values of the ratio length to diameter ratio, because the tension failure of the steel bar occurs.

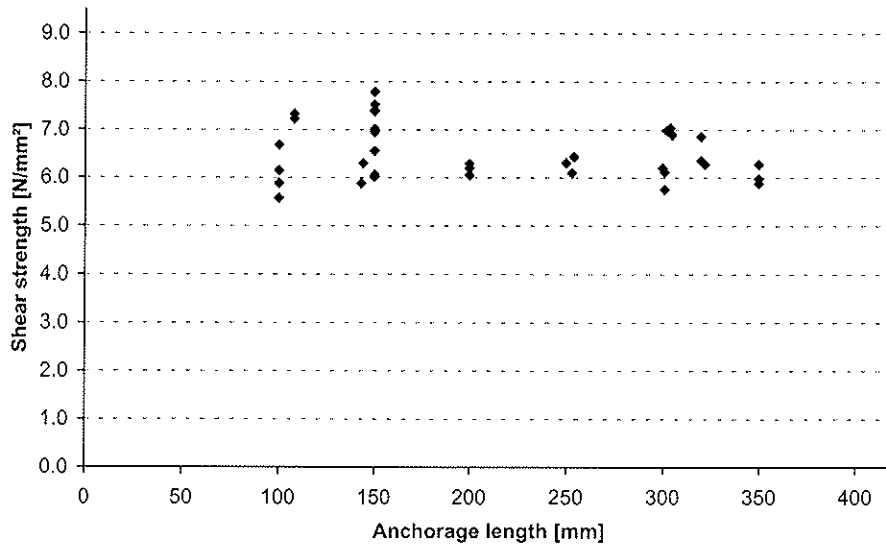


Figure 3.3: Relation between shear strength and anchorage length.
Hole diameter $d_a = 24$ mm, $n = 36$

The high tension stress - over the elastic behaviour - of the steel rods do not influence the timber strength. In case of a "to high" anchorage length the steel breaks outside of the glue-line.

3.4.1 Influence of the density

For the analysis of the influence of the density on the shear strength in the hole spruce timber with extreme density values was especially chosen. That way it was possible to have spruce timber elements with a density of 390 up to 570 kg/m³. The strength values from 30 tests with the hole diameter of 20 mm are shown in figure 3.4 and the results of 15 tests with the hole diameter 24 mm and an anchorage length of 150 mm are shown in figure 3.5.

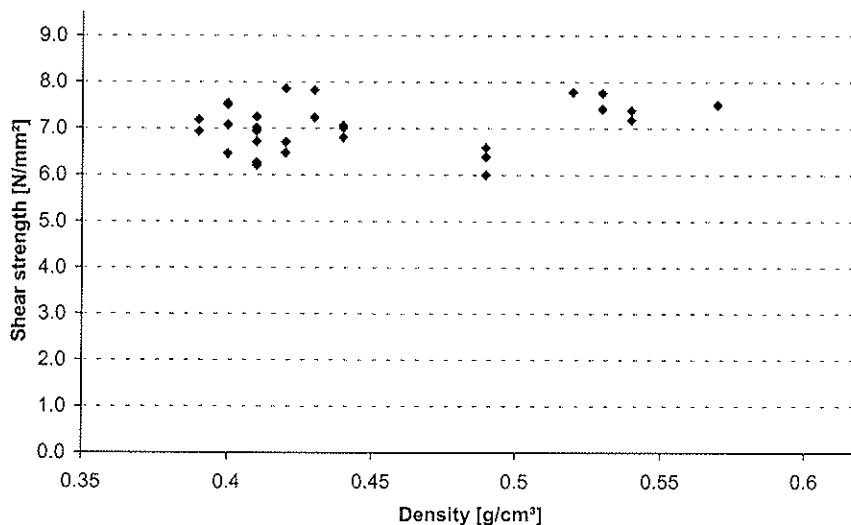


Figure 3.4: Relation between shear strength and density.
Hole diameter $d_a = 20$ mm, $n = 30$

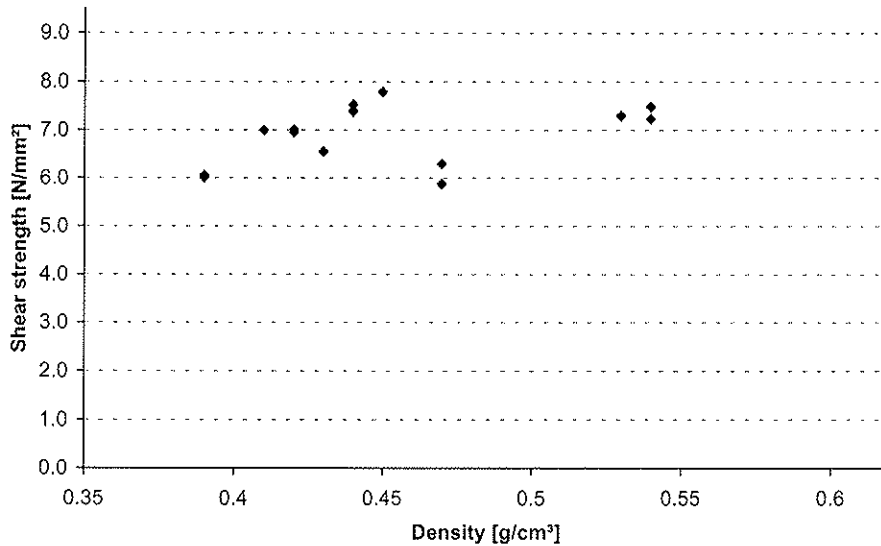


Figure 3.5: Relation between shear strength and density.

Hole diameter $d_a = 20$ mm, anchorage length = 150 mm, $n = 15$

In the figure 3.4 the influence of the density of the strength is non-existent. Also in figure 3.5 it is impossible to determine a clear influence of the timber density. The statistical analysis of all the results shows a very poor correlation between density and strength. In some cases it is possible to describe a trend for a relation between density and strength in the formula:

$$\tau \approx \rho^c \quad \text{with } c = 0,0 \dots 0,3 \quad (3.1)$$

Therefore on the basis of the results it is not possible to describe a clear influence of the density on the strength. The figures and the statistical evaluation show that the density has a slight influence on the strength.

3.4.3 Influence of hole-diameter

Figure 3.6 shows the results of 65 tests with different hole diameters. The density of the timber specimens varies between 0.39 and 0.45 t/m³.

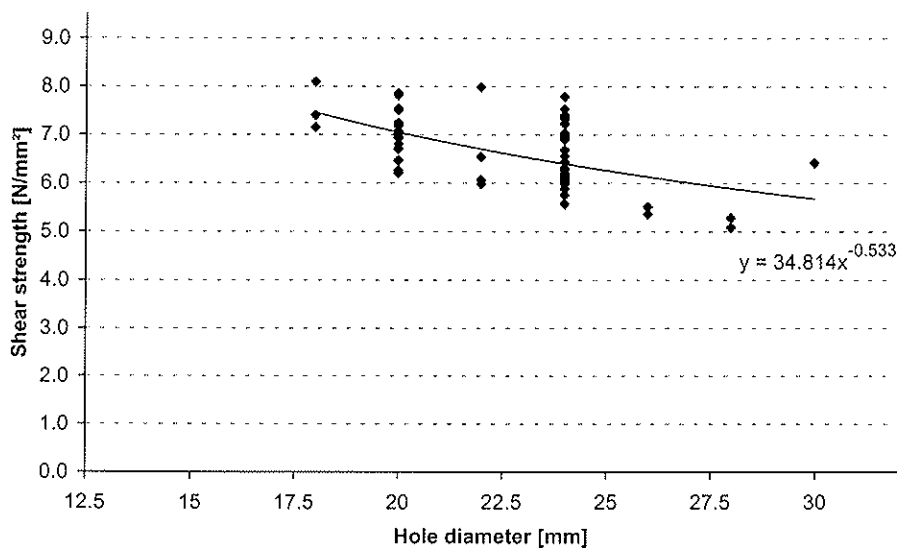


Figure 3.6: Relation between shear strength and hole diameter,
Hole diameter $d_a = 20$ mm, $n = 64$

The variation of the strength is proportional to the hole diameter with the exponent -0.5:

Figure 3.7 shows the results of about 174 tests regardless of anchorage length and density. The hole diameters vary from 12 up to 30 mm, the anchorage length from 50 up to 350 mm and the density from 0.39 up to 0.55 t/m³.

The continuous line in figure 3.7 corresponds to the curve

$$\tau = 32 \cdot d_a^{-0.5} \quad (3.2)$$

τ = shear strength in N/mm²

d_a = Hole diameter in mm

The formula (3.2) permits to describe the timber shear stress in the hole as a function of the hole diameter.

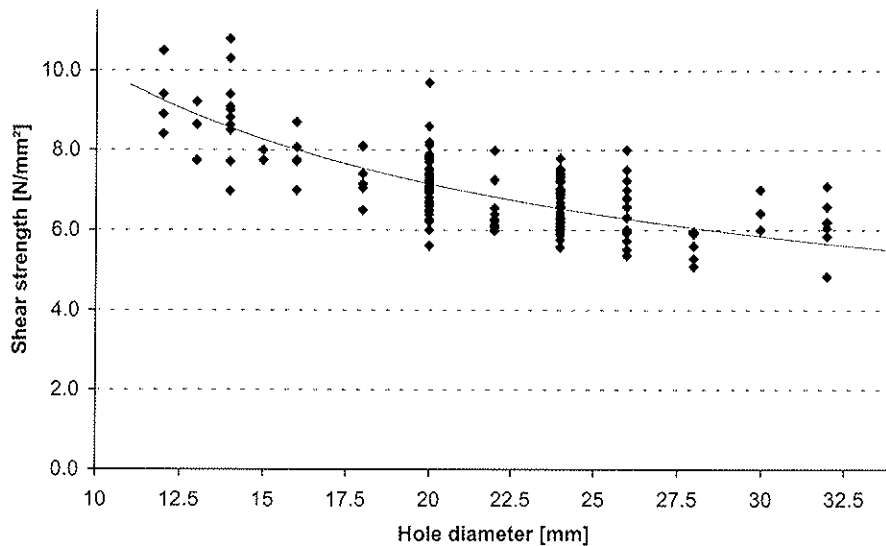


Figure 3.7: Relation between shear strength and hole diameter.
n = 174

3.4.4 Influence of the wood species

The described timber shear strength in the hole is a mechanical property of the timber and depends on the wood species. Only few tests were carried out with beech and oak timber and an important problem was the resistance of the glue. Due to the higher timber strength a higher stress in the glue-line than with spruce timber results. For this reason not all the tested glue systems are suitable for application on glued-in rods with other wood species than spruce.

Figure 3.8 shows the strength difference on spruce and beech timber. The number of results on values for beech timber is too small to give an exact evaluation of the results and to describe the strength of beech timber. But it is interesting that the strength values for beech timber are about 100 % higher than for spruce timber.

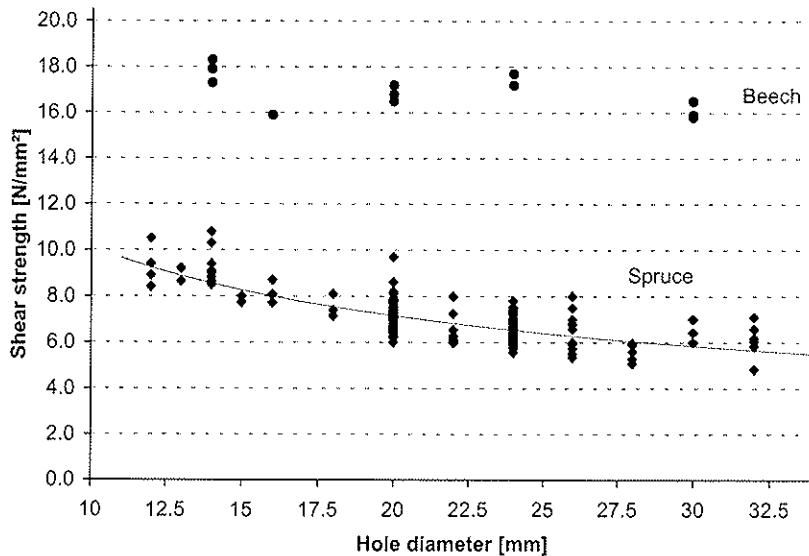


Figure 3.8: Relation between shear strength and hole diameter.
n (Spruce) = 174, n (Beech) = 16

4 Discussion and conclusions

4.1 General remarks

The requirement that the failure of the bond takes place as a timber failure permits to reach the optimal capacity of the bond. That way the requirement on the steel rods and the glue systems for glued-in rods are clearly defined.

The resistance of the bond is now given as a timber shear resistance in the hole. The results of the pull-out tests on glued-in rods with spruce timber show, that this strength is not depending of the length of the glue-line. This confirms the results from the numerical analysis of the static problem and the fact, that the shear stress is constant along the glue-line. The determination of a maximal length of the glue-line is principally not necessary because in case of a too high anchorage length the tensile strength of the rod can be reached. Tests were carried out with anchorage lengths up to 15 times the hole diameters.

The influence of the timber density is very slight. The results from several tests show a very bad correlation between strength and density. In some cases it was not possible to determine a correlation with the density. In other cases the correlation of the strength with the density was possible. This bad correlation can be written in form of exponent of the density: the exponent varies from 0.0 (no correlation) up to 0.3. The design rules of the informative annex A of prEN 1995-2 (1997-01-14) and of the informative annex A of prEN 1995-1-1 (final draft 2001-04-09) with the strength of the timber as function of the density with the exponent 1,5 can definitely not be confirmed or experimentally verified.

The timber strength depends on the diameter of the hole as shown in chapter 3.4.3. The reason for this probably is the size effect. The fact, that a very similar correlation between strength and the hole diameter has been founded on the figures 3.6 and 3.7 (with and without consideration of the variation of the density) confirms the assumption, that the influence of the density on the strength is very slight.

4.2 Suggestion for a design rule

The strength of the bond of glued-in rods perpendicular to the grain direction is given by the timber shear strength. This timber strength depends principally on the diameter of the hole. The influences of the timber density and of the anchorage length are very slight and can be disregarded.

The mean values of the timber strength in the hole of spruce timber with gluing perpendicular to the grain direction can be described with the formula 3.2. The characteristic values of the strength can be calculated as

$$\tau = 25 \cdot d_a^{-0.5} \quad (4.1)$$

Where: τ = shear strength in N/mm²

d_a = Hole diameter in mm

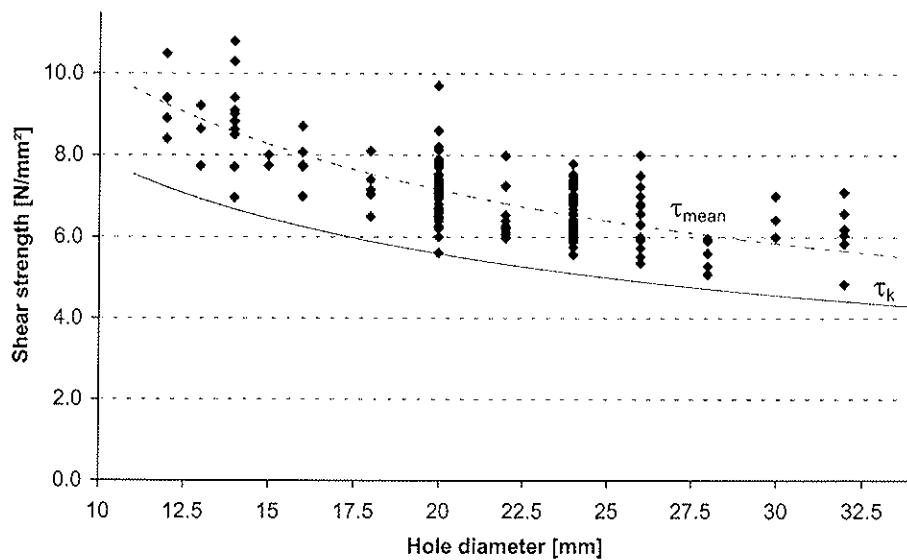


Figure 4.1: Experimental test results and suggestion for design rule,
n = 190

Figure 4.1 shows the results of 190 experimental pull-out tests with the curve of the proposed simple design rule.

That way it is possible to calculate the resistance of the bond for the introduction of forces into the timber with a single glued-in rod. The single glued-in rod should be considered as a single fastener. The design of joints or building elements with several glued-in rods should certainly consider the possibility of failures outside the single glued-in rod.

5 Bibliography

Kangas, J.: Design of joints based on in V-shape glued-in rods. CIB-W18A, Athens, Georgia, 1983.

Riberholt, H.: Glued bolts in glulam - Proposal for CIB Code. In Proceedings of the 21th Meeting of CIB-W18, CIB-W18A/21-7-2, Vancouver, 1988.

Turkowski, S. B.: Designing of glued wood structures joints on glued-in bars. In Proceedings of the Meeting of CIB-W18, CIB-W18A/22-7-13, Berlin, 1989.

- Zubarev, N. G.; Boitemirov, F. A.; Golovina, V. M.: Joints on glued-in steel bars present relatively new and progressive solution in terms of timber structure design. In Proceedings of the Meeting of CIB-W18, CIB-W18A/22-7-11, Berlin, 1989.
- Buchanan A. H.; Moos, P. J.; Townsend, P. K.: Reinforcing bars epoxy bonded in glue laminated timber. International timber engineering conference, Tokyo, 1990, p. 601-610.
- Turkowski, B.: Prefabricated joints of timber structures on inclines glued-in bars. International timber conference, London, 1991, p. 3.1143-3.157.
- Johansson, C.-J.; Serrano, E.; Gustafsson, P.J.; Enquist, B.: Axial strength of glued-in bolts. In Proceedings of the Meeting of CIB-W18, CIB-W18/28-7-9, Copenhagen, 1995.
- Bernasconi, A.: Tragverhalten von Holz senkrecht zur Faserrichtung mit unterschiedlicher Anordnung der Schub- und Biegearmierung, Holztechnologie ETH Zürich 96-3, Zürich, 1996.
- Gehri, E.: Background paper on glued-in rods, Axially loaded rod - failure of individual rod. Document CEN/TC 250/SC5:108rev., Zürich, 1997.
- Eurocode 5: Design of timber structures, Part 2: Bridges, Draft July 1997.
- Steinmetzler, J.: Krafteinleitung in das Holz mittels eingeleimter, axial beanspruchter Anker, Diplomarbeit Fachbereich Biologie der Universität Hamburg, 1998, 119 Seiten.
- Blass, H.J.; Lasekewitz, B.: Effect of spacing and edge distance on the axial strength of glued in rods. In Proceedings of the 32nd Meeting of CIB-W18, CIB-W18/32-7-2, Graz, 1999.
- Fabris, A.: Verhalten von Verbindungen mit axial beanspruchten, eingeleimten Stäben. In Verbindungstechnik im Holzbau, SAH Fortbildungskurs 2000, Lignum, Zürich, 2000.
- Eurocode 5: Design of timber structures, Part 1.1, General rules and rules for buildings, Final Draft prEN 1995-1-1, 2001-04-09.
- Fabris, A.: Verbesserung der Zugeigenschaften von Bauholz parallel zur Faser mittels Verbund mit profilierten Stahlstangen, Dissertation ETHZ Nr. 14050, Zürich, 2001.
- Bernasconi, A.: Axially loaded glued-in rods for high capacity joints - Behaviour and resistance. Proceeding of the Symposium on joints in timber structures, 55th Rilem annual week, Stuttgart, Germany, September 2001.

**INTERNATIONAL COUNCIL FOR RESEARCH AND INNOVATION
IN BUILDING AND CONSTRUCTION**

WORKING COMMISSION W18 - TIMBER STRUCTURES

**EMBEDDING CHARACTERISTICS ON FIBRE REINFORCEMENT
AND DENSIFIED TIMBER JOINTS**

P Haller

J Wehsener

T Birk

Faculty of Civil Engineering, University of Technology, Dresden

GERMANY

Presented by: P Haller

- H J Larsen questioned whether the difference in performance in the connection using different type of fibre glass versus aramid was a result of different fibre type or different volume of fibre.
- P Haller stated that the same weight of fibre was used; therefore, it was a fibre type effect.
- A Jorissen questioned about the improvements to tension perpendicular strength.
- P Haller responded that it would be even more efficient to reinforce for tension perpendicular strength; however, he did not have the numbers at hand.
- V Enjily asked about the cost.
- P Haller responded that with the machine shown large quantity of fibre could be produced at relatively low cost. Although Aramid would be expensive, this research aimed to optimise the connection. Densified wood was done in a hot press. Company doing such densification usually worked in electrical industry and wood can be densified also relatively cheaply.

Embedding characteristics on fibre reinforcement and densified timber joints

Peer Haller, Jörg Wehsener, Tilo Birk

Faculty of Civil Engineering, University of Technology, Germany

1 manufacture of densified wood

Densified wood was made of sawn, kiln dried spruce laminations of good quality. A grading according to knots, grain deviation and other characteristics was not done. The geometry of the section was 2500 x 140 x 100 mm. Moisture content before and after densification was 12 to 15% and 7 to 9% respectively. The initial density ranged from 380 to 530 kg/m³. The densification procedure took place in a conventional hot press.

The manufacturing of compressed wood was realized in three steps: heating, densification and cooling. In the first phase, the warming up of the specimen was done between the hotplates at a low pressure of 0.2 - 0.3 MPa. The heating time can be estimated roughly at 1 minute per mm thickness of the section. After having reached the necessary temperature throughout the section the plastification of the wood starts.

The plastification, which is related to the softening of the lignin, occurs at a temperature between 100°C and 160°C, so that the density of the wood can be increased easily due to the collapse of the cell walls under transverse pressure. The cells are folded by the thermo-mechanical densification and fixed by the available lignin matrix. The deformation has to be fixed by cooling in the compressed state. Physical and mechanical properties of densified wood strongly depend on pressure, moisture and time in this process.

When the temperature at the centre of the section reached 130 °C the compression started. During the densification process the internal stresses may lead to cracking or damage of the microstructure. The time for compression depends on the thickness of the section and amounts also to about 1 min/mm as a rule of thumb.

The pressure was increased to 2.5 MPa at constant temperature and maintained until the end of the compression.

The compressed wood is kept in this state before cooling for some minutes of „relaxation“. As wood remains still plastically deformable at 100 °C, it has to be cooled down under decreasing pressure to at least 80 °C. Therefore 1 min/mm thickness (densified) is chosen. The densified laminations had no visible checks or deformations with a final thickness of about 50%.

2 material

2.1 solid and densified wood

Determination of strength for bending, tension, compression and shearing

The carrying and deformation behaviour of solid and densified spruce was tested for 5 different types of loadings on 10 specimens each. A summary of the types of loadings, the configuration of the specimen, the density and rigidity as well as mechanical properties is given in table 1.

The execution of the tests took place according to DIN 52185 to 52188 and DIN 52192. For the measurement small clear specimen were stored up to the constant weight in normal climate (20/65) according to DIN 50014. The recording of measurement took place in an testing machine " Zwick " with a multiple displacement gauge.

The determination of the compression strength parallel to the grain (DIN 52185) was carried out with a test rate of 200 N/s (solid) and 400 N/s (densified). If the solid specimen fails perpendicularly to the test axis by shrinking of the cell layers, then glide layers are formed at an angle of 45° to the test axis of densified wood. These however fail in a brittle manner and in the area folded 45° by shear between the annual ring.

The determination of the bending strength (DIN 52186) took place in a three point bending test with a span of 300 mm. The loading rate was chosen 33,3 N/s. The failure mode of densified wood is brittle with short grain. Solid spruce wood dispose of a smaller Young's modulus and failure strength.

table 1 material properties

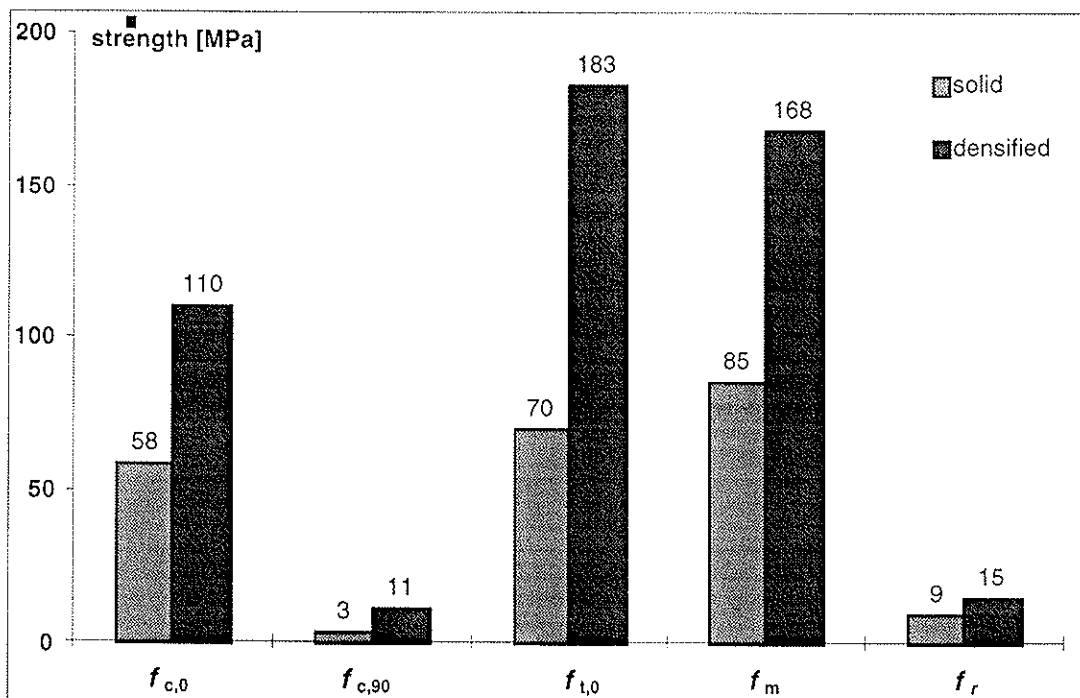
| | densification | $f_{c,0}$ | $f_{t,0}$ | f_m | $f_{t,90}$ | f_r |
|--|---------------|-----------|-----------|-------------|------------|---------|
| u [%] | 0% | 11,2 | 11,7 | 11,8 | 11,9 | 10,6 |
| | 50% | 11,0 | 10,6 | 12,2 | 12,0 | 9,4 |
| ρ [kg/m ³] | 0% | 420 | 421 | 389 | 425 | 403 |
| | 50% | 980 | 964 | 868 | 989 | 891 |
| geometry | 0% | 20x20x30 | 20x20x30 | 20x20x400 | 20x6x470 | 50 x 45 |
| | 50% | | | | | |
| ϵ [%] | 0% | 0,37 | 1,28 | f = 8,01 mm | 0,57 | |
| | 50% | 0,42 | 1,48 | f = 7,64 mm | 0,59 | |
| F_{max} [kN] | 0% | 20,9 | 1,0 | 1,49 | 8,9 | 19,6 |
| | 50% | 47,8 | 4,6 | 2,97 | 21,2 | 33,2 |
| Rm [N/mm ²] | 0% | 57,8 | 2,5 | 85,2 | 69 | 8,8 |
| | 50% | 122,0 | 1,1 | 168,5 | 183 | 14,7 |
| youngs modu- lus [N/mm ²] | 0% | 15429 | 195 | 12483 | 12000 | |
| | 50% | 27574 | 746 | 17694 | 31000 | |

The determination of the shear strength along the grain (DIN 52187) takes place in a special shearing device. The test rate was 2.0 (solid) and 3.0 mm/min (densified). Densified wood behaves stiffer and stronger.

The determination of the tensile strength (DIN 52188) parallel to the grain was executed with a test rate of 250 N/s. The failure of the solid wood was less brittle perpendicularly to the test axis, whilst for densified wood a brittle, shortgrain failure takes place.

The determination of the compression strength perpendicular to grain (DIN 52192) was carried out at a test rate of 15 N/s (solid) and 50 N/s (densified). Due to the thermo-mechanical compression in radial or tangential direction the rigidity increases considerably in comparison to the solid wood. Solid test specimen fail perpendicularly to the plane of the test axis by crushing of cell layers, while the densified wood samples show brittle shear failure between the annual rings.

figure 4 strength of solid and densified spruce wood

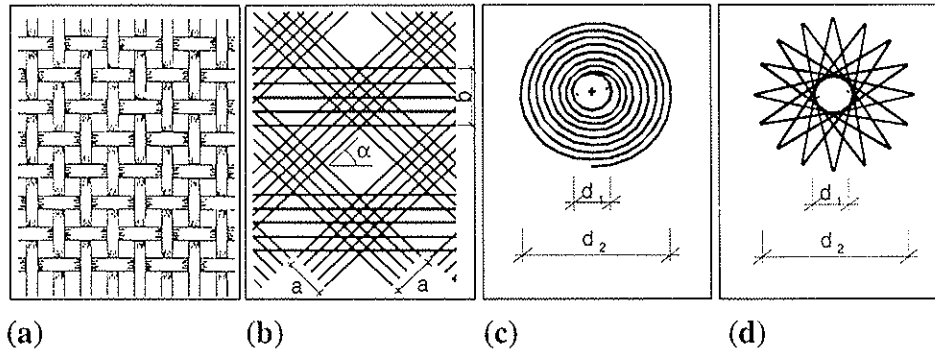


The comparison of the test results shows higher strength and rigidity for the densified wood samples. These samples fail more brittle at lower displacements than normal spruce. In figure 4 the average values of the different types of loading are summarized.

2.2 textile structures

Textile structures were made of multi-axial bonded fabric of various angles and so-called tailored fibre placements (TFP). The manufacturing of the multi-axial structures was done by means of a machine for techniques of stitch bonding which allows the lay up of bundles of rovings of various width. The angles are fixed to 0° and 90° and vary between $\pm 40^\circ$ and 90° . Figure 5 shows some examples of multi-axial textiles reinforcements and TFP-structures which were developed in collaboration with the Textile Institute of University of Technology, Dresden [8].

figure 5 examples of (a) woven fabric; (b) multi-axial stitch bonded fabric (diagonal fibre orientation $\alpha: \pm 40^\circ$); tailored fibre placements (TFP): (c) spiral, (d) star ($d_1 = 25$ mm, $d_2 = 100$ mm)



The TFP's permit an optimal orientation of the fibers with respect to mechanical stresses. These structure were hand made by sewing glass fibre rovings onto a thin non woven polypropylene serving as an application aid. Fibre properties can be seen in table 2 [10].

table 2 fibre properties [11]

| Material | yarn count [tex] | Young's modulus [N/mm ²] | modulus of rupture [cN/tex] |
|--|----------------------------------|--------------------------------------|---|
| E-glass-roving | 2400 | 75000 | 3100-7000 N/mm ² |
| polyethylene non woven | 0.2 (30 g/m ²) | | 80 N/5cm |
| woven fabric (E-glass) | 138 (204 g/m ²) | 12000 | 2400 N/mm ² |
| textile structure 1 (E-glass) set of warp threads: 20 rovings | 1200 (1048 g/m ²) | 12000 | 547 ($\pm 30^\circ$) 554 (90°) |
| textile structure 2 (E-glass) set of warp threads: 20 rovings | 1200 (1302 g/m ²) | 12000 | 547 ($\pm 35^\circ$) 554 (90°) |
| textile structure 3.1 (E-glass) set of warp threads: 5 rovings | 1200 (679 g/m ²) | 12000 | 864 ($\pm 40^\circ$) 1140 (90°) |
| textile structure 3.2 (E-glass) set of warp threads: 10 rovings | 1200 (1249 g/m ²) | 12000 | 542 ($\pm 40^\circ$) 600 (90°) |
| textile structure 3.3 (E-glass) set of warp threads: 20 rovings | 1200 (1581 g/m ²) | 12000 | 547 ($\pm 40^\circ$) 554 (90°) |
| textile structure 4 (E-glass) set of warp threads: 20 rovings | 1200 (1155 g/m ²) | 12000 | 547 ($\pm 45^\circ$) 554 (90°) |
| textile structure 5 (E-glass) set of warp threads: 20 rovings | 1200 (1063 g/m ²) | 12000 | 547 ($\pm 50^\circ$) 554 (90°) |

3 test procedure and results

3.1 test setup

Embedding tests according to DIN EN 383 were carried out on specimens made of clear spruce with a mean density of 380 kg/m^3 . Moreover, densified wood specimens with an average density of 980 kg/m^3 were subjected to the same test. The geometry was $350 \times 120 \times 10 - 70 \text{ mm}$ for loading parallel to grain. The diameter of the bolt was 22 and 25 mm, the edge and end distances were 3 times and 4 to 5 times respectively [9]. The textile reinforcement around the bolt hole had a minimum area of 7800 mm^2 or a diameter of 100 mm in case of the star and spiral TFP. The weight of the bi- and multi-axial bonded fabric was $679 \text{ g/m}^2 - 1581 \text{ g/m}^2$ with a yarn count of 1200 tex. All textile structures were applied by means of an epoxy resin cured at room temperature.

figure 6 specimen geometry for loading parallel (a) and perpendicular to grain (b)

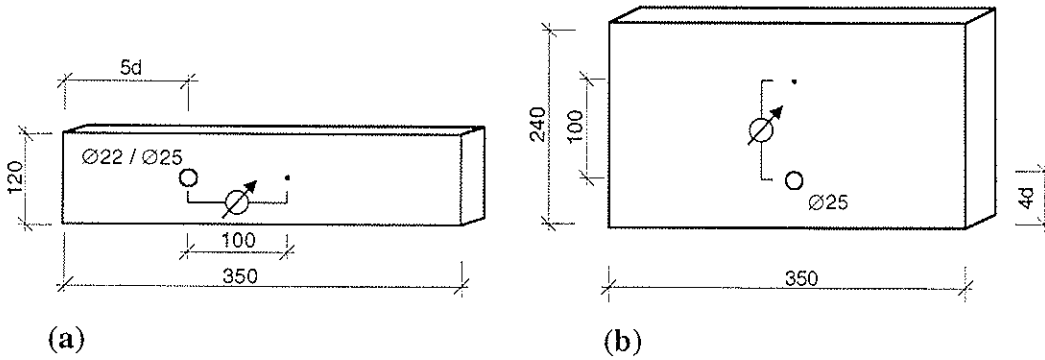


table 3 test parameter

| | parameter | material |
|---|---|---|
| test series I | Ratio of densification - undensified / unreinforced - undensified / reinforced - densified / unreinforced - densified / reinforced | woven fabric (204 g/m^2) epoxy resin dowel diameter ($\text{\O}22 \text{ mm}$) load controlled |
| test series II (a) (b) (c) | Ratio of reinforcement μ - number of textile rovings - thickness of wood - angle of textile fibres | textile structure 1-5 epoxy resin dowel diameter ($\text{\O}22 \text{ mm}$) load controlled |
| test series III (a) parallel to grain (b) perpendicular to grain | Orientation of the fibers - star, spiral, unsupported oval, supported oval, fanlike loop, cross loop, parallel loop | TFP-textile structure epoxy resin dowel diameter ($\text{\O}25 \text{ mm}$) constant cross head speed |

Cross head speed of the testing machine and loading procedure are chosen according to DIN EN 383 (test series I and II: load controlled, test series III: constant cross head speed).

Results were obtained for solid and densified spruce, bi- and multi-axial reinforcements with different ratios of reinforcement loaded parallel to grain as well as TFP's made of glassfibres which were in addition loaded perpendicular to grain. The displacement of the bolt w was measured by means of an inductive displacement transducer (see figure 6).

3.2 results

The tests showed that even small ratios of reinforcement prevent the samples from premature shear failure and that the textile still holds a split specimen together. The effect of reinforcement of the joint on the strength is illustrated in figure 7. Due to the densification and additional reinforcement of the wood the bearing capacity is more than tripled.

The results of the embedding test (figures 8-15) show an increase in load bearing capacity by a factor of 2.9 in case of densified wood with respect to normal solid spruce. All unreinforced specimens failed in a brittle way due to shear and splitting starting from the borehole. The embedding characteristics are intimately related to the density; an additional reinforcement of densified wood led to a further increase of the embedding strength of 35% and in many cases a significant ductility could be observed [2].

The ratio from thickness of wood and glass fibre laminate called the ratio of reinforcement μ .

$$\mu = t_{\text{reinf}} / t_{\text{wood}}$$

figure 7 load-carrying capacity of solid and densified spruce with and without textile reinforcement

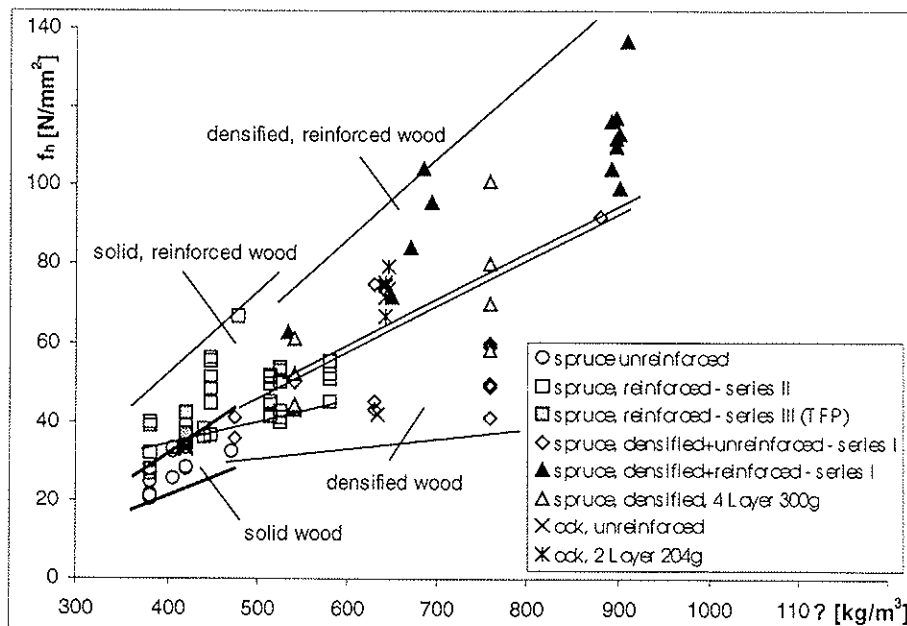


figure 8 load displacement curve of solid and densified spruce with and without textile reinforcement

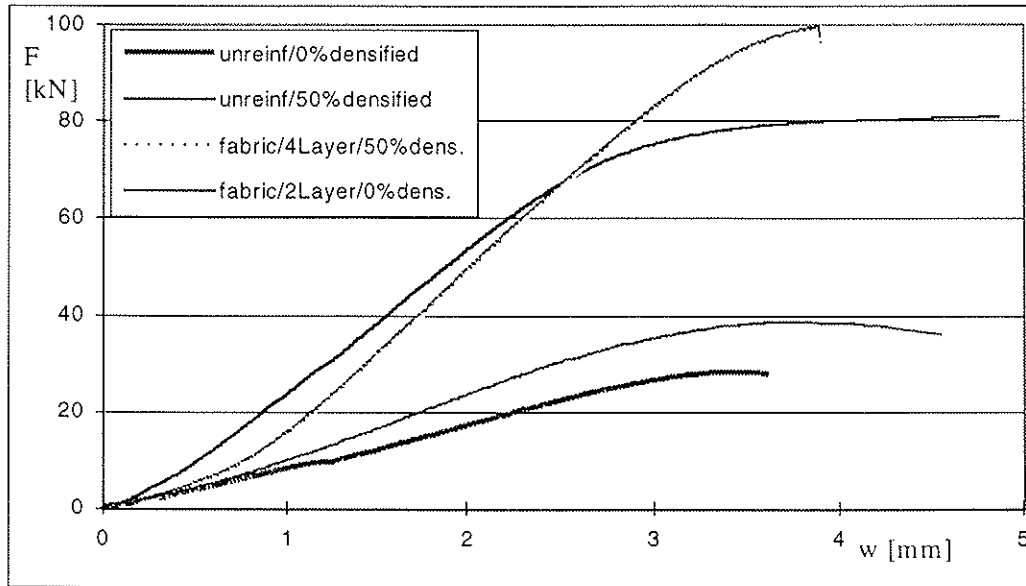


Figure 8 shows the load displacement behaviour of solid, unreinforced and densified, reinforced wood. The influence of the reinforcement on the stiffness is small. It improves however the load-carrying capacity and the failure behaviour of timber joint by prevention of shear- and splitting failure. All textile reinforced timber joints failed ductil. Figure 9 shows that with small ratio of reinforcement μ (textile structure 3.1) an increase of the load capacity was already achieved. A further increase of μ (textile structure 3.3) increased the load bearing capacity by the factor 1.8. The embedding strength f_h and the embedding modulus K_s are compared in figure 10.

figure 9 load displacement curves of reinforced wood with different number of textile rovings

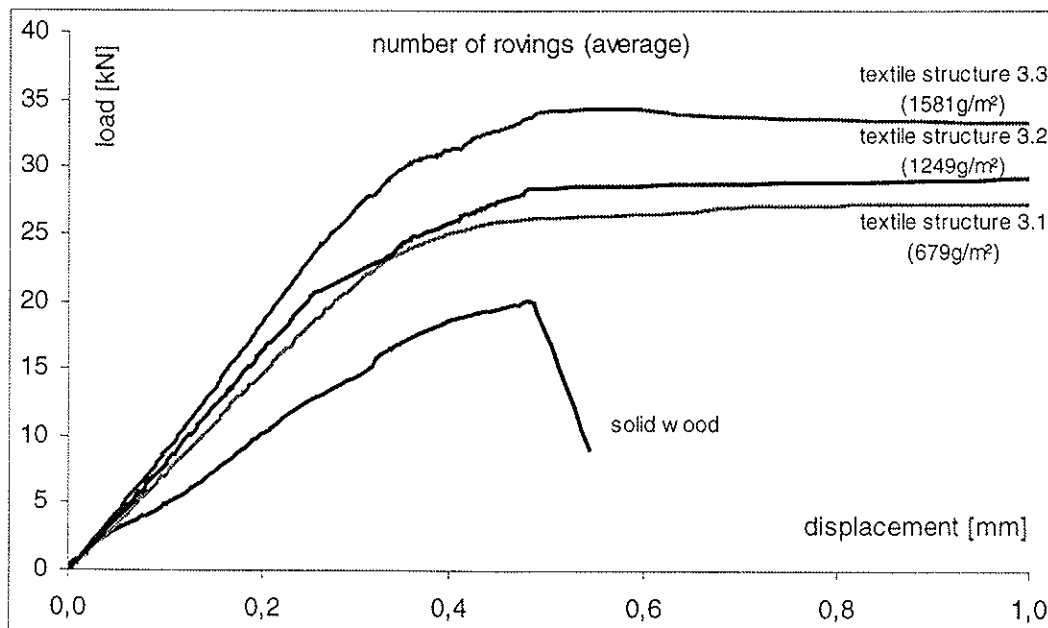
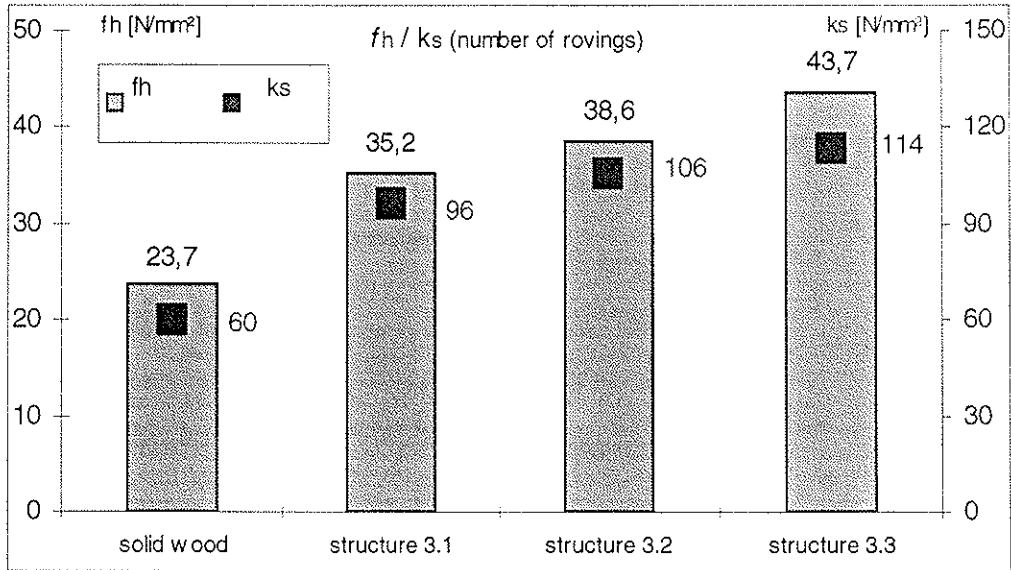


figure 10 embedding modulus K_s and embedding strength f_h for different number of textile rovings



The influence of the reinforcement depends on the ratio of reinforcement μ . Figure 11 and 12 show the load-carrying capacity of different wood thickness by the same reinforcement (textile structure 3.3). With a ratio of reinforcement $\mu < 0.075$ (wood 40 mm / reinforcement 3mm) a small increase of the load-carrying capacity is obtained. The influence of the reinforcement on the rigidity is relatively high with very thin wood specimens in relation to the reinforcement thickness. That failure is initiated in all cases by embedding.

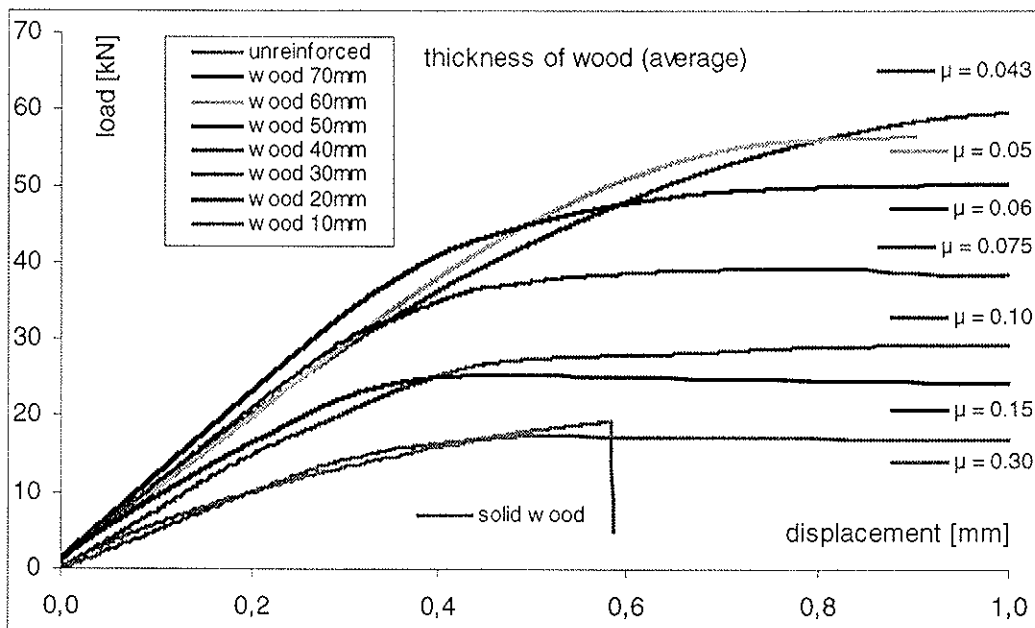


figure 11 load displacement curves for different ratios of reinforcement μ

figure 12 embedding modulus K_s and embedding strength f_h for different ratios of reinforcement (thickness of specimens: 10, 20, 30, 40, 50, 60, 70 mm)

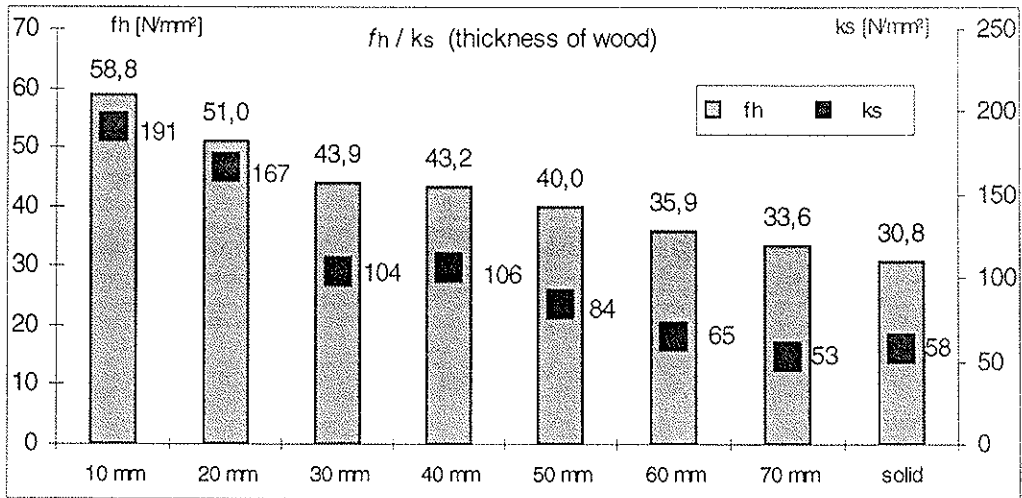
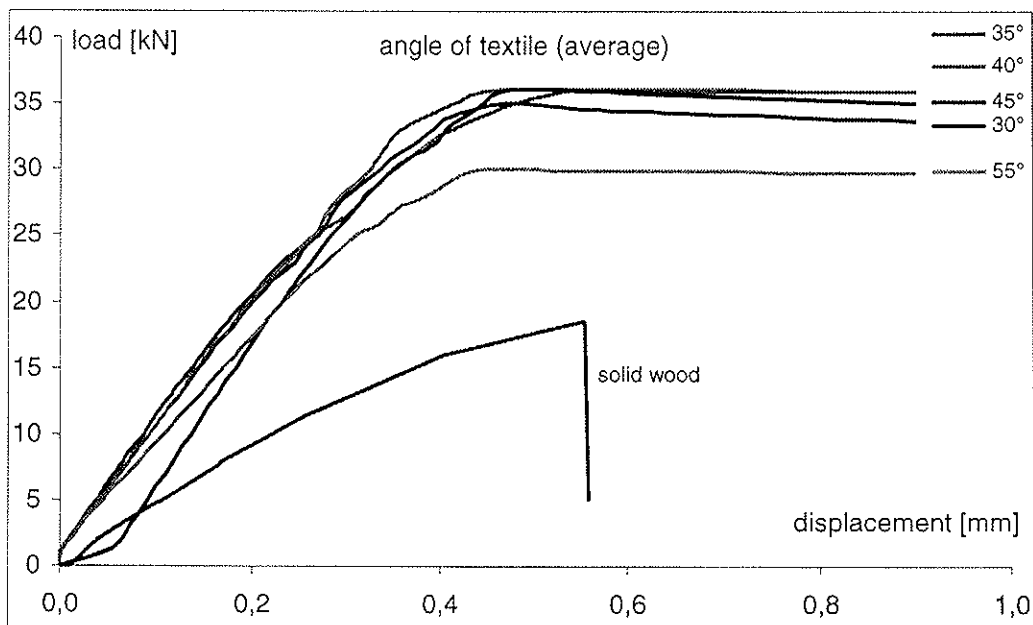


figure 13 load displacement curves for different angles of glass fibre directions (textile structures 1 (+/-30°) to 5 (+/-55°)



In a further test series multi-axial textile structures with different fibre angles from 30° to 55° were applied. The influence of the different fibre angles on the load carrying capacity and stiffness is rather small with this multi-axial textile structures. The failure occurs through replaces the separate roving around the dowel. Other textile structures (TFP) can support the occurring local stresses better. An increase of the load-carrying capacity is achieved on the average by factor 1.5, where the test series with + / - 45° achieved the best values.

figure 14 load displacement curves for different angles of glass fibre directions (textile structures 1 (+/-30°) to 5 (+/-55°); load controlled

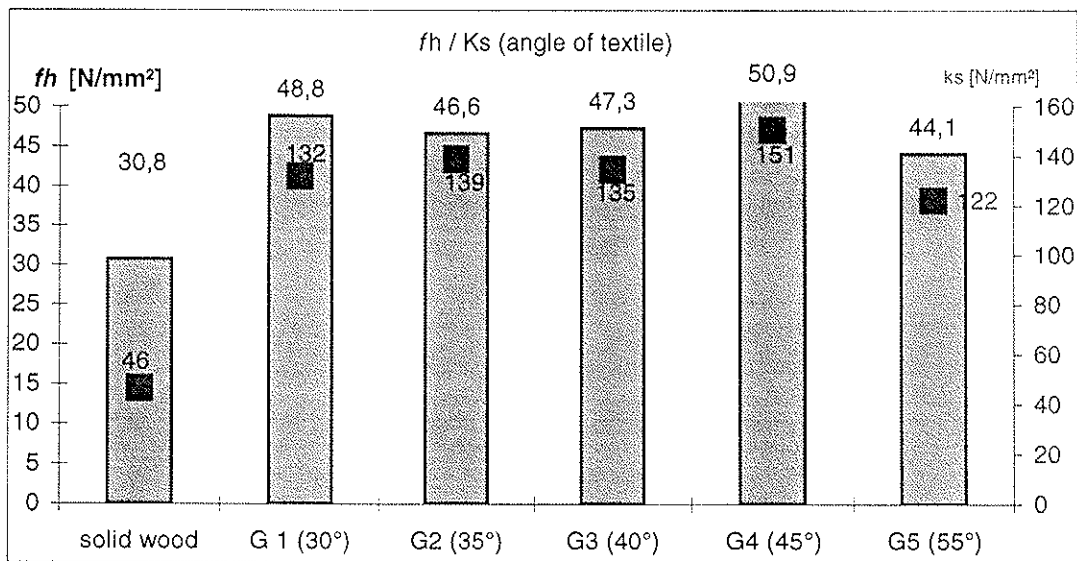


figure 15 embedding modulus K_s and embedding strength f_h for parallel (a) and perpendicular to the grain (b) loaded TFP-structures; travel constant controlled

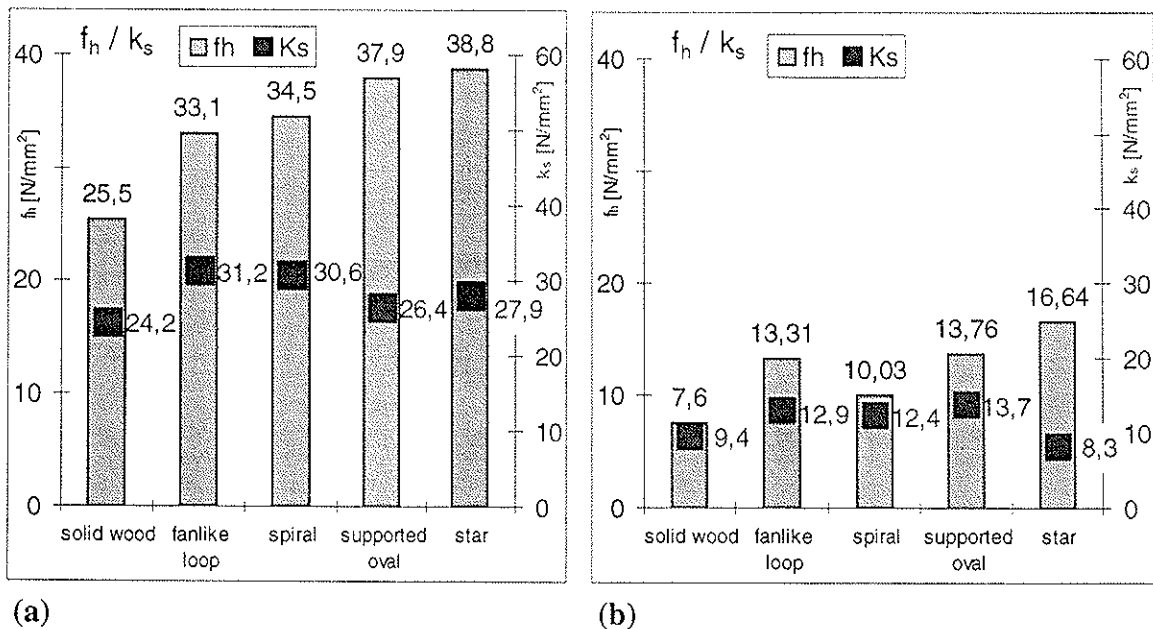


Figure 15 illustrates the effects of the calculated placement of reinforcing fibres. The embedding strength of dowels loaded parallel to the grain is raised to 150 %. The increase in strength is even doubled for loads acting perpendicular to grain. With respect to the stiffness the reinforcement proves to be more efficient with respect to this axis, too. Thus, failure due to exceeding the transverse tensile strength is prevented. In addition, the load-displacement curve shows a more ductile behaviour of the joint. The fracture behaviour is strongly affected by the type of TFP. The fanlike loop fails in a brittle way, whereas star and spiral TFP showed a very ductile behaviour.

table 4 results from embedding test: embedding strength from F_{max} according to EN 383;
(a) test series II, **(b)** test series II, **(c)** test series III

(a)

| | test (textile structure/ wood + laminat) | μ | $\bar{w}_{i,mod}$ [mm] | \bar{K}_s [mm] | \bar{F}_{max} [kN] | \bar{f}_h [N/mm ²] | ν [%] |
|---|--|----------|---------------------------|---------------------|-------------------------|-------------------------------------|--------------|
| I | unreinforced / 30mm solid wood | unreinf. | 0.25 | 49.0 | 28.6 | 32.5 | 5.6 |
| | woven 2 layer / 30+1.2mm solid wood | 0.040 | 0.26 | 64.2 | 38.6 | 43.8 | 8.2 |
| | unreinforced / 30mm densified wood 50% | unreinf. | 0.23 | 111.4 | 80.8 | 91.82 | 4.6 |
| | woven 4 layer / 30+2.4mm densified wood 50% | 0.080 | 0.35 | 99.0 | 99.6 | 113.2 | 11.5 |

(b)

| | test (textile structure/ wood + laminat) | μ | $\bar{w}_{i,mod}$ [mm] | \bar{K}_s [mm] | \bar{F}_{max} [kN] | \bar{f}_h [N/mm ²] | ν [%] |
|-----|---|----------|---------------------------|---------------------|-------------------------|-------------------------------------|--------------|
| IIa | unreinforced / 30mm | unreinf. | 0.184 | 67.9 | 20.6 | 30.8 | 8.8 |
| | textile structure 3.3 / 10+3mm | 0.300 | 0.152 | 66.1 | 17.9 | 62.6 | 7.2 |
| | textile structure 3.3 / 20+3mm | 0.150 | 0.127 | 120.9 | 27.2 | 53.7 | 10.6 |
| | textile structure 3.3 / 30+3mm | 0.100 | 0.175 | 105.0 | 31.9 | 43.9 | 11.0 |
| | textile structure 3.3 / 40+3mm | 0.075 | 0.204 | 126.9 | 44.0 | 46.5 | 12.0 |
| | textile structure 3.3 / 50+3mm | 0.060 | 0.190 | 84.1 | 46.6 | 40.0 | 8.9 |
| | textile structure 3.3 / 60+3mm | 0.050 | 0.214 | 64.7 | 48.1 | 34.7 | 7.2 |
| | textile structure 3.3 / 70+3mm | 0.043 | 0.256 | 53.3 | 53.9 | 33.6 | 9.6 |
| IIb | unreinforced / 30mm | unreinf. | 0.163 | 60.0 | 17.8 | 23.7 | 16.6 |
| | textile structure 3.1 / 30+3mm | 0.033 | 0.146 | 96.4 | 27.2 | 35.2 | 5.5 |
| | textile structure 3.2 / 30+3mm | 0.066 | 0.146 | 105.7 | 30.9 | 38.6 | 8.3 |
| | textile structure 3.3 / 30+3mm | 0.100 | 0.152 | 114.0 | 36.0 | 43.7 | 13.4 |
| IIc | unreinforced / 30mm | unreinf. | 0.184 | 67.9 | 20.6 | 30.8 | 8.8 |
| | textile structure 1 / 30+3mm | 0.100 | 0.148 | 131.8 | 35.4 | 48.8 | 13.7 |
| | textile structure 2 / 30+3mm | 0.100 | 0.135 | 138.7 | 33.8 | 46.6 | 12.1 |
| | textile structure 3.3 / 30+3mm | 0.100 | 0.141 | 134.7 | 34.3 | 47.3 | 8.2 |
| | textile structure 4 / 30+3mm | 0.100 | 0.136 | 150.8 | 36.9 | 50.9 | 7.3 |
| | textile structure 5 / 30+3mm | 0.100 | 0.158 | 122.0 | 32.0 | 44.1 | 8.0 |

(c)

| | test (textile structure/ wood + laminat) | μ | $\bar{w}_{i, mod}$ [mm] | \bar{K}_s [mm] | \bar{F}_{max} [kN] | \bar{f}_h [N/mm ²] | ν [%] |
|------|---|-------|----------------------------|---------------------|-------------------------|-------------------------------------|--------------|
| IIIa | unreinforced wood | 0.100 | 0.457 | 24.2 | 19.1 | 25.5 | 1.3 |
| | spiral | 0.100 | 0.392 | 31.2 | 25.9 | 34.5 | 3.4 |
| | star | 0.100 | 0.386 | 27.9 | 29.1 | 38.8 | 8.2 |
| | fanlike loop | 0.100 | 0.342 | 31.2 | 24.8 | 33.1 | 3.4 |
| | supported oval | 0.100 | 0.425 | 26.4 | 28.4 | 37.9 | 3.6 |
| IIIb | unreinforced wood | 0.100 | 0.646 | 9.4 | 7.1 | 7.06 | 4.8 |
| | spiral | 0.100 | 0.473 | 12.4 | 10.1 | 10.03 | 6.4 |
| | star | 0.100 | 0.533 | 8.3 | 16.8 | 16.64 | 9.7 |
| | fanlike loop | 0.100 | 0.453 | 12.9 | 13.3 | 13.31 | - |
| | supported oval | 0.100 | 0.427 | 13.7 | 13.6 | 13.76 | - |

4 references

1. Franzke, G., Offermann, P., Engler, Th., Abdkader, A., Schierz, M. (2001): *Erkenntnisse zur textilen Kennwertermittlung, geometrischer Modellierung und Fertigung textiler Bewehrungsstrukturen*. Textilbeton – 1. Fachkolloquium der SFB's 528 und 532, Aachen
2. Werner, H (1993): *Tragfähigkeit von Holz-Verbindungen mit stiftförmigen Verbindungsmitteln unter Berücksichtigung streuender Einflußgrößen*. Berichte der Versuchsanstalt für Stahl, Holz und Steine der Universität Fridericana in Karlsruhe, Karlsruhe
3. Haller, P. (1999): *Timber joints in joint research*. Final report of w.g. „timber joints“, COST C1, Semi-rigid timber joints - structural behaviour, modelling and new technologies
4. Larsen, H. J. (1996) *Glass fibre reinforcement of dowel-type joints*. Proceedings of the International Wood Engineering Conference, Vol. 2, New Orleans, USA
5. E. Gehri, E. (1997) *A steel-to-timber dowelled joint of high performance in combination with a high strength wood composite*. International Council for Building Research and Documentation, CIB-W18, Vancouver, Canada
6. Haller, P. (1999) *Textile reinforced timber joints and structures*. Materials for Buildings and Structures. EUROMAT – Volume 6, Weinheim, WILEY-VCH Verlag GmbH
7. Haller, P. (1997) Technische Textilien im Holzbau und ihre Möglichkeiten in der Verbindungstechnik. Bauen mit Textilien, Berlin: Ernst & Sohn
8. Godau, U., Diestel, O., Offermann, P. (1998) *Biaxial-verstärkte Mehrlagengestricke für die Kunststoffarmierung*. Technische Textilien, Frankfurt am Main, 41, S. 202-204
9. Haller, P., Wehsener, J. (1999) *Use of technical and densified wood for Timber joints* Proceedings, 1st International RILEM Symposium on Timber Engineering, Stockholm
10. Birk, T., Haller, P. (2001): *Textile Verstärkung von Holzbauteilen*. Textilbeton – 1. Fachkolloquium der Sonderforschungsbereiche 528 und 532, Aachen
11. Haller, P., Wehsener, J. (2000) *Entwicklung innovativer Verbindungen aus Pressholz und Glasfaserarmierung für den Ingenieurholzbau*, AiF-NR 11164 B / 1, Dresden

**INTERNATIONAL COUNCIL FOR RESEARCH AND INNOVATION
IN BUILDING AND CONSTRUCTION**

WORKING COMMISSION W18 - TIMBER STRUCTURES

GIROD - GLUED-IN RODS FOR TIMBER STRUCTURES

C Bengtsson

C-J Johansson

Wood Materials and Structures

SP Swedish National Testing and Research Institute

SWEDEN

Presented by: C Bengtsson

- H J Larsen questioned the timing for providing information for Eurocode 5. He also questioned the “scientific” ways to consider fatigue test for modelling both the parallel and perpendicular directions.
- C Bengtsson answered that this is an overview paper and the model could be used in both directions.
- J Kangas questioned the 0 to 90 degree interpolation shown on page 3 as it seemed to contradict Hankinson.
- J König and H.J. Larsen had further discussions on the provision of information for Eurocode 5.

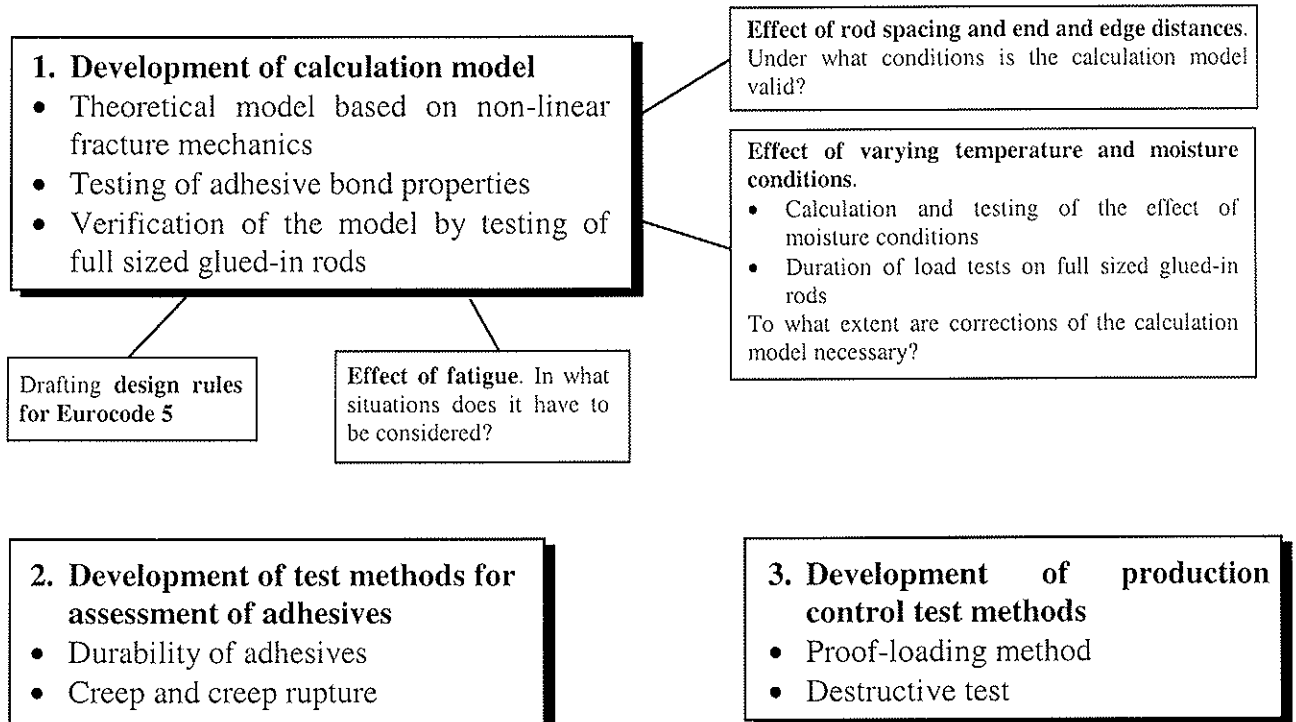
GIROD - Glued-in rods for timber structures

Charlotte Bengtsson and Carl-Johan Johansson

Wood Materials and Structures, SP Swedish National Testing and Research Institute, Sweden

1 Summary and introduction

Glued-in rods have been used during a number of years in several of the European countries which are active in timber engineering. They are economically, architecturally and industrially attractive means of transferring forces within a structure and of providing local reinforcement to critical zones of timber members. They also provide an important technology for the repair and upgrading of historically important timber structures which exist throughout Europe. Notwithstanding their importance, internationally accepted design rules for glued-in rods do not exist. This paper presents the main findings within the EU-project "Glued-in rods for timber structures" (GIROD). The project started in February 1998 and ended in March 2001. The paper is based on summaries written by the different partners in the project: Swedish National Testing and Research Institute (SP, coordinator), University of Lund (Sweden), TRADA Technology Ltd (UK), University of Karlsruhe (Germany) and FMPA in Stuttgart (Germany). Additionally, glulam- and adhesive producers from Sweden and Germany participated in the project. The main structure of the project is given below:



Within the GIROD-project the work is focused on rods glued-in with three different adhesive types: two-component epoxy (EP), two-component polyurethane (PUR) and

phenol-resorcinol-formaldehyde (PRF). Mainly steel rods were used within the project but also some fiber reinforced plastic rods (FRP) were tested.

The description of the GIROD-project given here is based on the project structure given above.

2 Objectives

The objective of the GIROD project is to provide the information required to prepare standards that will allow an increased, more advanced and more reliable use of glued-in rods in timber structures. When the project started the working plan was as follows:

1. Perform theoretical and experimental work leading to a calculation model for axially loaded glued-in rods based on the adhesive bond properties as well as the wood and rod material properties. This must take into account the effect of varying climatic and loading conditions as well as fatigue. This step will give information required by CEN.TC250/SC5 in the preparation of Eurocode 5 - Design of Timber Structures.
2. Develop test methods for the evaluation of adhesives for glued-in rods with respect to strength, durability, creep and creep rupture behaviour under different climatic conditions. This will support the work of CEN.TC193/SC1.
3. Derive test methods for the production control of structural glued-in rod connections. This will support the work of CEN.TC124/WG6.

3 Development of a calculation model

3.1 Proposal of an engineering formula

This work was performed by the University of Lund, Sweden. The objective was to establish a calculation model for the basic pull-out strength, that can be used as a basis for establishing design rules for glued-in rods and for creating a better understanding of the mechanical behaviour of glued-in rods. The work was organised in four parts:

1. Theoretical work on models for stress and strength analysis
2. Bond line tests of mechanical properties
3. Full scale joint test for calibration and verification
4. Verification of model and design equation proposal

The main aim was to propose a strength design method which fulfilled the following requirements:

- The method should be both general and simple, preferably just one or a few explicit equations.
- The equations should have a rational theoretical and physical basis.
- The method should give reasonably accurate strength predictions, on the average, and in general give predictions on the safe side.

The combined Volkersen-Fracture mechanics theory was used as a basis. The pull-out strength according this theory is determined by the geometry of the joint and by two bond line and material property parameters. It is proposed that these two parameters are determined by testing the pull-out strength of two sets of full-scale joints with different geometry (length and/or diameter) and loaded in "pull-compression". Given the two

material parameters, the equation for the “pull-compression” loading is used also for “pull-pull”. This gives a single and simple design equation, which according to theory gives “exact” predictions for the pull-compression loading and predictions on the safe side for pull-pull loading. For definition of the two loading modes see Figure 1a.

The above proposal is intended for adhesives that produce a tight contact to the rod. For adhesives with no bond to the rod and significant shrinkage (i.e. the PRF tested) no equation that fulfils the above basic goals has yet been found. For such adhesives it is proposed that testing is made as for the common adhesives, but no design equation is proposed, only a design rule saying that the load bearing capacity of joints with greater or equal rod diameter, greater or equal length, and greater or equal wood density may be assigned the same load bearing capacity as the tested joint.

For the loading case pull-compression:

$$\frac{P_f}{\pi d l} = \tau_f \frac{\tanh \varpi}{\varpi} \quad \text{where} \quad \varpi = \sqrt{\frac{l_{geo}}{l_m}} \quad (1)$$

where l_{geo} is a length parameter defined by the geometry of the joint and the rod to wood ratio for modulus of elasticity:

$$l_{geo} = \frac{\pi d l^2}{2} \left(\frac{1}{A_r} + \frac{E_r / E_w}{A_w} \right) \quad (2)$$

and l_m is a material property length parameter, which can be expressed as:

$$l_m = \frac{E_r G_f}{\tau_f^2} \quad (3)$$

The ratio E_r/E_w can be estimated in an approximate manner. The two parameters to be determined from tests are then τ_f and l_m . (It is thus no necessary to separate l_m into E_r , G_f and τ_f , although this in general is simple since E_r in general is known).

For a square shaped cross section with a centric location of the rod A_w is taken as a^2 , where a is the side length of the square. For other geometry $A_w = a^2$, where $a/2$ is the shortest distance from the center of the rod to an edge of the cross section. This shortest edge distance, $a/2$, may not be less than a distance determined in the project described in section 3.3, presumably $4d_r$. $P_f/(\pi d l)$ for arbitrary inclination, α , of the rod relative to grain may be determined by interpolation between the results for rods along the grain and perpendicular to the grain according to the Hankinson equation. The two material parameters must be determined for both rod to grain orientations.

Table 1. Test results for determination of material property parameters τ_f and l_m .

| Adhesive | d | l | a | l_{geo} | Failure load, P_f | $P_f/(\pi d l)$ | τ_f | l_m | G_f ¹⁾ |
|----------|-----|-----|-----|-----------|---------------------|-------------------|-------------------|-------|---------------------|
| | mm | mm | mm | mm | kN | N/mm ² | N/mm ² | mm | Nmm/mm ² |
| EPOXY | 16 | 160 | 115 | 4070 | 62.61 | 7.79 | 10.5 | 3600 | 1.89 |
| | 16 | 320 | 115 | 16300 | 77.36 | 4.81 | | | |
| PRF | 16 | 160 | 115 | 4070 | 63.83 | 7.94 | 8.9 | 11000 | 4.15 |
| | 16 | 320 | 115 | 16300 | 98.43 | 6.12 | | | |
| PUR | 16 | 160 | 115 | 4070 | 58.98 | 7.33 | 9.7 | 3960 | 1.77 |
| | 16 | 320 | 115 | 16300 | 74.09 | 4.61 | | | |

1) G_f calculated from l_m with the assumption $E_r=205000$ N/mm².

Test results for the pull-out strength at pull-compression loading are presented by Johansson (1999). The parameters τ_f and l_m (and G_f) were determined from these test results for the three adhesives investigated by use of the method described above. This evaluation is indicated in Table 1. The tests refer to loading along the grain and the ratio E_f/E_w was therefore set equal to 18.

The material combinations for which the material parameters were determined have been tested for several other joints, with other geometry and other type of loading. In Figures 1b-1d the design equation compared with those other test results are shown. Each mark in the diagrams represents mean values obtained from series with 6-10 tests in each series. The diagrams include tests carried out at SP with pull-pull loading and pull-compression loading. The diagrams also include tests made at FMPA with pull-pull loading of joints of varying size and shape. Both the results of timber in strength class C35 and three series with timber in strength class C24 are included. For epoxy and PUR, additionally, three previous series are included, see Aicher et al. (1999) and Gustafsson and Serrano (2001).

For the PRF the test results do not comply with the theoretical curve, but the diagram also shows a scattered picture, indicating that $P_f/(\pi dl)$ may hardly be described as a function of l_{geo} . The results found for PUR and epoxy are more appealing: the design equation gives reasonable predictions and the predictions are in most cases on the safe side.

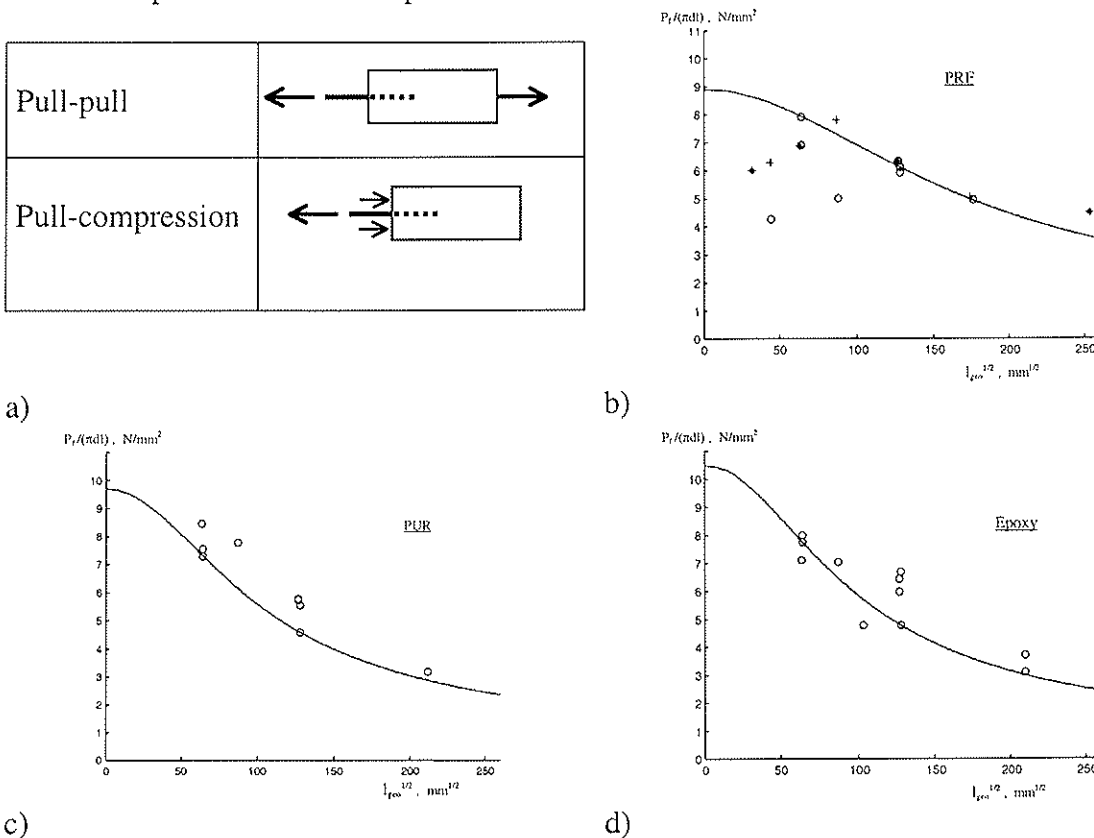


Figure 1. a) Definition of loading modes.
 $P_f/(\pi dl)$, N/mm^2 , versus square root of l_{geo} , $l_{geo}^{1/2}$, $mm^{1/2}$, for (Figures from Gustafsson and Serrano 2001.):
 b) PRF
 c) PUR
 d) EP

The different results found for the three adhesives are most probably related to the different ways in which the bondlines act. For PUR and epoxy there can be tensile stress (and very small deformation) in the critical region normal to the bond area. For the PRF there may be compressive stress (and significant deformation) normal to the bond area.

Above one single design proposal has been discussed. Possible modifications giving alternative, yet similar, proposals include:

- No consideration of grain to rod angle. Testing and all design made as for parallel orientation.
- No consideration of different loading conditions (pull-pull, pull-compression, pull perp. to beam). Testing and all design made as for pull-pull. Eq (1) replaced by the corresponding equation for pull-pull.

3.2 Effect of fatigue

This work was performed by TRADA Technology Ltd, UK. In the future, glued-in rods will be common in timber bridges, where fatigue may be a significant issue. The objective was to give an indication of whether or not the fatigue behaviour of glued-in rods may limit their use in certain applications, for instance in bridges. Bonded-in steel rod specimens were exposed to low frequency (approximately 1 Hz) cyclic tension fatigue ($R=0.1$) at fixed stress rates. The test configuration is shown in Figure 2a. Four distinct failure modes were observed through the tests: rod failure, failure in the adhesive (causing breakdown of the material in the bond-line itself), failure in the wood substrate and failure at the interface between timber and adhesive. The majority of the fatigue failure modes are relatively consistent with static test observations. From the results, it is apparent that fatigue does have the potential to cause damage in bonded-in rods, and that there is sufficient variation in failure modes to confirm that failure may be due to damage in any of the component materials (steel rod, adhesive or timber substrate) or breakdown of the timber to adhesive bond interface. The data obtained from the tests at $R=0.1$ (i.e. maximum tensile load = 10 x minimum tensile load) is presented in the form of cycles to failure versus load in Figures 2b-2d. It must be noted that observations and projected fatigue lives presented herein must be taken in the context of extrapolations based upon a limited data set, lacking confirmatory data at high numbers of load cycle ($>10^6$).

The work performed has demonstrated that fatigue performance is a significant factor in the performance of bonded-in rods and recommendations are made as to how further work, beyond the scope of GIROD, could improve understanding and design treatment of the fatigue behaviour of these types of connection. In relation to the stated objectives of the study, the experimental study has indicated that the fatigue behaviour of glued-in rods may limit their use in certain applications.

Some key conclusions that can be drawn from this limited experimental study are:

- The majority of fatigue failure modes were common to those observed in static test counterparts to the fatigue test specimens. Significant incidents of alternative failure modes were however also recorded, especially failures in the steel rods.
- It is apparent that different adhesive types behave in fundamentally different ways with respect to the fatigue performance and the eventual mode of failure at the fatigue ultimate limit state.

- Both the geometry of the test specimens and the adhesive type are important under the conditions of this test, but the general order of performance across the adhesive types was found to be consistent between specimen sets.
- The scope for further work to enhance the knowledge and design methods employed is very large.

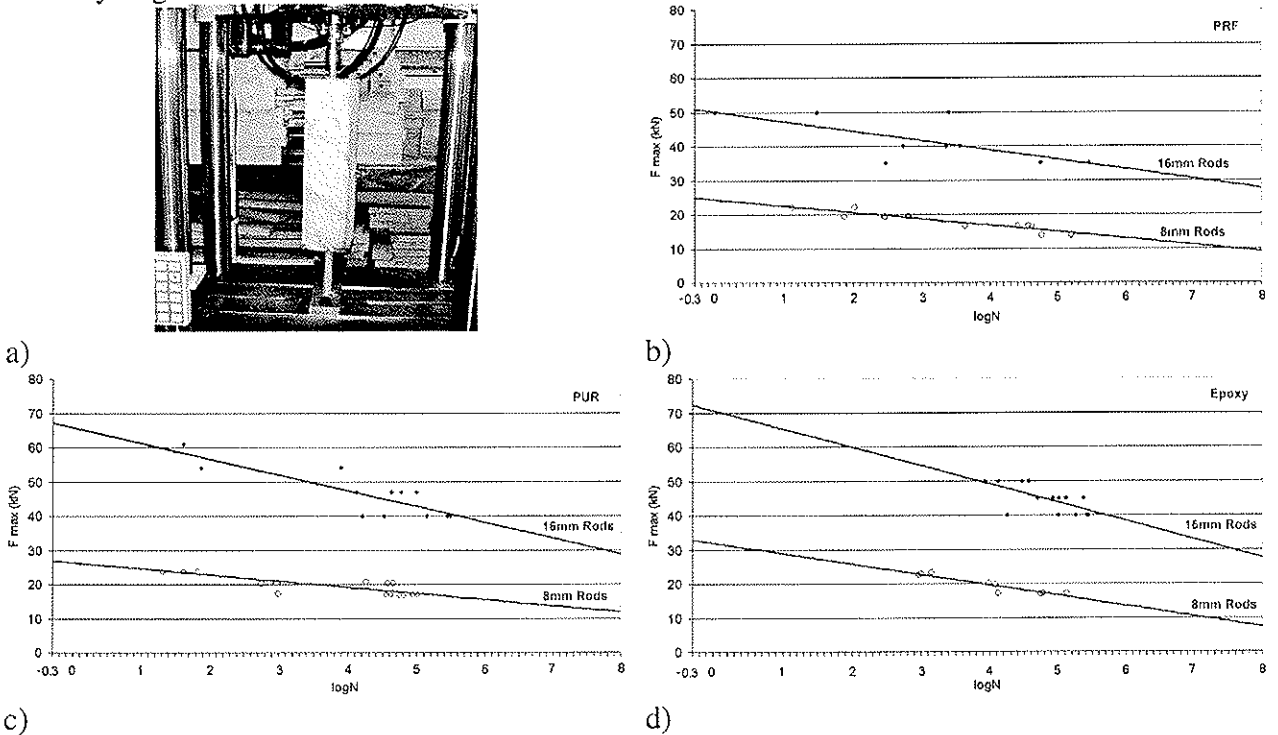


Figure 2. a) Test configuration for fatigue tests
 b) Cycles to failure versus load for PRF-bonded specimens.
 c) Cycles to failure versus load for PUR-bonded specimens.
 d) Cycles to failure versus load for EP-bonded specimens.
 (Figures from Bainbridge and Mettem 2001.)

A full description of failure mode-related fatigue performance basis of design would require further experimentation. To determine the full relationship with geometry and to verify the influence of R ratio and frequency upon the application of design methods based upon the observations drawn from the test set would be key to development of such development.

The results from this part of the work were presented thoroughly by Bainbridge et al. (2000) and Bainbridge and Mettem (2001).

3.3 Effect of rod spacing and edge distances

This work was performed by University of Karlsruhe, Germany. The objective of the work was to study and to quantify the effect of the spacing between rods and the distance to the timber edges on the axial and lateral load-carrying capacity. Tests were performed with rods glued-in parallel and perpendicular to the grain. The loading was axially as well as laterally. Furthermore, some theoretical investigations were carried out to describe the behaviour of glued-in rods depending on spacings and distances of rods.

Examples of results are: For rods glued-in parallel to the grain and loaded axially a rod-to-edge distance of 2.5 times the rod diameter and a spacing of 5 times the rod diameter is suggested. For rods glued-in perpendicular to the grain and loaded axially the load-carrying capacity decreased with increasing height of the beam or a descending ratio of the glued-in length to the height of the beam.

A part of this work was presented thoroughly by Blaß and Laskewitz (1999).

3.4 Effect of varying temperature and moisture conditions

This work was performed by FMPA in Stuttgart, Germany, University of Lund, Sweden and TRADA Technology Ltd, UK. Duration of load (DOL) tests on full-sized glued-in rod specimens were performed in different climates. An investigation concerning to what extent the axial strength of glued-in rods are affected by storage in constant and variable outdoor climates was also performed.

Storage in different variable sheltered outdoor climates without mechanical loading had very little effect on the residual strength in case of PRF. For PUR a strength loss of approximately 20% was obtained and for EP the residual strength increased with about 12%. Comparison was made to the residual strength after storage at 20°/65% RH. Storage of specimens at a constant elevated relative humidity of 85% delivered a drop in residual strength of 20% for PRF-bonded specimens.

Figure 3 summarises the DOL test results for full-sized glued-in rods carried out within the GIROD-project. The Madison curve is given as a reference curve. Also the time spans for load duration classes according to EC 5 are indicated in Figure 3. The EP-bonded specimens at 85% RH followed the Madison curve. At 50°C specially the PUR- but also the EP-bonded specimens displayed a strength drop with respect to time. This is mainly due to the thermo-mechanical properties of these adhesives.

An attempt was also made to derive k_{mod} values accounting for strength degradation with respect to load duration and service class. These results can be found in Aicher (2001).

3.5 Design rules for Eurocode 5

This work was performed by TRADA Technology Ltd, UK. The objective was to elaborate a proposal for design rules for glued-in rods based on the proposed calculation model, taking into account the information gained concerning influence of fatigue, rod spacing, time, temperature and moisture conditions.

The results of this part of the work are a guidance document style set of design rules drawn from the GIROD project and a condensed set of concise design rules more suited to consideration for incorporation in the body of EC5.

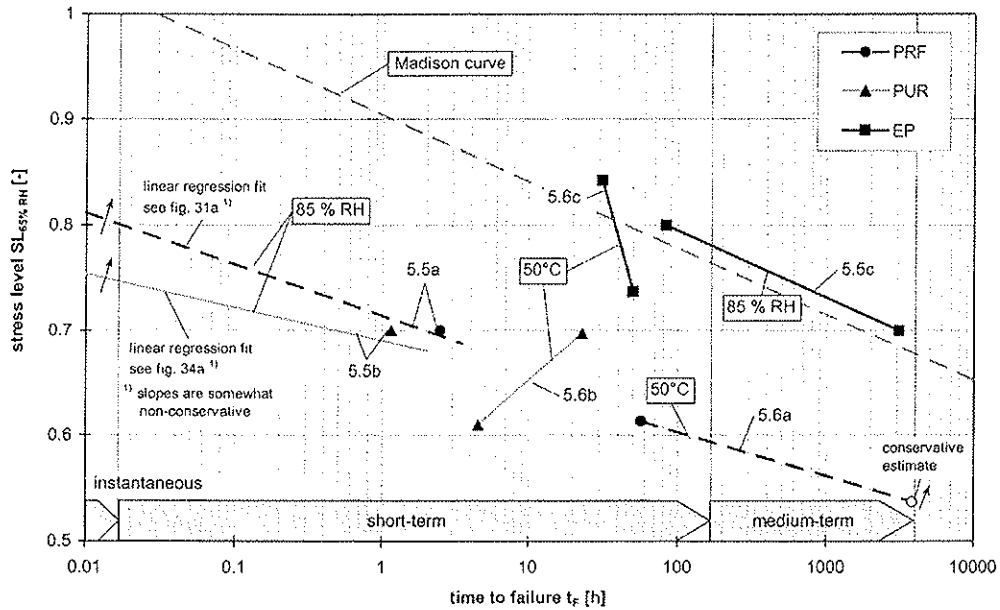
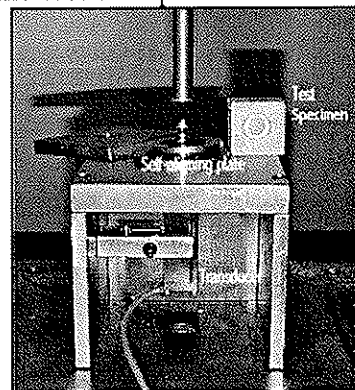
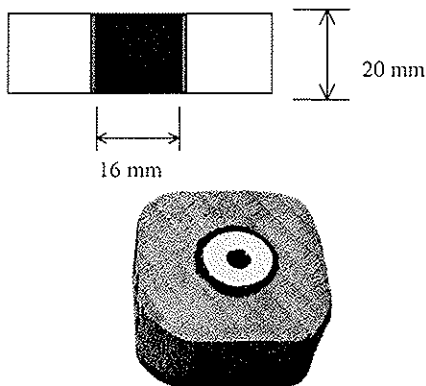


Figure 3. DOL behaviour of PRF-, PUR- and EP-bonded specimens with axially loaded glued-in threaded rods denoted by stress level (SL) versus time to failure (t_f) in wet or warm climate conditions. All stress levels are related to results obtained in ramp loading at 20°C/65% RH. (Figure from Aicher 2001.)

4 Development of test methods for adhesives

This work was performed by SP Swedish National Testing and Research Institute, Sweden. The objective was to develop test methods to evaluate the durability and the creep-rupture properties of adhesives for glued-in rods.

A possible test method for strength and durability of the adhesive for glued-in rods was developed. The suggested method consists of 40 x 40 x 20 mm beech blocks with glued-in 16 mm threaded rods which are tested in compression after different treatments (treatments A4 and A5 according to EN 302). The specimen and the test set-up are shown in Figure 4.



a) The test specimen.
 b) Test set-up for loading in compression.
 (Figures from Bengtsson and Johansson 2001.)

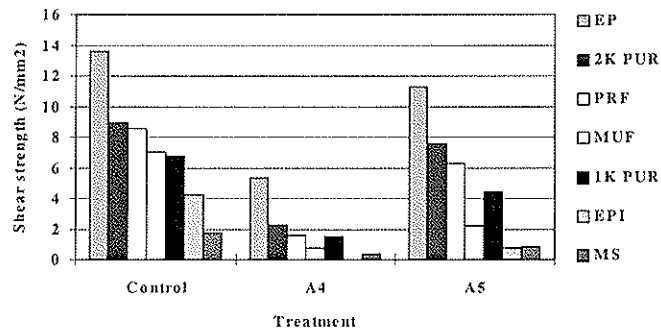


Figure 5. Shear strength (tested in compression). The shown values are average values of ten specimens in each group. (Figure from Bengtsson and Johansson 2001.)

To the three adhesives mainly studied within the GIROD-project, EP, PUR and PRF, four other adhesives were added. These were: melamine-urea-formaldehyde (MUF), one component polyurethane (1K PUR), emulsion-polymer-isocyanate (EPI) and a modified silyl-epoxy (MS). In this way, the suggested test method was applied for a large spectrum of adhesives with differing mechanical and durability properties. For each treatment and adhesive ten specimens were tested, which gave a total amount of 210 specimens.

If present shear strength test results, obtained with the suggested method, are compared with the requirements according to EN 301 (classification of phenolic and aminoplastic adhesives for load bearing timber) only the EP-bonded connections pass. The shear strength values are shown in Figure 5. However, comparison with the requirements according to EN 301 can be questionable as the suggested test specimens are very different from standard specimens prescribed in EN 301. As expected, cooking and testing in the wet state lead to very low shear strength of the glued connection. Bonding steel to wood puts extra strong requirements on the adhesive bond line as the wood swells while the steel rod is rigid.

A test method for creep-rupture testing of small glued-in rod specimens was also developed. The method is based on ASTM D 4680, see Figure 6. The specimens for this test method are of the same type as for the strength and durability tests, see Figure 4. Three load levels, 40%, 60% and 80% of the ultimate load, in three climates, 20°C/65% RH, 20°C/85% RH and 50°C/30% are studied. The three adhesives tested are very different. It therefore seems preferable to focus the evaluation of the test results on the absolute shear stress capacity instead of a stress level. The shear stress capacities versus median time to failure (median of ten specimens) for the specimens tested at the time of writing in all three climates are shown in Figure 7.

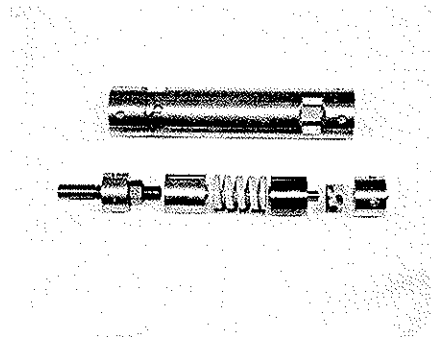
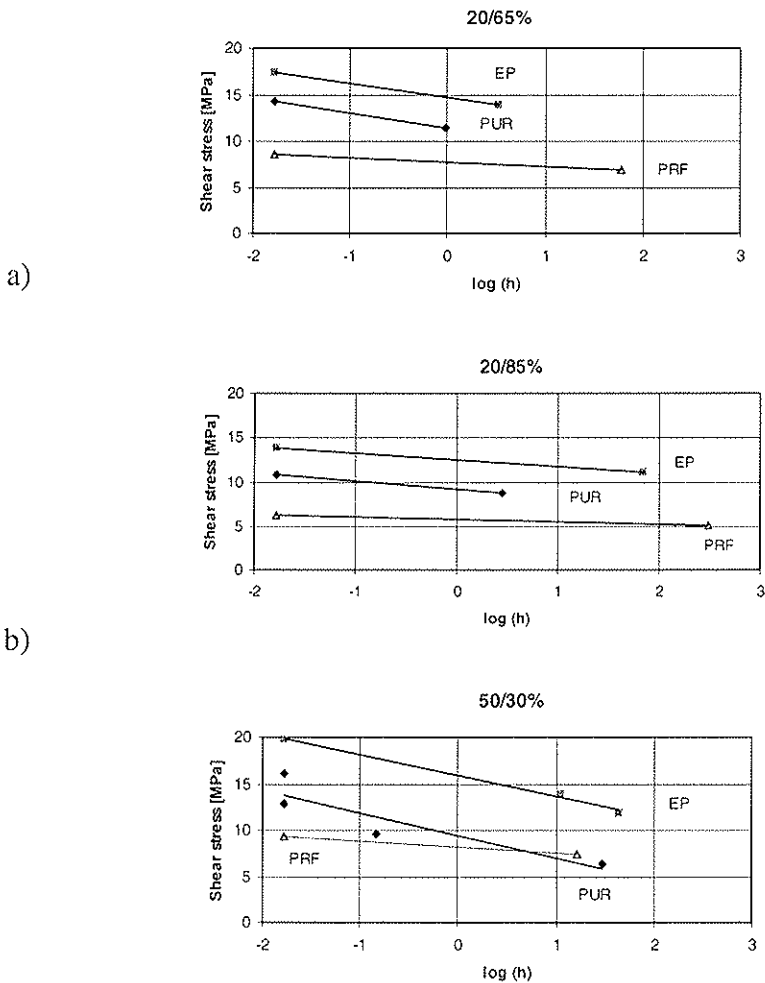


Figure 6. Creep-rupture testing device. (Figure from Bengtsson and Johansson 2001.)

In some cases comparison was made between the behaviour of small glued-in rod specimens and the behaviour of full-sized glued-in rod connections. These comparisons require further evaluation as the relationships are not simple.

Background for this part of the work can be found in Bengtsson and Johansson (2001).



c)
 Figure 7. Shear stress versus median time (hours) to failure in logarithmic scale for the three tested adhesives. (Figures from Bengtsson and Johansson 2001.)
 a) 20°C/65% relative humidity
 b) 20°C/85% relative humidity
 c) 50°C/30% relative humidity

5 Development of production control test methods

This work was performed by SP Swedish National Testing and Research Institute, Sweden. The objective of the work was to develop test methods which enable reliable and simple testing of glued-in rods for timber structures during production. The method/methods should be capable of revealing serious production errors, e.g. insufficient adhesive application, insufficient hardening, and other gluing errors. Two alternative test methods for full-sized glued-in rod connections have been studied: one destructive method and one proof-loading method.

Due to simplicity when testing it was decided to use a newly developed test method for testing glued-in rod connections. The method is a one-sided pull-out test (pull-compression). This method is suitable for production control. Four different proof-load levels, 50%, 65%, 80% and 90% of the short-term strength, were tested to try to find the maximum load that does not cause structural damage of the bond line. Specimens bonded with epoxy, on the average, reached higher pull-out loads after proof-loading until 80% and 90% than the specimens tested destructively. None of the tested groups of specimens displayed a decrease in pull-out strength after proof-loading to such high levels as 80% and 90%. The groups of specimens proof-loaded to 65% displayed a decreased pull-out strength. The reason for this behaviour was not explained within the present study.

Error detection was possible for coarse errors by proof-loading up to the 80% level. The induced errors in the present study were sometimes extreme errors. The selection of 80% as a suitable proof-load level is, however, still uncertain and must be further evaluated.

Generally, no relationship between the density of the wood surrounding the glued-in rod and the pull-out strength was found. This fact was also reported by others in the project and it needs to be further investigated.

The variation of the glue line thickness led to increasing pull-out loads for larger glue line thicknesses in case of EP and PUR, whereas for the PRF, which shrunk, the load-bearing capacity decreased.

As the destructive testing is done on specially produced test specimens, representative for a certain batch, the tests do not determine the reliability of the actual junction.

More details about this part of the work can be found in Bengtsson and Johansson (2000).

6 Conclusions

- A calculation model based on a combination of Volkersen theory and fracture mechanics gives good prediction of the pull-out strength for adhesives that bond to the rod such as PUR and EP. The pull-out strength is controlled by two material property parameters that can be easily determined in full-scaled pull-compression tests.
- Fatigue is a significant factor in the performance of glued-in rods and needs to be considered in applications like for instance bridges. Failure can occur in the rod, in the adhesive bond line, in the wood substrate and in the interface between wood and adhesive.
- The effect of rod spacing and edge distances have been clearly demonstrated and proposals to be used in design have been made.
- Storage without mechanical loading in variable outdoor climates had a strength reducing effect mainly on PUR-bonded rods. After storage in 85% RH the PRF-bonded rods were most affected.
- Glued-in rods have a DOL behaviour that can differ quite considerably from that of timber and other timber connections. In 85% RH the behaviour of EP-bonded rods behaved like the Madison curve while PRF and PUR had much shorter time to failure. At 50°C the PRF behaved in a better way than PUR and EP.

- It is questionable if the method developed for evaluation of the durability of adhesives for glued-in rods is suitable for the purpose. PRF, which is known to give very durable wood-to-wood bonding, obtains extremely low strength values after testing in wet conditions. It seems that the method punishes adhesives that do not bond to the rod.
- The creep-rupture test method developed for small specimens works well. The creep-rupture behaviour of small specimens compared to this behaviour for full-sized specimens will be further investigated.
- A simple production control test method based on proof-loading has been developed. It is able of detecting a number of serious production errors.

7 Acknowledgement

This research is sponsored by the European Commission (DG XII) through grant nr SMT 4-CT97-2199. SP also got a grant from NUTEK (Swedish National Board for Industrial and Technical Development). The financial support is gratefully acknowledged.

8 References

- Aicher, S.:** WP5 – Duration of load tests on full-sized glued-in rod specimens, Technical report for WP5, Project SMT4_CT97_2199 (GIROD), Otto-Graf-Institut, Stuttgart, Germany, 2001.
- Aicher, S., Gustafsson, P.J. and Wolf, M.:** Load-displacement and bond strength of glued-in rods in timber influenced by adhesive, wood density, rod slenderness and diameter. In Proceedings of the 1st RILEM symposium on Timber Engineering, September 1999, Stockholm, Sweden, pp 369-378.
- Bainbridge, R.J., Harvey, K., Mettem, C.J. and Ansell, M.P.:** Fatigue Performance of Bonded-in Rods in Glulam, Using Three Adhesive Types. CIB-W18/33-7-12, Proceedings of International Council For Building Research Studies And Documentation, Working Commission W18 - Timber Structures, Meeting Thirty-Three, Delft, Netherlands, August 2000.
- Bainbridge, R.J., Mettem, C.J.:** WP 6 – Effect of fatigue, technical report for WP6, Project SMT4_CT97_2199 (GIROD), TRADA Technology Ltd., High Wycombe, UK, 2001.
- Bengtsson, C., Johansson C.J.:** Test methods for glued-in rods for timber structures. . CIB-W18A, proceedings, Delft, Netherlands, 2000.
- Bengtsson, C., Johansson C.J.:** Glued-in rods – Development of test methods for adhesives. To be published in proceedings of the RILEM Symposium “Joints in Timber Structures” to be held in Stuttgart Sept. 12-14, 2001.
- Blaß, H.J., Laskewitz, B.:** Effect of Spacing and Edge Distance on the Axial Strength of Glued-In Rods. CIB-W18A, proceedings, Graz, Austria, 1999.
- Gustafsson P.J., Serrano E.:** Glued-in Rods for Timber Structures - Development of a Calculation Model, Technical report for WP1, Project SMT4_CT97_2199 (GIROD), Lund University, Lund, Sweden, 2001.
- Johansson, C.J.:** GIROD – Glued in rods for timber structures. WP 7 – Test methods for production control. Technical Report Nr SP-TR-1, SP, Borås, Sweden, 1999.

INTERNATIONAL COUNCIL FOR RESEARCH AND INNOVATION
IN BUILDING AND CONSTRUCTION

WORKING COMMISSION W18 - TIMBER STRUCTURES

CRITERIA FOR DAMAGE AND FAILURE OF DOWEL-TYPE JOINTS
SUBJECTED TO FORCE PERPENDICULAR TO THE GRAIN

M Yasumura
Department of Forest Resources Science
Shizuoka University

JAPAN

Presented by: M Yasumura

- V Enjily commented that the reversal loading should be considered as this is possible in some load cases.
- Smith asked why crack initiation prediction was not considered rather than cracked specimens.
- M Yasumura agreed from scientific perspective and maintained from practical/technical perspective the approach in this paper is correct.
- H J Blass commented that small cracks would always occur anyway.
- H J Larsen agreed.

Criteria for damage and failure of dowel-type joints subjected to force perpendicular to the grain

Motoi YASUMURA

Department of Forest Resources Science, Shizuoka University, Japan

1 Introduction

Fracture of timber under forces perpendicular to wooden grain is one of the most important criteria for the design of dowel type joints. This kind of failure has adverse effect on not only the load carrying capacity but also the ductility of joints that dominates the seismic behavior of timber structures. Current design procedure based on the yield theory assures only the load carrying capacity but does not predict the failure due to the fracture of wood. Therefore, bolted timber joints were tested under loading perpendicular to the grain, and the linear elastic fracture mechanics was applied to predict the failure of dowel type joints.

Japanese new building codes enforced in June 2000 stipulate the design method based on the damage limit and safety limit of building structures. Damage limit is the limit where no structural elements are damaged by the actions that may occur during the life of the building, and safety limit is the limit where the safety of structure is ensured during the extreme actions. This paper studies also the influence of the edge distance and height of beam on the damage and safety limit of bolted joints subjected to a force perpendicular to the grain.

2 Background

According to EN 383 (CEN, 1993), the embedding strength used for the yield theory is determined by the maximum embedding stress up to 5mm displacement. This procedure is appropriate for loading parallel to the grain as the embedding stress does not increase any more after the yielding of wood and keep almost constant value over 5mm displacement. Different from the embedding parallel to the grain, the embedding stress perpendicular to the grain continues to increase after the yielding as shown in Fig.1, and the embedding strength perpendicular to the grain obtained from 5mm displacement is much lower than the actual ultimate strength (Yasumura, M. and Sawata, K., 2000). To use this embedding stress up to 5mm displacement shall not only produce a conservative

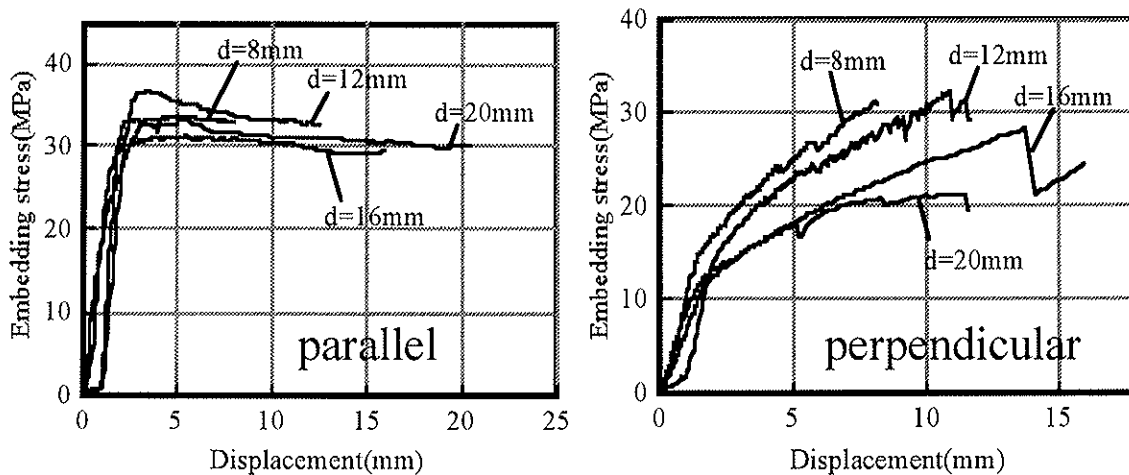


Fig.1 Stress-embedding displacement relationships parallel (left) and perpendicular (right) to the grain

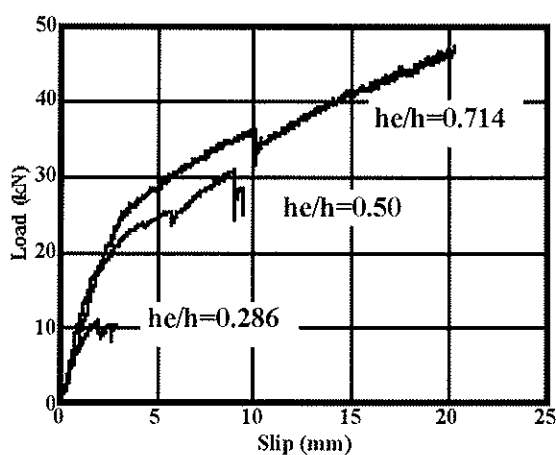


Fig.2 Load-slip relationships of bolted joints under loading perpendicular to the grain

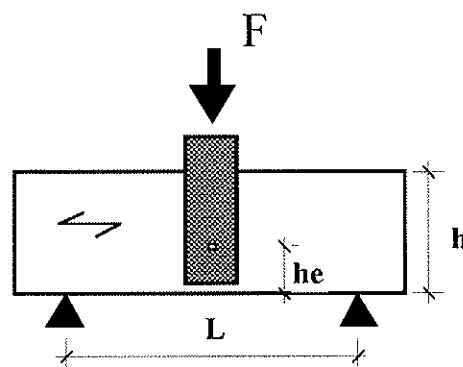


Fig.3 Outline of specimen

design value but also mislead the failure mode of joints subjected to a force perpendicular to the grain. The increase of the lateral force due to the embedding perpendicular to the grain shall cause the fracture of wood that does not always occur with 5mm embedding. Another fact we should notice on the failure of joints is that the cracks that initiated at the joint does not propagate immediately if the crack propagation is stable. Figure 2 shows the load displacement relationships of bolted joints with different edge distances and the same beam height loaded perpendicular to the grain as shown in Fig.3. The joint fails by fracture just after the yielding if the end distance is small, but the lateral load continues to increase remarkably if the edge distance is large in relation to the beam height. This is because the crack propagation is still stable even with a large split if the edge distance is

large in relation to the beam height. Lateral load continues to increase as the embedding stress perpendicular to the grain also does. Thus, the failure of joint subjected to a force perpendicular to the grain is governed by the critical crack length where the crack propagation becomes unstable. It is quite difficult however to determine the critical crack length from the experiments as it is hard to measure the crack propagation during the test. The relation between the lateral force and crack length can be easily calculated by using the linear elastic fracture mechanics (Yasumura, M. and Daudeville, L., 1996, 2000). In this study, critical crack length for the joints with different bolt geometry was obtained by means of LEFM, and the load carrying capacity calculated with these critical crack lengths were compared with the experimental results.

3 Specimen and test method

Specimens consisted of spruce glued laminated wood and 12mm thick steel side plates on both sides of the wooden member, connected with bolts 16mm in diameter (d). The glued laminated wood was made of laminae 30mm thick with an average density 440kg/m^3 . The quality of steel used for the side plates and bolts was JIS (Japanese Industrial Standard) SS 400. The pre-drilled holes of wooden members were equal to or slightly larger than the bolt diameters, and the diameters of the bolt holes of steel plates were 1mm larger than the bolt diameter. The thickness of the wooden member was kept 64mm ($4d$) for all specimen.

Table 1 Summary of specimens and comparison of experimental and simulated ultimate load (F_u). Experimental and simulated ultimate loads are those corresponding to up to 15mm slips and $10d$ crack length, respectively.

| Specimen | Member thickness (b) | Bolt diameter (d) (mm) | Span (L) | Height (h) | Edge distance (he) | he / h | Ultimate load (F_u) (kN) | | |
|----------|----------------------|------------------------|----------|------------|--------------------|--------|------------------------------|------------|-------|
| | | | | | | | Experiment | Simulation | ratio |
| S14-4 | 4d | 16 | 40d | 14d | 4d | 0.286 | 12.33 | 14.08 | 0.88 |
| S14-7 | 4d | 16 | 40d | 14d | 7d | 0.5 | 28.67 | 21.40 | 1.34 |
| S14-10 | 4d | 16 | 40d | 14d | 10d | 0.714 | 37.37 | 36.78 | 1.02 |
| L14-4 | 4d | 16 | 80d | 14d | 4d | 0.286 | 15.87 | 14.14 | 1.12 |
| L14-7 | 4d | 16 | 80d | 14d | 7d | 0.5 | 24.03 | 22.14 | 1.09 |
| L14-10 | 4d | 16 | 80d | 14d | 10d | 0.714 | 33.23 | 35.54 | 0.94 |
| L21-6 | 4d | 16 | 80d | 21d | 6d | 0.286 | 15.03 | 16.73 | 0.90 |
| L21-105 | 4d | 16 | 80d | 21d | 10.5d | 0.5 | 30.3 | 25.91 | 1.17 |
| L28-8 | 4d | 16 | 80d | 28d | 8d | 0.286 | 24.17 | 18.92 | 1.33 |
| L28-14 | 4d | 16 | 80d | 28d | 14d | 0.5 | 27.47 | 29.27 | 0.94 |

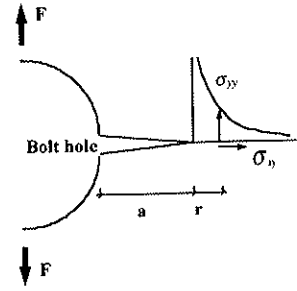
The outline of specimen is summarized in Table 1. Three specimens of each type were subjected to lateral loads as shown in Fig.3. The quasi-static compressive loads were applied to the steel side plates by a hydraulic jack on the center of wooden member. Relative displacement between the steel plates and wooden member was measured with two electric displacement transducers. The nuts were attached to the joints with little tightening.

4 Modeling and analysis

The crack propagation under the coupling of Mode I and Mode II can be calculated by using the stress intensity factor (K). The stress intensity factor in Mode I (K_I) and Mode II (K_{II}) can be calculated by following formula;

$$K_I = \lim_{r \rightarrow 0} \sigma_{yy}(r) \sqrt{2\pi r} \quad (1)$$

$$K_{II} = \lim_{r \rightarrow 0} \sigma_{xy}(r) \sqrt{2\pi r} \quad (2)$$



where, $\sigma_{yy}(r)$ and $\sigma_{xy}(r)$ are the tensile stress perpendicular to the grain and the shear stress at the distance r from the crack tip. The criterion for the crack propagation is generally expressed as follows;

$$\left(\frac{K_I}{K_{IC}} \right)^m + \left(\frac{K_{II}}{K_{IIC}} \right)^n = 1 \quad (3)$$

where, A is the crack length and K_{IC} and K_{IIC} are the critical stress intensity factors in Mode I and Mode II, respectively. The value of K_{IC} was set at $0.439 \text{MPa}\sqrt{\text{m}}$ from the previous study (Yasumura, M. and Daudeville, L., 1996) for spruce of the density of 440kg/m^3 . It is discussible what values should be taken for m , n and K_{IIC} . To make the problem simple, following values were assumed from the calibration between the experimental results of a single bolted joint and the simulation (Aicher, S., Schmidt, J and Brunold, S., 1995).

$$m = 1 \quad ; \quad n = 2 \quad ; \quad K_{IIC} = 4 K_{IC}$$

Tested joints were modeled with the finite elements. A half of the specimen was modeled considering the symmetry. The assumption for the modeling was the same as in the previous study (Yasumura, M. and Daudeville, L., 1999), the contact between the wood and the bolt was complete and there was no friction on them, and the plane stress

conditions were applied and there was no noticeable deformation of the bolt. Young's modulus of spruce was assumed to be 15,000 MPa in the longitudinal direction and 600 MPa in the transverse direction and the shear modulus and Poisson's ratio of 700 MPa and 0.5 were assumed, respectively.

Figure 4 shows the boundary conditions of the model. The bolt hole boundary was fixed in the radial direction but only in the positive direction and free in the tangential direction. The forced displacements were applied downwards at the right corner of the upper side. The FEM code CASTEM 2000 developed by the French Atomic Energy Commissariat (CEA) was used for the analysis.

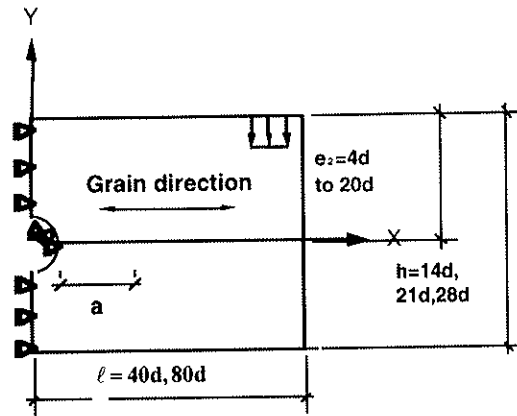


Fig.4 Boundary conditions

5 Results and discussion

5.1 Crack propagation

Figure 5 shows the relationships between the calculated lateral force ($F/(2b \cdot K_{Cl})$) and the crack length. For all types of specimen, lateral force just after the crack initiation differed very little regardless of the edge distance and beam height, and increased as the crack propagated. In the case of specimen with comparatively small edge distance ($he/h=0.286$), lateral force became almost constant with the crack length of 2 to 3d. For the specimen whose edge distance was a half of the beam height ($he/h=0.5$), lateral force became constant with the crack length of 3 to 6d except for the specimen with the beam height of 28d. In the specimen with beam height of 28d and edge distance of 14d, lateral force increased up to the crack length of 9d, and then became almost constant. In the case of the specimen with the beam height of 14d and edge distance of 10d, lateral force became almost constant with the crack length of 10d. Lateral force continued to increase at the crack length of 10d in the case of specimens with the beam height of 28d except for that with the edge distance of 8d..

5.2 Critical crack length

As we saw in 5.1, the crack propagation is stable up to certain crack length and then becomes unstable. We define this length as critical crack length. The critical crack length was 2 to 3d in the case that edge distance was comparatively small, and less than 10d in

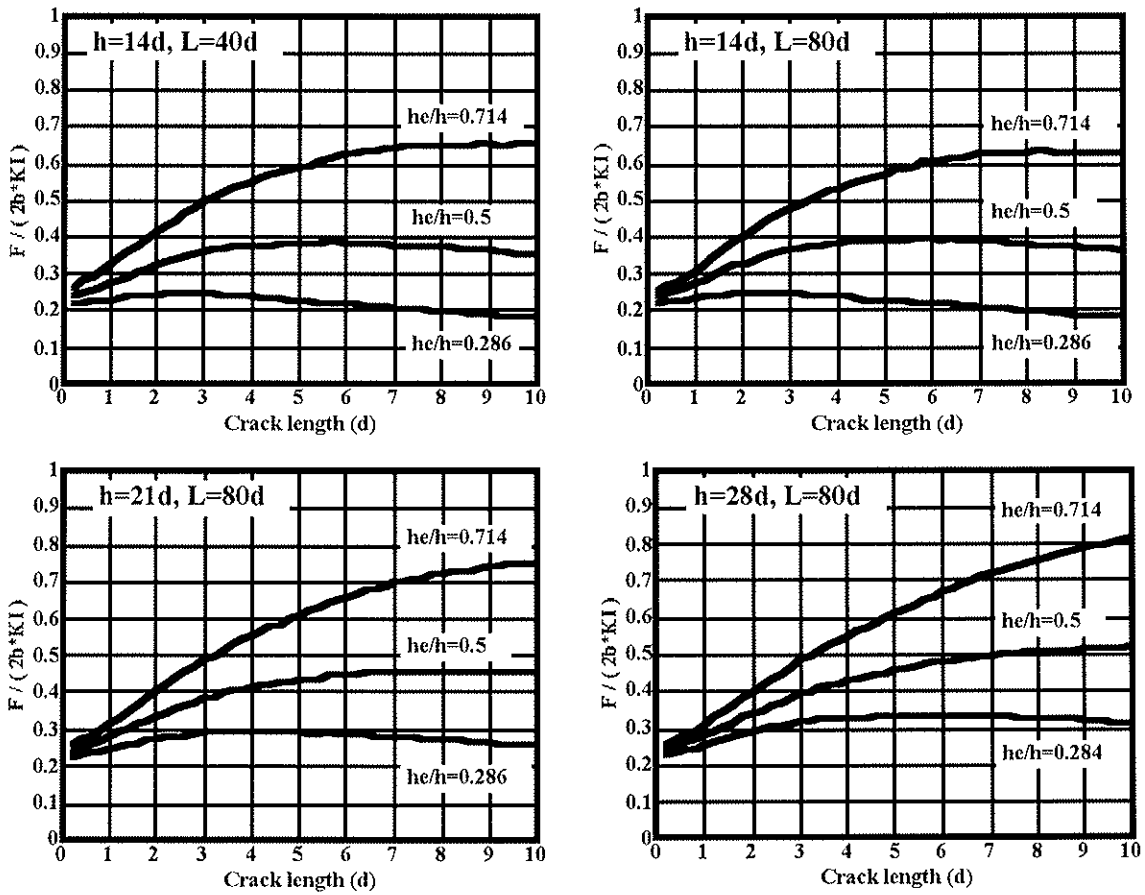


Fig.5 Relationships between lateral force and crack length

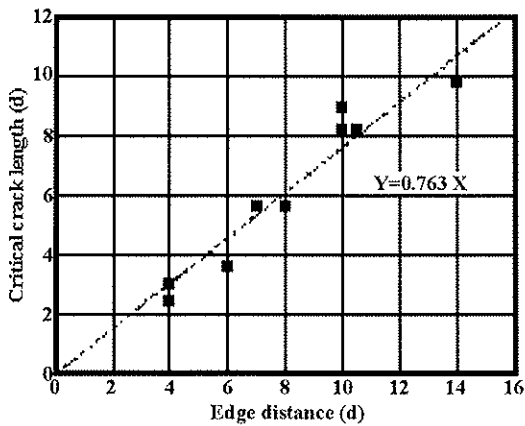


Fig.6 Critical crack length and edge distance

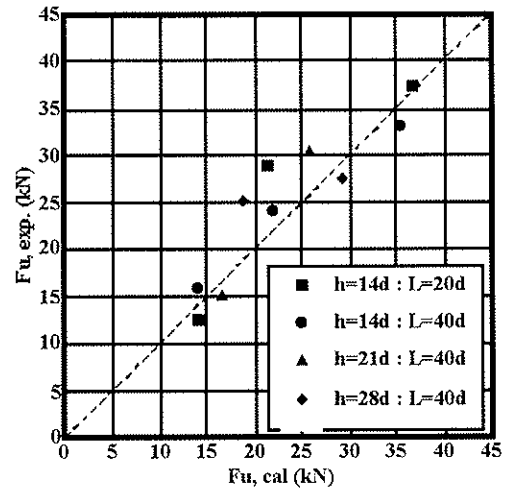


Fig.7 Comparison of calculated ultimate load with experimental results.

many cases, but it exceeded 10d when both beam height and edge distance were comparatively large.

Figure 6 shows the relationship between the critical crack length and edge distance. In this figure, the critical crack lengths larger than 10d are omitted. A strong correlation between the critical crack length and the edge distance was observed. Critical crack length (A_{cr}) is expressed with the edge distance (he) as follows;

$$A_{cr} = 0.763 he \quad (4)$$

5.3 Ultimate load

Calculated ultimate load by LEFM is compared with the experimental results in Table 1 and Fig.7. The experimental ultimate load was taken as the maximum load up to 15mm displacement according to EN26891 as some joints did not fail under 15mm displacement. The calculated ultimate load was obtained from those corresponding to the critical crack length with the critical stress intensity factor of $0.439\text{MPa}\sqrt{\text{m}}$ (Yasumura,M. and Daudeville,L., 1996). As the calculation was ceased with the crack length of 10d, some specimen did not attain to the ultimate load, but that load with the crack length of 10d was considered as the ultimate load.

Calculated ultimate load agreed comparatively well with the experimental results except for S14-7 and S28-8. The experimental results of these specimens were approximately 30% higher than the simulation for some reason.

5.4 Influence of edge distance

Figure 8 shows the relation between the calculated lateral force corresponding to the crack length of 0.5, 2, 4 and 10d. When the crack length was 0.5d, little difference was observed in lateral load for all specimen regardless of the edge distance, beam height and span of beam. Lateral load was close to that obtained from the embedding strength determined by 5% off-set. This means that we can not avoid small cracks around the yielding of wood with any fastener geometry if a dowel-type fastener is subjected to a force perpendicular to the grain, and that load is much lower than the load determined by the 5mm embedding. Lateral load at the crack length of 2d is higher than the load determined by 5% embedding, but lower than the load determined by 5mm embedding if the edge distance was smaller than a half of the beam height. This indicates that the joints can fail by fracture in the case of multiply joints whose spacing is not large enough if the edge distance is less than a half of the beam height. For the lateral load corresponding to crack length more than 4d, the influence of the height of beam is more remarkable. In the case of joints with the beam height of 14d, the joint can fail by fracture if the edge distance is smaller than one third of the beam height, but it never fails by fracture before the embedding attains to 5mm if the beam height is larger than 28d. We should notify that

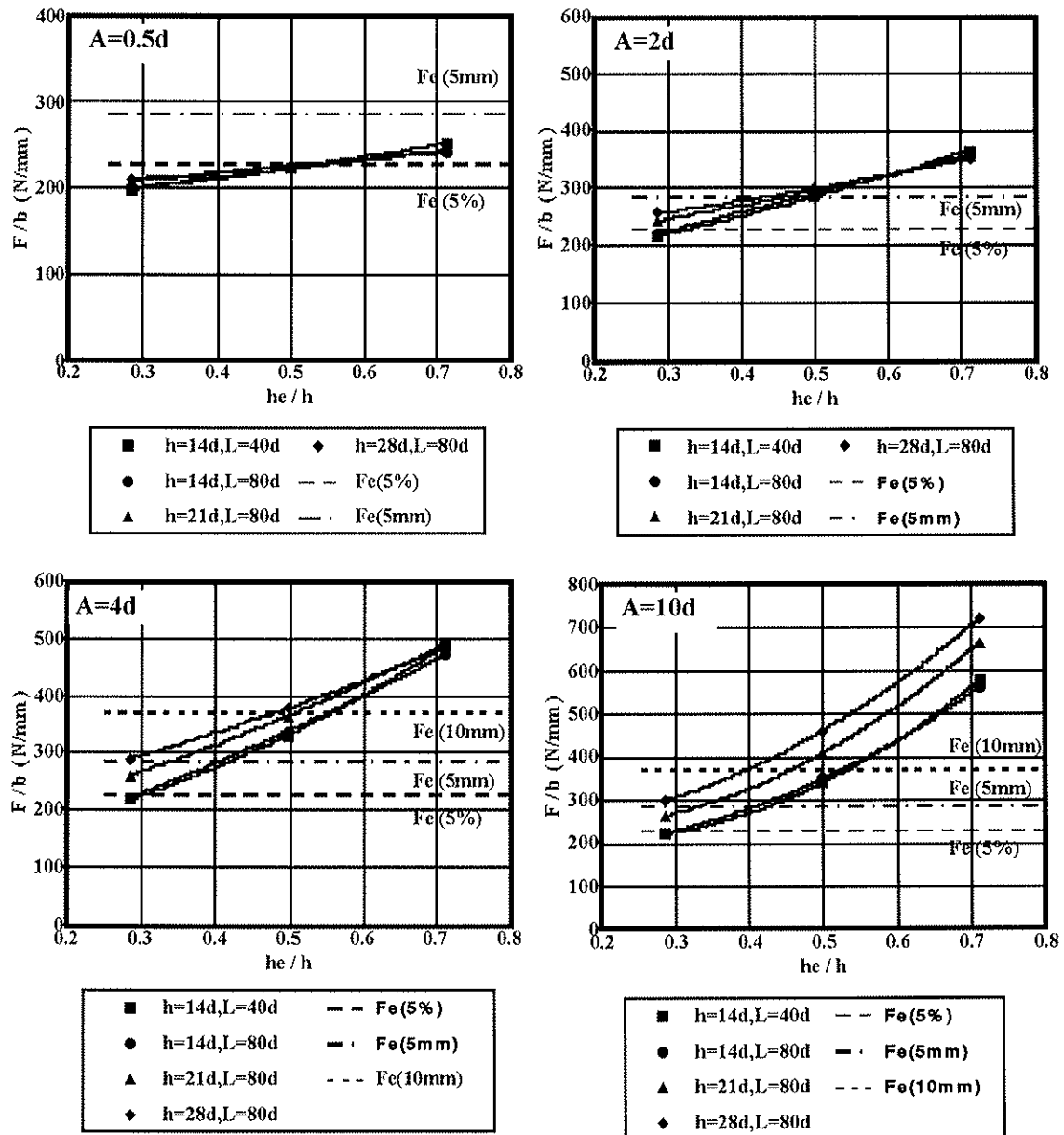


Fig. 8 Calculated ultimate strength (F/b) and he/h with the crack length (A) of 0.5, 2, 4, 10d.

the most joints fail finally by the fracture even though they do not fail before the embedding attains to 5mm.

5.5 Design proposal

A design formula for the failure of dowel-type joints was presented at the thirty-third CIB-W18 meeting in delft (Van der Put, T.A.C.M. and Leijten, A.J.M., 2000). The simplified formula for a dowel-type joint loaded on the center of beam is expressed as follows;

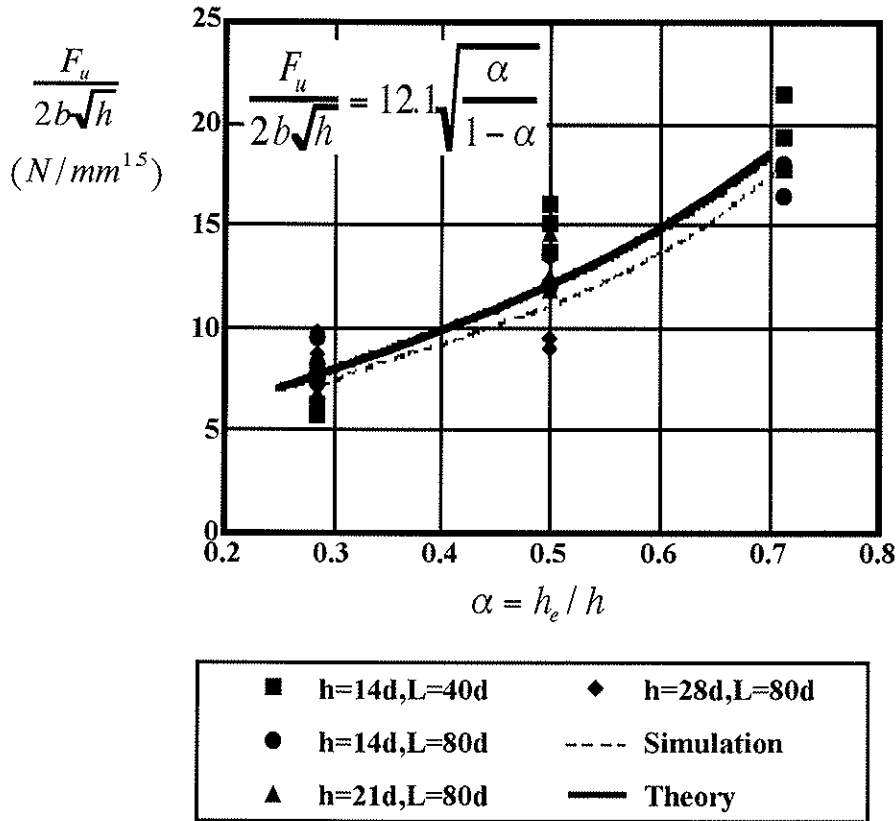


Fig.10 Comparison of the theoretical values with simulation and experimental results.

$$\frac{F_u}{2b\sqrt{h}} = C_1 \sqrt{\frac{\alpha}{1-\alpha}} \quad C_1 = \sqrt{\frac{GG_c}{0.6}} \quad (5)$$

Figure 10 shows the comparison of the calculated ultimate load by equation (5) with the experimental results and simulation. The value of C_1 obtained from the experiments was $12.1 \text{N/mm}^{1.5}$ and about 20% smaller than those proposed in that study. However the proposed formula agreed pretty well with the experimental and simulated values, and it seems this formula is appropriate to predict the failure of dowel type joints subjected to a force perpendicular to the grain if the value of C_1 is appropriately determined.

6 Conclusions

By comparing the experimental results with the LEFM analysis, it was found that we can not avoid a small crack around the yielding of wood for any geometry of fastener. Whether this crack propagates or not depends on the geometry of fastener. The crack propagation becomes unstable when the crack length attains to the critical crack length.

The critical crack length has a correlation with the edge distance, and approximately 0.76 times as large as the edge distance. The failure load of joint subjected to a force perpendicular to the grain can be obtained either by means of LEFM or design formula. The failure load is however much lower than the ultimate load determined by 5mm embedding stress if the edge distance is small, and much higher if the edge distance and beam height are comparatively large.

7 Acknowledgments

The author thanks Hiroshi Goto, graduate student of Shizuoka University, for his assistance in experiments and analysis.

8 References

- EN383: 1993: "Timber structures – Test methods – Determination of Embedding Strength and Foundation Values for Dowel Type Fasteners"
- Yasumura, M. and Sawata, K.: 2000: "Determination of Yield Strength and Ultimate Strength of Dowel –type Timber Joints", Proceeding of CIB-W18, Paper 33-7-1
- Yasumura, M. and Daudeville, L.: 1999: "Design and Analysis of Bolted Timber Joints under Lateral Force Perpendicular to Grain", Proceeding of CIB-W18, paper 32-7-3
- Aicher, S., Schmidt, J and Brunold, S.: 1995: "Design of Timber Beams with Holes by means of Fracture Mechanics, Proceeding of CIB-W18, paper 28-19-4
- Yasumura, M. and Daudeville, L.: 1996: "Fracture Analysis of Bolted Timber Joints under Lateral Force Perpendicular to the Grain", Mokuzaï Gakkaishi 42(3), pp225-233
- Yasumura, M. and Daudeville, L.: 2000: "Fracture of multiply-bolted joints under lateral force perpendicular to wooden grain", J. Wood Sci 46, pp187-192
- EN 26891:1991: "Timber structures; Joints made with mechanical fasteners; General principles for the determination of strength and deformation characteristics (ISO 6891:1983)
- Van der Put, T.A.C.M. and Leijten, A.J.M.: 2000: "Evaluation of Perpendicular to Grain Failure of Beams caused by Concentrated Loads of Joints", Proceeding of CIB-W18, paper 33-7-7

INTERNATIONAL COUNCIL FOR RESEARCH AND INNOVATION
IN BUILDING AND CONSTRUCTION

WORKING COMMISSION W18 - TIMBER STRUCTURES

INTERACTION BETWEEN SPLITTING AND
BLOCK SHEAR FAILURE OF JOINTS

A J M Leijten

J Kuipers

Delft University of Technology

A J M Jorissen

SHR-Timber Research and ABT Consulting Engineers

THE NETHERLANDS

Presented by: A Jorissen

- H J Blass commented that the load configuration reported here was different from previous papers.
- A Jorissen agreed and the results could not be compared.
- H J Blass stated that the splitting load perpendicular and block shear failures occurred at different planes; therefore, it was not surprising that there would be no interaction.
- I Smith asked how do you pick the points fitted on the line on figure 10 on the load parallel to grain axis.
- A Jorissen clarified that the data for different types of tests were plotted.

INTERACTION BETWEEN SPLITTING AND BLOCK SHEAR FAILURE OF JOINTS

A.J.M. Leijten,
J. Kuipers

Delft University of Technology, the Netherlands

A.J.M. Jorissen,

SHR- Timber Research and ABT Consulting Engineers, the Netherlands

Introduction

Recently, a new failure mode for connections was introduced in the draft Eurocode 5. It refers to timber failure along the circumference of the fastener pattern, so-called block-shear. This failure type mainly governs steel-to-timber connections with close spaced fasteners. The draft also contains a splitting failure criterion for connections loaded perpendicular to the grain as presented in paper CIB/W18/33-7-7. It is implicitly assumed that both criteria apply independently and therefore there is no interaction equation needed. Some experimental evidence is given in this paper to justify this approach.

Additional failure criteria for connections in Eurocode 5

Eurocode 5 (EC5) was revised during the last years based on comments of the member states. As a result of the discussion based on these comments, it was decided to add and modify a few criteria related to the strength capacity of connections. Particular when connections are loaded near end grain face and subjected to a force at an angle to the grain, the force components parallel and perpendicular to the grain can force separate failure modes. For the force component parallel to grain a failure criterion, known as the block shear, is introduced in EC5 based on French tests reported in [1]. Block shear is a brittle type of failure recognised by cracks along the circumference of the fastener area. A related phenomenon is shear plug failure as dealt with by Kangas [2]. Another criterion is the splitting strength of beams caused by a force component perpendicular to grain based on paper CIB/W18/33-7-7. No interaction

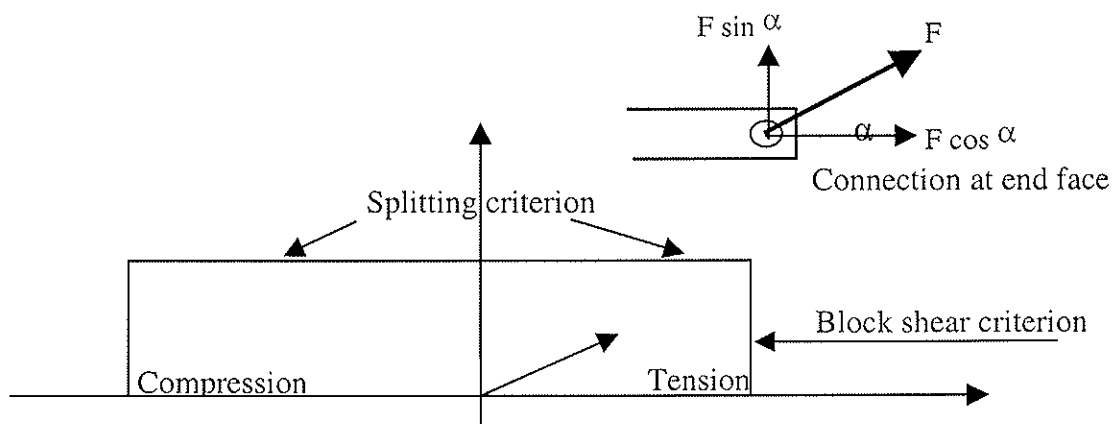


Figure 1: No interaction assumed between block shear and splitting criterion

between both criteria is assumed, Figure 1. The only experimental evidence as far as the author knows that supports and justifies this approach dates back to investigations by Kuipers [3] and Schippers [4] from 1960 and 1962, which deals with split-ring connections loaded at

various angles to the grain. The investigations were never published other than in a Dutch Stevin research report[3][4]. Below a summary is given of their research work.

Research results for split-ring connections.

The research projects by Kuipers [3] and Schippers [4] carried out in the late fifties/early sixties were related to the first draft of the Dutch timber design code dealing with split-ring connections. Many test series were performed with tension and compression joints, to obtain information about the influences of member thickness, spacing, and of end and edge distances. The connecting members were loaded all parallel to the grain. This situation occurs in many nodal points of trusses. However, in trusses some members are also loaded at an angle to the grain, specially those near the supports (diagonals). Available test data was only based on tests where a vertical member was connected to a horizontal beam, Figure 2. For connection with members loaded at other angles to the grain the Hankinson formula was

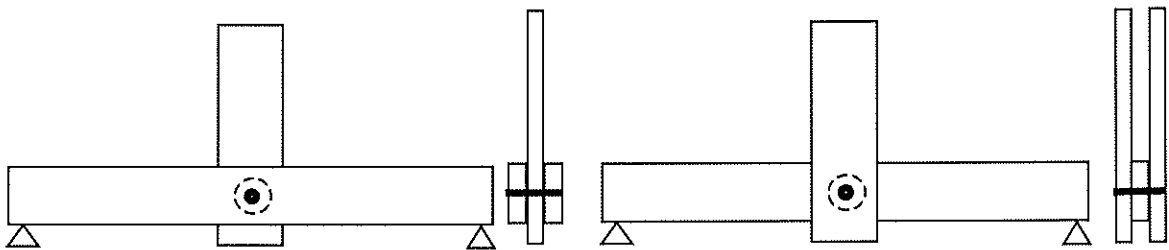


Figure 2: Perpendicular to grain test data available.

thought to apply for the off-axis strength of wood. This was felt unrealistic and did not reflect a close approximation of reality. The length of the horizontal beam in Figure 2 also affects the result. The aim of the research was to perform tests at an angle to the grain. As in many trusses the nodal points consist of so-called built up connections; the first tests performed were on little trusses like in Figures 3 and 4, where the connection studied was made with Spruce members while the others were with beech members. The test set up reflects a support situation. This set up was later replaced by the test set up of Figure 5, where the connections like the one of Figure 6 could be tested.

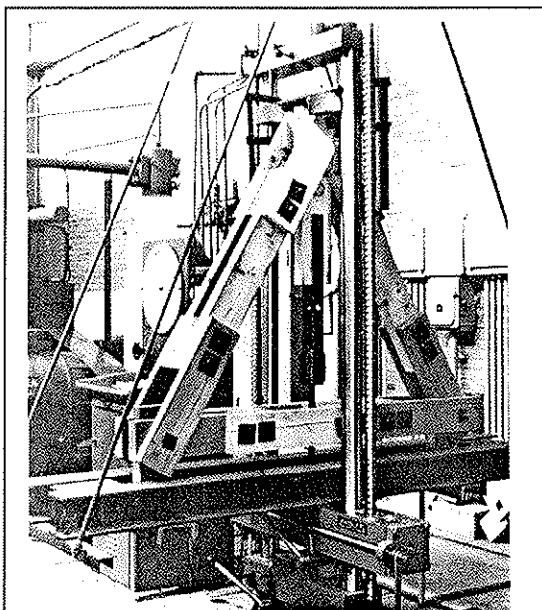


Figure 3: Test of truss support node

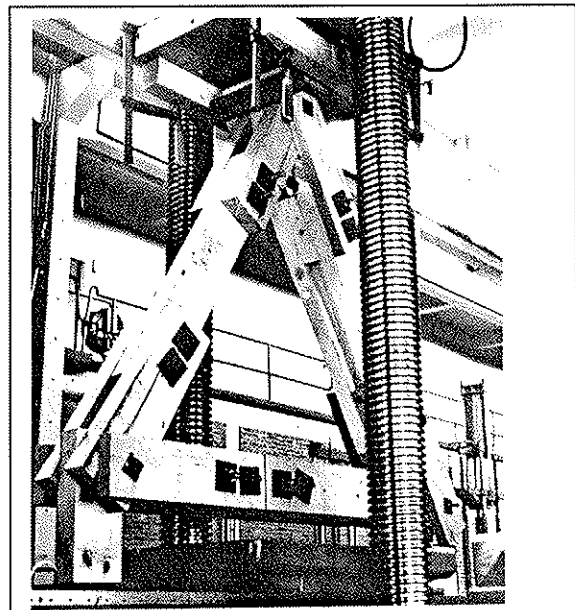


Figure 4: Failure at support node

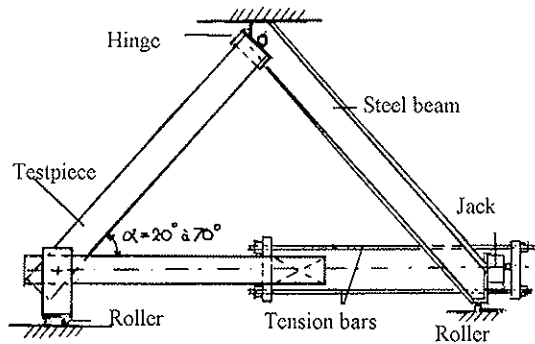


Figure 5: Test set up used by Kuipers [2] and Schippers [3].

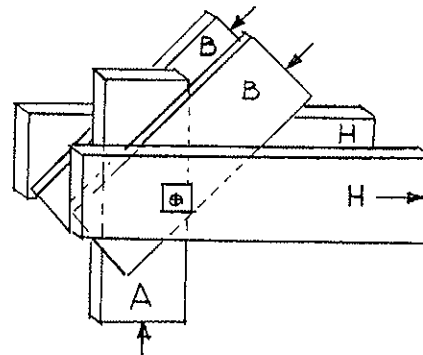


Figure 6: Detail of test arrangements for splitting connectors.

The members B in Figure 6 are the ones that are loaded at an angle to the grain, resulting in axial tensile or compressive forces in the members H and A respectively. The components perpendicular to the grain on both shear planes of these members are of equal magnitude but opposite direction. The forces have a splitting effect on this member B. In these tests it was observed that in many cases such splitting occurred without failure due to block shear or to compression failure.

Although much more tests were carried out with other size connectors, the attention is focused on the tests with 75 mm diameter TECO split-rings only. The test set-up shown in Figure 5 enables to change the angle of loading easily. For this reason most tests were performed with

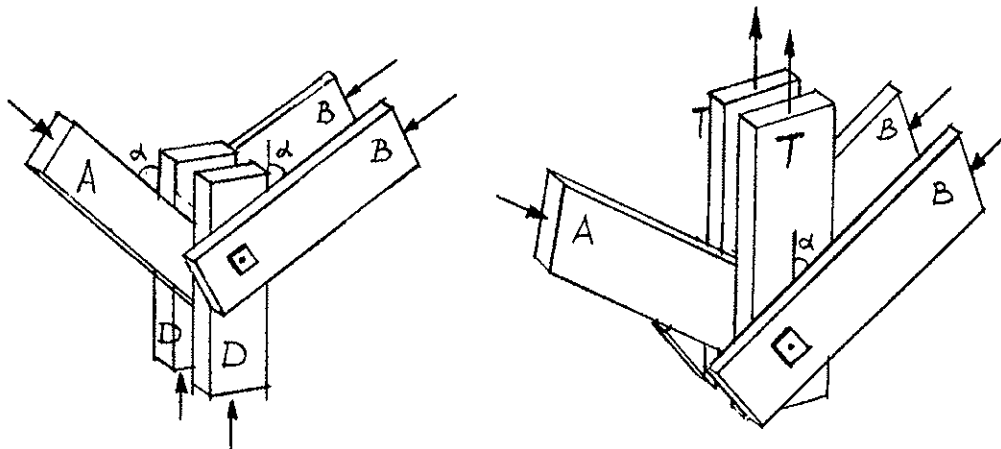


Figure 7: Two other test arrangements by Kuipers [2], see Figures 8 and 9

this type of test. More complex arrangements are given in Figures 7. Particular attention was given to the design of the members D and T of Figure 7, (8 and 9). These members are also loaded by a torque moment due to the opposite nature of the force component perpendicular to grain in respective shear planes of the connection. However, this effect is being neglected, as restraining neighbouring members do not allow much axial rotation, Figure 10, left.

As the researchers didn't care to much about the failure mode but just took the failure load associated with a certain geometry of the connection the code design rule implicitly take these failure modes into account, as does the EC5 rules. For other type of fasteners applied near the end of a beam, interaction between block shear and splitting perpendicular to grain might be possible and therefore need to be considered, Figure 10, right.

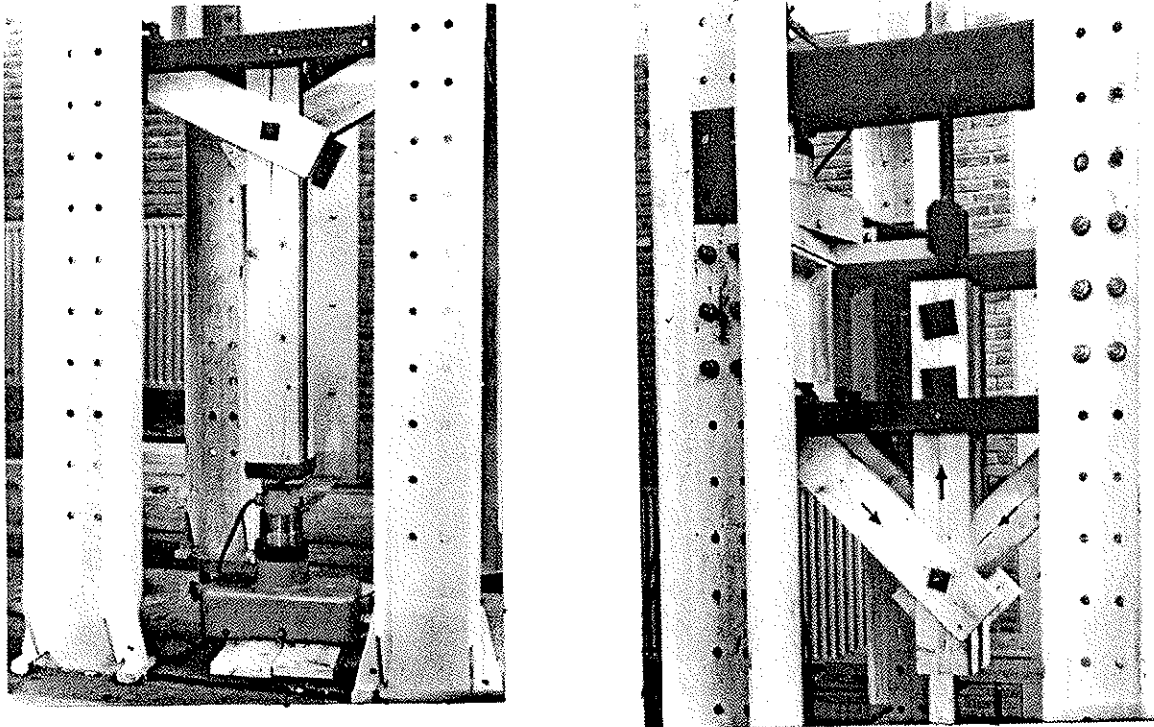


Figure 8: Compression (unloaded end)& splitting Figure 9: Tension (loaded end)& splitting

Obviously, there are differences between the splitting mode of both connections shown in Figure 10. The left part shows a connection with a split-ring connector. The failure shown is splitting and block shear failure of which usually one is governing. The splitting is caused by the opposite nature of the forces on both beam sides (shear planes). Similar, as shown in Figure 10 the forces transferred by the connection, for instance a nail plate, might cause either a block shear or splitting failure. Here the splitting is caused by the force components that both point in the same direction. When it is demonstrated that splitting and block shear exhibit no significant interaction for the left connection with split-ring connectors it might be assumed the same is valid for the other situation as well.

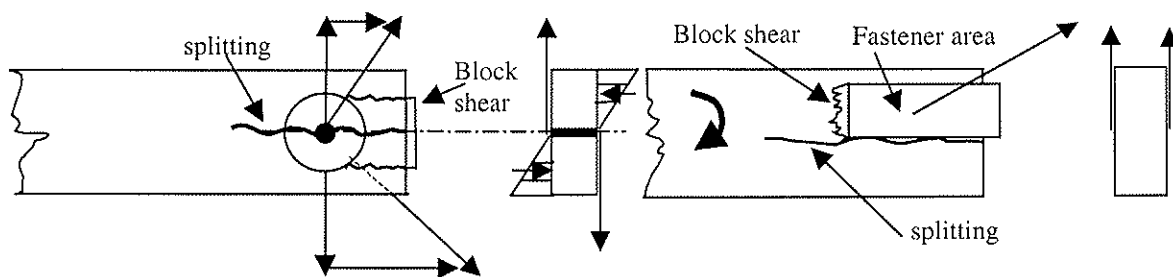


Figure 10: Left: Splitting forces in tests by Kuipers and Schippers. Right: interaction between splitting and block shear for other type of fasteners.

Test Results

In Figure 11 and Table 1 all relevant test results by Schippers [4] including tests by Kuipers [3] are presented for 75 mm diameter split-ring connectors. In all cases, the members subjected to forces perpendicular to the grain failed. The force to grain angle varied in the tensile quadrant from 30, 45, 60 and 70 degrees to 30, 45 and 60 degrees in the compressive quadrant. The line drawn in Figure 11, that connects the data points, is related to tests with the same timber dimensions, 58 mm thickness, and a connector end distance of 70 mm. If more than one test series for a given load to grain angle showed different results an intermediate

point was chosen based on the number of tests as for instance in the top left corner of Figure 11.

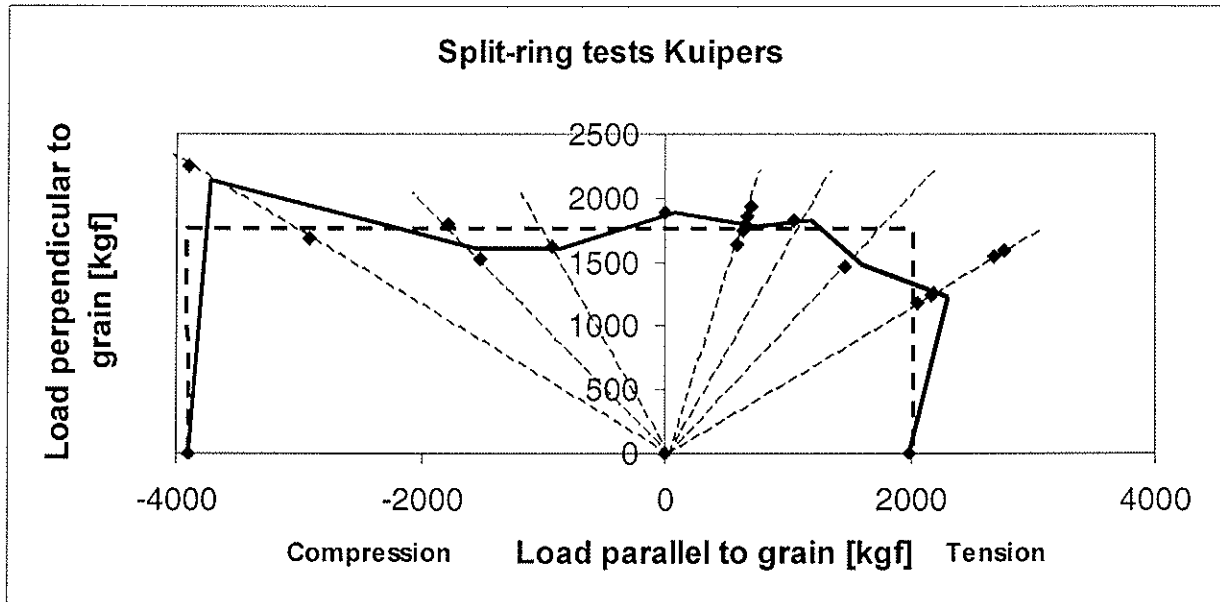


Figure 11: Summary of test results by Kuipers [3] and Schippers [4].

In Figure 11 a dashed line is drawn representing an approximation of the test results. It shows that the resistance against forces perpendicular to the grain, resulting in splitting, is hardly dependent of the force parallel to the grain, resulting in block shear. Apparently, there is no interaction.

Note the big difference between the tensile and compression strength, which apparently is much more than Eurocode 5 design rules envisage.

In their reports Kuipers and Schippers tried to model the connection strength by taking three parameters into consideration; the compression strength of the timber, splitting strength of the member, and the block shear at the end of the member, ignoring all mutual influences. Kuipers and Schippers showed that for the member loaded by perpendicular to grain forces the force with the smallest angle to grain governs the strength, see Figure 10 left. It also turned out that the component perpendicular to the grain is not much affected by the friction between the ring and the timber. The splitting criterion, the horizontal part of the dashed line in Figure 11, is actually slightly curved to fit the test data better. Reason is the friction between ring and the timber. However, the differences are not too big compared to the straight dashed line.

In the Dutch timber design code of 1971 the authors Kuipers and Vermeyden were very cautious and only allowed the connection compressive strength a benefit of 20% over the tensile strength although these tests showed a significant difference.

Table 1: Test results presented in Figure 11

| Number of tests | Member thickness | End distance | Axial Compression or Tension | Angle with grain | Strength [kgf] |
|-----------------|------------------|--------------|------------------------------|------------------|----------------|
| 5 | 58 | 70 | T | 45 | 2060 |
| 5 | 58 | 70 | T | 60 | 2110 |

| | | | | | |
|---|----|----|---|----|------|
| 5 | 58 | 70 | T | 70 | 1865 |
| 5 | 58 | 70 | T | 70 | 1905 |
| 5 | 58 | 70 | - | 90 | 1880 |
| 5 | 58 | 70 | C | 60 | 1875 |
| 1 | 58 | 70 | C | 45 | 2535 |
| 4 | 58 | 70 | C | 45 | 2155 |
| 4 | 58 | 70 | C | 30 | 4510 |
| 1 | 58 | 70 | C | 30 | 3360 |
| 5 | 58 | 65 | C | 0 | 3900 |
| 5 | 58 | 70 | T | 0 | 1990 |

CONCLUSION

It can be concluded that on the bases of the test results with split-ring connectors outlined above block shear and splitting failure can be considered as two independent failure mechanisms.

Recommendation

For the benefit of studying the effect of combined block shear and splitting failure of connections it would be an advantage to have a test standard that would provide guidance in testing at various angles to grain, see Kuipers [5]

Literature

- [1] Biger J.P., Boucquet J.F.,Racher P, Testing and designing the joints for the pavilion of Utopia, Proceedings of World Conference on Timber Engineering, WCTE2000, Whistler, BC, Canada, July 31-August 2, 2000.
- [2] Kangas, J. and Vesa, J., Design of timber capacity in nailed steel-to timber joints, Proceedings of CIB/W18/31-7-4, 1998.
- [3] Kuipers, Research of split-ring connections; connections with members loaded at an angle to the grain (in Dutch), Stevin report 4-60-1-HV-18, January 1960
- [4] Schippers, Test on uni-axial connections with TECO-split-rings; connection with members loaded at an angle to the grain (in Dutch), Stevin Report 4-62-1-HV-26, February 1962
- [5] Kuipers, J., Proposal for a basic test method for the evaluation of structural timber joints with mechanical fasteners and connectors, CIB-W18/4-7-1

INTERNATIONAL COUNCIL FOR RESEARCH AND INNOVATION
IN BUILDING AND CONSTRUCTION

WORKING COMMISSION W18 - TIMBER STRUCTURES

LIMIT STATES DESIGN OF DOWEL-FASTENER JOINTS –
PLACEMENT OF MODIFICATION FACTORS AND PARTIAL
FACTORS, AND CALCULATION OF VARIABILITY IN RESISTANCE

I Smith
University of New Brunswick
CANADA

G Foliente
CSIRO
AUSTRALIA

Presented by: I Smith

- H J Blass commented that the use of the expression of $F_y d^3/6$ assumed large strains in the fastener that might approach 45 degree. This would be true for thin fasteners not bolts.
- I Smith agreed and stated tests of actual fasteners such as bolts would be performed to calibrate the expression.

Limit states design of dowel-fastener joints – Placement of modification factors and partial factors, and calculation of variability in resistance

Ian Smith, University of New Brunswick, Canada
Greg Foliente, CSIRO, Australia

Introduction

Major overhauls of design code provisions for mechanical timber joints are in progress in Canada and Australia. The intent is to make strength calculations using mechanics based models, make expected failure modes transparent to designers, and lay a foundation for probability-based calibration of partial factors appearing on the resistance side of design equations. Strength calculations are based on the generic ‘limit state design’ equation:

$$R_d \geq N^* \dots\dots\dots (1a)$$

where:

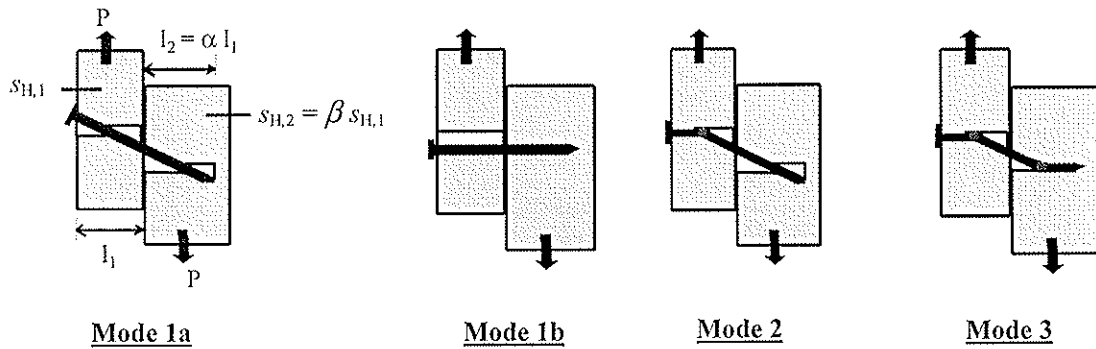
$$R_d = \text{factored design resistance} = (\phi k_1 \dots k_j n_f) R_k \dots\dots\dots (1b)$$

and ϕ = resistance factor (or $1/\gamma_m$, where γ_m is a materials partial coefficient), k_i = modification factor, n_f = number of fasteners, R_k = characteristic resistance per fastener, and N^* = factored design action effect. R_k values are typically near minimum, usually 5th percentile, values determined at reference conditions. Values of ϕ are typically assigned based on past experience to achieve ‘traditionally acceptable’ solutions in terms of the number of fasteners for various end-use applications (DeGrace 1986; McLain 1984). In Australia, values of ϕ factors are generally based on consideration of the state of current knowledge of structural performance (e.g., nailed joint vs. bolted joint) and the intended application of the structural joint (or structural role, i.e., primary or secondary element, in a house or in an engineered building).

Modification factors account for any deviations between design conditions and reference conditions for R_k . Key modification factors are those for duration of loading and climatic conditions. Without exception, modification factors are based on empirical evidence. In the past, most codes based duration of loading modification factors on the ‘Madison curve’ developed from a study on small clear Douglas fir bending specimens (Wood 1951). Currently the Canadian and US codes apply duration of loading adjustment that were derived from in-grade test data for softwood lumber to everything, including joints (Foschi et al. 1989). Eurocode 5 (CEN 1995) uses an experience based composite modification factor that accounts for the interactive effects of load and moisture histories during service. The Australian code is still based on the Madison curve.

Although details of its implementation differ from country to country, international practice has converged on use of Johansen’s yield model as the basis for calculations of the characteristic resistance per fastener, R_k (Johansen 1949; Larsen 1979). Both the fastener and the wood foundation upon which it bears are presumed to behave as ideal rigid plastic material. Model assumptions are the same as for the well-known limit analysis (plastic design) theory applied to steel frames. Figure 1 shows possible modes of failure for a single fastener joint loaded in single shear (equivalent modes exist for double shear joints). Geometric variables are fastener diameter and length of penetration in each member. Joint capacity increases as thickness of the members is increased up to the point where a mode 3 failure occurs. The governing mode is that giving the lowest estimate of the yield load P_Y . Failure can involve bearing failure in just one member or formation of a plastic hinge in just one member. Apart from Johansen’s own version (1949) there are various options regarding model equations (Whale et al. 1987; AFPA 1999; Blass et al. 1999; Smith et al. 2001).

This paper is concerned with the logic for placement of various factors that enter expressions for factored design resistance [Equation (1b)], and estimation of variability in yield strengths of joints.



• plastic hinge

Figure 1 – Failure modes for a single shear joint according to the Johansen theory

Yield equations and placement of factors within them

For simplicity this paper considers only the equations by Blass et al. (1999). These equations use the original Johansen expression for calculating the limiting mode 3 capacity. Mode 3 is attained only once fasteners attain a critical slenderness¹. For fasteners with insufficient slenderness to attain the full (mode 3) capacity, the strength is taken to be proportional to the ratio of actual to critical fastener slenderness. The Blass et al. (1999) equations for a single shear joint are:

- *Failure in the side member (Interpolation 1)*

$$P_Y = s_{H,1} d l_1 \Phi_1 \dots\dots\dots (2)$$

$$\text{where } \Phi_1 = 1 / [1 + \{(1+\beta) / \beta\}^{0.5}]$$

- *Failure in the main member (Interpolation 2)*

$$P_Y = s_{H,1} d l_1 \alpha \Phi_2 \dots\dots\dots (3)$$

$$\text{where } \Phi_2 = \beta / [1 + \{1+\beta\}^{0.5}]$$

- *Formation of plastic hinge in both members (Mode 3)*

$$P_Y = [4 M_Y s_{H,1} d]^{0.5} \Phi_3 \dots\dots\dots (4)$$

$$\text{where } \Phi_3 = [\beta / \{1 + \beta\}]^{0.5}$$

¹ Slenderness is the fastener's penetration into a joint member expressed as a ratio of its diameter.

In the above, d is fastener diameter and M_Y fastener yield moment. Other terms are as defined in Figure 1.

Let us suppose that it is required to predict the 5th percentile-based factored design strength of a joint, $P_{Y,d-0.05}$, based on the equations by Blass et al. There are various ways in which material properties, resistance factors and modification factors can be positioned in design equation to predict the factored design resistance R_d (or $P_{Y,d-0.05}$). Four alternative expressions for calculating the mode 3 strength of a single shear joint are used to illustrate this (ignoring any modification factors other than k_{nf} , k_{MC} and k_{DOL})²:

- Method 1 – *Resistance and modification factors placed external to calculation of P_Y :*

$$R_d = P_{Y,d-0.05} = \phi n_f k_{nf} k_{MC} k_{DOL} [4 M_Y s_{H,1} d \beta / \{1 + \beta\}]^{0.5} \dots\dots\dots (5)$$

where k_{nf} is a modification factor accounting for any effects from n_f on the capacity per fastener. This method is the concept underpinning current timber design code in Canada (CSA 1994). Values for M_Y are based on minimum specified yield properties of fasteners, while s_H values are 5th percentile embedment strengths or an approximation to them. A factor of 0.8 adjusting from short-term strength to ‘standard term’ duration of loading has been omitted here.

- Method 2 – *5th percentile s_H & resistance and modification factors placed internal to calculation of P_Y :*

$$R_d = P_{Y,d-0.05} = n_f k_{nf} [4 M_Y s_{H,1} \phi_{fastener} \phi_{wood} k_{MC} k_{DOL} d \beta / \{1 + \beta\}]^{0.5} \dots\dots\dots (6)$$

This is the form employed in Eurocode 5 (CEN 1995). It is understood that M_Y values used are based on minimum yield strength for fasteners such as bolts, while s_H values are 5th percentile embedment strengths.

- Method 3– *Normal distribution of P_Y & factors external to calculation of P_Y :*

$$R_d = P_{Y,d-0.05} = \phi n_f k_{nf} k_{MC} k_{DOL} P_{Y,av} (1 - 1.645 V_{PY}) \dots\dots\dots (7a)$$

² k_{MC} and k_{DOL} are the modification factors accounting for deviation from non reference conditions for moisture conditions and duration of the loading.

where $P_{Y,av} = [4 M_Y s_{H,1} d \beta / \{1 + \beta\}]^{0.5}$ (7b)

V_{Py} is the coefficient of variation for P_Y . Success of this method depends upon being able to estimate V_{Py} with reasonable accuracy. Average values of properties enter equation (7b). The theory for Generation of System Moments can be used to estimate $P_{Y,av}$ and V_{Py} (Appendix).

- Method 4 – Normal distribution of P_Y & factors internal to calculation of P_Y :

$$R_d = P_{Y,d-0.05} = n_f k_{inf} P_{Y,av} (1 - 1.645 V_{Py}) \dots\dots\dots (8a)$$

where $P_{Y,av} = [4 M_Y s_{H,1} \phi_{fastener} \phi_{wood} k_{DOL} k_{MC} d \beta / \{1 + \beta\}]^{0.5}$ (8b)

Average values of properties enter equation (8b) and the theory for Generation of System Moments can be used to estimate V_{Py} (Appendix, with the modification that $\phi_{fastener}$, ϕ_{wood} , k_{DOL} and k_{MC} be appropriately inserted in the numerator of the equations).

The issue, as discussed below, is which of the above-mentioned ways of estimating R_d are acceptable for code purposes.

Estimates $P_{Y,d-0.05}$ and $V_{Py,d}$ values

There have been numerous studies attesting to the ability of the Johansen model, and its derivatives, to accurately predict the average yield strength of timber joints with a single dowel-fastener (e.g. Daneff 1997; Ni 1997; Smith et al. 2001). Therefore, the ability to calculate average design strength, $P_{Y,d-av}$, is taken to be an uncontested issue. What is unresolved is how to reliably predict variability in $P_{Y,d}$, and thus how to predict characteristic values at low levels of exclusion. As already noted, 5th percentile characteristic values are of common interest. By using normalized 5th percentile values discussion of them is independent of specifics such as fastener diameter, fastener yield moment and the embedment strengths of members. Normalization is performed by expressing values as the ratio $P_{Y,d-0.05} / P_{Y,d-av}$, and using $V_{Py,d}$ the coefficient of variation in

$P_{Y,d}$. Only single shear joints are discussed here but conclusions will also apply to double shear joints.

Let us assume that joint yield strengths and all material properties entering yield equations are normally distributed (Appendix). It will be noticed from approximate Equations (A7), (A9) and (A12) that $V_{Py,d}$ are independent of geometric variables, but differ between failure modes. Figures 2 and 3 illustrate how $P_{Y,d-0.05} / P_{Y,d-av}$ and $V_{Py,d}$ vary as a function of the coefficient of variation for embedment strength $V_{sH,1}$. Values in those figures are a function of the form of the design equation, i.e. of Methods 1 to 4 [Equations (5) to (8), respectively]. In the case of Methods 1 and 2, $V_{Py,d}$ values were calculated assuming that 5th percentile values of s_H lie 1.645 standard deviations below average values (i.e. s_H is normally distributed). In the case of Methods 3 and 4, $V_{Py,d}$ is calculated using Equation (A7), (A9) or (A12), taking $V_{sH,1} = V_{sH,2}$ ($\beta_{nom} = 1.0$), $V_{My} = 0.05$ (based on various test data collected by the authors), and $V_{model} = 0.0$ or 0.1 . Assuming $V_{sH,1} = V_{sH,2}$ results in identical solutions for modes corresponding to Interpolation conditions [Equations (2) and (3)]. Effects of k_{MC} and k_{DOL} are neglected in the present discussion, i.e. results apply to a case where $k_{MC} = k_{DOL} = 1.0$. Under this circumstance, solutions are identical for Methods 1 and 2, and for Methods 3 and 4.

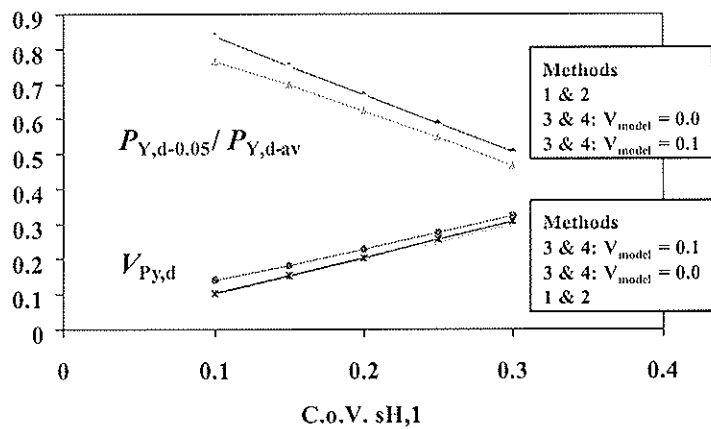


Figure 2 – Interpolation equations 1 & 2: effect of $V_{sH,1}$ on $P_{Y,d-0.05} / P_{Y,d-av}$ and $V_{Py,d}$

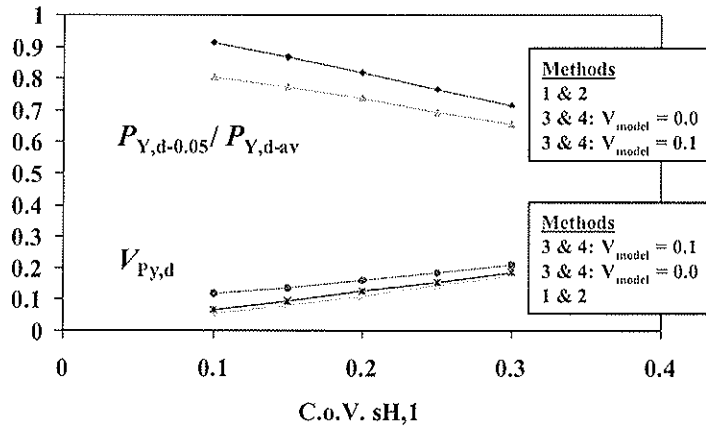


Figure 3 – Mode 3 equation: effect of $V_{sH,1}$ on $P_{Y,d-0.05}/P_{Y,d-av}$ and $V_{Py,d}$

Using Equations (A7) and (A9), $V_{Py,d}$ for ‘interpolation modes’ is not a function of fastener slenderness. It should be noted that this result would not hold if another version of the yield equations were adopted. As would be instinctively expected, $V_{Py,d}$ is lower for mode 3 than for interpolation modes. In general, joint yield strengths become less variable as slenderness of the fastener is increased, i.e. moving from failure modes 1a and 1b to mode 2 then to mode 3 (Figure 1). This is in agreement with numerous data collected by the authors (Smith et al. 2000) and others.

As seen in Figures 2 and 3, there is fairly strong dependence of $P_{Y,d-0.05}/P_{Y,d-av}$ and $V_{Py,d}$ on $V_{sH,1}$. In the case where model uncertainty is ignored, i.e. $V_{model} = 0.0$ (Methods 3 and 4), solutions from all Methods of formulating the design equation give comparable results. However, in the case where $V_{model} = 0.1$ (Methods 3 and 4), solutions from all Methods do not sensibly agree, with Methods 3 and 4 leading to the highest estimates of $V_{Py,d}$ and the lowest estimates of $P_{Y,d-0.05}$. As models can never be totally precise it is unwise to presume $V_{model} = 0.0$. The figures suggest another very simple approach can also work reasonably well. Test data available to the authors suggests that most often $0.2 < V_{sH} < 0.25$, which implies:

- For interpolation mode failures:

$$R_d = P_{Y,d-0.05} \approx 0.55 \phi_{nf} k_{nf} P_{Y,av} \dots\dots\dots (9)$$

- For mode 3 failures:

$$R_d = P_{Y,d-0.05} \approx 0.7 \phi n_f k_{nf} P_{Y,av} \dots\dots\dots (10)$$

The ratios of average strength suggested in Equations (9) and (10) are only indicative, but the appeal of such a simple approach is obvious. It should be noted that values of ϕ should differ in proportion to $V_{P_y,d}$.

Effect of using minimum rather than actual M_Y values

As mentioned previously, it is presumed in some design codes that the fastener yield moment M_Y should be calculated based on minimum specified yield strength of the fastener. This practice is most common for bolts. Daneff (1997) estimated that for SAE Grade 2 bolts, which are those commonly used in timber construction in Canada, the average yield strength in bending is between 514 and 437MPa (coefficient of variation ≤ 0.03 for bolts from one batch). The upper strength is for 6.35mm bolts and the lower strength for 25.4mm bolts. These values can be compared with 310MPa as specified in the Canadian timber design code (CSA 1994), i.e. the value actually being used by engineers. Ignoring the small variability in Daneff’s bolt strengths, it can reasonably be concluded that the actual M_Y of bolts is between about 1.4 and 1.67 times that being assumed in design. The implications of this are underestimation of joint strengths and in some cases prediction of the wrong failure mode. In cases where bolts are slender enough to develop a mode 3 failure, actual capacities are probably between 1.2 (25.4mm bolts) and 1.3 (6.35mm bolts) times those predicted. ‘Errors’ from this source are less for other failure modes degrading to zero for failure modes 1a and 1b, Figure 1.

Although it is likely that the effects of using minimum rather than actual M_Y values are much less for fasteners such as nails and wood screws, it is clear that efforts should be made to use realistic M_Y values.

Placement of $\phi_{fastener}$, ϕ_{wood} , k_{MC} and k_{DOL}

As already mentioned, there is divergence in practice regarding placement of resistance factors and ‘wood related’ modification factors within design equations. Placement of

ϕ_{fastener} and ϕ_{wood} internal to the calculation of P_Y as in Methods 2 and 4 [Equations (6) and (8)] is hard to justify as the practice will lead to variations in reliability levels between joints exhibiting the different yield modes in Figure 1. The importance of moisture condition and duration of loading modification factors (k_{MC} and k_{DOL}) is well established. Mechanics arguments dictate that the most logical placement of such factors is internal to the calculation of P_Y . The argument advanced, in North America at least, in support of having these modification factors external to the calculation of P_Y is that it leads to a consistent form of expression for calculating factored design resistances of members and joints. There is relatively little hard evidence on which to base values for k_{MC} and k_{DOL} but it has been clearly shown that moisture and duration of load effects are not independent (Mohammad and Smith 1996, 1997). A composite modification factor accounting for the combined influences of moisture and loading period, as in Eurocode 5 (CEN 1995), is clearly prudent. Table 1 lists Eurocode 5 values for k_{MC-DOL} . For a mode 3 failure, placing the adjustment factor external to the calculation of P_Y results in a reduction of up to 21 percent in the factored design resistance, compared to if the adjustment factor is internal to the calculation of P_Y (permanent load in service class 3). Mode 3 maximizes sensitivity to placement of k_{MC-DOL} within the design equation.

Table 1. Values of composite modification factor k_{MC-DOL} for solid and glued-laminated timber and plywood [based on Eurocode 5 (CEN 1995)]

| Load duration class | Services class 1 (MC < 12%) | Services class 2 (12% < MC < 20%) | Services class 3 (MC unlimited) |
|-----------------------------------|--------------------------------|--------------------------------------|------------------------------------|
| Permanent (>10 yrs.) | 0.60 | 0.60 | 0.50 |
| Long-term = (6 mo. to 10 yrs.) | 0.70 | 0.70 | 0.55 |
| Medium-term (1 wk. to 6 mo.) | 0.80 | 0.80 | 0.65 |
| Short-term (<1 wk.) | 0.90 | 0.90 | 0.70 |
| Instantaneous | 1.10 | 1.10 | 0.90 |

Note: MC = moisture content typical of solid timber in the service class.

Reliability analysis

It is anticipated that resistance factors, ϕ values, will be calibrated based on closed form first order reliability analysis as applied in the late 1970s to structural steel members and connections (Ravindra and Galambos 1978). The form of the associated design equation is:

$$R_d = n_f k_{inf} P_{Y,av} \exp(-0.55 \beta_j V_{Py}) \dots\dots\dots (11)$$

where β_j is the target reliability index for joints. Its value(s) will be selected based on fundamental considerations and to avoid major discrepancies between new and currently accepted factored design resistances. Although more advanced second order reliability analysis has been used for calibrating design equations for timber members (Foschi et al 1989), it is the opinion of the authors that such an approach is inconsistent with the state of engineering knowledge about strengths of timber joints (Smith and Foliente *in press*).

For design code purposes equation (1b), rather than equation (11), is likely to be used, in which case the resistance factor will be;

$$\phi = P_{Y,av} \exp(-0.55 \beta_j V_{Py}) / P_{Y,0.05} \dots\dots\dots (12)$$

assuming that 5th percentile values are the characteristic resistance level. As an illustration, suppose that β_j is 4.0, $P_{Y,av} / P_{Y,0.05}$ is 1.4 and V_{Py} is 0.2, then ϕ would be 0.58 which is in line with currently accepted values for timber joints.

Conclusions

Variability in yield strength of dowel-fastener joints depends upon the Johansen failure mode. Estimates of that variability should not only reflect the predicted failure mode but also uncertainly in accuracy of the Johansen model. The approach in the Appendix to this paper offers a relatively simple way of calculating variance and thus the coefficient of variation in yield strengths from variability in fastener yield moment and member embedment strengths.

Following the principle of mechanics-based design, the most appropriate format for factored resistance calculations that are based on Johansen type yield theory is:

$$R_d = P_{Y,d-0.05} = \phi n_f k_{inf} P_{Y,d-av} (1 - 1.645 V_{Py})$$

with $P_{Y,d-av}$ being calculated using embedment strengths that have been adjusted to account for effects such as the service environment and duration of the loading ($s_{H,1}$, k_{MC-DOL} , k_2

..... k_j). Adopting this format in a design code will have some practical implications, which should be carefully considered.

Follow-up work will involve Monte Carlo simulation to validate the use of the approximate equations to obtain the variability in P_Y and to conduct probability based calibration of the resistance factor ϕ for EYM-based equations in limit states design.

References

- AFPA. 1999. "General dowel equations for calculating lateral connection values", American Forest and Paper Association, Washington, DC, USA.
- Blass, H.J., Ehlbeck, J. and Rouger, F. 1999, "Simplified design of joints with dowel-type fasteners", Pacific Timber Engineering Conference, Rotorua, New Zealand, March 14-18, Forest Research Institute Limited, Rotorua, NZ, 3.275-3.279.
- CEN. 1995, "Eurocode 5: Part 1.1 Design of timber structures: General rules and rules for buildings", European Committee for Standardisation (CEN), Brussels, Belgium.
- CSA. 1994, "Engineering design in wood (limit states design)", CSA Standard 086.1-94, Canadian Standards Association, Toronto, ON.
- Daneff, G. 1997, "Response of bolted connections to pseudo-dynamic (cyclic) loading", MScFE thesis, University of New Brunswick, Fredericton, NB.
- DeGrace, R.F. 1986, "Commentary on CSA Standard 086.1-M84 Engineering design in wood (limit states design)", Special Publication 086.1.1-M1986, Canadian Standards Association, Toronto, ON.
- Foschi, R.O., Folz, B.R. and Yao, F.Z. 1989, "Reliability-based design of wood structures", Structural Research Series, Report No. 34, Department of Civil Engineering, University of British Columbia, Vancouver, BC.
- Hahn, G.J. and Shapiro, S.S. 1967, *Statistical Models in Engineering*, John Wiley and Sons, New York, NY.
- Johansen, K W. 1949, "Theory of timber connectors", Publication No. 9. International Association of Bridges and Structural Engineering, Bern, Switzerland, 249-262.
- Larsen, H.J. 1979, "Design of bolted joints", Proceedings International Council for Building Research Studies and Documentation: Working Commission W18 - Timber Structures, Bordeaux, France.
- McLain, T.E. 1984, "Mechanical fastening of structural wood members – design and research status", Proceedings of Workshop Structural Wood Research Needs, American Society of Civil Engineers, New York, NY: 31–70.
- Mohammad, M.A.H. and Smith, I. 1997, "Nail embedment responses of lumber and OSB: Influences of moisture conditioning", *Journal of the Institute of Wood Science*, 14(3): 131-139.
- Mohammad, M.A.H. and Smith, I. 1996, "Effects of multi-phase moisture conditioning on stiffness of nailed OSB-to-lumber connections", *Forest Products Journal*, 46(4): 76-83.
- Ni, C. 1997, "Behaviour of nailed timber joints under reversed cyclic load", PhD thesis, University of New Brunswick, Fredericton, NB.
- Ravindra, M.K. and Galambos, T.V. 1978, "Load and resistance factor design for steel", *ASCE Journal of the Structural Division*, 104(ST9): 1337-1353.

- Smith, I. and Foliente, G. *in press*, “LRFD of timber joints: International practice and future direction”, *ASCE Journal of Structural Engineering*.
- Smith, I., Craft, S. and Quenneville, P. 2001, “Design capacities of joints with laterally loaded nails”, *Canadian Journal of Civil Engineering*, 28(2): 282-290.
- Smith, I., Foliente, G.C. Syme, M. McNamara, R. and Seath C. 2000, “Development of limit states design method for timber joints – 2. Comparison of experimental results with EYM predictions”, BCE Doc 00/177, CSIRO Building, Construction and Engineering, Highett, Victoria, Australia.
- Whale, L.R.J., Smith, I. and Larsen, H.J. 1987, “Design of nailed and bolted joints - Proposals for the revision of existing formulae in draft Eurocode 5 and the CIB Code”, CIB-W18, Dublin, Ireland (paper 20-7-1).
- Wood, L.W. 1951, “Relation of strength of wood to duration of load”, Report No. R1916, US Forest Products Laboratory, Madison, WI.

Appendix - Expected Value and Coefficient of Variation of P_Y

For the purposes of demonstration, consideration is restricted to single shear joints. The expected (average) value, $E(\cdot)$, and variance, $\text{Var}(\cdot)$, of P_Y for particular failure mode can be estimated using the theory for Generation of System Moments (Hahn and Shapiro 1967). It is reasonable to presume that terms in Equations (2) to (4) are not correlated, and thus the expected value and variance can be determined from statistical distributions of $s_{H,1}$, M_Y , d , l_1 , α , β , Φ_1 , Φ_2 and Φ_3 . The mean value of P_Y for a mode of failure can be estimated by a curtailed multi-variable Taylor’s series that takes the form:

$$E(z) = h[E(x_1), E(x_2), \dots, E(x_n)] + \frac{1}{2} \sum_{i=1,n} \partial^2 h / \partial x_i^2 \text{Var}(x_i) \dots\dots\dots (A1)$$

where $\partial^2 h / \partial x_i^2$ denotes $\partial^2 h / \partial x_i^2$ evaluated at $E(x_r)$, i.e. $E(x_r)$ substituted for x_r , $r = 1, 2, \dots, n$. Variance of P_Y for a mode of failure can also be estimated by a multi-variable Taylor’s series that takes the form:

$$\begin{aligned} \text{Var}(z) &= \sum_{i=1,n} (\partial h / \partial x_i)^2 \text{Var}(x_i) + \sum_{i=1,n} (\partial h / \partial x_i) (\partial^2 h / \partial x_i^2) \mu_3(x_i) \\ &\approx \sum_{i=1,n} (\partial h / \partial x_i)^2 \text{Var}(x_i) \dots\dots\dots (A2) \end{aligned}$$

where $(\mu_3(x_i))$ is the third central moment of x_i . The approximate form of the equation for $\text{Var}(z)$ is adequate as distributions for $s_{H,1}$, M_Y , d , l_1 , α and β are approximately normal ($\mu_3(x_i) \approx 0.0$). The coefficient of variation is given by:

$$V_z = [\text{Var}(z)]^{0.5} / E(z) \dots\dots\dots (A3)$$

Using the relationship $\beta = s_{H,2} / s_{H,1}$, Equations (A2) and (A3) yield:

$$V_\beta = [V_{s_{H,1}}^2 + V_{s_{H,2}}^2]^{0.5} \dots\dots\dots (A4)$$

where $V_{s_{H,1}}$ and $V_{s_{H,2}}$ are the coefficients of variation for $s_{H,1}$ and $s_{H,2}$, respectively. Based on numerical simulation, it was found that for values of β that are of interest, reasonable approximations are:

$$V_{\Phi_1} \approx V_{\beta} / 6; \quad V_{\Phi_2} \approx V_{\beta}; \quad V_{\Phi_3} \approx V_{\beta} / 2 \quad \dots\dots\dots (A5)$$

Following from the above, the following are the expected values and coefficients of variation of P_Y for each failure mode:

- *Failure in the side member (Interpolation 1)*

$$E(P_Y) = E(s_{H,1}) E(d) E(l_1) E(\Phi_1) \quad \dots\dots\dots (A6)$$

$$V_{P_Y} \approx 1/6 [37V_{sh,1}^2 + V_{sh,2}^2]^{0.5} \quad \dots\dots\dots (A7)$$

where $E(\Phi_1) = 1 / [1 + \{(1+E(\beta)) / E(\beta)\}^{0.5}] \approx 1 / [1 + \{(1+\beta_{nom}) / \beta_{nom}\}^{0.5}]$, with β_{nom} being the nominal value of β .

- *Failure in the main member (Interpolation 2)*

$$E(P_Y) = E(s_{H,1}) E(d) E(l_1) E(\alpha) E(\Phi_2) \quad \dots\dots\dots (A8)$$

$$V_{P_Y} \approx 1/6 [V_{sh,1}^2 + 37V_{sh,2}^2]^{0.5} \quad \dots\dots\dots (A9)$$

where $E(\Phi_2) = E(\beta) / [1 + \{1+E(\beta)\}^{0.5}] \approx \beta_{nom} / [1 + \{1+\beta_{nom}\}^{0.5}]$.

- *Formation of plastic hinge in both members (Mode 3)*

$$E(P_Y) = 2 [E(M_Y) E(s_{H,1}) E(d)]^{0.5} E(\Phi_3) [1 - 1/32 (4V_{M_Y} + 5V_{sh,1}^2 + 4V_{sh,2}^2)] \\ \approx 2 [E(M_Y) E(s_{H,1}) E(d)]^{0.5} E(\Phi_3) \quad \dots\dots\dots (A10)$$

$$V_{P_Y} \approx 1/4 [4V_{M_Y}^2 + 5V_{sh,1}^2 + V_{sh,2}^2 + 4V_d^2]^{0.5} \quad \dots\dots\dots (A11)$$

where $E(\Phi_3) = [E(\beta) / \{1 + E(\beta)\}]^{0.5} \approx [\beta_{nom} / \{1 + \beta_{nom}\}]^{0.5}$, and V_{M_Y} and V_d are coefficients of variation for M_Y and d , respectively. Usually $V_d \approx 0.0$ and Equation (A11) simplifies to:

$$V_{P_Y} \approx 1/4 [4V_{M_Y}^2 + 5V_{sh,1}^2 + V_{sh,2}^2]^{0.5} \quad \dots\dots\dots (A12)$$

NOTES: 1) Expression (A9) as shown here is not fully consistent with approximation for V_{Φ_2} in equation (A5). This is because it is purely arbitrary which member is designated 1, and which member is designated 2. What is done makes equations (A7) and (A9) consistent. 2) There is always uncertainty associated with application of any model and that can be allowed for by adding appropriate terms to equations for V_{P_Y} . A term $36V_{model}^2$ should be added in Equations (A7) and (A9), and a term of $16V_{model}^2$ in Equations (A11) or (A12), these being placed under the root sign. V_{model} is the coefficient of variation associated with model accuracy. In the absence of better information, a value of 0.1 is initially suggested.

**INTERNATIONAL COUNCIL FOR RESEARCH AND INNOVATION
IN BUILDING AND CONSTRUCTION**

WORKING COMMISSION W18 - TIMBER STRUCTURES

DESIGN AND MODELLING OF KNEE JOINTS

J Nielsen

P Ellegaard

Department of Building Technology and Structural Engineering
Aalborg University

DENMARK

Presented by: J Nielsen

- H J Blass asked what spans were intended for these structures and how would one deal with different roof angles.
- J Nielsen answered 8 m to 10 or 11 m and most roof angles were 44 to 45 degrees.
- V Enjily asked what were the production problems with the double plates.
- J Nielsen answered the first plate was pushed in and then the second plate was slightly offset and pushed in. Alignment and wood compression problems were observed.
- H J Blass asked why thicker 2 mm plates were not used.
- J Nielsen answered such plates were not available.
- S Olsson commented that it seemed the timber structures had similar behaviour as steel structure (no cracking); however, by increasing the plate thickness the structure had brittle failure mode again. Was this desirable?
- J Nielsen answered that it was a problem identified by the truss manufacturer. It was a good solution to move the failure to the timber to obtain more ultimate use of the timber.
- J Kangas commented that the title promised too much and asked why existing models were not considered.
- J Nielsen agreed and stated that additional work would be needed to address the compression failure parallel to grain and crack failures. Rotational stiffness of plate was already included in the model and it could predict the deflections and forces. Refinements have been initiated to improve predictions.
- V Enjily commented that usually 4 small plates were used as a solution and bigger plates would be a good idea if manufacturing issues were resolved.
- J Nielsen agreed.
- F Lam commented that moving the failure mode to the wood would increase variability in the load capacity which would not be good from reliability perspective.
- B Källsner asked about the potential damage in the timber at the boundaries of the two-plate system.
- J Nielsen agreed and stated that same size plates were used to ensure second plate would not cause problem at the boundaries.

Design and Modelling of Knee Joints

Jacob Nielsen, Peter Ellegaard

Department of Building Technology and Structural Engineering
Aalborg University, Denmark

1 Abstract

The work on modified attic trusses has been continued at Aalborg University. 60 tests divided into 25 different test series are made on truss segments with a knee joint. The influence of type and number of plates, cutting of the timber members, and compound rafters have been tested. Some of the tests and the results are described in this paper. Finally a few load-displacements curves of the tests are compared to a numerical model.

2 Introduction

During the last 15 years modified attic trusses have been used for Danish buildings, see figure 1.

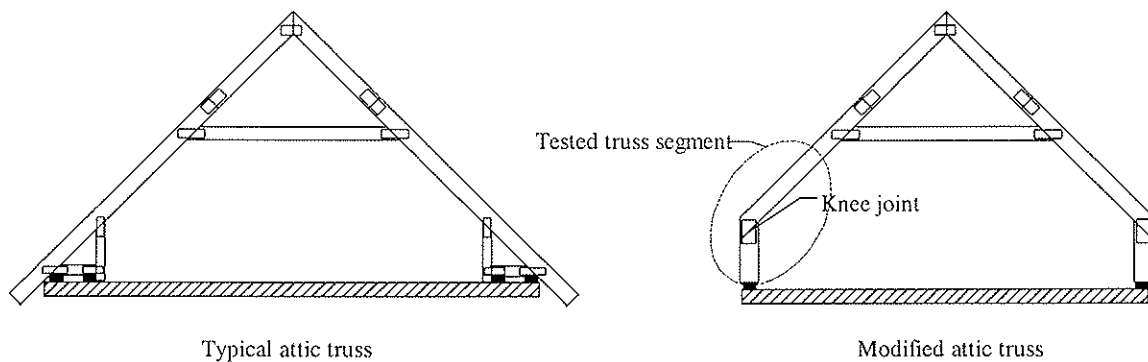


Figure 1: Shape of a typical attic truss and a modified attic truss.

The modified attic trusses are an attractive alternative to the typical trusses caused by better utilisation of the upper floor. The slope of the rafters is normally around 45° . However, the behaviour of the modified attic trusses is very dependent on the stiffness and the strength capacity of the knee joint, see figure 1 right. When the truss span is below 8 m the knee joints can be produced with punched metal plate fasteners. Above 8 m the knee joints have to be produced with steel gussets or nail-glued plywood, which are very costly connection types compared to punched metal plate fasteners.

In order to improve the design of the knee joints with punched metal plate fasteners the Department of Building Technology and Structural Engineering has cooperated since 1989 with the Association of Danish Manufactures of Roof Trusses.

In 1990 some full-scale static and dynamic tests have been performed on modified attic trusses with different designs of the knee joints. In addition to the full-scale tests a number of short-term tests were conducted on the truss segment including the knee joint, see figures 1 and 2.

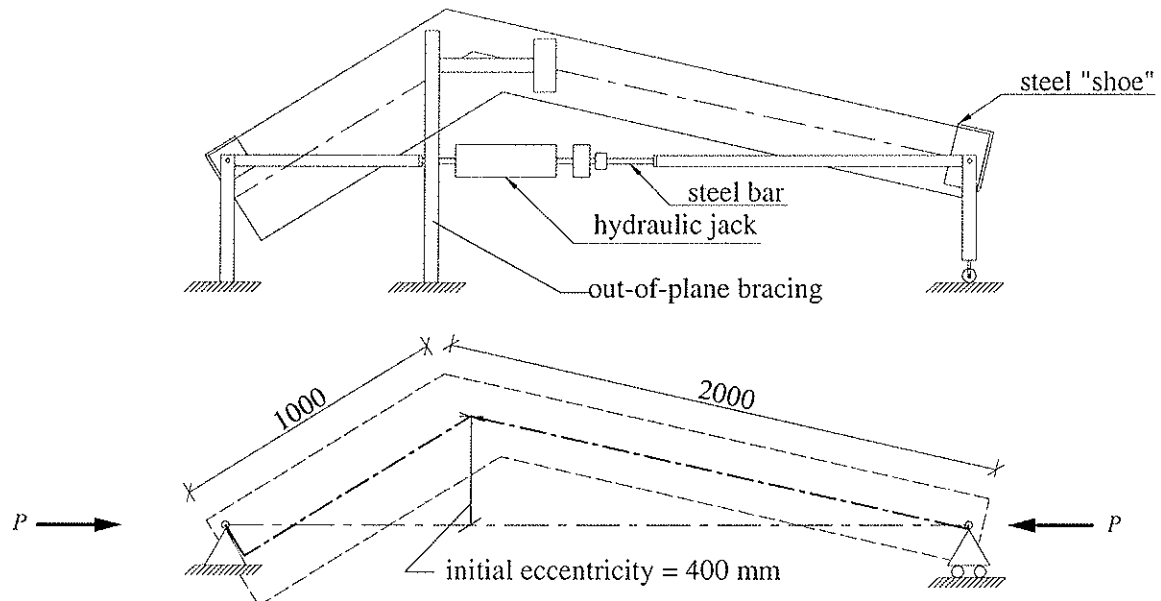


Figure 2: Test set-up of a truss segment. Dimensions in mm.

The average ultimate moment capacity of the knee joint designs with punched metal plate fasteners was found as 4.7 kNm with 45×220 mm leg and rafter. In some series the legs were designed with two parallel-connected timber beams increasing the leg width to 290 or 440 mm and causing an increased moment capacity of 8.3 and 11.6 kNm, respectively. In all cases the failure modes were affected by splitting in the wood and it was found that a location of punched metal plate fasteners close to the upper edge of the rafter prevents splitting of the rafter and increases the moment capacity significantly. The tests and some numerical analysis are described in Hansen et al. (1990) and Mortensen et al. (1992).

In the autumn of 2000 the work was continued with a number of experimental and numerical tests. The objectives of the work are twofold:

- to develop improved designs for knee joints with punched metal plate fasteners.
- to develop, calibrate and test a numerical model.

The experimental work was divided into two test programmes each with 30 tests. 15 different joint designs were tested in test programme 1. The experience of test programme 1 was used to design further 10 test series in test programme 2.

The dimensions of the test set-up give a combination of section forces at the joint, which corresponds to a modified attic truss, spanning 8 m, hinged at the legs and loaded with dead load only (roof and ceiling).

Each test specimen is loaded according to EN 26891.

Load-displacement curves of the tests are compared to the results from the numerical model. A detailed description of the whole work is given in Nørgaard et al. 2001.

3 Description of tests and results in test programme 1

Test programme 1 contained 15 different test series each with 2 tests, see figures 3, 4 and 5.

In each test series the joint design is different as the number, location and type of the punched metal plate fasteners were varied as well as the cutting of the beams at the joint. The size, location and type of the lower plates in the leg were not changed.

The rafters were made of one or two parallel-connected timber beams, i.e. the total dimension of the rafter was 45×245 mm. The legs were made of two or three parallel-connected timber beams, i.e. a total dimension of the leg of 45×360 mm, see figures 3, 4 and 5.

In general, two plate types from Mitek Inc. were used: GNA-20S and a GNT-150S. The plates have the following properties:

| Plate type | Thickness | Nail density | Nail length |
|------------|-----------|-----------------------|-------------|
| | mm | nails/cm ² | mm |
| GNA-20S | 1,0 | 1.47 | 8 |
| GNT-150S | 1,5 | 0.67 | 14 |

Table 1: Properties of the plate types used.

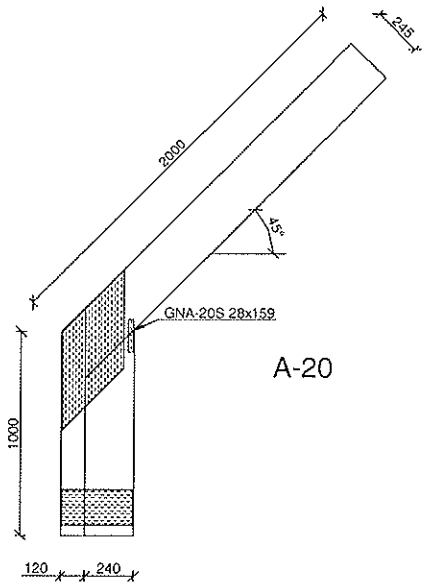
The same steel quality is used for both plate types, and the yield stress is at least 350 MPa.

The numbers 20 and 150 in the series name denote the plate type used in the knee joint and series with compound rafter were denoted r2. Two 174×350 mm GNT-150S plates are used to connect the legs 50 mm from the end.

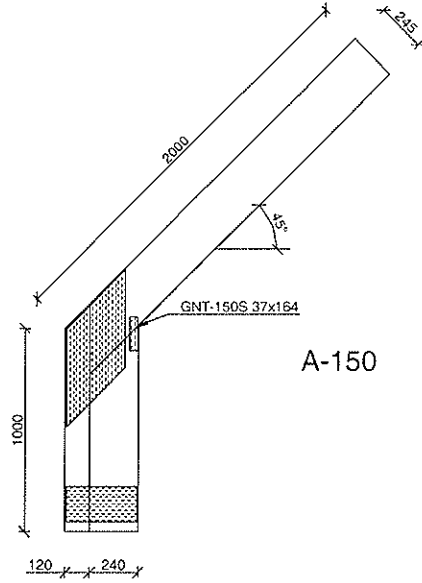
A large trapezoidal shaped plate was used as the primary connector in the knee joint for both plate types, see e.g. series A to E in figures 3 and 4. These plates are not standard and they were cut specially for this project. The dimensions of the vertical and the sloped plate edge were about 480×429 mm and 480×410 mm for the GNA-20S and GNT-150S, respectively.

Swedish spruce of strength class K24 (S10) was used. To get some knowledge of the stiffness properties of each timber member the E-modulus of the uncut timber beams (45×245 mm and 45×120) were measured according to EN 408. However, to save time the beams were conditioned at 85 % relative humidity, which gives an average moisture content about 16 % before the stiffness testing.

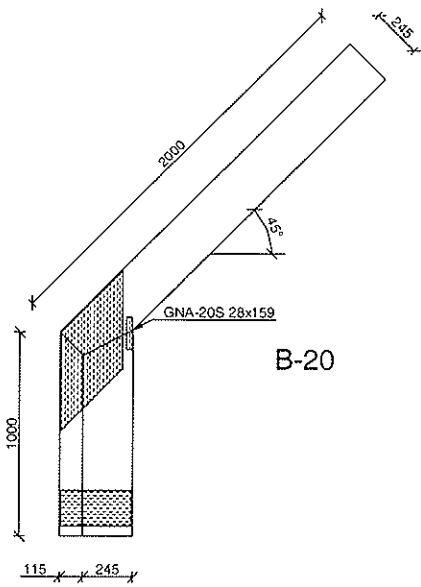
After measured E-modulus the test specimens were conditioned according to prEN1075 and cut and assembled at a truss plant.



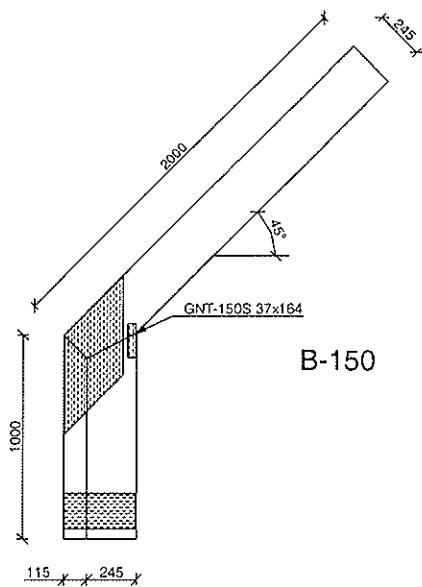
A-20



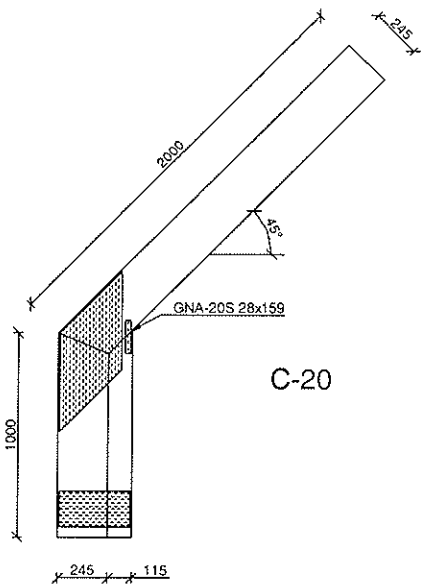
A-150



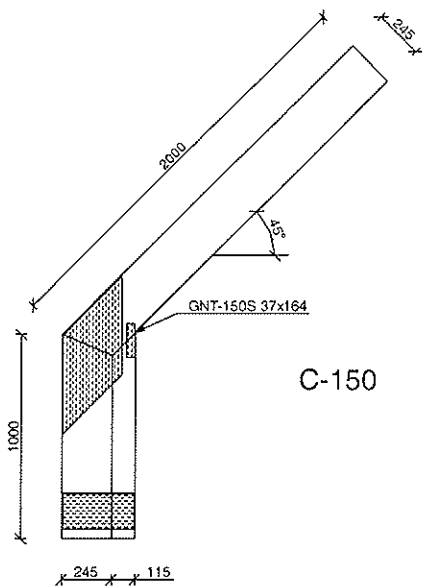
B-20



B-150



C-20



C-150

Figure 3: Series 1 - 6 in 15 test series of test programme 1. Dimensions in mm.

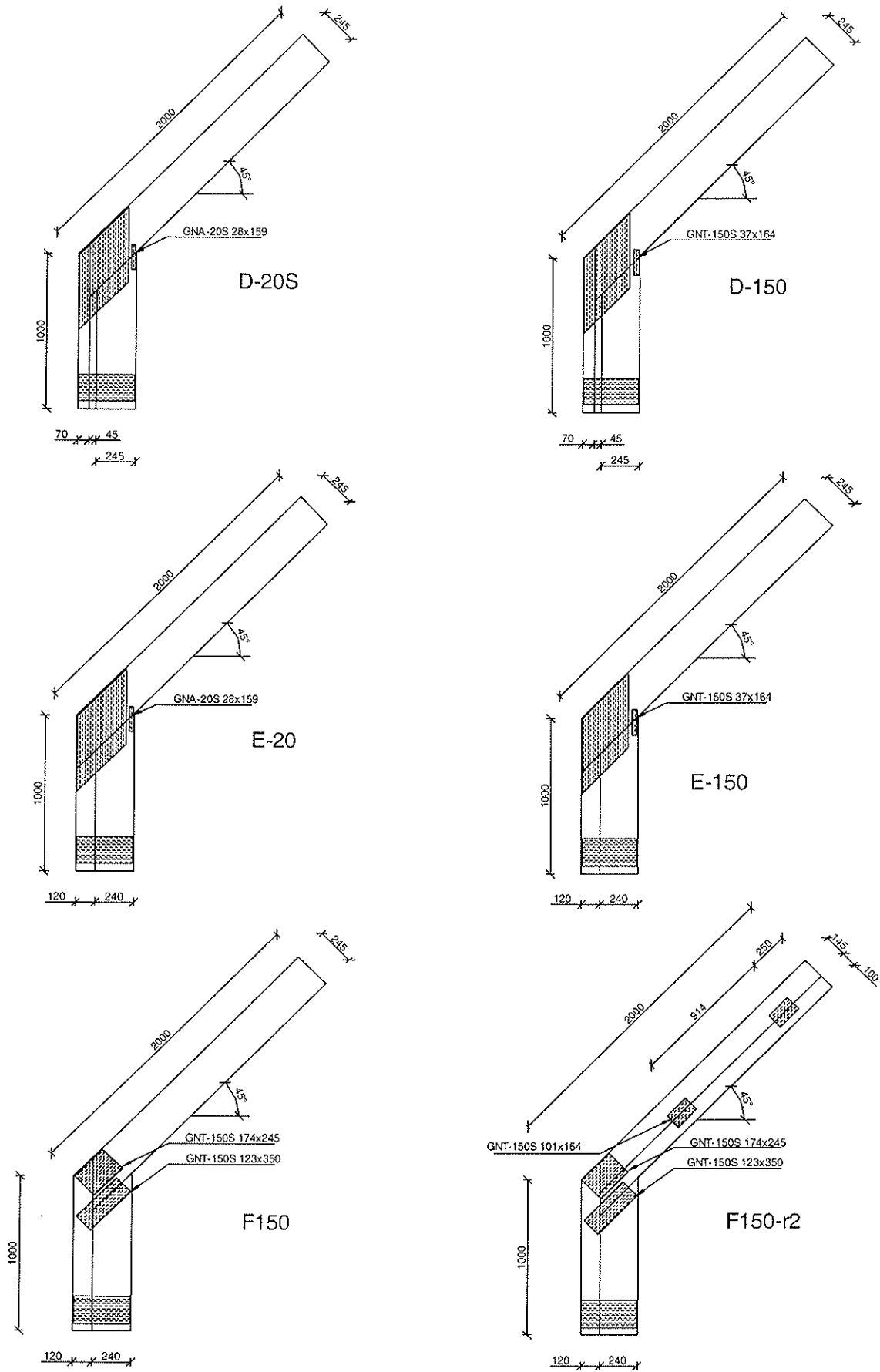


Figure 4: Series 7 - 12 in 15 test series of test programme 1. Dimensions in mm.

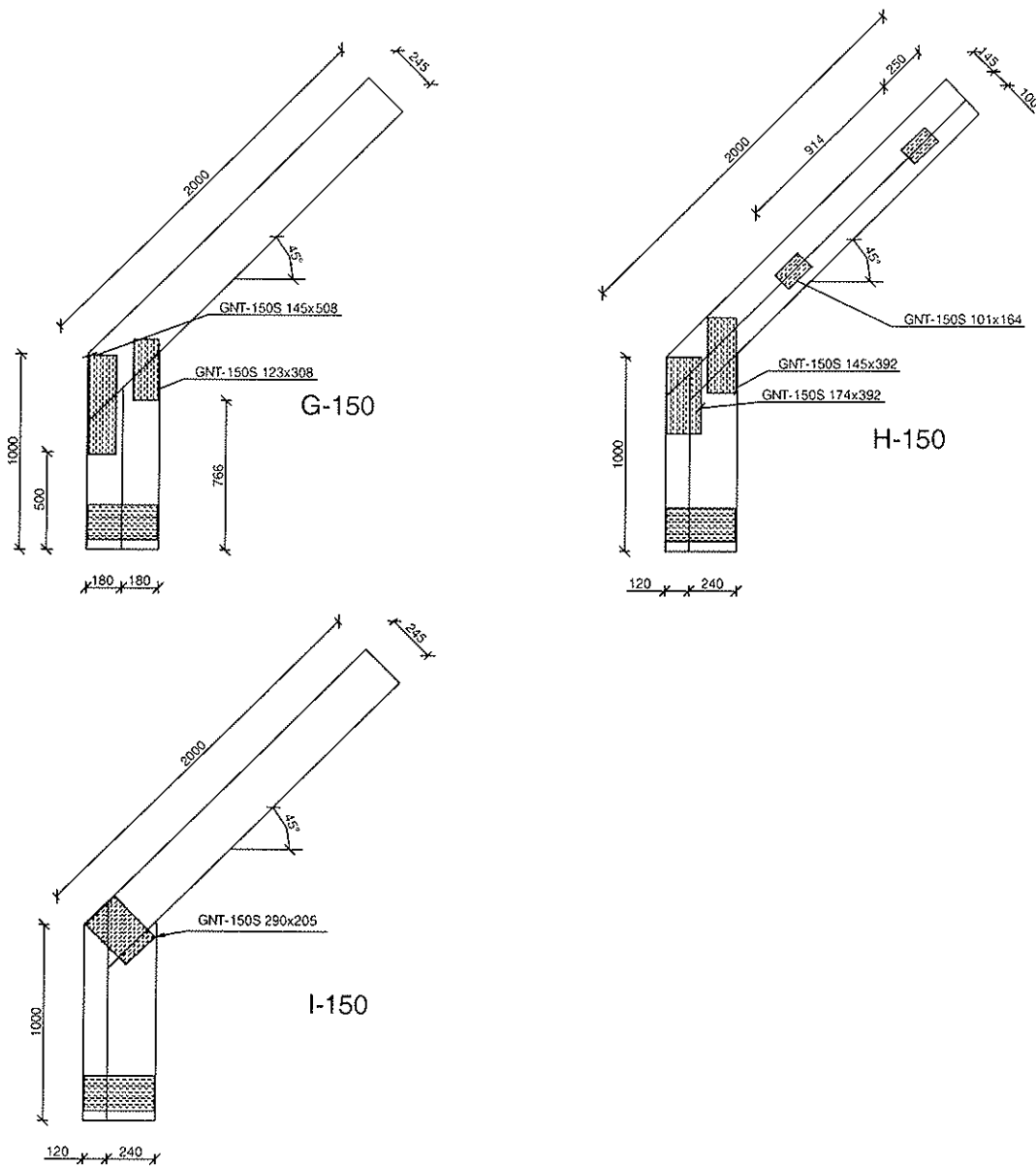


Figure 5: Series 13 - 15 in 15 test series of test programme 1. Dimensions in mm.

The designs of the knee joints are based on a brainstorm. Some of the test series e.g. test series B, C, and I are not optimal from a practical point of view and they only have theoretical interests.

3.1 Results

In table 2 the average failure load, the average failure moment, the failure type and load level at 5 and 10 mm displacement are given. The displacements are given as the horizontal movement of the rafter end, see the loading point on the rafter in figure 2. The failure moments are based on an initial eccentricity of 40 cm, see figure 2. The failure moments based on the deformed eccentricity are about 8 % higher.

During testing contact between the leg and the rafter was observed and further loading generated large compression deformations perpendicular to the grain at the contact zone of the rafter. Furthermore, close to failure, compression failure parallel to grain (kinking

band) was observed in the rafter just above the contact zone and hereafter only plastic deformations developed.

In table 2 the failure types for each series are denoted as follows: Sl: Splitting in the leg, Sr: Splitting in the rafter, P: Plate failure, W: Withdrawal of the nails and Tr: Tension failure in the rafter outside the plate area.

| Series | F_{max} KN | M_u kNm | Failure type | F_5 kN | F_{10} kN |
|-----------------|--|---------------------------------------|-------------------------------|--------------------------------------|---|
| A-150 | 35,3 | 14,1 | Sl | 10,4 | 20,0 |
| A-20 | 31,0 | 12,4 | P | 10,6 | 19,6 |
| B-150 | 38,0 | 15,2 | Sr | 11,7 | 21,3 |
| B-20 | 33,3 | 13,3 | W | 12,8 | 21,9 |
| C-150 | 38,6 | 15,4 | Tr | 10,4 | 20,5 |
| C-20 | 32,9 | 13,2 | W | 10,6 | 18,9 |
| D-150 | 33,9 | 13,6 | Tr | 11,1 | 20,5 |
| D-20 | 32,3 | 13,1 | P | 10,5 | 20,6 |
| E-150 | 40,5 | 16,2 | Tr | 12,1 | 22,7 |
| E-20 | 40,9 | 16,4 | Tr | 12,0 | 22,9 |
| F-150 | 28,6 | 11,5 | W | 8,7 | 17,1 |
| F-150-r2 | 29,3 | 11,8 | W | 7,1 | 14,0 |
| G-150 | 34,8 | 13,9 | W, Sr | 11,5 | 21,2 |
| H-150 | 35,5 | 14,2 | Tr, Sr | 11,3 | 20,1 |
| I-150 | 28,2 | 11,3 | W | 7,6 | 14,9 |

Table 2: Average failure load/moment, failure type and average load level at 5 and 10 mm displacement.

In general the deviation around the average was below 6% (note: only 2 tests).

By comparing series A to E the influence of the cutting and plate type can be found. Test series E obtained the maximum failure capacity and stiffness properties with both plate types and in these cases the failure occurred in the rafter just outside the joint area.

When comparing the influence of the plate types the thick plate GNT-150S increases the bearing capacity. However, the stiffness is not affected by the plate types, as the values of F_5 and F_{10} are almost the same.

By comparing F-150 and F-150-r2 the effect of two beams in the rafter is found. The bearing capacity is the same, but the stiffness is decreased by almost 20% in tests with a compound rafter.

4 Description of tests and results in test programme 2

Based on the results of test programme 1 further 10 test series were developed and 8 of the series are shown in figures 6 and 7. Additional tests of series E-150 and 3 new test series based on series E-150 were made. The influence of 290 and 360 mm leg width and 2 or 4 embedded plates at the knee joint was analysed, see figure 6. A “t” in the series name denotes “thin” leg width (290 mm) and “2P” denotes series with 2 embedded punched metal plate fasteners on each side.

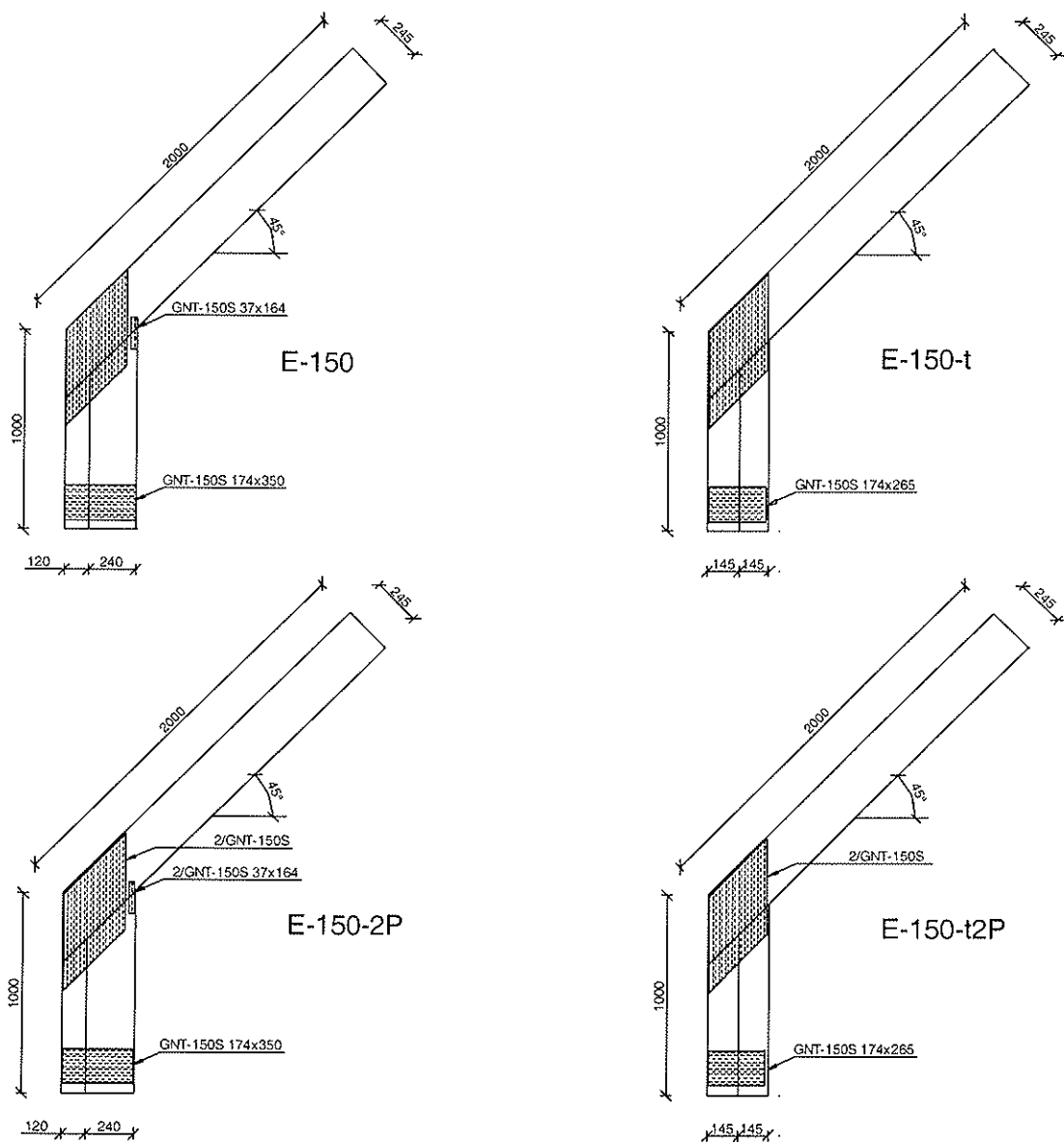


Figure 6: Series 1 - 4 in 8 test series of test programme 2. Dimensions in mm.

In series J a single-sloped plate was tested. Also in these series the influence of leg width and numbers of embedded plates was analysed, see figure 7.

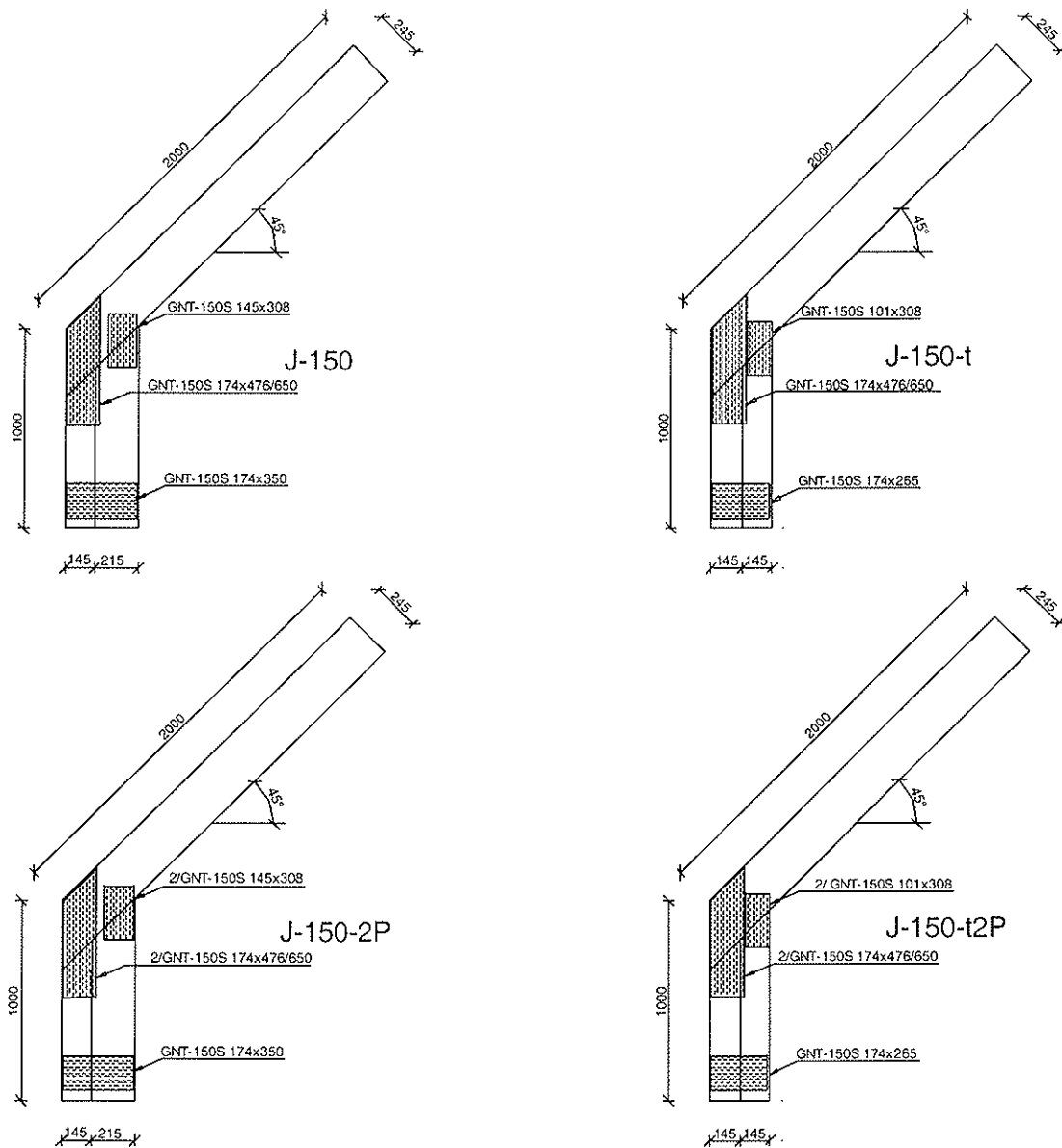


Figure 7: Series 5 - 8 in 8 test series of test programme 2. Dimensions in mm.

4.1 Results

In table 3 the average failure load, the average failure moment, the failure type and the load level at 5 and 10 mm displacement are given. The same observations as in test programme 1 were made.

Several production problems were encountered (bending of nails, wood crushing) when embedding 2 plates on each side of the timber, and if this joint is to be utilized the plate design and the embedding tool must be redesigned.

| Series | No tests | F_{max} kN | M_u kNm | Failure type | F_5 kN | F_{10} kN |
|-----------|----------|-----------------|--------------|--------------|-------------|----------------|
| E-150 | 4 | 45,6 | 18,2 | Tr, Sl | 11,3 | 21,7 |
| E-150-t | 4 | 40,8 | 16,3 | Tr, Sr | 10,3 | 19,5 |
| E-150-2P | 2 | 43,6 | 17,5 | Tr,Sl | 13,5 | 26,1 |
| E-150-t2P | 2 | 51,3 | 20,5 | Sl,Shr | 12,1 | 22,2 |
| J-150 | 4 | 42,5 | 16,9 | Tr,Sl | 11,1 | 21,3 |
| J-150-t | 4 | 35,2 | 14,1 | Tr,Sl,Sr | 9,9 | 19,2 |
| J-150-2P | 2 | 39,5 | 15,6 | Tr | 12,9 | 24,9 |
| J-150-t2P | 2 | 40,4 | 15,8 | Tr,Sr | 9,5 | 19,1 |

Table 3: Average failure load/moment, failure type and load level at 5 and 10 mm displacement.

In table 3 the failure types for each series are denoted as follows: Sl: Splitting in the leg, Sr: Splitting in the rafter, Shr: Shear failure parallel to grain in the rafter P: Plate failure, W: Withdrawal of the nails and Tr: Tension failure in the rafter outside the plate area.

In general the deviation around the average is around 5-10 %.

A decreased leg width decreases the average bearing capacity by 10-20 % in tests with one plate on each side. However, an increased capacity is observed in series E-150-t2P and J-150-t2P. In all tests the stiffness at 5 and 10 mm is increased by 10-20 % in tests with a “thin” leg.

The influence of 2 plates on each side is not obvious. In tests with 360 mm leg a “double plate” decreases the capacity and stiffness, however, in tests with 290 mm leg the “double plate” increases the capacity and stiffness.

In general a knee joint design with a trapezoidal punched metal plate fastener is a promising design type as it increases the bearing capacity to 16 and 18 kNm for the leg width of 290 and 360 mm, respectively. This is approximately twice the capacity obtained by the tests described in Mortensen et al. (1992).

5 Numerical analysis

The test series have been modelled by a finite beam element program called TRUSSLAB. The programme is described in detail in Ellegaard et al. (1999). However, the plate element has been further developed. The plate element consists of a number of small beam elements located over the joint line. In order to model yielding in tension and buckling in compression the stress-strain relation for these beams is non-linear, see figure 8. The axial force and the moment given at the ends of the beams determine the distribution of the axial stresses. The shear force is determined by establishing equilibrium.

The properties of the nail and plate elements have been calibrated by basic tensile, compression and shear tests, see Nørgaard et al. (2001) and Ellegaard (2000).

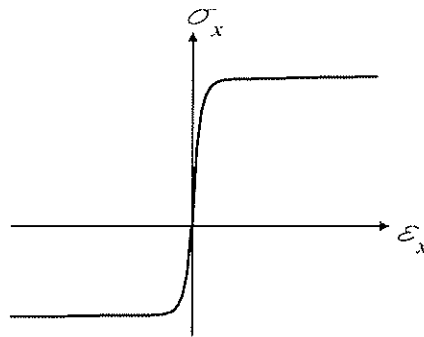


Figure 8: Stress-strain relation for axial stresses in beams in plate element.

In figures 9 to 12 the load-displacement curve from TRUSSLAB is compared with the test results in series E-150, E-150-t, J-150 and J-150-t. The thick solid line gives the numerical result.

The numerical results are based on the following:

- An average E-modulus of each of the timber parts (leg or rafter) within a series has been used.
- The second order displacements are added by increasing the output displacement by 8%.
- The initial position of the numerical load-displacement curve has been moved to the initial part of the reloading curves of the test results.
- The gap between the timber members is 1 mm.

In figure 9 to 12 it is seen that TRUSSLAB is able to predict the initial stiffness of the truss segment. However, during loading the model underestimates the deformation, which is caused by the fact that the timber is modelled by linear elastic Timoshenko beam elements and therefore is unable to model splitting and plastic deformation parallel to the grain at the compression zone. The compression between the timber members is modelled by contact elements with bi-linear properties.

In general, buckling and contact are obtained in the numerical model, but no plastic deformation perpendicular to the grain is obtained in the compression zone. This might be because the buckled beams of the plate element do not lose their load capacity after buckling, which is observed in basic compression tests.

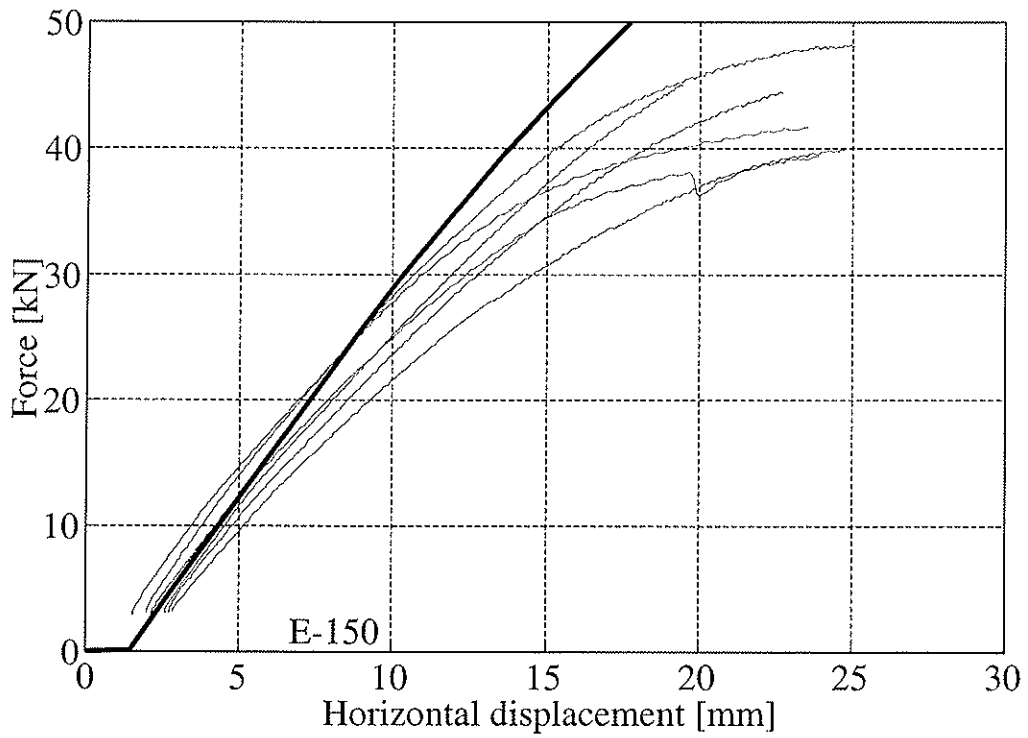


Figure 9: Load-displacement curves of series E-150.

The load-displacement curves for the (2+4) tests in series E150 in test programmes 1 and 2 are shown in figure 9.

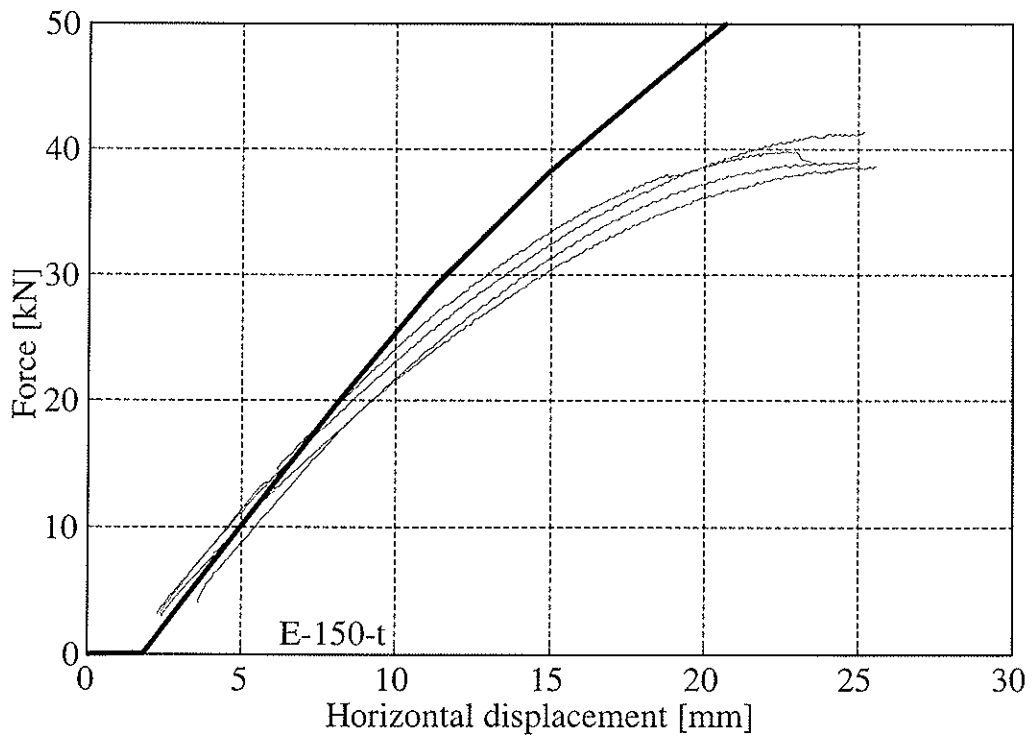


Figure 10: Load-displacement curves of series E-150-t.

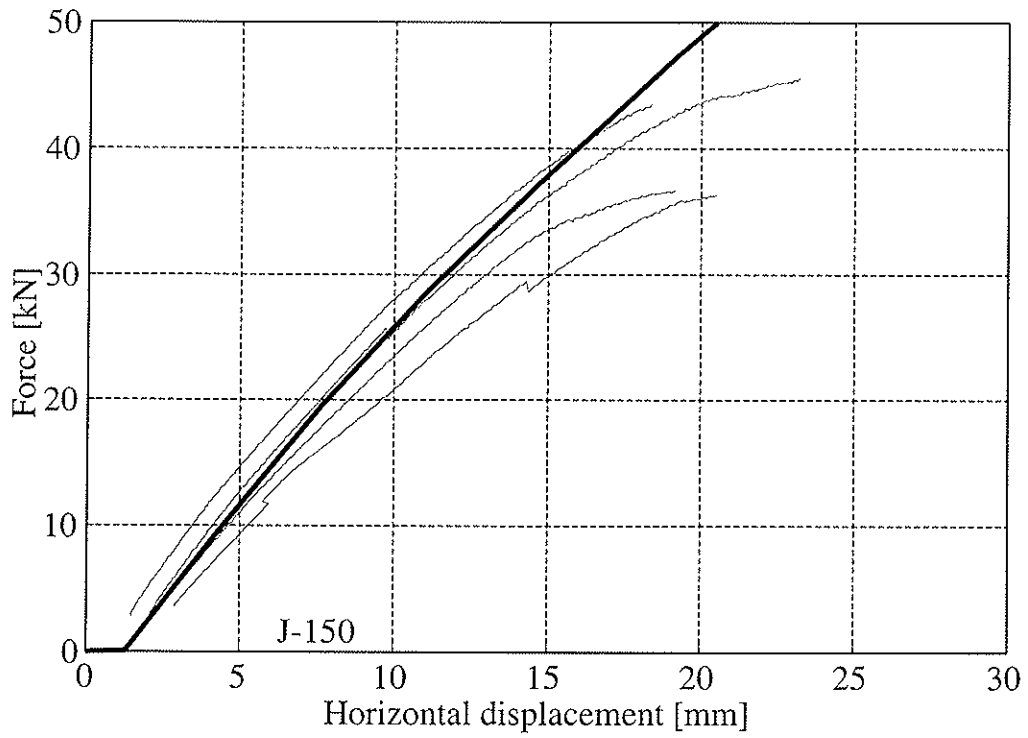


Figure 11: Load-displacement curves of series J-150.

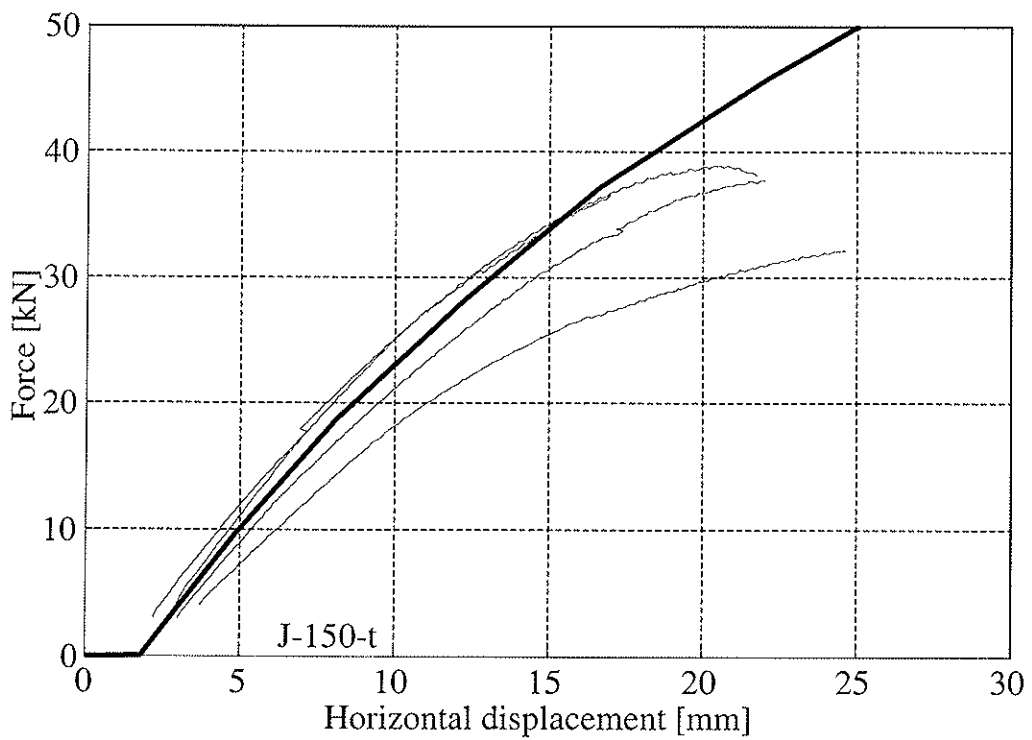


Figure 12: Load-displacement curves of series J-150-t.

6 Conclusion

Based on the results the following conclusions can be made:

- A knee joint design with a trapezoidal punched metal plate fastener is a strong and stiff joint type as the bearing capacity is doubled compared to the tests described in Mortensen et al. (1992). The above design gives a bearing capacity of 16 and 18 kNm for tests with 290 and 360 mm leg width.
- The influence of embedding 2 plates on each side of the joint is not clear and the production of these kinds of joints causes production problems.
- A numerical model is able to predict the initial stiffness of the joint types. At load levels above half the failure load the displacement is underestimated as modelling of wood with cracks and compression failure parallel to grain is not possible with TRUSSLAB.

7 References

Nørgaard M., Thomsen K. B., Strength and stiffness analysis of knee joints in modified attic trusses. (in Danish) Styrke- og stivhedsanalyse af hjørnesamlinger på trempelspær. B.Sc.-thesis, Aalborg University, March 2001.

Hansen F. T., Mortensen N. L., Hansen L. P. (1990), Full-scale Testing of Prefabricated Timber Frames Subjected to Static and Dynamic Load. Part no. 1, 2 and 3 (in Danish). ISSN 0902-7513 R9024, R9026 and R9128

Mortensen N. L., Kloch S., Strength and Stiffness of Knee Joints in Timber Frames, Aalborg University, December 1992. ISSN 0902-7513 R9247

Ellegaard P., Nielsen J. (1999), Advanced Modelling of Trusses with Punched Metal Plate Fasteners, Symposium Proceedings, RILEM Symposium on Timber Engineering 1999, Stockholm, Sweden., ISBN 2-912143-10-1.

Ellegaard P. (2000), Stiffness Analysis of Nail Plates, Proceedings of CIB-33, Delft, August 2000.

INTERNATIONAL COUNCIL FOR RESEARCH AND INNOVATION
IN BUILDING AND CONSTRUCTION

WORKING COMMISSION W18 - TIMBER STRUCTURES

TIMBER-STEEL SHOT FIRED NAIL CONNECTIONS AT ULTIMATE LIMIT STATES

R J Bainbridge
P Larsen
C J Mettem
TRADA Technology
P Alam
M P Ansell
University Of Bath
UNITED KINGDOM

Presented by: R J Bainbridge

- H J Blass asked why use the average values for the penetration depth of the head and point side nail.
- R J Bainbridge answered that it was a simplification as the penetration depth was governed by the explosive charge delivery and there would be fluctuation.
- H J Blass suggested that the minimum penetration depth should be considered for design.
- R J Bainbridge agreed.
- H J Larsen commented that the stated objective seemed to promise too much. He asked would anyone take up this connection method commercially. Also he questioned how much was the gain by using finch beams rather than timber in terms of economy and performance.
- R J Bainbridge answered the commercial aspect is a separate issue from this paper. The industry was encouraged by the potential use of lower grade timber.
- H J Blass stated that in Germany 3.2 mm nails driven with airgun have been available.
- H J Larsen commented that these systems have not been frequently used either.
- H J Blass asked what was the final angle of the failed nails.
- R J Bainbridge answered the angles were not measured and the information was not available at hand.
- H J Blass commented corrosion might be a problem as zinc coating could be damaged during installation.
- R J Bainbridge answered the manufacturer did not think it would be a problem.
- V Enjily commented that the distortion of timber after installation from moisture effects might be an issue.
- I Smith commented that the friction between timber and steel plate might change after installation thus influencing the performance.
- R J Bainbridge answered this was not considered in the initial study.
- J Ehlbeck asked which equation was used to predict the characteristic load R_k with reference to information on Page 7. This is an issue related to characteristic versus design loads.
- R J Bainbridge clarified that there was a misprint in Pg 7. The correct term should be characteristic values not design values (Fig 10).

Timber-Steel Shot Fired Nail Connections at Ultimate Limit States

Bainbridge, R.J., Principal Engineer, TRADA Technology, UK
Larsen, P., Project Engineer, TRADA Technology, UK
Mettem, C.J., Chief Research Engineer, TRADA Technology, UK
Alam, P., Postgraduate Student, University Of Bath, UK
Ansell, M.P., Senior Lecturer, University Of Bath, UK

Abstract

Composite timber/steel structural elements have the potential to combine the benefits of timber construction (ease of working, readily available resource, simple connection of ancillary components) with the strength and stiffness of structural steelwork.

Conventional flitch members constructed using bolts in clearance holes are time consuming and labour intensive. However, modern shot fired nails can be used to achieve an alternative connection, which is both fast and easy-to-achieve.

This paper presents findings from experimental trials of these fasteners in steel to timber joints and compares their performance to that modelled through application of the equations for dowel-type fastener joints presented in Eurocode 5: Part1-1.

1. Introduction

Conventional flitch members constructed using bolts in clearance holes are time consuming and labour intensive. However, a fast, easy-to-use, modern shot fired dowel connection system, capable of penetrating through both materials without pre-drilling, can be used with relatively thin gauge steel to produce more efficient and commercially viable alternatives. The concept is illustrated in Figure 1.

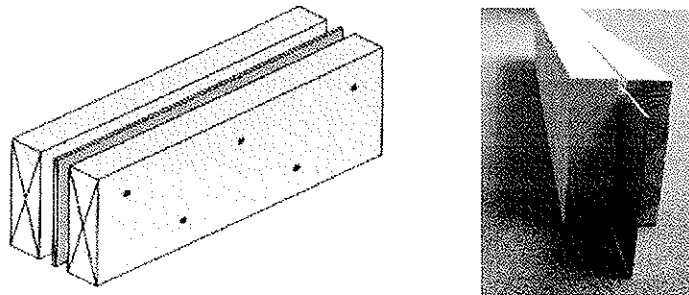


Figure 1 Conceptual and Prototype Timber / Steel Flitches Employing Shot Fired Nails

The work described herein is the part of a research and development project with the following stated aims:

- develop an identified value added use of UK grown softwood – especially Sitka spruce.
- show that innovation can work in the construction and timber industries, by delivering a commercially viable engineered timber product in joint partnership with members of the UK timber supply chain and fabricators.

The main application areas for modern steel-timber composites are envisaged to include:

- Floor and roof beams/trimmers/lintels.
- Post and beam construction.
- Footbridge beams and transoms.
- Bespoke structural joinery, conservatory construction.
- Portals and tied roof frames.
- In-situ restorations, including partially prefabricated kits.

2. System Basis and Considerations for Performance Prediction

The shot fired steel nail system used in this study comprises 3.6mm diameter high tensile steel nails (80 mm long), shot using an explosive charge nail gun, shown in Figure 2a. The nails are driven into a clamped lay-up of timber and steel plate with such force that the nails penetrate the steel undamaged and become friction welded to the plate in the process, as shown in the disassembled joint in Figure 2b. The force that drives the nails is controlled by the charge strength and can be varied for different applications.

The tested configuration in this paper comprised 47mm thick Sitka spruce (*Picea sitchensis*) and 6mm mild steel plate. In this configuration, the nails were found to penetrate the steel to an extent whereby the heads become sunk a few millimetres below the surface of the timber. This was found to be reasonably consistent throughout specimens. This results in a joint as described in Figure 2c, whereby the outer member thickness cannot be used to describe the thickness t_1 used in standard nail equations. The nails also have significant penetration on the pointside of the steel plate ($t_{1,b}$), as can be seen from the photograph in Figure 2b.

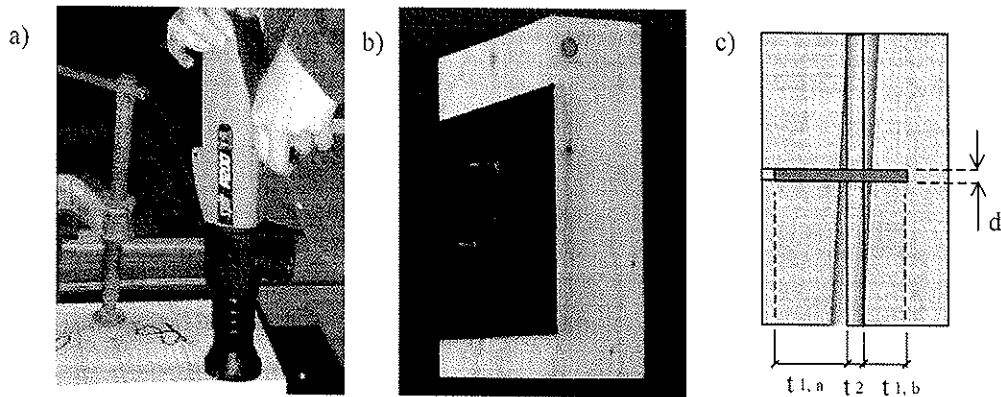


Figure 2 Shot Fired Nail System Used In Timber/Steel Connection

The shot fired joints differ from the traditional normal nail model as there is absolutely no tolerance hole in the steel plate, and furthermore a true rigid relationship is established between the plate and nail.

3. Experimental Investigations

The work reported herein is part of a technology demonstration project, which includes a limited test programme, performed to support the design and fabrication of prototypes. The initial tests comprised short-term ramp load tests, as described below, and duration of load tests, which are still in progress at the time of writing.

3.1 Ramp Load Tests To Failure

A small series of short-term joint tests were carried out on double-ended assemblies of this form of joint. The test specimens, manufactured from 47 x 195mm section, strength class C16 (machine graded) Sitka spruce, and 6 x 180 mm section steel plates, were assembled using 4 no 3.6mm diameter x 80mm long shot fired dowels, driven from one side only, as shown in Figure 3.

The test specimen was developed to reflect a target configuration in the flitch beam application. It is of note that this configuration employs non-standard nail spacings, as can be seen from Table 1.

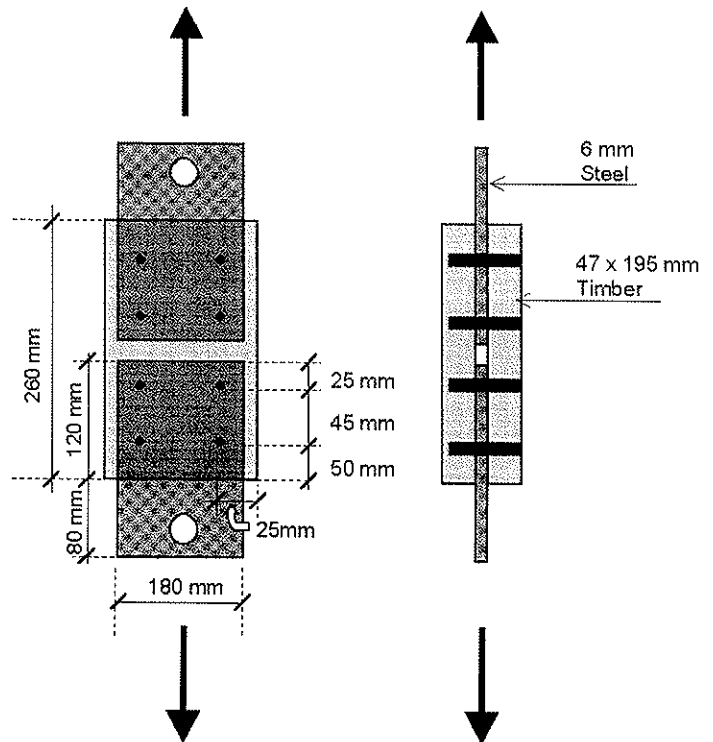


Figure 3 Schematic of Test Specimens

| Joint Type / Code Guidance | Nail Spacing (Load parallel To Grain) | | |
|--|---------------------------------------|--|------------------------------|
| | a ₁ parallel to grain | a ₂ perpendicular to grain | a ₃ loaded end |
| Shot Fired Nails (as reported herein) | 12 d | 40d | 14d |
| DDENV 1995-1-1 | predrilled holes | 7 d | 3d |
| | without predrilled holes | 10d | 5d |
| BS5268 Part 2 timber-to-timber | predrilled holes | 10d | 3d |
| | without predrilled holes | 20d | 10d |
| BS5268 Part 2 steel plate to timber | 14d | 7d | 14d |

Table 1 Comparison of Shot Fired Nail Spacings with Standard Nail Spacings

The samples were loaded to failure in tension. The load at failure was recorded in each case, together with load deformation recordings at each end of the test samples.

The results of the joint tests are summarised in Table 2 and load-deflection curves are shown in Figure 4.

| Specimen | Failure load (kN) | |
|----------|---------------------------------|--------------------------------------|
| | Total F _{ult,total} | per nail * F _{ult/dowel} |
| A1 | 20.02 | 5.00 |
| A2 | 22.29 | 5.57 |
| A3 | 21.14 | 5.29 |
| A4 | 22.53 | 5.63 |
| A5 | 19.86 | 4.97 |
| A6 | 16.11 | 4.03 |
| mean | 20.32 | 5.08 |

Notes:
* average based on assumed uniform load share between nails

Table 2 Summary of Tests in Ramp Load To Failure

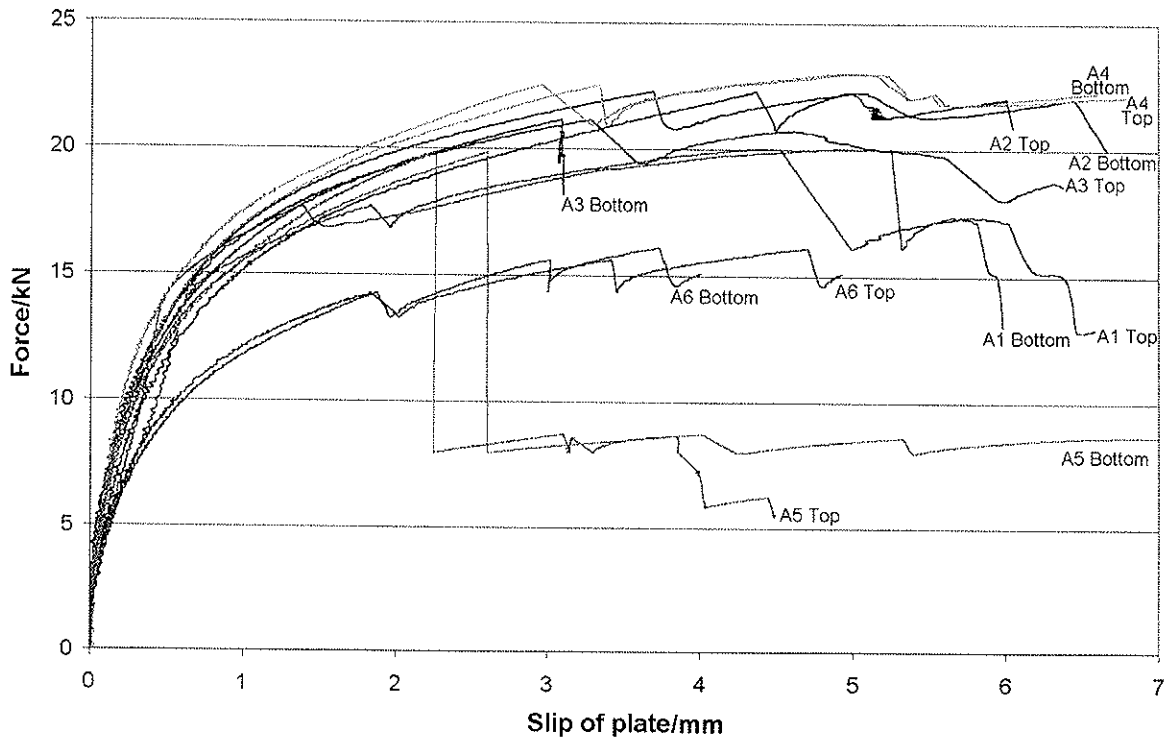


Figure 4 Load-Slip Curves For Short-term Load Tests

The modes of failure comprised substantial deformation of the nails (as evidenced in the opened joint in Figure 5), accompanied by eventual splitting along the grain in the timber. A selection of failed specimens is shown in Figure 6.

The distortions in the specimens further evidence the significant deformation throughout the nailed groups prior to eventual failure, suggesting a high degree of load sharing across the fasteners.

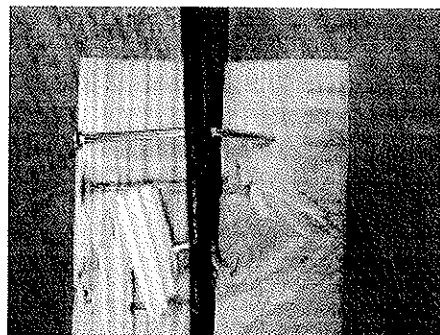


Figure 5 Nail Deformation in Failed Specimen

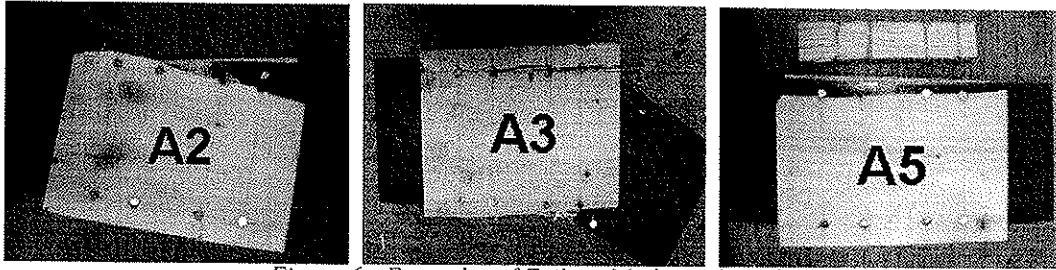


Figure 6 Examples of Failure Modes in Samples

The mean strength derived from the tests reflect a degree of variation in the ultimate capacities of these joints. The ultimate limit state design may be calculated from 5th percentile characteristic test values (F_k) modified by the material partial safety factor γ_m and the appropriate service class and duration of load factor k_{mod} . Derivation of these figures falls outside the scope of this paper. However, as the test set is to be used as a reference for a series of duration of load tests and assistance in design of a prototype bridge, an approximation of the 5th percentile characteristic value of the load-carrying capacity of the joint was calculated, assuming a normal distribution as in equation (1). Whilst it is appreciated that with a limited test set, the characteristic strength approximated will be a pessimistic value, it was deemed to be appropriate in this exercise.

$$F_k = k_p \left[F_{mean} - \left(k_n \sqrt{\frac{\sum (F - F_{mean})^2}{n-1}} \right) \right] = 3.72 \text{ kN/nail or } 14.88 \text{ kN/test joint} \quad (1)$$

k_p = the lesser of $450/\rho_{mean}$ and 1.0
 F_{mean} = mean value of F for the test series
 F = ultimate load in each test

ρ_{mean} = mean density of conditioned members at time of test
 k_n = Student-T factor related to n results for a 5 percentile probability level, (2.02 for n=6)
 n = number of tests in the test series

3.2 Duration of Load Tests

The short-term tests were used to determine the loads to be used in the DOL test, since these are performed at high fractions of the estimated short-term failure loads. Similar specimens to the short-term tests were tested through application of constant loads in the region of 70-80 % of the mean ultimate capacity in tension and maintaining this load until failure. The specimens were installed in purpose made, double-cantilever test rigs, located outside and under cover - a broad definition often applied to exemplify the Service Class 2. Dead weights were attached in order to induce axial load in the specimens. The dead weights were enclosed in waterproof jackets to avoid moisture uptake over the duration of the tests.

A similar method has been used previously to test bonded-in rod specimens [6] and relative humidity and air temperature in the test are known to be undoubtedly more severe than Service Class 1 and might even be considered as reflecting Service Class 3. The duration of load tests are still in progress at the time of writing, with the recorded failures and outstanding tests summarised in Table 3.

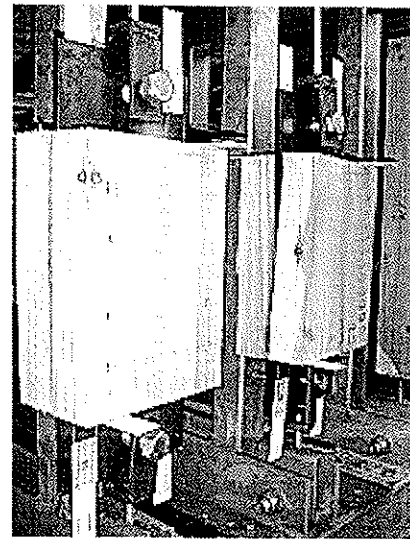


Figure 7 Duration of Load Tests

| | | | | | | | |
|------------------------------|-------|-------|-------|-------|-------|-------|-------|
| F (kN) | 18.68 | 18.18 | 18.15 | 18.00 | 17.96 | 17.65 | 16.37 |
| Time to Failure (hrs) | 21.2 | 72.5 | 140.8 | 140.8 | 70.8 | 72.8 | 120.4 |
| F (kN) | 15.98 | 15.96 | 15.63 | 15.62 | 15.42 | 14.03 | 14.03 |
| Time to Failure (hrs) | 143.0 | 50.5 | 166.3 | 120.5 | 146.3 | 143.4 | 863.3 |
| F (kN) | 14.02 | 14.02 | 14.00 | 14.00 | 13.99 | 13.98 | 13.97 |
| Time to Failure (hrs) | 100.0 | 292.0 | 118.5 | 22.3 | 28.3 | 196.5 | 723.8 |

Table 3 Summary of Duration of Load Results Obtained in Medium Term

4. Eurocode Equation Based Prediction of Strength

4.1 Lateral Load Carrying Capacity of Dowel Type Fasteners

There are two configurations in which this technique is practical - either a single shear steel to timber joint or in a three-member double shear joint, where the steel forms the inner member, as shown in Figure 8a and 8b respectively. The work described herein reflects the latter.

A series of dowel-type fastener design equations for steel to timber joints is presented in ENV 1995-1-1 [4]. In the case of single shear, these are differentiated with respect to the relationship of the fastener diameter (d) to steel plate thickness (t_{plate}), thus resulting in definition of a thin plate model ($t_{plate} \leq 0.5d$) or thick plate model ($t_{plate} \geq d$). In double shear with steel as the centre plate, there is no such differentiation, the calculation model being defined as shown in Figure 9.

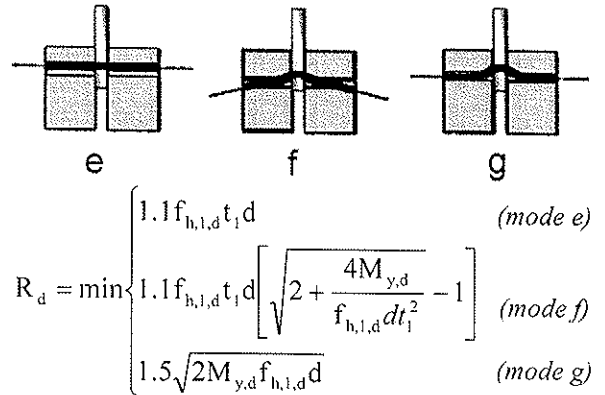
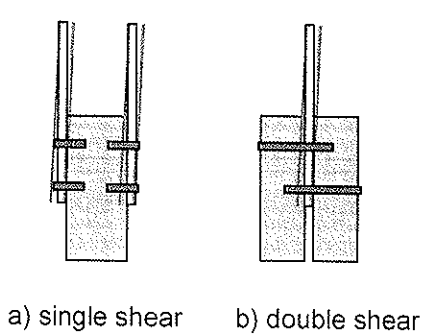


Figure 8 Alternative 3 Member Connection Configurations

Figure 9 Failure Models For Double Shear Steel-to-Timber Joints

Treatment of nails employs these basic equations, with t_1 taken for design purposes as the lesser of headside timber thickness and pointside penetration in double shear joints. It can be seen that selection of the lesser value of t_1 will result in a conservative estimation. A more realistic value of t_1 can be derived by taking t_1 as the mean of the headside member and pointside penetration. This also addresses the issue of variation of penetration and head embedment across the sample set. Thus, in the case of these specimens:

$$t_1 = 0.5 (t_{1,a} + t_{1,b}) = 0.5 (L_{nail} - t_2) \quad (2)$$

The characteristic embedding strength for non-pre-drilled nails (as in ENV1995-1-1 equation 6.3.1.2a) is derived from the expression:

$$f_{h,k} = 0.082 \rho_k d^{-0.3} \text{ N/mm}^2 \quad (3)$$

DDENV 1995 further advises that the yield moment of nails be derived for round nails produced from wire with tensile strength of 600 N/mm² from the expression:

$$M_{y,k} = 180 d^{2.6} \text{ Nmm} \quad (4)$$

The types of shot fired nails by necessity of their application method are of a higher grade steel, the ultimate tensile strength being in the order of 2000 N/mm² (yield = 1700 N/mm²). Therefore the general nail expression is not applicable for prediction of the strength of these nails. ENV 1995-1-1 further advises that the yield moment should be determined in accordance with prEN 409 [3] 'Determination of the yield moment for dowel type fasteners - Nails' and Annex A of EC5:1-1 [4] (for determination of 5-percentile characteristic values from test results and acceptance criteria for a sample). At the time of writing, the data from these nail tests was not available, but for the study presented in this paper, two alternative approaches to derivation of an approximate value were considered:

- enhancement of the yield moment derived from equation (4) based on the ratio of tensile strength (as in equation (5))

$$M_{y,k} = (f_k / 600) 180 d^{2.6} \text{ Nmm} \quad (5)$$

- adoption of the general bolt expression (as in equation (6)).

$$M_{y,k} = 0.8 f_{u,k} d^3 / 6 \quad (6)$$

Incorporation of the appropriate diameter and material properties results in calculated yield moments as summarised in Table 4. Based on these material values and employing material safety factor (γ_M) and k_{mod} values of 1.0 throughout the various combinations of equations 2-6, the projected values of characteristic capacity per shear plane (R_k) are summarised in Table 5.

| Equation | $180 d^{2.6}$ | $(f_k / 600) 180 d^{2.6}$ | $0.8 f_{u,k} d^2 / 6$ |
|-----------------|---------------|---|---|
| $M_{y,k}$ (Nmm) | 5031 | 16770 (based on ultimate strength) 14254 (based on yield capacity) | 12441 (based on ultimate strength) 10575 (based on yield capacity) |

Table 4 Calculated Characteristic Yield Moments

| Calculation Model Basis | | Predicted failure mode | Predicted R_k (N) | |
|------------------------------|---------------------------------|------------------------|-------------------------------|----------------------------|
| | | | Based on minimum t_1 (27mm) | based on mean t_1 (37mm) |
| Standard nail equation* | | g | 1192 | 1298 |
| Ratio modified nail equation | based on nail yield strength | f | 1650 | 1816 |
| | based on ultimate nail strength | f | 1765 | 1909 |
| Bolt Equation | based on nail yield strength | f | 1474 | 1677 |
| | based on ultimate nail strength | f | 1564 | 1748 |

* Will underestimate all modes where nail deformation is critical, due to higher than standard strength of nails used in tests

Table 5 Calculated Characteristic Capacity Per Shear Plane (using non-predrilled nails equations)

4.2 Modification Factors For Duration of Load

The effect of sustained actions on the performance of timber structures is treated through multiplication of the design capacity by k_{mod} , reflecting the load duration class and service class, as summarised in Table 6.

| Solid Timber | order of accumulated duration of load | k_{mod} | |
|--------------|---------------------------------------|-----------|------|
| | | SC1/SC2 | SC3 |
| Short Term | less than one week | 0.9 | 0.7 |
| Medium Term | 1 week - 6 months | 0.8 | 0.65 |

Table 6 Summary of Short and Medium-Term Load Duration and k_{mod} Treatment in EC5

5. Comparison of Test Results and Calculation Models

5.1 Characteristic Strength

The characteristic failure load obtained from the tests is compared with calculated results in Figure 10.

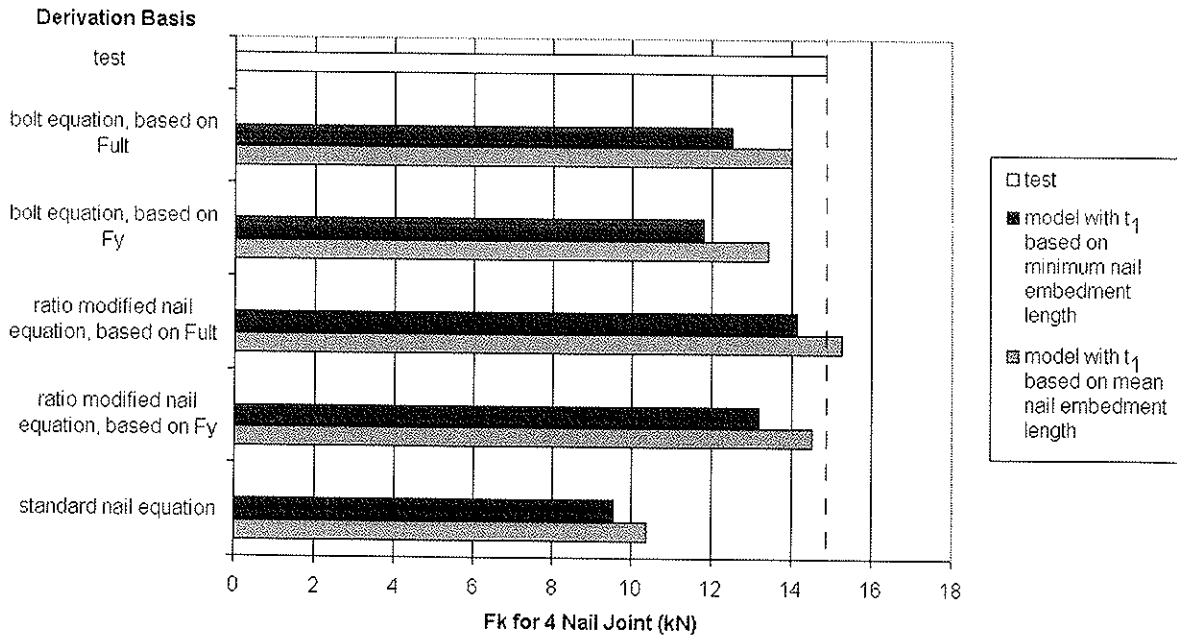


Figure 10 Characteristic Specimen Capacities Calculated From Dowel Type Fastener Models and Tests

It can be seen that the test strengths show a slightly higher short term joint capacity than that predicted by all models except that based on a nail equation modified by an ultimate capacity ratio in the fastener and employing the mean nail embedment length.

It is also apparent that the model which best reflects the values obtained from test is based upon a nail equation modified by a yield capacity ratio in the fastener and employing the mean nail embedment length. Thus, it is recommended that the following approach be used to calculate the characteristic capacity of these fasteners:

$$R_d = \min \begin{cases} 1.1 f_{h,1,d} t_1 d & (\text{mode } e) \\ 1.1 f_{h,1,d} t_1 d \left[\sqrt{2 + \frac{4M_{y,d}}{f_{h,1,d} d t_1^2}} - 1 \right] & (\text{mode } f) \\ 1.5 \sqrt{2M_{y,d}} f_{h,1,d} & (\text{mode } g) \end{cases}$$

where:

$$t_1 = 0.5 (L_{\text{nail}} - t_{\text{steel}}) \quad \text{mm} \quad (7)$$

$$f_{h,1,d} = k_{\text{mod}} 0.082 \rho_k d^{-0.3} / 1.3 \quad \text{N/mm}^2 \quad (8)$$

$$M_{y,d} = (f_{y,\text{nail}} / 600) 180 d^{2.6} / 1.1 \quad \text{Nmm} \quad (9)$$

5.2 Strength Under Sustained Actions

The tests performed only extend as far as the medium-term. These are compared with the projected performance on the basis of k_{mod} treatment (as in ENV1995-1-1 Table 3.1.7) of mean and characteristic capacities from the initial test set in Figure 11.

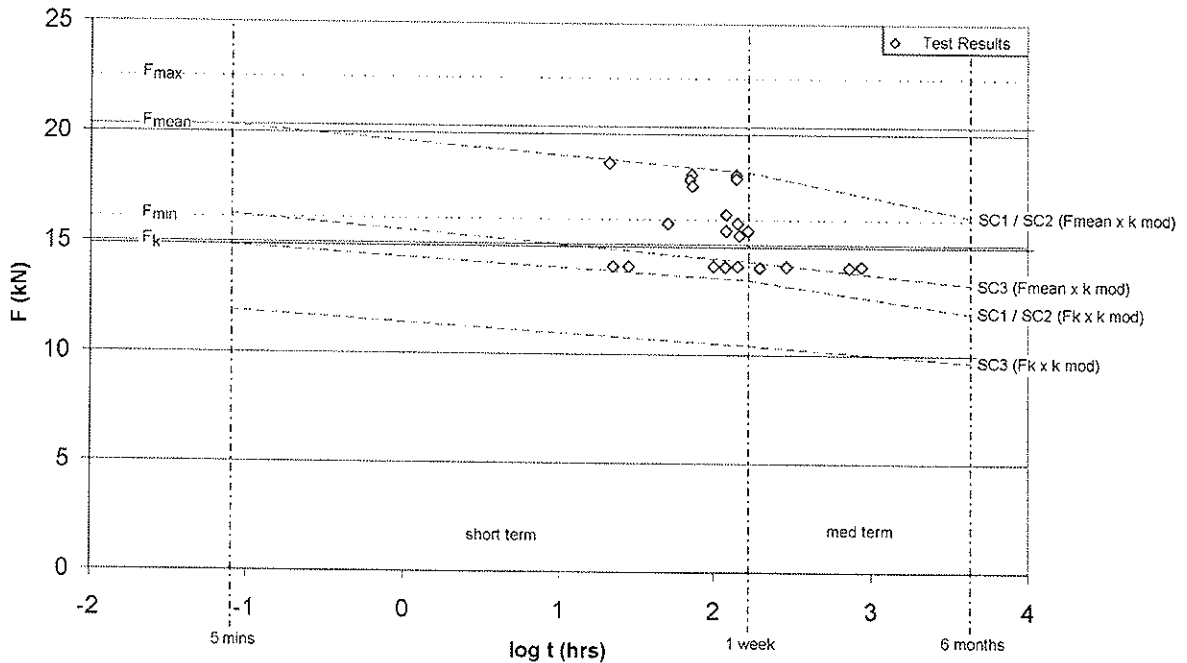


Figure 11 Summary of Load Duration Observations to Date.

As shown in Figure 11, the experimental evidence suggests that the performance of the specimens under sustained axial load exceeds the required level for application of the standard k_{mod} values in EC5 Part 1.1 for all three service classes.

It should be noted that although some of the results are very close to the projected curve for service class 1 and 2, in practice the design capacity would also be subject to material safety factors which are not included in this graph, hence the design criteria curves would be lower than those in Figure 11.

6. Showcase of Application in Prototype Footbridge

The application of this technology has also been showcased in the form of a small prototype footbridge structure. This has been manufactured from European Larch, another softwood produced in sufficient volume by the UK forest industries to be worthy of promotion for structural applications such as this. The overall length of the bridge is 5.1m and the width between the handrail posts is 1.2m. The main structure consists of 3 flich beams, each made of two timber pieces of 63 x 295mm section and one steel piece of 6 x 250mm

section (see Figure 12). Blocks of 63 x 295mm timber sections were installed at each end of the bridge, and at the third points of the span.

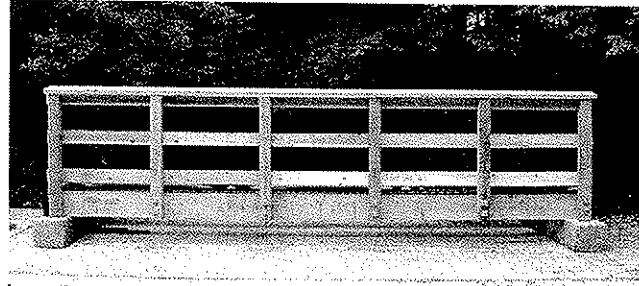
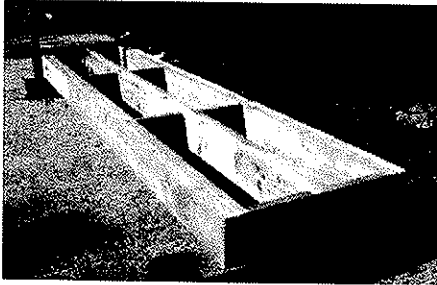


Figure 12 Technology Demonstration Prototype Footbridge

Handrail posts are of 100 x 100mm section timber and the rails are of 150 x 47mm section, except the top rail, which is made of 175 x 47mm section. The shot-fired nails were also used in some positions for an experimental connection between the handrail posts and the main beams, using the same shot-fire nail method. This time a recessed steel T section was employed, fixed to the face of beam members and recessed in a groove in the uprights, as shown in Figure 13.

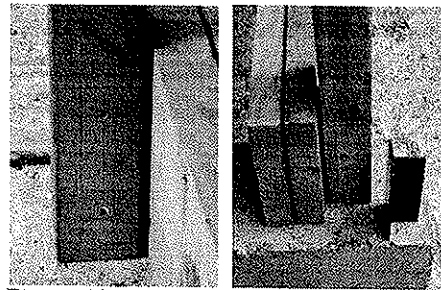


Figure 13 Hand Rail Upright Connection Employing Shot-fired Nail Fixing

7. Conclusions

Concerning the ultimate limit states performance of a non-standard shot-driven nail system for timber-to-steel connections, it has been found that:

- the characteristic strength demonstrated by tests of this particular nail system can be predicted using slightly modified versions of the nail equations in EC5:Part1.1
- in the absence of full nail bending data, the yield moment of this form of high tensile steel nails can be reasonably approximated for use in these situations by consideration of the ratio of the yield strength of the high tensile nail material to that of the standard reference nail (600 N/mm^2)
- the experimental evidence generated to date support the use of the k_{mod} values for timber published in EC5 to adequately describe the ultimate limit state performance of this type of connection under sustained loads

The system used has been shown to be both practical and efficient in its application to construct a prototype steel flitched timber footbridge, whereby the nails form an interconnection device within steel/timber composite members and are used to achieve connections between structural components.

Acknowledgements



Forestry Commission

This paper reports work performed as part of project TTL PIF 284, 'New Age Flitch – Case Study of Innovation Into Practice', which is co-sponsored by the Department of the Environment, Transport and the Regions (DETR), the Timber Research and Development Association (TRADA) and the Forestry Commission.

This project is also supported by Contributions-in-Kind from Forestry Civil Engineering, ITW Spit, James Callender and Son Limited, James Jones and Sons Limited, John Gordon and Son Limited and Walker Timber Ltd.

References

1. HILSON, B.O. (1995). Nailed Joints I. STEP Lecture C4, STEP Volume 1, STEP EUROFORTECH, Centrum Hout, Netherlands.
2. HILSON, B.O. (1995). Joints with Dowel Type Fasteners - Theory. STEP Lecture C3, STEP Volume 1, STEP EUROFORTECH, Centrum Hout, Netherlands.
3. BRITISH STANDARDS INSTITUTION (1993). BS EN 409 Timber Structures - Test Methods - Determination of the Yield Moment for Dowel Type Fasteners - Nails. BSI, London.
4. BRITISH STANDARDS INSTITUTION (1994). DD ENV 1995-1-1, Eurocode 5: Design of Timber Structures, Part 1.1 General Rules and Rules for Buildings. BSI, London.
5. BRITISH STANDARDS INSTITUTION (1996). BS 5268: Part 2. Structural Use of Timber, Part 2. Code of Practice for Permissible Stress Design, Materials and Workmanship. BSI, London.
6. BAINBRIDGE, R.J. and METTEM, C.J. (2000). Bonded-In Rods For Timber Structures -Test Observations With Impact Upon Development of Design Practice. 38th Annual Conference On Adhesion and Adhesives, Oxford, 5th April 2000.
7. SMITH, I., WHALE, L.R.J., ANDERSON, C. and HELD, L. (1984). Mechanical Properties of Nails and Their Influence on Mechanical Properties of Nailed Timber Joints Subjected to Lateral Loads. CIB-W18/17-7-1, Proceedings of International Council For Building Research Studies and Documentation, Working Commission W18 - Timber Structures, Meeting Seventeen, Rapperswil, Switzerland.

INTERNATIONAL COUNCIL FOR RESEARCH AND INNOVATION
IN BUILDING AND CONSTRUCTION

WORKING COMMISSION W18 - TIMBER STRUCTURES

SYSTEM EFFECT IN SHEATHED PARALLEL
TIMBER BEAM STRUCTURES

M Hansson

T Isaksson

Division of Structural Engineering

Lund University

SWEDEN

Presented by: M Hansson

- H J Blass asked about the first slide and how was the composite action taken into account.
- M Hansson explained that McCutcheon model took composite action into consideration.
- V Enjily asked about T&G floors and commented that it would be nice if the model could consider I-beam.
- M Hansson answered they were not considered in this study.
- H J Blass commented that uniformly distributed load was considered here and concentrated loads would be more important for the I-Beam case. He also question the term "Weakest" beam in the paragraph above Fig 8.
- M Hansson agreed that wording needed to be refined.
- F Rouger questioned why mean strength rather than minimum value was used in the single T-beam model stated in paragraph 3 on Page 10.
- P Glos commented that system effect is a function of the timber quality and only high quality of timber was considered in this study. One would get lower system factors compared to those obtained by Foschi.
- M Hansson agreed.
- A Jorissen asked would DOL also affect system behaviour.
- M Hansson answered that it was not considered.

System Effect in Sheathed Parallel Timber Beam Structures

Martin Hansson, Tord Isaksson
Division of Structural Engineering
Lund University, Sweden

1 Abstract

The paper presents a study on the system effect of sheathed timber structures, such as roof elements. For such structures Eurocode gives a system factor of 1.1. Using Monte Carlo simulations together with input from an experimental investigation of sheathed parallel timber beam structures, a parameter study of the system behaviour is performed. Parameters such as number and length of beams, type of connection between beam and sheathing and the variability in bending strength within and between members of the system are taken into account.

Systems are generated using Monte Carlo simulations and the system effect is evaluated by direct comparisons of strengths and by reliability methods, resulting in a calibration of the parameters in the code.

2 Introduction

The design of timber structures or systems is mainly based on the design of single elements. That is, the benefit of single elements interacting in a system is usually not taken into account.

This paper presents a study on the system effect for a flat roof or floor joist system, see Figure 1. Such a system is typically built up by beams of structural timber and a sheathing of plywood. The joint between the sheathing and beam can be nailed, screwed or glued resulting in a different effective bending stiffness.

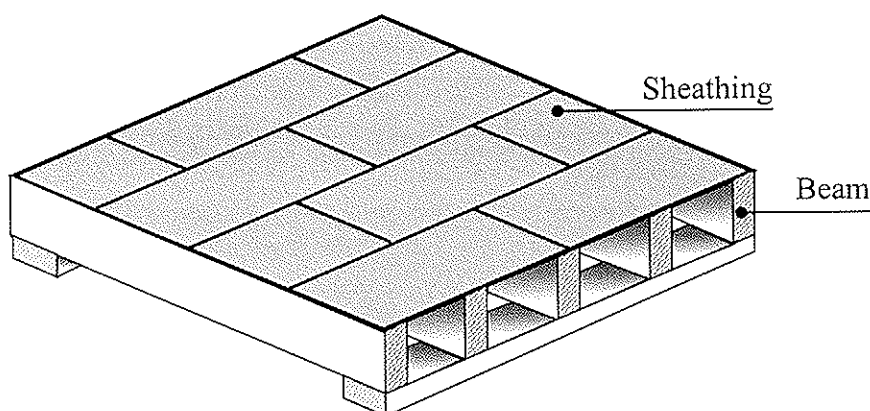


Figure 1. Example of timber system, a floor structure or a flat roof.

The increase in load carrying capacity of a system compared to a single member is mainly due to two factors. First, the positive correlation between stiffness and strength. That is, a beam of low strength also has a low stiffness, which means that this beam will carry less load. Secondly, the increase in load carrying capacity can be due to the load configuration effect, i.e. the probability of having the highest load at the weakest position of the system.

A system like the one shown in Figure 1 can be analysed in several ways. The simplest way is to define failure of the system as the failure of the first beam within the system. This corresponds to a series system. The load carrying capacity of the system, q , is given by eq. (1).

$$q = \min(q_i) \quad (1)$$

where

q_i is the maximum load on beam $i \{1:n\}$
 n number of beams in the system

If the sheathing is able to distribute the applied load so that all beams in the system reach their bending strength we have a perfect parallel system. The load carrying capacity of the system, q , is given by eq. (2). This results in a high system effect.

$$q = \sum_{i=1}^n q_i \quad (2)$$

The “true” behaviour should be somewhere between the values given by eqs. (1) and (2).

In Eurocode 5 a system strength factor, k_{ts} , is used to increase the single member design strengths. The following requirements should be fulfilled:

- The load-distribution system (the sheathing) is designed to support the applied permanent and variable loads.
- Each element of the load-distribution system (the sheathing) is continuous over at least two spans, and any joints are staggered.

For a roof or floor joist with a maximum span of 6 m and a load-distribution system of boards or sheathing the system strength factor k_{ts} equals 1.1.

Foschi et. al. (1989) presented a reliability study of a floor structure (or flat roof) and found, for Canadian conditions, a higher system effect factor compared to the one in Eurocode 5.

The present study of the system effect uses Monte Carlo simulations to generate systems and calculate their load carrying capacity. A parameter study of the system properties is performed together with an evaluation of the system effect using reliability methods and the code format.

3 Modelling of the system

The system studied in this paper is built up by beams of structural timber and a sheathing of plywood, see Figure 1. The sheathing can be nailed, screwed or glued to the beam.

3.1 Bending strength and modulus of elasticity of the beams

The bending strength is modelled using a statistical model of the variability within and between members, Isaksson (1999). The strength of a section i in beam j is given by eq. (3), see also Figure 2. The LN50step model, Isaksson (1999), is used in the simulation study.

$$f_{ij} = \exp(\mu + \tau_i + \varepsilon_{ij}) \quad (3)$$

where

μ is the logarithm mean of all weak sections in all beams.

τ_i is the difference between the logarithm mean of weak sections within a beam i and μ . The mean equals zero and the standard deviation is σ_τ .

ε_{ij} is the difference between weak section j in beam i and the value $\mu + \tau_i$. The mean equals zero and the standard deviation is σ_ε .

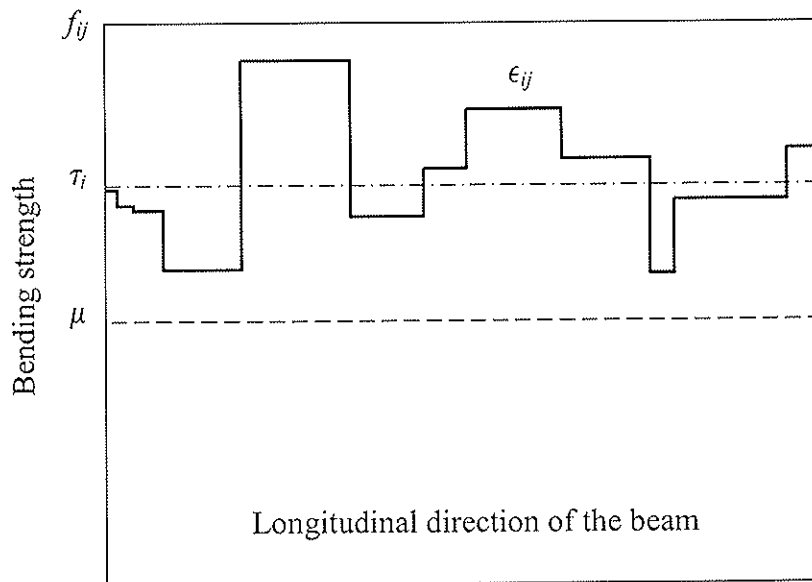


Figure 2. Modelling of longitudinal variation of bending strength, Isaksson (1999).

The length of a weak section is given by a gamma distribution $\Gamma(2.5445, 194.12)$, i.e. the mean length of a weak section is around 500 mm, Isaksson (1999).

The modulus of elasticity (*MOE*) of the beams is estimated by a linear regression, see eq. (4) (all values in MPa) and Figure 3. The *MOE* is assumed to be constant within each beam.

$$MOE = 185.58 \cdot f_m + 4323.1 \quad (4)$$

where f_m is the strength of the weakest section within each beam.

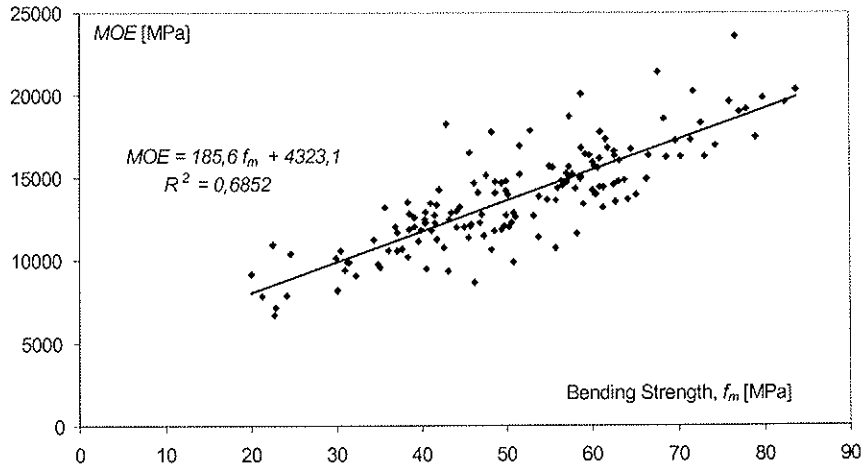


Figure 3. Relation between bending strength of weakest section and modulus of elasticity.

3.2 Composite cross sectional properties

The effective stiffness EI_e of the composite member (the T-beam), see Figure 4, is determined according to McCutcheon (1977), eq. (5). The expressions below give similar results to the ones in Eurocode 5.

$$EI_e = \frac{EI_r}{1 + f_\Delta \left(\frac{EI_r}{EI_u} - 1 \right)} \quad (5)$$

where

$$EI_r = EI_u + \frac{(EA_j)(EA_s)}{EA_j + EA_s} h^2$$

$$EI_u = EI_j + EI_s$$

$$f_\Delta = \frac{10}{(L_s \alpha)^2 + 10}$$

$$\alpha^2 = \frac{h^2 (k_n / s_n)}{EI_r - EI_u} \left(\frac{EI_r}{EI_u} \right)$$

$$h = \frac{h_j + h_s}{2}$$

- EI_e effective bending stiffness of a T-beam
- EI_r bending stiffness if the sheathing is rigidly connected to the beam
- EI_u bending stiffness of an unconnected beam and sheathing
- EI_j bending stiffness of a single beam
- EI_s bending stiffness of the sheathing (in the beam-direction)
- EA_j axial stiffness of the beam
- EA_s axial stiffness of sheathing (in the beam-direction)

- L_s clearance between boards in the sheathing in the beam direction (width of panel)
In this study set to 1.2 meter.
- k_n stiffness of connector between beam and sheathing
- s_n distance between nails/screws
- E_s Modulus of elasticity for sheathing. Deterministic value equal to 13 000 MPa.

The plywood thickness is set to 12 mm. Two out of five layers are in the direction of the main axis of the solid timber beams.

See also Figure 4.

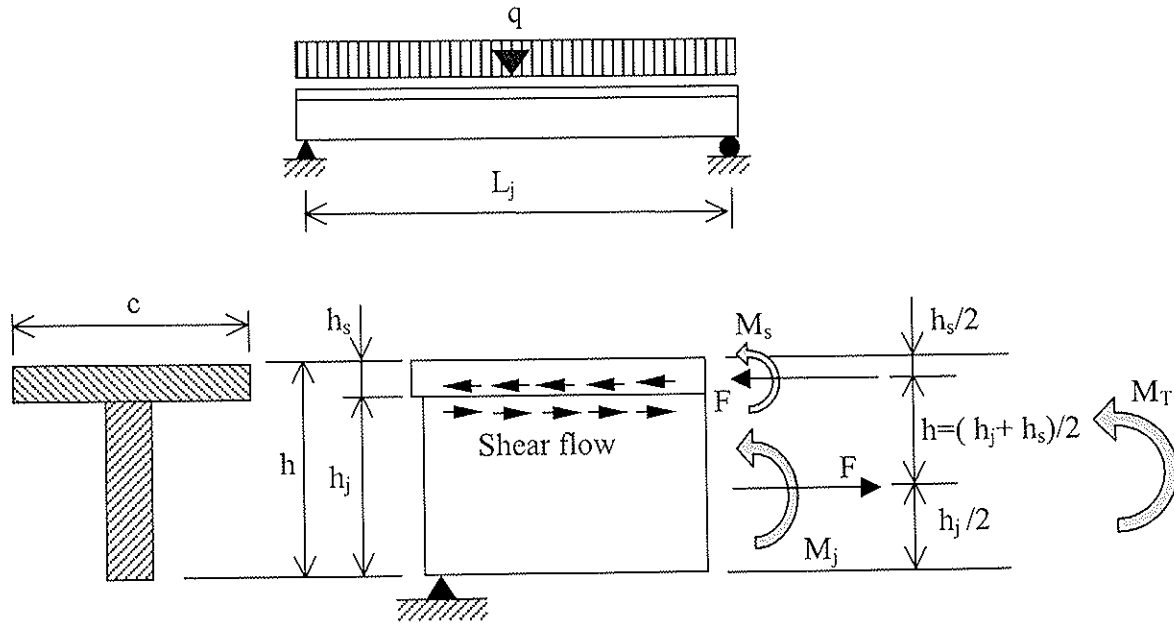


Figure 4. Behaviour of the T-beam.

The normal stresses are calculated according to Eurocode 5, see Figure 5. For the timber beam the stresses can be written according to eq. (6).

$$\sigma_j = \gamma_j \frac{E_j a_j}{EI_e} M_T \quad (6)$$

$$\sigma_{m,j} = \frac{E_j}{EI_e} \frac{h_j}{2} M_T$$

where

$$\gamma_j = 1$$

$$a_j = \frac{\gamma_s EA_s}{\gamma_s EA_s + EA_j} \frac{(h_j + h_s)}{2}$$

and

$$\gamma_s = \left(1 + \frac{\pi^2 EA_s s_n}{L_j^2 k_n} \right)^{-1}$$

L_j is the free span between supports.

The effect of clearance between boards in the sheathing on the bending strength of the T-beam is not included in study.

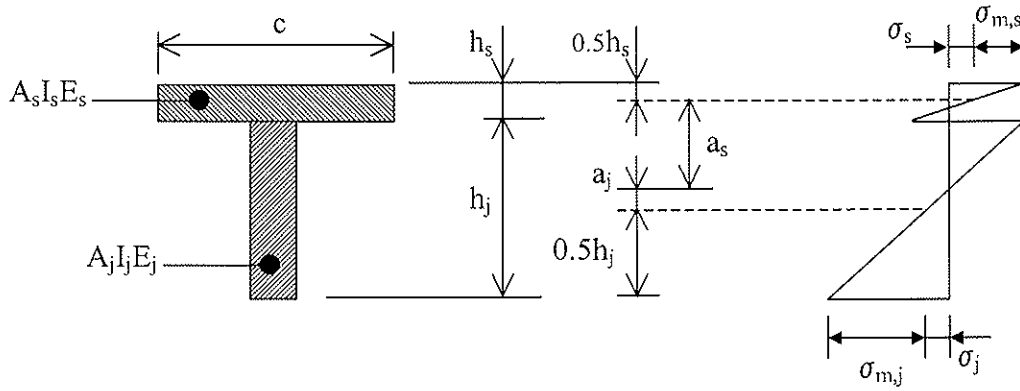


Figure 5. Normal stresses in the T-beam.

3.3 Beam-Spring model

The load distribution in the transverse direction to the beams is calculated using an analogue beam model according to Figure 6. This model was originally proposed by McCutcheon (1977, 1984) for analysing deflections of a system in the serviceability limit state. The springs were elastic brittle.

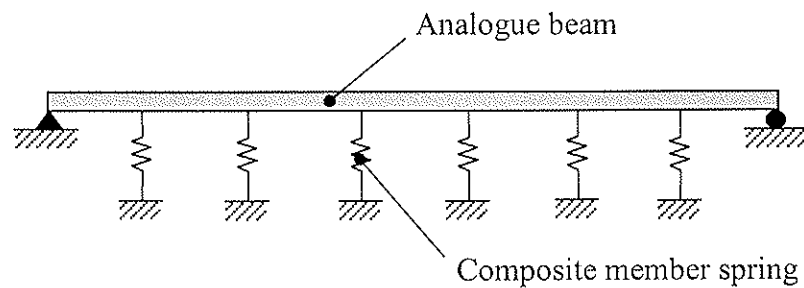


Figure 6. The beam - spring model. The ends are supported by walls.

In this study focus is on the ultimate limit state. To be able to account for the behaviour of a T-beam after first failure, the spring model is extended to be trilinear (Liu and Bulleit 1995), see Figure 7. After first failure of the beam, the remaining strength equals ΘR , where R is the original strength and Θ is reduction parameter. The stiffness of the spring after failure is ηK , where K is the stiffness of unbroken beam and η is a reduction parameter.

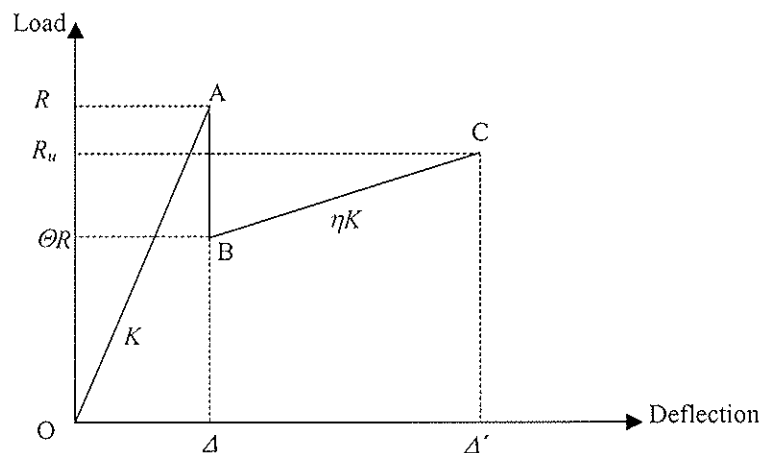


Figure 7. Load-Deformation curve for the spring, Liu and Bulleit (1995).

4 Experimental tests of systems

In an experimental investigation by Håkansson and Mauritz (1999) the system effect was studied. Three systems were built up and loaded to failure, see Figure 8. Prior to testing a parameter study was performed and the conclusion was that the spacing between the beams was the major influence on the system effect. The parameter study was based on a system model according to McCutcheon (1977, 1984) and a bending strength model by Isaksson (1999).

Before assembling the system the modulus of elasticity of each beam was measured according to EN 408 for the full span of 4 m and for the T-beam in the system, see Figure 9. The material for the beams (cross section $45 \times 145 \text{ mm}^2$) was Norway spruce – ungraded. The sheathing ($12 \times 1200 \times 2400 \text{ mm}^3$) was plywood, quality P30.

The beams and sheathing were screwed (diameter 4.2 mm, length 42 mm) with a spacing of 150 mm.

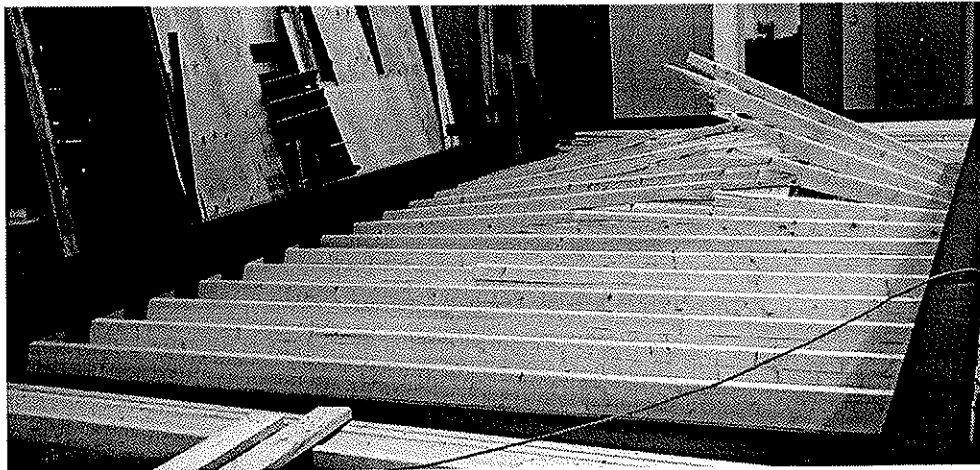


Figure 8. Experimental test of a system.



Figure 9. Measuring the stiffness of the T-beam.

For the three systems built up, the distribution of beam *MOE*'s throughout the system was kept as identical as possible. The uniform load was applied using an air balloon and the reaction force for each beam was measured enabling to see the load during the whole test.

One important input when simulating the behaviour of a system is the failure criteria. The test results indicate that the failure of any three beams or the failure of two neighbouring beams means the collapse of the system, i.e. the maximum load on the system is reached, see also Figure 8.

5 Simulation and Parameter study

5.1 Bending strength variation

The bending strength of a timber beam depends on the applied load and the bending strength variation along the beam (see Figure 10). The bending strength variation is implemented according to section 3.1. The bending strength has been determined for two different load configurations, a constant bending moment (weakest section) and a uniform load, f_q and f_M respectively (see Figure 10).

For the whole population (15 000) of simulated timber beams, the mean value and coefficient of variation (COV) for f_q and f_M for three different lengths (3, 4 and 5 m) are calculated, see Table 1. In order to reduce the variability between samples of beams due to the simulation, the shorter beams are “cut” out from the longer beams.

Table 2 shows the results from selecting the weakest beam in a group of 15 beams. This corresponds to weakest link theory without load sharing. Using the whole population of beams (see Table 1) 1000 groups can be generated. The table shows the 5th percentile, mean and COV for a span of 3, 4 and 5 m. Table 3 and 4 show results from groups with 10 and 5 beams respectively.

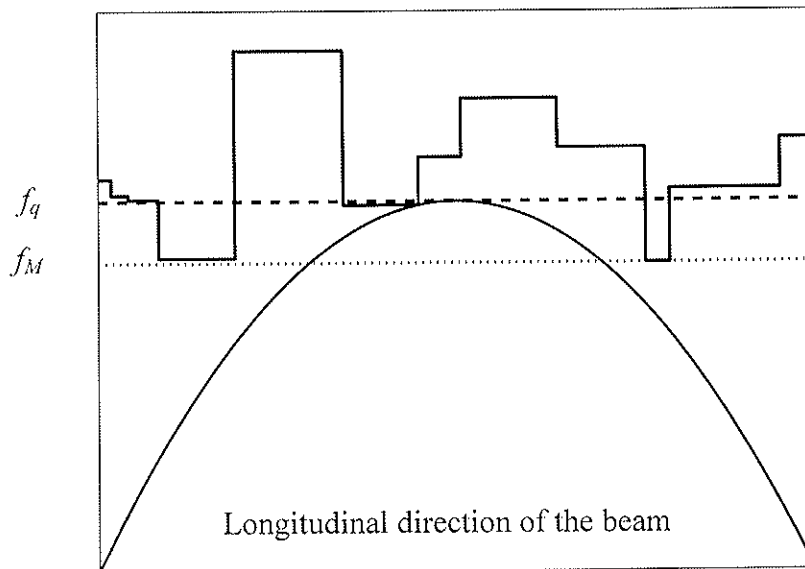


Figure 10. Evaluation of bending strength for different load configurations. q uniformly distributed load and M constant bending moment.

Table 1. The 5th percentile, mean bending strength and *COV* for the two load configurations (see Figure 10) for all beams (15000).

| L_j [m] | f_q | | | f_M | | |
|--------------|--------------------------------|---------------|-------------------|--------------------------------|---------------|-------------------|
| | 5 th perc. [MPa] | mean [MPa] | <i>COV</i> [%] | 5 th perc. [MPa] | mean [MPa] | <i>COV</i> [%] |
| 3 | 34.81 | 51.20 | 21.99 | 31.90 | 46.16 | 21.08 |
| 4 | 34.25 | 50.18 | 21.66 | 31.38 | 45.14 | 20.81 |
| 5 | 33.81 | 49.40 | 21.47 | 30.92 | 44.42 | 20.66 |

Table 2. The 5th percentile, mean bending strength and *COV* for the two load configurations (see Figure 10) for groups with 15 beams each (weakest link, no load sharing).

| L_j [m] | f_q | | | f_M | | |
|--------------|--------------------------------|---------------|-------------------|--------------------------------|---------------|-------------------|
| | 5 th perc. [MPa] | mean [MPa] | <i>COV</i> [%] | 5 th perc. [MPa] | mean [MPa] | <i>COV</i> [%] |
| 3 | 27.35 | 34.36 | 12.15 | 24.95 | 31.44 | 11.84 |
| 4 | 27.31 | 33.81 | 11.75 | 24.69 | 30.92 | 11.74 |
| 5 | 26.38 | 33.36 | 11.85 | 24.26 | 30.50 | 11.78 |

Table 3. The 5th percentile, mean bending strength and *COV* for the two load configurations (see Figure 10) for groups with 10 beams each (weakest link, no load sharing).

| L_j [m] | f_q | | | f_M | | |
|--------------|--------------------------------|---------------|-------------------|--------------------------------|---------------|-------------------|
| | 5 th perc. [MPa] | mean [MPa] | <i>COV</i> [%] | 5 th perc. [MPa] | mean [MPa] | <i>COV</i> [%] |
| 3 | 28.20 | 35.87 | 12.67 | 26.07 | 32.75 | 12.50 |
| 4 | 27.86 | 35.24 | 12.56 | 25.64 | 32.17 | 12.39 |
| 5 | 27.31 | 34.78 | 12.87 | 25.03 | 31.72 | 12.37 |

Table 4. The 5th percentile, mean bending strength and *COV* for the two load configurations (see Figure 10) for groups with 5 beams each (weakest link, no load sharing).

| L_j [m] | f_q | | | f_M | | |
|--------------|--------------------------------|---------------|-------------------|--------------------------------|---------------|-------------------|
| | 5 th perc. [MPa] | mean [MPa] | <i>COV</i> [%] | 5 th perc. [MPa] | mean [MPa] | <i>COV</i> [%] |
| 3 | 29.74 | 39.01 | 14.79 | 27.29 | 35.42 | 14.22 |
| 4 | 28.84 | 38.26 | 14.64 | 26.76 | 34.76 | 13.92 |
| 5 | 28.69 | 37.66 | 14.85 | 26.55 | 34.31 | 13.99 |

5.2 Parameter study

Using the beam-spring model and the material properties described in section 3, Monte Carlo simulations have been performed for a sheathed parallel timber beam structure. The intention is to reproduce the behaviour of systems similar to the experiments carried out by Håkansson and Mauritz (1999), see section 4.

In this paper the only failure criteria is bending failure in the timber beams. Other types of failures, such as shear failure, buckling of the sheathing or failure in the connectors, are not included in this study. The failure load for a system can be computed using the formulas for calculating the stresses in the beams, see section 3. The uniform load is increased until the bending stress σ is equal to the bending strength f_q (see Figure 10). The failure of the

system is defined as the failure of two neighbouring beams or the failure of any three beams, see section 4.

The output from the simulations is the 5th percentile and the mean failure load q_{sys} for the system and the corresponding COV , see Table 6. Every simulation in the parameter study is done for 1000 systems. The parameters studied are given in Table 5.

Included in Table 6, is the failure load $q_{weakest\ link}$ for a group of T-beams when no structural load sharing is employed. This is calculated using the mean value for f_q given in Table 2, Table 3 and Table 4 and transform it into a T-section for the parameters given in Table 6.

Further the values for the 5th percentile of the strength found in Table 1 is transformed into a T-section (q_{code}). This is in some sense what is done when designing a system according to the code.

Table 5. Input values to the parameter study.

| Parameter | Description | Reference value | Alternative values |
|-----------|--|-----------------|--------------------|
| Θ | Remaining bending strength of the beam at failure, see Figure 7. | 0.5 | 0.2 and 0.7 |
| η | Remaining stiffness of the beam at failure, see Figure 7. | 0.1 | 0.2 and 0.7 |
| f_A | Degree of rigidity between sheathing and timber beams, see eq. (5). $f_A = 0$ rigid connection $f_A = 1$ no connection | 0 and 1 | 0.5 |
| c | Centre to centre distance of the timber beams. [m] | 0.6 | 0.4 |
| n | Number of timber beams in each system. | 15 | 5 and 10 |
| L_j | Floor/roof span [m] | 4 | 3 and 5 |

6 Evaluation of the system effect

There are several possibilities of evaluating the system effect, from a simple comparison of means to a calibration of the code format. Below these evaluations are presented.

6.1 Comparison of means

A direct comparison of mean load carrying capacity for a system and for single beams can be made using the values in Table 6. The ratio between q_{sys} and $q_{weakest\ link}$ is given in the left column of the table. This ratio should not be understood as a system effect factor as the one found in the code but as a factor to be able to compare the effect of different parameters in the parameter study.

The following properties of the system results in a higher ratio (in no specific order):

- Low rigidity between sheathing and board (high f_A)
- Long span, L_j , of the system
- A low number of beams, n , in the system
- Higher stiffness after first failure in the broken beams (high η)
- Higher remaining bending strength after first failure of a beam (high Θ)

In general, systems with a weak connection between beam and sheathing results in a 15 to 20 % higher load carrying capacity for the system compared to the single beam. The more beams in the system the lower the effect. This is due to the higher probability of having a weaker beam when the number of beams in the system is increased. For systems where the sheathing is glued to the beam, the load carrying capacity is between 5 and 15 % higher for the system, again depending on number of beams in the system.

If the load carrying capacity for the simulated system with structural load sharing, q_{sys} is compared with the value q_{code} , no extra safety is found on this level. However the safety of the system is also depending of the variability in both q_{sys} and q_{code} .

Table 6. Parameter study of failure load for the system, q_{sys} . (The rows for $f_d=1$ are light shaded and the parameter values different to reference are dense shaded).

| System no | Parameter | | | | | | q_{sys}^* | | | $q_{weakest}^{**}$ link | $q_{sys}/$ $q_{weakest}$ link | q_{code}^{***} |
|-----------|-----------------|---------------|--------------|------------|------------|--------------|--|------------------------------|------------|------------------------------|-------------------------------------|--|
| | Θ [] | η [] | f_d [] | c [m] | n [] | L_j [m] | 5 th perc. [kN/m ²] | mean [kN/m ²] | COV [%] | mean [kN/m ²] | mean [] | 5 th perc. [kN/m ²] |
| 1 | 0.5 | 0.1 | 1 | 0.6 | 15 | 4 | 4.20 | 4.96 | 9.27 | 4.21 | 1.18 | 4.26 |
| 2 | 0.5 | 0.1 | 0 | 0.6 | 15 | 4 | 7.07 | 8.30 | 8.78 | 7.83 | 1.06 | 7.93 |
| 3 | 0.5 | 0.1 | 0.5 | 0.6 | 15 | 4 | 5.26 | 6.20 | 9.11 | 5.47 | 1.14 | 5.54 |
| 4 | 0.5 | 0.1 | 1 | 0.6 | 15 | 3 | 7.35 | 8.79 | 9.55 | 7.60 | 1.16 | 7.70 |
| 5 | 0.5 | 0.1 | 0 | 0.6 | 15 | 3 | 12.64 | 14.84 | 8.74 | 14.13 | 1.05 | 14.31 |
| 6 | 0.5 | 0.1 | 1 | 0.6 | 15 | 5 | 2.71 | 3.19 | 8.94 | 2.66 | 1.20 | 2.69 |
| 7 | 0.5 | 0.1 | 0 | 0.6 | 15 | 5 | 4.57 | 5.32 | 8.54 | 4.95 | 1.08 | 5.01 |
| 8 | 0.5 | 0.1 | 1 | 0.6 | 5 | 4 | 4.38 | 5.43 | 12.08 | 4.23 | 1.28 | 3.79 |
| 9 | 0.5 | 0.1 | 0 | 0.6 | 5 | 4 | 7.43 | 9.06 | 11.26 | 7.81 | 1.16 | 7.05 |
| 10 | 0.5 | 0.1 | 1 | 0.6 | 10 | 4 | 4.29 | 5.13 | 10.10 | 4.25 | 1.21 | 4.13 |
| 11 | 0.5 | 0.1 | 0 | 0.6 | 10 | 4 | 7.23 | 8.56 | 9.53 | 7.90 | 1.08 | 7.69 |
| 12 | 0.5 | 0.2 | 1 | 0.6 | 15 | 4 | 4.23 | 4.99 | 9.19 | 4.21 | 1.19 | 4.26 |
| 13 | 0.5 | 0.2 | 0 | 0.6 | 15 | 4 | 7.17 | 8.37 | 8.62 | 7.83 | 1.07 | 7.93 |
| 14 | 0.5 | 0.7 | 1 | 0.6 | 15 | 4 | 4.32 | 5.09 | 9.00 | 4.21 | 1.21 | 4.26 |
| 15 | 0.5 | 0.7 | 0 | 0.6 | 15 | 4 | 7.40 | 8.61 | 8.35 | 7.83 | 1.10 | 7.93 |
| 16 | 0.5 | 0.1 | 1 | 0.4 | 15 | 4 | 6.48 | 7.64 | 8.83 | 6.29 | 1.22 | 6.37 |
| 17 | 0.5 | 0.1 | 0 | 0.4 | 15 | 4 | 10.17 | 11.84 | 8.50 | 11.13 | 1.06 | 11.26 |
| 18 | 0.7 | 0.1 | 1 | 0.6 | 15 | 4 | 4.30 | 5.07 | 8.95 | 4.21 | 1.21 | 4.26 |
| 19 | 0.7 | 0.1 | 0 | 0.6 | 15 | 4 | 7.30 | 8.50 | 8.39 | 7.83 | 1.09 | 7.93 |
| 20 | 0.2 | 0.1 | 1 | 0.6 | 15 | 4 | 4.11 | 4.89 | 9.72 | 4.21 | 1.16 | 4.26 |
| 21 | 0.2 | 0.1 | 0 | 0.6 | 15 | 4 | 6.93 | 8.14 | 9.30 | 7.83 | 1.04 | 7.93 |

* Maximum load carrying capacity for simulated systems using the beam-spring model and trilinear load - deflection relationship and the failure criteria: two neighbouring beams or any three beams.

** Weakest link from a group of T-beams. Values for the strength of the solid timber are given in Table 2 to Table 4.

*** Strength values from the whole population of beams (see Table 1) are transformed to a T-section.

6.2 Calibration of the code format

The parameter study produced the 5th percentile, mean value and coefficient of variation for the ultimate load q_{sys} (kN/m²) of a system. This information can be used to calibrate the partial coefficient γ_m for a system. In this study the difference in *COV* for the load carrying capacity for the whole population of beams and for the system is taken into account. The Swedish code BKR 99 is used for the evaluation. For a more detailed presentation of the calibration procedure see for example Isaksson (1999).

The code format can be written as eq. (7). R is the resistance and S the action.

$$\frac{R_k}{\gamma_m \gamma_n} - \sum \gamma_i S_{ki} \geq 0 \quad (7)$$

γ_m , γ_n and γ_i are partial coefficients related to the material, safety class and action, respectively.

The characteristic strength is given by eq. (8).

$$R_k = C_k \kappa f_k a \quad (8)$$

where

- C_k uncertainty in the model
- κ reflects climate and duration of load (not included in this study, set to 1)
- f_k characteristic strength
- a dimension variable

The designing load combination according to BKR 99 (dominating variable load) is given by eq. (9).

$$S_d = \gamma_G G_k + \gamma_Q Q_k \quad (9)$$

where

- $\gamma_G = 1$
- $\gamma_Q = 1.3$
- G_k is the characteristic permanent load equal to its mean.
- Q_k is the characteristic variable load equal to the upper 98th percentile.

The probabilistic format for the strength can be written as a product of several stochastic variables, eq. (10). These variables are all assumed to be lognormally distributed.

$$R = C f a \kappa \quad (10)$$

where

- C uncertainty in the calculation model
- f strength
- a uncertainty in dimensions
- κ climate and duration of load parameter ($\kappa = 1$)

The product Cf is given by the simulations of systems. Since they are assumed to be log-normally distributed the means are related according to eq. (11).

$$\mu_R = \mu_C \mu_f \mu_a \quad (11)$$

The coefficient of variation of R is given by eq. (12).

$$COV_R^2 = COV_C^2 + COV_f^2 + COV_a^2 \quad (12)$$

The probabilistic format of the action can be written as eq. (13). The actions are assumed to be normally distributed.

$$S = Q_k(g\eta + q) \quad (13)$$

where

Q_k and G_k are characteristic values of the variable and permanent load respectively.

$$\eta = \frac{G_k}{Q_k}$$

$$g = \frac{G}{G_k} \in N(1, \sigma_g); \quad COV_g = COV_G$$

$$q = \frac{Q}{Q_k} \in N(\mu_q, \sigma_q); \quad COV_q = COV_Q$$

$$\mu_q = \frac{\mu_Q}{Q_k} = \frac{\mu_Q}{\mu_Q(1 + \Phi^{-1}(0.98)COV_Q)}$$

The probabilistic format given by the failure function is given by eq. (14)

$$g(R, S) = R - S = R - Q_k(g\eta + q) \quad (14)$$

Combining the code and probabilistic format results in the following failure function, eq. (15).

$$g(R, S) = R - \frac{R_d(g\eta + q)}{\gamma_G\eta + \gamma_Q} = 0 \quad (15)$$

The normalised variables R' , g' and q' are now introduced into the failure function, eq. (16).

$$\mu_R \exp(-R' COV_R) = R_d \frac{(\mu_g(1 - g' COV_g)\eta + \mu_q(1 - q' COV_q))}{\gamma_G\eta + \gamma_Q} \quad (16)$$

R' , g' and q' are substituted by $\alpha_R \beta$, $\alpha_g \beta$ and $\alpha_q \beta$ at the design point. β is the reliability index, set to be 4.3 in this study, and α are sensitivity factors. Since there are four unknowns in eq. (16) (α_R , α_g , α_q and μ_R), it must be solved iteratively.

The partial coefficient reflecting the material, γ_m , is given by eq. (17). γ_m is dependent on the relation between the coefficients of variation for the strength and the calculation model. However, the end result, the design value R_d , is independent of this relation. Thus, it is only a matter of giving a suitable value of COV_f . γ_n equals 1.1 for reliability index 4.3.

$$R_d = \frac{C_k f_k}{\gamma_m \gamma_n} \Rightarrow \gamma_m = \frac{C_k f_k}{R_d \gamma_n} \quad (17)$$

Table 6 shows the coefficient of variation COV for various assumptions regarding the model and behaviour of the system. As can be seen the COV is around 9.3 %. A system with few beams shows a little higher COV around 11.5 % and the length of the beams also has a minor influence on the COV .

Table 7 summarises the assumptions made regarding COV for the different parameters of the calibration. The target reliability index is 4.3 for both single members and a system.

Table 7. Summary of assumptions made for calibration.

| COV [%] | Single beam | System |
|--------------------------------|-------------|--------|
| Strength and model uncertainty | 21.5 | 9.3 |
| Strength | 20 | 8 |
| Model uncertainty | 7.9 | 4.7 |
| Geometry | 2 | 2 |
| Variable load | 40 | 40 |
| Permanent load | 5 | 5 |

Figure 11 shows the results of calibrating γ_m for single beams and for systems. As can be seen the single beam results in a higher partial coefficient, $\gamma_{m,single}$, than for the system, $\gamma_{m,system}$. This is due to the higher coefficient of variation for the single beam compared to the system. For timber structures the ratio α between variable load Q and the total load, $Q+G$, is typically above 0.5.

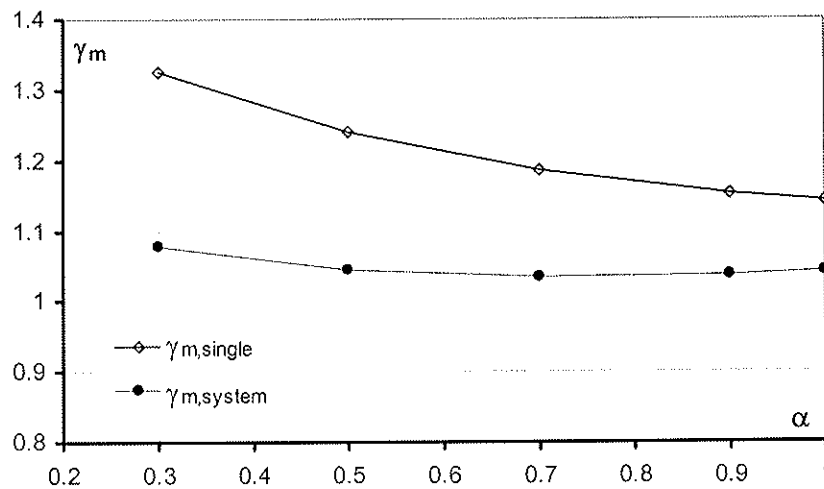


Figure 11. γ_m as function of α . $\alpha = \frac{Q_k}{Q_k + G_k}$

Returning to the code format and the equation for determining the designing strength, eq. (18). k_{Is} is the system effect factor. For a single beam $k_{Is} = 1$.

$$R_d = k_{Is} \frac{K_r f_{mk}}{\gamma_n \gamma_m} \quad (18)$$

γ_m for a single beam is given in the code. Using the following relation between design strength for a single beam and a beam in a system, the system factor can be evaluated, eq. (19).

$$R_{d,single} = \frac{K_r f_{mk}}{\gamma_n \gamma_{m,single}} \quad (19)$$

$$R_{d,system} = \frac{K_r f_{mk,sys}}{\gamma_n \gamma_{m,system}}$$

In this study $f_{mk,sys}$ is not evaluated and is set to f_{mk} .

$$R_{d,system} = k_{Is} R_{d,single} \Rightarrow \frac{1}{\gamma_{m,system}} = \frac{k_{Is}}{\gamma_{m,single}}$$

$$\Rightarrow k_{Is} = \frac{\gamma_{m,single}}{\gamma_{m,system}}$$

Figure 12 shows the system effect factor k_{Is} as a function of α (ratio between variable load and total load). The system effect decreases with increasing percentage variable load.

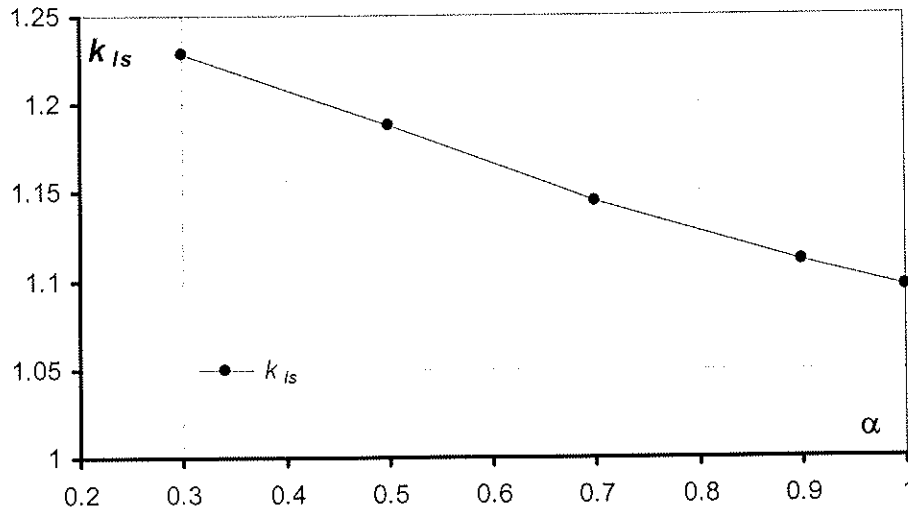


Figure 12. The system effect factor k_{Is} as a function of α .

For a typical timber system, α is somewhere between 0.4 and 1. In Thelandersson et al (1999) weighting for different intervals of α is suggested, see Table 8. If this weighting is used, k_{Is} equals 1.147.

Table 8. Weighting of structures according to the ratio between variable and total load, α

| Interval for α | Percentage of structures within the respective interval [%] |
|-----------------------|---|
| 0 – 0.4 | 0 |
| 0.4 – 0.6 | 20 |
| 0.6 – 0.8 | 60 |
| 0.8 - 1 | 20 |

7 Conclusions and further work

The present study uses a statistical model of variability of bending strength within and between beams to investigate the magnitude of the system effect for sheathed parallel timber beam structures.

Limited experimental investigations have shown that the failure criterion for a system corresponds to the failure of two neighbouring or any three beams.

The connector between the beam and sheathing influences the behaviour of the system in such away that a nailed connection gives a higher coefficient of variation of the system strength than a glued connection.

Compared to single beams where the coefficient of variation is around 20 %, the variation in strength of a system is around 10 %. The parameter study showed that the *COV* for the system is more or less independent of the studied parameters.

When calibrating the partial coefficient related to the material properties, γ_m , the low *COV* for the system results in a low γ_m . For a typical ratio between variable load and total load, the results indicate that the system effect factor k_{ls} , can be set equal to 1.15. This is based on the difference in *COV* for the load carrying capacity for the single solid timber beam and the structural system.

In the calibration of the system effect factor the reliability index for the system is set to 4.3. However in the code the reliability index is defined as the safety of the single member in this case the solid timber beam.

To be able to find a system effect factor that can be used in the code, further studies are needed.

8 References

BKR 99, 1998. *Boverkets Konstruktionsregler* (Swedish code, in Swedish). Boverket BFS 1993:58 and BFS 1998:39.

EN408. *Timber structures – Structural timber and glued laminated timber – Determination of some physical and mechanical properties.*

Eurocode 5. *Design of timber structures. – Part 1-1 : General rules and rules for buildings.* European Committee for Standardization, Bruxelles, Belgium.

Foschi R.O, Folz B.R. and Yao F.Z., 1989. *Reliability-Based Design of Wood Structures.* Structural Research Series, Report No. 34, Department of Civil Engineering, University of British Columbia, Vancouver, Canada.

Håkansson, T. and Mauritz, C., 1999. *System effects of wood structural systems* (in Swedish). Report TVBK-5100, Dept. of Structural Engineering, Lund University Sweden.

Isaksson, T., 1999. *Modelling the variability of bending strength in structural timber.* Report TVBK-1015, Dept. of Structural Engineering, Lund University Sweden.

Liu, W-F and Bulleit, W. M., 1995. *Overload behaviour of sheathed lumber systems.* ASCE Journal of Structural Engineering, vol 121, No 7.

McCutcheon, W. J., 1977. *Method for predicting the stiffness of wood-joist floor systems with partial composite action.* Research paper FPL 289, Forest products lab, U.S dept. of agriculture, Forest Service, Madison, Wisconsin.

McCutcheon, W. J., 1984. *Deflections of uniformly loaded floors: a beam-spring analog.* Research paper FPL 449, Forest products lab, U.S dept. of agriculture, Forest Service, Madison, Wisconsin.

Thelandersson, S., Larsen H. J., Östlund L., Isaksson T., Svensson S., 1999. *Reliability levels for timber and timber products used in construction* (in Swedish). Report TVBK-3039, Dept. of Structural Engineering, Lund University Sweden.

**INTERNATIONAL COUNCIL FOR RESEARCH AND INNOVATION
IN BUILDING AND CONSTRUCTION**

WORKING COMMISSION W18 - TIMBER STRUCTURES

**HIGH-STRENGTH I-JOIST COMPATIBLE GLULAM
MANUFACTURED WITH LVL TENSION LAMINATIONS**

B Yeh

T G Williamson

APA - The Engineered Wood Association

U.S.A.

Presented by: B Yeh

- G Schickhofer asked about the definition of beam and commented that with the LVL reinforcement the member behaved more like an I-beam. He also asked what were the volume factors used for the LVL and Glulam.
- B Yeh responded that different volume factors for the LVL and Glulam were used. The idea was to provide design values for designers.
- P Glos questioned the last conclusion in the paper on the relationship between beam bending strength and laminate strength.
- B Yeh stated that joint type would affect tensile strength of LVL because load transfer from lumber to LVL would not be the same as lumber to lumber; therefore, the relationship between beam bending strength and laminate tensile strength would be manufacturer dependent.
- M Yasumura asked about the size effect of the product.
- B Yeh stated that volume effect with exponent of 1/10 was used which would be appropriate for Douglas fir.
- G Schickhofer restated that the member behaved more like an I beam
- B Yeh stated that all beam failures were in the LVL (tension). This member had no failure in the finger joints.

High-Strength I-Joist Compatible Glulam Manufactured with LVL Tension Laminations

Borjen Yeh, Ph.D., P.E.
Thomas G. Williamson, P.E.
APA - The Engineered Wood Association, U.S.A.

Abstract

In recent years, the growing popularity of I-joists in residential construction has spawned strong demands for high-strength structural glued laminated timber (glulam) with I-joist compatible (IJC) depths in North America. Using the model prescribed in ASTM D3737, *Standard practice for establishing stresses for structural glued laminated timber*, APA - The Engineered Wood Association has developed glulam layup combinations using full-length (without end joints) laminated veneer lumber (LVL) as tension laminations to satisfy the market needs. These high-strength IJC glulam products have a characteristic flexural strength ($f_{m,g,k}$) of 43 MPa (6300 psi) and a mean modulus of elasticity ($E_{0,g,mean}$) of 14.5 GPa (2.1×10^6 psi), which represent the highest performance level that has ever achieved by the commodity glulam used in North America.

This paper describes the details of the layup combinations and the results of full-scale glulam beam confirmation tests. For quality assurance purposes, the required control values for the LVL tension laminations are established and reported. These layup combinations are being recognized by the evaluation service agencies of the major building codes in the United States.

Results obtained from this study suggested that relationship between the characteristic tensile strength of the LVL tension laminations ($f_{t,0,l,k}$) and the characteristic flexural strength of the glulam beams ($f_{m,g,k}$) is likely to depend upon not only the LVL, but the glulam manufacturers. It was noticed that the relationship between $f_{t,0,l,k}$ and $f_{m,g,k}$ did not necessarily follow the American National Standards Institute (ANSI) A190.1, *American National Standard for Wood Products -- Structural Glued Laminated Timber*. Therefore, the required $f_{t,0,l,k}$ value for QA purposes should be confirmed by LVL tension and full-scale glulam beam tests. Without the confirmation data, the $f_{t,0,l,k}$ should be assigned the same value as $f_{m,g,k}$.

1. Introduction

The development of high-strength layup combinations for I-joist compatible (IJC) structural glued laminated timber (glulam) was an interest of several glulam manufacturers in North America. This product is intended primarily for residential and light commercial and industrial buildings where the flexural strength or stiffness controls the design. Examples include floor or roof beams and garage door headers. The maximum depth for this product is typically limited to 457 mm (18 inches).

Based on the current glulam manufacturing specifications [1,2], the most common glulam produced in the United States has a characteristic (5th percentile with 75% confidence) flexural strength ($f_{m,g,k}$) of 35 MPa (5040 psi) with a mean modulus of elasticity ($E_{0,g,mean}$)

of 12.4 GPa (1.8×10^6 psi). In some instances, glulam beams manufactured from Southern pine can achieve a characteristic flexural strength ($f_{m,g,k}$) of 43 MPa (6,300 psi) and a mean modulus of elasticity ($E_{0,g,mean}$) of 14.5 GPa (2.1×10^6 psi), which represent the highest performance level that has ever achieved by the commodity glulam used in North America. In the working stress design, which is still the mainstream methodology used in wood design in the United States, these high-strength Southern pine glulam beams have an allowable flexural stress (F_b) of 21 MPa (3000 psi) with a beam MOE of 14.5 GPa (2.1×10^6 psi). This product is typically referenced as 30F-2.1E glulam in the marketplace and will be used in this paper.

These 30F-2.1E Southern pine glulam beams are limited to a maximum of 152 mm (6 inches) in width due primarily to the difficulty in manufacturing wider end joints with consistent quality at this strength level. In addition, a very high grade of E-rated Southern pine lumber required for the outer 10% of the tension zone for this high-strength glulam is getting difficult to procure.

Laminated veneer lumber (LVL) has been used in North American for more than 30 years. With improved technology in veneer grading, adhesives, and machining, LVL is known for its excellent load-carrying capacities and consistent quality. Since the grade and quality of each individual layer of veneers can be closely controlled in the LVL manufacturing processes, the variability in product properties is typically lowered than that of sawn lumber. Due to its unique manufacturing processes, LVL can be customized, just like glulam, to a wide variety of widths, thickness, and lengths. Most importantly, the end (scarf or lap) joints within the same veneer layer are staggered to minimize the strength reducing effect on the flexural and tensile strengths of LVL. Therefore, LVL is a natural choice for the tension lamination of high-strength glulam. In addition to its high tensile strength, the use of LVL tension laminations eliminates the need for high-strength and consistent-quality end joints in the glulam manufacturing.

APA has practiced the development of commercial glulam layup combinations for years using the GAP computer program that is recognized by the major building code evaluation services as an alternative method for determining design stresses of a given layup combination of glulam [3,4]. Even though the majority of glulam layup combinations developed by using GAP have been applied to sawn lumber laminations, prior experience showed that the GAP program could be used to predict the performance of hybrid glulam using LVL tension laminations [5]. This paper provides background information for the development of two 30F-2.1E IJC glulam layup combinations, both of which are now commercially available in the United States.

2. Objective

The main objective of this study was to develop high-strength 30F-2.1E IJC glulam layup combinations with LVL tension laminations. The maximum depth of the layup combinations was limited to 457 mm (18 inches). The layup combinations were developed using the GAP computer program and confirmed by full-scale beam tests. Results from this study were also intended for use to evaluate the relationship between the characteristic tensile strength of the LVL tension laminations and the characteristic flexural strength of the glulam beams.

3. Layup Development

Given the targeted design values at 30F-2.1E, and the specific depths of 241, 302, 356, and 406 mm (9-1/2, 11-7/8, 14, and 16 inches), which are I-joist compatible depths, APA staff developed the first layup combination using GAP. This layup combination, as shown in Table 1, was assigned a combination symbol of 30F-E2M2. It should be noted that the use of the Southern pine rather than other softwood species laminations in the core of the glulam ensures the highest design shear stress for commercial glulam.

Table 2 shows another 30F-2.1E layup combination, which was assigned a combination symbol of 30F-E2M3. The 30F-E2M3 layup combination has a maximum beam depth of 457 mm (18 inches).

Table 1. Layup combination for 30F-E2M2^(a)

| | | | | | | | |
|-------|------------|-------|------------|-------|-------------|-------|-------------|
| 44 mm | 2.4E LVL | 38 mm | 2.4E LVL | 44 mm | 2.4E LVL | 38 mm | 2.4E LVL |
| 38 mm | L1 2.3E/DF | 38 mm | L1 2.3E/DF | 36 mm | N1D 2.3E/SP | 33 mm | N1D 2.3E/SP |
| 35 mm | N2M8/SP | 34 mm | N2M8/SP | 36 mm | N2M8/SP | 33 mm | N2M8/SP |
| 35 mm | N2M8/SP | 34 mm | N2M8/SP | 35 mm | N2M8/SP | 33 mm | N2M8/SP |
| 34 mm | N2M8/SP | 34 mm | N2M8/SP | 35 mm | N2M8/SP | 33 mm | N2M8/SP |
| 34 mm | N2M8/SP | 34 mm | N2M8/SP | 36 mm | N2M8/SP | 33 mm | N2M8/SP |
| 34 mm | N2M8/SP | 34 mm | N2M8/SP | 36 mm | N1D 2.3E/SP | 33 mm | N1D 2.3E/SP |
| 35 mm | N2M8/SP | 38 mm | L1 2.3E/DF | 44 mm | 2.4E LVL | 38 mm | 2.4E LVL |
| 35 mm | N2M8/SP | 38 mm | 2.4E LVL | | | | |

406 mm (16 inches)

356 mm (14 inches)

302 mm (11-7/8 inches)

241 mm (9-1/2 inches)

^(a) Grade designations for the laminating lumber are in accordance with EWS Y117 [1] or AITC 117 [2].

Table 2. Layup combination for 30F-E2M3^(a)

| | | | | | |
|-------|-------------|-------|-------------|-------|-------------|
| 44 mm | 2.4E LVL | 44 mm | 2.4E LVL | 44 mm | 2.4E LVL |
| 34 mm | N1D 2.3E/SP | 38 mm | N1D 2.3E/SP | 34 mm | N1D 2.3E/SP |
| 34 mm | N1D 2.3E/SP | 35 mm | N2M8/SP | 34 mm | N2M8/SP |
| 34 mm | N2M8/SP | 35 mm | N2M8/SP | 34 mm | N2M8/SP |
| 33 mm | N2M8/SP | 34 mm | N2M8/SP | 33 mm | N2M8/SP |
| 33 mm | N2M8/SP | 34 mm | N2M8/SP | 33 mm | N2M8/SP |
| 33 mm | N2M8/SP | 34 mm | N2M8/SP | 33 mm | N2M8/SP |
| 33 mm | N2M8/SP | 34 mm | N2M8/SP | 33 mm | N2M8/SP |
| 34 mm | N2M8/SP | 35 mm | N2M8/SP | 33 mm | N2M8/SP |
| 34 mm | N1D 2.3E/SP | 35 mm | N2M8/SP | 34 mm | N2M8/SP |
| 34 mm | N1D 2.3E/SP | 38 mm | N1D 2.3E/SP | 34 mm | N1D 2.3E/SP |
| 44 mm | 2.4E LVL | 44 mm | 2.4E LVL | 44 mm | 2.4E LVL |

457 mm (18 inches)

406 mm (16 inches)

356 mm (14 inches)

| | |
|-------|-------------|
| 44 mm | 2.4E LVL |
| 36 mm | N1D 2.3E/SP |
| 36 mm | N2M8/SP |
| 35 mm | N2M8/SP |
| 35 mm | N2M8/SP |
| 36 mm | N2M8/SP |
| 36 mm | N1D 2.3E/SP |
| 44 mm | 2.4E LVL |

302 mm (11-7/8 inches)

| | |
|-------|-------------|
| 35 mm | 2.4E LVL |
| 34 mm | N1D 2.3E/SP |
| 34 mm | N2M8/SP |
| 35 mm | N2M8/SP |
| 34 mm | N2M8/SP |
| 34 mm | N1D 2.3E/SP |
| 35 mm | 2.4E LVL |

241 mm (9-1/2 inches)

^(a) see footnote to Table 1.

The 30F-E2M2 and 30F-E2M3 layup combinations were intended to follow the existing 30F-E2 layup combination recognized in ICBO ER-5714 [3] and NES NER-486 [4]. For modeling purposes, the “equivalent characteristic knot” required for GAP input for the 2.4E LVL tension lamination was conservatively assumed to be the same as those reported by Yeh [5] for the 2.0E LVL tension lamination. In addition, the “bending stress index value,” as documented in ASTM D3737 [6], for the 2.4E LVL tension lamination was conservatively assigned as 28 MPa (4,000 psi), which is the same as the value assigned to 2.3E sawn lumber lamination in accordance with ASTM D3737 [6].

Based on the layup combination given in Tables 1 and 2, and the input properties mentioned above, the properties for each beam depth were predicted by GAP, as shown in Tables 3 and 4 for 30F-E2M2 and 30F-E2M3, respectively.

Table 3. Predicted properties for 30F-E2M2 using GAP

| Depth | $f_{m,g,k}$ | $f_{t,0,g,k}$ | $f_{c,0,g,k}$ | $f_{c,90,g,mean}$ | $f_{v,g,k}$ | $E_{0,g,mean}$ |
|------------------------|----------------------|------------------------|------------------------|-----------------------|----------------------|------------------------|
| 406 mm (16 in.) | 47 MPa (6830 psi) | 18.5 MPa (2710 psi) | 24.5 MPa (3550 psi) | 7.4 MPa (1090 psi) | 4.3 MPa (630 psi) | 14.5 GPa (2.1 Mpsi) |
| 356 mm (14 in.) | 47 MPa (6870 psi) | 18.5 MPa (2690 psi) | 24.5 MPa (3590 psi) | 7.4 MPa (1090 psi) | 4.3 MPa (630 psi) | 14.5 GPa (2.1 Mpsi) |
| 302 mm (11-7/8 in.) | 48 MPa (7020 psi) | 20.0 MPa (2920 psi) | 26.0 MPa (3760 psi) | 7.4 MPa (1090 psi) | 4.3 MPa (630 psi) | 15.2 GPa (2.2 Mpsi) |
| 241 mm (9-1/2 in.) | 48 MPa (7020 psi) | 20.5 MPa (2970 psi) | 26.5 MPa (3850 psi) | 7.4 MPa (1090 psi) | 4.3 MPa (630 psi) | 15.2 GPa (2.2 Mpsi) |
| All ^(a) | 48 MPa (6930 psi) | 19.0 MPa (2730 psi) | 24.5 MPa (3610 psi) | 7.4 MPa (1090 psi) | 4.3 MPa (630 psi) | 14.5 GPa (2.1 Mpsi) |

^(a) For all depths after rounding in accordance with ASTM D3737 [6].

Table 4. Predicted properties for 30F-E2M3 using GAP

| Depth | $f_{m,g,k}$ | $f_{t,0,g,k}$ | $f_{c,0,g,k}$ | $f_{c,90,g,mean}$ | $f_{v,g,k}$ | $E_{0,g,mean}$ |
|------------------------|----------------------|------------------------|------------------------|----------------------|----------------------|------------------------|
| 457 mm (18 in.) | 49 MPa (7160 psi) | 20.0 MPa (2880 psi) | 25.5 MPa (3670 psi) | 5.9 MPa (850 psi) | 4.3 MPa (630 psi) | 14.5 GPa (2.1 Mpsi) |
| 406 mm (16 in.) | 47 MPa (6830 psi) | 20.5 MPa (3000 psi) | 24.5 MPa (3550 psi) | 5.9 MPa (850 psi) | 4.3 MPa (630 psi) | 14.5 GPa (2.1 Mpsi) |
| 356 mm (14 in.) | 47 MPa (6860 psi) | 21.5 MPa (3140 psi) | 25.0 MPa (3610 psi) | 5.9 MPa (850 psi) | 4.3 MPa (630 psi) | 14.5 GPa (2.1 Mpsi) |
| 302 mm (11-7/8 in.) | 48 MPa (7020 psi) | 23.0 MPa (3320 psi) | 26.0 MPa (3760 psi) | 5.9 MPa (850 psi) | 4.3 MPa (630 psi) | 15.2 GPa (2.2 Mpsi) |
| 241 mm (9-1/2 in.) | 48 MPa (7020 psi) | 22.5 MPa (3290 psi) | 26.5 MPa (3820 psi) | 5.9 MPa (850 psi) | 4.3 MPa (630 psi) | 15.2 GPa (2.2 Mpsi) |
| All ^(a) | 48 MPa (6930 psi) | 21.0 MPa (3050 psi) | 24.5 MPa (3520 psi) | 5.9 MPa (850 psi) | 4.3 MPa (630 psi) | 14.5 GPa (2.1 Mpsi) |

^(a) see footnote to Table 3.

4. Materials

4.1 LVL tension laminations

The 2.4E LVL products were manufactured by 2 different LVL plants. For the 30F-E2M2, the LVL products were manufactured using all G1 Douglas fir veneers of 2.5-mm (1/10-

inch) thick. On the other hand, the LVL products for 30F-E2M3 were manufactured using a combination of G1 and G2 Douglas-fir veneers of 3.2 mm (1/8 inch) in thickness. The veneers were graded using a machine grading setting specified in the Manufacturing Standard of each LVL plant. The veneer suppliers for each of the LVL plant were not the same. APA staff verified the veneer grades and witnessed the LVL manufacturing.

Given the difference in the LVL layup, veneer resource, and manufacturing parameters (glue spread rate, joint type, compression ratio, ... etc.) between these 2 LVL plants, the mechanical properties of the 2.4E LVL were not expected to be the same. Therefore, the tensile strength and long-span E of the LVL products were independently evaluated prior to the beam manufacturing in accordance with ASTM D4761 [7] and D5456 [8]. APA staff conducted the sampling and witnessed the LVL testing. Summary statistics for the LVL test results are given in Table 5.

Table 5. Summary statistics for 2.4E LVL

| | Tensile strength ^(a) , psi | | Long-span E ^(b) , psi | |
|------------------------------|---------------------------------------|----------------------|---|---|
| | For 30F-E2M2 | For 30F-E2M3 | For 30F-E2M2 | For 30F-E2M3 |
| N | 53 | 54 | 30 | 54 |
| Mean | 50 MPa (7190 psi) | 58 MPa (8460 psi) | 18.6 GPa (2.7 x 10 ⁶ psi) | 19.3 GPa (2.8 x 10 ⁶ psi) |
| COV | 0.124 | 0.080 | 0.054 | 0.046 |
| $f_{t,0,l,k}$ ^(c) | 38 MPa (5580 psi) | 50 MPa (7230 psi) | -- | -- |

^(a) Tested with a 4-ft gauge length in accordance with ASTM D5456 [8].

^(b) Tested with a span-to-depth ratio of 100 in accordance with ASTM D4761 [7].

As shown, the characteristic tensile strength ($f_{t,0,l,k}$ with a 4-ft gauge length) and mean long-span E ($E_{0,l,mean}$) for the LVL tension laminations manufactured for 30F-E2M3 were higher than the LVL manufactured for 30F-E2M2. In addition, the long-span E for the LVL tension laminations is substantially higher than the value of 16.6 GPa (2.4 x 10⁶ psi) used in the layup design, suggesting that the test beams are likely to have a higher $E_{0,g,mean}$ than the predicted values given in Tables 3 and 4.

It should be noted that according to the provisions of American National Standards Institute (ANSI) A190.1, *American National Standard for Wood Products -- Structural Glued Laminated Timber* [9], the required characteristic tensile strength of the tension lamination, $f_{t,0,l,k}$, can be correlated to the characteristic strength of the glulam beam, $f_{m,g,k}$, by a factor of 1.67/2.1 or 0.8. In other words,

$$f_{t,0,l,k} = 0.8 \times f_{m,g,k} \quad [\text{Eq. 1}]$$

Therefore, for a 30F glulam with a $f_{m,g,k}$ of 43 MPa (6300 psi), the required $f_{t,0,l,k}$ is 35 MPa (5010 psi). As noted from Table 5, the $f_{t,0,l,k}$ values for both LVL products meet this requirement for 30F glulam beams. However, the applicability of Equation 1 has been validated with glulam made of lumber tension laminations and its applicability with glulam made of LVL tension laminations has not been fully established.

4.2 Glulam beams

With the purpose of confirming the predicted $f_{m,g,k}$ and $E_{0,g,mean}$ of the glulam layups given in Tables 1 and 2, it was determined that full-scale glulam beam tests should be conducted. For 30F-E2M2, 15 glulam beams with a nominal dimension of 140 mm x 302 mm x 7010 mm (5-1/2 inches x 11-7/8 inches x 23 feet) and another 15 glulam beams with a nominal dimension of 140 mm x 406 mm x 9140 mm (5-1/2 inches x 16 inches x 30 feet) were manufactured by an APA glulam member.

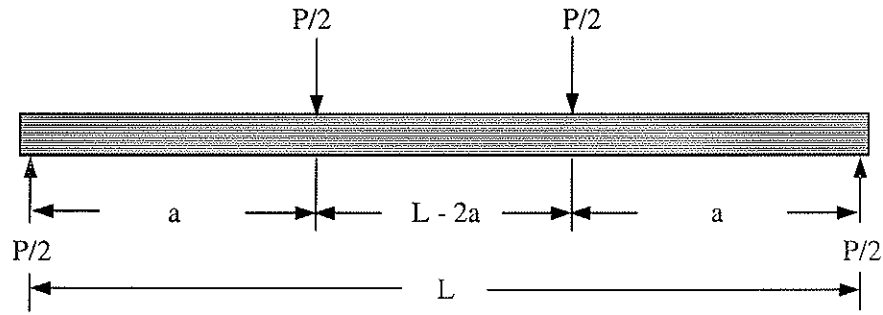
For 30F-E2M3, 17 glulam beams with a nominal dimension of 89 mm x 302 mm x 7010 mm (3-1/2 inches x 11-7/8 inches x 23 feet) and another 18 glulam beams with a nominal dimension of 178 mm x 457 mm x 10360 mm (7 inches x 18 inches x 34 feet) were manufactured by another APA glulam member. The choice of the glulam beam sizes was based on the consideration of the largest beam depths from Tables 1 and 2, and the predominant size of 302 mm (11-7/8 inches) in the market place.

All test beams were manufactured following the provisions of ANSI A190.1 [9]. Face bonding of the LVL to lumber was previously qualified in accordance with AITC 402, *Standard for Laminated Veneer Lumber (LVL) Used in Structural Glued Laminated Timber* [10]. A phenol resorcinol-type adhesive was used for all face bonding, while a melamine-formaldehyde adhesive was used for end (finger) joints of the lumber laminations. There were no end joints in the LVL laminations. The position of the end joints in each beam was random and not specifically excluded from the center one-half (high tensile stress) portion of the lamination. APA staff witnessed the beam manufacturing.

5. Test Methods and Data Analyses

All beam tests described in this paper were conducted at the APA Research Center in Tacoma, Washington, in February and May 2000. A four-point load method, as shown in Figure 1, was applied to test each beam using a constant span-to-depth ratio of approximately 21. This loading configuration resulted in a similar moment distribution as uniform loads, while giving a shear-free section between loading points. The test apparatus, including rocker-type reaction supports, reaction bearing plates and rollers, load bearing block, and load bearing rollers were set up following ASTM D198 [11]. A load button was installed between a 222-kN (50000-lbf) capacity load cell and load bearing block/rollers to function as a load-alignment device. Lateral supports were provided to avoid lateral buckling during testing.

Before testing, the cross-sectional dimensions of the beam were measured at loading points. The mean of the readings was used to calculate the sectional properties of the beam. A 9.5-mm (3/8-inch) hole was drilled at the neutral axis of the beam above one end reaction point. The same size of steel pin was then driven into the hole to provide a support for a stranded 890-N (200-lbf) capacity steel wire. A pulley was attached at the neutral axis above the other end of the reaction point. The wire was then tensioned between the steel pin and the pulley with a 445-N (100-lbf) dead weight. At the neutral axis of the midspan, a linear potentiometer (LP) with accuracy to 0.025 mm (0.001 inch) was attached on the beam. The frictionless shank of the LP was connected to the wire to measure beam deflections.



$L = 6400$ mm (21 ft); $a = 2286$ mm (7-1/2 ft) for the 302-mm (11-7/8-inch) deep beams
 $L = 8534$ mm (28 ft); $a = 3048$ mm (10 ft) for the 406-mm (16-inch) deep beams
 $L = 9144$ mm (30 ft); $a = 3353$ mm (11 ft) for the 457-mm (18-inch) deep beams

Figure 1. Schematic loading configuration for flexure tests

Load was applied by a hydraulic cylinder at a constant rate to fail the beam in flexure in about 10 minutes. Both load and deflection were continuously recorded by a computerized data acquisition system. At about 75% of the estimated maximum load, the LP was removed from the beam to prevent damage when the beam failed. The load was continuously recorded up to the ultimate load.

Based on the theory of elasticity, the modulus of rupture (MOR) and apparent modulus of elasticity (MOE) were calculated using the following equations:

$$\text{MOR} = \frac{3 P_{\text{ult}} a}{b d^2} + \frac{3 \omega \ell^2}{4 b d^2} \quad [\text{Eq. 2}]$$

$$\text{MOE} = \frac{\theta a (3 \ell^2 - 4 a^2)}{4 b d^3} \quad [\text{Eq. 3}]$$

where: MOR = modulus of rupture (MPa or psi),
 MOE = apparent modulus of elasticity (MPa or psi),
 P_{ult} = ultimate total load excluding the dead weight of the specimen (N or lbf),
 a = distance between the reaction to the nearest loading point (mm or in.),
 b = measured beam width (mm or in.),
 d = measured beam depth (mm or in.),
 ω = measured beam weight (N/mm or lbf/in.),
 ℓ = test span (mm or in.), and
 θ = slope of load vs. deflection plot below the proportional limit (N/mm or lbf/in.).

For determining the characteristic flexural stress of the beam, the MOR value calculated from Equation 1 was adjusted by a volume factor, C_v (as given in Equation 4), in accordance with the 1997 *National Design Specification for Wood Construction* [12].

$$C_v = \left(\frac{5.125}{b} \right)^{0.1} \left(\frac{12}{d} \right)^{0.1} \left(\frac{252}{\ell} \right)^{0.1} \quad [\text{Eq. 4}]$$

where: C_v = volume factor, and
 b, h, ℓ = as defined in Equations 2 and 3.

In addition, another adjustment factor was needed to account for the variation from the standard 12% moisture content. This moisture content adjustment factor, C_M , is shown in Equation 5 based on ASTM D2915 [13]. As a result, the adjusted MOR and MOE values given in this paper were determined by using Equations 6 and 7.

$$C_M = \frac{\alpha - \beta \times 12}{\alpha - \beta \times M} \quad [\text{Eq. 5}]$$

where: C_M = moisture content adjustment factor,
 M = actual moisture content of the beam, %,
 α = 1.75 for MOR and 1.44 for MOE, and
 β = 0.0333 for MOR and 0.02 for MOE.

$$\text{AdjustedMOR} = \frac{\text{CalculatedMOR (Eq. 2)}}{C_v} \quad [\text{Eq. 6}]$$

$$\text{Adjusted MOE} = \text{Calculated MOE from Eq. 3} \times C_M \text{ from Eq. 5} \quad [\text{Eq. 7}]$$

After the flexure tests, a 51-mm (2-inch) section was cut from each tested beam at about 457 mm (18 inches) away from each beam end to determine the beam moisture content, and density and specific gravity in accordance with the oven-drying method of ASTM D4442 [14] and D2395 [15], respectively. The mean of these two measurements was reported as the beam moisture content, and density and specific gravity. The mean density was used to calculate the beam weight for use in Equation 2, and the mean moisture content was used to calculate the moisture content adjustment factor based on Equation 5.

6. Results and Discussions

6.1 30F-E2M2 Glulam

All 30F-E2M2 glulam beams failed as a result of tension failure in the LVL tension lamination. Summary statistics for the 302-mm (11-7/8-inch) and 406-mm (16-inch) beam groups are given in Table 6.

Table 6. Summary statistics for 30F-E2M2 glulam beam tests

| | 406 mm (16 in.) | | | | 302 mm (11-7/8 in.) | | | |
|-------------|-----------------|-------------------|----------------------|------------------------|---------------------|-------------------|----------------------|------------------------|
| | MC | SG ^(a) | MOR ^(b) | MOE ^(c) | MC | SG ^(a) | MOR ^(b) | MOE ^(c) |
| N | 15 | | | | 15 | | | |
| Mean | 11.3% | 0.58 | 55 MPa (7980 psi) | 16.5 GPa (2.4 Mpsi) | 10.1% | 0.58 | 54 MPa (7900 psi) | 15.9 GPa (2.3 Mpsi) |
| COV | 0.025 | 0.013 | 0.070 | 0.039 | 0.030 | 0.029 | 0.066 | 0.028 |
| $f_{m,g,k}$ | | | 47 MPa (6860 psi) | | | | 47 MPa (6860 psi) | |

(a) Density based on weight and volume at beam test.

(b) Adjusted MOR based on Equation 6.

(c) Adjusted MOE based on Equation 7.

Based on the Smith-Satterthwaite statistical test [16], which is an alternate statistical t-test for equal/unequal sample sizes and/or non-homogeneous variances, the adjusted MOR data obtained from the 302-mm (11-7/8-inch) and 406-mm (16-inches) beam groups are not statistically significantly different at the 5%- α significance level. This is also evident from the observation that the mean and COV between these 2 beam groups are very similar. Therefore, it is justifiable to combine the data obtained from these 2 beam groups for deriving the characteristic flexural strength. Table 7 shows the summary statistics of the adjusted MOR and MOE based on the combined data.

Table 7. Summary statistics of combined data for 30F-E2M2

| | MOR ^(a) | | MOE ^(b) |
|--------------------|--------------------|-------------------|---------------------|
| | Normal | Lognormal | Normal |
| N | 30 | | |
| Mean | 55 MPa (7940 psi) | -- | 16.3 GPa (2.4 Mpsi) |
| COV | 0.067 | -- | 0.034 |
| $f_{m,g,k}$ | 48 MPa (6940 psi) | 48 MPa (6960 psi) | -- |
| SEE ^(c) | 2.4% | 2.1% | -- |

^(a,b) see footnotes to Table 6.

^(c) A standard error of estimate (SEE) of 5% or less is generally considered acceptable for engineered wood products.

The data distribution for the adjusted MOR is shown in Figure 2, which suggests that the data can be fitted well with either normal or lognormal distribution. The goodness-of-fit by the Kolmogorov-Smirnov statistical test indicates that both assumed distribution functions cannot be rejected at the 20% statistical significance level (the higher the significance level, the easier to reject the null hypothesis that assumes the test data can be characterized by the underlying empirical function). The Kolmogorov-Smirnov D for the test data was 0.11 and 0.12, respectively, for the normal and lognormal distributions, whereas the critical D at the 20% statistical significance level is 0.19 for 30 observations.

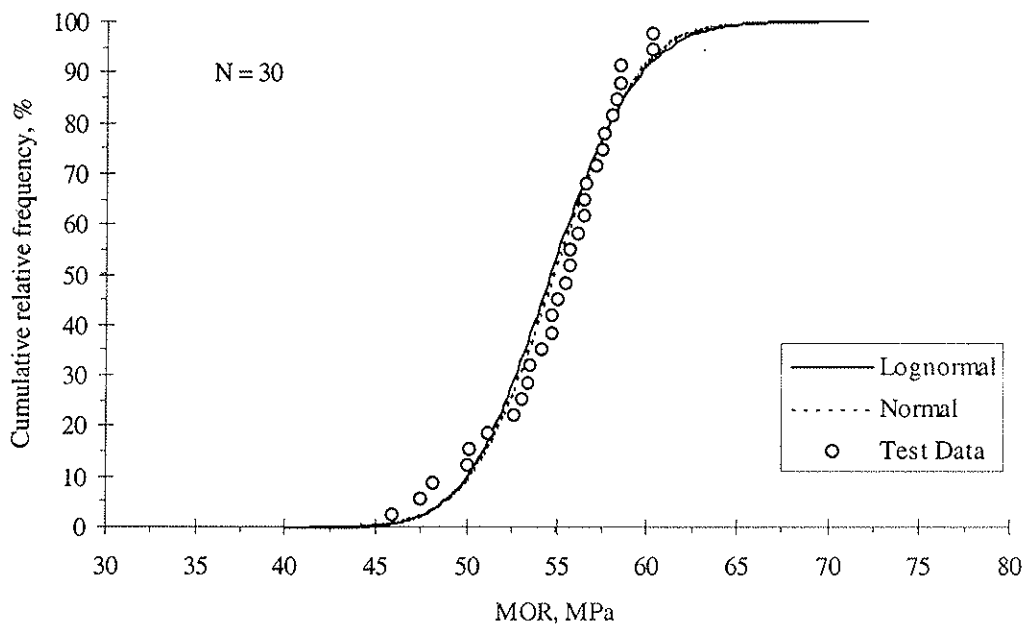


Figure 2. Adjusted MOR with empirical distribution functions overlaid for 30F-E2M2

As shown in Table 7, the characteristic flexural stress ($f_{m,g,k}$) is practically the same for both distribution functions. As a result, the $f_{m,g,k}$ value for the 30F-E2M2 layup combination can be estimated as 48 MPa (6940 psi). This $f_{m,g,k}$ value is identical to the value predicted by GAP (see Table 3), confirming the appropriateness of using GAP to predict the glulam beam performance with LVL tension laminations.

As also noted from Table 7, the $E_{0,g,mean}$ value obtained from full-scale beam tests was 16.3 GPa (2.4×10^6 psi). This value is significantly higher than the $E_{0,g,mean}$ value of 14.5 GPa (2.1×10^6 psi), as predicted by GAP (see Table 3), due primarily to the fact that the LVL tension laminations had an $E_{0,l,mean}$ value of 18.6 GPa (2.7×10^6 psi) (see Table 5) instead of the assumed 16.6 GPa (2.4×10^6 psi) used in the layup design.

6.2 30F-E2M3 Glulam

All 30F-E2M3 glulam beams also failed as a result of tension failure in the LVL tension lamination. However, there were 6 beams that were noted to have a questionable face bond between the LVL tension lamination and the adjacent lumber lamination. Summary statistics for the 302-mm (11-7/8-inch) and 457-mm (18-inch) beam groups are given in Table 8.

Table 8. Summary statistics for 30F-E2M3 glulam beam tests

| | 457 mm (18 in.) | | | | 302 mm (11-7/8 in.) | | | |
|-------------|-----------------|-------------------|----------------------|------------------------|---------------------|-------------------|----------------------|------------------------|
| | MC | SG ^(a) | MOR ^(b) | MOE ^(c) | MC | SG ^(a) | MOR ^(b) | MOE ^(c) |
| N | 18 | | | | 17 | | | |
| Mean | 12.4% | 0.60 | 59 MPa (8520 psi) | 17.0 GPa (2.5 Mpsi) | 11.4% | 0.60 | 56 MPa (8100 psi) | 17.6 GPa (2.6 Mpsi) |
| COV | 0.051 | 0.027 | 0.060 | 0.034 | 0.025 | 0.030 | 0.085 | 0.058 |
| $f_{m,g,k}$ | | | 52 MPa (7520 psi) | | | | 47 MPa (6750 psi) | |

(a,b,c) see footnotes to Table 6.

The adjusted MOR data obtained from the 302-mm (11-7/8-inch) and 457-mm (18-inch) beam groups are not statistically significantly different at the 5%- α significance level based on the Smith-Satterthwaite statistical test [16]. Therefore, it is justifiable to combine the data obtained from these 2 beam groups for deriving the characteristic flexural strength. Table 9 shows the summary statistics of the adjusted MOR and MOE based on the combined data.

Table 9. Summary statistics of combined data for 30F-E2M3

| | MOR ^(a) | | MOE ^(b) |
|--------------------|--------------------|-------------------|---------------------|
| | Normal | Lognormal | Normal |
| N | 35 | | |
| Mean | 57 MPa (8315 psi) | -- | 17.3 GPa (2.5 Mpsi) |
| COV | 0.076 | -- | 0.034 |
| $f_{m,g,k}$ | 49 MPa (7150 psi) | 50 MPa (7190 psi) | -- |
| SEE ^(c) | 2.5% | 2.1% | -- |

(a,b,c) see footnotes to Table 7.

Figure 3 shows the data distribution for the adjusted MOR, which suggests that the data can be fitted well with either normal or lognormal distribution. The goodness-of-fit by the Kolmogorov-Smirnov statistical test indicates that both assumed distribution functions cannot be rejected at the 20% statistical significance level. The Kolmogorov-Smirnov D for the test data was 0.11 and 0.12, respectively, for the normal and lognormal distributions, whereas the critical D at the 20% statistical significance level is 0.18 for 35 observations.

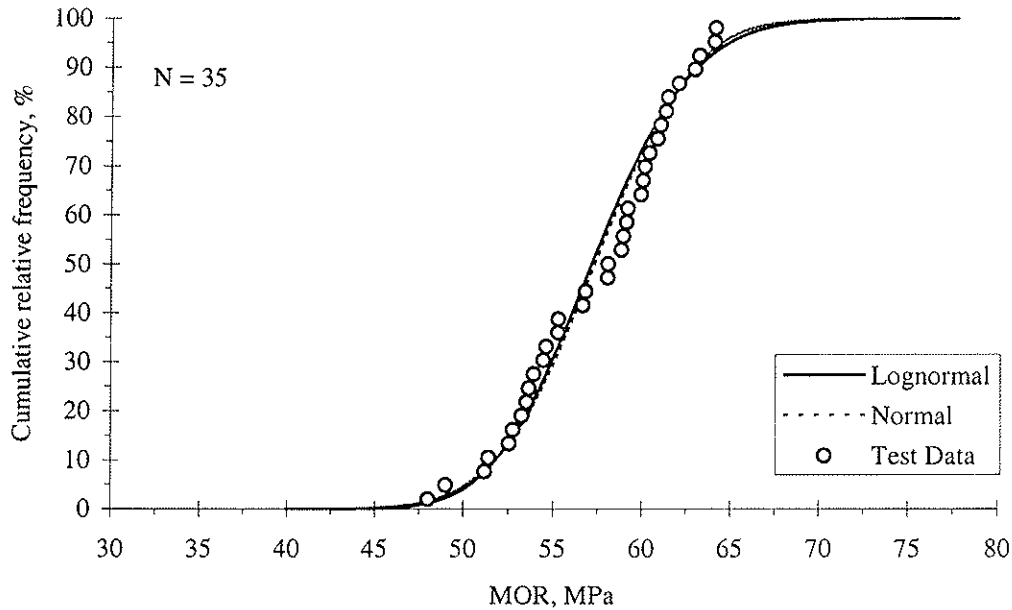


Figure 3. Adjusted MOR with empirical distribution functions overlaid for 30F-E2M3

The characteristic flexural stress ($f_{m,g,k}$) is practically the same for both distribution functions, as shown in Table 9. As a result, the $f_{m,g,k}$ value for the 30F-E2M3 layup combination can be estimated as 49 MPa (7150 psi). This $f_{m,g,k}$ value is very similar to the value of 48 MPa (6930 psi) predicted by GAP (see Table 4). In addition, the $E_{0,g,mean}$ value obtained from full-scale beam tests was 17.3 GPa (2.5×10^6 psi). This value is significantly higher than the $E_{0,g,mean}$ value of 14.5 GPa (2.1×10^6 psi), as predicted by GAP (see Table 4), due primarily to the high $E_{0,l,mean}$ value from the LVL tension laminations.

6.3 Relationship between $f_{t,0,l,k}$ and $f_{m,g,k}$

Based on Tables 5, 7, and 9, the relationship between $f_{t,0,l,k}$ and $f_{m,g,k}$ can be expressed as follows:

$$\text{For 30F-E2M2} \quad f_{t,0,l,k} = 0.8 \times f_{m,g,k} \quad [\text{Eq. 8}]$$

$$\text{For 30F-E2M3} \quad f_{t,0,l,k} = 1.0 \times f_{m,g,k} \quad [\text{Eq. 9}]$$

In other words, the relationship between the characteristic tensile strength of the LVL tension laminations and the characteristics flexural strength of the glulam beams does not necessarily follow the relationship prescribed in ANSI A190.1 [9] (see Equation 1). It was originally theorized that the high ratio for 30F-E2M3 might have been associated with the

questionable face bond between the LVL tension lamination and adjacent lumber lamination, as previously noted. It was suspected that the questionable glue bond might have caused an incomplete stress transfer between the inner laminations and the LVL tension lamination, thereby demanding a higher share of tensile stress on the LVL tension lamination.

This hypothesis, however, could not be substantiated in 2 other similar testing programs conducted for the same glulam manufacturer soon after the completion of this study. The glue bond did not have any problems in those 2 studies. However, the relationship between the characteristic tensile strength of the LVL tension laminations and the characteristic flexural strength of the glulam beams was the same as that described by Equation 9. Likewise, another similar testing program conducted for the same glulam manufacturer who produced the 30F-E2M2 glulam tested in this study showed a consistent relationship as that described in Equation 8. Details of those 3 studies will be reported in the near future.

Results obtained from this study suggested that relationship between the characteristic tensile strength of the LVL tension laminations ($f_{t,0,l,k}$) and the characteristic flexural strength of the glulam beams ($f_{m,g,k}$) is likely to depend upon not only the LVL, but the glulam manufacturers. It was noticed that the relationship between $f_{t,0,l,k}$ and $f_{m,g,k}$ did not necessarily follow ANSI A190.1 [9]. Therefore, the required $f_{t,0,l,k}$ value for QA purposes should be confirmed by LVL tension and full-scale glulam beam tests. Without the confirmation data, the $f_{t,0,l,k}$ should be assigned the same value as $f_{m,g,k}$.

6.4 Control Values for 30F-E2M2 and 30F-E2M3

As the LVL tension laminations are crucial to the glulam beam performance, control values for the LVL should be established for quality control purposes when the layup combinations given in Tables 1 and 2 are implemented in production. Based on the full-scale beam test results given in Tables 7 and 9, it appears that the beam performance can be justified at $f_{m,g,k}$ of 48 MPa (6940 psi) and $E_{0,g,mean}$ of 16.3 GPa (2.4×10^6 psi) for 30F-E2M2, and $f_{m,g,k}$ of 49 MPa (7140 psi) and $E_{0,g,mean}$ of 17.3 GPa (2.5×10^6 psi) for 30F-E2M3, provided that the control values for the LVL tension laminations are established based strictly on the LVL test results given in Table 5. However, as the targeted $f_{m,g,k}$ and $E_{0,g,mean}$ are limited to 43 MPa (6300 MPa) and 14.5 GPa (2.1×10^6 psi), respectively, the control values for the LVL tension laminations can be adjusted accordingly.

In lack of further supporting data, the required LVL characteristic tensile strength based on a 4-ft gauge length may be established based on Equations 8 and 9. In other words, the $f_{t,0,l,k}$ value should be required at 43 MPa (6300 psi) $\times 0.8 = 34$ MPa (5040 psi) for 30F-E2M2. On the other hand, the $f_{t,0,l,k}$ value should be required at 43 MPa (6300 psi) for 30F-E2M3. Apparently, the required LVL long-span E can be established at 16.6 GPa (2.4×10^6 psi) as the glulam beam MOE is very predictable using GAP or the transformed section method.

7. Conclusions

The following conclusions are supported by the results obtained from this study:

- LVL could be used as tension laminations for high-strength glulams up to, but not limited to, an $f_{m,g,k}$ value of 43 MPa (6300 psi) and $E_{0,g,mean}$ value of 14.5 GPa (2.1×10^6 psi).
- The layup combinations given in Tables 1 and 2 could meet the values given above provided that the LVL tension laminations are properly quality-controlled.
- It is also important to recognize that relationship between $f_{i,o,l,k}$ and $f_{m,g,k}$ is likely to depend upon not only the LVL, but the glulam manufacturers. Therefore, the required $f_{i,o,l,k}$ value for QA purposes should be confirmed by LVL tension and full-scale glulam beam tests. Without the confirmation data, the $f_{i,o,l,k}$ should be assigned the same value as $f_{m,g,k}$.

8. References

1. APA - The Engineered Wood Association. 2000. *Glulam Design Properties and Layup Combinations*. EWS Y117. Tacoma, WA.
2. American Institute of Timber Construction. 1993. *Standard Specifications for Structural Glued Laminated Timber of Softwood Species*. AITC 117-93 -- Manufacturing. Englewood, CO.
3. ICBO Evaluation Service, Inc. 2000. *EWS glued laminated timber combinations and the "GAP 2000" computer program for determining design stresses*. Evaluation Report No. ER-5714.
4. National Evaluation Service, Inc. 2000. *EWS glued laminated timber combinations and "GAP" computer program for determining design stresses*. Evaluation Report No. NER-486.
5. Yeh, B.J. 1996. *Using computer models to predict the performance of structural glued laminated timber*. In Proceedings of the International Wood Engineering Conference, 1:136-143. New Orleans, LA.
6. American Society for Testing and Materials. 2000. Standard test method for establishing stresses for structural glued laminated timber (glulam). ASTM D3737. *Annual Book of ASTM Standards*. Philadelphia, PA.
7. American Society for Testing and Materials. 2000. Standard test methods for mechanical properties of lumber and wood-base structural material. ASTM D4761. *Annual Book of ASTM Standards*. Philadelphia, PA.
8. American Society for Testing and Materials. 2000. Standard specification for evaluation of structural composite lumber products. ASTM D5456. *Annual Book of ASTM Standards*. Philadelphia, PA.
9. American National Standards Institute. 1992. *American National Standard for Wood Products - Structural Glued Laminated Timber*. ANSI A190.1. New York, NY.
10. American Institute of Timber Construction. 1992. *Standard for Laminated Veneer Lumber (LVL) Used in Structural Glued Laminated Timber*. AITC 402. Englewood, CO.
11. American Society for Testing and Materials. 2000. Standard methods of static tests of timbers in structural sizes. ASTM D198. *Annual Book of ASTM Standards*. Philadelphia, PA.
12. American Forest & Paper Association. 1997. *National Design Specification for Wood Construction*. Washington, D.C.

13. American Society for Testing and Materials. 2000. Standard practice for evaluating allowable properties for grades of structural lumber. ASTM D2915. *Annual Book of ASTM Standards*. Philadelphia, PA.
14. American Society for Testing and Materials. 2000. Standard test methods for direct moisture content measurement of wood and wood-base materials. ASTM D4442. *Annual Book of ASTM Standards*. Philadelphia, PA.
15. American Society for Testing and Materials. 2000. Standard test methods for specific gravity of wood and wood-based materials. ASTM D2395. *Annual Book of ASTM Standards*. Philadelphia, PA.
16. Miller, I and J.E. Freund. 1977. Probability and Statistics for Engineers, 2nd Edition. Prentice-Hall, Inc., Englewood Cliffs, NJ.

**INTERNATIONAL COUNCIL FOR RESEARCH AND INNOVATION
IN BUILDING AND CONSTRUCTION**

WORKING COMMISSION W18 - TIMBER STRUCTURES

**EVALUATION OF GLULAM SHEAR STRENGTH
USING A FULL-SIZE FOUR-POINT TEST METHOD**

B Yeh

T G Williamson

APA - The Engineered Wood Association

U.S.A.

Presented by: B Yeh

- I Smith asked about the nature of the failure mode.
- B Yeh answered that the failure was typically in the late and early wood band. The flat or quarter sawn lumber will have an influence however this was not controlled in the production.
- F Lam asked would deeper beams be also considered.
- B Yeh stated that there were no plans to consider deeper beams as they would typically span long distances and bending would govern.

Evaluation of Glulam Shear Strength Using A Full-Size Four-Point Test Method

Borjen Yeh, Ph.D., P.E.

Thomas G. Williamson, P.E.

APA - The Engineered Wood Association, U.S.A.

Abstract

The shear strengths of structural glued laminated timber (glulam) have been traditionally evaluated in the United States based on the procedures set forth in ASTM Standards D3737 and D2555 using small block shear values of clear wood specimens. For most glulam products, the design shear stresses so derived are conservative. In recent years, the demand to optimize the design shear stress has been increased due to a higher design shear stress offered by competing structural wood composites, such as laminated veneer lumber (LVL) and parallel strand lumber (PSL).

Since 1997, APA has conducted a series of full-size shear tests on glulam manufactured with Douglas fir, Southern pine, and Spruce-Pine-Fir. A four-point load method with a clear distance between the edge of the reaction bearing plate to the edge of the nearest curved load bearing block of at least 2 times the specimen depth was used to test all specimens. Based on this experience, the full-size shear test method has been adopted in ASTM D3737 as a standard test method for determining the horizontal shear strength of glulam. This paper provides detailed descriptions of the test methods, experimental results, and data analyses.

The test results obtained from this study indicate that the characteristic shear strength values based on full-size shear tests are approximately 70% of the values determined from small block shear tests. However, the allowable horizontal shear stress could be increased by a factor of at least 1.25, including a 10% reduction to allow for occasional seasoning checks. This increase can be attributed in part to the difference in the procedures used to derive the design value between the full-size and small block shear tests.

1. Introduction

Glued laminated timber (glulam) has been extensively used in North America in both residential and nonresidential applications. Nonresidential uses include commercial and industrial buildings, marinas, transmission structures, and pedestrian, highway, and railroad bridges. While most applications are controlled by bending stress or stiffness, there are situations in which horizontal shear is the controlling design stress. Examples include heavily loaded floor beams, bridge stringers, and cantilever or continuous beams.

In the United States, the design (allowable) shear stresses for glulam have been traditionally determined based on the procedures set forth in ASTM D3737 [1] and D2555 [2] using small block shear values of clear wood specimens. The shear reduction factor customarily applied to test results of small scale block shear specimens is 1/4.1, which is composed of the effects of load duration (10/16) and stress concentration (4/9), and a factor of safety (8/9).

In recent years, however, information has been generated, indicating that the allowable shear stresses so derived are overly conservative for glulam when compared to the results of full-size shear tests [3,4,5]. Based on the available data, it has been determined that the stress concentration factor of 4/9 is only applicable to small block shear specimens and should be removed from the reduction factor for use with the results of full-size shear tests. It has been further determined that the factor of safety should be revised to be the same as the allowable flexural stress (10/13). Combining this with the duration of load factor of 10/16 results in a net reduction factor of 1/2.1 that can then be applied to the 5th percentile shear results obtained from full-size glulam shear tests to establish design shear values.

Since 1997, APA has conducted a series of full-size shear tests on glulam manufactured with Douglas fir, Southern pine, and Spruce-Pine-Fir. This report provides detailed descriptions of the test methods, experimental results, and data analyses.

2. Objective

The main purpose of this study was to systematically evaluate the shear strengths of glulam for various wood species used in the manufacture of glulam in North America based on a full-size four-point test method.

3. Materials

Three major wood species used in the manufacture of glulam in North America, these being Douglas fir (DF), Southern pine (SP), and Spruce-Pine-Fir (SPF), were identified for testing in this study. As the primary goal was to evaluate the shear strengths, it was essential to fail as many glulam specimens in shear as possible. In addition, it was considered critical that the specimen dimension should be sufficiently large so as to prevent the shear stress distribution from being affected by the interaction of the compressive stress perpendicular to grain.

Consequently, a specimen depth of approximately 457 mm (18 in.) with a simply supported test span (from the center of support to the center of support) of 3048 mm (10 ft) was selected, resulting in a span-to-depth ratio of approximately 6.7. This specimen dimension was also selected to represent the boundary size in which the allowable shear stress governs the design of typical residential floor beam construction [6]. It can be expected that either bending or deflection will control the design as the span-to-depth ratio increases.

All specimens were manufactured using full-length laminations without any end joints to induce failures in shear, but not at an end joint, in the critical tension zone of the test beams. The manufacturing processes followed the provisions of American National Standards Institute (ANSI) A190.1, *American National Standard for Wood Products -- Structural Glued Laminated Timber* [7]. Wet-use adhesives were used for face bonding of the laminations. APA staff was present during the lumber selection and manufacturing for all test specimens.

A series of glulam beams, as shown in Table 1, were tested at the APA Research Center in Tacoma, Washington, in the as-received indoor conditions without any moisture pre-

conditioning. The layups for these beams are shown in Table 2, which were designed to achieve a targeted 70% failure rate in shear using the test method selected.

Table 1. Specimen cross sections

| Species | DF | | SP | | SPF |
|------------|-----------------------|----------------------|------------------------|------------------------|------------------------|
| Replicates | 39 | 40 | 42 | 40 | 40 |
| Net width | 171 mm (6-3/4 in.) | 79 mm (3-1/8 in.) | 171 mm (6-3/4 in.) | 79 mm (3-1/8 in.) | 105 mm (4-1/8 in.) |
| Net depth | 457 mm (18 in.) | 457 mm (18 in.) | 454 mm (17-7/8 in.) | 454 mm (17-7/8 in.) | 429 mm (16-7/8 in.) |

Table 2. Specimen layups

| Species | Tension zones | | | Core | Compression zones | | |
|---------|---------------|--------------|-------------|--------------|-------------------|--------------|---------------|
| DF | 1 - 302-26 | 1 - L1 | 1 - L2 | 6 - L3 | 1 - L2 | 1 - L1 | 1 - 302-26 |
| SP | 1 - 302-26 | 1 - N1D14 | 2 - N1D8 | 5 - N2M8 | 2 - N1D8 | 1 - N1D14 | 1 - 302-26 |
| SPF | 1 - 302-24 | 1 - 1.8E3 | -- | 8 - 1.4E2 | -- | 1 - 1.8E3 | 1 - 302-24 |

This shear failure rate was estimated by equating the predicted 25th percentile of the bending strength to the anticipated 95th percentile of the shear strength of the glulam. The bending strength of the glulam was predicted by using the GAP computer program that was developed by APA and is recognized by the major building code evaluation services as an alternative method for determining design stresses of a given layup combination of glulam [8]. The shear strength of the glulam was estimated based on the authors' experience and the information obtained from the literature [3,9,10,11].

The layups shown in Table 2 were based on commercially available combinations except that the tension laminations were generally up-graded to increase the probability of shear failure. The shear-critical core laminations were all carefully selected as being "on-grade." The laminations used for manufacturing the specimens were Douglas fir grown west of the Cascade Mountains, Southern pine grown in Southern Alabama and Southern Arkansas-Northern Louisiana, and Spruce-Pine-Fir grown in Southeast British Columbia, Canada. The actual sub-species of the species group were not microscopically determined.

4. Test Methods

A four-point load method, as shown in Figure 1, was applied to test all specimens. In this case, the four-point load method is considered superior to the center-point load method as the compressive stress perpendicular to grain under the load point is reduced to 1/2 of the compressive stress perpendicular to grain under the center-point load. This test setup significantly alleviates the wood crushing under the load point, which could interfere with the shear stress distribution in the specimen [9].

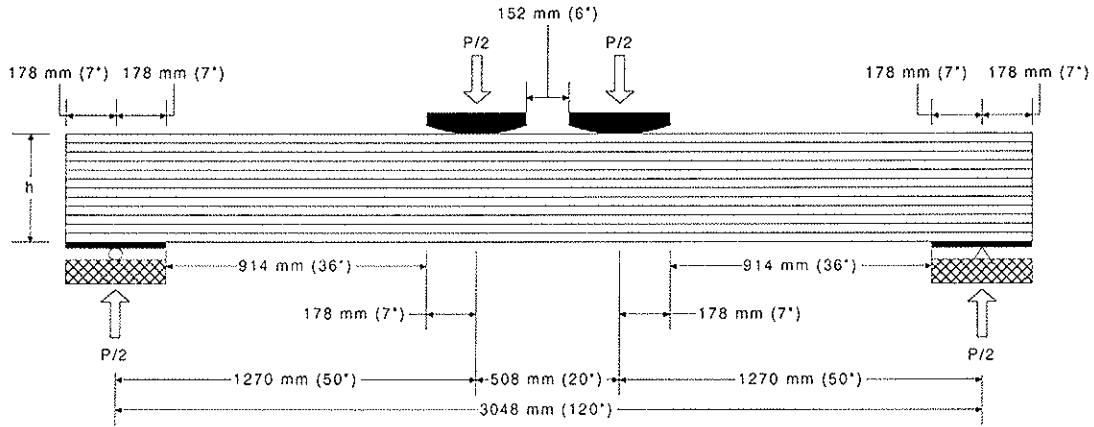


Figure 1. Test setup (see Table 1 for the depth, h , of each tested species)

The test apparatus, including rocker-type reaction supports, reaction bearing plates and rollers, load bearing blocks, and load bearing rollers were set up following ASTM D198 [12]. The curved load bearing blocks had a chord length of 356 mm (14 in.) and a radius of curvature of 711 mm (28 in.). The clear distance between the edge of the bearing plate to the edge of the nearest load bearing block was 914 mm (36 in.) for all specimens, which was at least 2 times the specimen depth. This clear distance was regarded as critical to prevent the shear stress distribution from being influenced by the compressive stress perpendicular to grain [9]. All specimens were cut to the exact length of 3404 mm (134 in.) and no overhangs were allowed. Load was applied by a hydraulic cylinder at a constant rate so as to reach the ultimate load in about 10 minutes. Load readings were continuously recorded by a computerized data acquisition system up to the ultimate load. The deflection readings were not recorded.

5. Analysis Methods

Based on the theory of elasticity, the flexural (f_b) and shear (f_v) stresses at the time of specimen failure were calculated using the following equations:

$$f_b = \frac{3 P_{ult} a}{b h^2} \quad [\text{Eq. 1}]$$

$$f_v = \frac{3 P_{ult}}{4 b h} \quad [\text{Eq. 2}]$$

where:

f_b = flexural stress, MPa (psi),

f_v = shear stress, MPa (psi),

P_{ult} = ultimate total load, N (lbf),

a = distance between the reaction point to the nearest loading point, mm (in.),

b = measured beam width, mm (in.), and

h = measured beam depth, mm (in.)

The flexural stress of each specimen, as calculated from Eq. 1, was adjusted by a volume factor, C_v , in accordance with the *National Design Specification for Wood Construction* [13]. In addition, as the members were not pre-conditioned prior to testing, the moisture

content adjustment factor, C_M , as shown in Eq. 3 based on ASTM D2915 [14], was used to adjust the test results to the standard 12% moisture content.

$$C_M = \frac{C_1 - C_2 \times 12}{C_1 - C_2 \times M} \quad [\text{Eq. 3}]$$

where:

- C_M = moisture content adjustment factor,
- M = actual moisture content of the specimen, %,
- C_1 = 1.75 for f_b and 1.33 for f_v , and
- C_2 = 0.0333 for f_b and 0.0167 for f_v .

After testing, a 51-mm (2-in.) section was cut from each tested specimen at approximately 305 mm (12 in.) in from each beam end. The laminations other than the core laminations (L3 for DF, N2M8 for SP, and 1.4E2 for SPF) were then removed from these end sections. The resulting sections, which represented the core laminations, were then used to determine the moisture content and specific gravity of each beam in accordance with the oven-drying method of ASTM D4442 [15] and D2395 [16], respectively.

6. Results and Discussions

6.1 Modes of failure

The summary of the failure modes for each tested species is shown in Table 3. Typically, the shear failure was initiated at one end of the specimen near the neutral axis or in the bottom half of the cross section, which is consistent with the observations reported by Freas and Selbo [10]. The patterns of failure surface were similar for all tested species. In general, the failure surface followed a growth ring along the late wood and early wood interface of a flat-grained lamination and in some cases then jumped over to the adjacent growth rings or laminations.

Table 3. Summary of failure modes

| Modes of failure | Percentage of specimens failed in each mode | | | | | Total |
|------------------|---|----------------------|-----------------------|----------------------|-----------------------|-------|
| | DF | | SP | | SPF | |
| | 171 mm (6-3/4 in.) | 79 mm (3-1/8 in.) | 171 mm (6-3/4 in.) | 79 mm (3-1/8 in.) | 105 mm (4-1/8 in.) | |
| Shear | 82% | 73% | 62% | 92% | 43% | 70% |
| Flexure | 18% | 22% | 38% | 8% | 57% | 29% |
| Bearing | 0% | 5% | 0% | 0% | 0% | 1% |

From Table 3, the overall percentage of shear failure is 70%, which coincides with the anticipated shear failure rate previously mentioned. However, due to the relatively low percentage of shear failure for SPF, the test results were highly censored when the analysis is performed using all data combined. Therefore, it is necessary to conduct a censored data analysis for each species and tested width.

For the censored data analysis, the uncensored mean and standard deviation can be estimated by using the maximum likelihood estimators (MLEs) described in Lawless [17]. The estimates of the uncensored statistics from the highly censored data are critical due to the fact that although the uncensored mean is expected to be higher than the censored

mean, the uncensored standard deviation might be also higher than the censored standard deviation. As a result, the characteristic value (5th percentile with 75% confidence) based on the uncensored data may or may not be actually higher than the value determined from the censored statistics.

6.2 Shear and flexural strengths

Table 4 shows the summary statistics for the moisture content and specific gravity of the core materials obtained from all specimens. The summary statistics for the calculated shear and flexural strengths after being adjusted to the standard moisture content of 12% are given in Table 5. The flexural strengths have been further adjusted by a volume factor. It should be noted that the dead weight of the specimen was not included in the calculations. In addition, the calculated shear and flexural strengths represented the stress states at failure and might not represent the ultimate shear and flexural strengths unless the specimen happened to fail in the specific mode.

Table 4. Summary statistics for moisture content and specific gravity^(a)

| | DF | | SP | | SPF |
|---------|-----------------------|----------------------|-----------------------|----------------------|-----------------------|
| | 171 mm (6-3/4 in.) | 79 mm (3-1/8 in.) | 171 mm (6-3/4 in.) | 79 mm (3-1/8 in.) | 105 mm (4-1/8 in.) |
| N | 39 | 40 | 42 | 40 | 40 |
| Mean MC | 11.4% | 11.5% | 11.0% | 10.3% | 14.5% |
| Mean SG | 0.43 | 0.43 | 0.51 | 0.47 | 0.40 |

^(a) Based on the oven-dry weight and as-received volume of the core laminations only.

Table 5. Summary statistics for shear and flexural strengths^(a)

| | | DF | | SP | | SPF |
|----------------------------|------|------------------------|------------------------|------------------------|------------------------|------------------------|
| | | 171 mm (6-3/4 in.) | 79 mm (3-1/8 in.) | 171 mm (6-3/4 in.) | 79 mm (3-1/8 in.) | 105 mm (4-1/8 in.) |
| Shear failure only | | | | | | |
| N | | 32 | 29 | 26 | 37 | 17 |
| f_v | Mean | 4.40 MPa (639 psi) | 4.66 MPa (676 psi) | 5.38 MPa (780 psi) | 5.24 MPa (760 psi) | 4.34 MPa (630 psi) |
| f_b | | 48.9 MPa (7095 psi) | 48.0 MPa (6957 psi) | 59.8 MPa (8669 psi) | 55.7 MPa (8075 psi) | 51.8 MPa (7507 psi) |
| f_v, f_b | COV | 0.070 | 0.085 | 0.098 | 0.092 | 0.130 |
| All failure modes combined | | | | | | |
| N | | 39 | 40 | 42 | 40 | 40 |
| f_v | Mean | 4.33 MPa (628 psi) | 4.60 MPa (667 psi) | 5.41 MPa (785 psi) | 5.22 MPa (757 psi) | 4.18 MPa (616 psi) |
| f_b | | 48.1 MPa (6970 psi) | 47.4 MPa (6868 psi) | 60.1 MPa (8718 psi) | 55.5 MPa (8045 psi) | 50.6 MPa (7341 psi) |
| f_v, f_b | COV | 0.089 | 0.086 | 0.100 | 0.092 | 0.112 |

^(a) Calculated stresses adjusted for moisture content and volume effect (f_b only) at time of specimen failure.

The data distribution for those specimens that failed in shear is shown in Figure 2 with an empirical normal distribution function overlaid. It should be noted that there was one 79-mm (3-1/8-in.) wide DF specimen that was noted to contain an off-grade ring shake that

extended from the wide face into the thickness at an angle less than 45 degrees from the wide face, which is not permitted by industry standards [18]. This specimen ultimately failed at the lowest shear value of 3.35 MPa (486 psi) among all 40 specimens of the same size, including those that failed in a flexural or bearing mode. Although this test result can be statistically quantified as an outlying observation at the 5% significance level in accordance with ASTM E178 [19], it was still included in the data analysis to be conservative. Similarly, the SPF specimen that failed at the lowest adjusted shear strength of 2.88 MPa (418 psi) was included in the data analysis even though it can also be statistically justified as an outlying observation.

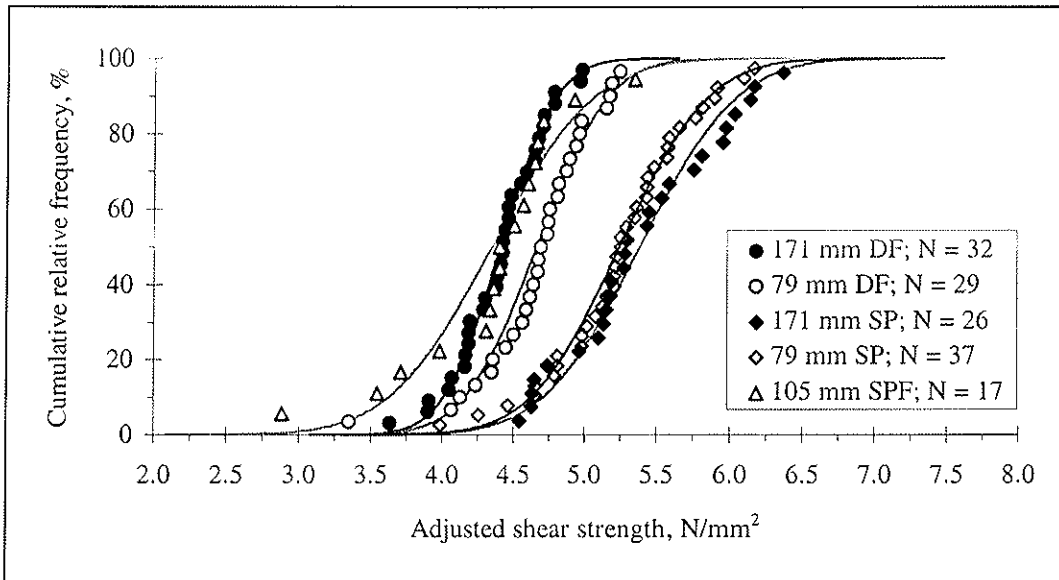


Figure 2. Shear strengths with an empirical normal distribution function overlaid

Using the MLE method, the uncensored mean and standard deviation for the shear strength of each tested width were calculated based on all data combined (censored data), as shown in Table 6. When compared to the results obtained from the specimens that failed in shear (see Table 5), the MLE method in general gives a comparable mean and COV.

Table 6. Estimated statistics from the censored data analyses using the MLE technique

| | DF | | SP | | SPF |
|------------------------|-----------------------|-----------------------|-----------------------|-----------------------|-----------------------|
| | 171 mm (6-3/4 in.) | 79 mm (3-1/8 in.) | 171 mm (6-3/4 in.) | 79 mm (3-1/8 in.) | 105 mm (4-1/8 in.) |
| Normal Distribution | | | | | |
| Mean | 4.43 MPa (642 psi) | 4.73 MPa (686 psi) | 5.66 MPa (821 psi) | 5.26 MPa (763 psi) | 4.66 MPa (676 psi) |
| COV | 0.070 | 0.082 | 0.110 | 0.090 | 0.122 |
| Lognormal Distribution | | | | | |
| Mean | 4.43 MPa (642 psi) | 4.74 MPa (687 psi) | 5.67 MPa (822 psi) | 5.26 MPa (763 psi) | 4.72 MPa (684 psi) |
| COV | 0.073 | 0.090 | 0.115 | 0.094 | 0.144 |

According to the statistics given in Tables 5 and 6, the parametric estimates of the shear strength at the 5th percentile with 75% confidence (characteristic values) can be determined following the procedures given in ASTM D2915 [14]. The characteristic value for each tested species will be discussed below.

7. Characteristic Shear Strength

7.1 Douglas fir glulam

Table 7 shows the estimated characteristic values for DF glulam based on normal and lognormal distribution functions. The assumed normality for both distribution functions cannot be rejected at the 20% statistical significance level for all tested species and widths in accordance with the Kolmogorov-Smirnov test statistics (the higher the significance level, the easier to reject the null hypothesis assuming the same distribution). In fact, the characteristic values determined from both types of distribution functions are generally similar.

Table 7. Parametric estimates of the characteristic shear strengths for DF glulam

| | 171 mm (6-3/4 in.) | | | 79 mm (3-1/8 in.) | | |
|----------------------------|--------------------|-------------------------------------|-----------------------|-------------------|-----------------------|-------------------------------------|
| | N | Characteristic value | | N | Characteristic value | |
| | | Normal | Lognormal | | Normal | Lognormal |
| Shear failure only | 32 | 3.83 MPa (555 psi) | 3.85 MPa (558 psi) | 29 | 3.92 MPa (569 psi) | 3.91 MPa (568 psi) |
| All failure modes combined | 39 | 3.62 MPa (525 psi) | 3.63 MPa (527 psi) | 40 | 3.88 MPa (562 psi) | 3.88 MPa (562 psi) |
| MLE estimates | 39 | 3.86 MPa (560 psi) | 3.84 MPa (557 psi) | 40 | 4.02 MPa (583 psi) | 3.96 MPa (574 psi) |

As noted from Table 7, the characteristic values for DF, as derived from the shear-failure-only data and the MLE method, are all higher than the values determined from the all-failure-modes-combined data. From a statistical viewpoint, the values obtained from the MLE method can be inferred as being better than the conservative estimates calculated from the censored data (all failure modes combined). Therefore, it is justifiable to establish the characteristic shear value for each tested width based on the lower value between the MLE estimates and the characteristic value determined from the shear-failure-only data. As a result, the characteristic shear value of 3.83 MPa (555 psi) based on the normal distribution and 3.91 MPa (568 psi) based on the lognormal distribution was determined, respectively, for the 171-mm (6-3/4-in.) and 79-mm (3-1/8-in.) wide specimens. These values are significantly lower (approximately 30%) than the characteristic value of 5.50 MPa (798 psi) derived from the small block shear values given in ASTM D2555 [2] and adjusted to the standard moisture content of 12%.

Using the reduction factor of 1/2.1 (see Section 1), the allowable shear stress can be calculated as 3.83/2.1 or 1.83 MPa (265 psi) for 171-mm (6-3/4-in.) wide and 3.91/2.1 or 1.87 MPa (270 psi) for 79-mm (3-1/8-in.) wide DF glulam. Due to the small difference in the allowable shear stress between the tested widths, a single allowable value of 1.83 MPa (265 psi) was established for DF glulam of all widths. This value is significantly higher (approximately 35%) than the allowable shear value of 1.35 MPa (195 psi) based on the characteristic shear strength of the small block shear (5.50 MPa or 798 psi) multiplied by the reduction factor of 1/4.1 (see Section 1). This increase can be attributed in part to the difference in the adjustment factors used to derive the allowable shear stress based on full-size and small block shear test results.

7.2 Southern pine glulam

Table 8 shows the estimated characteristic values for SP glulam based on normal and lognormal distribution functions. As noted from Table 8, the characteristic values for SP, as derived from the shear-failure-only data and the MLE method, are not always higher than the values determined from the all-failure-modes-combined data. For example, for the 171-mm (6-3/4-in.) wide specimens, the characteristic value determined from the all-failure-modes-combined data is higher than the value obtained from the shear-failure-only data due in part to the large difference in the sample size. As the characteristic value based on the all-failure-modes-combined data can be regarded as a conservative estimate of the actual shear strength, it is prudent in this case to use such a value for deriving the characteristic shear strength even though the use of a higher value based on the MLE method may be justifiable.

Table 8. Parametric estimates of the characteristic shear strengths for SP glulam

| | 171 mm (6-3/4 in.) | | | 79 mm (3-1/8 in.) | | |
|----------------------------|--------------------|-------------------------------------|-----------------------|-------------------|-------------------------------------|-----------------------|
| | N | Characteristic value | | N | Characteristic value | |
| | | Normal | Lognormal | | Normal | Lognormal |
| Shear failure only | 26 | 4.39 MPa (636 psi) | 4.46 MPa (646 psi) | 37 | 4.35 MPa (631 psi) | 4.38 MPa (635 psi) |
| All failure modes combined | 42 | 4.43 MPa (642 psi) | 4.48 MPa (650 psi) | 40 | 4.34 MPa (629 psi) | 4.37 MPa (634 psi) |
| MLE estimates | 42 | 4.52 MPa (655 psi) | 4.48 MPa (650 psi) | 40 | 4.39 MPa (636 psi) | 4.36 MPa (632 psi) |

As a result, the characteristic shear value can be estimated as 4.43 MPa (642 psi) for 171-mm (6-3/4-in.) wide and 4.34 MPa (629 psi) for 79-mm (3-1/8-in.) wide SP glulam based on the normal distribution. These values are approximately 25% lower than the characteristic value of 5.66 MPa (820 psi) derived from the small block shear values given in ASTM D2555 [2] and adjusted to the standard moisture content of 12%.

Again, the allowable shear stress can be calculated as 2.10 MPa (305 psi) for 171-mm (6-3/4-in.) wide and 2.07 MPa (300 psi) for 79-mm (3-1/8-in.) wide SP glulam using the reduction factor of 1/2.1. Due to the small difference in the allowable shear stress between the tested widths, a single value of 2.07 MPa (300 psi) was assigned to SP glulam of all widths. This value is approximately 50% higher than the allowable shear value of 1.38 MPa (200 psi) based on the characteristic shear strength of the small block shear (5.66 MPa or 820 psi) multiplied by the reduction factor of 1/4.1 (see Section 1).

7.3 Spruce-Pine-Fir glulam

As the difference in the allowable shear stress between the tested widths for both DF and SP was negligible, only one net width, 105 mm (4-1/8 in.), was tested for SPF. This width was selected based on the available resource at the glulam plant fabricating the SPF specimens. Note that the width effect on the shear strength of SPF glulam was previously reported as insignificant in another study [11].

The estimated characteristic values for SPF glulam based on normal and lognormal distribution functions are given in Table 9. As noted from Table 9, the characteristic

values for SPF, as derived from the MLE method, are all higher than the values determined from the censored data (all failure modes combined). In addition, the characteristic value determined from the all-failure-modes-combined data is higher than the value based on the shear-failure-only data. As the characteristic value based on the all-failure-modes-combined data can be regarded as a conservative estimate of the actual shear strength, it is appropriate to use such a value for deriving the characteristic shear strength even though the use of a higher value from the MLE method is justifiable.

Table 9. Parametric estimates of the characteristic shear strengths for SPF

| | 105 mm (4-1/8 in.) | | |
|----------------------------|--------------------|---------------------------|--------------------|
| | N | Characteristic value | |
| | | Normal | Lognormal |
| Shear failure only | 17 | 3.23 MPa (469 psi) | 3.26 MPa (473 psi) |
| All failure modes combined | 40 | 3.38 MPa (490 psi) | 3.40 MPa (493 psi) |
| MLE estimates | 40 | 3.61 MPa (524 psi) | 3.48 MPa (504 psi) |

Therefore, the characteristic shear value for the SPF glulam can be estimated as 3.38 MPa (490 psi) based on the normal distribution. This value is approximately 20% lower than the characteristic value of 4.10 MPa (595 psi) derived from the small block shear values given in ASTM D2555 [2] and adjusted to the standard moisture content of 12%.

Again, the allowable shear stress can be calculated as 1.62 MPa (235 psi) for SPF glulam using the reduction factor of 1/2.1. This value is approximately 60% higher than the allowable shear value of 1.00 MPa (145 psi) based on the characteristic shear strength of the small block shear (4.10 MPa or 595 psi) multiplied by the reduction factor of 1/4.1.

7.4 Allowance for checking

An important consideration when establishing the design shear stress for large dimension timber is the allowance for checking or splits which may occur in service. Although the degree of in-service checking normally observed for glulam, as compared to sawn timber, is considerably less severe, it has been a common practice for the glulam industry in the U.S. to publish reduced allowable shear stresses to account for possible in-service checking. The APA Glulam Technical Advisory Committee adopted a 10% reduction in 1997 to allow for checking based on full-size shear test results and the past industry practice.

Note that seasoning checks in glulam most commonly occur along the first glueline adjacent to an outer lamination due to the exposure of the larger surface area of the outer lamination to the environment. However, at a given cross section along the beam length, the shear stress at the first glueline is significantly lower than the shear stress at the neutral axis and varies with beam depth. Therefore, the 10% checking allowance should permit typical in-service checks (occurring at the first glueline) that are considerably deeper than 10% of the glulam width without impairing the structural integrity of the member.

In addition, checks frequently occur in the radial direction of a lamination and do not coincide with the shear surface, which typically occurs along growth rings. This is distinctly different from sawn lumber joists whose checks often occur near the neutral axis in the radial direction of the growth rings and are mostly likely to coincide with the

maximum shear plane. As such, the 10% checking allowance is likely to still be conservative even when a 10% deep check does occur at the neutral axis of a glulam beam that is controlled by shear.

7.5 Procedural calibration factors

The characteristic shear strength and allowable shear stress for glulam have been traditionally developed in the U.S. based on the provisions given in ASTM D3737 [1] using the small block shear data published in ASTM D2555 [2]. For SPF glulam, the calculated values for all sub-species in the SPF species group are in the range of 1.00 to 1.07 MPa (145 to 155 psi). As the actual sub-species for the SPF glulam tested in this study was not determined, the ratio between the minimum and maximum calculated shear stresses for this species group, 1.00/1.07, was used to adjust the characteristic and allowable shear values derived above to account for the possibility that the actual tested sub-species might have been the higher strength sub-species, such as Black spruce, Jack pine, and/or Lodgepole pine. It should be noted that the species calibration factor is equal to 1.0 for both DF and SP glulam.

According to the discussions given above, Table 10 compares the characteristic and allowable shear values derived from this study with those previously published based on the traditional small block shear values. The variation in the new and previously published values can be regarded as the difference in the procedures used to derive the design value between the full-size and small block shear tests. Then, when generalized, this information can be used as a calibration factor for adjusting the design values derived from small-clear block shear data.

Table 10. Procedural calibration factor

| | DF | | SP | | SPF | |
|----------------------------------|-----------------------|--------------------------------------|-----------------------|--------------------------------------|--------------------------------------|--|
| | $f_{v,g,k}$ | Allowable | $f_{v,g,k}$ | Allowable | $f_{v,g,k}$ | Allowable |
| Full-size shear ^(a) | 3.83 MPa (555 psi) | 1.66 MPa (240 psi) ^(b) | 4.34 MPa (629 psi) | 1.86 MPa (270 psi) ^(b) | 3.16 MPa (458 psi) ^(c) | 1.35 MPa (195 psi) ^(b,c) |
| Small block shear ^(d) | 5.50 MPa (798 psi) | 1.35 MPa (195 psi) | 5.66 MPa (820 psi) | 1.38 MPa (200 psi) | 4.10 MPa (595 psi) | 1.00 MPa (145 psi) |
| Ratio | 0.70 | 1.23 | 0.77 | 1.35 | 0.77 | 1.35 |

^(a) Based on the results obtained from this study.

^(b) Reduced by 10% to allow for checking.

^(c) Adjusted for the sub-species effect.

^(d) Based on ASTM D3737 and D2555.

It is noted that the three species tested in this study represent about 85% of total glulam production in North America today. Since it is not feasible to conduct full-size shear tests on all species used in the manufacture of glulam in the U.S., it was decided that the lowest ratio given in Table 10 could be used to determine the shear stress for those species not tested. As a result, the characteristic shear strength and allowable shear stress for the species other than DF, SP, and SPF can be established by multiplying the small block shear value by the procedural calibration factor of 0.70 and 1.25, respectively. The allowable shear stress derived using this procedural calibration factor includes a 10% allowance for checking.

7.6 Limitations on use of results

It is very important to realize that these new allowable shear values obtained from this study are intended to be limited to prismatic glulam members subjected to typical dead, live, snow, wind, and earthquake loads only. The allowable shear stresses for impact or cyclic loading, such as may occur in bridges or crane rail applications, have not been evaluated. Neither have the effects of these higher shear stresses been accounted for in the design of non-prismatic members which are typically subjected to an interaction of shear stresses with other stresses. For these applications, the previously published shear values, which have been proven adequate through years of experience, should be retained for design use.

8. Conclusions

The following conclusions are based on the results obtained from this study:

- The setup used in this study can be used to evaluate the shear strength of full-size glulam. ASTM D3737 adopted this test method in October 2000 as an alternative standard test method for determining the horizontal shear strength of glulam. Since then, this test method has been used by other researchers in the United States for evaluating glulam shear strength of ponderosa pine with equally satisfactory results [20].
- The width effect on the characteristic shear strength was determined to be negligible for DF and SP glulam members and assumed to be negligible for all other species.
- The characteristic shear strength and allowable shear stress for the species other than DF, SP, and SPF can be established by multiplying the small block shear value by the procedural calibration factor of 0.70 and 1.25, respectively. The allowable shear stress derived using this procedural calibration factor includes a 10% allowance for checking.
- Results obtained from this study have been accepted by the major building code agencies in the U.S. and the new allowable shear values are being used by the wood engineering community.

9. References

1. ASTM, *Standard practice for establishing stresses for structural glued laminated timber (glulam)*, ASTM D3737-99, Philadelphia, PA, 2000.
2. ASTM, *Standard test methods for establishing clear wood strength values*, ASTM D2555-98, Philadelphia, PA, 2000.
3. Rammer D.R. and L.A. Soltis, *Experimental shear strength of glued laminated beams*, Research Report FPL-RP-527, Forest Products Lab., Madison, WI, 1994.
4. ICBO Evaluation Service, Inc., Report No. 5100, Whittier, CA, 1995.
5. SBCCI Public Safety Testing and Evaluation Services, Inc., Report No. 9625, Birmingham, AL, 1996.
6. APA - The Engineered Wood Association, *Glued laminated timber design tables*, Tacoma, WA, 2001.

7. American National Standards Institute, *American National Standard for Wood Products - Structural Glued Laminated Timber*, ANSI A190.1, New York, NY, 1992.
8. National Evaluation Service, Inc., *EWS glued laminated timber combinations and "GAP" computer program for determining design stresses*, Report No. NER-486, 2000.
9. Keenan, F.J. and K.A. Selby, *The shear strength of Douglas-fir glued laminated timber beams*, University of Toronto, Toronto, ON, 1973.
10. Freas, A.D. and M.L. Selbo, *Fabrication and design of glued laminated wood structural members*, Technical Bulletin No. 1069, Forest Products Lab., USDA, Madison, WI, 1954.
11. Keenan, F.J. and B. Kyokong, *Shear strength of spruce glued-laminated timber beams*, Canadian Journal of Civil Engineering, 12: 661-672, 1985.
12. ASTM, *Standard test methods of static tests of lumber in structural sizes*, ASTM D198-99, Philadelphia, PA, 2000.
13. American Forest & Paper Association, *National Design Specification for Wood Construction*, Washington, D.C, 1997.
14. ASTM, *Standard practice for evaluating allowable properties for grades of structural lumber*, ASTM D2915-98, Philadelphia, PA, 2000.
15. ASTM, *Standard test methods for direct moisture content measurement of wood and wood-base materials*, ASTM D4442-92, Philadelphia, PA, 2000.
16. ASTM, *Standard test methods for specific gravity of wood and wood-base materials*, ASTM D2395-93, Philadelphia, PA, 2000.
17. Lawless, J.F., *Statistical models and methods for lifetime data*, John Wiley and Sons, New York, NY, 1982.
18. American Institute of Timber Construction, *Lumber grading for glued laminated timber*, Inspection Bureau Memorandum 3, Englewood, CO, 1984.
19. ASTM, *Standard practice for dealing with outlying observations*, ASTM E178-94, Philadelphia, PA, 2000.
20. Hernandez, R. Personnel communications, USDA Forest Products Laboratory, Madison, WI.

INTERNATIONAL COUNCIL FOR RESEARCH AND INNOVATION
IN BUILDING AND CONSTRUCTION

WORKING COMMISSION W18 - TIMBER STRUCTURES

DESIGN MODEL FOR FRP REINFORCED GLULAM BEAMS

M Romani

H J Blaß

Lehrstuhl für Ingenieurholzbau und Baukonstruktionen

University of Karlsruhe (TH)

GERMANY

Presented by: M Romani

- V Enjily asked about the manufacturing issues.
- M Romani answered that it would be similar to normal glulam manufacturing and no problem for the manufacturer.
- A Jorissen asked about the improvement of stiffness.
- M Romani answered that the stiffness improvements (15%) were less than strength improvements (34%). It would be similar to normal glulam manufacturing and no problem for the manufacturer.
- B Yeh commented that there have been much activities in the US in this area.
- H J Blass commented that they were aware of the US groups but information exchange was only in one direction.
- B Yeh asked about volume effect.
- H J Blass answered that it was not considered in this study.
- I Smith commented that one of the US patents dealt with the process of "hairing-up". In this study and in the University of Maine study, it seemed that this was not required.
- F Lam asked whether pre-pregnated fibre glass could be considered.
- M Romani answered no but thicker glass may be needed.
- G Schickhofer asked whether shear failure would become an issue.
- M Romani answered no shear failures were observed.

Design model for FRP reinforced glulam beams

M. Romani and H.J. Blaß
University of Karlsruhe (TH), Germany

1 Abstract

For several years possibilities to reinforce glulam beams parallel to the grain to increase bending and axial stiffness and ultimate load have been investigated. One method is to use Fibre-Reinforced Plastics (FRP) as a tensile reinforcement. Fibres used were glass fibres, aramid fibres and carbon fibres.

At the University of Karlsruhe a research project was carried out where the load-deformation behaviour of reinforced glulam beams was studied. Thin carbon FRP and aramid FRP were used as reinforcements. Within this research project a design model was developed taking into account the plastic behaviour of timber loaded in compression parallel to the grain. This paper presents the design model and test results of beams loaded to failure to verify the design model.

2 Introduction

Glulam beams loaded by bending moments fail at the tension side at the position of knots or finger joints. Due to this failure mode glulam beams are mainly reinforced at the tension side to strengthen the weak cross-sections.

The reinforcement for glulam beams should have a high modulus of elasticity (MOE) and a large tensile strain at failure. Materials considered in the past were steel, glass fibre reinforced plastic (GFRP) and since a few years carbon fibre reinforced plastic (CFRP) and aramid fibre reinforced plastic (AFRP). Fibre reinforced plastic (FRP) has the advantage of a high MOE – although generally lower than steel – and a high tensile strength. The disadvantage of steel is the low yield strength leading to plastic deformations before the timber fails. FRP reinforcements do not show this behaviour.

An effective reinforcement leads to a plastic behaviour on the timber compression side. In unreinforced glulam beams this effect hardly occurs and design models therefore do not take into account this effect. For FRP reinforced beams therefore different design models are necessary.

3 Structure and failure modes of reinforced glulam beams

Figure 1 shows the types of cross section studied. 30 beams of type 1 and 8 beams of type 2 were loaded to failure. In practice, for reasons of fire safety or for esthetical reasons a facing consisting of a load carrying timber lamination is applied below the reinforcement (type 1). Nevertheless 8 beams without a timber facing were tested to study the influence of the timber facing on the load deformation behaviour. The width of the reinforcement always equals the width of the cross section.

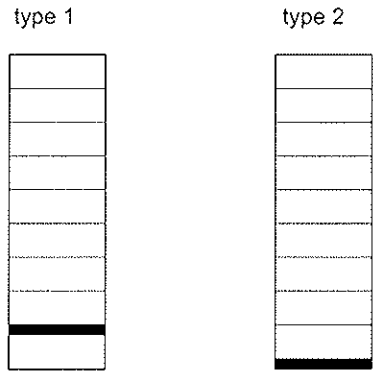


Figure 1: Cross section of the test specimens

For reinforced glulam beams different failure modes are possible. Assuming constant MOE, constant tensile and compressive strength and a linear-elastic-ideal-plastic stress-strain relationship within a cross section the following failure modes are considered.

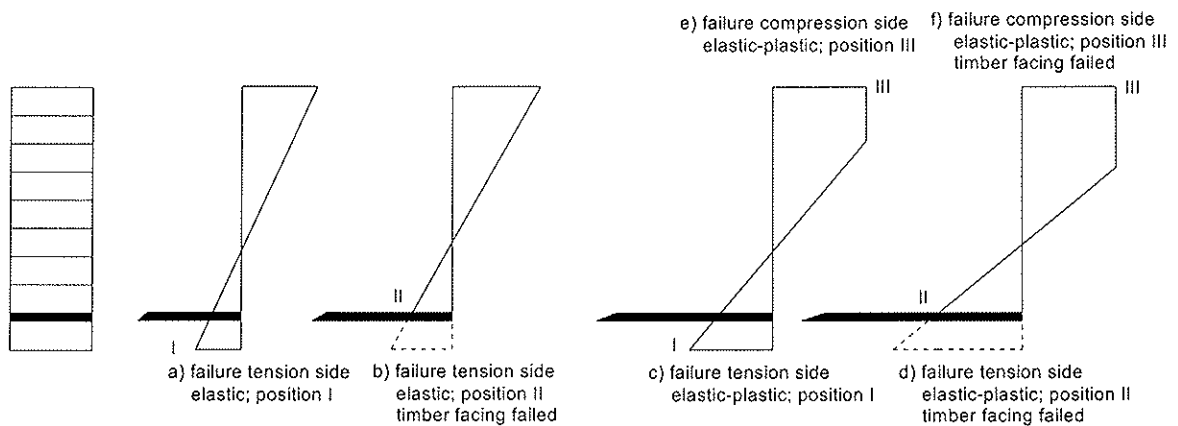


Figure 2: Failure modes

Global failure modes at the tension side:

- Mode a: Failure of the timber facing while the cross section is in a linear-elastic state
- Mode b: Failure above the reinforcement while the cross section is in a linear-elastic state
- Mode c: Failure of the timber facing while the cross section is in a linear-elastic-ideal-plastic state
- Mode d: Failure above the reinforcement while the cross section is in a linear-elastic - ideal-plastic state

Failure at the compression side by a defined ultimate compression strain:

- Mode e: Compressive failure before the timber facing fails in tension
- Mode f: Compressive failure after the timber facing failed in tension with subsequent tensile failure above the reinforcement

Using a tensile reinforcement the compressive stress will exceed the timber tensile stress in beams loaded in bending. Therefore plastic deformations are more probable in beams with tensile reinforcement. Using both, compressive and tensile reinforcement the linear modes will mostly occur due to the reduction of the plastic area in the compressive zone.

4 Design model

Figure 3 illustrates the notation and the assumed stress-strain relation. The design model reduces the calculation to unreinforced glulam beams by using absolute geometrical factors α_i and general factors k_i . These factors allow to calculate geometrically similar cross sections by calculating just once these factors α_i and k_i .

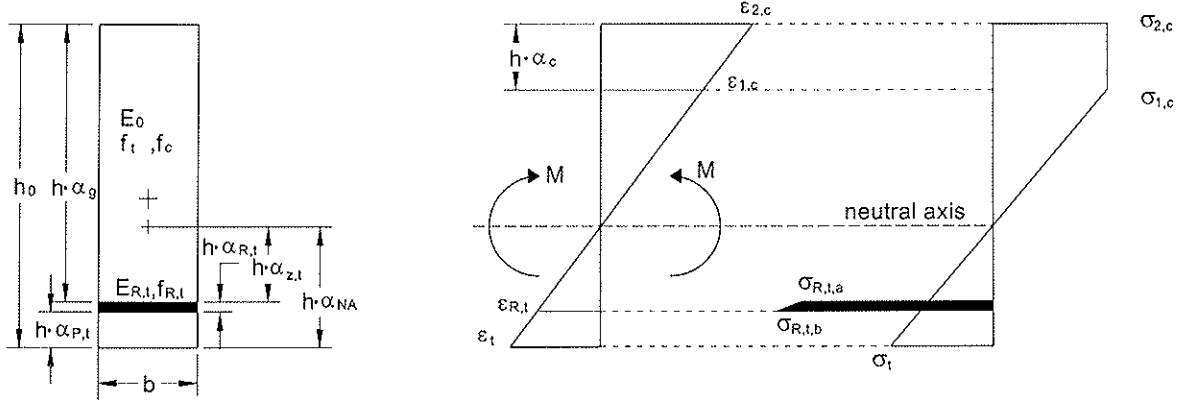


Figure 3: Notation and stress-strain relationship of a type 1 cross section with plastic compression area

Dimensionless factors α_i :

$$\alpha_i = \frac{h_i}{h} \quad (1)$$

Ratio of the timber compressive to tensile strength:

$$k_f = \frac{f_c}{f_t} = \frac{\epsilon_{c,u}}{\epsilon_{t,u}} \quad (2)$$

Abbreviation:

$$k_t = \frac{E_{R,t}}{E_0} - 1 \quad (3)$$

The effective height h is the remaining height of the cross section. With intact timber facing h is equal to h_0 . After failure of the timber facing the effective height h is reduced by the height of the timber facing.

4.1 Calculation of the load carrying capacity

Because of the non-linear stress distribution, an ultimate moment instead of an ultimate stress is used to express the load carrying capacity. This ultimate moment depends on the failure mode (see figure 2). Failure at the tension side is assumed when the outermost timber fibre of the effective cross section has reached the ultimate strength f_t or the ultimate strain $\epsilon_{t,u}$, respectively. The strain at the compression side is limited to the ultimate compression strain $\epsilon_{c,u}$. Below the strain $\epsilon_{1,c}$ the timber behaves linear-elastic (see Figure 3).

The equilibrium of the resulting forces in the cross-section yields the position of the neutral axis $h \cdot \alpha_{NA}$. After failure of the timber facing the neutral plane changes. The absolute parameters α_i then relate to the reduced height $h = h_0 - h_{p,t}$. Separate equations for cross-sections with or without timber facing are used, because of the different position of the outermost timber fibre below or directly above the reinforcement.

The ultimate moment of a reinforced glulam beam is calculated as:

$$M_u = f_t \cdot W \cdot k_{M,Mode} \quad (4)$$

where: $k_{M,Mode}$ is a failure mode based factor (see figure 2)

$$W = \frac{b \cdot h^2}{6}$$

h: effective height of the beam
f_t: bending strength

The design model is an extension of a design model for tensile bending failure of cross sections without timber facing presented by Ehlbeck and Colling (1987).

4.1.1 Tensile failure

Bending tensile failure is equivalent to reaching the ultimate tensile strain $\varepsilon_{t,u} = \varepsilon_t$ at position I or position II, respectively. According to the observations during the tests failure at position II occurs after failure and subsequent separation of the timber facing (then $h = h_0 - h_{p,t}$) along the beam length.

Mode a ($h = h_0$; $\sigma_{1,t} = f_t$; $\sigma_{1,c} \leq f_c$):

$$\alpha_{NA} = \frac{1}{2} \cdot \frac{1 + \alpha_{R,t} \cdot k_t \cdot (2 \cdot \alpha_{P,t} + \alpha_{R,t})}{1 + \alpha_{R,t} \cdot k_t} \quad (5)$$

$$k_{M,a} = \frac{2}{\alpha_{NA}} \cdot \left[(1 - \alpha_{NA})^3 + \alpha_{NA}^3 - k_t \cdot (\alpha_{z,t}^3 - (\alpha_{z,t} + \alpha_{R,t})^3) \right] \quad (6)$$

Mode b ($h = h_0 - h_{p,t}$; $\sigma_t = f_t$; $\sigma_{1,c} \leq f_c$):

$$\alpha_{NA} = \frac{1}{2} \cdot \frac{1 + \alpha_{R,t} \cdot k_t \cdot \alpha_{R,t}}{1 + \alpha_{R,t} \cdot k_t} \quad (7)$$

$$k_{M,b} = \frac{2}{\alpha_{z,t}} \cdot \left[(1 - \alpha_{NA})^3 + (1 + k_t) \cdot \alpha_{NA}^3 - k_t \cdot \alpha_{z,t}^3 \right] \quad (8)$$

Mode c ($h = h_0$; $\sigma_t = f_t$; $\alpha_c \geq 0$):

$$\alpha_{NA} = \frac{1}{(1 + k_f)^2} \cdot \left[k_f - \alpha_{R,t} \cdot k_t + \sqrt{(\alpha_{R,t} \cdot k_t - k_f)^2 + \alpha_{R,t} \cdot k_t \cdot (1 + k_f)^2 \cdot (\alpha_{R,t} + 2 \cdot \alpha_{P,t})} \right] \quad (9)$$

$$\alpha_c = 1 - \alpha_{NA} \cdot (1 + k_f) \quad (10)$$

$$k_{M,c} = 2 \cdot k_f \cdot \left[3 \cdot \alpha_c \cdot \left(1 - \alpha_{NA} - \frac{\alpha_c}{2} \right) + (1 - \alpha_{NA} - \alpha_c)^2 \right] - 2 \cdot \frac{k_t}{\alpha_{NA}} \cdot (\alpha_{z,t}^3 - (\alpha_{z,t} + \alpha_{R,t})^3) + 2 \cdot \alpha_{NA}^2 \quad (11)$$

Mode d ($h = h_0 - h_{p,t}$; $\sigma_t = f_t$; $\alpha_c \geq 0$):

$$\alpha_{NA} = \frac{1}{(1 + k_f)^2} \cdot \left[k_f + \alpha_{R,t} \cdot (k_f \cdot (1 + k_f) - k_t) + \sqrt{(\alpha_{R,t} \cdot k_t - k_f)^2 + \alpha_{R,t}^2 \cdot k_t \cdot (1 - k_f^2)} - 2 \cdot \alpha_{R,t} \cdot k_f \cdot (1 + k_f) \right] \quad (12)$$

$$\alpha_c = 1 + k_f \cdot \alpha_{R,t} - \alpha_{NA} \cdot (1 + k_f) \quad (13)$$

$$k_{M,d} = 2 \cdot \left[k_f \cdot \left(3 \cdot \alpha_c \cdot \left(1 - \alpha_{NA} - \frac{\alpha_c}{2} \right) + (1 - \alpha_{NA} - \alpha_c)^2 \right) - k_t \cdot \alpha_{z,t}^2 + \frac{\alpha_{NA}^3}{\alpha_{z,t}} \cdot (1 + k_t) \right] \quad (14)$$

Considering a plastic behaviour of a not reinforced cross-section in the compression zone, the factor $k_{M,0}$ according to Ehlbeck and Colling (1987) may be used to calculate the necessary height of a not reinforced beam with the same ultimate moment. The factor $k_{M,0}$ is based on the assumption of a failure at the tension side.

$$h_{M,unrein} = h \cdot \sqrt{\frac{k_{M,Mode}}{k_{M,0}}} \quad (15)$$

where

$$k_{M,0} = \begin{cases} k_f \cdot \frac{3 - k_f}{1 + k_f} & k_f \leq 1 \\ 1 & k_f > 1 \end{cases} \quad (16)$$

The factor $k_{M,0}$ takes into account that plastic strains are also possible in a not reinforced timber cross section. Inserting $k_{M,0}$ into equation (4) yields the ultimate moment of an unreinforced cross section considering plastic behaviour in the compression zone.

In general, the effect of a plastic compression zone in unreinforced glulam beams is neglected. For a comparison between reinforced and not reinforced glulam beams, however, the same assumptions for the behaviour in the compression zone are made.

For a tensile failure first the timber facing fails (mode a, mode c). When a load increase is possible the global tensile failure starts above the reinforcement (mode b, mode d). Figure 4 shows the tensile failure history.

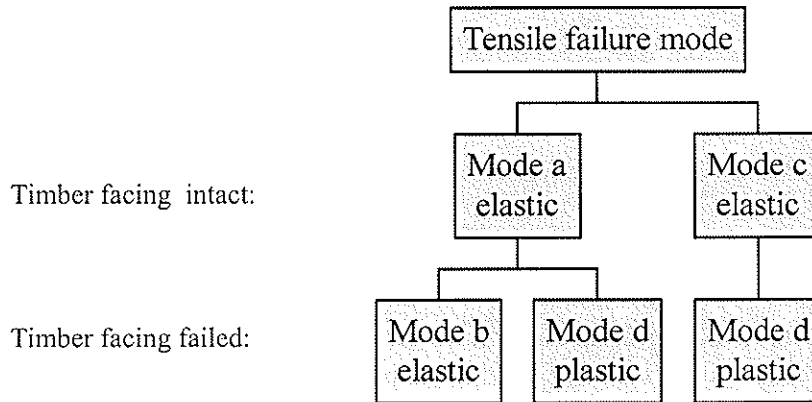


Figure 4: Tensile failure history

The highest ultimate moment depends on the possibility of a load increase after failure of the timber facing.

4.1.2 Compressive failure

The compressive failure depends on the ultimate strain $\varepsilon_{c,u} = \varepsilon_{2,c}$ at the outermost fibre of the compression zone. A condition for a compressive failure is that no tensile failure occurs, i.e. $\varepsilon_{t,l} \leq \varepsilon_{t,u}$.

$$\psi = \frac{\varepsilon_{2,c}}{\varepsilon_{1,c}} \quad (17)$$

Mode e ($h = h_0$; $\alpha_c \geq 0$, $\varepsilon_{t,u} \geq \varepsilon_t$):

$$\alpha_{NA} = \frac{1}{(\psi - 1)^2} \cdot \left[1 - 2 \cdot \psi - \psi^2 \cdot \alpha_{R,t} \cdot k_t + \psi \cdot \sqrt{2 \cdot \psi + \psi^2 \cdot \alpha_{R,t}^2 \cdot k_t \cdot (k_t + 1)} \right. \\ \left. + 2 \cdot \alpha_{P,t} \cdot (\psi - 1)^2 \cdot \alpha_{R,t} \cdot k_t - 1 + \alpha_{R,t} \cdot k_t \cdot (2 - \alpha_{R,t}) \cdot (2 \cdot \psi - 1) \right] \quad (18)$$

$$\alpha_c = \frac{(1 - \alpha_{NA}) \cdot (\psi - 1)}{\psi} \quad (19)$$

$$k_{M,e} = \frac{2 \cdot k_f}{1 - \alpha_c - \alpha_{NA}} \cdot \left[3 \cdot \alpha_c \cdot \left(1 - \frac{1}{2} \cdot \alpha_c - \alpha_{NA} \right) \cdot (1 - \alpha_c - \alpha_{NA}) + (1 - \alpha_c - \alpha_{NA})^3 \right. \\ \left. + \alpha_{NA}^3 + k_t \cdot (\alpha_{NA} - \alpha_{P,t})^3 - k_t \cdot \alpha_{z,t}^3 \right] \quad (20)$$

$$\varepsilon_{t,u} \geq \varepsilon_{2,c} \cdot \frac{\alpha_{NA}}{1 - \alpha_{NA}} \quad \text{with } \varepsilon_{t,u} = \frac{f_t}{E_0} \quad (21)$$

Mode f ($h = h_0 - h_{P,t}$; $\alpha_c \geq 0$, $\varepsilon_{t,u} \geq \varepsilon_t$):

By setting $\alpha_{P,t}$ equal to zero and inserting the adjusted α_i in the equations for mode e, the equations for mode f result. This is possible because the modes e and f are independent of the tension stress since no tensile failure occurs. This is checked using equation (22).

$$\varepsilon_{t,u} \geq \varepsilon_{2,c} \cdot \frac{\alpha_{NA} - \alpha_{R,t}}{1 - \alpha_{NA}} \quad \text{with } \varepsilon_{t,u} = \frac{f_t}{E_0} \quad (22)$$

Compression failure is defined as reaching of the ultimate compression strain at the outermost compression fibre at position III. The ultimate compression strain is a defined value. This value is higher than the strain at which a timber fibre begins to behave plastically.

Figure 5 shows the compression failure history.

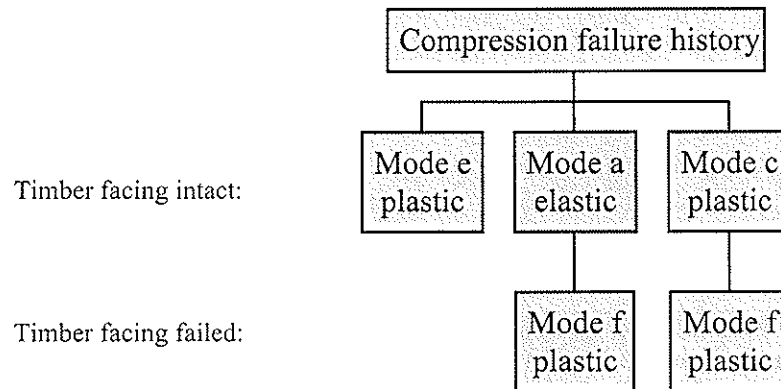


Figure 5: Compression failure history

4.2 Calculation of the bending stiffness

The stiffness is calculated according to the theory of composite cross sections in the linear-elastic state (according to the position of the neutral axis for modes a and b). Plastic deformations are not considered, since the stiffness is used for serviceability limit states. Stiffness in the linear-elastic state:

$$ef(EI) = \sum n_i \cdot I_i + n_i \cdot A_i \cdot z_i^2 = k_{EI} \cdot E_{0,g} \cdot I \quad (23)$$

$$k_{EI} = \alpha_g^3 + n_t \cdot \alpha_{R,t}^3 + \alpha_{P,t}^3 + 12 \cdot \alpha_g \cdot \left(\frac{1}{2} + \frac{\alpha_{R,t} + \alpha_{P,t}}{2} - \alpha_{NA} \right)^2 + 12 \cdot n_t \cdot \alpha_{R,t} \cdot \left(\alpha_{z,t} + \frac{\alpha_{R,t}}{2} \right)^2 + 12 \cdot \alpha_{P,t} \cdot \left(\alpha_{NA} - \frac{\alpha_{P,t}}{2} \right)^2 \quad (24)$$

with $I = \frac{b \cdot h^3}{12}$

α_{NA} : according to mode a or mode b (with $\alpha_{P,t} = 0$)

The factor k_{EI} indicates the stiffness increase of reinforced beams. For not reinforced beams the following height of the cross section is necessary to reach the same bending stiffness:

$$h_{EI,u} = h \cdot \sqrt[3]{k_{EI}} \quad (25)$$

5 Experimental study

30 reinforced glulam beams of type 1 and 8 beams of type 2 were tested to failure. Table 1 summarises the FRP properties, table 2 the adhesives being used and table 3 the test program.

Table 1: FRP

| Shortcut. | Type of FRP | Tensile MOE ¹⁾ mean value [N/mm ²] | Tensile strength ¹⁾ mean value [N/mm ²] | Thickness $h_{R,t}$ [mm] | Width b [mm] |
|-----------|-------------|---|--|--------------------------------|--------------------|
| L1 | CFRP | 173.000 | 3.050 | 1,2 | 100 |
| L2 | CFRP | 304.000 | 1.680 | 1,4 | 50 |
| L3 | AFRP | 74.000 | 995 | 1,8 | 132 |
| L4 | CFRP | 199.000 | 2.570 | 1,4 | 100 |

¹⁾ from tension specimen of 50 mm width, average of 5 specimens

Table 2: Adhesives

| Shortcut | Name of product | Manufacturer / distribution |
|----------|--------------------------|-----------------------------|
| K1 | Sikadur-30 | Sika Chemie GmbH |
| K2 | Ispo Concretin SK 41 | ispo GmbH |
| K3 | Collano Purbond HB 110 | Ebnöther AG |
| K4 | Dynosol S-199 with H-629 | Dyno Industries A.S. |

For the test specimens it was decided to use timber with a low MOE and a low density in order to maximise the reinforcement effect. The MOE and the density of every single board

was determined before the glulam production. The boards with the smallest MOE and density values were arranged in the outer areas of the cross-section. The mean dynamic MOE of the boards was 9800 N/mm² for MS 10 (according to German Standard DIN 4074) boards which correspond to strength class C24 according to EN 338.

The tests were performed as four point bending tests with a span of 4,20 m and a distance of 1,35 m from the support to the loading point. The thickness of the timber facing was 34 mm (Tr-5;Tr-6) and 35 mm (Tr-1 to Tr-4).

Table 3: Test programme for bending tests

| Test series | Number of specimens | Grade of laminations | Grade of timber facing | Mean height/width h_0/b [mm] | FRP (number of layers) | Adhesive | Finger joint |
|-------------|---------------------|----------------------|------------------------|--------------------------------|------------------------|----------|--------------|
| Tr-1 | 5 | MS7 / MS10 | MS7 / MS10 | 308/100 | L1 (1) | K2 | no |
| Tr-2 | 5 | MS7 / MS10 | MS7 / MS10 | 312/100 | L4 (2) | K2 | no |
| Tr-3 | 5 | MS10 | MS10 | 308/100 | L1 (1) | K2 | yes |
| Tr-4 | 5 | MS10 | MS10 | 312/100 | L4 (2) | K2 | yes |
| Tr-5 | 5 | MS10 / MS17 | MS17 | 312/100 | L3 (4) | K3 | yes |
| Tr-6 | 5 | MS10 / MS17 | MS10 | 312/100 | L3 (4) | K3 | yes |
| Tr-7 | 5 | MS10 | - | 308/100 | L1 (1) | K3 | yes |
| Tr-8 | 3 | MS10 | - | 310/100 | L4 (2) | K3 | yes |

The specimens of the test series Tr-1 to Tr-6 first failed due to tensile/bending failure of the timber facing. After the first failure, the load generally could be increased. The timber facing of test specimens with CFRP (FRP L1 and L4) delaminated after failure. The timber facing of test specimens with AFRP (FRP L3) partly failed at two locations and delaminated less than with CFRP. Table 4 shows the test results.

Table 4: Test results

| Test series | Tr-1 | Tr-2 | Tr-3 | Tr-4 | Tr-5 | Tr-6 | Tr-7 | Tr-8 |
|---|----------------|----------------|----------------|-------------------------|----------------|-------------------------|----------------|----------------|
| F_{max} [kN] | 44,1 | 57,7 | 43,0 | 58,1 | 60,5 | 59,1 | 49,8 | 66,5 |
| $M_{u,mean}$ [kNm] | 59,5 | 77,9 | 58,1 | 78,4 | 81,7 | 79,8 | 67,2 | 89,8 |
| $f_m = M_{u,mean}/W$ [N/mm ²] | 37,6 | 48,0 | 36,7 | 48,3 | 50,4 | 49,2 | 42,5 | 56,1 |
| COV [%] | 12,5 | 4,7 | 13,0 | 5,9 | 6,8 | 3,5 | 5,0 | 6,9 |
| Deflection [mm] | 70,2 | 86,6 | 64,0 | 97,5 | 88,6 | 83,2 | 61,7 | 74,8 |
| COV [%] | 16,1 | 6,5 | 33,4 | 5,8 | 12,1 | 6,6 | 4,8 | 12,3 |
| Failure at (number) | K (5) | K (5) | K (3) F (2) | K (1) F (3) T (1) | F (3) A (2) | K (1) F (2) A (2) | K (2) F (3) | K (2) F (1) |
| Failure mode (number) | c (1) d (4) | d (4) f (1) | c (3) d (2) | d (5) | c (3) d (2) | d (4) f (1) | d (5) | d (3) |
| efMOE [N/mm ²] | 10.400 | 11.400 | 10.300 | 11.500 | 12.700 | 12.200 | 11.100 | 13.100 |
| COV [%] | 5,9 | 4,2 | 1,7 | 5,0 | 4,5 | 2,3 | 3,6 | 0,9 |

K: knot
F: finger joint

T: timber
A: abort of test

In Figure 6 the load-deflection curve of test specimen Tr-3.4 is presented with a first failure at the timber facing, a consequent global failure starting above the reinforcement after 30 % load increase.

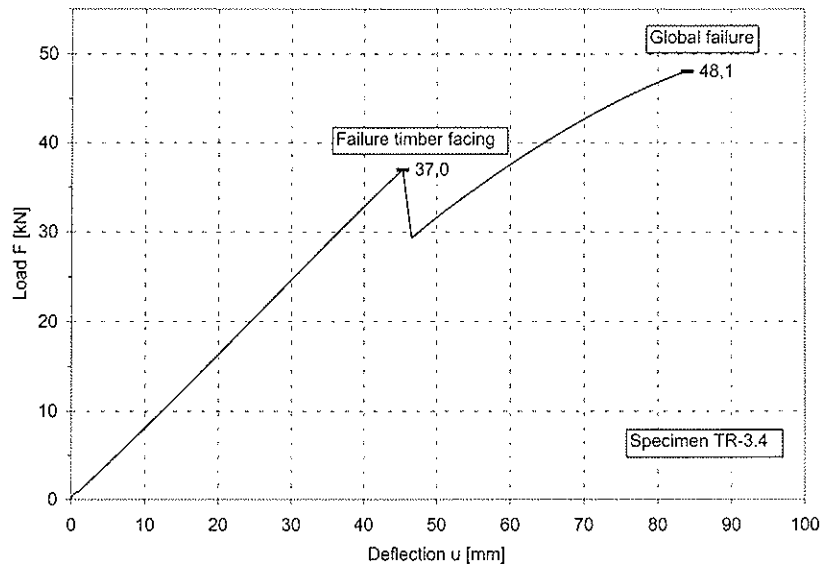


Figure 6: Load deflection curve of test specimen Tr-3.4

6 Comparison of the Design model with the test results

The calculation model allows to design reinforced beams according to Eurocode 5. As input values for the glulam strength and MOE the values according to glulam BS 11 of the German National Application Document for Eurocode 5 are applied. This strength class is very similar to GL 24. For the modes e and f $\epsilon_{2,c}$ was set to 1,3 times $\epsilon_{1,c}$.

Table 5: Material properties for the calculation model

| | f_t [N/mm ²] | f_c [N/mm ²] | k_f [-] | MOE [N/mm ²] |
|---------------------|-------------------------------|-------------------------------|--------------|-----------------------------|
| Glulam BS11/GL24 | 24,0 (= $f_{m,g,k}$) | 24,0 (= $f_{c,0,g,k}$) | 1,00 | 11.500 |
| CFRP L1 | 3.050 | - | - | 173.000 |
| AFRP L3 | 995 | - | - | 74.000 |
| CFRP L4 | 2.570 | - | - | 199.000 |

Because of $f_t = f_c$ only modes c, d, e and f are possible.

The design model relates to a beam cross-section. Because of the not complete delamination of the timber facing for different adhesive-FRP combinations, the assumption of a complete delamination over the length of the beam is conservative.

The comparison shows a mean ratio of about 1,49 between the load-carrying capacity in the test and the governing calculated characteristic load-carrying capacity. The characteristic value of that ratio based on the single test results is 1,24, the minimum value from 38 tests is 1,18. Taking into account the unfavourable lamination properties, the calculation model yields conservative values of the beam bending capacity.

Table 6: Ultimate Moment capacity according to the calculation model

| Mode | | Tr-1 | Tr-2 | Tr-3 | Tr-4 | Tr-5 ¹⁾ | Tr-6 ¹⁾ | Tr-7 | Tr-8 |
|------|--|-------|-------|-------|-------|--------------------|--------------------|-------|-------|
| c | $M_{u,c}$ [kNm] | 43,0 | 51,9 | 43,0 | 51,9 | 49,9 | 49,9 | NP | NP |
| | α_c [-] | 0,042 | 0,109 | 0,040 | 0,108 | 0,091 | 0,091 | | |
| | $M_{u,mean}/M_{u,c}$ [-] | 1,38 | 1,50 | 1,35 | 1,51 | 1,64 | 1,60 | | |
| d | $M_{u,d}$ [kNm] | 37,4 | 50,1 | 37,2 | 49,8 | 48,4 | 48,4 | 46,3 | 60,1 |
| | α_c [-] | 0,066 | 0,176 | 0,064 | 0,177 | 0,173 | 0,173 | 0,059 | 0,158 |
| | $M_{u,mean}/M_{u,d}$ [-] | 1,59 | 1,55 | 1,56 | 1,57 | 1,69 | 1,65 | 1,45 | 1,49 |
| e | $M_{u,e}$ [kNm] | 49,2 | 53,6 | 53,0 | 53,5 | 52,6 | 52,6 | NP | NP |
| | α_c [-] | 0,122 | 0,128 | 0,121 | 0,128 | 0,127 | 0,127 | | |
| | $\sigma_{t,required}$ [N/mm ²] | 28,0 | 24,9 | 28,1 | 24,9 | 25,6 | 25,6 | | |
| f | $M_{u,f}$ [kNm] | 51,9 | 59,6 | 55,8 | 59,6 | 57,9 | 57,9 | 51,4 | 58,9 |
| | α_c [-] | 0,124 | 0,133 | 0,123 | 0,133 | 0,131 | 0,131 | 0,123 | 0,133 |
| | $\sigma_{t,required}$ [N/mm ²] | 27,0 | 22,8 | 27,1 | 22,8 | 23,7 | 23,7 | 27,3 | 22,8 |

NP: Mode not possible

¹⁾ The MS 17 timber lamella was not considered.

A comparison of the failure modes c and d shows higher values for the mode c failure. The ultimate moment of mode c is the proper value according to the failure history. A load increase after failure of the timber facing seems not possible. This is in contradiction with the observed failure behaviour of the test specimens. A reason for this is that the design model for mode d just takes into account the geometrical change as a result of the failure of the timber facing into and assumes a beginning failure directly above the reinforcement at position II. In reality there are crack effects at knots or finger joints above the reinforcement before a global failure occurs. The "real position II" is at the beginning of the global failure above the assumed position II. Further investigations for this unknown "real position II" are necessary.

In Table 7 a fictitious MOE as a parameter for the bending stiffness of the test series and the calculated MOE values are summarised. For every board used in the glulam beams the dynamic, lengthwise MOE was measured before glulam production. The calculated MOE of the beams were determined using the MOE of every single board with the theory of composite cross section for the elastic state. In row 1 the measured values of the test specimens, in rows 2 and 3 the calculated values of the reinforced and unreinforced beams are presented.

Table 7: Calculated MOE versus MOE of the test series

| | | Tr-1 | Tr-2 | Tr-3 | Tr-4 | Tr-5 | Tr-6 | Tr-7 | Tr-8 |
|---|---|--------|--------|--------|--------|--------|--------|--------|--------|
| 1 | $MOE_{rein.,test}$ [N/mm ²] | 10.400 | 11.400 | 10.300 | 11.500 | 12.700 | 12.200 | 11.100 | 13.100 |
| 2 | $MOE_{rein.,calc}$ [N/mm ²] | 10.100 | 11.100 | 10.300 | 12.000 | 13.500 | 12.900 | 11.100 | 13.700 |
| 3 | $MOE_{unrein.,calc}$ [N/mm ²] | 9.100 | 8.700 | 9.200 | 9.300 | 11.500 | 10.800 | 9.400 | 9.300 |
| 4 | 1 / 2 [-] | 1,03 | 1,03 | 1,00 | 0,96 | 0,94 | 0,95 | 1,00 | 0,96 |
| 5 | 1 / 3 [-] | 1,14 | 1,31 | 1,12 | 1,24 | 1,10 | 1,13 | 1,18 | 1,41 |

The calculated values of the fictitious MOE with the composite theory assuming a stiff connection between the reinforcement and the glulam show a good agreement with the test results.

7 Summary

For the calculation of the load-carrying capacity and stiffness of tensile reinforced glulam beams a model is derived taking into account the plastic behaviour of glulam loaded in compression parallel to the grain. The model is based on an analytic solution and allows a simple calculation without any iteration steps based on design values of non-reinforced glulam. Different failure modes of FRP reinforced glulam beams are considered. Test results with reinforced beams loaded to failure show that the proposed model leads to conservative values of the load-carrying capacity. This is especially true considering the low quality of the timber used in the tests.

The test specimens mainly failed at the tension side. With a different cross-section set-up reinforced beams are possible failing in a more ductile way on the compression side. The test specimens mostly showed a significant load increase after failure of the timber facing. This was mainly caused by an effective reinforcement even after a bending failure above the FRP layer. Further research will quantify this effect and permit a more economic use of FRP reinforced glulam.

References

Blaß HJ and Romani M (2000) Trag- und Verformungsverhalten von Verbundträgern aus Brettschichtholz und faserverstärkten Kunststoffen. Forschungsbericht der Versuchsanstalt für Stahl, Holz und Steine, Abt. Ingenieurholzbau der Universität Karlsruhe

Ehlbeck J and Colling F (1987) Tragfähigkeit von Glasfaser-Verbund-Profilen verstärkten Brettschichtholzträgern. Forschungsbericht der Versuchsanstalt für Stahl, Holz und Steine, Abt. Ingenieurholzbau der Universität Karlsruhe

**INTERNATIONAL COUNCIL FOR RESEARCH AND INNOVATION
IN BUILDING AND CONSTRUCTION**

WORKING COMMISSION W18 - TIMBER STRUCTURES

MOISTURE INDUCED STRESSES IN GLULAM CROSS SECTIONS

J Jönsson
Dept. of Structural Engineering
Lund University

SWEDEN

Presented by: J Jönsson

- A Jorissen commented about the MOE difference between the outside and inside of the specimen.
- J Jönsson clarified that it was the annual ring direction effect.

Moisture induced stresses in glulam cross sections

Johan Jönsson
Dept. of Structural Engineering
Lund University, Lund, Sweden

Abstract

Preliminary results from an experimental investigation to determine the internal stress state perpendicular to grain in glulam were presented at the CIB meeting in Delft, see Jönsson and Svensson, (2000). Further results from this research are presented in this paper together with improvements of the experimental methodology. The modifications concern digital camera equipment for strain measurements with better optics, fixtures for holding the camera, the method of releasing the deformation and the technique to moisture seal specimens. Altogether the changes in methodology has made the testing more rational and increased the reliability of the measurements. However, repetition of tests made before these improvements have confirmed the results presented in the previous paper.

Three categories of tests are presented where strain and stress distribution in the cross grain direction are determined. The different categories are specimens seasoned in constant humidity, specimens exposed to an artificial single climate change and specimens exposed to natural climate outdoors under shelter. Results for seasoned specimens show that internal stresses exist in glulam without the presence of moisture gradients. Results for specimens with induced moisture gradient show that the stresses become larger when moistening from a specific climate A to another climate B than when drying from B to A. The largest stress level found in the tests was about 0,6 MPa. The last category of test (natural climate) shows a large variation in strains and stresses. The tensile stress level in the outer part of the glulam cross section exceeds the characteristic strength of 0,5 MPa during a period of approximately 80 days.

1 Introduction

Due to the hygroscopic behaviour of wood, the variations in surrounding climate indoors as well as outdoors will impose continuous moisture changes in wood elements. The case when relative humidity and temperature are constant is very rare. The change in moisture state often affects untreated wood in a negative way, with respect to shape stability, change in mechanical properties parameters and increased creep. These effects are rather well documented and they are accounted for in timber design codes in a reasonable manner. Another effect related to moisture exposure is internal stresses perpendicular to grain caused by moisture gradients. This is normally not considered in design of timber structures. The presence of moisture gradients leads to tension and compression stresses which may combine with stresses perpendicular to grain caused by external loading. According to Ranta-Maunus (2001) moisture action should be treated as a variable load to be combined with other load effects. In recent years the study of the influence of moisture gradients has been quite intensive see e.g. Aicher and Dill-Langer (1997), Svensson and Toratti (1997).

The most common type of failure for timber structures in practice is actually caused by tension perpendicular to grain. Failure modes in tension perpendicular to grain are difficult to predict correctly in many situations, and one of the main complications is the influence

of moisture induced internal stresses. To predict the magnitude of moisture induced stresses correctly is difficult due to the complex material response of wood when it is exposed to moisture changes. Numerical methods based on complex constitutive models are often used, but systematic experimental verification of such models are uncommon. The purpose of the present research is to measure moisture induced stresses in wood cross sections under moisture action. The results will be used to verify and develop models, which can predict moisture induced stresses in a reliable way.

2 Material and method

2.1 Test specimen

All specimens used in the experiment were sawn from glulam beams with the standard size 90x270 mm. The beams contain 6 lamellae of Norway Spruce. The glulam beams were manufactured by Moelven Töreboda Limträ AB, Sweden and taken directly from the production line. The thickness of the test specimens was chosen to 16 mm, giving the specimens the dimensions $h=270$, $w=90$ and $t=16$ mm. Only specimens more or less free from knots were used. Markers, white dots on a black background were glued along each short side of the specimens see figure 1. These markers are measuring points and enable deformation measurement using a digital camera technique, described in the next section.

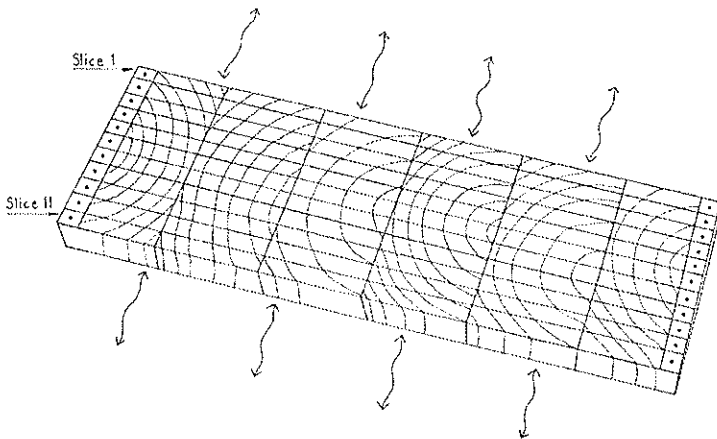


Figure 1. Test specimens sawed into eleven slices.

Prior to testing, the specimens are placed in different climates until they reach equilibrium. After this they are moisture sealed on four sides, ensuring one-dimensional moisture transport, when placing them in a different climate see figure 1. For the surface perpendicular to the grain a special moisture sealing tape was used. On the two remaining sides sealing was made with silicone. A 5-millimetre rubber plate was placed between the specimens and a package of specimens was tightened with two straps ensuring that the tape stays in place, see figure 2.

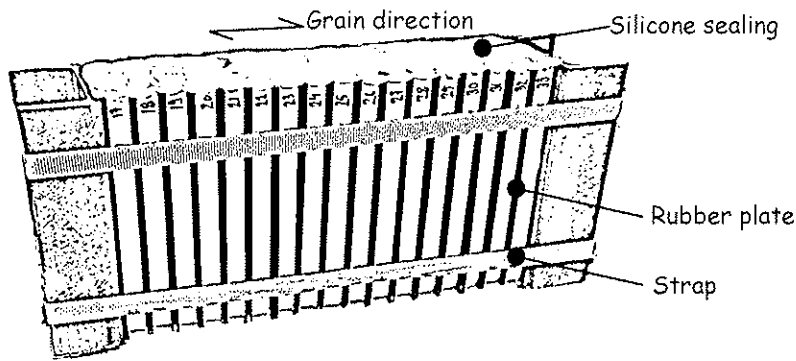


Figure 2. Moisture sealing of the specimens.

2.2 Measuring released deformations

Deformations were measured with a contact free technique, using a digital camera as measuring device. The specimens were photographed, just before and just after sawing into slices, with a band saw. The slices were put together after sawing with a thin strip of steel between them, before taking the second photo. This strip has the same thickness as the saw notch and was used for two different reasons 1) to prevent the slices to interlock with each other, giving non accurate deformations 2) to replace the saw notches and thereby give the test specimens the original size, which is important when comparing the photos. The wooden slices are approximately 7 mm wide and from each test specimen eleven slices are sawn, implying that deformations were measured at eleven discrete points. The photographed images are then processed in a commercial computer program, Matlab[®] with an image process application, developed by Heyden (1996). With this application the positions of the markers on the specimens are determined for both images.

The positions of the markers are determined in the following way. The user points out the marker" manually" with the help of the computer mouse. The program then scans an area, which includes a certain number of pixels outside the white marker. A limit intensity between black and white is preset in the program. The area of the marker is defined where the intensity is greater or equal to the limit. The position of the centroid of the marker area is calculated with each pixel weighted with respect to its output intensity. In the image plan there is also 22 reference markers, 11 markers on both sides of the test specimen. These markers are placed in a fix position, and are used to determine a scale factor when comparing the two images before and after sawing into slices. When comparing the reference length between the two images, there is a small significant difference, in the range of 0.2-0.3 pixels where the larger length is recorded in the second image. The reason for this is unknown, but is probably related to the function of the camera. To compensate for this, the lengths in the second image are scaled with a factor determined from the reference markers, this makes the lengths in both images comparable when calculating the strain. Deformations in each slice were calculated from the change of position for the two markers. Due to the chosen location of the markers, end effects on the internal stress field are included in the measured result. *The stresses*, later presented, *are* calculated directly from these measurements and are therefore the average stress (σ) in each slice given as

$$\sigma = \varepsilon E(u) = \frac{\Delta l}{l} E(u) \quad (1)$$

where ε is the released strain, E the modulus of elasticity as a function of moisture content, Δl is the length change and l is the initial length between the two markers. The modulus of elasticity was measured with a dynamic method in each individual slice and then

transformed to a static modulus of elasticity, see Jönsson and Svensson (2000). The average stresses based on the released strain over the measuring length should be corrected for end effects since the stress is zero at the ends of the specimen. The real stress in the central part of the specimen is therefore higher than the average stress determined from equation (1). Such corrections are not made for the results presented later in this paper. According to Alhassani (1999), who measured internal stresses in circular logs with similar methods, the correction for end effects in logs can be made by using an effective length equal to about 75% of the measuring length instead of l in equation (1). This means that the maximum stress is about 30% higher than the average stress over the measuring length. This correction is not necessarily valid in this case since the orientations of material directions as well as the geometry are different, but could be seen as an indication of the order of magnitude for the correction. A more detailed analysis of the end effects in this case will be made in future presentations of results from the present research.

The moisture content in each slice is determined using the oven method. This means that the weight in each slice is measured directly after sawing and after being placed in an oven (100 degrees Celsius) for approximately 48 hours. The moisture content (mc) is calculated according to

$$mc = \frac{\Delta w}{w_{dry}} 100 \quad (2)$$

where Δw is the difference between the weight before and after drying and w_{dry} the weight after drying. There must be force and moment equilibrium in the test specimens. This is not initially obtained for several reasons: incorrectness in the measuring of the dynamic modulus of elasticity, incorrect translation from the dynamic modulus of elasticity to static modulus of elasticity and errors when measuring the width and height in each thin slice. The final result is obtained by adjusting the stress distribution under the condition that the force and moment equilibrium is fulfilled. The correction is in the range of approximately 0,03-0,05 MPa, and is mainly due to a translation of the measured values. This evaluation of the correction is based on 374 test results.

2.3 Camera equipment, experimental work and accuracy of measurement

A digital camera is used to measure deformations. The camera is a Nikon D1 with a total of 2.6 millions pixels. The photo taken has 2000 pixels in width and 1312 pixels in height. There are a number of file formats, in which the photo can be saved, raw, tiff, jpeg etc. Different file formats requires different file spacing due to the degree and method of compression. In this work the file format jpeg is used. The resolution i.e. the number of pixels per millimetres is dependent on three factors, namely the size of the specimens, the cameras distance from the specimen and the total amount of pixels. In the present application the resolution is about 7 pixels per millimetre. Nikon D1 has one major advantage compared to other digital cameras, since it is possible to use replaceable lenses. A macro lens was used and gives an image, which is more or less non-distorted. Using an ordinary lens means that distances are not invariant with respect to position in the image plan. This means that a length in reality becomes different whether it is in the centre or periphery of the taken photo.

As mentioned earlier one photo before and one after sawing was taken, the camera was placed in a copying easel and adjusted so the camera always stays in the same position see figure 3. For all photos, the light, shutter time and diaphragm were the same. It is theoretically possible to determine the position of markers to within 1/256 of pixel length,

due to the fact that there are 256 grey-scales from black to white. But according to Heyden (1999) it is more reasonable to believe that the resolution is 1/100-1/10 of a pixel. This means that when determining a specific length between two markers in the image plane, the resolution becomes, in the worst case, 1/50-1/5 of a pixel. When determining the current resolution in this study, the random errors in measurements were evaluated from eleven pairs of images of the same object with 11 fixed reference lengths in each image, i.e. 110 measured values. The error was found to be normally distributed with a zero mean and a standard deviation of 1/9 pixel. The corresponding error of strain is also normally distributed with zero mean and standard deviation of 0.006 %, when using the measuring length 1830 pixels. Using typical values for the modulus of elasticity in the outer and inner part of the specimens i.e. 150 and 400 MPa, the standard error in stress then becomes 0.009 and 0.024 MPa respectively.

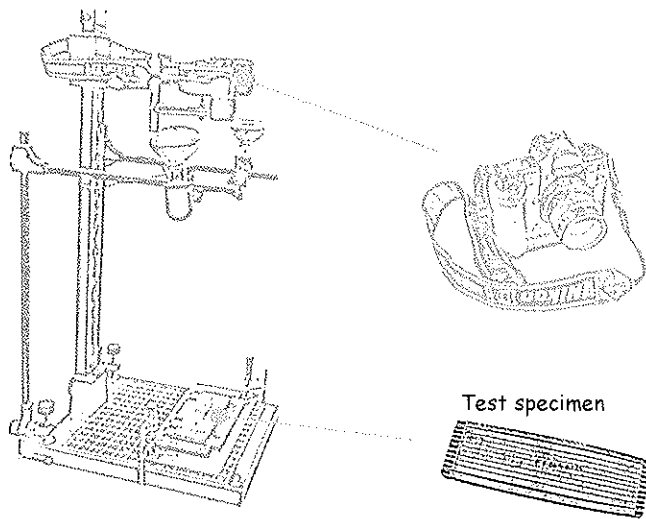


Figure 3. The camera was placed in a copying easel when taking photos.

3 Test program

The test program are separated in 3 different categories A, B and C; seasoned specimens, specimens exposed to an artificial single climate change and specimens exposed to natural climate.

A: In the first category the specimens were seasoned in 40 and 80% relative humidity (RH), 20 C° for about four months. These tests are to study strain/stress state present in specimens without moisture gradients.

B: The specimens in the second group were also seasoned in RH 40 and 80%, 20 C° and then moisture sealed. After this a climate change took place, i.e. specimens seasoned in RH 40% where put in RH 80% and vice versa. It is here possible to evaluate the influence of moisture gradient perpendicular to the grain direction on the strain/stress distribution.

C: In the last category the specimens were seasoned in RH 60%, 20 C° corresponding to a moisture content of approximately 12%, then moisture sealed and placed outdoors under shelter. The specimens were not exposed to rain or sun during the test period. This test was designed to evaluate the influence of “real conditions”. In this case the test started out in the winter and the test is still in progress.

Table 1 Test program

| Test category | Seasoned in relative humidity | Climate exposure | Total number of specimens | Specimens tested each time | Day of testing |
|---------------|-------------------------------|------------------|---------------------------|----------------------------|---|
| A | 40% | - | 14 (10)* | - | - |
| | 80% | - | 14 (12)* | - | - |
| B | 40% | 80% | 14 | 2 | 1,3,5,6,11,24,38 |
| | 80% | 40% | 14 | 2 | 1,3,5,7,11,24,38 |
| C | 60% | Natural. climate | 60 (30)** | 2 | 0,3,11,20,33,42,62,69,76,90,104,118,132,146,161 |

*When sawing the seasoned specimens into slices some of them were broken due to microscopic checks and were rejected.

**The testing of this category is not finished when writing this paper 010505.

4 Results and discussion

Category A, seasoned specimens

Figure 4 to 6 shows the internal strain and stress distribution determined in specimen seasoned in RH 40% and 80%. When the glulam beams were manufactured in the factory the moisture content were between 10-14%. When the test specimens were seasoned in RH 40% and RH 80% desorption and absorption, respectively, occurred. The shrinkage/swelling is larger in the tangential direction than in the radial direction. This is a possible explanation for the observed stress state for the seasoned specimens. For the case RH 40% the outermost part of the specimens is constrained from shrinkage by the middle, which results in the internal stresses presented in figure 4 (right). For the other case RH 80% the result will be the opposite as shown in figure 5 (right). The largest tensile stress, approximately 0,2 MPa was found in this case.

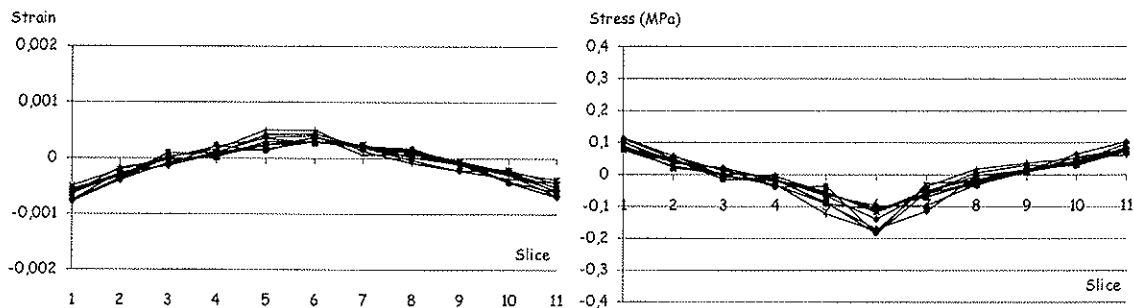


Figure 4. Internal strain (left) and stress (right) for 12 different specimens seasoned in RH 40%.

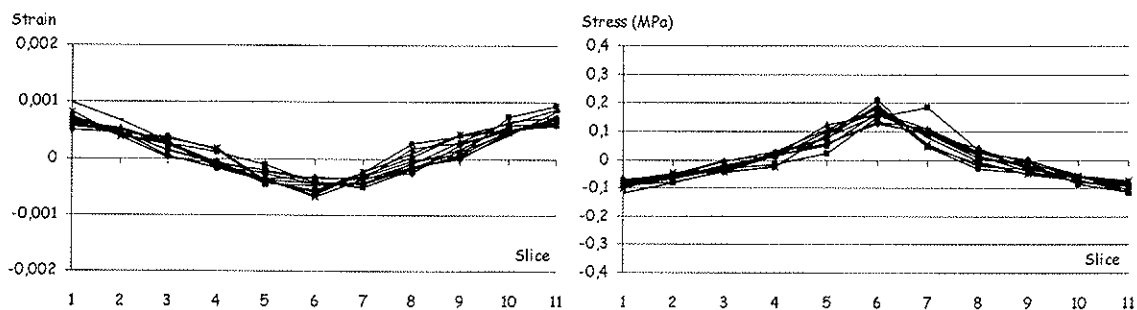


Figure 5. Internal strain (left) and stress (right) for 12 different specimens seasoned in RH 80%.

Category B, artificial single climate step, RH 40% to 80%

Figure 6 shows the distributions in moisture content in each slice during the tested period. The inner part of the specimens is not initially responding to the moistening in the outer part, according to figure 8 it takes about 11 days until the inner part is affected. It can also be observed that the shape of the curves differs a great deal compared to the opposite test i.e. drying the specimens from RH 80% to 40% see figure 9. The differences in the moisture content between adjacent slices i.e. moisture gradients create strain and stress distributions according to figure 7 to 8.

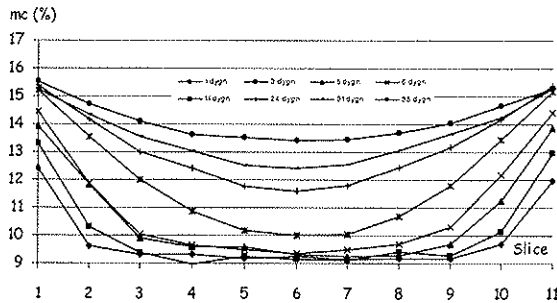


Figure 6. Moisture content after day 1,3,5,6,11,24 and 38. Climate variation from RH 40% to RH 80%.

Figure 7 (left) shows three measured specimens at day 3, 11 and 38. This figure reveals that after 3 days the strains in the outermost slices reach high levels, the inner part seems to have a constant strain level. With increasing time the inner part of the specimen becomes more affected and the constant level is replaced with a local maximum strain value and at this time the strain level in the outer part is decreasing. After 38 days the moisture gradient is reduced and the strain level in the entire specimen decreases. Figure 7 (right) shows the corresponding internal stress distribution and the same pattern is shown. The stresses are however more irregular due to the influence of the modulus of elasticity in each slice. The maximum tension and compression stress during the tested period are 0,56 and 0,72 MPa respectively.

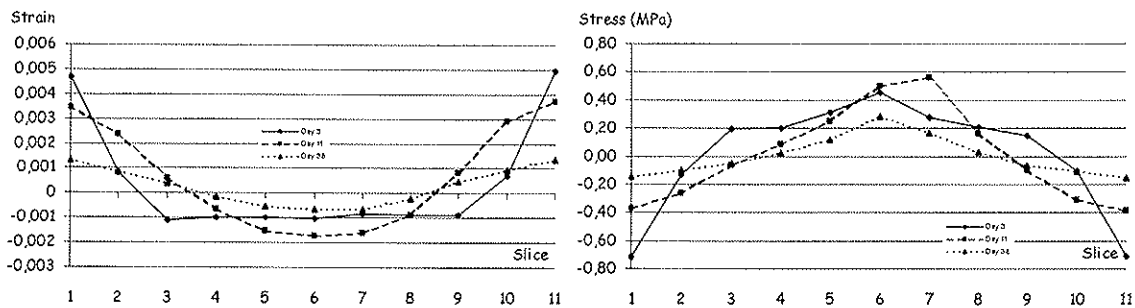


Figure 7. Internal strain (left) and stress (right) for specimen tested day 3, 11 and 38. Climate variation from RH 40% to RH 80%.

Figure 8 shows how strain and stress varies in the outer slice 1,11 and the middle slice 6 with increasing time. Each value is taken as the average between two measured specimens see table 1.

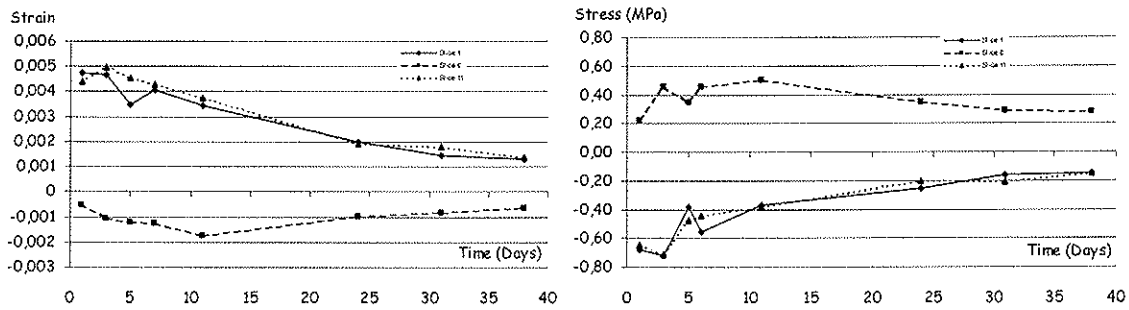


Figure 8. Internal strain (left) and stress (right) in slice 1, 6 and 11 versus time. Climate variation from RH 40% to RH 80%.

Category B, artificial single climate step, RH 80% to 40%

The moisture distributions displayed in figure 9 show a different pattern than figure 6 when it comes to the shape of the curves. It seems that the inner part of the specimen is affected earlier during drying, than during absorption.

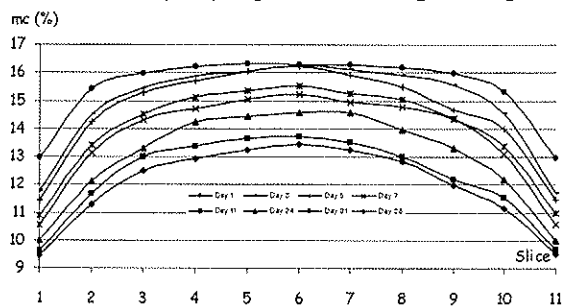


Figure 9. Moisture content after day 1,3,5,7,11,24 and 38. Climate variation from RH 80% to RH 40%.

For this test group the internal strain distribution is the opposite and the outer part wants to contract. Tensile stress arises in the outermost slices and compression stress occurs in the middle. The strain distribution in figure 10 shows the same pattern as figure 7, but less pronounced in the middle part. Drying specimens give lower stresses than moistening. The largest stresses in these two test groups differ in the outer and inner part approximately by a factor 2 and 3 respectively. The maximum tension and compression stress during the tested period are 0,33 and 0,25 MPa respectively

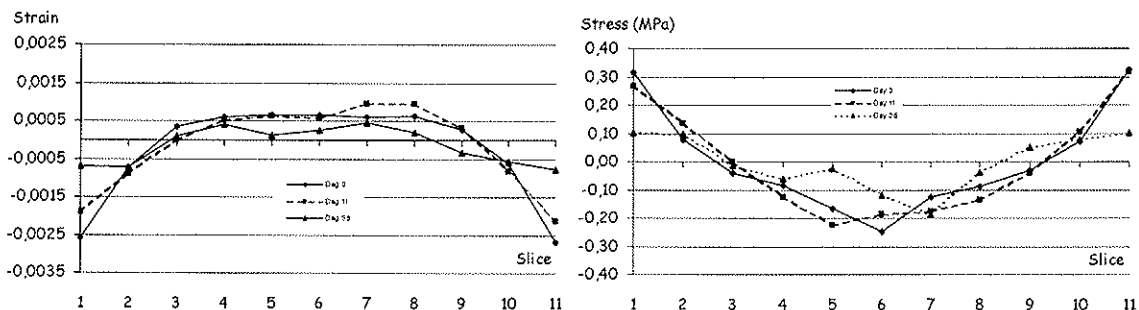


Figure 10. Internal strain (left) and stress (right) for specimen tested day 3, 11 and 38. Climate variation from RH 80% to RH 40%.

Figure 11 illustrates the absolute value of the difference between the moisture content in slice 1 and 2 for the two tests in category B versus time for testing. It can be seen that the

difference in moisture content are almost the same the first days. After the initial phase the difference between adsorption and desorption can clearly be seen i.e. a hysteresis effect. One reason for this is that desorption isotherms give a greater difference in moisture content than the corresponding adsorption isotherms for a given relative humidity change.

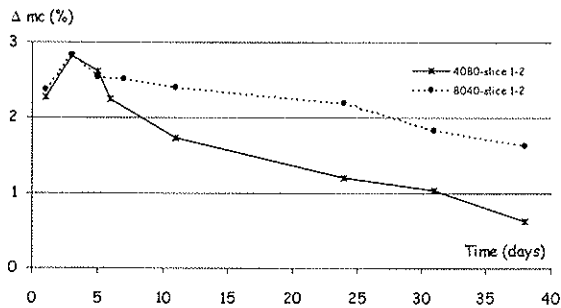


Figure 11. The difference between moisture content (moisture gradient) in slice 1 and 2 versus time.

Figure 12 below shows how strain and stress vary in the outer slice 1,11 and the middle slice 6 with increasing time. Each value is taken as the average between two measured specimens see table 1.

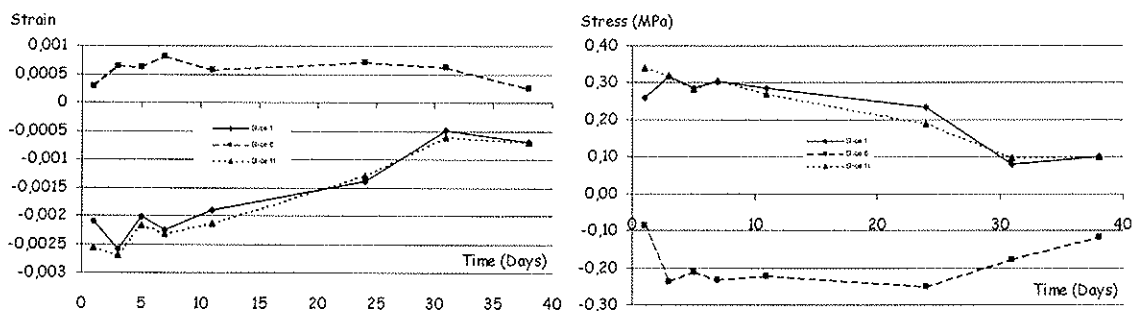


Figure 12. Internal strain (left) and stress (right) in slice 1, 6 and 11 versus time. Climate variation from RH 80% to RH 40%.

Category C, natural climate

The glulam specimens are placed outdoors but sheltered from rain and sun. The test started out in November the 16 and the last value recorded for this paper was April the 26. Figure 13 and 14 below shows data logged by an electronic thermohygrograph called Testostore 171-3. Temperature and relative humidity are logged each hour during the tested period. It is shown from data that 73% of the time the RH was above 90%, the mean RF was almost 92%.

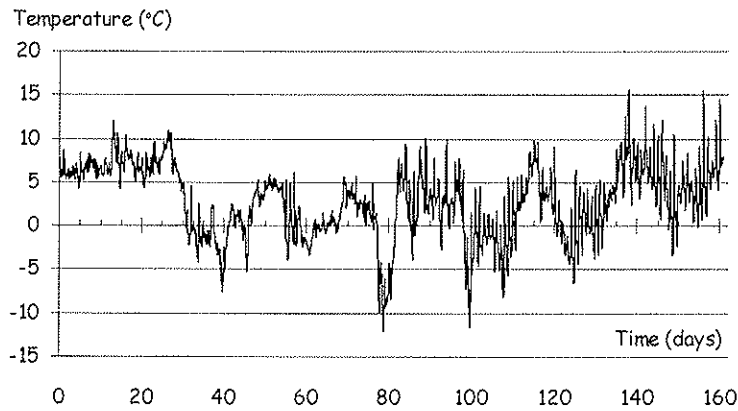


Figure 13. Temperature versus time, natural climate

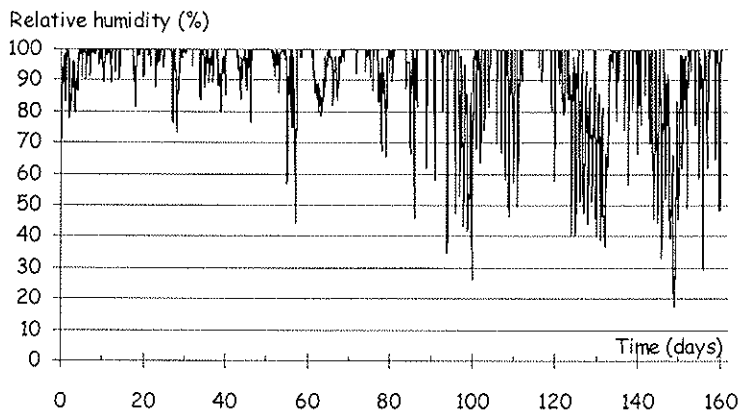


Figure 14. Relative humidity versus time, natural climate

The moisture content, strain and stress distribution in specimens exposed to natural climate is shown for 15 different occasions shown in figure 15, 16 and 17 (left). Figure 15, 16 and 17 (right) show the results for slices 1,6 and 11 versus time. The value in each slice is taken as the average measured values between 2 slices. There is a large fluctuation in strain and stress in the slices during the test period. According to figure 16 the strain in the outer slice varies between $-2,2$ and $5,7$ ‰ and in the middle slice from $-1,9$ to 0 ‰. The corresponding stress in figure 17 varies from $-0,65$ to $0,32$ and 0 to $0,85$ MPa.

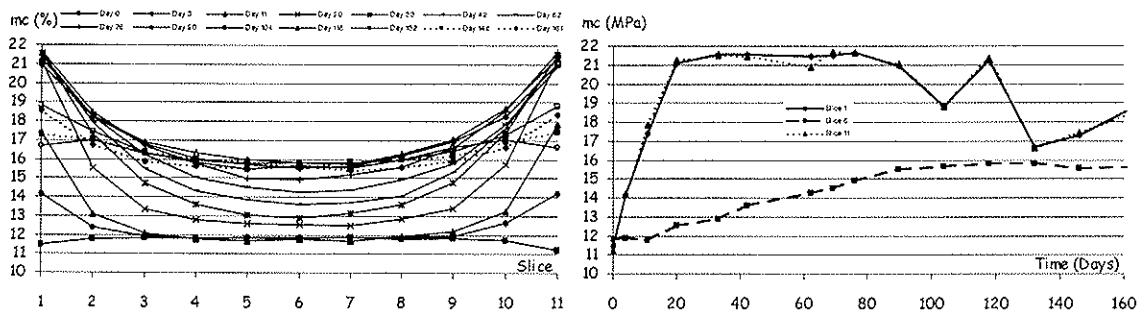


Figure 15. Moisture content after day 0,3,11,20,33,42,62,69,76,90,104,118,132,146 and 161 (left) and moisture content in slice 1, 6 and 11 versus time (right), natural climate.

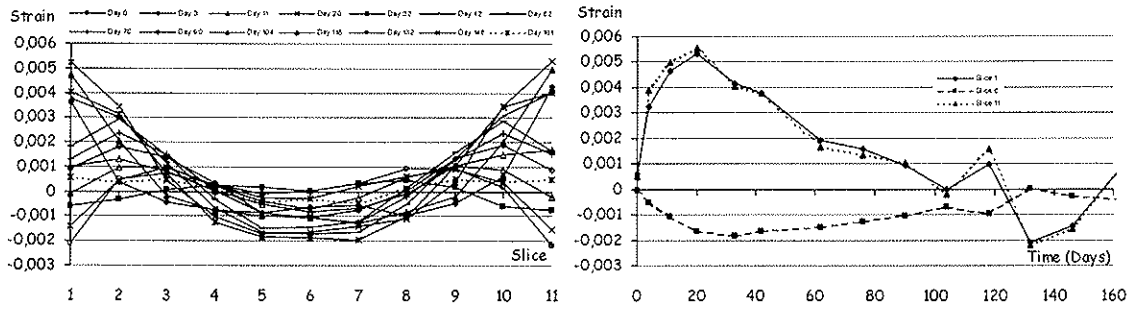


Figure 16. Internal strain for specimen tested day 0,3,11,20,33,42,62,69,76,90,104,118,132,146 and 161 (left) and internal strain in slice 1, 6 and 11 versus time (right), natural climate.

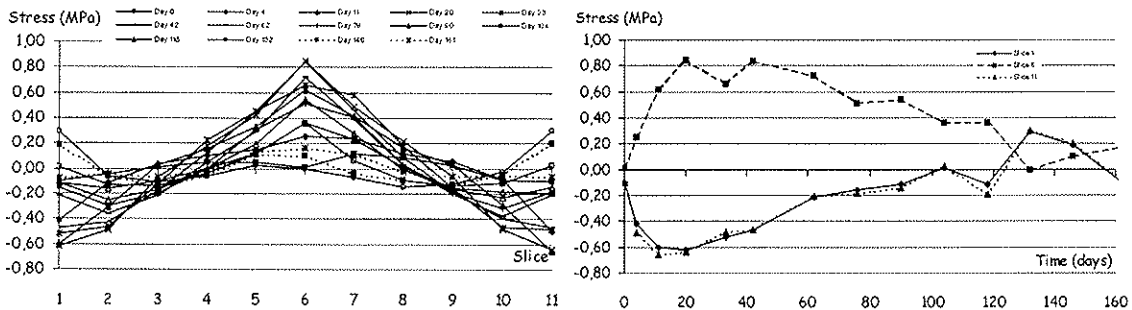


Figure 17. Internal stress for specimen tested day 0,3,11,20,33,42,62,69,76,90,104,118,132,146 and 161 (left) and internal stress in slice 1, 6 and 11 versus time (right), natural climate.

Figure 18 is a “simplification” of figures 16 and 17, only showing selected test results. When observing only the outer part of the specimen it is evident that the initial behaviour follows the same pattern as for moistening specimens in Category B. From approximately day 69 to day 104 the relative humidity is decreasing and the specimens are drying, this can be seen in specimens tested at day 104 where the strain is negative and tension stresses are developed. After day 104 the relative humidity is increasing again giving compression stresses in the outer part (day 118). Once again the specimen are drying, from day 118 to day 132. The moisture content has dropped almost 10%, giving large tensile stresses in outer parts and approximately zero (-0,005 MPa) stresses in the middle. The last recorded days shows an increase in relative humidity, the strain and stress has once more changed signs (day 161).

According to the Swedish code the characteristic value for tension perpendicular to grain is set to 0,5 MPa. This value was exceeded for approximately 80 days, during a total testing period of 161 days, see figure 17 (right).

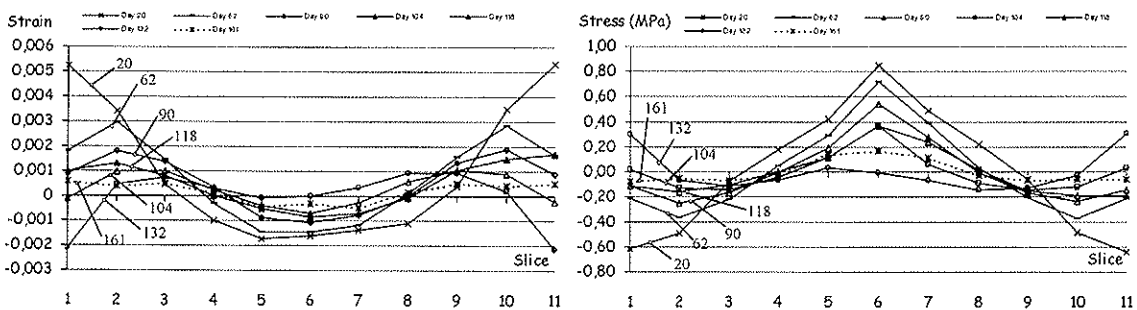


Figure 18. Internal strain (left) and internal stress (right) for specimen tested day 20,62,90,104,118,132 161, natural climate.

Conclusions

The stress values given below refer to average stresses along slices disregarding end effects. The maximum stress levels in the cross section are significantly higher. A preliminary estimate is that the stresses may be about 30 % larger than the values quoted below. The following conclusions can be drawn from the tests.

- Significant internal stresses were found in seasoned specimens with uniform moisture content.
- The maximum tension and compression stress for seasoned specimens is of the order 0,2 MPa.
- For specimens with induced moisture gradient, the stresses become larger for moistening from a specific climate RH 40% to another climate RH 80% than for drying from RH 80% to RH 40%.
- The tensile stresses are twice as high and the compressive stresses are three times higher under moistening between RH 40 % and 80 % than under drying or vice versa.
- The largest tension stress level observed was about 0,6 MPa, which is larger than the characteristic tensile strength perpendicular to the grain.
- Specimens exposed to natural climate outdoors under shelter show a large fluctuation in released strains and internal stresses during a 160-day period from November to April.
- The stress level varied in the outer part of the cross section from –0,65 to 0,32 MPa and from 0 to 0,85 MPa in the middle part.
- The tensile stresses exceeded 0,5 MPa during a period of 80 days, out of a total testing period of 160 days.
- The main conclusion is that moisture induced stresses must always be taken into account in one way or another for failure modes involving tension perpendicular to grain.

References

- Aicher, S., Dill-Langer, G. 1996. Influence of cylindrical anisotropy of wood and loading conditions on off-axis stiffness and stresses of a board in tension perpendicular to the grain. *Otto-Graf-Journal*, Vol. 7.
- Aicher, S., Dill-Langer, G. 1997. Climate induced stresses perpendicular to the grain in glulam. *Otto-Graf-Journal*, Vol. 8.
- Blass, H.J, Schmid, M. 1998. Tensile strength perpendicular to grain according to EN 1193 Proceedings CIB W18/31, paper 31-6-6, Savonlinna, Finland.
- EN 1193:1998. Timber structures- Structural timber and glued laminated timber – Determination of shear strength and mechanical properties perpendicular to the grain.
- Görlacher, R. 1986. A dynamic method for determining elastic properties of wood. Proceedings CIB W18/19, paper 19-6-6, Florence, Italy.
- Jönsson, J., Svensson, S. 2000. Internal stresses in the cross-grain direction of wood induced by climate variation. Proceedings CIB W18/33, paper 33-12-1, Delft,

Netherlands.

Ranta-Maunus, A. 2001. Effects of climate and climate variations on strength. Lecture, Timber engineering, Lund, Sweden.

Svensson, S., Toratti, T. 1997. Mechanical response of wood perpendicular to grain when subjected to changes of humidity. Wood Science and Technology. In press.

**INTERNATIONAL COUNCIL FOR RESEARCH AND INNOVATION
IN BUILDING AND CONSTRUCTION**

WORKING COMMISSION W18 - TIMBER STRUCTURES

**LOAD CARRYING CAPACITY OF NAIL-LAMINATED TIMBER
UNDER CONCENTRATED LOADS**

V Krämer

H J Blass

Lehrstuhl für Ingenieurholzbau und Baukonstruktionen

University of Karlsruhe

GERMANY

Presented by: V Krämer

- S Thelandersson commented that there was agreement with displacement but what about strength.
- V Krämer answered that the exact bending capacity was not known and linear elastic behaviour was assumed. In the second step realistic load-slip behaviour of the nails would be needed.
- I Smith commented the in service nail might loosen and gaps might occur. He asked how could these moisture related effect be taken into consideration.
- V Krämer answered that work has been initiated to test nail connections.
- H J Blass added that this would only be a limited study as the system was intended to be used in building not bridges.
- I Smith added that empirical rules were available for bridges.
- G Schickhofer commented that nail laminated deck is in EC5 therefore study with regard to gaps would be important.
- V Krämer agreed.
- V Enjily commented that he saw the benefits and asked whether such system would be intended for low quality timber.
- H J Blass explained that in effect high quality timber would be used.

Load Carrying Capacity of Nail-Laminated Timber under Concentrated Loads

V. Krämer, H. J. Blass

Lehrstuhl für Ingenieurholzbau und Baukonstruktionen

Universität Karlsruhe

Germany

1 Introduction

A laminated timber element is a plane structural component composed of single, edgewise-oriented lamellas. These lamellas are mechanically jointed usually by nails, alternatively by dowels made of hardwood. In the following, only nail-laminated timber elements are considered, which are mechanically jointed by nails and loaded by central concentrated loads.

The aim of a research project was to derive design-equations for the effective bending stiffness, for the resulting bending stresses, and for the nail loads. It would have been quite expensive to obtain the design-equations by running a large number of tests. This is why the tests were simulated on the computer. For the simulations, the parameters ℓ/h (span / height of the element), the nail diameter, and the nail spacing were varied. The simulations were conducted on the basis of realistic stiffness-values of the lamellas and of the nails. The lamellas were generated on the basis of Görlacher [1], the nails on the basis of the deformation characteristics given in EC5 [2]. To guarantee statistically reliable results, 36 different systems of nail-laminated timber elements were simulated. Each system of the nail-laminated timber elements was simulated 500 times. The design equations were derived from the results of these 18,000 simulations.

The results of the design equations show a good agreement with the results of 6 tests.

2 Basis of the Simulations

2.1 Lamellas

The strength and stiffness properties of the lamellas were simulated on the basis of the work of Görlacher and Colling [3]. Investigations of lamellas used in glued laminated timber served as a basis for these simulations. A virtual lamella ($l = 4.5\text{m}$) is subdivided into 30 segments with a length of 15 cm each. The values of MOE, the Knot Area Ratio (KAR) and the density are assigned to each single segment. The distribution of the MOE-values within a simulated lamella is shown as an example in figure 1.

According to Glos [4], the values of the simulated lamellas correspond to strength class C24 [5].

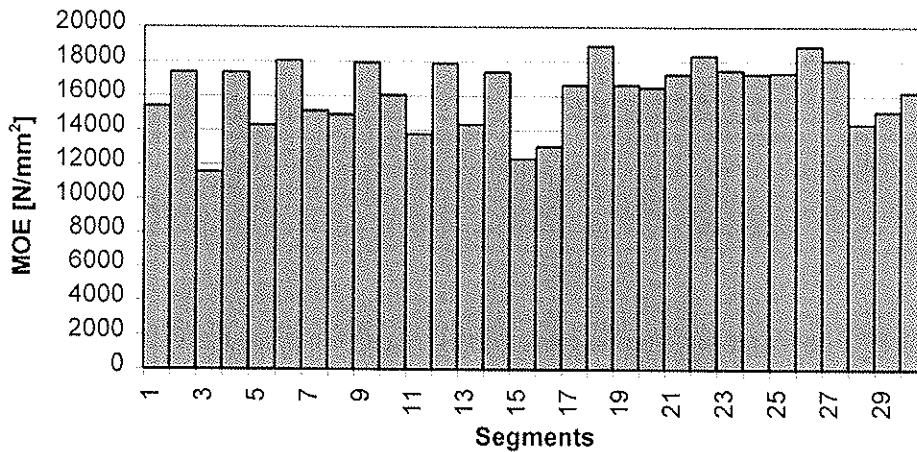


Figure 1 Example of the simulated within member variability of a lamella ($\text{MOE}_{\text{mean}} = 15959 \text{ N/mm}^2$)

2.2 Dimensions of the nail-laminated timber elements

The nail-laminated timber elements (NLTE) were simulated as simply supported beams (see figure 2). The span (ℓ) of the NLTE was kept constant at 3.6 m. The depth (h) of the lamellas was varied in the range of 140, 160 and 180 mm. Consequently, the ℓ/h -ratios ranged from 20 up to 25.7, which are close to the ratios used for floors [6]. The width (t) of the lamellas was varied in the range of 30 mm, 35 mm, and 40 mm.

To keep the computing time at a reasonable level, each virtual NLTE consisted of 30 lamellas.

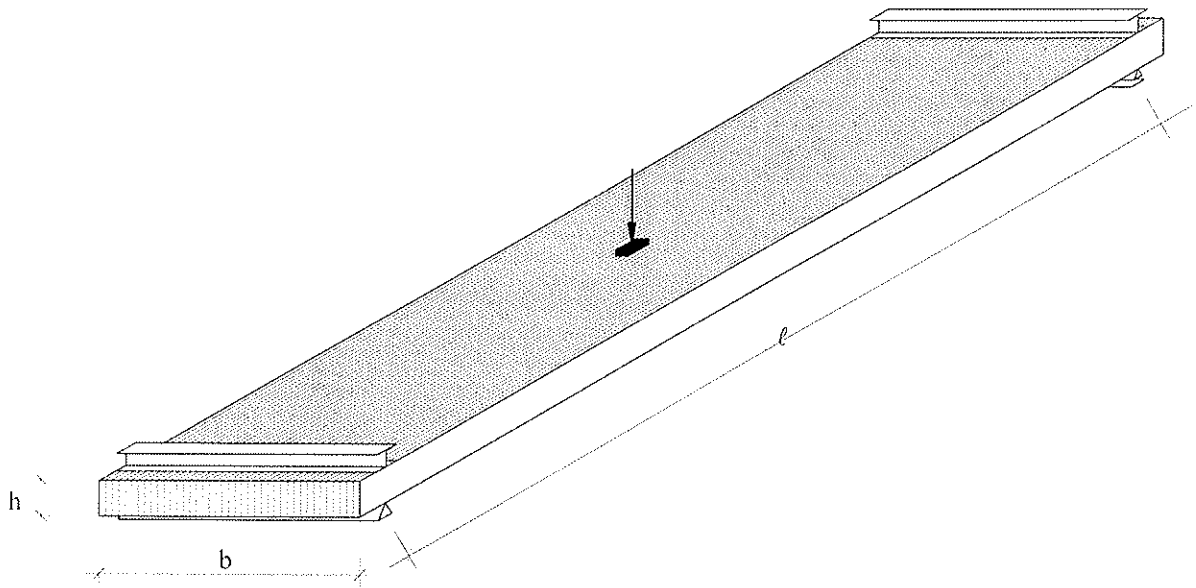


Figure 2 Nail-laminated timber element

2.3 Nails

The simulation of the nails was conducted on the basis of a nailed double shear timber to timber connection. The nail length consequently resulted as three times the lamella width. With the available smooth nails commonly used, the nail diameter (d_N) then depends on the width (t) of the lamella. The dimension of the nails corresponded to dimensions given in DIN 1151 [7] and in DIN 1143 [8]. For example, for $t = 30$ mm the nail 3.4 x 90 mm is used. The nails are assumed to be arranged in a zigzag pattern, as shown in figure 3.

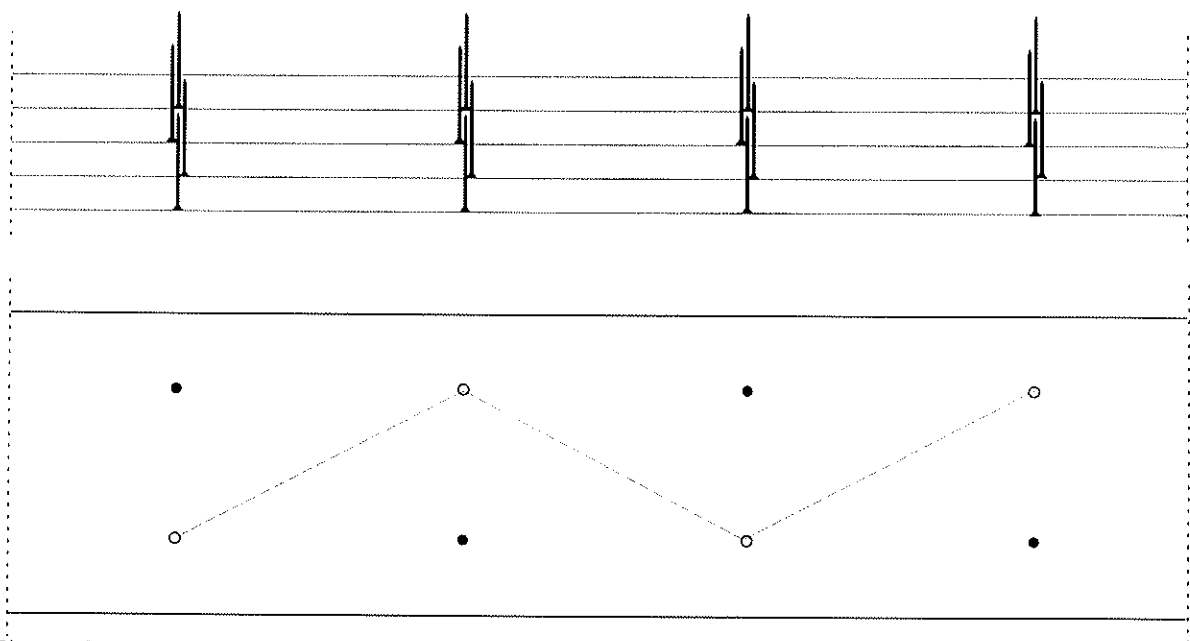


Figure 3 Nail arrangement

3 Finite Element Model

A grid was chosen as the mechanical model of the NLTE. The girders in longitudinal direction represent the lamellas. The shear stiffness of the nails was modelled by the bending stiffness of the girders in transverse direction. The lamellas of the NLTE are supported in x-, y-, and z-direction (left end) and in y-, and z-direction (right end).

The NLTE's were loaded with a single load of 1.0 kN. To simulate the spatial distribution of a single load (approximately 5cm/5cm), the single load was subdivided into 6 parts. The assembly of the mechanical model of the NLTE is shown in figure 4.

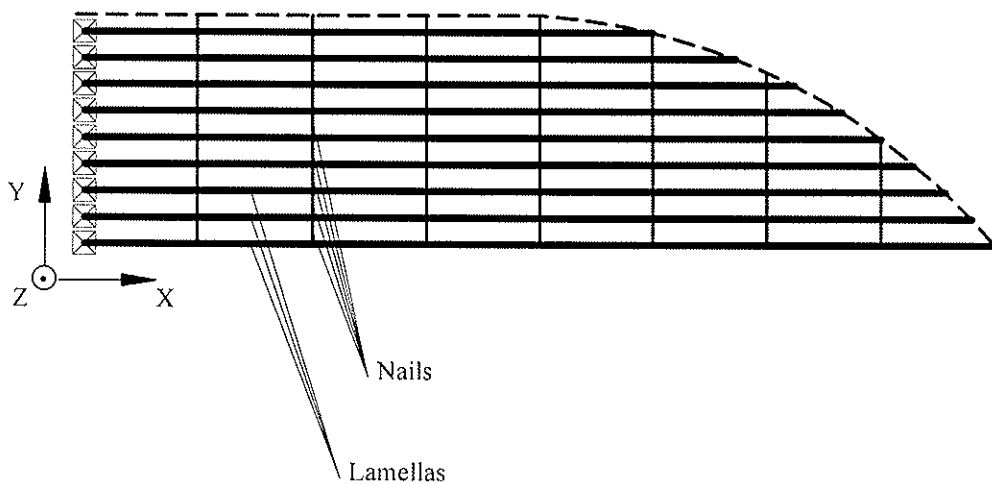


Figure 4 Mechanical model of the NLTE

3.1 Simulation of the NLTE

First, the files with the material properties of the lamellas and of the nails were generated. The files for the FE-calculation were generated on the basis of these material properties and on chosen geometric values of the NLTE. The calculations were performed with the FE- program ANSYS. Due to the fact that the calculations were linear-elastic, the results could be linearly extrapolated. Table 1 shows the parameters of 36 different simulated NLTE-systems [9]. 500 simulations were calculated and evaluated for each of the 36 NLTE-systems.

Table 1 Simulation table

| No. | Spacing (Nail) a1 [mm] | Height (Lam.) h [mm] | Width (Lam.) t [mm] | Diameter (Nail) d [mm] |
|-----|---------------------------|-------------------------|------------------------|---------------------------|
| 1 | 75 | 140 | 30 | 3,4 |
| 2 | 75 | 140 | 35 | 3,8 |
| 3 | 75 | 140 | 40 | 4,2 |
| 4 | 75 | 160 | 30 | 3,4 |
| 5 | 75 | 160 | 35 | 3,8 |
| 6 | 75 | 160 | 40 | 4,2 |
| 7 | 75 | 180 | 30 | 3,4 |
| 8 | 75 | 180 | 35 | 3,8 |
| 9 | 75 | 180 | 40 | 4,2 |
| 10 | 150 | 140 | 30 | 3,4 |
| 11 | 150 | 140 | 35 | 3,8 |
| 12 | 150 | 140 | 40 | 4,2 |
| 13 | 150 | 160 | 30 | 3,4 |
| 14 | 150 | 160 | 35 | 3,8 |
| 15 | 150 | 160 | 40 | 4,2 |
| 16 | 150 | 180 | 30 | 3,4 |
| 17 | 150 | 180 | 35 | 3,8 |
| 18 | 150 | 180 | 40 | 4,2 |
| 19 | 225 | 140 | 30 | 3,4 |
| 20 | 225 | 140 | 35 | 3,8 |
| 21 | 225 | 140 | 40 | 4,2 |
| 22 | 225 | 160 | 30 | 3,4 |
| 23 | 225 | 160 | 35 | 3,8 |
| 24 | 225 | 160 | 40 | 4,2 |
| 25 | 225 | 180 | 30 | 3,4 |
| 26 | 225 | 180 | 35 | 3,8 |
| 27 | 225 | 180 | 40 | 4,2 |
| 28 | 300 | 140 | 30 | 3,4 |
| 29 | 300 | 140 | 35 | 3,8 |
| 30 | 300 | 140 | 40 | 4,2 |
| 31 | 300 | 160 | 30 | 3,4 |
| 32 | 300 | 160 | 35 | 3,8 |
| 33 | 300 | 160 | 40 | 4,2 |
| 34 | 300 | 180 | 30 | 3,4 |
| 35 | 300 | 180 | 35 | 3,8 |
| 36 | 300 | 180 | 40 | 4,2 |

4 Evaluation of the Simulations

For each of the 36 NLTE's the 95%-fractile-values of the bending stresses of the lamellas and of the nail loads and the mean-values of the deformations were determined. The design equations were derived from these 95%-fractile- and mean-values.

4.1 Bending stresses of the lamellas

The maximum bending stress of lamellas in a NLTE under a centric single load can be calculated using equation 1:

$$\sigma_B = \frac{M}{W_{ef}} \text{ [N/mm}^2\text{]} \quad (1)$$

The bending moment is calculated according to equation 2:

$$M = \frac{F \cdot \ell}{4} \text{ [Nmm]} \quad (2)$$

where F is the concentrated load in midspan and ℓ is the span of the NLTE.

The effective section modulus W_{ef} resulted as:

$$W_{ef} = \frac{t \cdot h \cdot \ell}{4,5 \cdot a_1^{0,3}} \quad (3)$$

where t and h are the width and the depth of the lamellas [mm]

ℓ is the span of the NLTE [mm]

a_1 is the nail spacing [mm]

4.2 Nail loads

The nail loads depend on the parameters ℓ/h and a_1 . Thus, the equation to calculate the nail loads are given as:

$$F_{Na} = F \cdot \frac{\left(\frac{\ell}{h}\right)^{2/3} \cdot a_1^{0,8}}{8,5} \text{ [N]} \quad (4)$$

where

F is the concentrated load [kN]

ℓ is the span of the NLTE [mm]

h is the depth of the lamellas [mm]

a_1 is the nail spacing [mm]

4.3 Deformation of the NLTE

The elastic displacement of the NLTE under a concentrated load is calculated with equation 5:

$$v = \frac{F \cdot \ell^3}{48 \cdot E \cdot I_{ef}} \text{ [mm]} \quad (5)$$

The modulus of elasticity is assumed as the mean value of the simulated MOE-values and resulted as 12600 N/mm². The effective second moment of area of the NLTE cross section I_{ef} was determined as:

$$I_{ef} = \frac{t \cdot h^2 \cdot \ell^{0,86}}{0,9 \cdot a_1^{0,4}} \quad (6)$$

where

- ℓ is the span of the NLTE [mm]
- t/h are the width and the depth of the lamellas [mm]
- a_1 is the nail spacing [mm]

5 Validating tests

A total of 6 tests were conducted to validate the simulation results. The test parameters are shown in table 2.

Table 2 Test Parameters

| Test No. | Span (Element) ℓ [m] | Spacing (Nail) a_1 [mm] | Depth (Lam.) h [mm] | Width (Lam.) t [mm] | Diameter (Nail) d [mm] |
|----------|------------------------------|------------------------------|--------------------------|--------------------------|-----------------------------|
| 1 | 3,75 | 150 | 190 | 35 | 3,8 |
| 2 | 4,50 | 150 | 155 | 28 | 3,1 |
| 3 | 4,50 | 150 | 140 | 30 | 3,4 |
| 4 | 3,75 | 75 | 180 | 28 | 3,1 |
| 5 | 3,75 | 150 | 180 | 28 | 3,1 |
| 6 | 3,60 | 225 | 180 | 28 | 3,1 |

The material properties (density, MOE, KAR and moisture content) of 248 lamellas were determined and used for simulating the tests in advance. Thus, the position and the material properties of each lamella in the NLTE were known.

Figure 5 shows the comparison of 248 values of MOE (lamellas) with 248 simulated mean values of MOE.

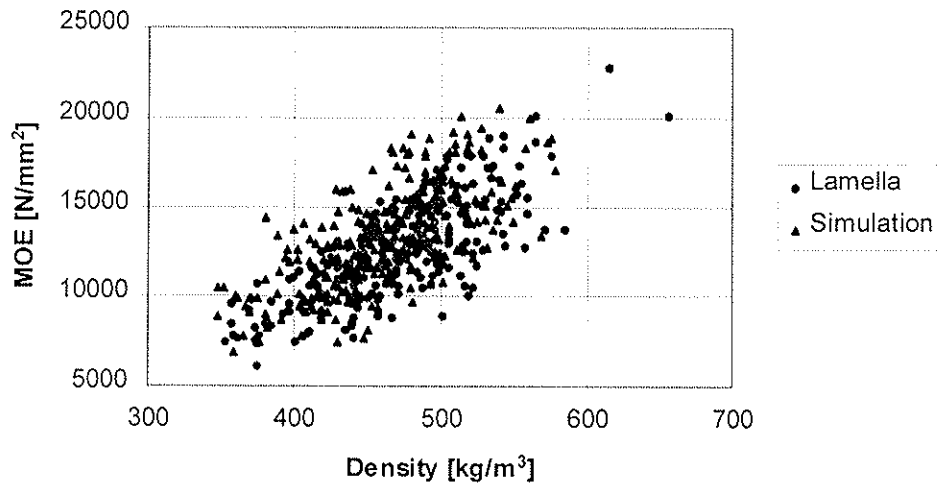


Figure 5 Comparison of measured and simulated values of MOE versus density

The test results agreed with the results of the simulations. The comparison of the test results, the simulations result, and the results of the design equations for the vertical displacement under a load of 5.0 kN is shown in figure 6.

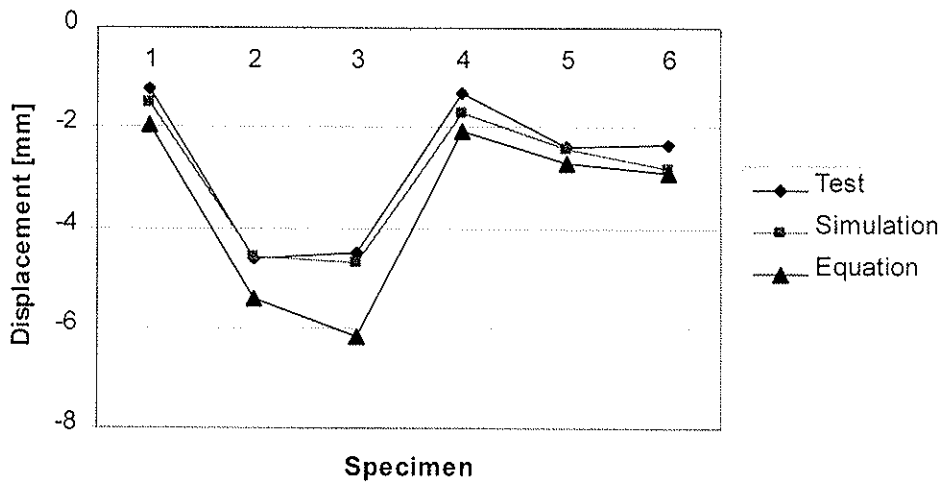


Figure 6 Comparison of the results of the tests, simulation, and equation

6 Summary

A mechanically laminated timber element (NLTE) is a plane structural component which is made of single, edgewise-oriented lamellas. The lamellas are mostly jointed by nails.

The aim of a research project was to derive design-equations for the bending stiffness, for the bending stresses of the lamellas, and for the action effects of the nails. The design-equations were derived from the simulation of thousands of nail-laminated timber elements. In these simulations, the parameters ℓ/h (span / height of the element), the diameter of the nails, and the nail spacing were varied. The simulations were conducted on the basis of realistic stiffness-values of the lamellas and the nails. The lamellas were generated on the basis of the work of Görlacher, the nails on the basis of the slip moduli given in EC5. To guarantee statistically reliable results, 36 different systems of nail laminated timber elements were simulated. Each system of nail-laminated timber elements was simulated 500 times. The design equations were derived from the 95%-fractile-values and from the mean-values of 18,000 simulations.

The results of the design equations were compared with the test results and demonstrated good agreement with each other.

7 References

- [1] R. Görlacher: Klassifizierung von Brettschichtholzlamellen durch Messung von Longitudinalschwingungen; 4.Folge – Heft 21, Berichte der Versuchsanstalt für Stahl, Holz und Steine der Universität Fridericiana in Karlsruhe; 1990
- [2] DIN V ENV 1995 Teil 1 -1 (Eurocode 5): Entwurf, Berechnung und Bemessung von Holzbauwerken, Teil 1-1: Allgemeine Bemessungsregeln, Bemessungsregeln für den Hochbau; Ausgabe Juni 1994
- [3] F. Colling: Tragfähigkeit von Biegeträgern aus Brettschichtholz in Abhängigkeit von festigkeitsrelevanten Einflußgrößen; 4.Folge – Heft 22, Berichte der Versuchsanstalt für Stahl, Holz und Steine der Universität Fridericiana in Karlsruhe; 1990
- [4] P. Glos: Maschinelle Festigkeitssortierung von frisch eingeschnittenem Schnittholz; Bericht Nr. 95507, Institut für Holzforschung der Universität München; 1997
- [5] DIN EN 338: Bauholz für tragende Zwecke, Festigkeitsklassen; Ausgabe Juli 1996
- [6] Brettstapelbau-Bausystem, Handbuch, Hiwo Holzindustrie Waldburg zu Wolfegg GmbH & Co. KG; November 1997
- [7] DIN 1151: Drahtstifte rund; Ausgabe April 1973
- [8] DIN 1143-1: Maschinenstifte, rund lose, Ausgabe August 1982
- [9] M. Haberer: Die Querverteilung von Lasten an Brettstapelelementen; Vertieferarbeit am Lehrstuhl für Ingenieurholzbau und Baukonstruktionen, Universität Karlsruhe; Juni 2000

**INTERNATIONAL COUNCIL FOR RESEARCH AND INNOVATION
IN BUILDING AND CONSTRUCTION**

WORKING COMMISSION W18 - TIMBER STRUCTURES

**DETERMINATION OF SHEAR STRENGTH VALUES FOR GLT
USING VISUAL AND MACHINE GRADED SPRUCE LAMINATIONS**

G. Schickhofer
Graz University of Technology

AUSTRIA

Presented by: G Schickhofer

- H J Larsen commented that standard test methods for shear strength were available and asked whether such test have been performed with the point that the standard test would be more cost effective.
- G Schickhofer answered that EN408 test configuration was not tried.
- H J Larsen commented that one should not standardise complicated beam test methods if cheaper tests were available.
- G Schickhofer agreed but stated that real glulam behaviour would also be important.
- P Glos commented that he agreed with the results in general; however, there appeared to be some contradiction of results between the visually graded and the machine stress rated timber of the same strength class with reference to the general conclusion in the paper.
- G Schickhofer agreed and explained only a limited sample size of 15 specimens were available.
- P Glos commented that the conclusions should be qualified with limited sample size.
- B Yeh commented that he agreed with the concept that shear strength should be tensile strength independent. He questioned the use of overhang in the test which could increase the measured shear strength.
- G Schickhofer answered that only a small overhang was used and it was chosen via the optimisation step to reduce the compression perpendicular to grain stresses in the wood near the support. Tests comparing 50 mm and 500 mm of overhang did not show increases.
- B Yeh asked how the I-section was made with the web centered.
- G Schickhofer answered that there was no manufacturing problem.

Determination of Shear Strength Values for GLT using Visual and Machine Graded Spruce Laminations

G. Schickhofer
Graz University of Technology, Austria

1 Abstract

The aim of this research project was to conduct tests to determine load-based shear strength values for GLT components subject to bending load. In order to achieve this objective it was necessary to develop a suitable test set-up for glued laminated timber. Although extensive research of the literature revealed that such tests have been conducted for solid timber, the lack of standardised test set-ups is equally a problem in this area. Recent analyses have been performed by B. Yeh, T.G. Williamson and G. Schickhofer and B. Obermayr on glued laminated timber. On the basis of preliminary tests on 24 glulam beams (I-cross section, rectangular cross section with reinforced edge zones, $h = 320$ mm, $h = 608$ mm) and finite element analyses aimed to optimise the load introduction area and the cross-sectional form, further tests were based on an I-cross section. Visually and machine graded laminations were used to build the cross-section of the test pieces (S10, S13, MS10, MS13 and MS17 in accordance with ON DIN 4074). A total of 75 test glulam pieces were analysed (5 series with different glulam strength classes) taking into account the optimised three-point loading test set-up with central load introduction (single-span, three-point loading test setup), 5 pieces taking into account an overlap on both sides of 500 mm, and 10 pieces taking into account a two-span, five-point loading test setup. With the aid of the results it was not possible to confirm the formal correlation between shear strength of glued laminated timber $f_{v,g}$ and the tensile strength of the laminations $f_{t,0,1}$ in accordance with EN 1194/1999. Rather, in contrast to the normative rising shear strength values with increasing glulam strength classes, a reduction in shear strengths was displayed. It would seem appropriate to discuss the EN correlation.

2 Introduction

Bending MOE and flexional strength constitute two major properties for the design of GLT components subject to bending stress. However, these are not the only two figures; shear strength and the allowable values for shear for a bending-stressed component are also important properties in the design process. Very frequently, it is shear that must be verified as the decisive factor for cross section. However, the figures available in the national design standards are mostly based on shear tests on small clear wood specimens. Nevertheless, it is clear that tests on small specimens cannot do justice to the actual load on a beam subject to bending stress. The shear design properties derived from these tests are thus of only limited informative value with respect to the shear design process for a beam subject to bending stress. EN 1194 “Timber structures – glued laminated timber – strength classes and

determination of characteristic values” defines the material properties of glued laminated timber as functions of the characteristic tensile strength or the mean tensile MOE of a lamination. According to EN 1194 [1], the characteristic bending strength for glued laminated timber is:

$$f_{m,g,k} = 7.0 + 1.15 * f_{t,0,l,k}$$

This function (basic model) was developed on the basis of numerous tests [15]. In contrast, there are no sufficient investigations available for determining the characteristic shear strength, and for this reason it has been necessary to have recourse to strength values in existing standards in order to derive the function of EN 1194 [1]:

$$f_{v,g,k} = 0,32 * f_{t,0,l,k}^{0,8}$$

The objective is to verify the extent to which this function – shear strength of glued laminated timber dependent on lamination tensile strength – represents the actual stress-based shear behaviour of glued laminated timber, whereby, given the load situation, it should be noted inter alia that the tensile strength of the lamination will only constitute an insufficient parameter for determining the shear strength value. In order to obtain shear properties that do justice to the load, it is necessary to abandon shear tests on small specimens and to define a corresponding shear test configuration.

3 State of knowledge and research

3.1 Solid timber

A work by F. Lam, H. Yee and J.D. Barrett [6] used a five-point bending test configuration, with the test beam being stressed in the middle of the span with a single load. The investigation used 100 specimens of dimensions 38 x 185 x 3000 mm for each of the wood types Douglas Fir, Hem Fir and Spruce-Pine-Fir. One half of the specimens were tested with a span to depth ratio of 5:1 and the other half at a ratio of 6:1. The contribution made by shear force on the middle support is 2.2 times higher than the amount of shearing force on the end supports. Thus, using the classical theory of elasticity, there is a calculated maximum shear stress value of $\tau_{max,classical} = 33 * P / 64 * b * d$. Fig. 1 shows the selected test set-up for a span to depth ratio of 6:1. As a result of the work, the following table 1 shows the mean values for shear strength resulting from the tests for all three wood types for $l = 5h$ and $6h$. It should be noted that there is a reduction of shear strength for a larger $l:h$ ratio, which is due to the influence of the volume. The low shear failure rate of only 40% (!) of all tests was not satisfactory.

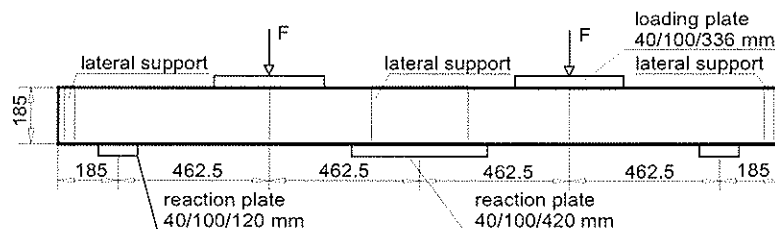


Fig. 1 Two span five point loading test configuration for a span to depth ratio of 5:1

| | | Experimental Results Median Failure Stresses [N/mm ²] ¹⁾ | |
|--------------|-----------------|--|----------------|
| | | Test Span to Specimens Depth Ratio | |
| | | L:H = 5:1 (5D) | L:H = 6:1 (6D) |
| Wood species | Douglas-Fir | 9,47 | 8,61 |
| | Hem-Fir | 7,82 | 6,20 |
| | Spruce-Pine-Fir | 7,65 | 6,70 |

¹⁾ Table 4 of the CIB-paper 28-6-1 [6] refer to the shear failures only [F. Lam]

Tab. 1 Experimental results in accordance to table 4 of the CIB-paper 28-6-1 [6]

B. Madsen [11] carried out a broad series of tests on bridge ties – 200 new undapped ties, 60 new dapped ties, 200 old dapped ties, 20 untreated and un-framed ties – in order to determine the shear strength of Douglas Fir solid timber bridge ties of 240 x 290 x 3660 mm (new ties) and 3960 mm (old ties). Using two different configurations (see Fig. 2) and after conducting 1033 tests (four series) under a proof load of 220 kN and 250 kN, a total of 338 ties failed as a result of bending and only 53 ties revealed shear failure. In all the series, B. Madsen found that the ties had a greater shear strength than bending strength under load. For the 452 tests based on the configuration with a 761 mm cantilever at each end measured from the middle of the outer loading plate to the end of the tie (See. Fig. 2), B. Madsen specifies an 0.7% fractile level for shear strength of > 4.7 N/mm² (6 shear failures). Taking into account the shear test set-up without cantilever, 557 tests resulted in 47 shear failures and a 5% fractile value for the Douglas Fir ties of 4.5 N/mm². The importance of a beam cantilever on the increase of shear strength under load was also noted. B. Madsen [11] speaks of conservative and hence uneconomic allowable shear stress properties in the “Code for engineering design in wood (CSA-086)”. These are still based on block shear tests on small clear wood specimens and thus not on the actual stress situation of a beam subject to bending stress.

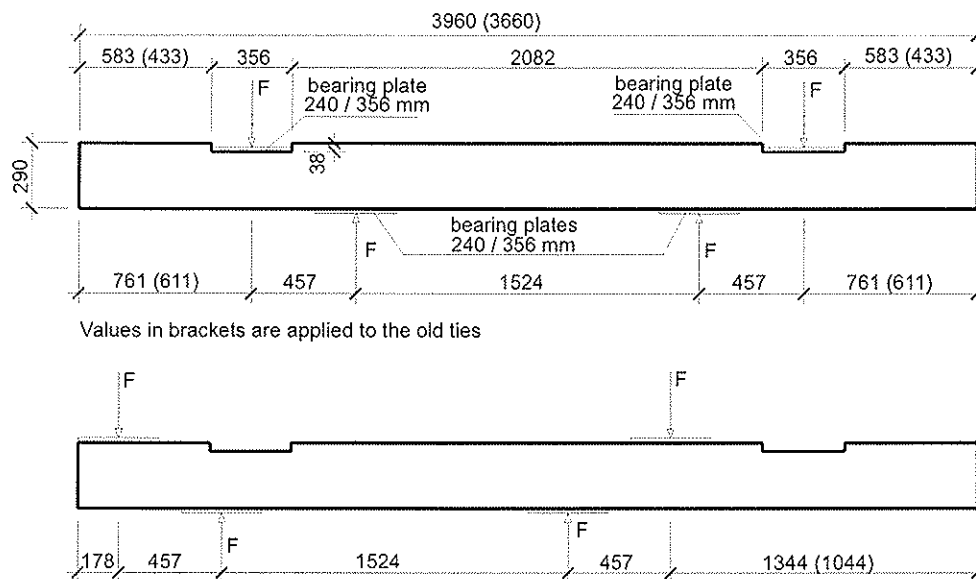


Fig. 2 Testing set-up in accordance to the CIB-paper 28-6-2 [11]

D.R. Rammer and D.I. McLean [13] in their work examined the influence of wood moisture content and wood splits on shear strength of structural timbers subject to bending stress. These investigations were conducted on the wood types Douglas Fir (DF), Engelmann Spruce (ES) and Southern Pine (SP) with cross section dimensions from 51 x 102 mm to 102 x 356 mm, taking into account a single-span three-point (span to depth ratio = 5:1) and a two-span five-point (2 x 5:1) bending test set up. In total, 1279 failure tests were carried out. The tests on DF, SP and ES with a wood moisture content of $\geq 20\%$ using the two-span five-point bending test set up revealed an influence of volume for all three wood types and hence a decline of the mean shear strength value with increasing beam volume.

| Cross Section [mm/mm] | Shear Strength [N/mm ²] |
|--------------------------|--|
| 51 / 102 | 12,76 |
| 51 / 203 | 10,71 |
| 102 / 203 | 11,27 |
| 102 / 305 | 8,33 |
| 102 / 356 | 7,39 |

Tab. 2 Shear strength of Southern Pine (12 % moisture content) in accordance to table 3 of the IWEC'96 paper by Rammer / McLean [13]

Table 2 shows the influence of beam volume. Related to the cross section 102 x 356 mm, there is an increase of 73% of the mean shear strength value for the cross section 51 x 102 mm at a wood moisture content of 12%. In addition, the influence of wood moisture content specifically on the material property shear strength was confirmed. For Southern Pine, there resulted a $f_{v,50,dry} : f_{v,50,green}$ factor of between 1.25 and 1.59 differing according to cross section. According to D.R. Ramer and D.I. McLean, the comparison of the present results with those from tests on Southern Pine glued laminated timber shows a similar behaviour with respect to the influence of volume and shear area. The shear strength values for solid timber are slightly lower and, as a result of the greater tendency to crack, have a greater spread than for glued laminated timber. With respect to the influence of cracks on shear strength, D.R. Rammer and D.I. McLean found that although there was a reduction in strength as the fault area resulting from cracks increased for DF, nevertheless the determination of crack fault areas and failure areas following the failure of the beam proved to be difficult. The low shear failure rate for Southern Pine was 35%(!) and 48%(!) for Douglas Fir.

R.H. Leicester and F.G. Young [9] conducted tests on LVL specimens with a cross section $W \times H = 120 \times 45$ mm. The test set-up was a three-point and a five-point test set up with a span to depth ratio of 6:1. In the three-point set up with $L:H = 6:1$, shear failure occurred in all 70 specimens, with a mean shear strength of **5.4 N/mm²** (COV=0.08). In the five-point test set up, only 2 of the 14 specimens suffered shear failure, resulting in a calculated mean shear stress value of 7.6 N/mm² at a bending strength of 50 N/mm².

The aim of the work by U. Korin [5] was to develop a shear test set-up to determine shear strength of structural timbers of construction element size subject to bending stress. In order to achieve this, a total of 50 structural timbers with a cross section of 45 (40) x 95 mm in 5 types of wood were tested in two test set-ups – three-point (span to depth ratio $\approx 5:1$) and five-point (span to depth ratio = 5,5:1). It was found that the I-cross section constitutes an ideal cross section shape for obtaining high shear failure rates. The I-cross section proposed by U. Korin [5] was achieved by cutting a groove of dimensions $t = 3\text{mm}$ and $b_{slot} = 0.3 \times b$ on both sides along the neutral axis of the rectangular cross section. This left an undisturbed

cross section width of $0.4 \times b$. The shear failure rate was 72% (18 of 25 tested specimens) for the three-point shear test set-up with I-cross section, and 68% (17 of 25) for the five-point set-up with rectangular cross section.

B. Madsen [10] developed a testing machine to determine the shear strength of solid timber – known as the “shear tester” – and used this machine to conduct a broad test programme. He was primarily concerned with the influence of the size of the specimens, the rate of loading increases, the wood moisture content, the state of the annular rings and the failure shapes on shear strength. Using a test of 1120 specimens (14 series of 80 specimens each) with different specimen dimensions (length, width, thickness), it was possible to show very clearly the marked influence of volume on shear strength. B. Madsen proposes a reference specimen dimension of 35 x 140 x 560 mm for his test set-up. The important influence of wood moisture content on shear strength was demonstrated using two series of 100 specimens each ($u = 25\%$ and $u = 12\%$). Three series with a total of 400 specimens were used to investigate the influence of the orientation of the annular rings – flat, diagonal, vertical – as related to the cross section of the specimen. B. Madsen was unable to determine any significant influence. The values are summarised in the following table.

| | N [-] | $f_{v,05}$ [N/mm ²] | $f_{v,50}$ [N/mm ²] |
|----------------|----------|------------------------------------|------------------------------------|
| Flat Grain | 185 | 3,6 | 5,7 |
| Diagonal Grain | 89 | 4,3 | 5,7 |
| Vertical Grain | 126 | 3,8 | 5,9 |

Tab. 3 Number of specimens and percentiles of strength of different grain orientation in accordance to [10]

Using 379 failure results, the influence of failure shape – longitudinal failure with torn fibres, failure along the annular rings, failure triggered by properties of the wood such as knots, combination of longitudinal failure and annular ring failure, failure in the jaws and no failure – on shear strength was also investigated. Different shear strength properties resulted depending on the failure form – and the influencing factors. **This relationship could accordingly also apply to different grading classes.**

V.R. Ordonez-Candelaria and R. Davalos-Sotelo [12] also used the shear test set-up of B. Madsen [10] for their shear investigations of Mexican Pine. A total of 794 specimens of varying dimensions – 35 x 140 mm, 35 x 190 mm, 35 x 240 mm, each 560 mm in length, and with two different wood moisture contents – 14% +/- 3% and at fibre saturation point – were examined. The influence of wood moisture content and volume and the failure form on shear strength was also confirmed in this work.

H.G. Larsen [7] in his work pointed out that block shear tests are not suitable for determining the shear strength of beams because of the unequal stress distribution. He proposes determining shear strength of beams subject to bending stress with I-cross section in order to obtain the desired high shear failure rate.

3.2 Glued laminated timber

The aim of the research project by B. Yeh and T.G. Williamson [18] was to determine the characteristic shear strength properties for glued laminated timber made up of Douglas Fir, Southern Pine and Spruce-Pine-Fir. As with F. Lam, H. Yee, J.D. Barrett [6] and B. Madsen [11], the article by B. Yeh and T.G. Williamson [18] points out the current unacceptable situation, namely the determination of allowable shear properties taking into account a reduction factor of 4.1 (based on small scale block shear specimens). On the basis of a three-point loading test set-up (see Fig. 3) with a span to depth ratio of 6,7:1 (for series with DF and SP) and 7.1:1 (SPF), 201 beams were tested up to failure in 1996 and 1997. Of these, 141 beams (70,1%) suffered a shear failure mostly in the neutral axis and in the lower area of the beam along an annular ring at the point of transition between early and late wood. All the glued laminated timber beams were structured symmetrically, with lower grading classes being used in the core area at risk of shear failure, while specifically visually sorted tension laminations without dove tail joints were used for the edge laminations subject to tensile stress. Two series each of widths $b = 79,4$ mm (40 DF, 40 SP) and $b = 171.5$ mm (39 DF, 42 SP) were tested for the two wood species Douglas Fir and Southern Pine. Since the influence of width proved negligible once the results had been obtained, only one series (40 SPF) with a beam width of $b = 104,8$ mm was tested for the wood species Spruce-Pine-Fir. After the tests had been conducted and evaluated, B. Yeh and G.T. Williamson, using a reduction factor of 2.1 (including the safety factor and a factor for the duration of the effect of the load), a 10% reduction to take into account possible cracks and a 7 % reduction to take into account the effect of the wood species group for SPF, specified allowable shear stress values for glued laminated timber: 3.83 N/mm^2 (characteristic value, account only taken of shear failures)/2.1/1.1 - $\rightarrow 1.65 \text{ N/mm}^2$ for Douglas Fir (DF), 4.35 N/mm^2 (characteristic value, account only taken of shear failures)/2.1/1.1 - $\rightarrow 1.88 \text{ N/mm}^2$ for Southern Pine (SP), and 3.38 N/mm^2 (characteristic value, account taken of all failure forms)/2.1/1.1/1.07 - $\rightarrow 1.35 \text{ N/mm}^2$ for SPF. **On the basis of the results obtained, it is proposed that the allowable shear stress values be raised by 25% as compared with the properties obtained from the block shear tests.**

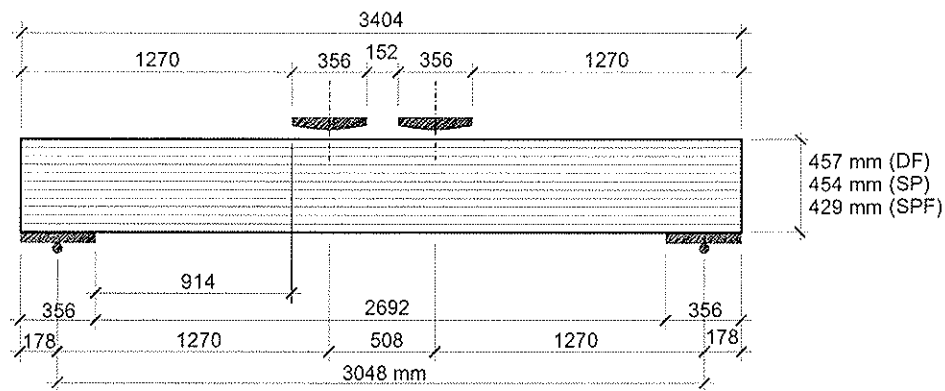


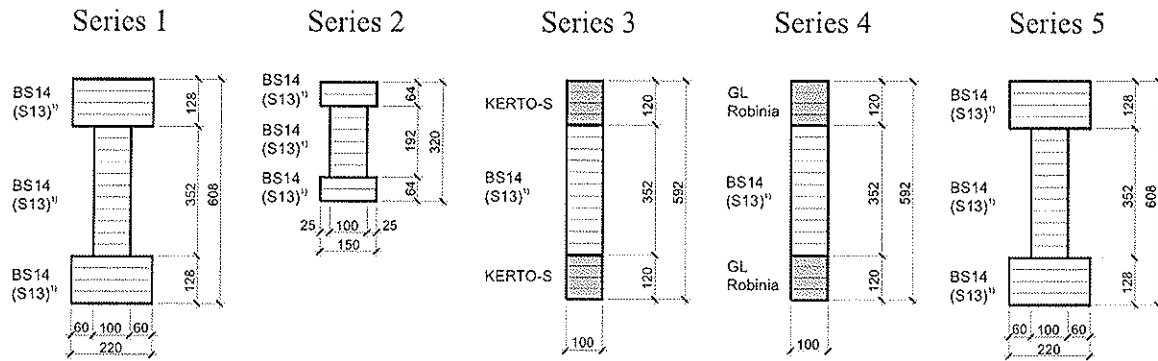
Fig. 3 Test setup in accordance to the CIB-paper 31-12-3 (not presented) [18]

3.3 Development of an optimised test configuration to determine the shear strength of glued laminated timber [16]

Almost all the research work draws attention to the unsuitability of using the results from block shear tests to draw conclusions about shear design values for structural timber or glued laminated timber beams subject to bending stress. Both for structural timber and for glued laminated timber, there is on the one hand no standardised shear test configuration for testing beams of construction element sizes with standardised specimen dimensions, nor on the other hand are there the necessary modification factors and functions, for which reason a comparison with results from known work is regarded as being of little value. There is wide correspondence in the span to depth ratio of a shear test configuration. This ranges between $l : h =$ predominantly 5:1 to maximum 7,1:1. With respect to the optimum choice of cross section, H.J. Larsen [7] and U. Korin [5] refer to the importance of an I-cross section for a standard shear test configuration in order to achieve a high shear failure rate. B. Yeh and T.G. Williamson [18] achieve the advantages of the I-cross section through the symmetrical structure of the glued laminated timber cross section and the reinforcement of the edge zones by using specific tension laminations. The works taken into account also show that the mean shear strength properties with a wood moisture content of roughly 12% are between 25% and 60% above the shear strength properties for solid timber at a wood moisture content $\geq 20\%$ (and up to fibre saturation point). In addition, the available research work shows a marked influence of volume for solid timber cross sections of 51 x 102 mm to 102 x 356 mm and for 35 x 140 mm to 35 x 240 mm. Consequently, the following conditions have been derived from the literature for the development of the proposed standard shear test configuration for glued laminated timber [16]:

- A span to depth ratio of $l : h = 5:1$ was selected.
- The cross section selected was an I-cross section or a rectangular profile with reinforcement of edge zones.
- In order to determine the influence of volume for glued laminated timber, two beam heights of $h = 608$ mm and $h = 320$ mm were taken into account.
- The measured wood moisture content of the test glued laminated timber beams was, as a result of manufacture and in accordance with the standards, 12% +/- 2%.
- Impairment of the test results as a result of unexpected cracks close to the supports were excluded or were not taken into consideration, since no significant wood moisture content differences were registered between manufacture and laboratory.

In order to specify and optimise a shear test configuration for glued laminated timber, a total of 24 glued laminated timber beams (5 test series) of construction element size were tested. A comprehensive presentation of the results can be found in the articles by G. Schickhofer and B. Obermayr [research report] [16]. The cross sections of the 5 test series are shown in the following figure 4 and table 4.



¹⁾ BS14 (S13) ≈ GL28 (C30)

Fig. 4 Cross sections of the five test series in accordance to the CIB-paper 31-21-1 [16]

| | Number of specimens | Cross section | Test configuration | Symmetrical build-up of the cross section ¹⁾ flange web |
|----------|---------------------|-----------------|------------------------------|--|
| Series 1 | 6 | I-cross section | Config. 1 ²⁾ | GL28 spruce GL28 spruce |
| Series 2 | 6 | I-cross section | Config. 1 | GL28 spruce GL28 spruce |
| Series 3 | 3 | rectangular | opt. Config. 2 ³⁾ | KERTO-S GL28 spruce |
| Series 4 | 3 | rectangular | opt. Config. 2 | GL Robinia GL28 spruce |
| Series 5 | 6 | I-cross section | opt. Config. 2 | GL28 spruce GL28 spruce |

¹⁾ BS14 (S13) ≈ GL28 (C30)

²⁾ Configuration 1 was presented in CIB-W18 1998 / paper 31-21-1 [16]

³⁾ The optimised configuration 2 (extension of the support-plate, shift of the roller bearing, introduction of an overlap was also presented in CIB-W18 1998 / paper 31-21-1 [16]

Tab. 4 Test series in accordance to the CIB-paper 31-12-1 [16]

The tests carried out on the first two series (series 1 and series 2 = 12 beams) already showed the efficiency of the I-cross section as the standard cross section for a shear test configuration. Of the 12 beams, only one beam broke as a result of bending – caused by a large spike knot. With all the other beams, shear failure or a failure combination resulting from shear and compression perpendicular to the grain (in the transitional area between lower flange and web) or tension perpendicular to the grain in the transitional area between top flange and web close to the supports) occurred. Thanks to the location and dimensions of the support plates for configuration I [16] for series 1 and 2, a high local compression stress perpendicular to the grain occurred in the transitional area between lower flange and web. The finite element analyses revealed a compression stress perpendicular to the grain of around -6.0 N/mm^2 for a resulting flat load on a loading plate of $F_{\text{res}} = 400 \text{ KN}$ (in the area of the failure loads). This

compression stress perpendicular to the grain applies at the beam end in the middle line of the cross section between lower flange and web. These concentrations of compression stress perpendicular to the grain at the end of the beam are due to a lack of overlap in configuration I. A further finite element analysis showed the influence of these compression stress perpendicular to the grain on failure behaviour. The distribution of compression stress perpendicular to the grain over the web lamination width from $-6,0 \text{ N/mm}^2$ (middle of web) to $> -8,0 \text{ N/mm}^2$ (edge of web) resulted in shear stresses in the annular rings of a magnitude of $3,5 \text{ N/mm}^2$ to $4,0 \text{ N/mm}^2$. As a result of this, the failure probability along the annular rings increases (the sliding of the late wood rings on the early wood rings).

The following table shows the test results for series 1 ($h = 608 \text{ mm}$) and series 2 ($h = 320 \text{ mm}$).

| Series | Depth [mm] | All Specimens | | Specimens with shear-failure | | Specimens with shear-failure | |
|--------------|------------|---------------|-----------------------------------|------------------------------|-----------------------------------|------------------------------|-----------------------------------|
| | | Specimens [-] | $f_{v,g,50}$ [N/mm ²] | Specimens [-] | $f_{v,g,50}$ [N/mm ²] | Specimens [-] | $f_{v,g,50}$ [N/mm ²] |
| 1 | 608 | 6 | 4,18 | 5 | 4,10 | 5 | 3,53 |
| 2 | 320 | 6 | 4,94 | 6 | 4,94 | 6 | 4,38 |
| Δ [%] | | | 18,2 | | 20,5 | | 24,1 |

Tab. 5 Test results of series 1 and 2 (test configuration 1)

The examination of the shear stress values in the middle of the beam at the time of failure (breaking load) shows a mean value of $f_{v,g,50} = 4.18 \text{ N/mm}^2$ for $h = 608 \text{ mm}$ and a mean value of $f_{v,g,50} = 4.94 \text{ N/mm}^2$ for $h = 320 \text{ mm}$. This difference of 18.2% between the mean values for series 1 and for series 2 also reveals an influence of volume for glued laminated timber.

The tests on series 1 and series 2 had shown that the following assumptions for a standard shear test configuration 1 had been chosen correctly:

- The selection of an I-cross section for the test beams lead to a high (and desirable) shear failure rate;
- The three-point loading test configuration with an individual load introduction (3-point load configuration) and a span to depth ratio of 5:1.

In contrast, problems arose as a result of the high compression stress perpendicular to the grain between lower flange and web occurring at the end of the beams. Consequently, the support area was optimised following a further finite element analysis. The measures were as follows:

- Extension of the support plate from $l = 250 \text{ mm}$ to $l = 350 \text{ mm}$;
- Shift of the roller bearing inwards;
- Introduction of an overlap of 50 mm.

These measures achieved a balanced compression stress perpendicular to the grain of roughly -3.0 N/mm^2 (middle of web) in the support area. On the basis of this optimised configuration 2, a further 12 beams were tested in the form of three test series (series 3 and series 4: rectangular cross section, series 5: I-cross section). The following table shows the results of series 5. The results for series 3 and series 4 are to be found in the literature [16].

| Series | Depth [mm] | All Specimens | | Specimens with shear-failure | | Specimens with shear-failure | |
|--------|---------------|------------------|--------------------------------------|------------------------------|--------------------------------------|------------------------------|--------------------------------------|
| | | Specimens [-] | $f_{v,g,50}$ [N/mm ²] | Specimens [-] | $f_{v,g,50}$ [N/mm ²] | Specimens [-] | $f_{v,g,50}$ [N/mm ²] |
| 5 | 608 | 6 | 4,33 | 6 | 4,33 | 6 | 3,92 |

Tab. 6 Test results of series 5 (optimised test configuration 2)

4 Load-appropriate shear strength values for glued laminated timber

As already mentioned in chapter 3.2, only a few investigations of glued laminated timber are available. Accordingly, it must be assumed that the shear function in product standard EN 1194 [1] has a basis that is insufficiently secured through tests. The same is probably also true for the shear function for structural timber pursuant to EN 338. On the contrary, these functions are derived relationships without, in particular, sufficient knowledge of the influence of different strength classes on shear strength properties. In order to have a greater insight into the problem of shear for glued laminated timber, it is therefore necessary to conduct shear tests on configurations with a suitable load.

On the basis of the present optimised shear test configuration (optimised test configuration 2), a test programme for determining load-appropriate shear strength properties for glued laminated timber was organised within the framework of a further research project at the Graz University of Technology, with the following aspects to the fore:

- Verification of the shear test configuration optimised within the framework of preliminary tests and the finite element analysis of usability with respect to a standard configuration for series tests capable of being laid down as official standard.
- Proof of sufficiently high shear failure ratio when using the present optimised test configuration.
- Determination of the influence of the visual and machine strength grading of glued laminated timber laminations (determination of the essential lamination properties for the wood species in question, spruce: tensile strength, tensile MOE, density) on shear strength and shear failure form of glued laminated timber.
- Consideration of different glued laminated timber strength classes BS11v (visually from S 10), BS 11 (by machine from MS 10), BS 14 (visually from S 13), BS 16 (by machine from MS 13) and BS 18 (by machine from MS 17) and a presentation of the results in the form of major relationships (tensile strength of laminations to shear strength of beam).

- Clarification of the influence of different configurations on the shear behaviour under stress and the failure forms. Using the optimised three-point load test configuration, the question arises of whether higher shear strength values are to be expected from a three-point loading configuration with overlap (beam overlap: 500 mm) or a two-span five-point loading configuration (continuous beam).
- Comparison of the shear strength properties obtained from the test with the design properties laid down by national regulations. In addition, the aim is to check the accuracy of the shear function in EN 1194 and in EN 338.
- Presentation, description and analysis of the failure forms in order to achieve a better understanding of the failure mechanism.
- The influence of different cross section structures in terms of the opposing position of the top lower flange lamination and the bottom web lamination on shear strength properties.

5 Test programme

The entire test programme is shown in the following table 7 in total, in addition to the 5 preliminary test series already available (24 glued laminated timber beams) – series 1 to series 5 – used to determine an optimised test configuration, a further 90 glued laminated timber beams of construction element size were tested in the form of 7 test series.

| Series | Specimens | Subseries | Grading Classes | Grading Method | Free span [mm] | Beam depth [mm] | Test configuration |
|--------|-----------|-----------|-----------------|----------------|----------------|-----------------|---|
| 5 | 6 | | BS14 | visual | 3040 | 608 | optimised single-span three-point loading setup |
| 6 | 15 | 5 5 5 | BS11 | visual | 3040 | 608 | optimised single-span three point loading setup |
| 7 | 15 | 5 5 5 | BS14 | visual | 3040 | 608 | |
| 8 | 15 | 6 7 2 | BS11 | masch. | 3040 | 608 | |
| 9 | 15 | 5 5 5 | BS16 | masch. | 3040 | 608 | |
| 10 | 15 | 5 5 5 | BS18 | masch. | 3040 | 608 | |
| 11 | 5 | | BS11 | masch. | 3040 | 608 | opt. single-span three-point loading setup with overlap |
| 12 | 10 | | BS11 | masch. | 2 x 1565 | 320 | two-span five-point loading setup |

Tab. 7 Test programme

5.1 Test configurations

For the three-point load beam without overlap, 5 series were tested: series 6 with BS11v (visual), series 7 with BS 14 (visual), series 8 with BS 11 (machine), series 9 with BS 16 (machine) and series 10 with BS 18 (machine). Each series comprises 15 beams and is broken down into 3 sub-series of 5 specimens each (with the exception of series 8), which differ by virtue of different lamination layers. Thus 75 three-point load beams without overlap were tested. The evaluation also takes into account series 5 with 6 beams. This was tested within

the framework of the development of the test configuration [16] and is identical with series 7 both in terms of structure and in terms of glued laminated timber strength class, namely BS 14 (visual). In series 11, a further 5 three-point load beams were tested but with an overlap of 500 mm. This series was manufactured using MS 10 laminations (machine) and is thus to be ascribed to strength class BS 11 (machine). 10 continuous beams were tested in series 12. The cross section height in this series was 320 mm, in contrast with the beam height of 608 mm for all other series. Like series 11, series 12 was also manufactured using MS 10 lamination (machine graded) – hence BS 11 (machine graded). The following shows the test configurations and cross section structures.

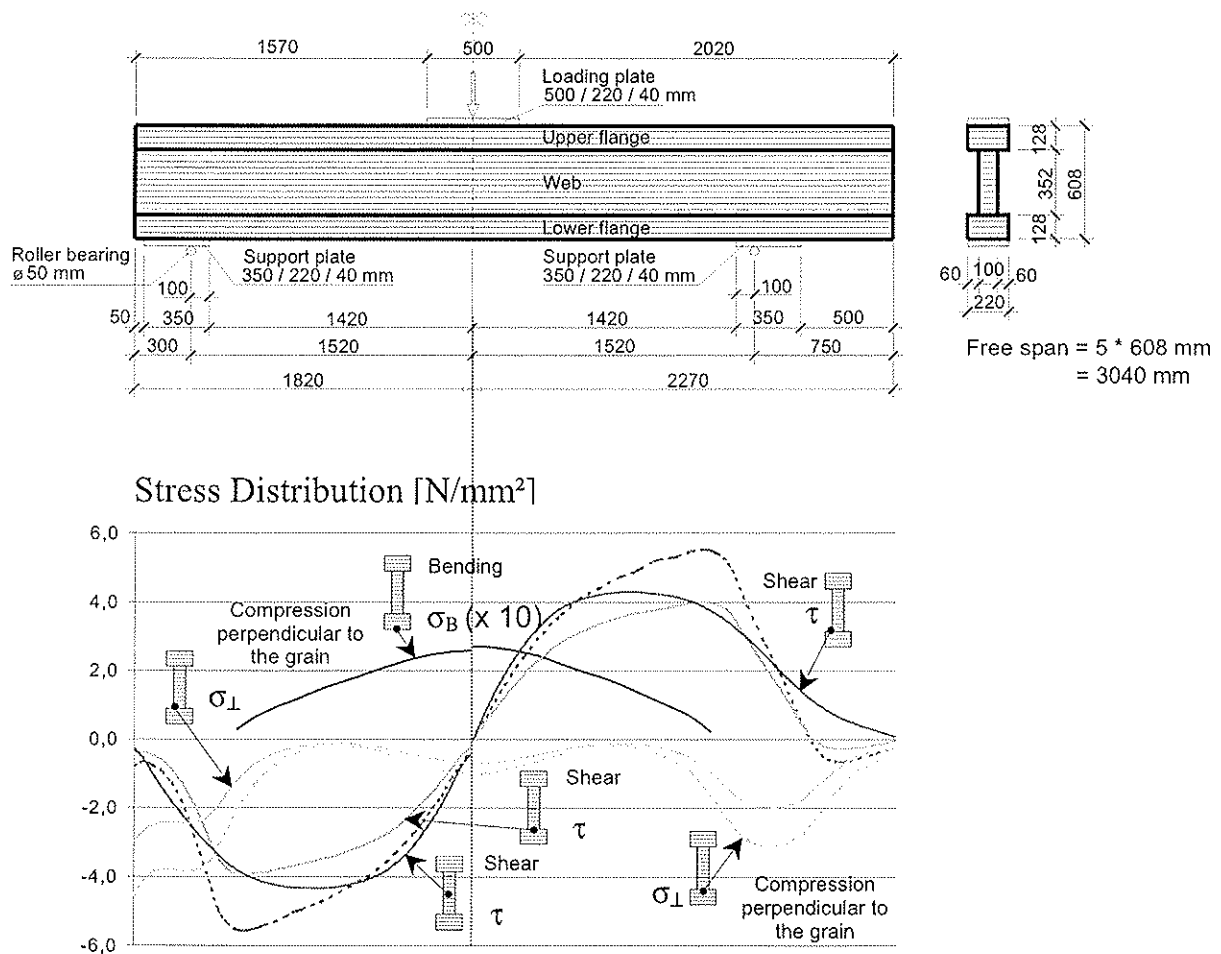


Fig. 5 Stress distribution for the single-span beams with and without overlap

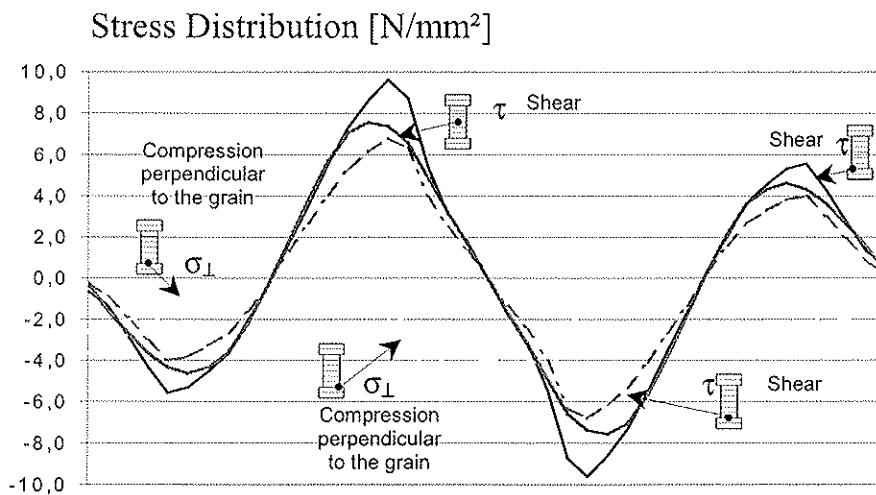
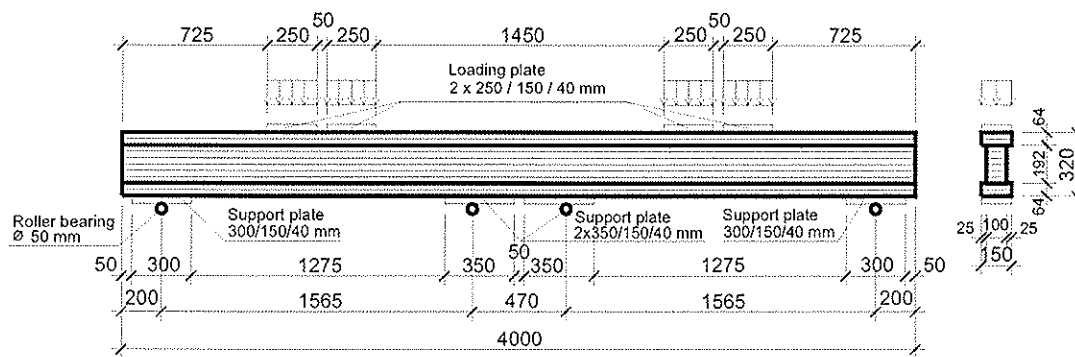


Fig. 6 Stress distributions for the continuous beam

5.1.1 Series 6 to series 10

The primary objective of all five test series was to achieve a high shear failure rate in order to confirm the configuration selected and to be able to put forward this configuration as a possible standard configuration for EN 1194 and EN 408. In all five series, account was also taken of the structure of the beams in terms of the orientation of the annular rings, in order in particular to investigate the influence of the opposing position of the top lower flange lamination and the bottom web lamination. In addition, a major objective was to identify the influence of the glued laminated timber strength classes on the relevant shear strength values. Series 8, 9 and 10 were expected specifically to provide information on this point. The objective was also to be able to verify the relationship given in EN 1194 between shear strength of the glued laminated timber and lamination tensile strength.

5.1.2 Series 11 and series 12

In series 11, a further 5 three-point load beams were tested, but with an overlap of 500 mm. This series was manufactured using laminations of grading class MS 10 (hence glued laminated timber strength class BS 11 \approx GL 24 pursuant to EN 1194) and was expected to help clarify whether the given overlap influences shear strength. In series 12, 10 continuous beams were tested. In contrast to the other series ($h = 608$ mm), the cross section height of this series was 320 mm. The beams were manufactured using laminations of grading class MS

10 (hence glued laminated timber strength class BS 11 \approx GL 24). This series was intended to determine the increased influence of the continuous beam effect on shear strength.

5.5 Starting material

The starting material consisted of 176 specimens of spruce from an austrian sawmill with a cross section of 150 x 35 mm.

The tensile tests were carried out in accordance with the regulations to EN 408. The free test length was 2860 mm. The required measurements for determining the modulus of elasticity were carried out by means of inductive transducers and a test length of 5*w., i.e. 750 mm on two opposite points.

| Pro- perties | Cross section [mm/mm] | Grading Classes ¹⁾ | Speci- mens | Normal-Distribution | | | Log-Normal- Distribution | Weibull- Distribution (2p) |
|---------------------|-----------------------------|----------------------------------|----------------|----------------------------|------------------------------|------------|-----------------------------|----------------------------------|
| | | | | 5% [N/mm ²] | mean [N/mm ²] | COV [-] | 5% [N/mm ²] | 5 % [N/mm ²] |
| Density | 150 / 35 | S10 | 45 | 385 | 451 | 0,09 | | |
| | | S13 | 45 | 383 | 443 | 0,08 | | |
| | | MS13 | 45 | 406 | 475 | 0,09 | | |
| | | MS17 | 41 | 433 | 506 | 0,09 | | |
| Tensile MOE | 150 / 35 | S10 | 45 | 8242 | 10969 | 0,15 | 8506 | 7360 |
| | | S13 | 45 | 8664 | 12810 | 0,20 | 8980 | 8297 |
| | | MS13 | 45 | 12162 | 13813 | 0,07 | 12261 | 11297 |
| | | MS17 | 41 | 13654 | 16352 | 0,10 | 13874 | 12530 |
| Tensile strength | 150 / 35 | S10 | 45 | 10,45 | 21,83 | 0,32 | <u>12,62</u> | 9,95 |
| | | S13 | 45 | <u>16,66</u> | 34,83 | 0,32 | 18,94 | 16,45 |
| | | MS13 | 45 | 18,31 | 32,78 | 0,27 | <u>20,47</u> | 16,68 |
| | | MS17 | 41 | 25,57 | 44,51 | 0,26 | <u>28,04</u> | 23,48 |

¹⁾ Grading classes in accordance to DIN 4074-1; machine grading was done with GRADEMASTER 403

Tab. 8 Test data of the starting material

5.3 Conduct of the shear tests

The shear tests were carried out in the Experimental Laboratory for Structural Engineering at the Graz University of Technology under the direction of K. Kernbichler.

The load was applied at a constant advance speed via the load piston. The speed was 0.1 mm/sec. This ensured compliance with the requirement of EN 408 that the maximum load be reached within (300 +/- 120) sec. when determining bending strength, and for the determination of shear strength.

Figs. 7 and 8 show the optimised test structure (I-cross section, stress-optimised beam geometry, 40 mm thick support plates and eccentric roller bearings).

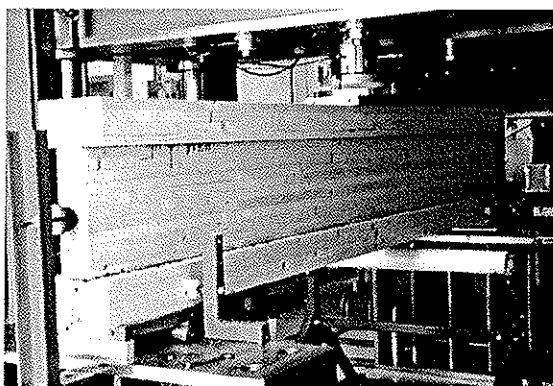


Fig. 7 Optimised test configuration

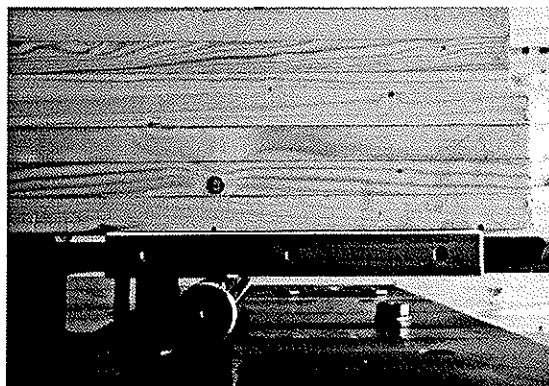


Fig. 8 Support and eccentric roller bearing

5.4 Test results and assessment

Thanks to the cross section structure selected and the optimised test configuration – three-point load beam, continuous beam – a shear failure rate over all series (series 6 to series 12) of **82 %** was achieved. Only in series 7 (BS 14 \approx GL 28) did a compression perpendicular to the grain failure of the upper flange in the area of the loading plates occur on 40% of the test beams. This was associated with the upper flange cracking open in the middle in the longitudinal direction. In the other series, this failure was avoided by specifically selecting “upper flange laminations” with higher density and annular ring density and a corresponding arrangement – right-hand side facing downwards. As a result of these measures, series 9 to 12 achieved (more or less) a 100% shear failure. As a result of the high shear failure rate, it can be concluded that the selected optimised shear test configuration combined with a specific I-cross section structure appears suitable for the definition of a standardised shear test configuration.

5.5 Shear strength

On the basis of the individual results of the 7 individual test series set out in the schedule, the statistical properties set out in the following table – 5% fractile value, mean value and variation coefficient – were calculated on the basis of different distribution functions.

Test results of the visual graded laminations built-up GLT beams

| Series | All / Shear | Grading Class | Normal-Distribution | | | Log-Normal-Distribution | | | Weibull-Distribution (2p) | |
|--------|-------------|---------------|----------------------|----------------------|-------|-------------------------|----------------------|-------|---------------------------|----------------------|
| | | | 5% | mean | COV | 5% | mean | COV | 5 % | mean |
| | | | [N/mm ²] | [N/mm ²] | [-] | [N/mm ²] | [N/mm ²] | [-] | [N/mm ²] | [N/mm ²] |
| 6 | All | BS11v | 3,79 | 4,42 | 8,61 | 3,78 | 4,40 | 9,27 | 3,90 | 4,48 |
| 6 | Shear | BS11v | 3,65 | 4,36 | 9,82 | 3,65 | 4,34 | 10,45 | 3,73 | 4,42 |
| 5+7 | All | BS14 | 3,63 | 4,22 | 8,43 | 3,63 | 4,20 | 8,90 | 3,59 | 4,26 |
| 5+7 | Shear | BS14 | 3,46 | 4,20 | 10,73 | 3,47 | 4,18 | 11,29 | 3,45 | 4,26 |
| 5+6+7 | All | visual | 3,69 | 4,30 | 8,70 | 3,68 | 4,28 | 9,22 | 3,68 | 4,35 |
| 5+6+7 | Shear | visual | 3,55 | 4,27 | 10,25 | 3,56 | 4,25 | 10,84 | 3,56 | 4,33 |

Test results of the machine graded laminations built-up GLT beams

| Series | All / Shear | Grading Class | Normal-Distribution | | | Log-Normal-Distribution | | | Weibull-Distribution (2p) | |
|------------------|-------------|-----------------|----------------------|----------------------|-------|-------------------------|----------------------|-------|---------------------------|----------------------|
| | | | 5% | mean | COV | 5% | mean | COV | 5 % | mean |
| | | | [N/mm ²] | [N/mm ²] | [-] | [N/mm ²] | [N/mm ²] | [-] | [N/mm ²] | [N/mm ²] |
| 8 | All | BS11 | 3,76 | 4,17 | 6,09 | 3,77 | 4,17 | 6,00 | 3,60 | 4,20 |
| 8 | Shear | BS11 | 3,77 | 4,10 | 4,80 | 3,78 | 4,09 | 4,77 | 3,68 | 4,12 |
| 9 | All | BS16 | 3,67 | 4,11 | 6,51 | 3,69 | 4,11 | 6,57 | 3,59 | 4,15 |
| 10 | All | BS18 | 3,14 | 3,84 | 11,09 | 3,17 | 3,82 | 11,43 | 3,12 | 3,90 |
| 5+6+7+ 8+9+10 | All | 81 single beams | 3,53 | 4,16 | 9,17 | 3,54 | 4,15 | 9,57 | 3,47 | 4,21 |
| 12 | All | BS11 | 3,86 | 5,64 | 19,13 | 3,98 | 5,65 | 20,36 | 3,80 | 5,72 |

Tab. 9 Shear strength values for the different test series and GLT strength classes

5.5.1 Three-point load beam

For the two glued laminated timber strength classes made of visually graded laminations – series 6: BS 11v \approx GL 24, series 7: BS 14 \approx GL 28 – the mean values for the shear strength properties tend to be higher than for the high glued laminated timber classes. Compared with the mean value $f_{v,g,50} = 4.21 \text{ N/mm}^2$ over the series 5 to 10, there was a 6.4% higher mean value at $f_{v,g,50} = 4.48 \text{ N/mm}^2$ for BS 11v (\approx GL 24) for the lowest strength class and a mean value 7.4% lower at $f_{v,g,50} = 3.90 \text{ N/mm}^2$ for the highest strength class BS 18 (\approx GL 36). This result of the test is shown in figure 9. This clearly shows the falling tendency of the shear strength properties. A reason for this can be derived from the different failure forms and causes.

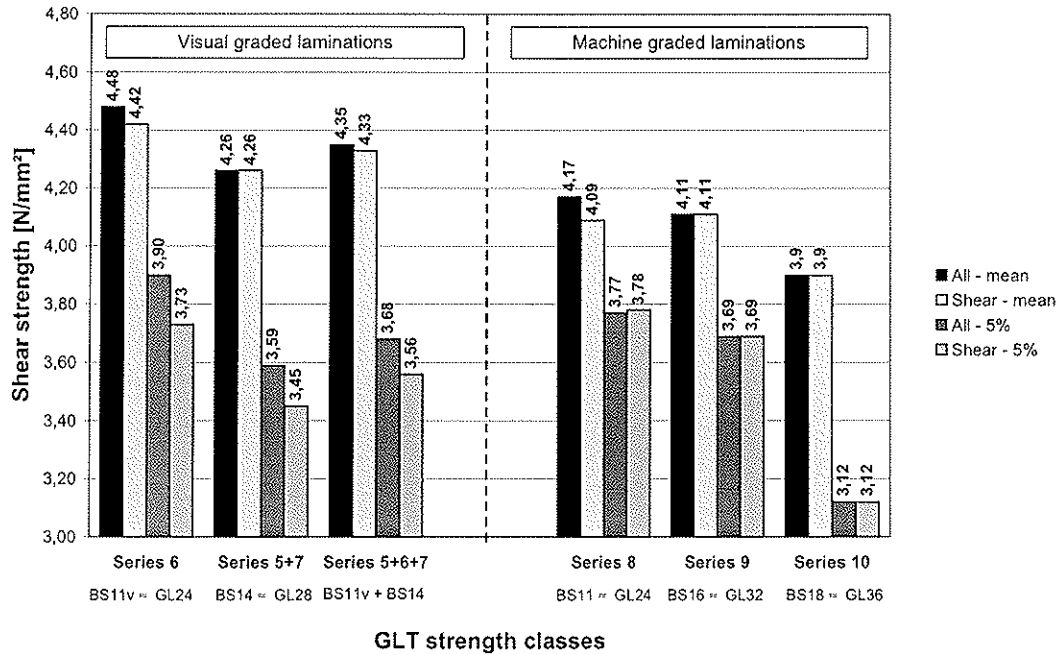


Fig. 9 Relationship between GLT grading classes and GLT shear strength

5.5.2 Three-point load beam with overlap

The small number of test beams with an overlap of 500 mm ($N = 5$) prevented statistical evaluation. The arithmetic mean of the shear strength of series 11 (BS 11 with overlap) is $f_{v,g,50} = 3.97 \text{ N/mm}^2$. At -7.8%, this is substantially below the mean value of series 8 at $f_{v,g,50} = 4.17 \text{ N/mm}^2$. The small size of the specimen means that it is not possible to make any general statements about the influence of a cantilever on shear strength. However, it can be assumed that with the present geometry dimensions, an overlap of 500 mm appears to be too small in order to have any positive effect on an increase of shear strength.

5.5.3 Continuous beam, two-span five-point set-up

The appendix to the present paper sets out a summary in tabular form of the results from the continuous beam tests. This shows clearly that a total failure of these beams did not occur immediately upon the first crack, but only after a certain load history in the form of a bending failure. The first crack around the middle support was a shear failure in each of the 10 beams. The remaining area up to the edge of the beam meant that the load bearing capacity could continue to increase. Taking into account the **first cracks (shear failures around the central support)**, series 12 results in a mean value of $f_{v,g,50} = 5.72 \text{ N/mm}^2$. Related to the mean value of series 8 ($f_{v,g,50} = 4.17 \text{ N/mm}^2$, likewise BS 11 \approx GL 24), but without taking into account the influence of volume ($h_{\text{three-point}} = 608 \text{ mm}$, $h_{\text{five-point}} = 320 \text{ mm}$), series 12 reveals a mean value 37% higher than for series 8.

5.6 Failure mechanisms

Fundamentally, the 4 following failure forms occurred:

- Shear failure
- Bending failure
- Compression and Tension perpendicular to the grain failure of the upper flange (load introduction area)
- Tension perpendicular to the grain between upper flange and web (bearing area, top).

5.6.1 Shear failure

A typical shear failure is characterised by a reciprocal shift of the two beam parts separated by the failure. A friction surface is created along the transition from early to late wood along an annular ring. The failure line, however, may jump over to adjacent annular rings and can also continue in adjacent laminations.

5.6.2 Bending failure

A failure as a result of bending commences around the middle of the lower flange. Mostly, it begins at a spike knot, which weakens the cross section at the point that is subject to the highest bending load.

5.6.3 Compression and tension perpendicular to the grain failure of the upper flange

A failure of the upper flange as a result of compression perpendicular to the grain under the loading plate occurs if the upper flange is too soft. In this case, the edges of the loading plate cut into the upper flange, causing considerable compression. As a further consequence, the web shifts into the soft upper flange, which arches downwards over the web and as a result tension stress perpendicular to the grain occurs on the upper side of the upper flange, ultimately capable of leading to the cracking open of the upper flange longitudinally.

5.6.4 Tension perpendicular to the grain between upper flange and web

As the finite element analysis showed, tension arises at right angles to the fibre at the ends of the beams at the transition between the web and the upper flange and is increased by the large deformations of the upper flange in the load introduction area. The considerable deformation under the loading plate causes the ends of the upper flange to bend upwards. However, the unity of the web and the lower flange is not impaired by the compression and remains very rigid as compared with the upper flange. The tension stresses perpendicular to the grain arising in this way lead to a failure as a result of the low tension strength perpendicular to the grain of the timber (see figure 10).



Fig. 10 Failure caused by tension perpendicular to the grain between the upper flange and the web

6 Importance of the results for the shear function in EN 1194 and effects on national standards

The shear function specified in EN 1194: 1999, appendix A/Table A.1

$$f_{v,g,k} = 0.32 * f_{t,0,l,k}^{0.8}$$

has thus not been confirmed. The relationship therein between the shear strength of the glued laminated timber $f_{v,g,k}$ and the tensile strength of the timber laminations $f_{t,0,l,k}$ should be withdrawn. As is shown in the following diagram, shear strength – contrary to the specifications in the standard – falls with increasing tensile strength of the timber laminations.

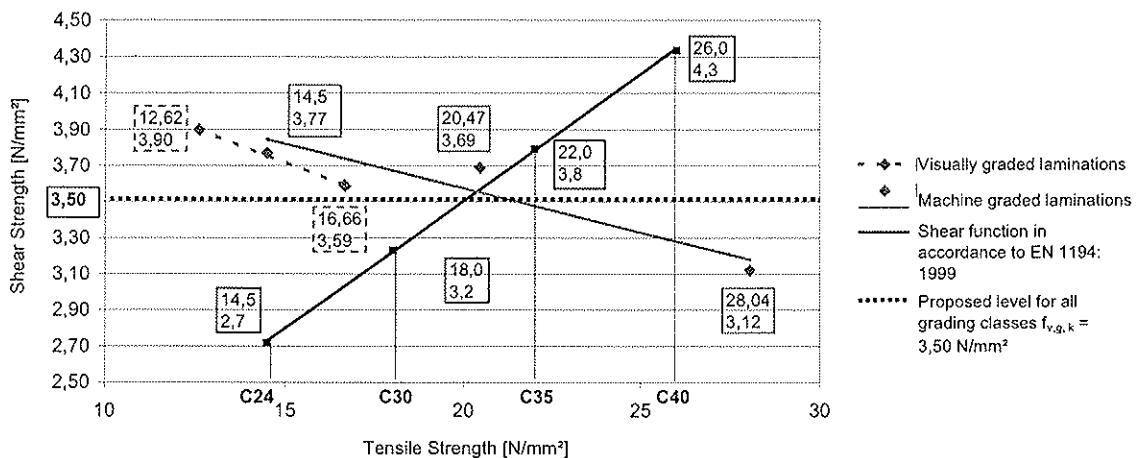


Fig. 11 Relationship between the shear strength of GLT and the tensile strength of the laminations

It is therefore to be assumed that it is not the tensile strength of the timber laminations but rather microscopic and macroscopic timber features (“friction surface” between early and late wood, knottiness) that influence the shear strength properties. In this connection, reference is made to the contributions by P. Glos and M. Tratzmiller [3] and D. Larsson et al [8]. From this it can be concluded that higher knottiness in the trunk core area must be associated with high shear properties in these zones. It was possible to confirm this indirectly with our own results presented here. The lower glued laminated timber strength classes had higher shear

strength values than the high strength classes. A reason is probably to be found in the grading parameter knottiness for timber laminations. Grading classes S10 and MS10 usually have greater knottiness than grading classes S13 and MS13 or MS17. At the same time, the yield of high lamination strength classes increases with the distance from the pith, indicating that the location of the cut timber in the trunk cross section has a decisive influence on strength class and hence on the mechanical and physical properties. Coniferous wood cut close to the pith is usually associated with the following characteristics: high knottiness, low tensile and bending strength and MOE, low density, large width of annular rings but a high shear strength and a high shear modulus. The presence of higher shear properties in the area close to the pith is probably primarily due to the following causes:

- A higher so-called “dowelling effect” resulting from the higher knottiness in the core area;
- The following illustration shows the failure surfaces of shear failures with differing knottiness. The knots at right angles to the annular ring surfaces (= failure surface) can be clearly seen. These act like a dowel and thus have the effect of increasing shear strength. This may also be a possible plausible reason for the decline in shear strength as the strength of glued laminated timber increases.

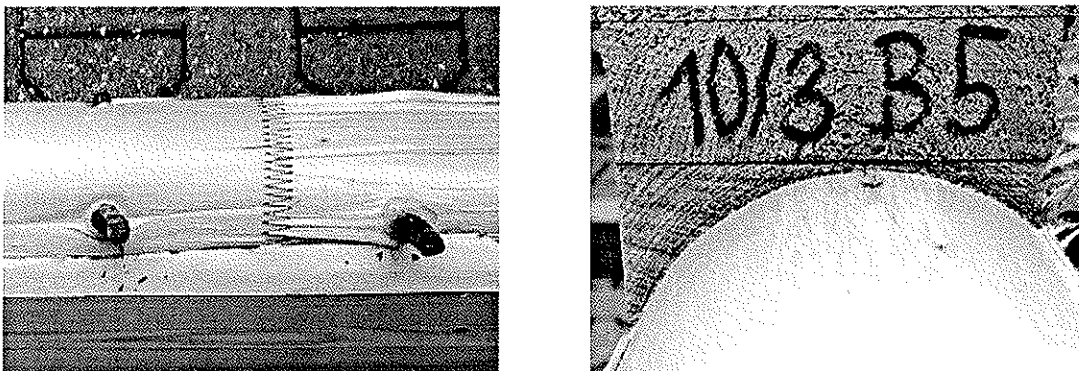


Fig. 12 Failure surface with (‘dowelling effect’) and without knots

Other causes may be:

- A larger number of resistant late wood shear zones in the case of tangential cuts (possible shear area in failure condition);
- Larger surface and hence larger shear area between the early and late wood zones within one annular ring;

On the basis of the known work and our own research results presented here, the following can be proposed for the European standardisation work:

- Establishment of a standardised shear test configuration appropriate to the load in order to determine the shear strength values for glued laminated timber. A three-point load beam with I-cross section is recommended [16];
- Using the said shear test configuration and the recommended I-cross section structure, a shear failure rate of over 82% (for series 9, 10 and 11, even 100%) could be achieved.

- The relationship laid down in the standard between shear strength of the glued laminated timber beam and the tensile strength of the laminations could not be confirmed. On the contrary, increasing glued laminated timber strength class is associated with a decrease of shear strength values.
- For continuous beams (with the exception of the areas at the end supports) higher shear strength values can be assumed in corresponding load situations in the glued laminated timber (loads causing compression perpendicular to the grain).
- It is recommended that the relationship $f_{v,g,k} = 0.32 * f_{t,0,l,k}^{0.8}$ laid down in the standard be deleted and at least a constant shear strength value be formulated for all strength classes (of one wood species). For the coniferous wood species spruce, this could be in the range of around $f_{v,g,k} = 3.50 \text{ N/mm}^2$. On the basis of this value, this would result for glued laminated timber classes GL24 and GL28 in an increase of around 22.9% and around 8.6% respectively, and a reduction of around -8.6% and around -22.9% for GL32 and GL36 respectively.
- The failure is essentially influenced by timber properties of relevance to shear strength (form and condition of the shear area = usually the area of transition between early and late wood).
- It was not possible to demonstrate that shear strength properties are influenced by different cross section structures in terms of the opposing position of the top lower flange lamination and the bottom web lamination.

7 Acknowledgement

I appreciate the Technical Commission of the Austrian GLT Association and first of all the European President of GLT Association Mr H. Stingl, since they enabled us (G. Schickhofer, B. Obermayr, G. Rauchlatner) to do this piece of work. Moreover I want to give my thanks also to the Experimental Laboratory for Structural Engineering of the TU Graz, above all K. Kernbichler and J. Linder, since they assisted our project decisively. Discussion with E. Gehri from the ETH Zurich helped us a lot on our way. Of course I want to thank everybody for the interest taken in our work.

Thanks also to M. Augustin / Lignum Research Graz for preparing the figures and tables of this paper.

8 Literature

- [1] EN 1194: 'Timber Structures - Glued laminated timber - Strength classes and determination of characteristic values', April 1999.
- [2] Foschi, R.O.: 'Longitudinal Shear Design of Glued Laminated Beams', CIB-W18-Meeting, Paper 18-12-2, Beit Oren, Israel, June 1985.
- [3] Glos, P., Tratzmiller, M.: 'Erzeugung von höherwertigem Bauschnittholz aus Starkholz', Allgemeine Forstzeitung / Der Wald, 22 / 1996, page 1230-1231
- [4] Görlacher, R., Kürth, J.: 'Determination of Shear Modulus', CIB-W18-Meeting, Paper 27-10-1, Sydney, Australia, July 1994.

- [5] Korin, U.: 'Determination of the Shear Strength of Timber', International Wood Engineering Conference '96, New Orleans, Louisiana, USA, Proceedings Vol. 2, page 91-95, 1996.
- [6] Lam, F., Yee, H., Barrett, J.D.: 'Shear Strength of Canadian Softwood Structural Lumber', CIB-W18-Meeting, Paper 28-6-1, Copenhagen, Denmark, April 1995.
- [7] Larsen, H.J.: 'Determination of Shear Strength and Strength Perpendicular to Grain', CIB-W18-Meeting, Paper 20-6-3, Dublin, Ireland, September 1988.
- [8] Larsson, D. et al: 'Mechanical properties of sawn timber from Norway spruce', *Holz als Roh- und Werkstoff*, 56 (1998), Springer, page 331-338
- [9] Leicester, R.H., Young, E.G.: 'Shear Strength of Continuous Beams', CIB-W18-Meeting, Paper 24-10-1, Oxford, United Kingdom, September 1991.
- [10] Madsen, B.: 'In-Grade Testing and Results', in 'Structural behaviour of Timber, Timber Engineering Ltd., North Vancouver, Canada/BC, ISBN 0-9696162-0-1, page 102-107, 1992.
- [11] Madsen, B.: 'Shear Strength of Douglas Fir Timber', CIB-W18-Meeting, Paper 28-6-2, Copenhagen, Denmark, April 1995.
- [12] Ordonez-Candelaria, V.R., Davalos-Sotelo, R.: 'Shear Strength of Mexican Pine', International Wood Engineering Conference '96, New Orleans, Louisiana, USA, Proceedings Vol. 2, page 104-111, 1996.
- [13] Rammer, D.R., McLean, D.I.: 'Recent Research on the Shear Strength of Wood Beams', International Wood Engineering Conference '96, New Orleans, Louisiana, USA, Proceedings Vol. 2, page 96-103, 1996.
- [14] Riberholt, H.: 'Comparison of a shear strength design method in Eurocode 5 and a more traditional one', CIB-W18-Meeting, Paper 21-12-4, Parksville, Canada, September 1988.
- [15] Schickhofer, G.: 'Development of Efficient Glued Laminated Timber', CIB-W18-Meeting, Paper 29-12-1, Bordeaux, France, August 1996.
- [16] Schickhofer, G., Obermayr, B.: 'Development of an Optimised Test Configuration to Determine Shear Strength of Glued Laminated Timber', CIB-W18-Meeting, Paper 31-21-1, Savonlinna, Finland, August 1998.
- [17] Stieda, C.K.A.: 'Planar Shear Capacity of Plywood in Bending', CIB-W18-Meeting, Paper 16-4-1, Lillehammer, Norway, May/June 1983.
- [18] Yeh, B., Williamson, T.G.: 'Shear Strength of Structural Glued Laminated Timber based on Full-size Flexure Tests', CIB-W18-Paper 31-12-3 (not presented), August 1998.

Appendix

The following table A.1 shows the results from 5 series with three-point load beam “without overlap” and series 11 of the three-point load beam with 500 mm overlap.

| Specimens | Failure | Fracture Force | Weight | Density | Moisture Content | Density at 12% MC | f_v | f_v |
|------------|-------------------|----------------|--------|----------------------|------------------|----------------------|-----------------------------|----------------------|
| | | | | | | | (at the middle of the beam) | (at the crack) |
| | [-] | [kN] | [kg] | [kg/m ³] | [%] | [kg/m ³] | [N/mm ²] | [N/mm ²] |
| S 6 / 1 B1 | Shear | 306,60 | 135,00 | 405,24 | 10,30 | 408,69 | 3,46 | 2,81 |
| S 6 / 1 B2 | Bending, Shear | 420,00 | 141,20 | 423,85 | 9,80 | 428,52 | 4,74 | |
| S 6 / 1 B3 | Bending | 407,40 | 143,40 | 430,46 | 11,50 | 431,54 | 4,59 | |
| S 6 / 1 B4 | Shear | 423,40 | 150,80 | 452,67 | 11,30 | 454,26 | 4,77 | 4,18 |
| S 6 / 1 B5 | Shear | 411,70 | 146,80 | 440,67 | 10,77 | 443,38 | 4,64 | 4,29 |
| S 6 / 2 B1 | Shear | 425,30 | 136,90 | 410,95 | 13,70 | 407,45 | 4,80 | 4,73 |
| S 6 / 2 B2 | Comp. perpend. UF | 397,60 | 148,10 | 444,57 | 11,87 | 444,86 | 4,48 | |
| S 6 / 2 B3 | Shear | 378,70 | 144,45 | 433,61 | 11,10 | 435,56 | 4,27 | 4,11 |
| S 6 / 2 B4 | Shear | 404,70 | 144,45 | 433,61 | 11,20 | 435,35 | 4,56 | 3,71 |
| S 6 / 2 B5 | Shear | 392,30 | 152,50 | 457,78 | 11,97 | 457,84 | 4,42 | 3,60 |
| S 6 / 3 B1 | Shear | 327,80 | 135,20 | 405,84 | 12,30 | 405,24 | 3,70 | 3,01 |
| S 6 / 3 B2 | Shear | 403,60 | 142,80 | 428,66 | 11,70 | 429,30 | 4,55 | 3,70 |
| S 6 / 3 B3 | Shear | 403,00 | 141,65 | 425,21 | 12,20 | 424,78 | 4,54 | 4,36 |
| S 6 / 3 B4 | Comp. perpend. | 403,80 | 140,80 | 422,65 | 10,80 | 425,19 | 4,55 | |
| S 6 / 3 B5 | Shear | 373,10 | 140,20 | 420,85 | 10,90 | 423,17 | 4,21 | 3,42 |
| S 7 / 1 B1 | Shear | 356,40 | 149,70 | 449,37 | 11,43 | 450,65 | 4,02 | 3,27 |
| S 7 / 1 B2 | Comp. perpend. UF | 387,60 | 145,05 | 435,41 | 11,17 | 437,22 | 4,37 | |
| S 7 / 1 B3 | Shear | 376,50 | 150,40 | 451,47 | 11,87 | 451,77 | 4,25 | 4,24 |
| S 7 / 1 B4 | Shear | 398,60 | 147,15 | 441,72 | 10,83 | 444,30 | 4,49 | 3,66 |
| S 7 / 1 B5 | Comp. perpend. UF | 375,30 | 151,00 | 453,27 | 11,83 | 453,66 | 4,23 | |
| S 7 / 2 B1 | Shear | 318,20 | 148,50 | 445,77 | 11,13 | 447,71 | 3,59 | 3,14 |
| S 7 / 2 B2 | Shear | 286,50 | 149,20 | 447,87 | 12,53 | 446,68 | 3,23 | 3,19 |
| S 7 / 2 B3 | Comp. perpend. UF | 391,60 | 145,80 | 437,66 | 14,20 | 432,85 | 4,42 | |
| S 7 / 2 B4 | Tension UF-Web | 377,20 | 148,10 | 444,57 | 12,60 | 443,23 | 4,25 | |
| S 7 / 2 B5 | Comp. perpend. UF | 365,30 | 147,45 | 442,62 | 11,63 | 443,44 | 4,12 | |
| S 7 / 3 B1 | Shear | 387,30 | 147,55 | 442,92 | 11,33 | 444,40 | 4,37 | 4,20 |
| S 7 / 3 B2 | Shear | 414,80 | 150,50 | 451,77 | 12,23 | 451,25 | 4,68 | 4,11 |
| S 7 / 3 B3 | Tension UF-Web | 374,90 | 145,60 | 437,06 | 12,47 | 436,04 | 4,23 | |
| S 7 / 3 B4 | Comp. perpend. UF | 377,30 | 148,40 | 445,47 | 11,97 | 445,53 | 4,25 | |
| S 7 / 4 B1 | Comp. perpend. UF | 365,80 | 151,00 | 453,27 | 13,07 | 450,85 | 4,12 | |
| S 8 / 1 B1 | Tension UF-Web | 412,20 | 145,70 | 437,36 | 10,97 | 453,44 | 4,65 | |
| S 8 / 1 B2 | Shear | 357,70 | 145,25 | 436,01 | 12,00 | 453,39 | 4,03 | 3,53 |
| S 8 / 1 B3 | Shear | 384,00 | 149,20 | 447,87 | 9,97 | 465,05 | 4,33 | 4,16 |
| S 8 / 1 B4 | Shear | 343,00 | 145,75 | 437,51 | 10,07 | 455,30 | 3,87 | 3,49 |
| S 8 / 1 B5 | Tension UF-Web | 373,00 | 143,75 | 431,51 | 9,83 | 448,32 | 4,21 | |
| S 8 / 1 B6 | Bending | 410,20 | 142,75 | 428,51 | 10,23 | 444,30 | 4,63 | |
| S 8 / 2 B1 | Shear | 392,40 | 141,20 | 423,85 | 9,90 | 439,92 | 4,42 | 4,36 |
| S 8 / 2 B2 | Shear | 357,80 | 137,95 | 414,10 | 10,07 | 430,60 | 4,03 | 3,53 |
| S 8 / 2 B3 | Shear | 343,50 | 143,15 | 429,71 | 11,03 | 447,18 | 3,87 | 3,74 |
| S 8 / 2 B4 | Shear | 360,00 | 143,75 | 431,51 | 11,10 | 448,64 | 4,06 | 4,05 |
| S 8 / 2 B5 | Shear | 379,20 | 145,00 | 435,26 | 11,75 | 452,06 | 4,28 | 4,22 |
| S 8 / 2 B6 | Comp. perpend. UF | 359,00 | 145,45 | 436,61 | 11,47 | 453,97 | 4,05 | |
| S 8 / 2 B7 | Shear | 352,40 | 146,50 | 439,76 | 9,00 | 457,42 | 3,97 | 3,88 |
| S 8 / 3 B1 | Shear | 347,70 | 141,95 | 426,11 | 10,90 | 443,32 | 3,92 | 3,27 |
| S 8 / 3 B2 | Shear | 379,80 | 146,50 | 439,76 | 9,50 | 456,74 | 4,28 | 3,96 |

| Specimens | Failure | Fracture Force | Weight | Density | Moisture Content | Density at 12% MC | f_v (at the middle of the beam) | f_v (at the crack) |
|-------------|---------|----------------|--------|----------------------|------------------|----------------------|--------------------------------------|-------------------------|
| | [-] | [kN] | [kg] | [kg/m ³] | [%] | [kg/m ³] | [N/mm ²] | [N/mm ²] |
| S 9 / 1 B1 | Shear | 372,30 | 156,64 | 470,20 | 10,07 | 474,74 | 4,20 | 4,14 |
| S 9 / 1 B2 | Shear | 369,00 | 150,32 | 451,23 | 9,87 | 456,04 | 4,16 | 4,10 |
| S 9 / 1 B3 | Shear | 347,40 | 152,56 | 457,96 | 11,43 | 459,26 | 3,92 | 3,78 |
| S 9 / 1 B4 | Shear | 370,10 | 156,46 | 469,66 | 12,10 | 469,43 | 4,17 | 3,65 |
| S 9 / 1 B5 | Shear | 346,80 | 152,66 | 458,26 | 10,77 | 461,07 | 3,91 | 3,76 |
| S 9 / 2 B1 | Shear | 396,50 | 154,88 | 464,92 | 9,83 | 469,96 | 4,47 | 4,22 |
| S 9 / 2 B2 | Shear | 339,30 | 154,43 | 463,57 | 10,53 | 466,98 | 3,83 | 3,77 |
| S 9 / 2 B3 | Shear | 398,10 | 156,85 | 470,83 | 10,47 | 474,44 | 4,49 | 3,65 |
| S 9 / 2 B4 | Shear | 389,90 | 153,20 | 459,88 | 12,07 | 459,72 | 4,40 | 3,58 |
| S 9 / 2 B5 | Shear | 362,90 | 150,80 | 452,67 | 11,40 | 454,03 | 4,09 | 3,33 |
| S 9 / 3 B1 | Shear | 367,20 | 153,29 | 460,15 | 12,80 | 458,31 | 4,14 | 3,37 |
| S 9 / 3 B2 | Shear | 340,20 | 147,80 | 443,67 | 12,87 | 441,74 | 3,84 | 3,46 |
| S 9 / 3 B3 | Shear | 358,10 | 151,70 | 455,37 | 13,27 | 452,48 | 4,04 | 3,28 |
| S 9 / 3 B4 | Shear | 318,60 | 153,26 | 460,06 | 14,03 | 455,39 | 3,59 | 2,92 |
| S 9 / 3 B5 | Shear | 396,20 | 157,76 | 473,56 | 12,93 | 471,36 | 4,47 | 4,13 |
| S 10 / 1 B1 | Shear | 306,40 | 172,08 | 516,55 | 11,80 | 517,07 | 3,45 | 3,19 |
| S 10 / 1 B2 | Shear | 385,40 | 171,02 | 513,37 | 12,23 | 512,78 | 4,35 | 4,32 |
| S 10 / 1 B3 | Shear | 348,80 | 163,91 | 492,03 | 12,93 | 489,74 | 3,93 | 3,20 |
| S 10 / 1 B4 | Shear | 367,80 | 166,94 | 501,12 | 13,80 | 496,61 | 4,15 | 4,14 |
| S 10 / 1 B5 | Shear | 373,70 | 167,44 | 502,62 | 12,77 | 500,69 | 4,21 | 4,15 |
| S 10 / 2 B1 | Shear | 309,50 | 158,89 | 476,96 | 12,03 | 476,89 | 3,49 | 3,07 |
| S 10 / 2 B2 | Shear | 383,40 | 163,55 | 490,95 | 12,07 | 490,77 | 4,32 | 3,80 |
| S 10 / 2 B3 | Shear | 370,20 | 164,57 | 494,01 | 12,03 | 493,93 | 4,17 | 4,12 |
| S 10 / 2 B4 | Shear | 287,70 | 168,27 | 505,11 | 12,60 | 503,60 | 3,24 | 2,64 |
| S 10 / 2 B5 | Shear | 276,30 | 168,27 | 505,11 | 11,97 | 505,19 | 3,12 | 2,90 |
| S 10 / 3 B1 | Shear | 363,30 | 174,01 | 522,34 | 13,77 | 517,72 | 4,10 | 3,33 |
| S 10 / 3 B2 | Shear | 379,20 | 165,81 | 497,73 | 11,53 | 498,90 | 4,28 | 4,22 |
| S 10 / 3 B3 | Shear | 335,10 | 166,73 | 500,49 | 12,30 | 499,74 | 3,78 | 3,49 |
| S 10 / 3 B4 | Shear | 330,60 | 167,13 | 501,69 | 12,60 | 500,19 | 3,73 | 3,15 |
| S 10 / 3 B5 | Shear | 294,50 | 167,30 | 502,20 | 12,00 | 502,20 | 3,32 | 2,91 |
| S 11 / B1 | Shear | 317,40 | | | 12,73 | | 3,58 | 3,44 |
| S 11 / B2 | Shear | 397,40 | | | 12,47 | | 4,48 | 3,93 |
| S 11 / B3 | Shear | 287,00 | | | 12,67 | | 3,24 | 2,85 |
| S 11 / B4 | Shear | 345,10 | | | 12,57 | | 3,89 | 3,74 |
| S 11 / B5 | Shear | 370,80 | | | 11,53 | | 4,18 | 3,68 |

Tab. A.1 Test results of series 6, 7, 8, 9, 10 and 11

The following table A.2. shows the shear stress values in the middle of the cross section of the continuous beams. Since in most cases the failure of the beam did not occur immediately upon the first crack, and instead it was possible to increase the load, all the strength values at which cracks occurred are listed.

| Specimen | | 1 st crack | 2 nd crack | 3 rd crack | 4 th crack | 5 th crack |
|----------|-------------------------------------|-----------------------|-----------------------|-----------------------|-----------------------|-----------------------|
| S12 B1 | Failure | Shear | Shear | Shear | Shear | Bending |
| | Failure Force [kN] | 265,6 | 346,8 | 436,7 | 438,6 | 430,8 |
| | $f_{v,middle}$ [N/mm ²] | 3,75 | 4,89 | 6,16 | 6,19 | 6,08 |
| S12 B2 | Failure | Shear | | | | |
| | Failure Force [kN] | 440,6 | | | | |
| | $f_{v,middle}$ [N/mm ²] | 6,22 | | | | |
| S12 B3 | Failure | Bend.+Shear. | | | | |
| | Failure Force [kN] | 506,5 | | | | |
| | $f_{v,middle}$ [N/mm ²] | 7,15 | | | | |
| S12 B4 | Failure | Shear | | | | |
| | Failure Force [kN] | 426,5 | | | | |
| | $f_{v,middle}$ [N/mm ²] | 6,02 | | | | |
| S12 B5 | Failure | Shear | Bending | | | |
| | Failure Force [kN] | 503,9 | 492,1 | | | |
| | $f_{v,middle}$ [N/mm ²] | 7,11 | 6,94 | | | |
| S12 B6 | Failure | Shear | Bending | | | |
| | Failure Force [kN] | 386,7 | 476,0 | | | |
| | $f_{v,middle}$ [N/mm ²] | 5,46 | 6,72 | | | |
| S12 B7 | Failure | Shear | Shear | | | |
| | Failure Force [kN] | 400,0 | 417 | | | |
| | $f_{v,middle}$ [N/mm ²] | 5,64 | 5,88 | | | |
| S12 B8 | Failure | Shear | Shear | | | |
| | Failure Force [kN] | 372,1 | 465,6 | | | |
| | $f_{v,middle}$ [N/mm ²] | 5,25 | 6,57 | | | |
| S12 B9 | Failure | Shear | Bending | Shear | Bending | |
| | Failure Force [kN] | 385,5 | 422,6 | 447,1 | 459,9 | |
| | $f_{v,middle}$ [N/mm ²] | 5,44 | 5,96 | 6,31 | 6,49 | |
| S12 B10 | Failure | Shear | Shear | Bending | | |
| | Failure Force [kN] | 305,9 | 346,5 | 425,5 | | |
| | $f_{v,middle}$ [N/mm ²] | 4,32 | 4,89 | 6,00 | | |

Tab. A.2 Test results of series 12

INTERNATIONAL COUNCIL FOR RESEARCH AND INNOVATION
IN BUILDING AND CONSTRUCTION

WORKING COMMISSION W18 - TIMBER STRUCTURES

MECHANICALLY JOINTED BEAMS
POSSIBILITIES OF ANALYSIS AND SOME SPECIAL PROBLEMS

H Kreuzinger
Technische Universität München

GERMANY

Presented by: H Kreuzinger

- A Jorissen questioned why a zero shear zone existed in Figures 13 and 14 in the paper.
- H Kreuzinger stated that this was a beam with two parts and the zone of zero shear corresponded to the area where there was no shear connector between the two parts.

Mechanically Jointed Beams

Possibilities of Analysis and some special Problems

Heinrich Kreuzinger
Technische Universität München

1. Introduction

Mechanically jointed beams have a higher load capacity than the sum of the single beams. One beam must be situated over the other beam and the connectors must transport shear forces from one to the other beam. Figure 1 shows a simple bridge with a „flitch beam“. The single beams may also be laminates, horizontally or vertically situated like shown in figure 2.



Figure 1: Flitch beam

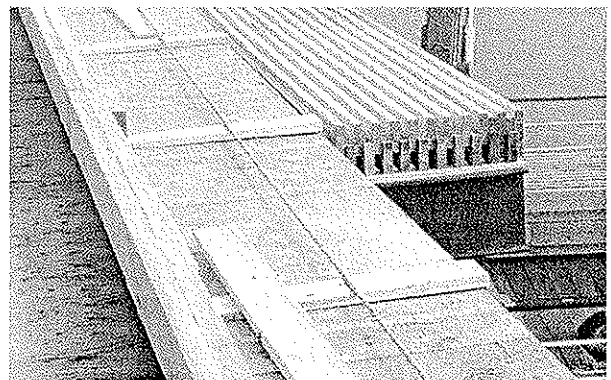


Figure 2: Mechanically jointed laminates

Regarding cross sections made of two parts - the situation is presented in figure 3:

- a) two beams jointed with shear connectors
- b) a framework with two flanges, connected by the diagonals
- c) vertically situated laminates, jointed by nails or screws

The three cross sections have the same definitions:

- a (m) the distance of the axes of the single parts 1 and 2
- k (MN/m²) stiffness of the shear connection K/e with
 K (MN/m): stiffness of one connector, e (m): distance of the connectors
 The distance e of the connectors in direction of the axis may be changing. There may be also few strong connectors or a lot of weak connectors.

- EI_1 (MNm²) bending stiffness of part 1
- EA_1 (MN) stretching stiffness of part 1
- EI_2 (MNm²) bending stiffness of part 2
- EA_2 (MN) stretching stiffness of part 2

If the bending stiffness of the single beams is zero there is the situation of framework with hinges

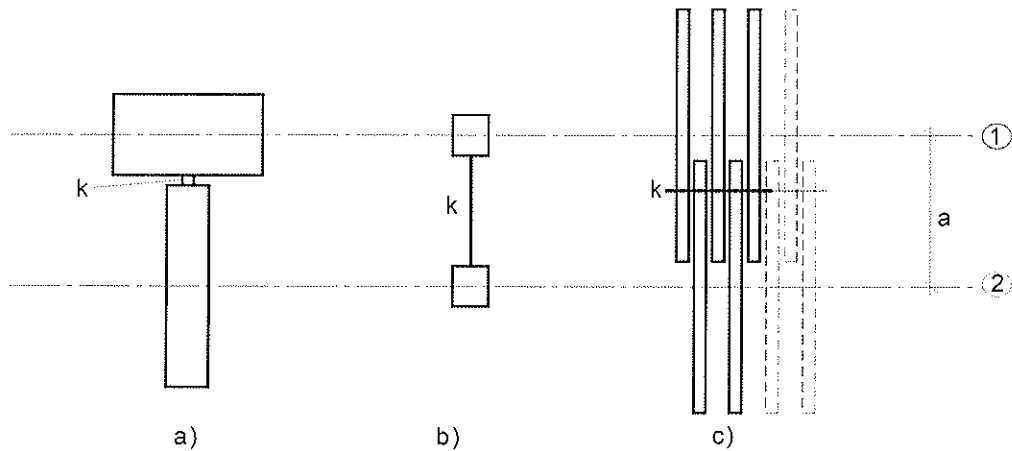


Figure. 3: cross sections

The connection is not only necessary to transport the shear forces from one part to the other but also to have the same deformation w of the two parts. Cross sections made of more than two parts are also possible. An example are the ribs of shells like shown in the figures 4a and 4b. The formulas for a approximation of cross sections with more than two parts are given in E DIN 1052, Mai 2000 /1/.

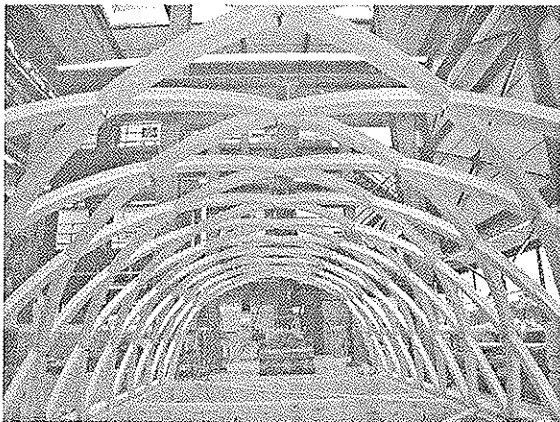


Figure 4a: ribbed timber shell /3/

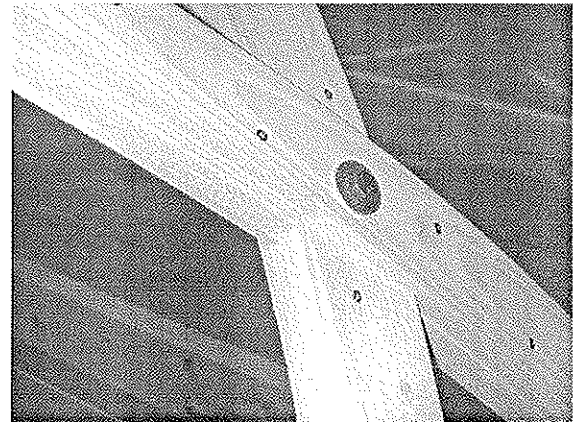


Figure 4b: node /3/

2. Calculation

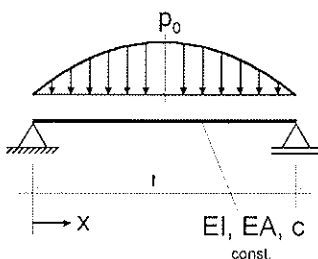
2.1 General

Each part is regarded as a beam. The shear deformation of the single parts is neglected and the classic theory of bending of beams is valid. The different deformations of the beams on the place of the connectors give forces in the connectors. The differential equations of the problem are known /4/, /6/.

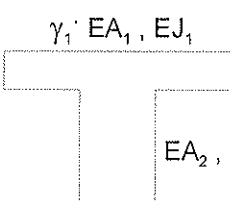
2.2 Analytical solution

For single supported beams with constant cross section and connection along the length and sinuslike load along the axis the analytical solution is very simple, given in the codes EC5 /2/ and DIN 1052 /1/. To use this solution for other systems it is necessary to estimate a length in order to compare the given situation with the sinuslike situation. The length may be the distance between the points where the bending moment is zero. But for to know this situation it is necessary to know the solution!

The following formulas are given in the mentioned codes. In the middle there is the real cross section, on the left side there are the formulas with the reduced stiffness $\gamma_1 EA_1$ of part 1 and on the right side there are the formulas with the reduced stiffness $\gamma_2 EA_2$ of part 2. The results of both sides are of course the same.



$$p = p_0 \cdot \sin \frac{\pi}{\ell} \cdot x$$

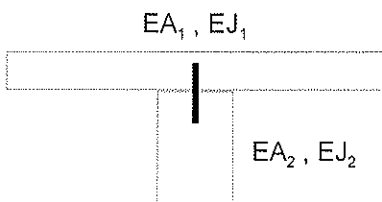


$$\gamma_1 = \frac{1}{1 + \frac{\pi^2 \cdot EA_1}{\ell^2 \cdot c}}$$

$$a_1 = a \cdot \frac{EA_2}{\gamma_1 EA_1 + EA_2}$$

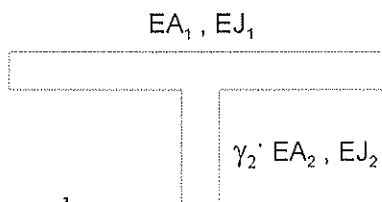
$$EJ_1 + EJ_2 + a^2 \cdot \frac{\gamma_1 EA_1 \cdot EA_2}{\gamma_1 EA_1 + EA_2}$$

$$t_o = \frac{Q}{efEJ} \cdot \gamma_1 EA_1 \cdot a_1 = \frac{Q}{efEJ} \cdot EA_2 \cdot a_2$$



$$a_1 + a_2 = a$$

$$efEI =$$



$$\gamma_2 = \frac{1}{1 + \frac{\pi^2 \cdot EA_2}{\ell^2 \cdot c}}$$

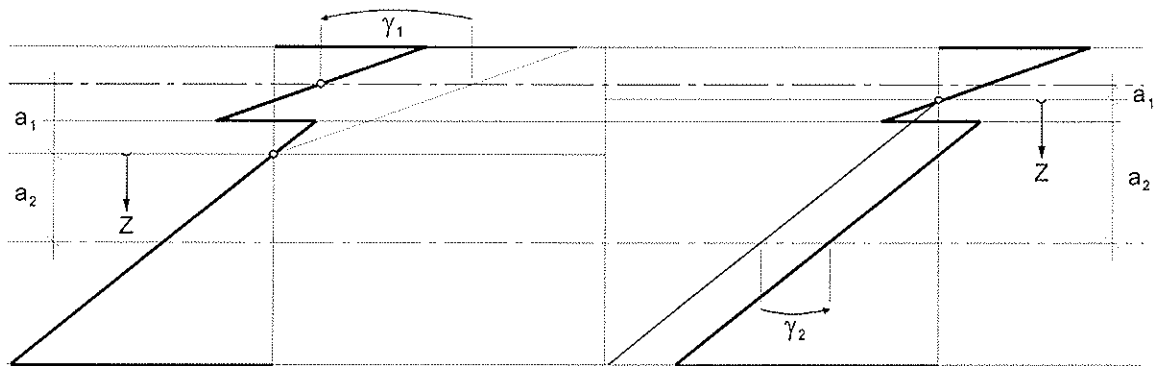
$$a_1 = a \cdot \frac{\gamma_2 EA_2}{EA_1 + \gamma_2 EA_2}$$

$$EJ_1 + EJ_2 + a^2 \cdot \frac{EA_1 \cdot \gamma_2 EA_2}{EA_1 + \gamma_2 EA_2}$$

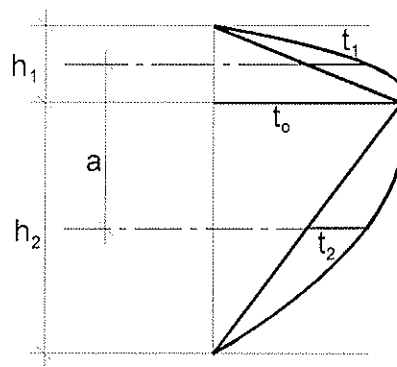
$$t_o = \frac{Q}{efEJ} \cdot EA_1 \cdot a_1 = \frac{Q}{efEJ} \cdot \gamma_2 EA_2 \cdot a_2$$

stress:

$$\sigma = \frac{M}{ef EJ} \cdot z \cdot E$$



shear flow:



$$t_1 = \frac{Q}{efEI} \cdot EI_1 \cdot \frac{1,5}{h_1} \quad t_2 = \frac{Q}{efEI} \cdot EI_2 \cdot \frac{1,5}{h_2}$$

2.3 Calculation with programs for framed structures

The parts of the construction are regarded as a beam. The connection is simulated by members /5/.

2.4 Sandwich analogy

The differential equations of a mechanically jointed beam built by two parts are identically with the differential equations of two beams with the same deformation w : one beam A with a bending stiffness EI_A and an other beam B with a bending stiffness EI_B and a shear stiffness S . Figure 5 shows the situation.

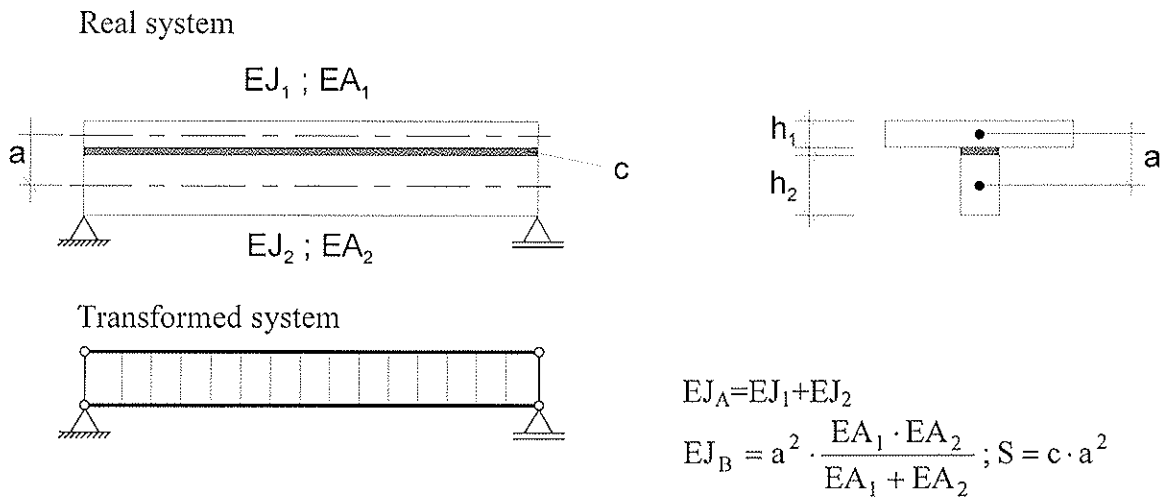


Figure 5: Sandwich analogy

This method is shown in the draft of DIN 1052, Mai 2000 /1/. The calculation for different loads, boundary conditions and changing cross sections is possible with simple beam programs.

The calculation of the transformed system results in:

Beam A: V_A, M_A

Beam B: V_B, M_B

To go back in the real system the following calculation is necessary:

Bending moment in the parts $M_i = M_A \cdot \frac{EI_i}{EI_A}$

Shear force in the parts $V_i = V_A \cdot \frac{EI_i}{EI_A}$

The stresses σ and τ may be calculated by the rules of the classic theory of beams.

Normal forces in the parts $N_i = M_B \cdot \frac{1}{a}$

Shear flow between the parts $t_o = V_B \cdot \frac{1}{a}$

3. Special problems

The differential equations for an element of a beam like figure 6 are:

a: $p_x + N' = 0$ b in c': $M'' + p_z - m' = 0$

b: $p_z + V' = 0$ $M'' + p_z^E = 0$

c: $m + V - M' = 0$ $p_z^E = p_z - m'$

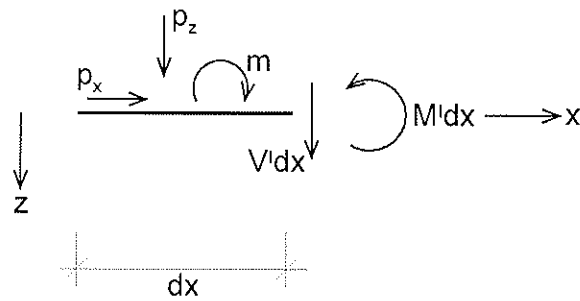


Figure 6: beam element dx

The load m results from the shear flow with the excentricity e (fig. 7). The bending moment - but not the shear force V - produced by m may be the same produced by $p_z^E = m'$. This is important for the interpretation of the shear forces V . The equation b results in:

$$V' = -p_z = -p_z^E - m' \quad (\text{and not } V' = -p_z^E!)$$

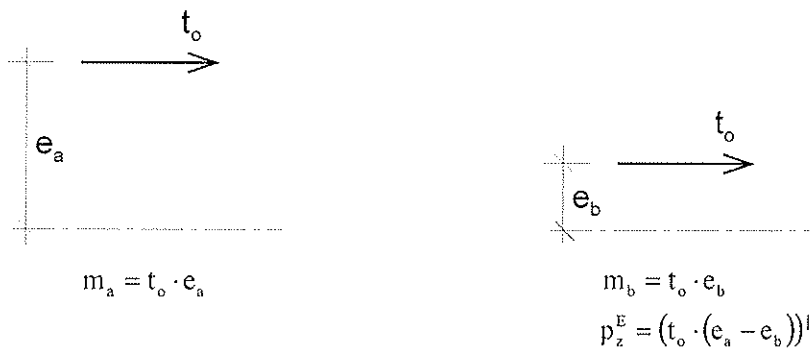


Figure 7: load m or p_z^E

If the shear flow t_o is in the position of a_1 , the following equations and figure 8 show the distribution.

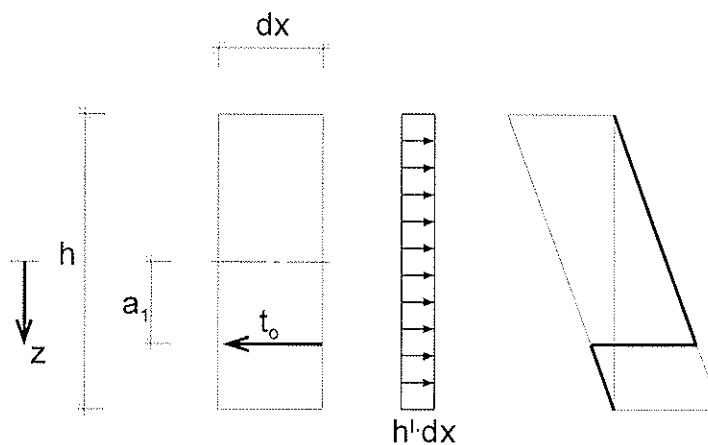


Figure 8: distribution of shear force t

It is surprising, that the position of the shear connection has no influence on the result. Whether the analytical solution or the sandwich analogy have a possibility to regard the position. Reasonable for this effect is the neglect of the shear deformation of the single parts. The position of the shear connection influences the shear forces $V_{1,\text{sum}}$ and $V_{2,\text{sum}}$.

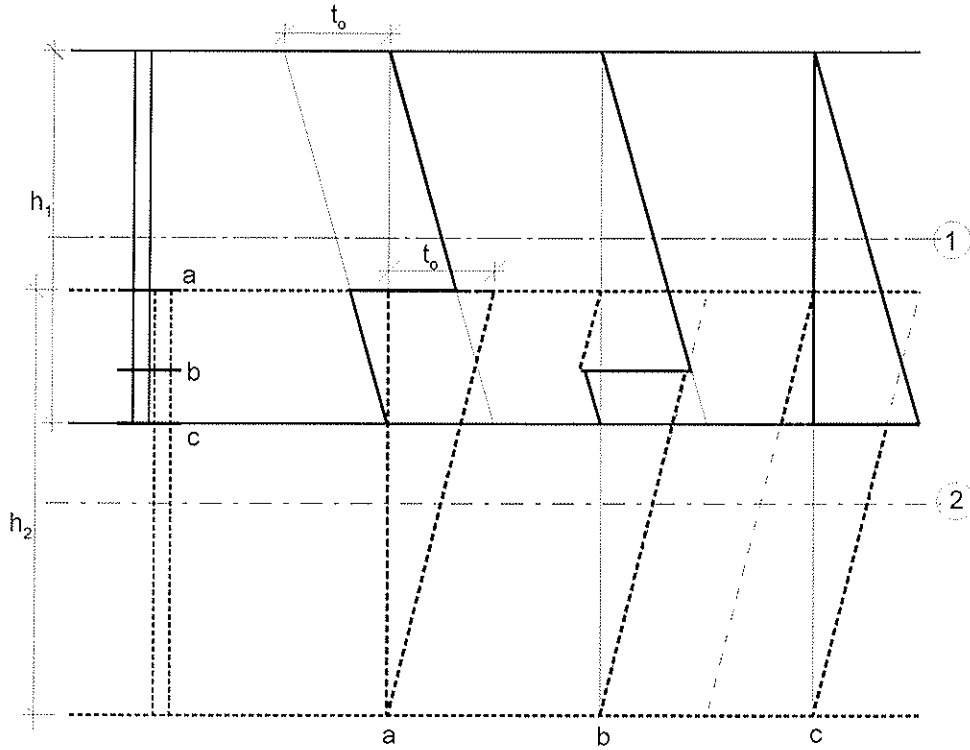
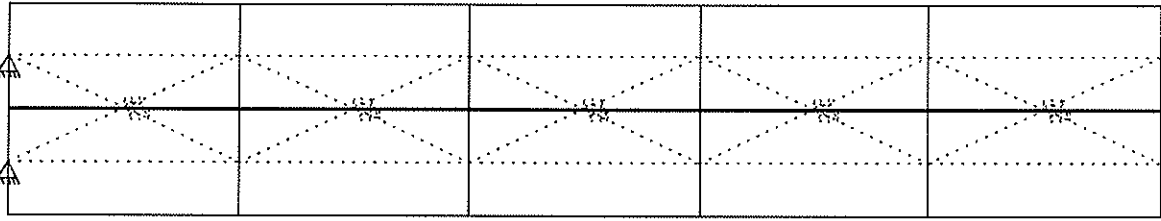
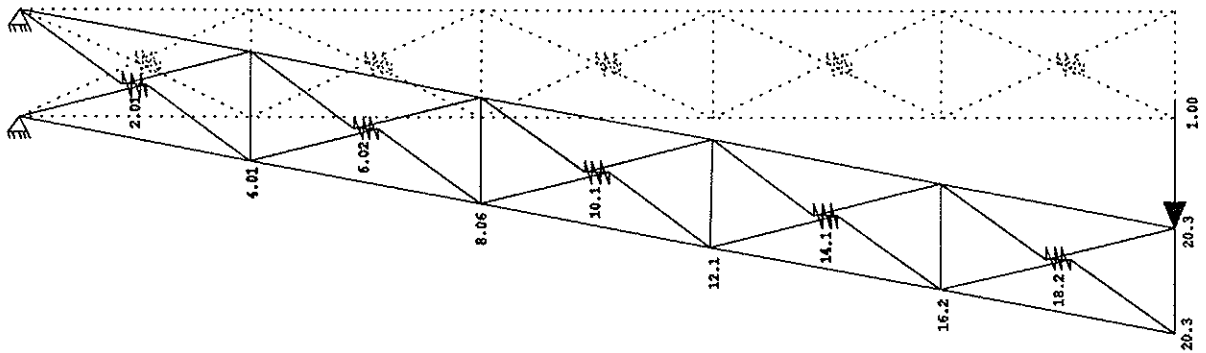


Figure 9: position of the shear connector

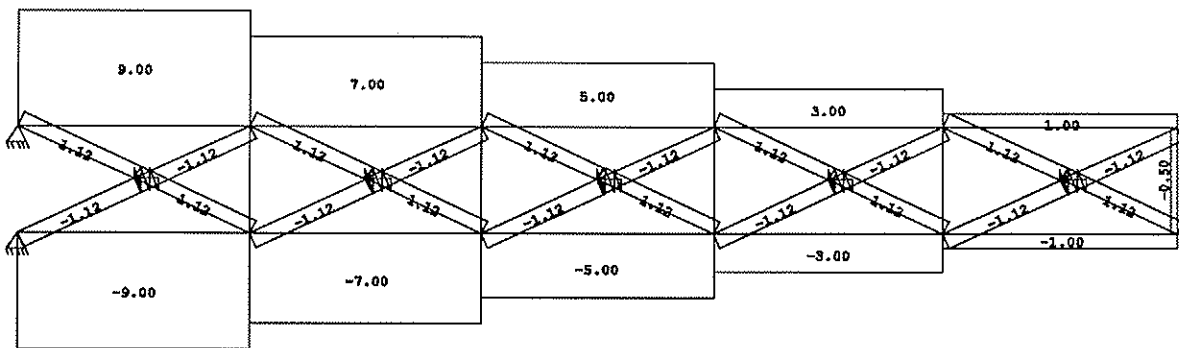
This phenomena is also shown in the example of figure 10. A framework has different situations of the diagonals (figures 10a and 10b) with a spring to transport the shear forces. The normal forces in the lower flange and the upper flange are equal in both models, also the deformation.



Querschnitte
Struktur



Verschobene Struktur aus LF 1
Knotenverschiebung Y in mm, Lastfall 1 (Max=20.3)
Struktur
Knotenlast Y, Lastfall 1, 1 cm = 0.500 kN



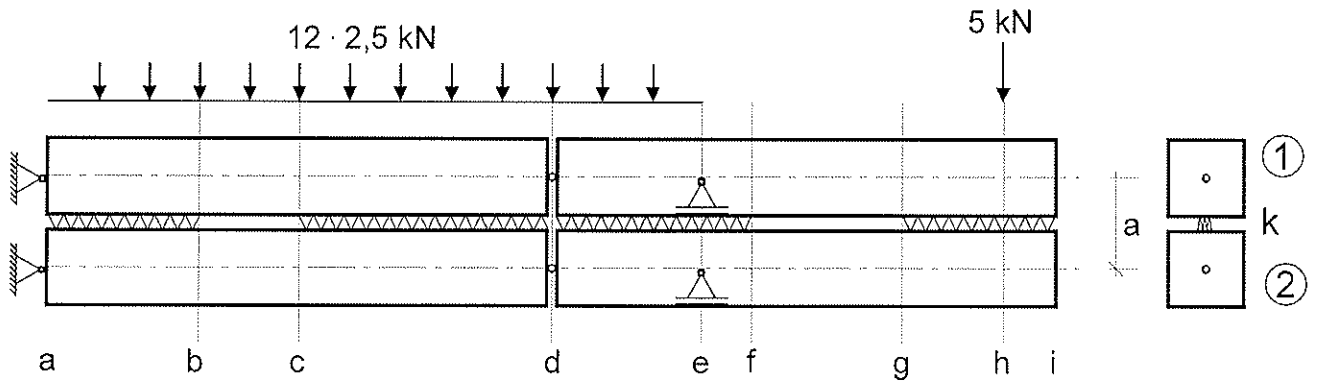
Fachwerknormalkraft, Lastfall 1, 1 cm = 5.00 kN



Figure 10a: truss girder

3. Example

Two beams (figure 11) are mechanically jointed in the range from a to b, c to f and g to i. The single beams have hinges in a and d, the supporting is in a and e. The supporting in a does not allow deflections of the beams in the direction of the axis but there is no bending moment. Between a and f there are single loads and also in h there is a single load.



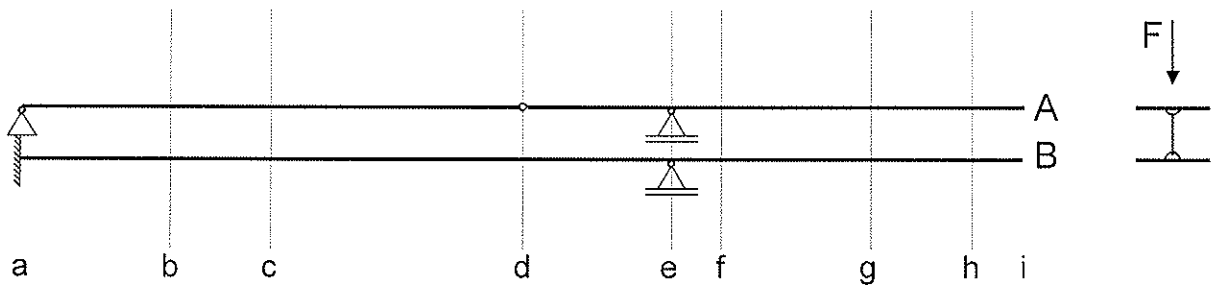
$$EI_1 = EI_2 = 1,66 \text{ MNm}^2$$

$$EA_1 = EA_2 = 400 \text{ MN}$$

$$a = 0,2 \text{ m} \quad l_{ac} = 6,5 \text{ m} \quad l_{ei} = 3,5 \text{ m}$$

$$k = 5 \text{ MN/m}^2$$

Figure 11: real system



$$EI_A = EI_1 + EI_2 = 2,66 \text{ MNm}^2$$

$$EI_B = a^2 \cdot EA_1 \cdot EA_2 / (EA_1 + EA_2) = 8 \text{ MNm}^2$$

$$S = k \cdot a^2 = 5 \cdot 0,2^2 = 0,2 \text{ MN}$$

Figure 12: transformed system

Obviously the analytical solution of paragraph 2.2 does not work here.

The transformation from the real system to the calculation system (figure 12) using the sandwich analogy results in:

Beam A: The bending stiffness is the sum of the stiffness of the single parts, the shear stiffness is infinite.

Beam B: The bending stiffness results from the stiffness and the distance of the two beams, the shear stiffness (figure 13) from the stiffness k from the connectors and the distance a .

The same deformation of the beams is obtained by a rigid member between the nodes of beam A and B (figure 12, right side). To avoid differences due to this connection it is necessary to use single forces in the nodes and not distributed load.

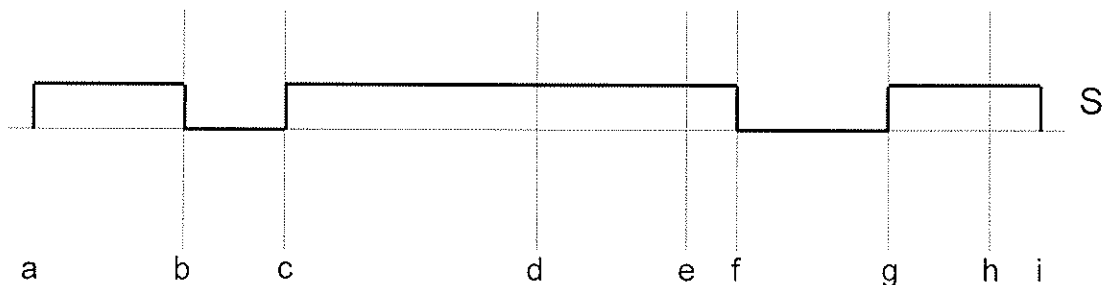


Figure 13: Distribution of shear stiffness S

The calculation of the coupled beams is resulting in the bending moments M_A and M_B and also in the shear forces V_A and V_B (figure 14).

The transformation back to the real system allows to have the bending moments M_1 and M_2 , the shear forces V_1 and V_2 in the two parts and the shear flow between the two parts. It is to mention that the total vertical forces $V_{1,sum}$ and $V_{2,sum}$ result from V_1 , V_2 and $t_0 a$.

Results:

a The bending moment M_B gives the normal forces in the support points

$$Z_1 = \frac{M_B}{a} = \frac{9,3}{0,2} = 46,5 \text{ kN} = D_2$$

The bending moment in the two parts is 0 because there is a hinge.

The supporting reaction is $3,59 + 10,53 = 14,12 \text{ kN}$

b to c V_B is 0 because there is no shear stiffness. M_B must be constant.

d In the two beams there is no bending moment.

e The supporting force is $11,57 + 6,12 + 4,3 - 1,12 = 20,87 \text{ kN}$. Together with the supporting force in a the vertical equilibrium is o. k.

f to g V_B is 0 because there is no shear stiffness. M_B must be constant.

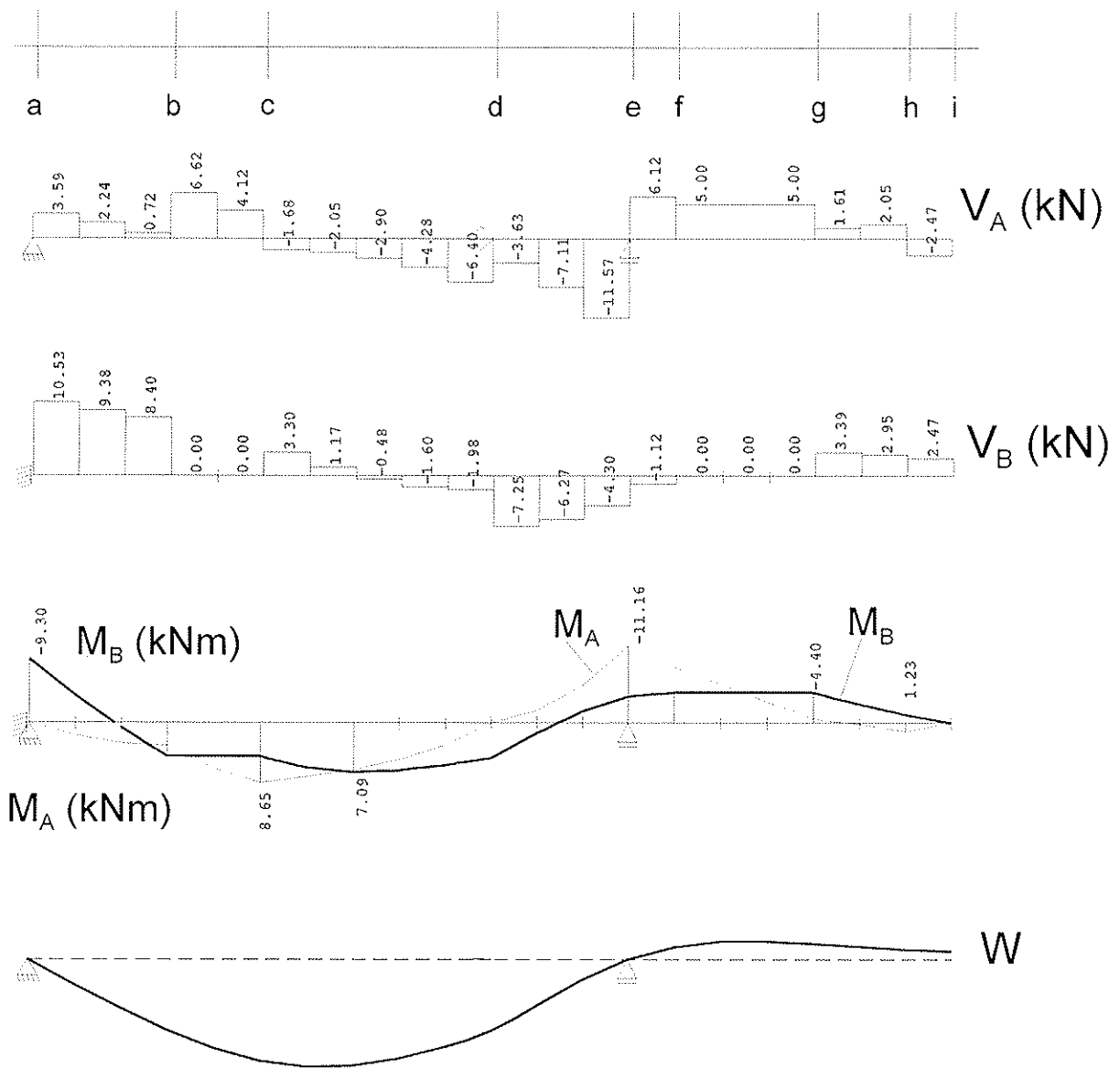


Figure 14: results: V_A , V_B , M_A , M_B and w

- h Between h and i there is no shear force and no bending moment but there are stresses. Figure 15 shows the values.

$$M_1 = M_A \cdot \frac{EI_1}{EI_A} \quad \sigma_{1,M} = \frac{M_1}{W_1} \quad V_1 = V_A \cdot \frac{EI_1}{EI_A} \quad t_1 = \frac{V_1}{h_1} \cdot 1,5$$

$$N_1 = \frac{-M_B}{a} \quad \sigma_{1,N} = \frac{N_1}{A_1} \quad t_0 = \frac{V_B}{a}$$

The resulting vertical shear force in section 1 is:

$$V_{I,\text{sum}} = t_0 \cdot h_1 \cdot \frac{1}{2} + V_I = V_B \cdot \frac{h_1}{2 \cdot a} + V_A \cdot \frac{EI_1}{EI_A}$$

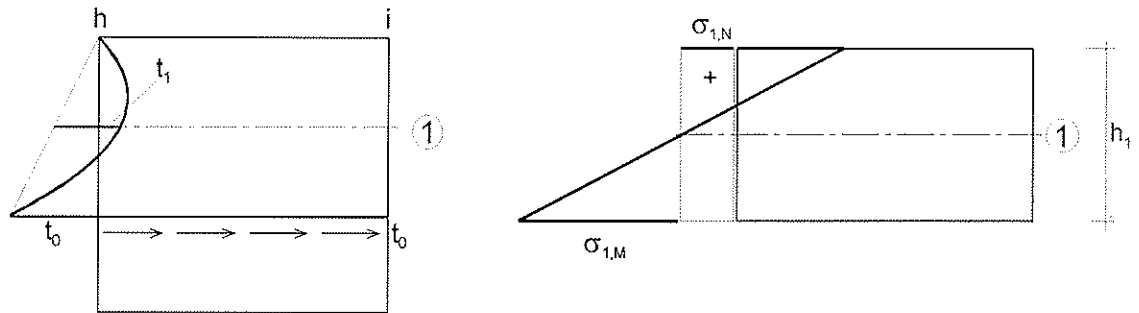


Figure 15: shear flow and stress

5. Summary

The connections of mechanically jointed beams are quite different. For example there are nails, screws or notches. They are arranged continuously or on single points along the length of the beam. The beam itself may be supported like a simple beam or may be part of a system. All these must be taken into account by calculation.

For calculation different methods are available:

- The analytic solution, given in the codes, is strongly valid only for single supported beams with constant cross section and connection along the length sinuslike load.
- Frameworksystems allow to calculate more complicated systems.
- Regarding the deformation of the connectors as a shear deformation, it is possible to do the calculation with beams with bending- and shear stiffness (sandwich analogy).

To use the different methods and to interpret the results, the knowledge of the different distribution of shear forces over the cross section is necessary. The basic case is a beam with a shear flow as load. The shear flow in the direction of the axis acts in a distance to the axis.

There are also some peculiar problems with single loads or different boundary conditions. An examples was shown by using the calculation method with the sandwich analogy.

For cross sections built with two parts the sandwich analogy is theoretical correct. For cross sections consisting of more than two parts, the sandwich analogy is a good approximation calculation. The real system is also transformed in the two girders A and B like shown in figure 5. The bending stiffness of beam A is the sum of the bending stiffness of the single beams, the bending stiffness of the beam B results from the stretching stiffness and the distance of the single beams. The shear stiffness S is calculated with the values of the stiffness of the connection and the shear module of the parts. The formulas are documented in E DIN 1052, Mai 2000, Annex F.

6. References

- /1/ Entwurf DIN 1052, Mai 2000, Entwurf, Berechnung und Bemessung von Holzbauwerken, Allgemeine Bemessungsregeln und Bemessungsregeln für den Hochbau, E DIN 1052:2000-05
- /2/ EC 5, DIN V ENV 1995-1: Entwurf, Berechnung und Bemessung von Holzbauwerken, Teil 1: Allgemeine Bemessungsregeln, Bemessungsregeln für den Hochbau, Deutsche Fassung, Oktober 1993
- /3/ Natterer, J.; Burger, N.; Müller, A.; Natterer, Jo.: Holzrippendächer in Brettstapelbauweise, Bautechnik 77(2000), H.11, S. 783-792, Verlag Ernst & Sohn, Berlin
- /4/ Kreuzinger, H.: Träger und Stützen aus nachgiebig verbundenen Querschnittsteilen. In: Arbeitsgemeinschaft Holz e.V. (Hrsg.): Step 1: Holzbauwerke nach Eurocode 5 - Bemessung und Baustoffe. 1. Aufl. Fachverlag Holz Düsseldorf, 1995, S. B11/1-B11/9
- /5/ Kneidl, R.; Hartmann, H.: Träger mit nachgiebigem Verbund - Eine Berechnung mit Stabwerksprogrammen. In: Bauen mit Holz (1995) S. 285-290
- /6/ Schelling, W.: Zur Berechnung nachgiebig zusammengesetzter Biegeträger aus beliebig vielen Einzelquerschnitten. In: Ehlbeck, J.; Steck, G. (Hrsg): Ingenieurholzbau in Forschung und Praxis, Karlsruhe: Bruderverlag, 1982, 155-162
- /7/ Platten, Scheiben und Schalen, ein Berechnungsmodell für gängige Statikprogramme, Bauen mit Holz, 1/1999, S. 34-39, Bruderverlag
- /8/ Kreuzinger, H.: Flächentragwerke; Platten, Scheiben und Schalen, Berechnungsmethoden und Beispiele. In: Informationsdienst Holz, Brücken aus Holz, Konstruieren-Berechnen-Ausführen, 1999, 42-60

**INTERNATIONAL COUNCIL FOR RESEARCH AND INNOVATION
IN BUILDING AND CONSTRUCTION**

WORKING COMMISSION W18 - TIMBER STRUCTURES

**A SIMPLIFIED PLASTIC MODEL FOR DESIGN OF PARTIALLY ANCHORED
WOOD-FRAMED SHEAR WALLS**

B Källsner

Träteknik - Swedish Institute for Wood Technology Research

U A Girhammar

Liping Wu

Department of Applied Physics, Umeå University,

SWEDEN

Presented by: B Källsner

- V Enjily asked how was the shear wall fixed to the foundation.
- B Källsner said that the practice in Sweden was not clear.
- V Enjily commented that the assumptions in the model were not realistic with respect to the directions of the nail forces as the walls are subject to both racking and overturning.
- B Källsner agreed that the model did not fully describe the real case; however, equilibrium conditions were met and the model worked well.
- V Enjily commented that ring shank nails were used which might not be realistic as the failure mode would be biased towards pull through failure.
- B Källsner answered that the fasteners showed plastic behaviour. Failure in the nails were nail withdrawal and sometimes pull through were observed.
- S Thelandersson commented that in Sweden one or two stories to med rise houses wind loads would be important. In the one to two stories houses simple metal plate anchorages were used. For the higher houses the calculations would become a problem. He also commented that the model presented was elegant; however, one must be careful with the assumptions as the assumed force distribution might be different from reality.

A simplified plastic model for design of partially anchored wood-framed shear walls

Bo Källsner

Träteknik - Swedish Institute for Wood Technology Research, Sweden

Ulf Arne Girhammar and Liping Wu

Department of Applied Physics, Umeå University, Sweden

Abstract

This is an introductory paper in which the structural behaviour and design of partially anchored wood-framed shear walls are studied.

A simplified plastic model is proposed for design in the ultimate limit state. The model covers only static loads and can only be applied when mechanical fasteners with plastic characteristics are used.

A few tests of shear walls have been conducted in which the influence of vertical loads and anchorage of bottom rail was investigated. A comparison between measured and calculated load-carrying capacities indicates that the proposed model is suitable for design purposes.

1 Introduction

1.1 Background

Shear walls are constructed in different ways depending on local traditions. They can be prefabricated in a factory or built on site. The prefabricated shear walls can consist of one or several wall assemblies of different sizes. The structural behaviour of wall diaphragms is to a large extent determined by the sheathing-to-timber joints and how the diaphragms are connected to the surrounding structure. Of particular importance is the anchoring of the shear wall to the substrate. Sometimes tie-downs are used for anchorage of the end studs of the shear wall. On other occasions only the bottom rail is anchored to the substrate. Due to economic reasons the building industry, at least in the Nordic countries, desires to reduce the number of tie-downs, nails and screws to a minimum.

In Eurocode 5 a simplified method for the design of wall diaphragms is given. When this method is used, the code stipulates that the tensile studs at the end of the diaphragm must be anchored to the substrate or secured against uplift by vertical actions.

An alternative method for the design of wall diaphragms, in Eurocode 5, is to determine the racking resistance by testing according to test standard EN 594. This standard stipulates that the bottom rail of the shear wall is bolted to the test rig and uplift is resisted by the sheathing-to-timber joints and also by the vertical loads on the top rail of the wall panel. Since the end stud on the tensile side of the wall panel is not directly anchored to the base of

the test rig, this stud will normally be subjected to substantial vertical displacement. Consequently, the structural behaviour will deviate considerably from what is assumed in the simplified calculation procedure. This means that the sheathing-to-timber joints located along the bottom rail on the tension side of the test panel will be subjected to vertical tensile forces which strive to draw the sheet apart from the bottom rail. This redistribution of the fastener forces will result in a lower racking capacity for a tested wall diaphragm according to EN 594 than for a diaphragm designed according to the simplified theory with a fully anchored tensile stud.

In an ongoing Nordic project, dealing with the design of wood-based diaphragm structures, it has become obvious that there is a need for developing a general method for simplified design which can be used for wall diaphragms that are incompletely anchored to the substrate. In this introductory paper the principles of a possible method is presented.

1.2 Objective

The main objective of this study is to present a simplified method for design of wood-framed shear walls that can be used for various boundary conditions between the wall diaphragm and the substrate. The following requirements are made on the model:

- it should be suitable for calculation by hand
- it should explain the structural behaviour of the shear wall in the ultimate limit state
- it should handle the influence of adjacent wall and floor diaphragms
- it should give results that are somewhat on the safe side
- it should lead to economical structures.

1.3 Limitations

The simplified model can only be applied on shear walls where the sheet material is fixed by mechanical fasteners to the frame members and where these sheathing-to-timber joints show plastic behaviour.

The model covers only static loads in the ultimate limit state. The model can not be used for determination of deformations in the serviceability state.

In this introductory paper shear walls with openings are not dealt with.

In some cases there are risks of brittle failure modes in the shear walls. An example of such a failure mode is when cracks occur in the frame members due to small edge distances of the fasteners. The influence of such failure modes is treated incompletely.

2 Models for simplified design of fully anchored shear walls

The purpose of this section is to present two simplified methods for design of fully anchored shear walls, that are commonly used in the Nordic countries and which may contribute to a better understanding of the structural behaviour of such walls. By a fully anchored shear wall is meant a wall where the vertical stud on the tension side is fully anchored to the substrate.

2.1 Elastic model

A typical part of a shear wall is shown in Figure 1. An elastic model suitable for calculation by hand has been presented by Källsner et. al (1995). The model is based on the following assumptions:

- the shear wall is fully anchored to the substrate
- the frame members are rigid and hinged to each other
- the sheet is rigid
- the load-displacement relationships of the sheathing-to-timber joints are linear-elastic until failure.
- the displacements are small compared with the width and height of the sheet.

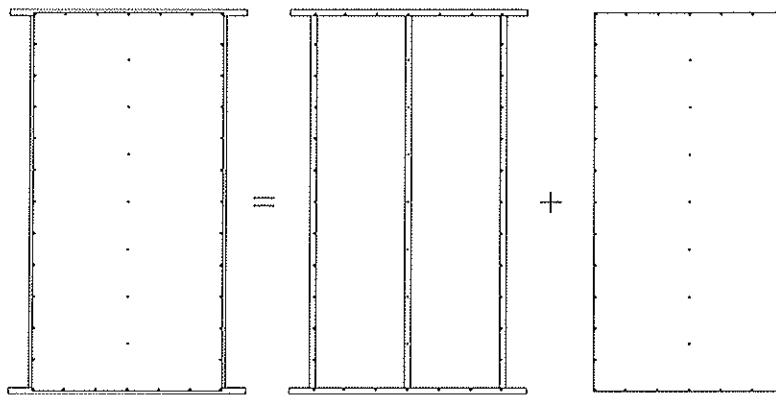


Figure 1: A shear wall unit built up of a timber frame and a sheet.

In order to determine the forces acting upon the individual fasteners, the displacement of the sheet relative to the frame members must be formulated. In Figure 2, a static model of the wall unit in the unloaded and loaded states is shown. The studs have been given the rotation γ and the sheet the rotation φ in relation to their original positions. The coordinate axes x and y refer to the centre of gravity (CG) of the fasteners.

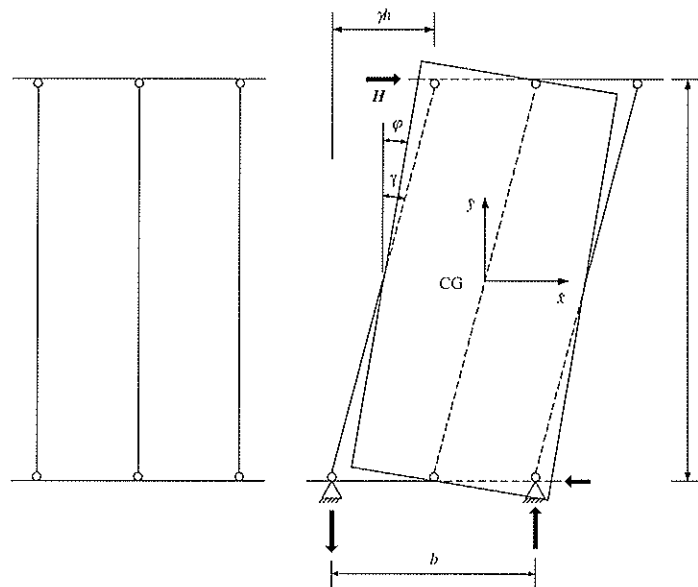


Figure 2: Static model of a shear wall unit in unloaded and loaded states.

Using the principle of the minimum of the potential energy of the structure the angles φ and γ are derived as:

$$\varphi = \frac{1}{K} Hh \frac{1}{\sum_{i=1}^N \hat{x}_i^2} \quad (1)$$

$$\gamma = \frac{1}{K} Hh \left(\frac{1}{\sum_{i=1}^N \hat{x}_i^2} + \frac{1}{\sum_{i=1}^N \hat{y}_i^2} \right) \quad (2)$$

where K denotes the slip modulus of the fasteners, (\hat{x}_i, \hat{y}_i) denotes the coordinates of fastener number i and N denotes the total number of fasteners. The horizontal displacement of the top rail is given by:

$$u = \gamma h = \frac{1}{K} Hh^2 \left(\frac{1}{\sum_{i=1}^N \hat{x}_i^2} + \frac{1}{\sum_{i=1}^N \hat{y}_i^2} \right) \quad (3)$$

Denoting the shear capacity of each sheathing-to-timber joint by F , the horizontal load-carrying capacity H of the wall unit becomes

$$H = \frac{F}{h \left(\frac{\hat{x}_{\max}}{\sum_{i=1}^N \hat{x}_i^2} + \frac{\hat{y}_{\max}}{\sum_{i=1}^N \hat{y}_i^2} \right)} \quad (4)$$

where $(\hat{x}_{\max}, \hat{y}_{\max})$ are the coordinates of the fastener which is the most remote one from the center of gravity of the fasteners.

For the shear wall in Figure 1, the calculated distribution of the fastener forces is shown in Figure 3.

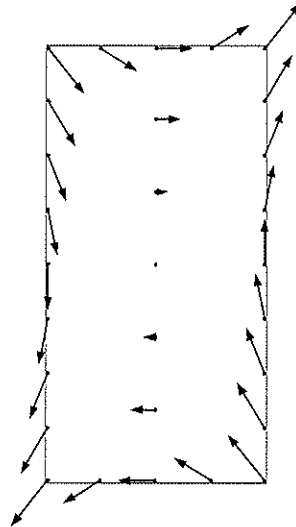


Figure 3: Force distribution on the sheet according to a linear elastic model.

2.2 Plastic model

In the elastic analysis, a linear elastic load-displacement relationship until failure was assumed. From tests of nailed joints it is well known that the load-slip curves are often characterised by plastic deformations. Methods for determination of the lower and upper bounds of the plastic load-carrying capacity of a shear wall have been presented by Källsner et al (1995). The following assumptions are made:

- the shear wall is fully anchored to the substrate
- the frame members are rigid and hinged to each other
- the sheet is rigid
- the load-displacement relationships of the sheathing-to-timber joints are completely plastic.
- the displacements are small compared with the width and height of the sheet.

2.2.1 Lower bound method

A lower bound of the plastic load-carrying capacity of a shear wall can be obtained by assuming a force distribution that fulfils the conditions of force and moment equilibrium and where the force on each fastener is at most equal to the plastic capacity of the fastener. For a wall unit as in Figure 1, where the distance of the fasteners along the edges is constant, it is possible to find a simple force distribution according to Figure 4. Each edge fastener, except those in the corners, may be assumed to carry the same plastic load F parallel to the edge. Each corner fastener is assumed to carry one load component $F/2$ parallel to each of the associated sides of the sheet. The fasteners in the centre stud are assumed not to carry any load. With the chosen force distribution, which corresponds to a pure shear flow along the edges of the sheet, the horizontal load-carrying capacity H is

$$H = n F \quad (5)$$

where n = number of fastener spacings along the top rail

F = load-carrying capacity of a fastener loaded in shear

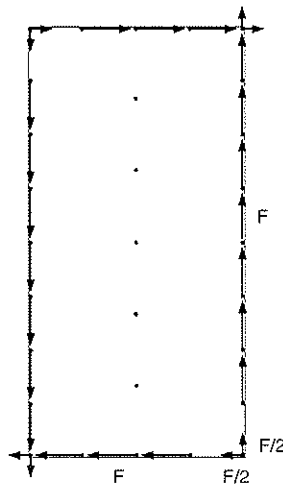


Figure 4: Force distribution on the sheet according to a plastic lower bound model.

2.2.2 Upper bound method

An upper bound of the plastic load-carrying capacity of a shear wall can be obtained using the principle of virtual work, by making the internal work of all the fasteners equal to the work of the external force. In the formulation of the internal work, each timber member can be regarded as a rigid body rotating around its own centre of rotation on the sheet. The true plastic load-carrying capacity of a shear wall is obtained when the internal work of all the fasteners reaches its minimum value. The principle is demonstrated in Figure 5 for the previously studied wall unit, where the assumed positions of the centre of rotations (CR) and the matching fastener forces are shown.

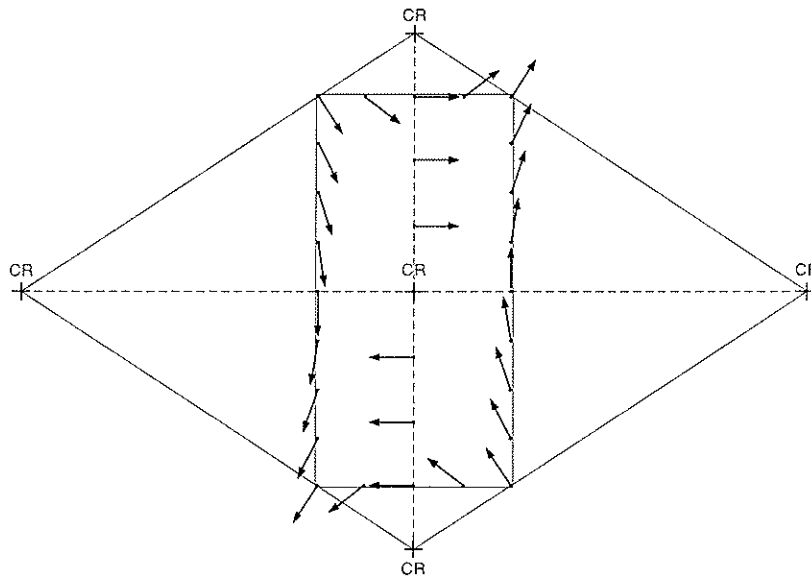


Figure 5: Force distribution on a sheet according to a plastic upper bound model.

2.3 Elastic versus plastic model

For the fastener configuration shown in Figure 1, the elastic model and the plastic lower bound model give almost the same load-carrying capacity for the shear wall. The distribution of the fastener forces is, however, fairly different as is evident from Figure 3 and Figure 4. In the ultimate limit state the force distribution according to the plastic lower bound model can be justified for different reasons. One reason is that the joints between the timber members often tend to yield which means that the force components perpendicular to the length direction of the timber members can not be fully built up. Another reason is that at high loads some bending deformations in the timber members can almost always be seen, that also lead to reduced force components perpendicular to the timber members.

3 Simplified design model for partially anchored shear walls

3.1 Basic assumptions

For design of partially anchored shear walls a plastic lower bound method, see section 2.2.1, is proposed in this study. This means that a force distribution is chosen that fulfils the conditions of force and moment equilibrium for each timber member and sheet. The following basic assumptions are made:

- the sheathing-to-timber joints, referring to the vertical studs and the top rail, are assumed to transfer shear forces only parallel to the timber members
- the sheathing-to-timber joints, referring to the bottom rail, are assumed to transfer forces both parallel and perpendicular to the bottom rail
- compressive forces can be transferred via contact between adjacent sheets.

In order to obtain simple expressions for the racking resistance of the shear walls, the fasteners are assumed to be continuously distributed along the timber members. The load-carrying capacity of the fasteners is consequently given in force per unit length. In all the examples presented below, it is assumed that the fastener spacing around the perimeter of the sheets is constant.

3.2 Fully anchored leading stud

Shear walls with a fully anchored leading stud, i.e. walls where the end stud at the load-application-point is fully anchored to the substrate, can be designed according to the principles given in section 2.2.1. For a shear wall consisting of four sheets, the force distribution can be chosen as in Figure 6. In the upper part of the figure, the external and internal forces acting on the frame members are shown. In the lower part of the figure, the internal forces acting on the sheets are shown. All timber members and all sheets are in force and moment equilibrium. The force distribution corresponds to a pure shear flow. From a horizontal equilibrium equation for the top rail, the racking resistance H of the shear wall is obtained as

$$H = f_p l \quad (6)$$

where l = length of the wall

f_p = plastic fastener capacity per unit length of timber member

From a vertical equilibrium equation for the leading stud, the anchorage force F_a is obtained as

$$F_a = f_p h \quad (7)$$

The load case shown in Figure 6, is identical to the case where a diagonal force is applied on a shear wall with no anchorage of the leading stud.

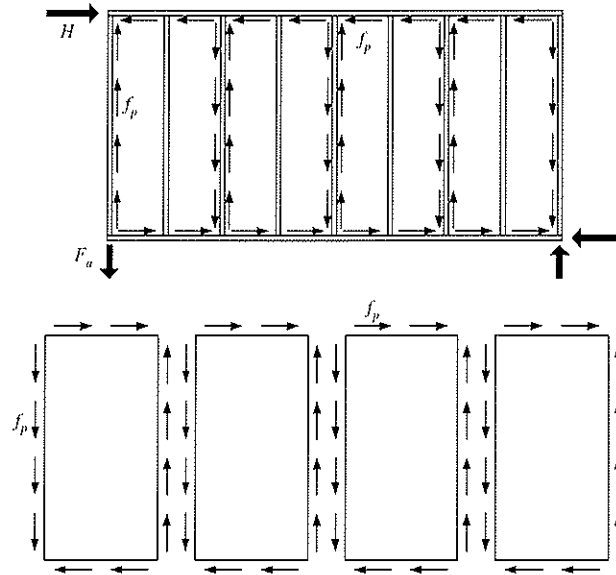


Figure 6: Forces acting on the timber frame and the sheets in the case of a fully anchored leading stud.

3.3 Fully anchored bottom rail - no vertical loads

A shear wall where the bottom rail is fully anchored to the substrate will now be studied. The leading stud is assumed to be completely free from the substrate and the framing joints are assumed to not transfer any tensile forces. The forces acting on the wall in the ultimate limit state are assumed to be distributed according to Figure 7. The forces acting along the lower part of the wall are shown in a section immediately above the bottom rail and represent the sheathing-to-timber joints. The factor μ opens for the possibility of using reduced strength properties when the fastener forces act perpendicular to the sheet edges. If nothing else is said, it is assumed that $\mu = 1$ in this paper. The notation l_{eff} is used to indicate that this length of the wall is fully effective for horizontal load transfer.

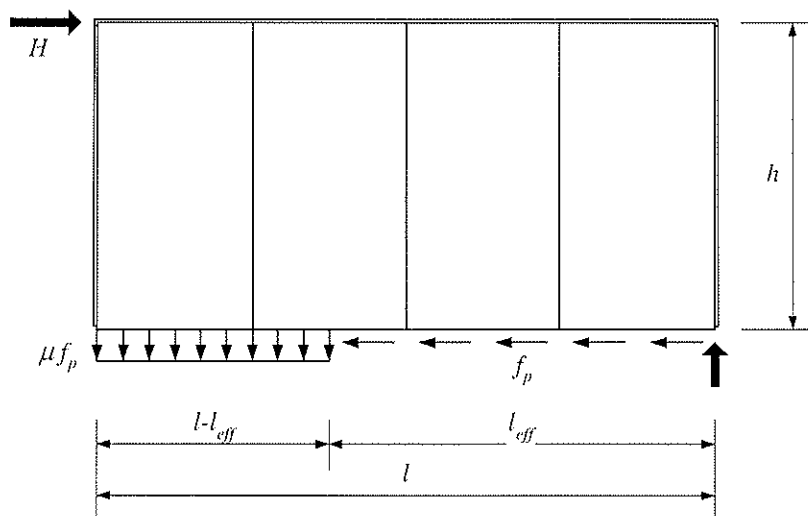


Figure 7: Forces acting on a shear wall in the case of a fully anchored bottom rail.

Moment equilibrium around the lower right corner of the wall diaphragm gives

$$H h = \mu f_p (l - l_{eff}) \left(\frac{l + l_{eff}}{2} \right) \quad (8)$$

Force equilibrium in horizontal direction gives

$$H = f_p l_{eff} \quad (9)$$

By introducing the notation

$$\alpha = \frac{l}{h} \quad (10)$$

and using equations (8) and (9) the effective wall length can be calculated as

$$l_{eff} = l \left(\sqrt{1 + \left(\frac{1}{\alpha \mu} \right)^2} - \frac{1}{\alpha \mu} \right) \quad (11)$$

The anchorage force is obtained as

$$F_u = \mu f_p (l - l_{eff}) \quad (12)$$

It is easy to show that this anchorage force is always less than the anchorage force $f_p h$ corresponding to a fully anchored leading stud according to equation (7). This means that the transferred shear flow between the sheets and the frame members is always less than the plastic fastener capacity f_p . The shear wall in Figure 7, will consequently work as a rigid body and the load-carrying capacity is determined by the plastic failure mechanism along the bottom rail.

By studying the force and moment equilibrium of the individual sheets in Figure 7, it is obvious that the proposed model will only work if compressive forces are transferred between the adjacent sheets. Since one of the basic assumptions of the simplified model was (see section 3.1) that the vertical studs can only transfer shear forces parallel to the timber members, the compressive forces must be transferred by direct contact between the sheets.

An alternative way of analysing shear walls with a fully anchored bottom rail is to assume that no compressive forces can be transferred between adjacent sheets. This leads to a stress distribution of the type shown in Figure 8. The force and moment equilibrium of each sheet is studied starting from the left end of the wall (see the right part of Figure 8). The unknown quantities $b_{1,eff}$, H_1 and V_1 are determined using the equations (9)-(11) and replacing l by b . When the force and moment equilibrium of the second sheet from the left is studied the force V_1 must be considered in the equations. For further details see equation (15) in section 3.5. The load-carrying capacity of the shear wall is obtained as the sum of horizontal forces acting on the top of the sheets.

The calculated effective wall length l_{eff} according to equation (11) is given in Table 1 for shear walls built up of different number of sheets. As is evident from equation (11), the distance $l - l_{eff}$ over which the anchorage force acts is always less than h . For the case of no contact between the adjacent sheets, the lengths l_{eff} and $l - l_{eff}$ are shown in the two last columns of Table 1. The load-carrying capacity of a shear wall is only slightly lower if it is assumed that there is no contact between the sheets.

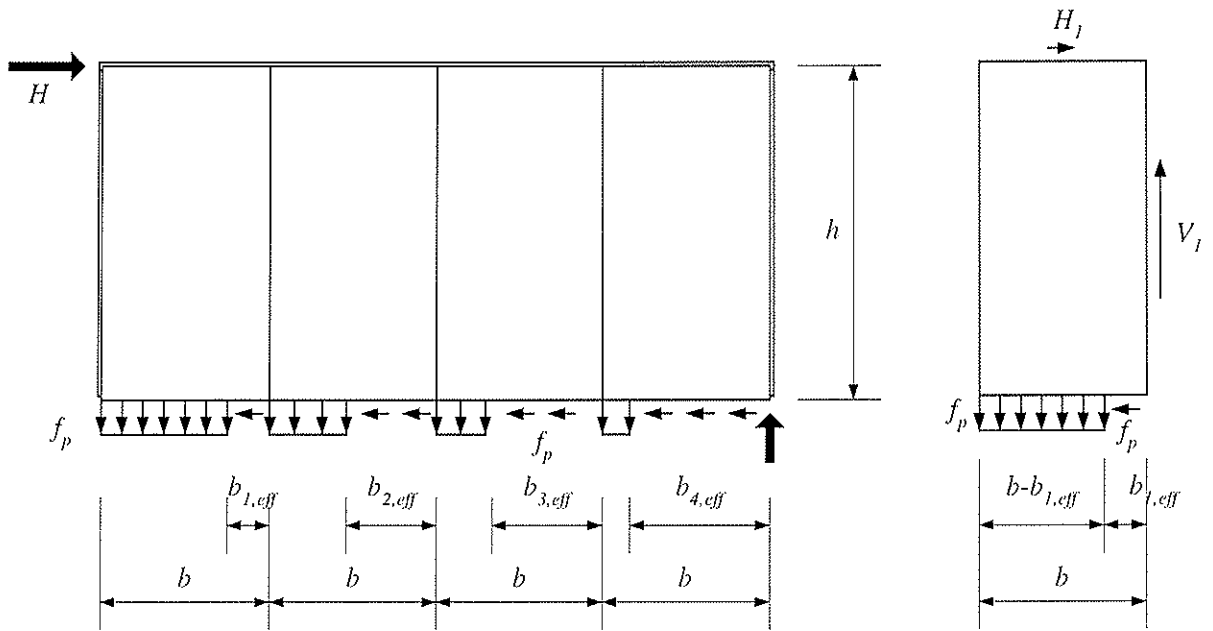


Figure 8: Fully anchored bottom rail. Force distribution in the case of no contact between the sheets.

Table 1: Effective wall lengths in the cases of contact and no contact between the sheets ($h/b=2$ and $\mu=1$).

| Number of sheets | Contact | | No contact | |
|------------------|-----------|---------------|------------|---------------|
| | l_{eff} | $l - l_{eff}$ | l_{eff} | $l - l_{eff}$ |
| 1 | $0,24 b$ | $0,76 b$ | $0,24 b$ | $0,76 b$ |
| 2 | $0,83 b$ | $1,17 b$ | $0,79 b$ | $1,21 b$ |
| 3 | $1,61 b$ | $1,39 b$ | $1,51 b$ | $1,49 b$ |
| 4 | $2,47 b$ | $1,53 b$ | $2,33 b$ | $1,67 b$ |
| 5 | $3,39 b$ | $1,61 b$ | $3,22 b$ | $1,78 b$ |
| 6 | $4,32 b$ | $1,68 b$ | $4,15 b$ | $1,85 b$ |

3.4 Not anchored bottom rail - vertical loads

Vertical loads in the form of dead load have normally a large influence on the load-carrying capacity of shear walls. The distribution of these loads depends to a large extent on the rigidity of the structure above the wall. If that structure is flexible the loads will be relatively uniformly distributed over the wall. If the structure is rigid the loads will be concentrated to the uplift points of the shear wall.

A shear wall with no vertical anchorage and with distributed vertical loads V according to Figure 9 is studied. In the upper part of the figure the external and internal forces acting on the frame members are shown. In the lower part of the figure the internal forces acting on the sheets are shown. For small loads V , the shear flow in all sheathing-to-timber joints will be less than the plastic shear flow f_p and the shear forces can be determined by systematically analysing the equilibrium of each sheet from the left to the right in the figure.

Thus, the horizontal force components acting on the top and bottom of the sheets are obtained by studying the moment equilibrium of each sheet. The studied load case in Figure 9 is of course trivial as long as the plastic shear flow f_p has not been attained in any point. The wall will in this case work as a rigid body and the load-carrying capacity H of the shear wall can directly be determined by studying the moment equilibrium of the whole wall.

If the plastic shear flow is attained in a point within the shear wall the calculations become more complicated. The force distribution within the previously investigated shear wall is in Figure 10 shown for the case when the plastic shear flow has just been attained in the whole of the sheet furthest to the right. The two vertical loads V furthest to the right are now transferred directly to the substrate since the sheet can not carry any more loads. The wall consisting of the three sheets to the left will work as a rigid body while there will be a plastic failure mechanism in the sheet furthest to the right. The load-carrying capacity H is calculated by summation of the horizontal forces acting on the top of each sheet.

In order to simplify design of shear walls it is possible to produce diagrams of the type shown in Figure 11. Relationships between load-carrying capacity H and vertical load V are given for shear walls assembled of 1 to 4 sheets. The bold lines in the small figures indicate where the plastic shear flow f_p has been attained in the sheathing-to-timber joints.

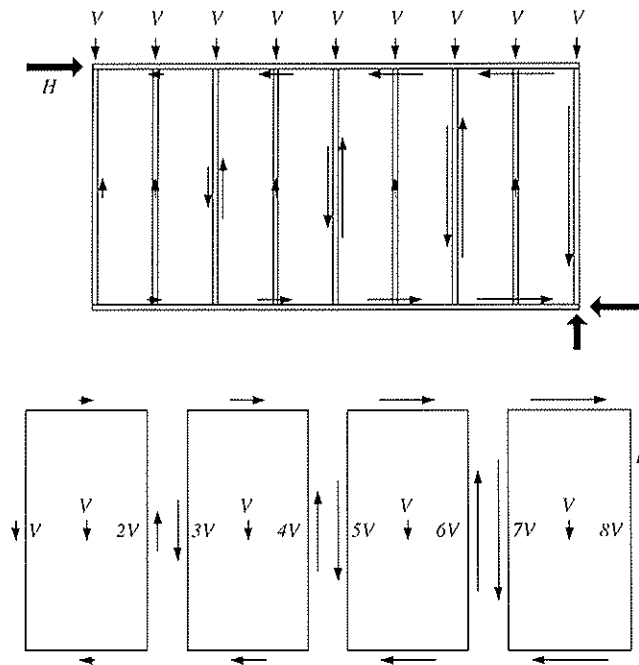


Figure 9: Forces acting on the timber frame and the sheets in the case of no vertical anchorage. The plastic shear f_p flow has not been attained.

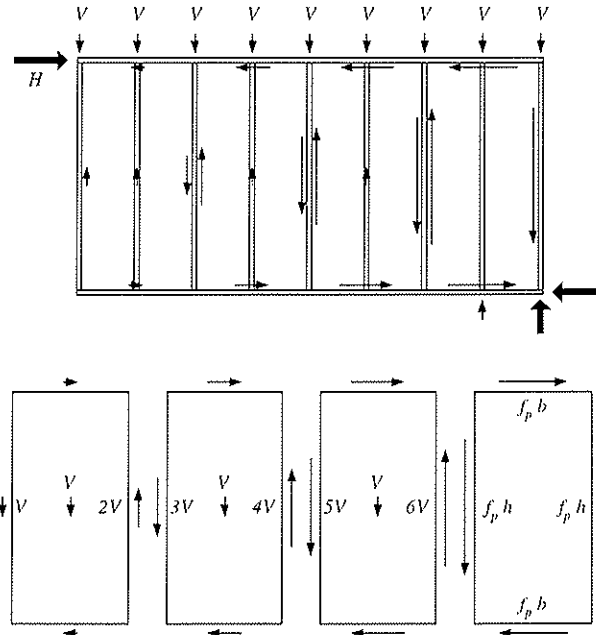


Figure 10: Forces acting on the timber frame and the sheets in the case of no vertical anchorage. The plastic shear flow f_p has been attained in the sheet furthest to the right.

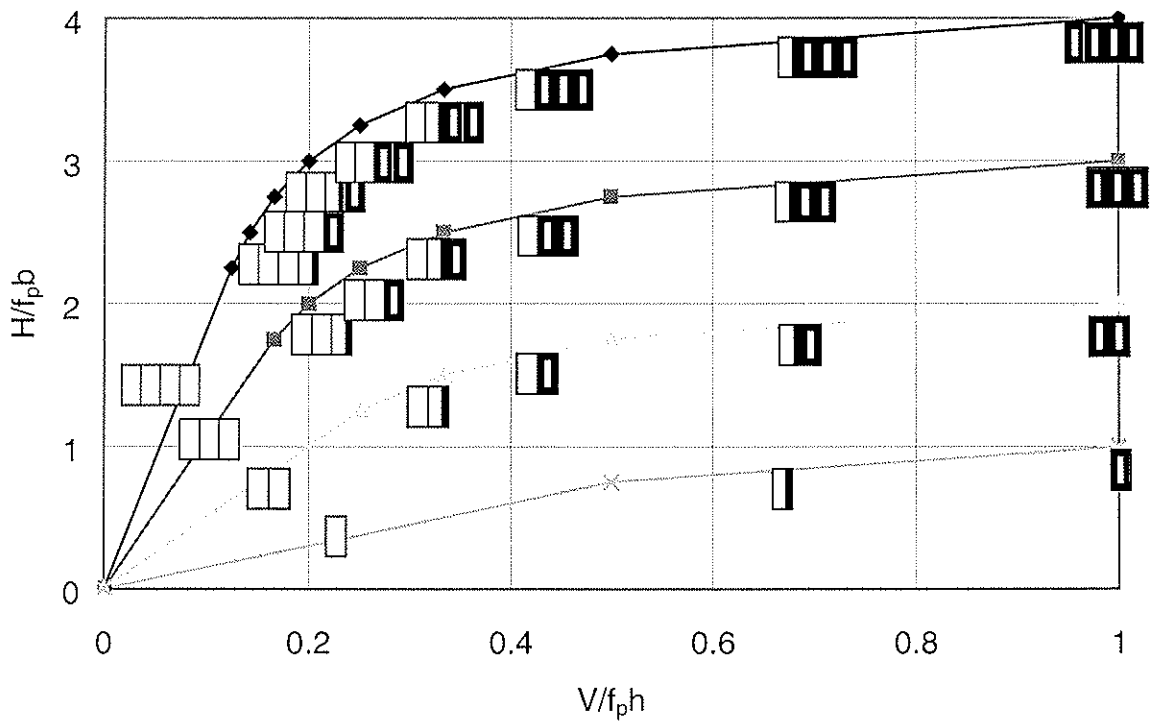


Figure 11: Relationships between load-carrying capacity H and vertical load V in the case of no anchorage. All studs are loaded, $h/b = 2$ and $\mu = 1$. The progress of plastification in the walls is indicated by the bold lines in the small figures.

3.5 Fully anchored bottom rail - vertical loads

The shear wall in section 3.3 will now be analysed when a vertical load is acting on the leading stud. The assumed forces acting on the wall are shown in Figure 12. The vertical load V can be expressed by the factor β defined as

$$\beta = \frac{V}{f_p h} \quad (13)$$

The case $\beta = 1$ corresponds to a fully anchored leading stud. A moment equation around the lower right corner of the wall gives

$$H h - V l = \mu f_p (l - l_{eff}) \left(\frac{l + l_{eff}}{2} \right) \quad (14)$$

From the equations (9), (10), (13) and (14) the effective wall length is obtained as

$$l_{eff} = l \left(\sqrt{1 + \left(\frac{1}{\alpha \mu} \right)^2} + \frac{2\beta}{\alpha \mu} - \frac{1}{\alpha \mu} \right) \quad (15)$$

The value of the factor β in equation (15) may not be larger than unity. If $\beta < 1$ then the expression within parenthesis in equation (15) will always be less than unity. This means that the transferred shear flow between the sheets and the studs is always less than the plastic shear flow f_p . An alternative design procedure would have been to systematically study the moment equilibrium of each sheet from the left end of the wall to the right one, as in section 3.3.

Relationships between the load-carrying capacity H and the vertical load V are given in Figure 13 for shear walls consisting of different number of sheets. It is assumed that the depth-to-width ratio of a sheet $h/b = 2$ and $\mu = 1$. For $V = 0$ the same racking load is obtained as was given in Table 1.

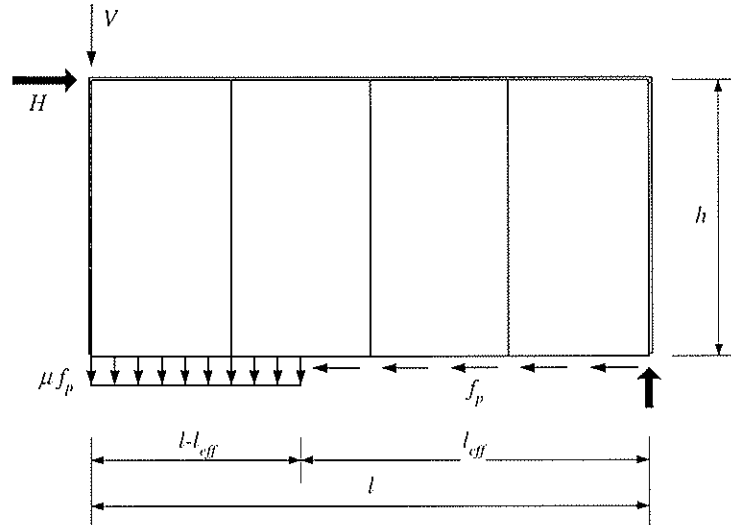


Figure 12: Forces acting on a shear wall in the case of a fully anchored bottom rail and a vertical load on the leading stud.

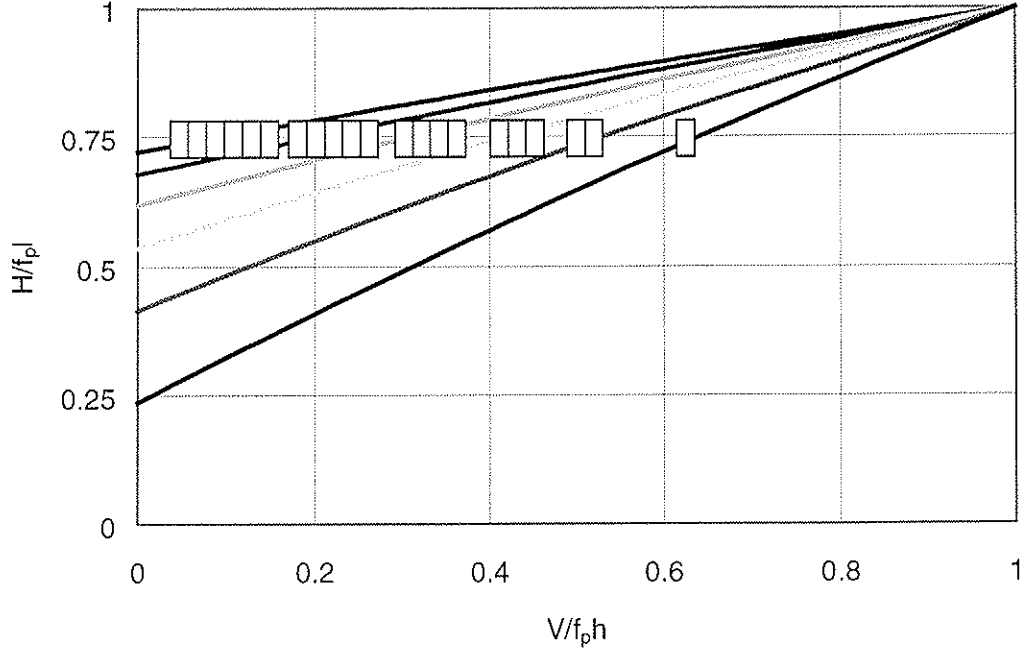


Figure 13: Relationships between load-carrying capacity H and vertical load V in the case of a fully anchored bottom rail. Only the leading stud is loaded, $h/b = 2$ and $\mu = 1$. The small figures indicate the number of sheets in the shear walls.

We will now study a load case where the vertical load V acting on the leading stud has been replaced by a vertical load V acting on each stud according to Figure 14. The forces are assumed to be transferred in the same way as previously was described. This means that it is assumed that the plastic shear flow has not been attained along any of the vertical studs. Consequently for the sheathing-to-timber joints furthest to the right, the shear force must fulfil the condition

$$\mu f_p (l - l_{eff}) + (n_v - 1)V \leq f_p h \quad (16)$$

where n_v = number of vertical loads V .

Now the moment equilibrium of the shear wall can be expressed as

$$H h - n_v V \frac{l}{2} = \mu f_p (l - l_{eff}) \left(\frac{l + l_{eff}}{2} \right) \quad (17)$$

By introducing the factor κ

$$\kappa = \frac{n_v V}{f_p h} \quad (18)$$

and using the equations (9), (10), (17) and (18) the effective wall length is obtained as

$$l_{eff} = l \left(\sqrt{1 + \left(\frac{1}{\alpha \mu} \right)^2 + \frac{\kappa}{\alpha \mu}} - \frac{1}{\alpha \mu} \right) \quad (19)$$

If condition (16) is not fulfilled, the expression for the effective length l_{eff} becomes fairly complicated. In such cases, a reasonable approximation is to determine l_{eff} according to

equation (19) for those vertical loads where plasticity starts in the different sheets and then use linear interpolation between these points. The relationship between load-carrying capacity H and vertical load V from such a calculation is presented in Figure 15 for a shear wall consisting of 4 sheets. As a comparison the results from a calculation with a shear wall without vertical anchorage are shown. The bold lines in the small figures show where a plastic shear flow has been attained in the sheathing-to-timber joints.

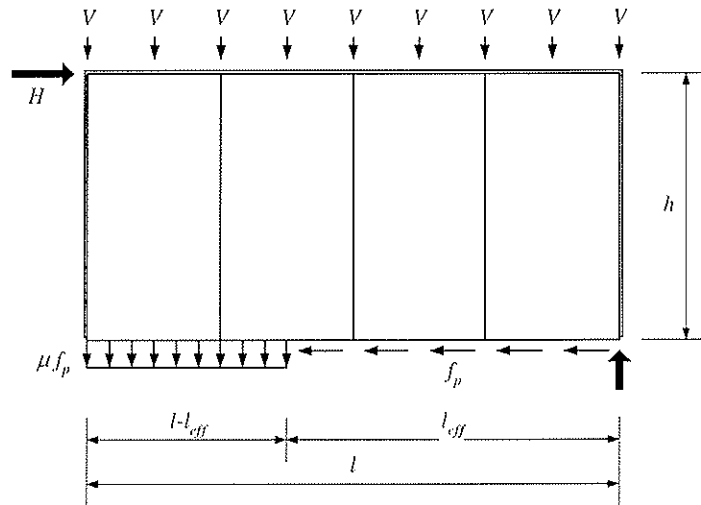


Figure 14: Forces acting on a shear wall in the case of a fully anchored bottom rail and vertical loads on all studs.

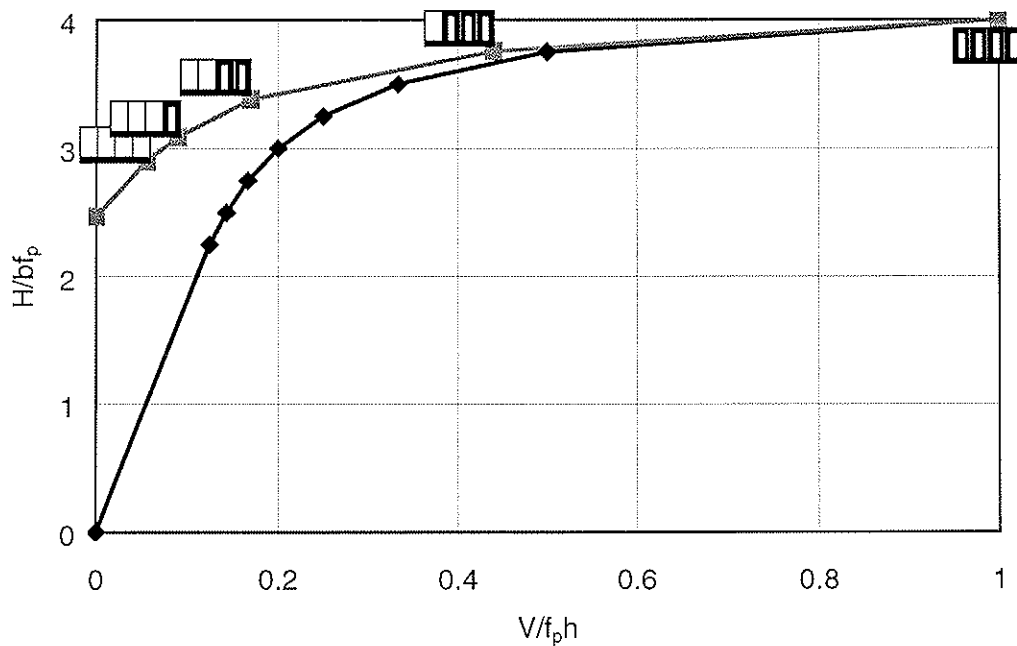


Figure 15: Relationships between load-carrying capacity H and vertical load V . The upper curve refers to the case of a fully anchored bottom rail. The lower curve refers to the case of no anchorage. All studs are loaded, $h/b = 2$ and $\mu = 1$. The progress of plastic flow in the walls is indicated by the bold lines in the small figures.

4 Experimental work

4.1 Tests of shear walls

Some introductory racking tests of shear walls have been conducted, where the influence of different kind of anchorage and load configurations has been investigated. A few tests of shear walls with openings were also conducted but the results of those will not be reported here. The test results are preliminary and need to be further evaluated.

A specification of shear walls tested is shown in Table 2. All walls tested consisted of four sheets of fibreboard fastened to a timber frame where the centre distance between the studs was 600 mm. The supplier of the medium density fibreboard was Masonite AB in Sweden. The thickness of the fibreboard was 8,0 mm and the size of the sheets was 1200 x 2400 mm. The dimension of the frame members was 45 x 120 mm and the timber quality corresponded to C24.

For the sheathing-to-timber connections, annular ringed shank nails of dimension 50 x 2,3 mm were used. The nails were attached by a handheld nailing gun. The distances between the fasteners were 100 mm along the perimeter of the sheets and 200 mm along the vertical centre lines of the sheets. The nominal edge distance was 11,25 mm along the vertical studs and 22,5 mm along the bottom and top rails. For each framing joint two annular ringed shank nails of dimension 90 x 3,1 mm were used. These nails were applied in the grain direction of the vertical studs.

The horizontal load was applied by a hydraulic jack in line with the top rail except for the first test specimen where the load was applied diagonally. A deformation speed of 8 mm/min was used. This corresponds to a time to failure of about 5 minutes. The vertical loads were applied manually by hydraulic jacks. The test specimens were prevented from slipping along the substrate by a horizontal support that was in contact with the end of the bottom rail.

Some observations regarding the tests should be given. The positions of the nails deviated in many cases considerably from the nominal ones. This resulted sometimes in splitting of the frame members due to small edge distances. In other cases local edge failures occurred around some of the nails in the fibreboard. The behaviour of the sheathing-to-timber joints was often somewhat brittle. The nails were sometimes torn to pieces.

After the testing of the first three walls it was observed that there had been some contact between one of the sheets and the support. It is possible that this had a slight effect on the load-carrying capacity of the walls.

Some test results are presented in Table 3. Measured load-carrying capacities are given in the second column. Test specimen 1 served as a reference test for the other tests. The load was in this case applied in the diagonal direction of the wall diaphragm but the horizontal load component is given in the table. Using equation (6), the plastic shear flow is obtained as $f_p = 51,7 / 4,8 = 10,8$ kN/m. In the third column of the table, the theoretical load-carrying capacities are given. The simplified model in section 3 has in this case served as a basis for the expressions. The calculated load-carrying capacities in the fourth column of the table have been obtained by inserting numerical values in the expressions. Finally, in the last column of the table, the ratios between measured and calculated load-carrying capacity are shown.

Table 2: Specification of shear walls tested

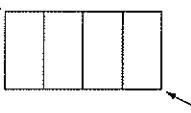
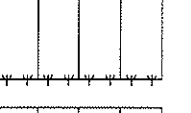
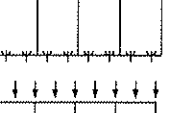
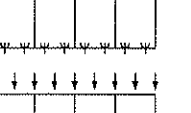
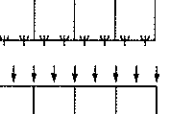
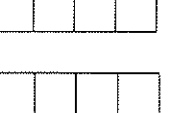
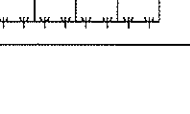
| Test wall | Load configuration | Anchored bottom rail | Vertical load V [kN] |
|-----------|---|--------------------------|------------------------|
| 1 |  | No | |
| 2 |  | Yes | |
| 3 |  | Yes No framing joints | |
| 4 |  | Yes | 1,29 $(0,05 f_p h)$ |
| 5 |  | Yes | 3,23 $(0,125 f_p h)$ |
| 6 |  | No | 6,46 $(0,25 f_p h)$ |
| 7 |  | Yes | 12,9 $(0,50 f_p h)$ |

Table 3: Measured and calculated load-carrying capacities.

| Test wall | Load-carrying capacity H | | | $\frac{H_{measured}}{H_{calculated}}$ |
|-----------|----------------------------|--------------|-----------------|---------------------------------------|
| | Measured [kN] | Theoretical | Calculated [kN] | |
| 1 | 51,7 | $4,00 f_p b$ | | 1,00 (reference) |
| 2 | 33,2 | $2,47 f_p b$ | 31,9 | 1,04 |
| 3 | 29,4 | $2,47 f_p b$ | 31,9 | 0,92 |
| 4 | 50,1 | $2,86 f_p b$ | 37,0 | 1,35 |
| 5 | 52,5 | $3,22 f_p b$ | 41,6 | 1,26 |
| 6 | 48,2 | $3,25 f_p b$ | 42,0 | 1,15 |
| 7 | 53,1 | $3,29 f_p b$ | 42,5 | 1,25 |

The difference between test specimen 2 and 3 was that the nails in the framing joints were removed along the bottom rail in specimen 3. The reason for doing so was to study the influence of the frame member connections on the load-carrying capacity. The tests indicate these joints contribute to about 10 percent higher load-carrying capacity.

The obtained ratios between measured and calculated load-carrying capacity are according to Table 3 in the range between 0,92 and 1,35. The lowest ratios are obtained for those test walls that are not subjected to any vertical load. A possible explanation is that these walls are subjected to high tensile forces in the sheathing-to-timber connections along the bottom rail, which might lead to more brittle failures.

5 Design aspects

The transfer of forces within a shear wall is strongly dependent on how the timber frame and the sheet material are assembled and how the diaphragm is connected to the surrounding structures. Of particular interest is the anchoring of the shear wall to the substrate.

The presented simplified model is based on the assumption that the sheathing-to timber joints have a plastic behaviour. In reality there will almost always be parts of the shear wall that have a somewhat brittle behaviour. It is, however, important that the brittle failure modes do not dominate the behaviour of the structure. Brittle failure modes can occur as a consequence of

- small edge distances for the fasteners
- small distances between the fasteners
- brittle material properties of the fasteners
- bad anchorage of the bottom rail
- openings in the shear wall

6 Conclusion

The basic principles of a simplified plastic model for design of incompletely anchored wood-framed shear walls have been presented. The model can be used if the sheet material is fixed by mechanical fasteners and if these sheathing-to-timber joints show plastic behaviour. The model can only be applied on static loads in the ultimate limit state.

Some introductory tests of shear walls have been conducted where the bottom rail was completely fixed to the substrate or free with respect to vertical displacements. Some of the tests included vertical loads. The test results indicate that there is a reasonable agreement between measured and calculated load-carrying capacities.

The model explains the structural behaviour of incompletely anchored wood-framed shear walls and is suitable for calculations by hand. The model can be used to analyse the influence of 3-dimensional load transfer within a building.

7 Future work

The simplified method has so far only been checked against some introductory experiments. The intention is to repeat these experiments with specimens that have been manufactured under more controlled conditions.

The behaviour of a shear wall is to a large extent governed by the anchorage of the bottom rail. In most of the tests performed so far the bottom rail has been completely fixed to the substrate. Results from tests performed under more realistic boundary conditions are needed.

In order to consider the 3-dimensional behaviour of a timber framed building, more data is needed regarding the mechanical properties of the joints between different diaphragms within the building.

When shear walls are tested brittle failure modes can often be observed. It is important to give design rules that reduce the occurrence of such types of failure.

In this paper the simplified model has only been applied on walls without openings. Some work has already been done in order to extend the model to include the influence of openings, but the model must be developed further in this respect.

Finally there is a need to develop more diagrams and tables that can facilitate a structural design.

8 References

Draft prEN 1995-1-1, Eurocode 5 – Design of timber structures – Part 1-1: General rules and rules for buildings, Final draft May 2001.

EN 594:1995, Timber structures – Test methods – Racking strength and stiffness of timber frame wall panels.

Andreasson, S., 2000, Three-dimensional interaction in stabilisation of multi-storey timber frame building systems, Lund University, Report TVBK-1017, Lund.

Källsner, B., 1984, Panels as wind-bracing elements in timber-framed walls, Swedish Institute for Wood Technology Research, Report No. 56, Stockholm.

Källsner, B. and Lam F., 1995, Diaphragms and shear walls, *Holzbauwerke nach Eurocode 5 - STEP 3*, Arbeitsgemeinschaft Holz e. V., Düsseldorf, pp 15/1-15/19.

INTERNATIONAL COUNCIL FOR RESEARCH AND INNOVATION
IN BUILDING AND CONSTRUCTION

WORKING COMMISSION W18 - TIMBER STRUCTURES

THE EFFECT OF THE MOISTURE CONTENT
ON THE PERFORMANCE OF THE SHEAR WALLS

Shiro NAKAJIMA
Building Research Institute

JAPAN

Presented by: S Nakajima

- H J Blass asked what types of nails were used and whether they had corrosion protection.
- S Nakajima stated that smooth shank nails were used and small amount of rust was observed as they did not have any corrosion protection. He agreed that this might lead to increase in capacity in the nail tests.
- V Enjily commented that the test method for panel shear will be changed in CEN and received clarification that the service class order referred to the Japanese case.
- S Nakajima agreed that international harmonisation of service class order should be considered in the future.

The effect of the moisture content on the performance of the shear walls

Shiro NAKAJIMA
Building Research Institute, JAPAN

1 Abstract

Plywood sheathed or OSB sheathed shear walls were constructed by the 2X4-construction system and tested in two environments, 20°C, 65% R.H. and 20°C, 90% R.H. to clarify the effect of the moisture contents on the racking strength and stiffness of the shear walls. The nail joints of the shear walls and the sheathing materials were also test in the two environments to clarify the effect of the moisture contents on the strength and deformation properties of the nail joints and the panel shear properties of the sheathing materials. The reduction of the yield strength of the plywood sheathed shear walls after being conditioned in the atmosphere of 20°C and 90% R.H. was 15% and that of the OSB sheathed shear walls was 10%. The test results suggested that the durability of the shear walls against water might not be adequately evaluated by the current evaluation method.

The yield strength and the initial stiffness of the shear walls were estimated from the strength and stiffness properties of the nail joints and the sheathing materials. The results of the calculation suggested that the simplified calculation method described in the 2X4 designers' manual does not sufficiently predict the effect of the moisture contents on the performance of the shear walls.

2 Introduction

The moisture contents of wooden materials and components affect on the strength and stiffness properties of the joints and the shear walls of wooden structures (Arima et.al. 1981). In most cases the strength and stiffness properties of the joints and the shear walls are evaluated from the test results of the test pieces that are conditioned in the standard condition, temperature 20°C and relative humidity 65%. Wooden structures are used under various humidity and temperature. And the performance of the joints and the shear walls of these structures should be properly evaluated according to the conditions in which they are used.

On the other hand the species or the grades of the lumbers that compose the shear walls will affect on the performance of the shear walls. The effect of the performance of the materials on the performance of the shear walls should also be clarified to enable the optimal use of the materials.

“Methods for stipulating the allowable stress, and elastic modulus of framing and sheathing materials” were announced in 1998 by the former Ministry of Construction (Japan 2X4 Home Builders Association, 1998). Three service classes, service class 1, service class2 and service class3 were proposed at that time.

Service class 1 is the environments in which structural members are directly exposed to the outside or could be perpetually exposed to moisture. The representative temperature and

relative humidity for this service class are 20°C and 95%. Service class 2 is the environments in which structural members are indirectly exposed to the outside or could be intermittently exposed to moisture as sheathing materials of exterior wall, roof or floor. The representative temperature and relative humidity for this service class are 20°C and 85%. Service class 3 is the environments other than those of service class 1 and 2. The representative temperature and relative humidity for this service class are 20°C and 65%. The above-mentioned methods require structural materials and components to be tested according to the conditions they are used.

In Japan the allowable shear strengths of the shear walls constructions by the 2X4-construction system were decided by analyzing the test data of the series of shear wall tests conducted in 1975 (Building Research Institute 1975). In the process of calculating the allowable shear strengths of the shear walls, the strength modification factors were multiplied to the shear strength to give safety factors for the durability issues of the sheathing materials against water. Table 1 shows the values of these strength modification factors. Most of these values were derived from the test results of the lateral nail resistance test of the nailed joints. The strength reductions of the nailed joints after experiencing three cycles of wet and dry procedures were mainly considered when deciding the values for the modification factor. The modification factors were not directly derived from the test data of the shear walls.

Table 1 The shear strength modification factors for sheathed shear walls

| Sheathing Type | Modification factor |
|--|---------------------|
| Plywood 9mm in thickness | 1.00 |
| Plywood 7.5mm in thickness | 1.00 |
| Insulation board 12mm in thickness | 0.75 |
| Particleboard 12mm in thickness | 0.85 |
| Hard board 5mm in thickness | 0.65 |
| Hard board 7mm in thickness | 0.90 |
| Hard cement particle board 12mm in thickness | 0.75 |
| Gypsum board 12mm in thickness | 0.75 |

As there are limitations in the capacity of the testing facilities in most cases it is difficult to condition full size shear walls in a certain atmosphere. And of course it is quite difficult to conduct a full size shear wall test in a chamber controlled to a certain temperature and humidity. For these reasons the durability of the shear walls against water should be evaluated from the durability performance of the composing materials and joints. The object of this research is to evaluate the performance of the shear walls and estimate the effect of the moisture contents on the performance of the shear walls from performance of the nail joints and the sheathing panels.

3 Testing

3.1 Racking test of shear walls

3.1.1 Test specimens

Figure 1 shows the size and assembly of the shear walls. The types and grades of the materials are also described in this figure. The shear walls were 2460mm in height and 948mm in width and sheathed with 9.0mm thick CSP plywood panels (JAS Grade S-2) or 9.5mm thick OSB panels (JAS Grade S-4).

The moisture contents and the specific gravity of the structural lumbers and the sheathing

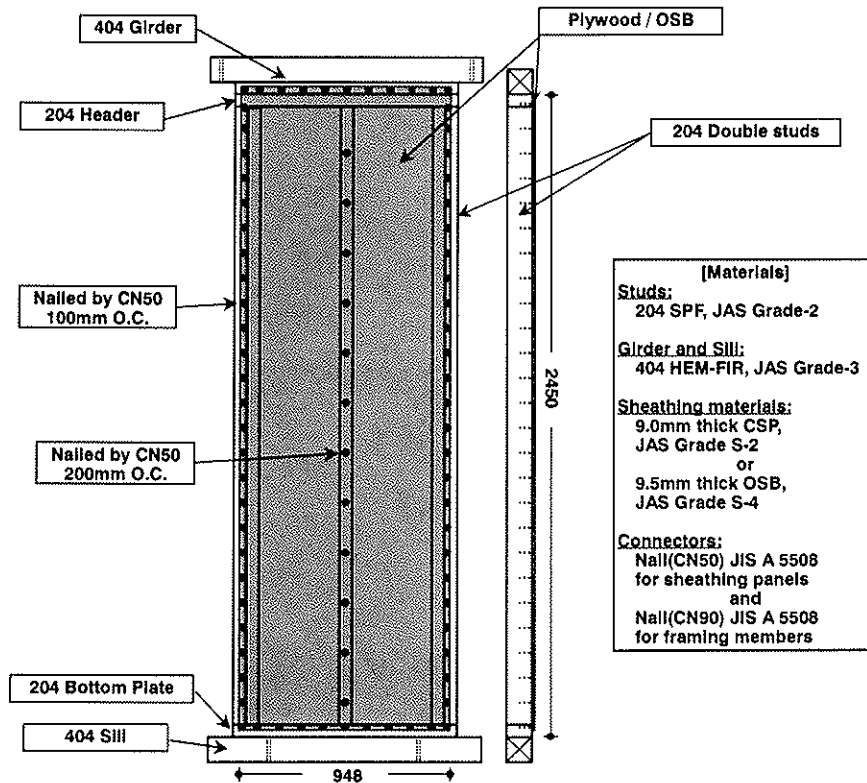


Figure 1 Size and assembly of the shear wall test specimens.

panels were measured before assembling the test specimens. The specific gravities of the lumbers composing every test specimens were controlled so that there would be no significant difference among the average specific gravities of the lumbers composing each test specimen.

The test specimens were assembled following the specification stipulated in the Notification no.56, "Establishment of technical standards for ensuring structural safety of wood frame construction (Ministry of construction, 1982)".

3.1.2 Testing methods

10 plywood sheathed test specimens and 10 OSB sheathed test specimens were tested to evaluate the racking strength and stiffness. Half of the test specimens were conditioned in a chamber controlled to 20°C and 90% R.H and another half of test specimens were conditioned in a chamber controlled to 20°C and 65% R.H. The relative humidity 90% was chosen considering the maximum controllable relative humidity of the chamber. So the temperature 20°C and relative humidity 90% dose not exactly represent the environment of the service class 1. This temperature and relative humidity represent the intermediate circumstance of service class 1 and service class 2. All test specimens were controlled in the chamber until the change of the mass of

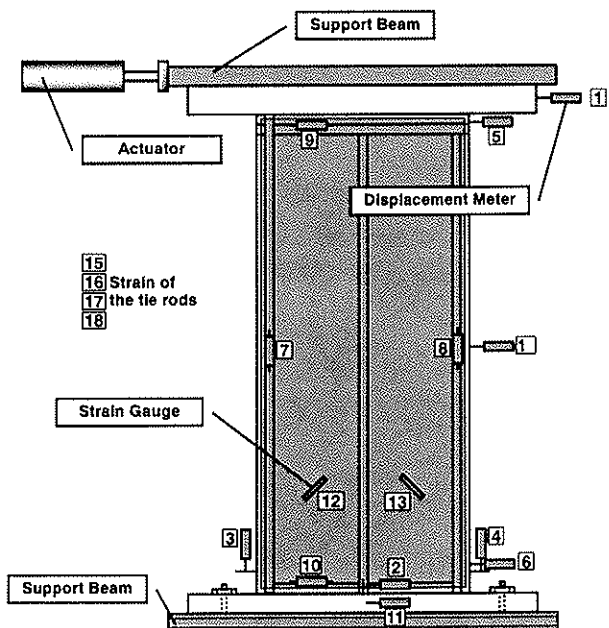


Figure 2 Test set-up for the racking test.

the sample test specimens (lumbers, plywood panels and OSB panels) over 24 hours were less than 1%.

The shear walls were tested to evaluate their racking strength and stiffness under cyclic loading. The loading schedule is shown in figure 3. The loading schedule follows the ISO TC165 protocol for joints (ISO/DIS 16670). The ultimate deformation of the test

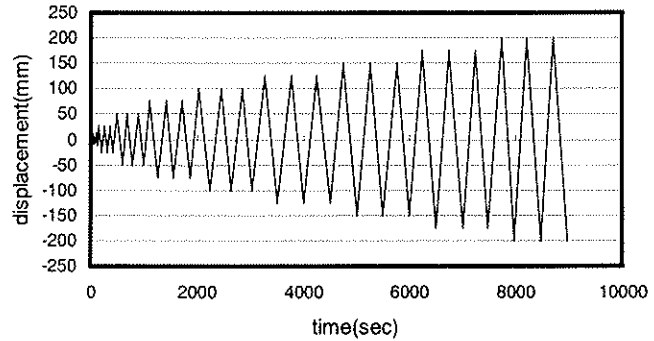


Figure 3 Loading Schedule.

specimens was experimentally known to be approximately 125mm. A single cycle reversed-cyclic load was applied at 1.25%, 2.5%, 5.0%, 7.5% and 10.0% levels of the ultimate deformation. And three cycles of reversed-cyclic load was applied at 20%, 40%, 60%, 80%, 100%, 120% (continue) level of the ultimate deformation. The loading velocity was approximately 80mm/min.

The load was applied to the top girder of the test specimens. Figure 2 shows the details of the test setup. Lateral load was applied to the shear walls using the tie rods. The horizontal movements of the test specimens were measured at the top, bottom and middle of the walls and the lateral movements of the test specimens were measured at the bottom of the studs. The relative movement of the sheathing panels against the framing members and the strain of the sheathing panels were also measured to evaluate the slip of the nail joints and the deformation of the sheathing panels.

3.2 Panel shear test of panels

3.2.1 Test specimens

20 pieces of plywood panels and OSB panels were tested to evaluate their panel shear modulus of rigidity and panel shear strength. Figure 4 shows the size and shape of the test specimens. The panel size is 600mm in length and 400mm in width. The size and shape of the test specimens almost follow the regulation stipulated in the final draft of prEN 798 (Final draft prEN 789 1995). After bonding two sets of rails on both sides of the panels the test specimens were conditioned in a chamber. Half of the test specimens were conditioned to constant mass in an atmosphere of temperature 20°C and relative humidity 65% and half of them were conditioned in an atmosphere of temperature 20°C and relative humidity 90%.

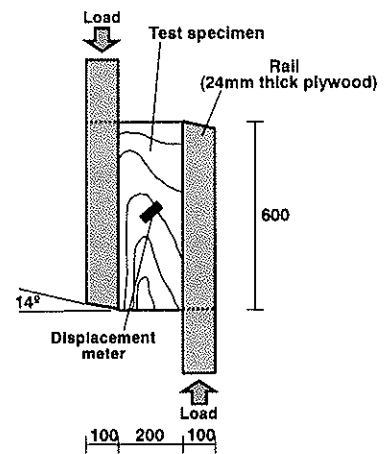


Figure 4 Test specimens for the panel shear test.

30 pieces of gypsum boards were tested in the same way. One-third of them were conditioned in an atmosphere of temperature 20°C and relative humidity 65% and another one-third of them were conditioned in an atmosphere of temperature 20°C and relative humidity 80%. The rest of the test specimens were conditioned in an atmosphere of temperature 20°C and relative humidity 90%.

3.2.2 Testing methods

The testing methods stipulated in Annex B of the final draft of prEN 798 was used as the testing method. The load was applied in a constant rate and the maximum load was

reached within about 300 seconds. The deformation of the test piece was measured at the center on each side of the test piece, using transducers.

3.3 Reverse-cyclic test of nail joints

3.3.1 Test specimens

Three types of nail joint test specimens, plywood connected to the stud (204) by nails (CN50), OSB connected to the stud (204) by nails (CN50) and gypsum board connected to the stud (204) by nails (GNF40) were tested to evaluate the performance of the nail joints. Figure 5 shows the size and shape of the test specimens. The size of the sheathing materials was 250mm in length and 100mm in width. The sheathing materials were nailed on the edge-wise sides of the stud (204) with four nails.

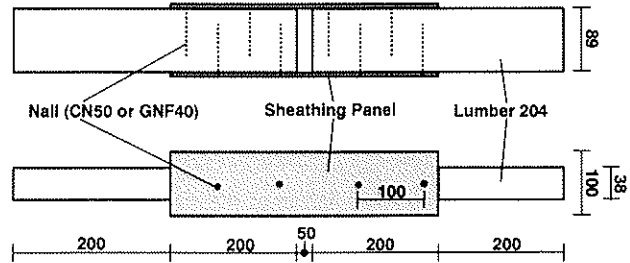


Figure 5 Test specimens for the reverse-cyclic test of nail joints.

20 test specimens were prepared for every nail joints type. After nailing the sheathing panels to the studs the test specimens were conditioned in a chamber. Half of the plywood nailed test specimens and OSB nailed test specimens were conditioned to constant mass in an atmosphere of temperature 20°C and relative humidity 65% and half of them were conditioned in an atmosphere of temperature 20°C and relative humidity 90%. And half of the gypsum board nailed test specimens were conditioned in an atmosphere of temperature 20°C and relative humidity 65% and half of them were conditioned in an atmosphere of temperature 20°C and relative humidity 80%.

3.3.2 Testing methods

Both ends of the studs (204 lumber) were connected to the testing equipment and the reverse-cyclic load was applied to the test specimens. The loading schedule followed the ISO/DIS 16670 protocol. The slip between the sheathing materials and the studs were measured, using transducers.

4 Results and discussion

4.1 Moisture condition of the test specimens

During conditioning the test specimens the weight of the samples of the 204 lumber, plywood and OSB were monitored. Figure 6 shows the weight increase ratio of each sample. The samples conditioned in an atmosphere of temperature 20°C and relative humidity 65% had no significant weight increase (or decrease). The weight of the samples conditioned in an atmosphere of temperature 20°C and relative humidity 90% increased in the first 15 days and the weight became almost constant after conditioning 30 days. The weight increase ratio of the plywood and the OSB was around 20% and that of the lumbers was around 12%. The moisture contents of these materials after conditioned in the humid atmosphere were almost 25%.

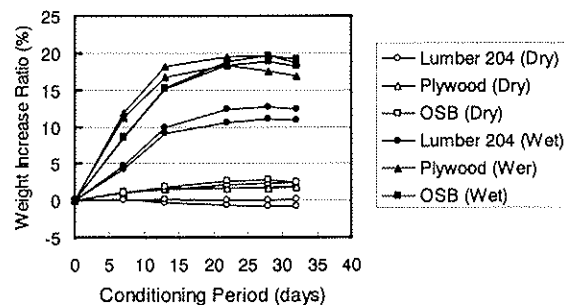


Figure 6 Weight increase ratio of the sample test specimens.

4.2 Test results of the racking tests of shear walls

The typical load - true displacement curves of the shear walls are shown in figure 7. The true displacement d_{true} is calculated by the following formula:

$$d_{true} = disp_1 - disp_2 - \frac{disp_3 - disp_4}{w \times h} \quad \text{--- (1)}$$

where,

h is the height of wall (2450mm).

w is the width of the wall (910mm).

$disp_n$ is the displacement measured by transducer no. n .

The first reversed cycles were used to derive the envelope curves. The strength properties and the deformation properties of the shear walls were evaluated from the envelope curves. Yield strength (P_y), yield deformation (D_y), ultimate strength (P_u), ultimate deformation (D_u) and initial stiffness (K) were derived using the calculation methods shown in figure 8.

The test results of the plywood sheathed shear walls and the OSB sheathed shear walls are summarized in table 2 and table 3. The average P_y , D_y , P_u , D_u and K and their coefficient of variation are tabulated in both tables.

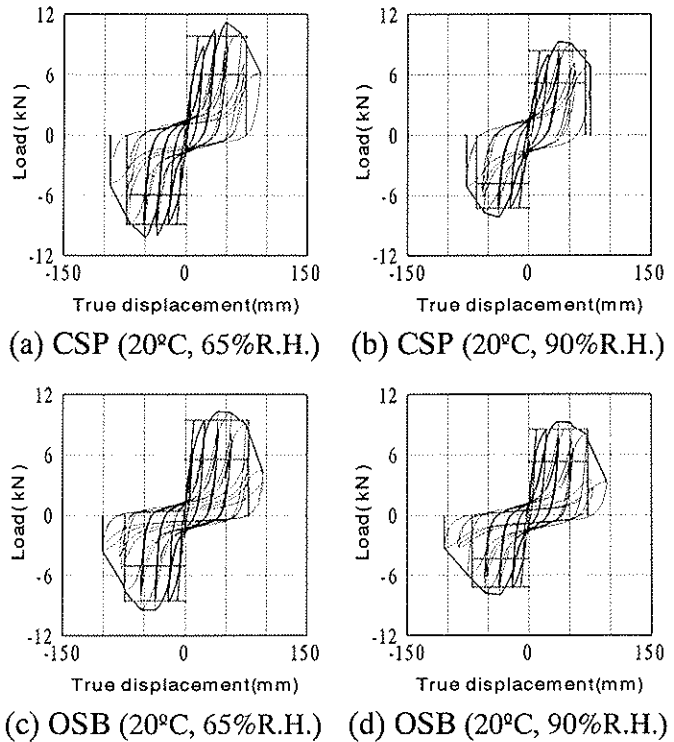


Figure 7 Representative load - true displacement curves of the shear walls.

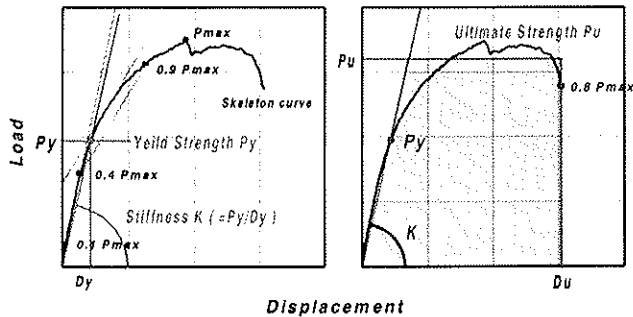


Figure 8 Calculation methods for P_y , D_y , P_u , P_y and K .

The weight of the shear walls increased more than 10% after being conditioned in the atmosphere of 20°C and 90% R.H. The increase ratio was almost same between the plywood sheathed shear walls and the OSB sheathed shear walls. The thickness swelling of the two materials was not same and the thickness swelling of the OSB panels was more than 20% when that of the plywood panels was less than 10%.

The reduction of the yield strength of the plywood sheathed shear walls after being conditioned in the atmosphere of 20°C and 90% R.H. was 15% and that of the OSB sheathed shear walls was 10%. The reduction of the ultimate strength was 13% for the plywood sheathed shear walls and 9% for the OSB sheathed shear walls. The reduction of the initial stiffness of the plywood sheathed shear walls was 21% and the initial stiffness of the OSB sheathed shear walls increased 5% after being conditioned in the atmosphere of

20°C and 90% R.H. As mentioned above the strength modification factors for the plywood sheathed shear walls is 1.00 and that for the OSB sheathed shear walls is 0.85. The effect of the repetitive dry and wet condition and other factors should be considered before making a conclusion though the modification factor 1.00 for plywood seems to be too high and the modification factor 0.85 for OSB seems to be too conservative.

The reduction of the ultimate deformation was 5% for the plywood sheathed shear walls and 8% for the OSB sheathed shear walls. The ductility of the plywood sheathed shear walls and the OSB sheathed shear walls seems to be almost same in both dry and wet conditions.

Table 2 Summary of the test results of the plywood sheathed shear walls.

| | (1) 20°C , 65% | (2) 20°C , 90% | (2)/(1) |
|----------------------|----------------|----------------|---------|
| Weight (kg) | 34.24 (4.2%) | 38.56 (4.8%) | 1.13 |
| Panel thickness (mm) | 9.25 (1.1%) | 9.91 (1.7%) | 1.07 |
| Py (kN) | 5.70 (3.8%) | 4.85 (3.5%) | 0.85 |
| Dy (mm) | 11.01 (6.3%) | 11.79 (9.1%) | 1.07 |
| Pu (kN) | 8.93 (2.7%) | 7.72 (4.7%) | 0.87 |
| Du (mm) | 94.44 (2.9%) | 89.88 (4.5%) | 0.95 |
| K (kN/cm) | 5.25 (5.0%) | 4.17 (7.4%) | 0.79 |

Note: The figures shown in the parenthesis are the coefficient of variation.

Table 3 Summary of the test results of the OSB sheathed shear walls.

| | (1) 20°C , 65% | (2) 20°C , 90% | (2)/(1) |
|----------------------|----------------|----------------|---------|
| Weight (kg) | 39.68 (3.7%) | 44.02 (5.2%) | 1.11 |
| Panel thickness (mm) | 9.85 (1.4%) | 12.04 (4.0%) | 1.22 |
| Py (kN) | 5.95 (6.6%) | 5.36 (8.7%) | 0.90 |
| Dy (mm) | 9.43 (11.3%) | 8.25 (19.9%) | 0.88 |
| Pu (kN) | 9.42 (3.2%) | 8.57 (7.8%) | 0.91 |
| Du (mm) | 92.25 (9.0%) | 84.57 (11.5%) | 0.92 |
| K (kN/cm) | 6.39 (5.8%) | 6.70 (17.1%) | 1.05 |

Note: The figures shown in the parenthesis are the coefficient of variation.

As the failure mode and the yield mode of the nailed joints would affect on the yield strength and the ultimate strength of the shear walls the failure mode of each nail joint was recorded after the test. Figure 9 shows the occurrence of each failure mode. The punching out failure mode seems to be more dominant when the test specimens are in the wet condition. And the nail pull through failure mode seems to be dominant when the test specimens are in the dry condition.

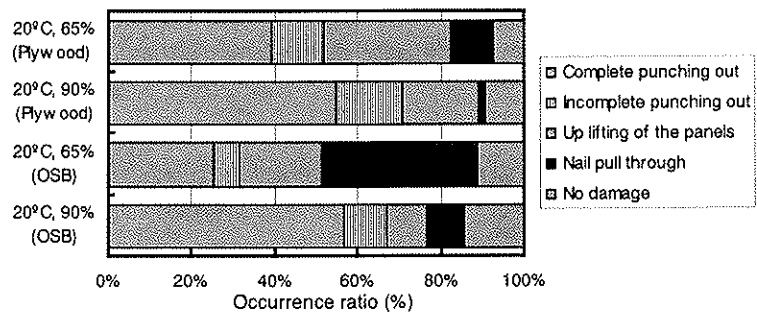


Figure 9 Failure mode of the nail joints.

4.3 Test results of panel shear test of plywood, OSB and gypsum board

The load - shear deformation curve of the panel shear tests of the plywood, OSB and gypsum board are shown in figure 10 and the test results are summarized in table 4 and 5.

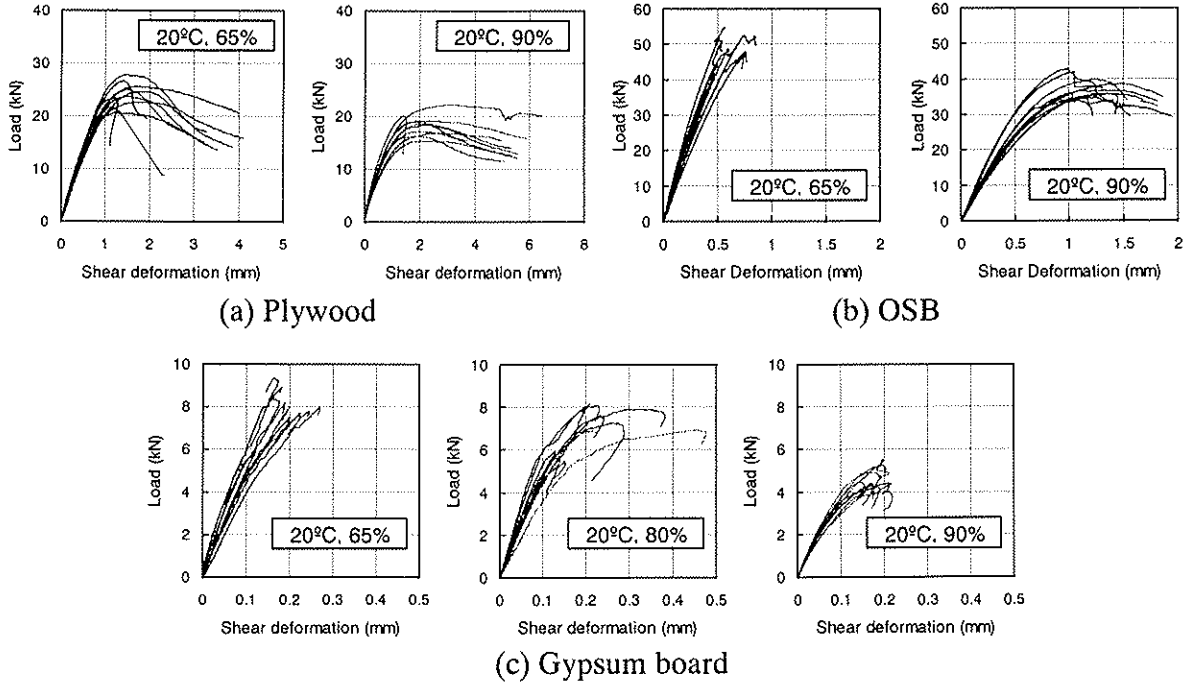


Figure 10 Load - shear deformation curve.

The panel shear strength was calculated from the following formula:

$$f_p = \frac{F_{max} \cos 14^\circ}{lt} \quad \text{--- (2)}$$

where:

- F_{max} is the maximum load.
- l is the length of the test specimens.
- t is the thickness of the test specimens.

The panel shear modulus of rigidity was calculated from the following formula:

$$G_p = \frac{0.5 \cos 14^\circ (F_2 - F_1) l_1}{(u_2 - u_1) lt} \quad \text{--- (3)}$$

where:

- $F_2 - F_1$ is the increment of load on the straight-line portion of the load-deflection curve. And F_1 is approximately 10% and F_2 is approximately 40% of the maximum load F_{max} .
- $u_2 - u_1$ is the increment of deflection corresponding $F_2 - F_1$.
- l_1 is the length of the displacement meter or gauge.

The reduction of the panel shear modulus of rigidity due to the wet condition was 24% for plywood and 43% for OSB and the reduction of the panel shear strength was 24% for plywood and 23% for OSB. Both sheathing materials particularly OSB becomes more ductile when it is in a wet condition.

No reduction of the panel shear modulus of rigidity of gypsum board was observe when the board was conditioned in the atmosphere of 20°C, 80% R.H. and 23% reduction was observed when the board was conditioned in the atmosphere of 20°C, 90% R.H. The panel shear strength of the gypsum board was reduced to 15% after conditioned in the atmosphere of 20°C, 80% R.H. and 44% after conditioned in the atmosphere of 20°C, 90% R.H.

Table 4 Summary of the panel shear properties of plywood and OSB.

| Properties | Material | Conditioning atmosphere | | (2)/(1) |
|------------------------------------|----------|-------------------------|---------------|---------|
| | | (1) 20°C, 65% | (2) 20°C, 90% | |
| Shear modulus of rigidity (Gpa) | Plywood | 0.46 (7.6%) | 0.35 (15.0%) | 0.76 |
| | OSB | 1.65 (13.7%) | 0.94 (13.1%) | 0.57 |
| Shear strength (MPa) | Plywood | 4.11 (9.2%) | 3.11 (11.0%) | 0.76 |
| | OSB | 8.30 (7.7%) | 6.40 (7.9%) | 0.77 |
| Increase ratio of weight (%) | Plywood | 1.0 (9.7%) | 9.2 (5.4%) | - |
| | OSB | 1.1 (18.1%) | 8.7 (4.0%) | - |

Note: The figures shown in the parenthesis are the coefficient of variation.

Table 5 Summary of the panel shear properties of the gypsum board.

| Properties | Conditioning atmosphere | | | (2)/(1) | (3)/(1) |
|---------------------------------|-------------------------|---------------|---------------|---------|---------|
| | (1) 20°C, 65% | (2) 20°C, 80% | (3) 20°C, 90% | | |
| Shear modulus of rigidity (Gpa) | 0.69 (16.6%) | 0.69 (17.4%) | 0.53 (10.0%) | 1.00 | 0.77 |
| Shear strength (MPa) | 1.07 (7.6%) | 0.91 (13.4%) | 0.60 (10.4%) | 0.85 | 0.56 |
| Increase ratio of weight (%) | 0.83 (12.3%) | 3.11 (4.0%) | 6.63 (3.7%) | - | - |

Note: The figures shown in the parenthesis are the coefficient of variation.

Table 6 Summary of test results of the reverse-cyclic test of nail joints.

| Properties | Material | Conditioning atmosphere | | (2)/(1) |
|------------------------------|--------------|-------------------------|----------------|---------|
| | | (1) 20°C, 65% | (2) 20°C, 90%* | |
| P_y (N/nail) | Plywood | 461 (11.0%) | 534 (5.2%) | 1.16 |
| | OSB | 516 (22.4%) | 644 (7.2%) | 1.25 |
| | Gypsum board | 206 (12.2%) | 210 (11.6%) | 1.02 |
| P_u (N/nail) | Plywood | 739 (12.5%) | 923 (4.6%) | 1.25 |
| | OSB | 807 (24.1%) | 989 (8.6%) | 1.23 |
| | Gypsum board | 331 (13.7%) | 316 (9.2%) | 0.95 |
| K (N/cm/nail) | Plywood | 6470 (12.8%) | 6380 (24.1%) | 0.99 |
| | OSB | 8680 (28.2%) | 14400 (24.0%) | 1.65 |
| | Gypsum board | 2370 (27.1%) | 3850 (17.6%) | 1.62 |
| D_y (mm) | Plywood | 0.75 (22.1%) | 0.94 (24.4%) | 1.25 |
| | OSB | 0.63 (20.6%) | 0.48 (9.2%) | 0.76 |
| | Gypsum Board | 0.94 (27.2%) | 0.58 (16.0%) | 0.62 |
| D_u (mm) | Plywood | 12.1 (10.7%) | 11.6 (10.6%) | 0.96 |
| | OSB | 13.4 (18.6%) | 12.5 (9.0%) | 0.93 |
| | Gypsum board | 12.5 (14.1%) | 12.4 (21.1%) | 0.99 |
| Increase ratio of weight (%) | Plywood | 0.0 | 10.0 | - |
| | OSB | 0.0 | 12.0 | - |
| | Gypsum board | -1.0 | 3.0 | - |

Note: The figures shown in the parenthesis are the coefficient of variation.

* 'Gypsum board - nail - stud' test specimens was conditioned in the atmosphere of 20°C, 80%R.H.

4.4 Test results of reverse-cyclic test of nail joints

The first reversed cycles were used to derive the envelope curves. The strength properties and the deformation properties of the nail joints were evaluated from these envelope curves. Yield strength (P_y), yield deformation (D_y), ultimate strength (P_u), ultimate deformation (D_u) and initial stiffness (K) were derived using the calculation methods shown in figure 8.

The test results are summarized in table 6. The yield shear strengths of the plywood nail joints and the OSB nailed joints in the wet condition (condition in the atmosphere of 20°C, 90%R.H.) were almost 10% higher than the yield shear strengths measured in the normal condition. Similar test results was reported in 1975 (Arima et.al. 1975). It was reported that the lateral nail resistance of the plywood increased almost 20% after immersed in the water at normal temperature for 24 hours and the lateral nail resistance of the particleboard increased almost 10% after the same treatment. Thickness swelling of the materials or the physical changes of the materials is considered to be the reason for this but the conclusion should be based on further research works.

4.5 Estimation of P_y and K of the shear walls

The shear strength and the initial stiffness of the plywood sheathed shear walls and the OSB sheathed shear walls were estimated from the simplified calculation method described in the 2X4 designers' manual (Japan 2X4 Builders Association, 1998).

The yield strength was calculated from the following formula:

$$P_{ycal} = P_{ynail} \times s \quad \text{--- (4)}$$

where:

P_{ycal} is the calculated yield strength of the shear walls.

P_{ynail} is the yield strength of the nail joints.

s is number of the nails calculated from the following formula:

$$d = \text{minimum}\{m-1, (n-1) \cdot w/h\}$$

where:

m is the number of the nails nailed either on the left or right edge of the shear wall.

n is the number of the nails nailed either on the top or bottom edge of the shear wall.

w is the width of the shear wall.

h is the height of the shear wall.

The initial stiffness was calculated from the following formula:

$$\frac{1}{K_{cal}} = \frac{2 \times h}{K_{nail}} \times \left\{ \frac{1}{h(m-1)} + \frac{h}{w^2(n-1)} \right\} + \frac{h}{Gwt} \quad \text{--- (5)}$$

where:

K_{cal} is the calculated initial stiffness of the shear walls.

K_{nail} is the initial stiffness of the nail joints.

G is the panel shear modulus of rigidity of the sheathing materials.

t is the thickness of the sheathing materials.

The results for the plywood sheathed shear walls are summarized in table 7. The reduction of the initial stiffness of the shear walls due to the wet condition could be predicted by the simplified calculation method but the reduction ratio was no well estimated. And the reduction of the yield strength due to the wet condition could not be predicted by the simplified calculation method. The characteristic of the nail joints

should be reviewed before making a conclusion but roughly speaking the simplified calculation method described in the 2X4 designers' manual seems not to be a good predictor to evaluate the effect of the moisture contents on the shear walls.

Table 7 Summary of the results of the calculation.

| Properties | | Conditioning atmosphere | | (2)/(1) |
|-------------|------------|-------------------------|---------------|---------|
| | | (1) 20°C, 65% | (2) 20°C, 90% | |
| P_y (kN) | Measured | 5.70 | 4.85 | 0.85 |
| | Calculated | 4.44 | 5.15 | 1.16 |
| K (kN/cm) | Measured | 5.25 | 4.17 | 0.79 |
| | Calculated | 5.66 | 5.05 | 0.89 |

5 Conclusion

The reduction of the yield strength, ultimate strength and initial stiffness of the plywood sheathed shear walls after being conditioned in the atmosphere of 20°C and 90% R.H. was 15%, 13% and 21%. The reduction of the yield strength and ultimate of the OSB sheathed shear walls after being conditioned in the atmosphere of 20°C and 90% R.H. was 10% and 9%. And the initial stiffness of the OSB sheathed shear walls increase 5% after conditioned in the atmosphere of 20°C and 90% R.H. The current modification factor for the water durability issues of the shear walls should be reviewed as 1.00 for plywood seems to be too high and 0.85 for OSB seems to be too conservative.

The reduction of the panel shear modulus of rigidity due to the wet condition was 24% for plywood and 43% for OSB and the reduction of the panel shear strength was 24% for plywood and 23% for OSB. Both sheathing materials particularly OSB becomes more ductile when it is in a wet condition.

The yield shear strengths of the plywood nail joints and the OSB nailed joints in the wet condition were almost 10% higher than the yield shear strengths measured in the normal condition. Thickness swelling of the materials or the physical changes of the materials is considered to be the reason for this but the conclusion should be based on further research works.

The reduction of the initial stiffness of the shear walls due to the wet condition could be predicted by the simplified calculation method but the reduction ratio was not well estimated. The reduction of the yield strength due to the wet condition could not be predicted by the simplified calculation method. The simplified calculation method described in the 2X4 designers' manual seems not to be a good predictor to evaluate the effect of the moisture contents on the shear walls.

Reference

Arima, T., Sato, M., Mashita, K., 1981. Studies on the evaluation methods for long-term performance of wood-based materials and elements. Report of the Building Research Institute. No.95. pp.42-61.

Building Research Institute MOC 1975. 'Annual Report of the General Technology Development Project – Development of the Construction Methods for the Small Scale Wooden houses'. Building Research Institute MOC.

Nakajima S, 2000. The Effect of the moisture contents on the strength and stiffness properties of nailed joints and shear walls. Proceedings of the World Conference on Timber Engineering, Whistler, Canada, Vol.1. pp.1.1.3-1-1.1.3-8.

Japan 2X4 Builders Association. 1998. 'Structural Design Guidelines for Wood Frame Construction'.

The Building Center Japan. 1996. 'Establishment of Technical Standards for Ensuring Structural Safety of Wood Frame Construction'.

ISO/DIS 16670. Timber structure – Joints made with mechanical fasteners – Quasi-static reversed-cyclic test method. International Organization for Standardization, Geneva, Switzerland.

EN 789. Timber structure – Test methods – Determination of mechanical properties of wood based panels. European Committee for Standardization, Brussels, Belgium.

EN 894. Timber structures – Test methods – Racking strength and stiffness of timber frame wall panels. European Committee for Standardization, Brussels, Belgium.

INTERNATIONAL COUNCIL FOR RESEARCH AND INNOVATION
IN BUILDING AND CONSTRUCTION

WORKING COMMISSION W18 - TIMBER STRUCTURES

EVALUATION OF DAMPING CAPACITY OF TIMBER STRUCTURES
FOR SEISMIC DESIGN

M Yasumura
Department of Forest Resources Science
Shizuoka University

JAPAN

Presented by: M Yasumura

- A Ceccotti commented that that the 2% damping is only for the test specimens. For structural design of real structures, 5% damping would be appropriate because other energy dissipation components might not be considered in the test specimens.
- M Yasumura agreed.
- B Dujic commented that the suggested 2% damping should be model dependent. A sophisticated hysteretic model can use this.
- M Yasumura agreed and suggested that for the simpler model higher damping level should be used.
- P Glos questioned the loading rate effect on nail joints.
- M Yasumura stated that the nail joints test showed higher loading rate effects compared to shear wall tests. This can be explained because the speed of each nail in a wall test and the displacement of each nail in a wall tests were not always the same as those in the individual nail test. In the wall test the speed referred to the movement between the top of the wall and the support.
- L Daudeville asked and received clarification on the relationship between energy dissipation versus the loading rate.

Evaluation of damping capacity of timber structures for seismic design

Motoi YASUMURA

Department of Forest Resources Science, Shizuoka University, Japan

1. Introduction

Linear equivalent response method is one of the seismic design methods to ensure the structural safety of buildings against severe earthquake motion. This design method was introduced to Japanese new building codes in June 2000. Different from the equivalent energy method, it does not need the behavior factor (q) which depends on a lot of experiences and highly engineering judgements. The major parameter required for the linear equivalent response method is a force-displacement relationship and the equivalent damping of the structure. The equivalent viscous damping ratio obtained from the static reversed cyclic test is generally applied to determine the equivalent damping of the structure.

The structural behavior of wood-framed construction against horizontal loads is highly dependent on those of shear walls. Therefore, monotonic and reversed cyclic loading tests were conducted on wood-framed shear walls to obtain the parameters for determining the hysteretical model of shear walls. Pseudo-dynamic test was also conducted on the same type of shear walls and the experimental results were compared with the calculation by non-linear earthquake response analysis and the equivalent linear response analysis.

Viscous damping is one of the issue difficult to determine. In general damping factor of 2 to 5% is assumed for dynamic analysis. In this study, high-speed loading test was conducted to determine the damping factor of wood-framed shear walls. It was found that the loading rate has an effect on the lateral resistance at the horizontal displacement of 10 to 70mm, but it makes no influence on the load carrying capacity of shear walls.

2. Specimens

Specimen had wooden frames of 1.82m and 2.44m height sheathed with 9.5mm thick spruce plywood on one side as shown in Fig.1. Sheathing materials were connected to frames of nominal two-by-four lumbers of S-P-F Standard with JIS A5508 CN50 nails (50.8mm length and 2.87mm diameter). Nails were spaced 100mm in the perimeters of a sheet material and 200mm on the central support. Studs were spaced 455mm and connected to bottom and double top plates with CN90 nails (88.9mm length and 4.11mm diameter). End studs were doubled and

respectively for all the specimens.

The loading system was the same as static test except that each displacement increment of the actuator was calculated on line based on the previous load response.

3.3 High-speed test

To investigate the influence of loading rate on the mechanical properties of shear walls, high-speed tests were conducted on wood-framed shear walls. Loading system was the same as the static tests except that the loading girder of four-by-four was replaced by four-by-eight. Lateral forces were applied at the end of girder with the constant velocity of 0.05mm/sec. and 500mm/sec. Lateral force was applied in one direction until the horizontal displacement attained to 180mm. Three specimens were tested for each velocity.

4. Dynamic analysis

4.1 Hysteretical model

A hysteretical model as shown in Fig.2 was assumed for the dynamic analysis of wood framed structures. This model includes;

- 1) Loading on the primary curves up to the maximum load
- 2) Loading on the primary curves over the maximum load
- 3) Unloading from the peak on the primary curve
- 4) Reloading with soft spring
- 5) Reloading toward the previous peak with hard spring
- 6) Unloading from the inner peak
- 7) Reloading toward the peak without slips

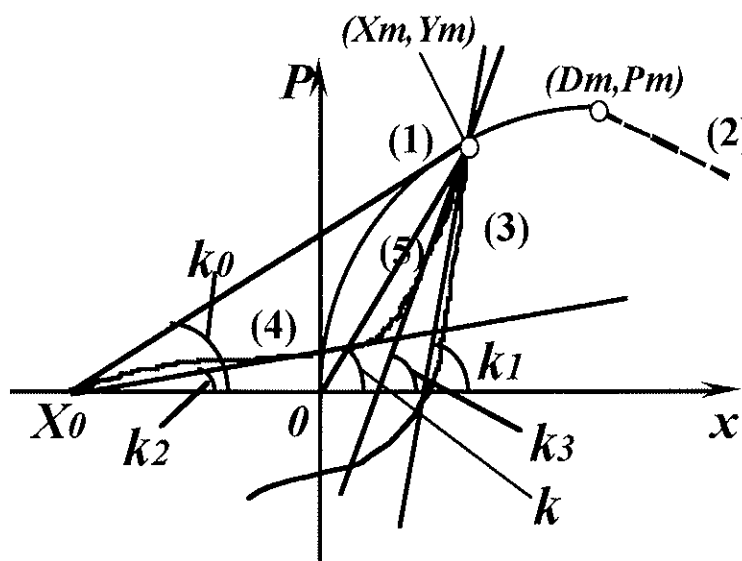


Fig.2 Hysteretical model for wood-framed shear walls

The parameters were determined from the experimental results of the reversed cyclic loading test of shear walls. The primary curves up to the maximum load (1) and those over the maximum load (2), are expressed as follows;

$$P = (P_0 + C_2x)(1 - e^{-\frac{C_1x}{P_0}}) \quad (1)$$

$$P = Pm - C_3|x - Dm| \quad (2)$$

The primary curves over the maximum load was obtained as the straight line determined by the drawn through the points corresponding to Pmax and 0.8Pmax.

Unloading stiffens (3) and the reloading stiffness toward the previous peak (5) were based on the inclination of the straight line determined by the drawn through the origin and the peak on the primary curve (k_0). Reloading stiffness with soft spring (4) was based on the inclination of the straight line determined by the drawn through the peak on the primary curve and the crossing point of the X-axis.

$$k_1/k = C_4Xm + 1 \quad (3)$$

$$k_2/k_0 = 1 - C_5|Xm - X_0|^{C_6} \quad (4)$$

$$k_3/k = C_7Xm + 1 \quad (5)$$

4.2 Time-history earthquake response analysis

Time-history earthquake response analysis was conducted on the wood framed shear walls. Single-degree-of-freedom lumped mass model was applied. The input earthquake ground motions were based on the records of N-S components of the 1940 El Centro and the 1995 JMA Kobe. The accelerograms were linearly scaled to have the maximum acceleration of 0.4 and 0.6g for El Centro NS and 0.4 and 0.5g for JMA Kobe NS. The damping factor and mass were assumed as 2% and 5000kg respectively for all the specimens.

4.3 Equivalent linear response analysis

Equivalent damping was obtained by comparing pseudo-dynamic test results and equivalent linear response analysis. Linear response was calculated by using the stiffness giving the maximum response in pseudo-dynamic test with different damping factor, and the damping factor that gave the same maximum response in pseudo-dynamic test was obtained for each specimen.

5. Results and discussions

5.1 Comparison of non-linear analysis and pseudo-dynamic test results

Figure 3 show the comparison of horizontal displacement response between non-linear time-

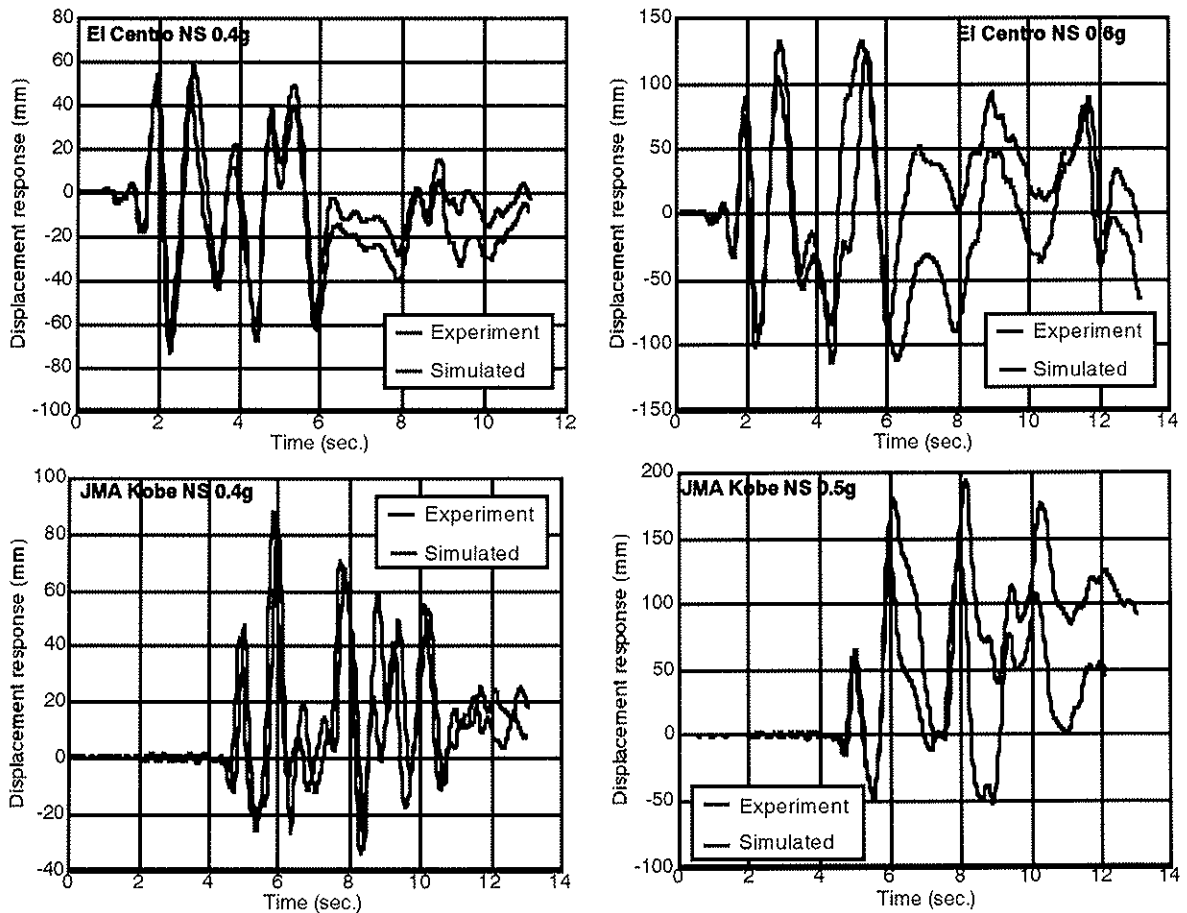


Fig.3 Comparison of displacement response between non-linear analysis and Pseudo-dynamic test results

history earthquake response analysis and pseudo-dynamic test results. They show that the calculated displacement response by non-linear analysis agreed comparatively well with the experimental results except for that of JMA Kobe NS scaled to 0.5g. In the response with JMA Kobe NS 0.5g, the shape of response resembled each other but the simulated results slipped upward.

Figure 4 shows the comparison of force-displacement relationships at the top of wall between non-linear time-history earthquake response analysis and pseudo-dynamic test results. They show that the calculated force-displacement relationships by non-linear analysis agreed also comparatively well with the experimental results. In the response with JMA Kobe NS 0.5g, the simulated lateral force tended to be smaller than the experimental results. This is because we apply the reversed cyclic test results to simulate the envelop curves where the effects of cyclic loading is significant in a large displacement.

5.2 Effects of loading rate

Figure 5 shows the load-displacement relationships at the top of the shear wall at the loading rate of 0.05mm/sec. and 500mm/sec. The figure shows the average value of three specimens. There were little difference in load-displacement relationships up to 10mm between loading rate

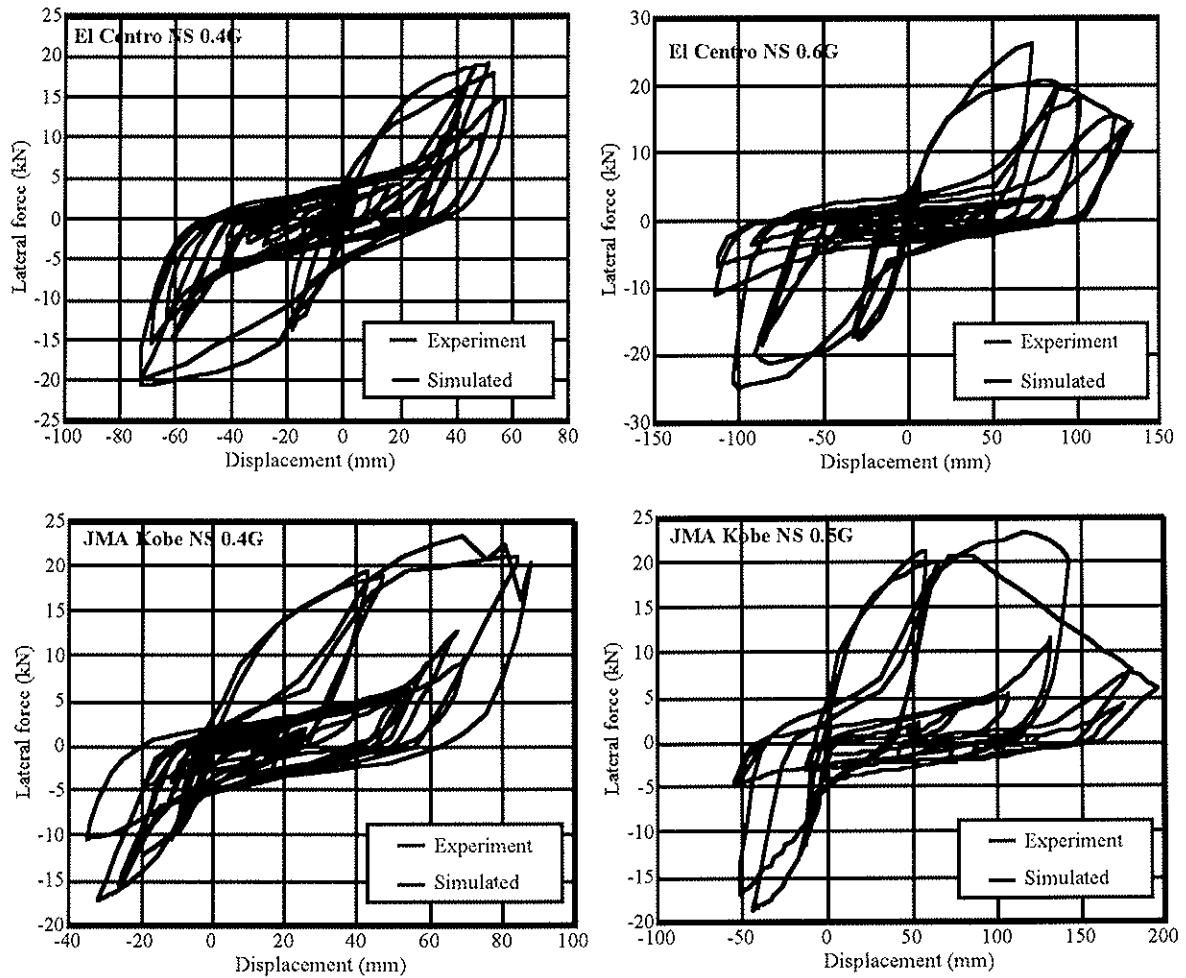


Fig.4 Comparison of load-displacement relationships between non-linear analysis and Pseudo-dynamic test results

of 0.05mm/sec. and 500mm/sec. As the displacement increased, the specimen of the loading rate of 500mm/sec. showed higher load than that of loading rate of 0.05mm/sec. As the load approached the maximum, the difference of lateral loads between the specimens of loading rate of 0.05mm/sec. and 500mm/sec.was quite insignificant.

Figure 6 shows the viscous damping (c) obtained by comparing test results of 0.05mm/sec. and 500mm/sec.loading, and Fig.7 shows the damping factor (h) for each displacement calculated by the equation (6) assuming mass (m) equals to 5000kg. Viscous damping (c) increased as the displacement increased and showed the maximum value at the horizontal displacement of 35mm. Then it decreased gradually and became null value at the displacement of 100mm. The damping factor calculated with the mass of 5000kg showed similar tendency. It showed the value of 2.5% at the displacement of 10mm, the maximum value of 5.5% at the displacement of 35mm, and null value at the displacement of 100mm.

These results indicate that we can expect 2 to 5% damping factor up to horizontal displacement of approximately 70mm (story drift of 1/35), but we can not expect viscous damping at a large deformation in wood-framed shear walls.

5.3 Equivalent viscous damping ratio

Figure 9 shows the equivalent viscous damping ratio obtained from the second and third cycles in reversed cyclic loading test. Equivalent viscous damping ratio obtained from the second and third cycles was approximately 10% when the displacement was comparatively small. It increased as the displacement was larger, and showed maximum value of 18% at the peak displacement of 110mm. Equivalent viscous damping (h_{eq}) of plywood sheathed shear wall is expressed by the following formula;

$$h_{eq} = 0.1062(D/D_y)^{0.1516} \quad (6)$$

where, D and D_y are the horizontal displacement and yield displacement ($D_y=10\text{mm}$).

5.4 Equivalent linear response analysis

Damping factor for the equivalent linear response was obtained by comparing linear time history earthquake analysis and pseudo-dynamic test results. Figure 10 shows the damping factor calculated by the linear response analysis that gave the same maximum response as pseudo-dynamic test result, and the equivalent viscous damping ratio obtained from the second and third cycles in reversed cyclic test. Damping factor obtained from the comparison of linear response and pseudo-dynamic test results was approximately 15% regardless of seismic input and magnitude except for JMA Kobe 0.4g. In JMA Kobe 0.4g, the

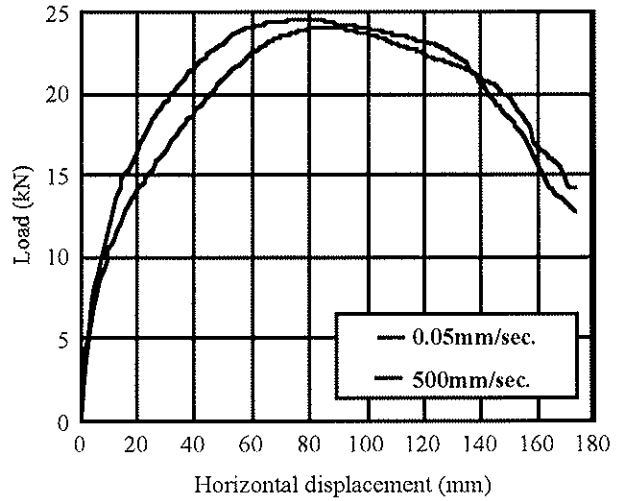


Fig.5 Load-displacement relationship in high speed loading test

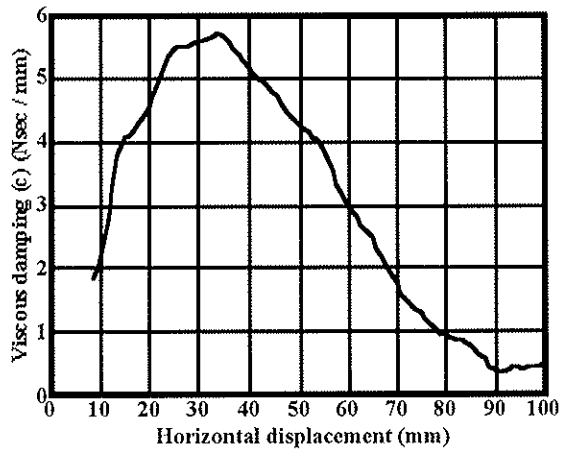


Fig.6 Viscous damping (c) obtained from high speed test

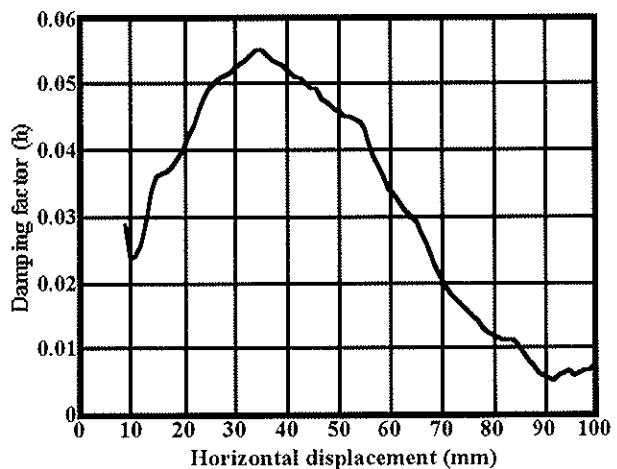


Fig.7 Damping factor (h) obtained from high speed test

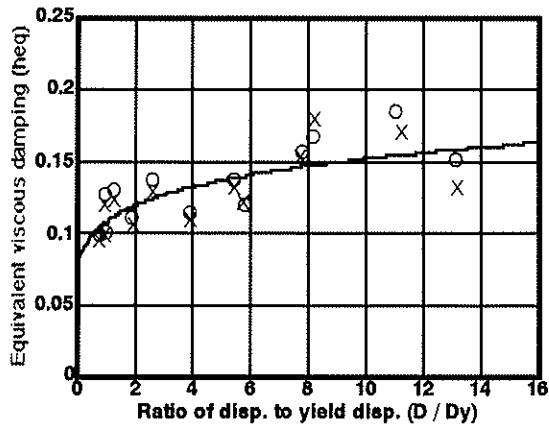


Fig. 8 Equivalent viscous damping ratio

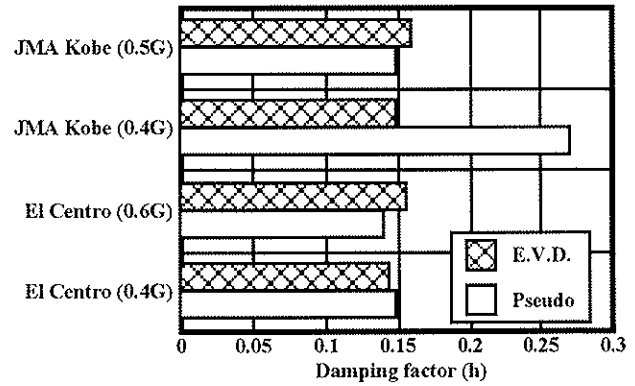


Fig. 7 Comparison of damping factor obtained from pseudo-dynamic test with E.V.D.

obtained damping factor was somehow much larger than equivalent viscous damping. This results shows that the equivalent linear response method represents well the non-linear seismic response in general, however special consideration should be taken for some kind of seism.

6. Conclusions

Simulation by Non-linear time-history earthquake analysis agrees comparatively well with pseudo-dynamic test results. This kind of model is appropriate for predicting seismic behavior of wood-framed shear walls. Equivalent linear response method using equivalent viscous damping ratio also gives generally good approximation to determine the maximum displacement response, however special consideration should be take for some kind of seism. High speed test of shear walls showed that we can expect 2 to 5% damping factor up to horizontal displacement of approximately 70mm (story drift of 1/35), but we can not expect viscous damping at a large deformation in wood-framed shear walls.

7. Acknowledgements

The author thanks Maiko Suzuki, former graduate student of Shizuoka University, for her assistance of testing of shear walls and analysis.

8. References

- Yasumura, M. and Kawai, N. 1997. Evaluation of Wood Framed Shear Walls subjected to Lateral Load, CIB-W18, 30th meeting, paper 30-15-4
- EN 12512. 1997. Timber Structures - Test Methods - Cyclic Testing of Joints Made with Mechanical Fasteners.
- Yasumura, M., Kawai N.1998. Estimating Seismic Performnce of Wood-framed Structures,

Proceedings of 5th WCTE, Vol.2, 564-571

Kawai,N.1999. Prediction Methods for Earthquake Response of Shear Walls, Proceedings of PTEC.

Yasumura, M. 2000, Dynamic Analysis and Modeling of Wood-framed shear walls, Proceedings of WCTE 2000,Vol.2,7.1.3-1-7.1.3-8

INTERNATIONAL COUNCIL FOR RESEARCH AND INNOVATION
IN BUILDING AND CONSTRUCTION

WORKING COMMISSION W18 - TIMBER STRUCTURES

INFLUENCE OF THE STRENGTH DETERMINING FACTORS ON THE
FIRE RESISTANCE CAPABILITY OF TIMBER STRUCTURAL MEMBERS

I Totev

D Dakov

University of Architecture, Civil Engineering and Geodesy, Sofia,

BULGARIA

Presented by: I Totev

- H J Blass asked how were the beams graded for the thickness.
- I Totev answered that they were cut.
- J König stated that the knots on the edge should be positive effect.
- I Totev agreed but stated that if the knots had been located originally away from the edge, the burnt member might have knots nearer to the edge.
- J König asked about the load level in relation to the code.
- I Totev clarified that the load level was related to Bulgaria standard.
- A Jorrissen commented on the low Coefficient of Determination <0.5 in Figures 8 and 9.
- I Totev agreed and stated only 15 specimens were used.
- J König commented that the charring depth was found to be greater on the tension side in this paper; this meant state of stress had some influence on the charring rate. However, the Swedish tests (7 years ago) showed state of stress did not have influence on charring rates.
- I Totev stated that the tension side might have caused some of the char to fall of and might expose more wood to the fire.

Influence of the Strength Determining Factors on the Fire Resistance Capability of Timber Structural Members

Ivan Totev, Dimitar Dakov
University of Architecture, Civil Engineering and Geodesy, Sofia, Bulgaria

1. Introduction

The main objective of this research is to obtain data for the influences of the strength determining factors on the fire resistance of softwood beams, subjected to bending. It was researched the relationship between growth rate and charring rate. It is easy to be established the number of growth rings. It allows rapid approximate assessment of the fire resistance through relationship between growth rate and charring rate.

Knots and fissures are important factors for assessment of the behaviour of the timber elements in fire conditions as well.

2. Loading on beams and parameters recorded during the tests

The tests were carried out in the Laboratory of the Faculty for fire and accidental safety of Higher institute for training of officers and scientific activity of Ministry of Internal Affairs. Leaning of the beam over furnace's borders and loading is shown in Figure 1. The loading consisted of two concentrated forces applied to the beams to the third points of their effective span of 2320 mm.

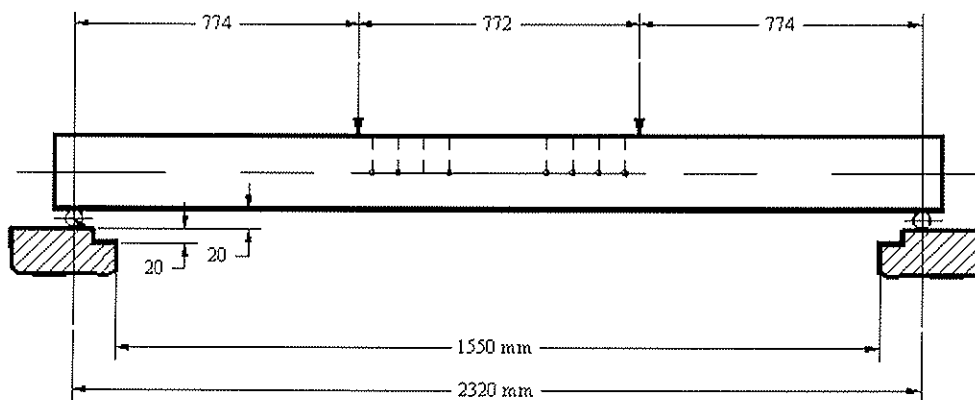


Figure 1 Test layout

The specimens were exposed three sides to heating condition satisfying standard temperature-time curve:

$$\theta_g = 345 \cdot \log_{10} (8 \cdot t + 1) + 20 \text{ } ^\circ \text{C} \quad (1)$$

where θ_g - gas temperature in furnace;

t - time [min]

It was recorded during the test:

- deflection of the beam under the loading at room temperature;
- temperatures were recorded at three points in furnace and at 8 different points into the beam every 2 minutes [1]:

Either fracture or deflection greater than 10 cm (1/23 l) was adopted as the end of the fire resistance.

Basic dates for the beams and some test results are given In Table 1.

Table 1 Beams data and test results

| № | b mm | h mm | g kg/m ³ | n | E _n MPa | b _t mm | h _t mm | t _{ing} min | P _f min | β _b mm/sec | β _h mm/sec | β _{b,l} mm/sec | β _{h,l} mm/sec |
|----|---------|---------|------------------------|----|-----------------------|----------------------|----------------------|-------------------------|-----------------------|--------------------------|--------------------------|----------------------------|----------------------------|
| 1 | 2 | 3 | 4 | 5 | 6 | 7 | 8 | 9 | 10 | 11 | 12 | 13 | 14 |
| 1 | 124 | 120 | 477 | 10 | 9580 | 84.2 | 96.9 | 3.4 | 32.0 | 0.62 | 0.72 | 0.70 | 0.81 |
| 2 | 99 | 130 | 419 | 10 | 9820 | 63.6 | 106.6 | 2.5 | 35.7 | 0.50 | 0.66 | 0.53 | 0.70 |
| 3 | 92 | 93 | 430 | 7 | 11590 | 67.4 | 79.5 | 3.2 | 16.0 | 0.77 | 0.84 | 0.96 | 1.05 |
| 4 | 110 | 111 | 367 | 5 | 6850 | 79.3 | 91.9 | 3.5 | 23.4 | 0.66 | 0.82 | 0.77 | 0.96 |
| 5 | 119 | 125 | 379 | 5 | 7430 | 88.3 | 103.5 | 3.3 | 23.9 | 0.64 | 0.90 | 0.75 | 1.05 |
| 6 | 90 | 97 | 473 | 14 | 16000 | 64.7 | 81.1 | 2.0 | 24.7 | 0.51 | 0.64 | 0.56 | 0.70 |
| 7 | 114 | 118 | 399 | 10 | 7370 | 89.9 | 95.4 | 3.3 | 20.8 | 0.58 | 1.09 | 0.69 | 1.30 |
| 8 | 103 | 97 | 392 | 8 | 8830 | 77.8 | 73.9 | 3.8 | 19.3 | 0.65 | 0.88 | 0.81 | 1.10 |
| 9 | 112 | 117 | 409 | 7 | 10770 | 89 | 98.7 | 3.3 | 18.8 | 0.61 | 0.97 | 0.74 | 1.18 |
| 10 | 87 | 88 | 371 | 5 | 6690 | 64.2 | 73 | 2.9 | 15.0 | 0.76 | 1.00 | 0.94 | 1.24 |
| 11 | 115 | 120 | 442 | 8 | 8100 | 93 | 107.2 | 2.8 | 20.3 | 0.54 | 0.63 | 0.63 | 0.73 |
| 12 | 104 | 109 | 423 | 6 | 12000 | 79.4 | 92 | 3.3 | 20.8 | 0.59 | 0.82 | 0.71 | 0.98 |
| 13 | 98 | 96 | 382 | 5 | 8400 | 79.8 | 78.4 | 3.0 | 20.0 | 0.46 | 0.88 | 0.54 | 0.74 |
| 14 | 114 | 95 | 453 | 11 | 13750 | 78.7 | 59.3 | 3.0 | 28.0 | 0.63 | 1.04 | 0.71 | 1.17 |
| 15 | 94 | 97 | 384 | 8 | 10680 | 68 | 77.3 | 4.0 | 21.6 | 0.60 | 0.66 | 0.74 | 0.81 |

3. Analyses of test results

3.1 Causes which govern the limit of fire resistance

3.1.1 Deflection criterion

Ten centimetre deflections were reached by three beams - № 1, № 10 and № 14. This deflection was reached by beam №1 after 32 minute. Beam №1 had high modulus of elasticity and density. Its knot and fissures complied with quality-class grade according to DIN 4074 [2] and grade 50 by BS CP112 [3]. The beam №10 had low modulus of elasticity and reached deflection of 10 cm after 15 minute. The beam №14 was similar to the beam №1 and had 28 minutes fire resistance.

3.1.2 Different types of destruction

The rest 12 beams can be divided into three groups according to main reason for their destruction:

- knots were the cause for fracture in 9 cases – some of them given in Figure 2, 3 and 4



Figure 2 Fracture of beam № 3



Figure 3 Fracture of beam № 7



Figure 4 Fracture of beam № 15

- the fracture of two beams was induced by fissures with width of 5 mm. Beam №12 is given in Figure 5.



Figure 5 Fracture of the beam № 12

- the fracture of beam №5 was caused by separation of the pith from the rest part of the cross section – Figure 6



Figure 6 Fracture of the beam № 5

3.2 Relationship between modulus of elasticity, charring rate and growth rate.

3.2.1 Relationship between growth rate and modulus of elasticity

The tests results allowed to establish relationship between growth rate and modulus of elasticity. Correlation between these two parameters is shown in Figure 7. The following relationship was established through linear regression:

$$E = 4551 + 669 \cdot n \quad (2)$$

where E – modulus of elasticity;

n – number of the growth rings per 25 mm.

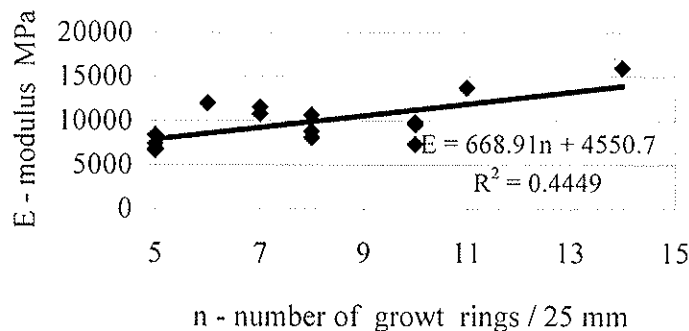


Figure 7 . Relationship between the number of growth ring per 25 mm and modulus of elasticity E

The correlation coefficient for this relationship is 0.67, which is due to the limited number of tests.

3.2.2 Relationship between growth rate and charring rates.

The charring rate β was calculated according to ENV 1995 -1-2 [4] without reducing the fire resistance with time to ignition. The charring rate on bottom edge of the beam is greater than the charring rates on the two faces. In [5], [6] and [7] the authors explained this effect with the stress distribution – the greater the stresses – the greater the charring rates are. We suppose that the level of strains is important, too. The strains produce intensive fracture of the charcoal layer and thus the thermal protection of the bottom of the beam is diminished and charring rate is speeded up.

$$\beta_h = (h - h_t) / P_f \quad (3)$$

$$\beta_b = (b - b_f) / P_f \quad (4)$$

where β_h and β_b are the charring rates on the bottom and lateral sides of a beam;

b and h – width and depth of the initial cross section of the tested beam;

b_f and h_f – width and depth of the section after the fire test;

P_f – fire resistance – duration of the fire test.

We can define precisely the charring rate when we take into account the real period when wood is on fire. This period starts after the ignition of the beam.

The charring rates $\beta_{1,b}$ and $\beta_{1,h}$ are defined when the time of ignition is taken into account:

$$\beta_{1,h} = (h - h_f) / (P_f - t_{\text{ing}}) \quad (3a)$$

$$\beta_{1,b} = (b - b_f) / (P_f - t_{\text{ing}}) \quad (4a)$$

where $\beta_{1,h}$ and $\beta_{1,b}$ are charring rates on bottom and lateral sides of a beam;

b and h – width and depth of the initial cross section of a tested beam;

b_f and h_f – width and depth of the section after the fire test;

P_f – fire resistance – duration of the fire test

The relationship between the growth rate and $\beta_{1,h}$ and $\beta_{1,b}$ are presented in Figure 8 and Figure 9.

The following relationships are obtained using linear regression:

$$\beta_{1,b} = 0.89 - 0.023.n \quad (6)$$

$$\beta_{1,h} = 1.29 - 0.0385.n \quad (7)$$

The correlation coefficient is about 0.5.

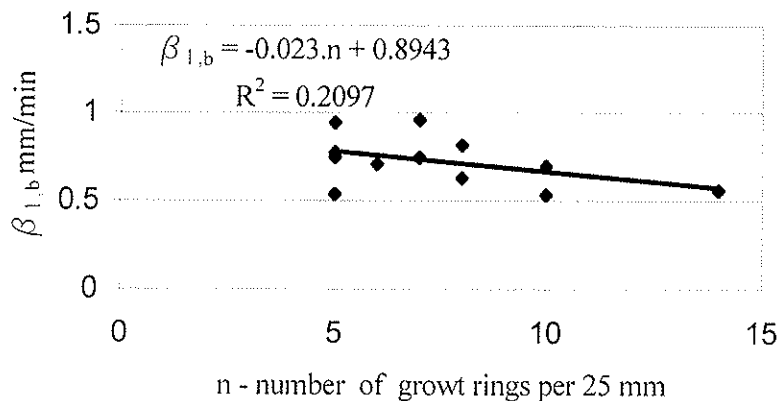


Figure 8. Relationship between the number of growth rings per 25 mm and charring rate $\beta_{1,b}$

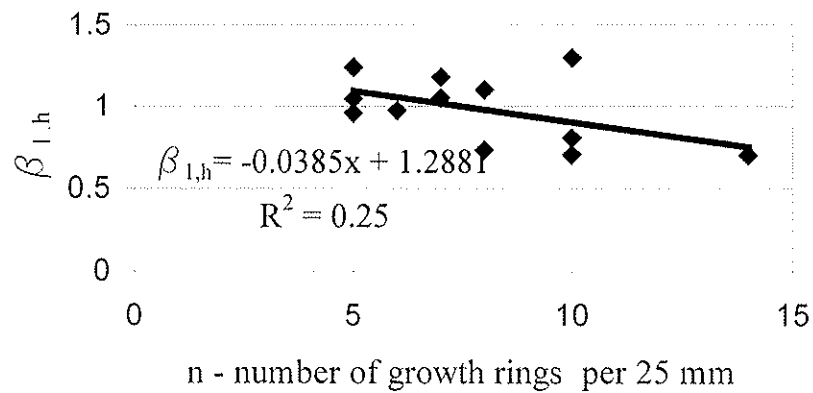


Figure 9 Relationship between the number of growth ring per 25 mm and charring rate $\beta_{1,h}$

3.3 Assessment of the knot influence on the fire resistance

The knots are the basic strength-reducing factor. The knots, which are situated near by the bottom of the beams, are particularly unfavourable. In BS CP112 the term “margin knots” is introduced for knots, which are situated outside of the central half of the lateral faces of the beam. There is the stronger limitation for their sizes. There is no similar differentiation for knots according their position in DIN 4074. The effective section after the fire tests is smaller than the initial one. That lead to increasing the relative influence of the knots and they get closer to the dangerous end areas.

Grading were carried out according both DIN and BS CP112 for all beams before and after the tests. The results were :

- five of the beams did not changed their grades in both standards after the test;
- five of them changed their grade after the test when one of the standards was used and kept its grade when other was used;
- the last five beams changed grades after test in both standards.

Influence of re – grading was checked out by comparative calculations of fire resistance. These calculations are performed using following assumptions:

- an overall load reducing coefficient $\eta_{fi} = 2$;
- diminished load-bearing capability of the remaining part of the cross section was assessed by the simplified method with β_o and with the sophisticated method with reduced strength;

The results of these calculations compared with fire resistance reached in the tests are shown in Table 2. Values displayed in column 5 and 6 are calculated without re-grading the beams after the tests. Generally, all predictions are relatively close to the tests results. However, the using of re-grading technique in some crucial cases of beams with many knots gives more accurate prediction than conventional methods do.

The fire resistance is influenced by the distance between the bottom edge of the beams and knots t_c (Figure 10). These distances and their corresponding fire resistance of 6 beams whit the shortest t_c are shown in Table 3. It seems that the value of the distance [mm] is close to the value of the fire resistance [min]. Because of a limited number of data it is not possible to do quantitative assessment of the relationship between the distance t_c and the fire resistance..

Table 2 Comparison of experimental fire resistance with calculated ones.

| | Fire resistance [in minutes] obtained by | | | | | | |
|----------------|--|-------------------|------------------|--------------------|-------------------------|------------------|--------------------|
| | experiment | simplified method | | | reduced strength method | | |
| | | re-grading | | without re-grading | re-grading | | without re-grading |
| | DIN | BS | P _{fd1} | P _{fb1} | P _{fd2} | P _{fb2} | P _{fb2} |
| N ₀ | P _{fe} | P _{fd1} | P _{fb1} | P _{fb1} | P _{fd2} | P _{fb2} | P _{fb2} |
| 1 | 2 | 3 | 4 | 5 | 6 | 7 | 8 |
| 1 | 32 | 30 | 30 | 30 | 34 | 34 | 34 |
| 2 | 36 | 24 | 20 | 20 | 30 | 24 | 30 |
| 3 | 16 | 15 | 15 | 15 | 18 | 20 | 18 |
| 4 | 23 | 24 | 24 | 24 | 30 | 30 | 30 |
| 5 | 24 | 30 | 30 | 30 | 34 | 34 | 34 |
| 6 | 25 | 20 | 20 | 20 | 24 | 24 | 24 |
| 7 | 21 | 28 | 28 | 28 | 32 | 32 | 32 |
| 8 | 19 | 15 | 20 | 20 | 20 | 24 | 26 |
| 9 | 19 | 20 | 20 | 24 | 26 | 26 | 32 |
| 10 | 15 | 15 | 18 | 18 | 18 | 24 | 24 |
| 11 | 20 | 20 | 22 | 22 | 24 | 26 | 32 |
| 12 | 21 | 18 | 24 | 24 | 24 | 24 | 24 |
| 13 | 20 | 15 | 22 | 22 | 18 | 26 | 26 |
| 14 | 28 | 18 | 20 | 24 | 20 | 24 | 26 |
| 15 | 22 | 22 | 15 | 22 | 26 | 20 | 26 |

Table 3 Comparison of distance t_c with fire resistance



Figure 10 Distance from edge to a margin knot

| N ₀ | t_c | P _f |
|----------------|-------|----------------|
| 3 | 16 | 16 |
| 4 | 15 | 23 |
| 5 | 20 | 24 |
| 8 | 17 | 19 |
| 9 | 10 | 19 |
| 13 | 14 | 20 |

4. Conclusions

Relationships are obtained between the number of growth rings, charring rates and the modulus of elasticity. Estimations for fire-resistance of existing timber structures are possible because it is easy to determine the number of growth rings. The distance between the knots and bottom edge of the beam is a useful bit of information about expected fire-resistance. Re-grading of the beams helps us in carrying out the correct assessment. Methods that predict fire resistance based on data about growth rate, disposition and size of knots and fissures could be developed. They could be employed by insurance companies when assessing the fire risk of existing timber structures.

5. Acknowledgement

The authors wish to thank their colleagues in the Laboratory of Faculty of fire and accidental safety for their contribution to the test.

This work is made with financial support of the National Foundation for scientific research.

REFERENCES

1. Todorov, I and Totev, I : Full scale fire resistance test on timber girders, Annuaire de l'Universite d'architecture, de genie civil e de geodesie, Sofia, Fascicule VII, 1998 (in Bulgarian) .
2. DIN 4047 Güte bedingungen für Bauschnitholz (Nadelholz).
3. BS CP112 British Standard Code of Practice for the structural use of timber. The council for codes of practice. British Standard Institution, London.
4. ENV-1995-1- 2 Eurocode 5 Design of timber structures, Part 1.2 General rules. Supplementary rules for structural fire design.
5. R.J. Dayeh and D.R. Syme – Behaviour of glulam beams in fire, Proceedings of International seminar “Building te Future” , Brighton, UK, 1993.
6. Knublauch,E und Rudolphi, R : Der Abbrand als Grunlage zur teoretischen Vorausbestimmung der Feuerwiederstandsdauer von Holzbautailen. Bauen im Holz , 73/71, S. 590-593.
7. Sheer, C , Thorsten, K. und Meyer-Ottens, C. : Rechnerische Brandschutzbemessung unbedeckter Hozbauteile . Bautechnik 69 (1992) Heft4, S. 179 – 189.

INTERNATIONAL COUNCIL FOR RESEARCH AND INNOVATION
IN BUILDING AND CONSTRUCTION

WORKING COMMISSION W18 - TIMBER STRUCTURES

CROSS SECTION PROPERTIES OF FIRE EXPOSED
RECTANGULAR TIMBER MEMBERS

J König

B Källsner

Träteknik – Swedish Institute for Wood Technology Research

SWEDEN

Presented by: J König

- H J Blass asked whether EC 5 part 5 will have only one simplified method.
- J König answered no. The project team made a proposal but it was rejected.
- R Marsh asked why not apply an adjustment factor to the current method.
- J König answered keeping the reduced properties method would be more logical and accurate. More importantly accurate values to be used in the method would be critical.
- A Jorissen questioned about structures exposed to real fire.
- J König answered that standard fire scenario was used as real fire would be too complicated.
- R Marsh agreed that this was only an indicative method and could not be used to deal with real fire situations.

Cross section properties of fire exposed rectangular timber members

Jürgen König and Bo Källsner

Träteknik – Swedish Institute for Wood Technology Research, Sweden

Summary

The Fire Part of Eurocode 5 gives the option of using methods of different complexity for the determination of the uncharred residual cross section and the reduction of strength and stiffness parameters. By using advanced methods of heat transfer calculations, using the thermal properties of wood and the char layer given in Draft prEN 1995-1-2, it is shown that the notional charring rates given in the code are reasonable, allowing the designer to disregard corner roundings. This paper gives the background of the different methods for the reduction of strength and stiffness. Advanced calculations using the thermo-mechanical properties of timber given in Draft prEN 1995-1-2, show that the reduced cross section method gives fairly accurate results for members in bending, while it is unsafe in relation to the advanced method for members in compression or tension. The reduced properties method, however, is unsafe for members in bending, compression and tension.

1 Introduction

The Fire Part of Eurocode 5 (ENV 1995-1-2) gives simplified rules for the determination of the uncharred residual cross section and the reduction of strength and stiffness parameters. For the determination of the charring depth, an increased charring rate is used in order to take into account the effect of increased charring at cross-section corners. Following a proposal by König (1998), in Draft prEN 1995-1-2 this charring rate is called the notional charring rate.

For the reduction of strength and stiffness parameters, in both ENV 1995-1-2 and Draft prEN 1995-1-2 two simplified methods are given:

1. reduced cross-section method
2. reduced properties method.

While in the reduced cross-section method the reduction of the strength and stiffness properties is replaced by an equivalent reduction of the cross section (that is a so-called zero-strength layer is introduced), the reduced properties method, in general, is more applicable and precise by giving modification factors for strength and stiffness parameters.

The first method using a reduced (or effective) residual cross section gives lower mechanical resistance than the second one using reduced properties. The reason is that the methods are based on different assumptions. The intention of the second method was to be

more precise, and that the designer should get a bonus by using it instead of the first more simple one. König (1998) argued for preference of the reduced properties method and proposed to skip the reduced cross-section method in the code.

In the following, the basis of both methods is discussed. Performing an advanced analysis using thermal and thermo-mechanical properties given by König et al. (2000) and Källsner et al. (2000), now introduced in an informative annex of Draft prEN 1995-1-2, for some specific cross sections new modification factors for fire are derived and compared with the simplified methods.

2 Notional charring rates

2.1 Values of Eurocode 5

The Fire Part of Eurocode 5 gives two charring rates (using the notation of Draft prEN 1995-1-2):

- The *basic charring rate* β_0 for one-dimensional charring (i.e. one-dimensional heat transfer)
- The *notional charring rate* β_n including the effect of increased charring adjacent to corners of the cross section and fissures often occurring in solid timber sections.

The notional charring rate should be the preferred alternative for designers since it is not necessary to take into account the corner roundings when calculating cross section quantities such as area, section modulus and second moment of area.

For softwood, i.e. solid and glued laminated timber, the charring rates are given in table 1.

Table 1 — Basic and notional charring rates for softwoods

| | β_0 | β_n | β_n/β_0 |
|------------------------|-----------|-----------|-------------------|
| | mm/min | mm/min | |
| Glued laminated timber | 0,65 | 0,7 | 1,08 |
| Solid timber | 0,65 | 0,8 | 1,23 |

The main fields of application of the basic charring rate are glued laminated timber decks where the heat flux is one-dimensional, and very large cross sections when the corner roundings are taken into account separately.

In solid timber cross sections heat flux is predominantly two-dimensional. In small cross sections as they are used in timber frame construction, the effect of corner roundings becomes important in an early stage of the fire exposure. While small timber frame members normally are kiln-dried such that the effect of fissures on charring can be neglected, this is normally not the case regarding large solid timber members where the effect of fissures can be considerable.

2.2 Calculations

A thermal analysis was performed as described by Källsner et al. (2000) of timber cross sections fire exposed on four sides with the following sizes:

200 mm × 800 mm

140 mm × 300 mm
 100 mm × 200 mm
 45 mm × 120 mm

The first two of these cross sections would normally be glued laminated beams, while the last two would be typical solid timber members. The element size of the grid used in the thermal analysis was 2,5 mm.

The temperature at the char-line was assumed as 300°C and the residual cross section was determined for specified times of fire exposure. The calculations showed that the charring depth of the narrow sides was somewhat greater than the charring depth of the wide sides. For each of these residual cross sections a notional charring depth was determined such that the section modulus W and second moment of area I respectively of the simplified rectangular (notional) cross section were the same as for the “real” residual cross section. Calculating W and I the element size of the grid was 1,25 mm. The results are shown in figure 1 as the ratio of charring rates β_n and β_0 versus time.

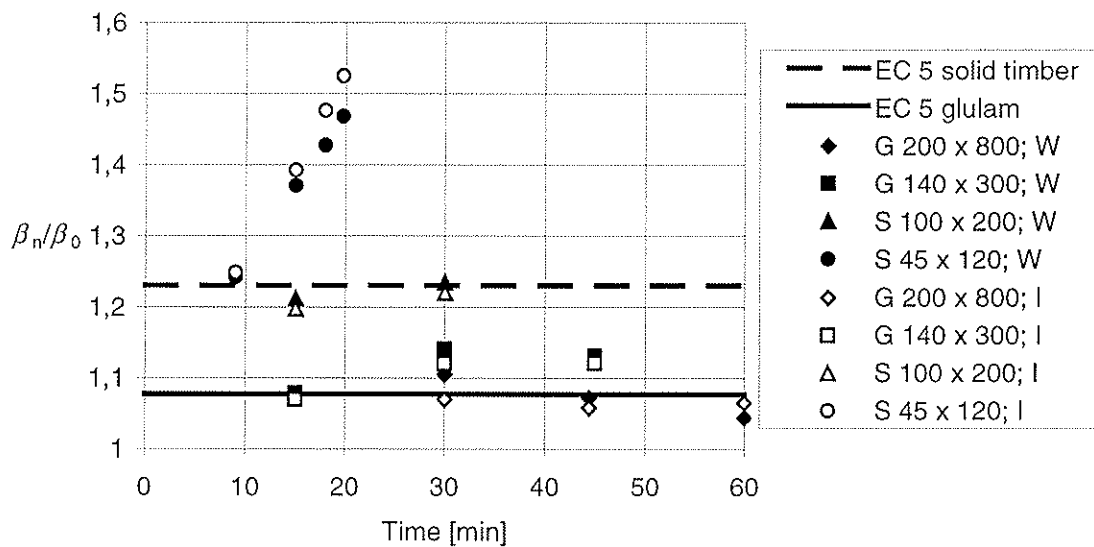


Figure 1 — Charring rate ratios vs. time: Comparison of calculated values with Eurocode 5 for solid (S) and glued-laminated (G) timber cross sections exposed on four sides

The results show that the choice of notional charring rates of Eurocode 5 is a reasonable simplification. Drying fissures in the wood, that can be expected in cross sections of solid timber of size 100 mm × 200 mm and more, were not modelled. Such drying fissures would cause increased charring adjacent to the fissures, giving somewhat higher values than calculated. Several of the data points for cross section 45 mm × 120 mm seem to give non-conservative results, however they are based on charring depths of more than ten millimetres and should be beyond limit of interest. Normally failure would occur after 10 minutes. Since such small cross sections normally are kiln-dried, they would not suffer from drying fissures, which would require additional increase of the notional charring rate.

3 Reduction of strength and stiffness parameters

3.1 The reduced cross section method

The reduced cross section method adopted by ENV 1995-1-2 was presented by Schaffer et al (1986). The effect of temperature within a zone of about 40 mm below the char layer was replaced by a zero-strength layer, while the remaining part of the residual cross section was assumed to exhibit unreduced strength and stiffness. Using the criterion of equal section moduli, the thickness of the zero-strength layer was calculated as 0,3 inches (7,6 mm). The value adopted by Eurocode 5 (ENV 1995-1-2) was 7 mm. It was assumed that this reduction is fully effective after 20 minutes, and that the thickness of the zero-strength layer increased linearly during the first 20 minutes of fire exposure.

In the calculation by Schaffer et al. (1986) strength and stiffness profiles in the member adjacent to the char layer according to Schaffer (1984) were used, see figure 2 which is a reconstruction from Schaffer (1984).

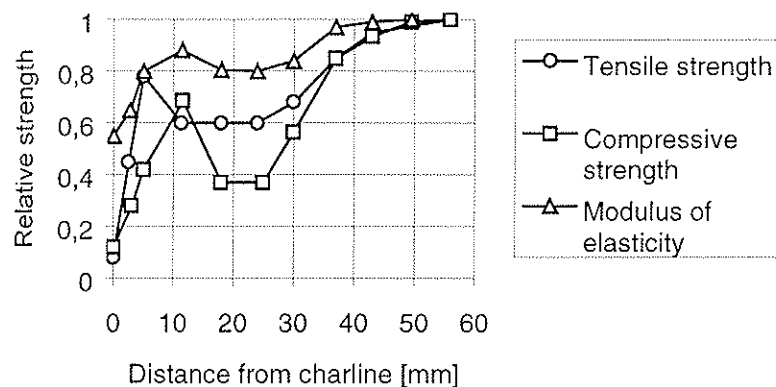


Figure 2 — Relative modulus of elasticity and compressive and tensile strength vs. distance from char-line (Reconstructed from Schaffer, 1984)

The curves were derived from temperature-dependent values of strength and modulus of elasticity, using the temperature profile in the wood, and were corrected with respect to the influence of the moisture content profile. The curves have a minimum at a distance of about 20 to 25 mm below the char-layer, where the temperature in the wood is about 100°C. Closer to the char-layer the values are increasing again due to the drying of the wood before they reach minimum values at the char-line.

3.2 The reduced properties method

The reduced properties method (in ENV 1995-1-2 called reduced strength and stiffness method) is based on the strength and stiffness values provided by Glos et al. (1990) and was introduced in DIN 4102 Part 4 (1994). While DIN 4102 uses relationships of reduction factors of properties as a function of the *mean temperature in the residual cross section*, ENV 1995-1-2 uses relationships between the reduction of properties, i.e. the modification factor for fire $k_{\text{mod,fi}}$, as a function of the section factor p/A_r

where

p perimeter of the fire exposed sides of the residual cross section in m

A_r area of the residual cross section in m^2 .

The reason of this modification, made in analogy to design rules used for steel structures, was to prevent potential confusion about the difference of mean temperatures of a cross section and local temperatures in cross sections described by temperature profiles.

3.3 Calculations

Using the reduction of mechanical properties given in annex B of the first draft of prEN 1995-1-2 for compressive and tensile strength¹ and modulus of elasticity, for the cross sections of section 2 modification factors for fire $k_{\text{mod,fi}}$ were calculated for cross sections exposed on four sides for bending, tensile and compressive strength. As above in 2.2, for the geometrical and mechanical properties analysis the element size of the grid was 1,25 mm. The strength properties of the members used in the calculation are shown in table 2.

Table 2 — Properties of members used in the calculation

| Member size | Strength class | Bending strength | Local compressive strength | Local tensile strength | Strength ratio |
|-------------|----------------|----------------------------|----------------------------|----------------------------|----------------|
| mm × mm | | f_m N/mm ² | f_c N/mm ² | f_t N/mm ² | f/f_t |
| 200 × 800 | GL 32h | 36,8 | 44 | 36,8 | 1,20 |
| 140 × 300 | GL 32h | 39,4 | 44 | 39,4 | 1,12 |
| 100 × 200 | C 30 | 37,5 | 44 | 37,5 | 1,17 |
| 45 × 120 | C 30 | 39,2 | 44 | 39,2 | 1,12 |

Since in prEN 1995-1-2 the strength for fire design is based on the twentieth percentile of the strength at normal temperature, the fifth percentile values were multiplied by 1,15 for glulam and 1,25 for solid timber. Further, the size factor according to prEN 1995-1-1 was used, given as

$$k_h = \left(\frac{600}{h}\right)^{0,1} \quad \text{for glued laminated timber} \quad (1)$$

$$k_h = \left(\frac{150}{h}\right)^{0,2} \quad \text{for solid timber.} \quad (2)$$

The simplified strain-stress relationship according to figure 3 was used, where f_c is the clear wood compressive strength, see König et al. (2000).

The clear wood compressive strength of spruce and pine is normally in the range from 40 to 50 N/mm². From Thunell (1941), for wood with a moisture content of 12 %, the following relationship between compressive strength f_c in N/mm² and dry density $\rho_{0,12}$ in kg/m³ can be derived, see figure 4:

$$f_c = 0,114 \rho - 9 \quad (3)$$

Here the local compressive strength was taken as 44 N/mm². Since the bending strength values are smaller than 44 N/mm², no plastic flow occurred at normal temperature. Therefore, the tensile strength of the beams was put equal to the bending strength.

¹ The co-ordinate of the temperature-tensile strength relationship given as (100; 0,63) should be changed to (100; 0,65), which is the correct result of the calibrations reported in the background literature.

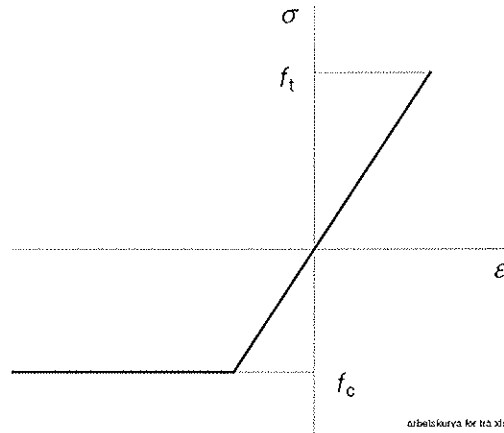


Figure 3 — Simplified strain-stress relationship for wood

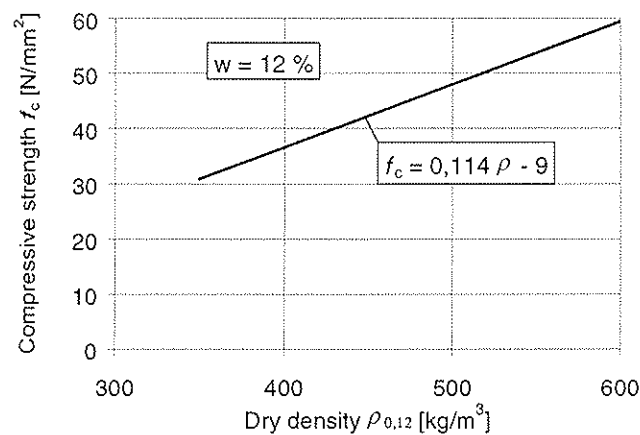


Figure 4 — Compressive strength vs. density according to Thunell (1941)

The calculated strength reduction factors were compared with those according to the reduced properties method and the reduced section method, see figure 5. Using the reduced cross section method, the reduction of strength of the residual cross section was expressed as the ratio W_{ef}/W_r where W_r and W_{ef} are the section moduli of the residual cross section and the effective residual cross section respectively.

The load ratios, see figure 6, were calculated as

$$\frac{R_{fi}}{R} = \frac{W_r}{W} k_{mod,fi} \quad (\text{reduced properties method}) \quad (3)$$

and

$$\frac{R_{fi}}{R} = \frac{W_r}{W} \frac{W_{ef}}{W_r} = \frac{W_{ef}}{W} \quad (\text{reduced cross section method}) \quad (4)$$

respectively where the first term is the effect of charring and the second term is the effect of strength reduction.

The results show that, with the exception of the initial phase of the fire exposure, the values of the reduced properties method are higher than the values according to the reduced cross section method, as anticipated in ENV 1995-1-2.

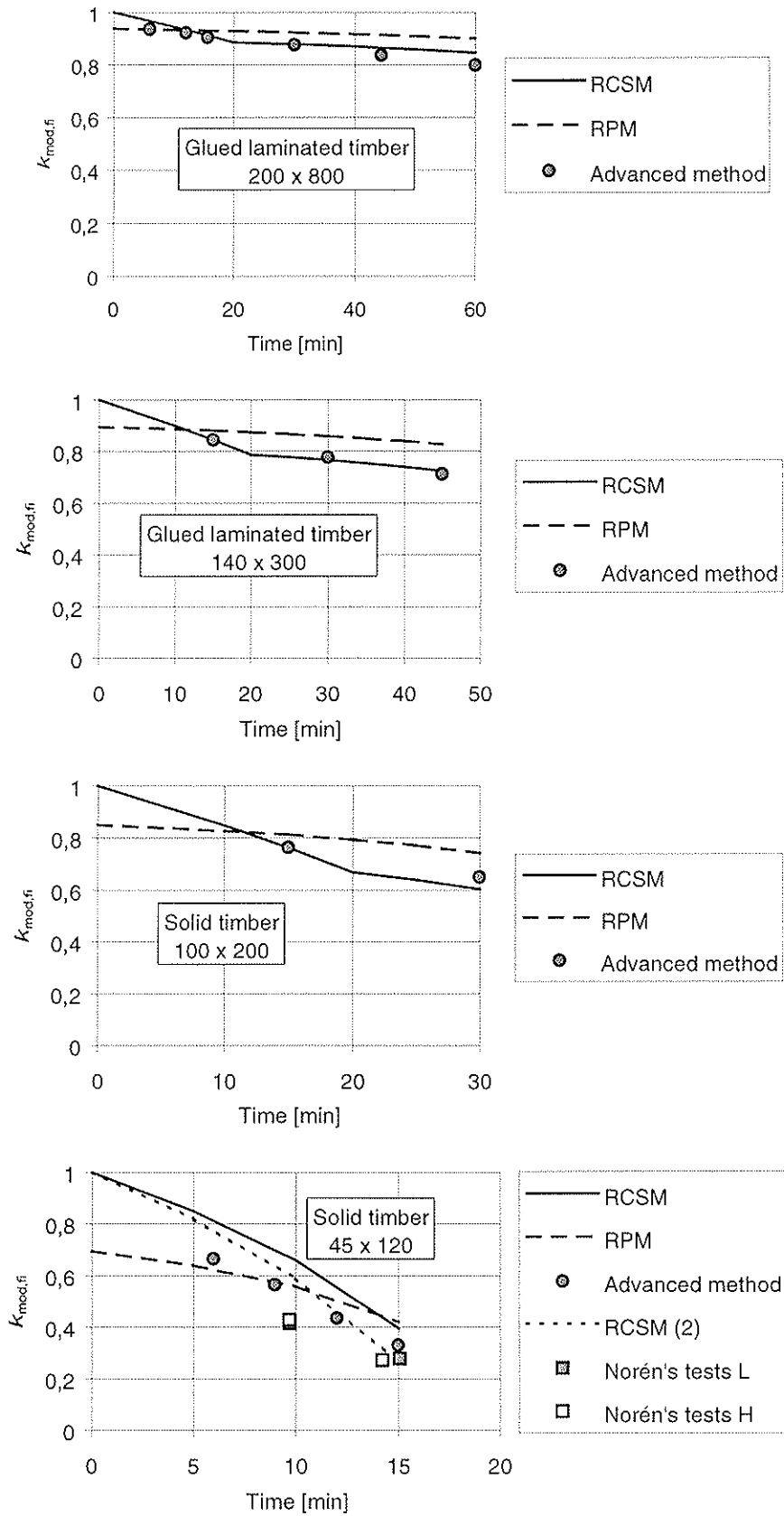


Figure 5 — Comparison of calculated (advanced method) modification factors for fire in bending with values according to reduced properties method (RPM) and reduced cross section method (RCSM) of ENV 1995-1-2 for exposure on four sides

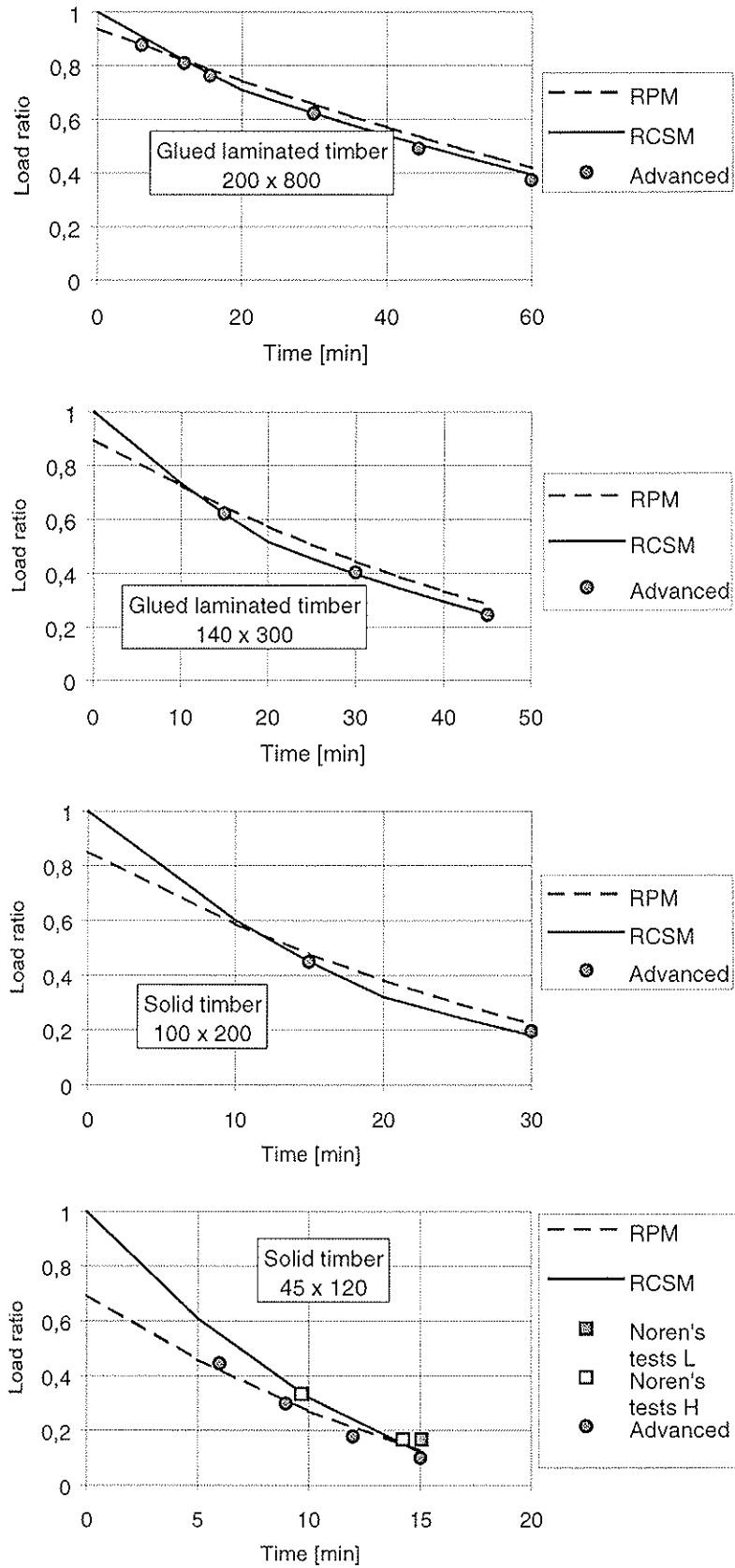


Figure 6 – Load ratio vs. time for bending. Comparison of calculated (advanced method) values with values according to reduced properties method (RPM) and reduced cross section method (RCSM) of ENV 1995-1-2 for exposure on four sides

Comparing the results of the reduced cross section method with the calculated values according to the advanced method, it can be seen that the assumption of 7 mm as the thickness of the zero-strength layer is reasonable, see figure 5. For small cross sections such as 45 mm × 120 mm, however, it would be better to assume that the reduction by 7 mm is fully effective earlier than after 20 minutes. The second curve shown in figure 5 (dotted) is shown assuming a linear increase to 7 mm during the first 15 minutes of fire exposure. For cross sections of size 45 mm × 120 mm also the experimental results by Norén (1988) are shown, where L and H refer to timber of low and high grade respectively, see below. For other cross sections, no test results are available in literature, since normally no cold mechanical properties of specimens have been determined.

From the graphs of figure 6, showing relationships between the load ratio and time, it can be seen that the differences between the different methods are not as pronounced as in figure 5, since the effect of charring is dominating. For cross sections of size 45 mm × 120 mm also the experimental results by Norén (1988) are shown.

For cross sections in bending, in figure 7, the calculated modification factor for fire are compared with the values of ENV 1995-1-2. It is obvious that the section factor p/A_r , representing a measure of the degree of heating, is not an adequate parameter describing the physics well, see discussion below.

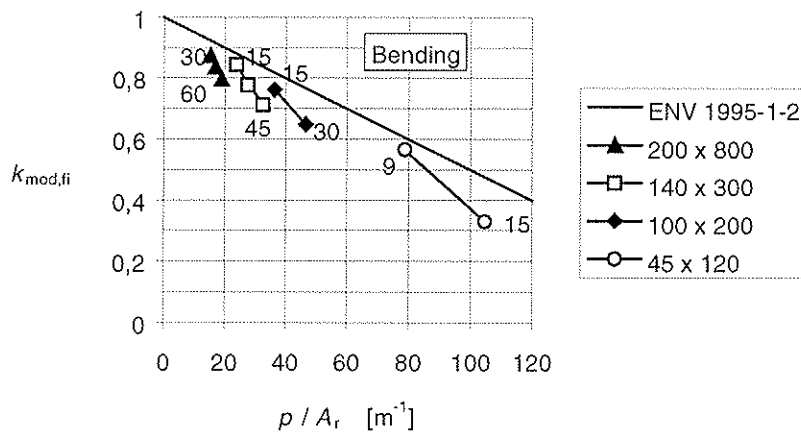


Figure 7 — Modification factor for fire versus section factor – Comparison of calculated values with ENV 1995-1-2. The figures in the graph refer to time of fire exposure

Comparing the fire performance of timber members with and without knots, Norén (1988) found that timber quality has a very small effect on fire resistance of load bearing timber members, with a slightly better performance of low grade timber with large knots. A sensitivity study was done for cross sections 200 mm × 800 mm and 45 mm × 120 mm, to determine the effect of varying tensile strength when the compressive strength was kept constant, and vice versa. The results can be seen in figure 8 and 9. Within the normal interval of compressive strength from 40 to 50 N/mm², the influence of varying compressive strength is negligible. When the compressive strength was kept constant, increasing tensile strength gives a small decrease of the modification factor for fire, being in line with the results of Norén (1988).

The relationships for explicit strength values shown in figure 8 and 9 can be expressed as relationships between the modification factor $k_{mod,fi}$ and the strength ratio of compressive and tensile strength f_c and f_t . The figure shows also, along the horizontal axis, strength

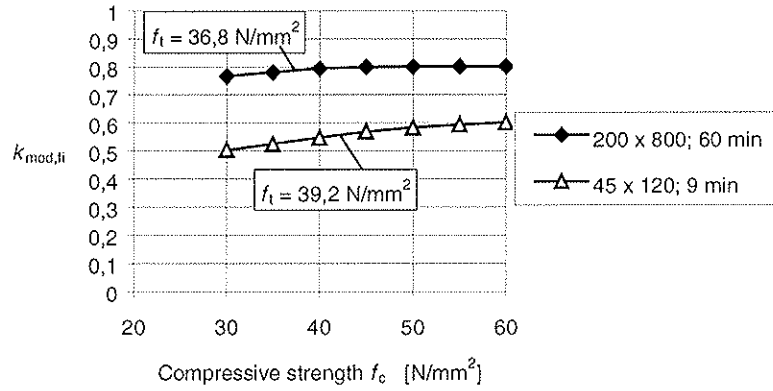


Figure 8 — Effect of compressive strength on modification factor for fire for bending for two cross sections

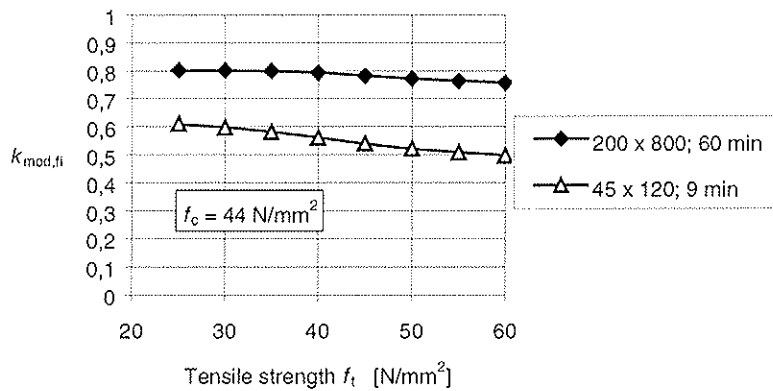


Figure 9 — Effect of tensile strength on modification factor for fire for bending for two cross sections

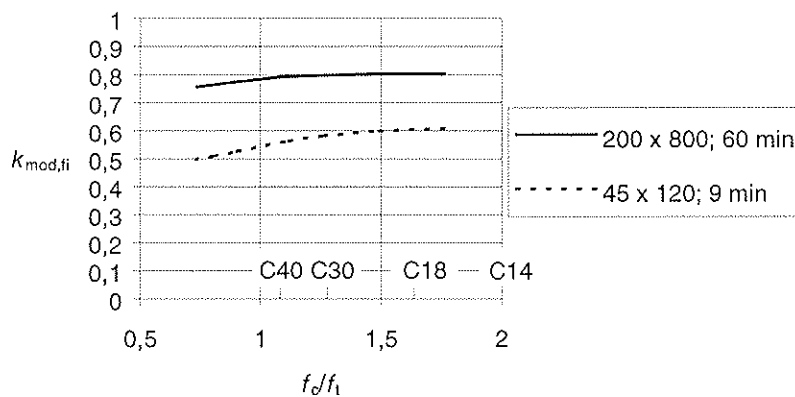


Figure 10 — Effect of strength ratio on modification factor for fire for bending for two cross sections

ratios f_c/f_t for some strength classes between C14 and C40 according to EN 338, see table 3, giving the characteristic values for compression and tension parallel to grain for both solid timber according to EN 338 and homogenous glued laminated timber according to EN 1194. Since all strength ratios are greater than unity, no plastic flow would occur at

normal temperature. With the assumptions of table 2, the strength ratios assumed in the calculations are 1,22 for the large glued laminated cross section of figure 10 and 1,12 for the small solid timber cross section. While the results of figures 5 and 6 are representative for all strength classes of glued laminated timber, somewhat greater values are possible for low strength classes of solid timber.

Table 3 — Characteristic strength values for compression and tension parallel to grain for some strength classes according to EN 338 and EN 1194

| Strength class | $f_{c,0,k}$ N/mm ² | $f_{t,0,k}$ N/mm ² | $f_{c,0,k}/f_{t,0,k}$ |
|----------------|----------------------------------|----------------------------------|-----------------------|
| C14 | 16 | 8 | 2,00 |
| C18 | 18 | 11 | 1,64 |
| C30 | 23 | 18 | 1,28 |
| C40 | 26 | 24 | 1,08 |
| GL24h | 24 | 16,5 | 1,45 |
| GL28h | 26,5 | 19,5 | 1,36 |
| GL32h | 29 | 22,5 | 1,29 |
| GL36h | 31 | 26 | 1,19 |

For tension and compression the calculated modification factors are shown for a glued laminated cross section of 140 mm × 300 mm, see figure 11 and 12. They deviate considerably from the values of both methods given by ENV 1995-1-2. The total effect on the load ratio is shown in figure 13 and 14.

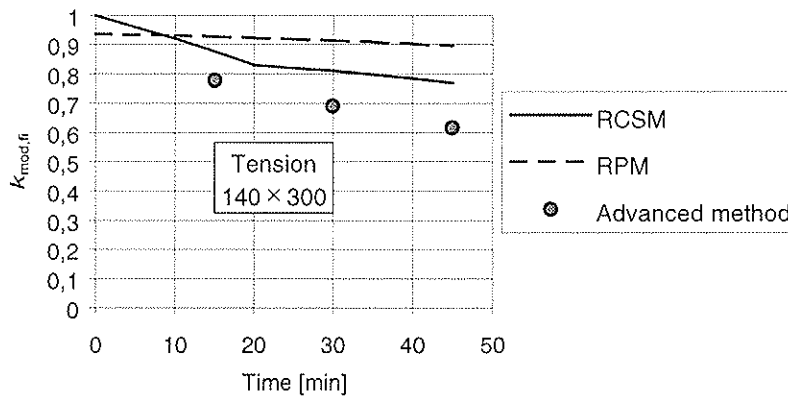


Figure 11 — Comparison of calculated (advanced method) modification factors for fire in compression with values according to reduced properties method (RPM) and reduced cross section method (RSCM) of ENV 1995-1-2

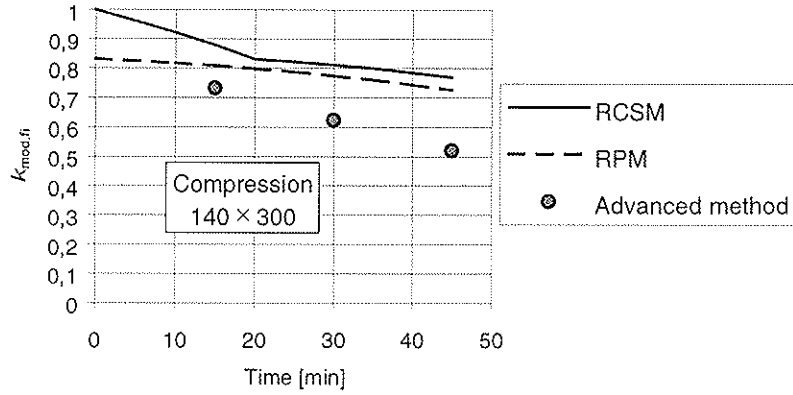


Figure 12 — Comparison of calculated (advanced method) modification factors for fire in compression with values according to reduced properties method (RPM) and reduced cross section method (RCSM) of ENV 1995-1-2

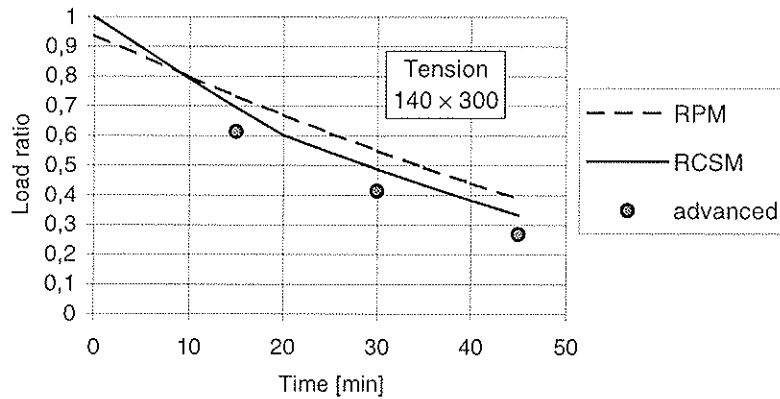


Figure 13 — Load ratio vs. time for tension. Comparison of calculated (advanced method) values with reduced properties method (RPM) and reduced cross section method (RCSM) according to ENV 1995-1-2

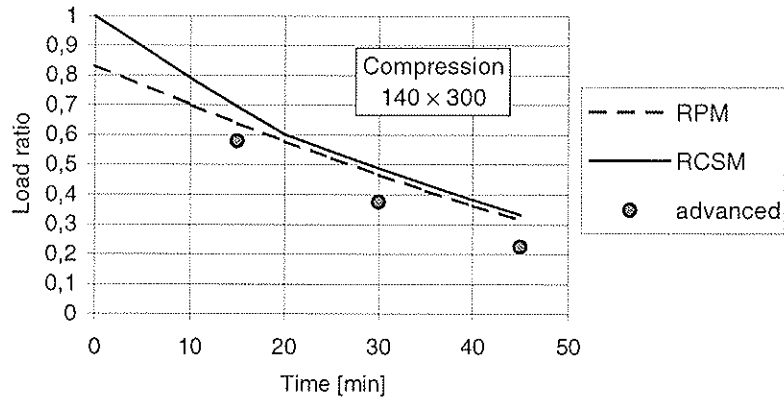


Figure 14 — Load ratio vs. time for compression. Comparison of calculated (advanced method) values with reduced properties method (RPM) and reduced cross section method (RCSM) according to ENV 1995-1-2

4 Discussion and conclusions

4.1 Notional charring rates

In order to simplify the determination of the residual cross section, Eurocode 5 gives the option of applying notional charring rates and preventing tedious calculations taking into account corner roundings. The values given by ENV 1995-1-2 and Draft prEN 1995-1-2 are reasonable approximations.

4.2 Strength and stiffness parameters

Above, two alternative simplified methods of taking into account the reduction of strength and stiffness parameters of the residual cross section are compared with the advanced method given in Draft prEN 1995-1-2. It has been shown that there exists good agreement of the reduced cross section method and the advanced method for members in bending. The intention of the somewhat more sophisticated reduced properties method was that the designer should get an extra bonus by “better”, that is more precise and “economic” results. However, comparing these values with those according to the advanced method, it seems doubtful if these “more precise” values are still safe. In tension and compression, both methods are unsafe. Using the reduced cross section method, the zero-strength layer should be increased further. For practical reasons, however, it should be avoided to use different effective cross sections dependent on the type of action effect.

The advantage of the reduced properties method is that it is, or could be, more applicable and precise. The format of the method allows that modification factors for fire are derived for other cases than rectangular cross sections exposed on three or four sides, see for example modification factors for fire given in Draft prEN 1995-1-2 for timber members in insulated wall and floor assemblies, or for glued laminated beams exposed to parametric fires. Here the introduction of a zero-strength layer would not allow a simple solution. For timber cross sections exposed on four sides (and probably also for exposure on three sides), there is a need to derive correct modification factors for fire such that non-conservative results are prevented.

Contrary to steel sections, where the section factor is a good measure for the steel temperature, which is almost the same in the entire cross section, the temperature conditions of timber sections are much different. In timber cross sections large temperature and moisture gradients occur, and the size of the zones not affected by elevated temperature plays an important role, as well as the time of fire exposure. The reduced properties method cannot be used for the calculation of timber members exposed on one side, e.g. laminated timber decks. In this case, new relationships between the modification factor for fire $k_{mod,fi}$ and the section factor p/A_r should be derived. Here, however, the reduced cross section method is applicable.

In this paper, a comparison is made of modification factors for fire and load ratios versus time with results according to the advanced method. Only for small cross sections of size 45 mm × 120 mm a comparison was possible with experimental results by Norén (1988). Unfortunately no other experimental results are found in literature. Even though a large number of tests have been carried out of timber beams in bending exposed to fire on three or four sides, no information is available on predicted normal temperature strength of the specimens.

In general, there is a need of carrying out more fire tests in order to obtain more robust results. For special cases, more knowledge is needed. Especially for combined glued

laminated timber with outer laminations of a higher grade, a greater decrease of load-bearing capacity can be expected when exposed to fire than shown here.

5 References

- DIN 4102 Teil 4 (03/94), Brandverhalten von Baustoffen und Bauteilen; Zusammenstellung und Anwendung klassifizierter Baustoffe Bauteile und Sonderbauteile. DIN Deutsches Institut für Normung e.V. 1994
- Draft prEN 1995-1-2, Eurocode 5 – Design of timber structures, Part 1-2 Structural fire design, First draft October 2000
- EN 338:1995, Structural timber – Strength classes. CEN –European Committee for Standardization
- EN 1194:1999, Timber structures – Glued laminated timber – Strength classes and determination of characteristic values. CEN –European Committee for Standardization
- ENV 1995-1-2:1994, Eurocode 5 – Design of timber structures, Part 1-2 Structural fire design
- Glos, P. and Henrici, D., 1990, Festigkeit von Bauholz bei hohen Temperaturen. Institut für Holzforschung der Universität München.
- Källsner, B. and König, J., 2000, Thermal and mechanical properties of timber and some other materials used in light timber frame construction. CIB W18 Paper 33-16-3
- König, J., 1998, Revision of ENV 1995-1-2: Charring and degradation of strength and stiffness. CIB W18, Paper 31-16-1
- König, J. and Walleij, L., 2000, Timber frame assemblies exposed to standard and parametric fires – Part 2: A design model for standard fire exposure. Swedish Inst. for Wood Technology Research, Report I0001001
- Norén, J., 1988, Failure of structural timber when exposed to fire. Proc. of Int. Conf. on Timber Engineering, Vol. 2, 397-406, Seattle
- Schaffer, E. L., 1984, Structural fire design: Wood. Forest Products Laboratory. Res. Paper FPL 450. Madison
- Schaffer, E. L., Bender, D. A. and Woeste, F. E., 1986, Strength validation and fire endurance of glued-laminated timber beams. Forest Products Laboratory. Res. Paper FPL 467. Madison
- Thunell, B., 1941, Hållfasthetsegenskaper hos svenskt furuvirke utan kvistar och defekter. Royal Swedish Institute for Engineering Research, Proceedings No. 161, Stockholm

**INTERNATIONAL COUNCIL FOR RESEARCH AND INNOVATION
IN BUILDING AND CONSTRUCTION**

WORKING COMMISSION W18 - TIMBER STRUCTURES

PULL-OUT TESTS ON GLUED-IN RODS AT HIGH TEMPERATURES

A Mischler

A Frangi

Swiss Federal Institute of Technology, Zurich

SWITZERLAND

Presented by: A Mischler

- H J Blass asked why the behaviour of the glued-in rod at 80°C and 100°C did not coincide with data from the manufacturer.
- A Mischler agreed with the observation. He stated that steel plates might have been used on the manufacturer tests as compared to the wood-adhesive-steel interaction of the glue-in rod connections. He commented that the manufacturer test results could not be relied upon.
- S Olsson commented on the Kollmann diagram and asked whether residual stresses in wood be a means to explain the observations.
- A Mischler responded that this was a moisture effect according to Kollmann
- V Enjily stated that he agreed with S. Olsson comment
- J König commented on the effect of moisture and temperature on MOE. He stated that oven tests were under steady state condition. Kollmann was able to keep the specimens moist although there was some surface drying in the specimens. In fire situation one would experience transient conditions with movement of moisture front and it would be more complicated. He also stated that temperature and shear strength relationships are available in the Euro Code.
- S Thelandersson commented about more test with ISO fire and asked how much wood would be needed to protect the glued-in rod for ISO fire test.
- A Mischler responded that models in the Euro Code could be used to estimate the amount of wood needed and then ISO fire test could be conducted to confirm.
- J Kangas commented that in the Finnish V-connections brittle behaviour was not observed. With angle across the grain type fasteners used in the Finnish V-connections, it was not possible to obtain the cylindrical failures.

Pull-out tests on glued-in rods at high temperatures

Adrian Mischler, Andrea Frangi

Swiss Federal Institute of Technology, Zurich, Switzerland

1 Introduction

Connections and reinforcements with glued-in steel rods are becoming more and more important in timber engineering. The load-carrying behaviour of this connection type at room temperature is investigated in many research projects.

Not only the knowledge of the resistance at room temperature is needed but, in some cases, also the fire resistance of a connection. At present, there is only little information available about the fire resistance of this connection type. One problem is that the different adhesives are more or less sensitive to high temperature. Therefore, the fire resistance of these connections has to be investigated.

This paper presents results of tests at different temperatures with axially loaded rods glued in glued laminated timber parallel to the grain.

2 Experimental Investigations

2.1 Specimen an Configuration

The tests were carried out during a diploma thesis [1] at the ETH in Zürich. The specimen consisted of glued laminated timber GL 24 with a moisture content of 12%. As the pull-out resistance is affected by the timber around the drilled hole and not by the timber properties of the whole specimen, the timber density was determined from the individual lamella containing the rod. The mean wood density of the 10 specimens tested at room temperature was 414 kg/m^3 with a coefficient of variation of 5.7%. The threaded rods with an outer diameter of 12 mm correspond to strength class 8.8 (tensile strength 800 N/mm^2 , yield strength 640 N/mm^2). The hole diameter in the timber was 16 mm. The adhesive was an Epoxy: GSA produced by ASTORit AG, CH-8840 Einsiedeln. To avoid splitting of the timber, there was a free length of 60 mm without bond between the timber and steel rod (see figure 1). The subsequent anchorage length was 160 mm. The effect of the free length is described in [2].

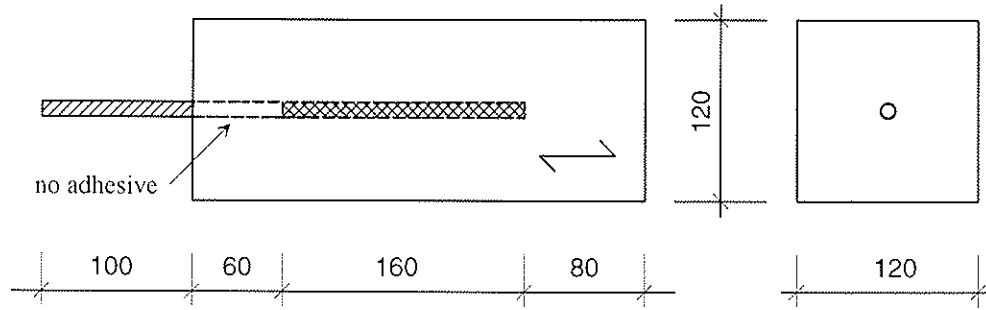


Figure 1: Dimensions of the test specimens

The loading arrangement is shown in figure 2. The tests were performed by pulling out the bar under counter-pressure on the end face of the timber. The load was applied by a constant displacement. The load as well as the displacement were continuously measured.

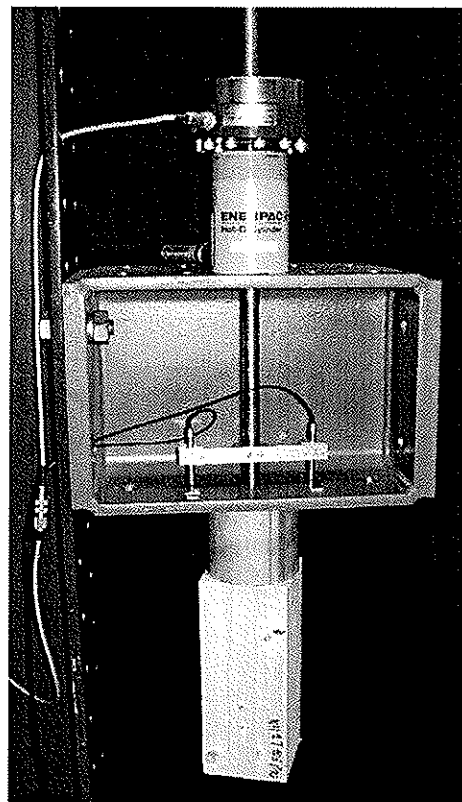


Figure 2: Test arrangement

2.2 Heating the test specimen

The specimens were heated in an oven to the corresponding temperature. The temperature in the timber was continuously measured during the heating and during the loading of the specimen. A typical heating curve is shown in figure 3. The temperature measure points 1 and 2 are in the middle of the timber cross section.

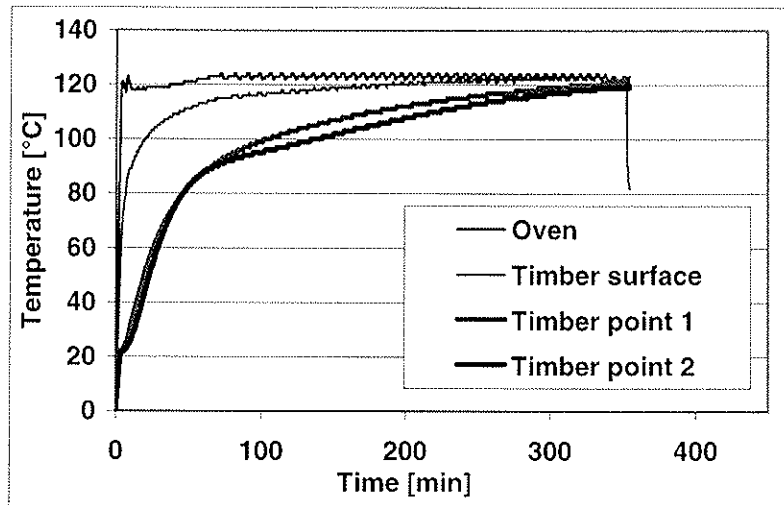


Figure 3: Typical heating curve

2.3 Testing Programme and test results

Seven series of 10 specimens each were to be tested. The specimens were heated before testing at the following temperatures:

20°C, 75°C, 85°C, 95°C, 105°C, 120°C, 175°C

The shear strengths in the bond line are given in Table 1. Figure 4 shows the effect of the test temperature on the shear strength. The shear strength f_v is defined in formula (1):

$$f_v = \frac{F_u}{d_h \cdot \pi \cdot \ell_a} \quad (1)$$

Where: F_u Ultimate failure load
 d_h Diameter of the hole in the timber
 ℓ_a Anchorage length

Table 1: Tests results [1]

| Test temperature | Number of tests | Mean shear strength in bond line [N/mm ²] | Coefficient of variation [%] |
|------------------|-----------------|---|------------------------------|
| 20°C | 10 | 6.95 | 9.10 |
| 75°C | 9 | 5.14 | 9.94 |
| 85°C | 10 | 5.20 | 7.74 |
| 95°C | 8 | 4.51 | 6.94 |
| 105°C | 10 | 2.21 | 8.16 |
| 120°C | 10 | 1.99 | 10.9 |
| 175°C | 10 | 1.26 | 18.3 |

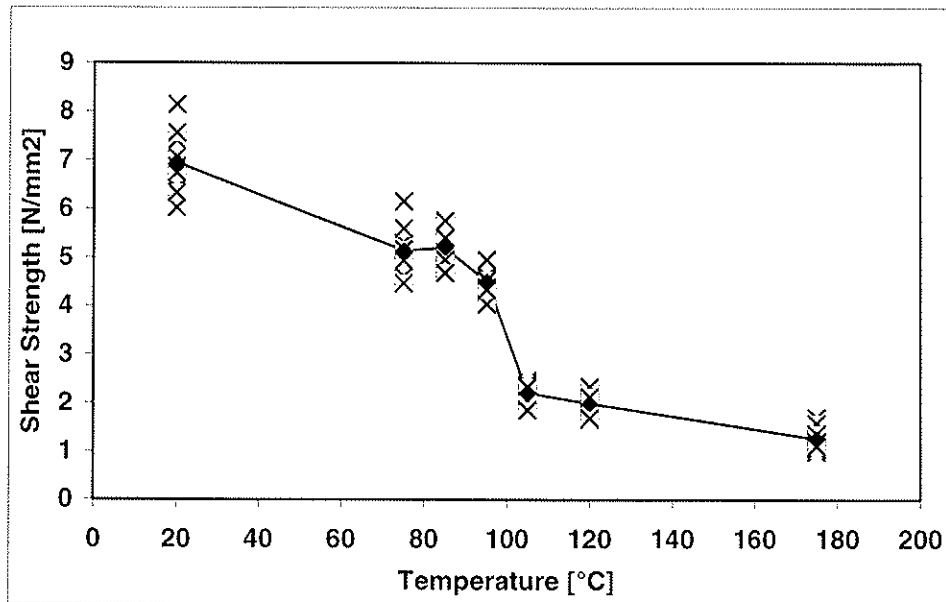


Figure 4: Shear strength in the bond line versus test temperature.

2.4 Failure modes

2.4.1 Test temperature 20°C

The specimens tested at 20°C showed a brittle failure of the epoxy adhesive (figure 5). The individual failure loads laid between 50.9 kN and 65.5 kN. At this load level, the elongation of the steel bar M12 was between 2.9 and 3.71 %. The adhesive was not able to follow the large strains of the steel bar. A brittle failure of the adhesive resulted, even if the shear strength of the adhesive was not reached yet.

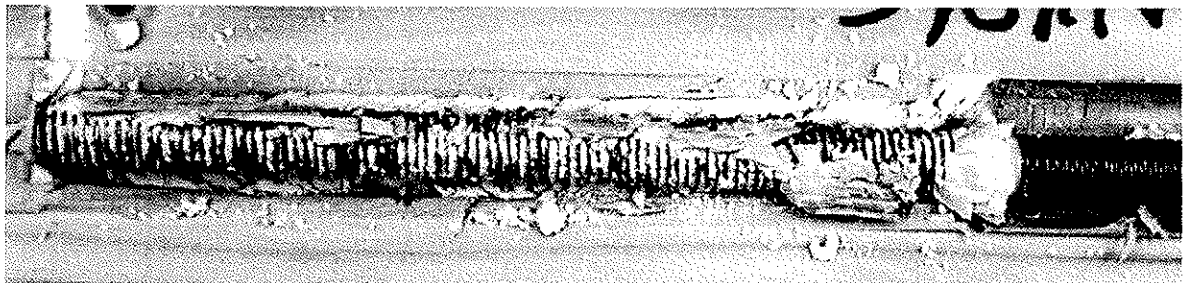


Figure 5: Typical failure at 20°C.

2.4.2 Test temperature 75°C

The specimens tested at 75°C showed a shear failure of the timber (figure 6). The steel bar with the adhesive was pulled out as an entire cylinder. The surface of the epoxy was covered with timber.

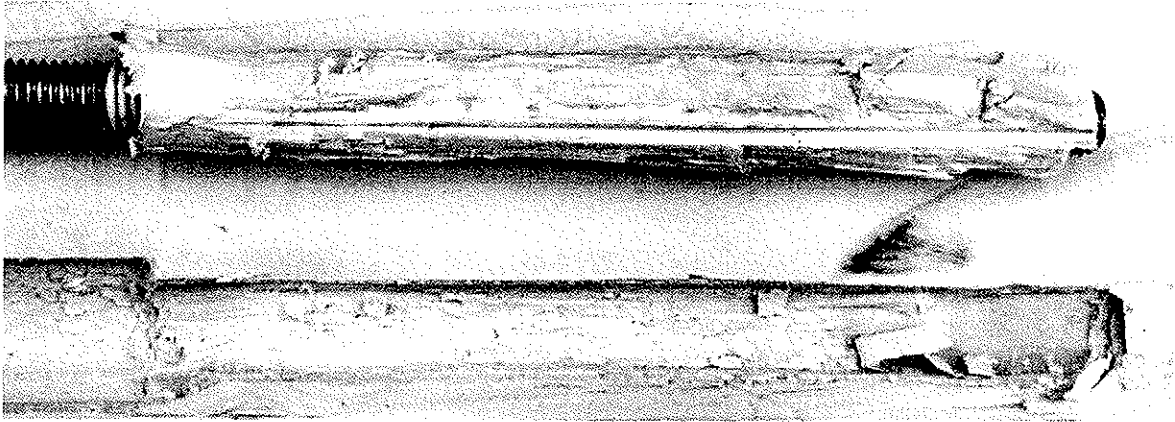


Figure 6: Typical failure at 75°C.

2.4.3 Test temperature 85 and 95°C

Between 75°C and 95°C, the location of the failure moved from the timber to the adhesive. Again, the adhesive was pulled out as an entire cylinder but there was only little timber at the adhesive (figure 7). The mean failure load was higher at 85°C than at 75°C. A possible reason for this fact is that the stiffness of the epoxy is reduced at higher temperature levels, what could help to reduce the shear tension concentrations at the ends of the anchorage length.

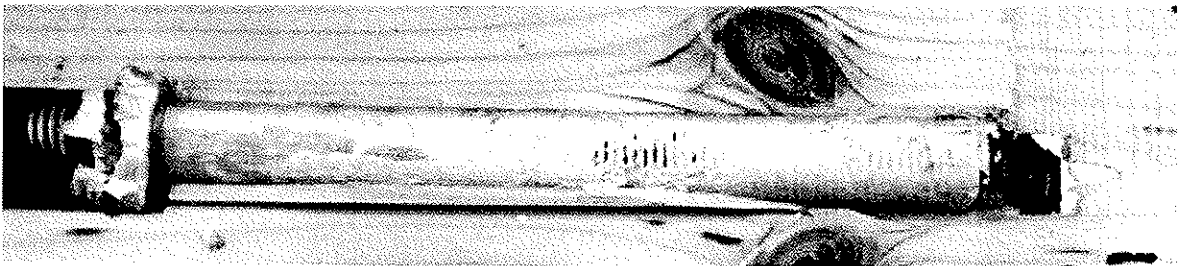


Figure 7: Typical failure at 95°C.

2.4.4 Test temperature 105, 120 and 175°C

At temperatures higher than 100°C, the epoxy adhesive was converted. The colour changed from white to yellow-pink. The epoxy could be crushed to powder by hand. Therefore, its strength was reduced considerably. In the tests, the epoxy adhesive was no more pulled out as an entire cylinder, but it was partly removed from the steel bar (see figure 8).



Figure 8: Typical failure at 105°C.

3 Temperature behaviour of the timber and of the epoxy adhesive

3.1 Timber

Pull out tests on self-tapping screws were carried out to study the behaviour of the timber at different temperatures. The tested screws had an outer diameter of 8 mm and a length of 100 mm. The threaded length was 74 mm. The screw and the dimensions of the specimens are shown in figure 9 and 10. The withdrawal shear strength was calculated without considering the length of the screw point which is 6 mm. Therefore, the effective anchorage length was 68 mm as shown in figure 9. The results are given in table 2 and figure 11.

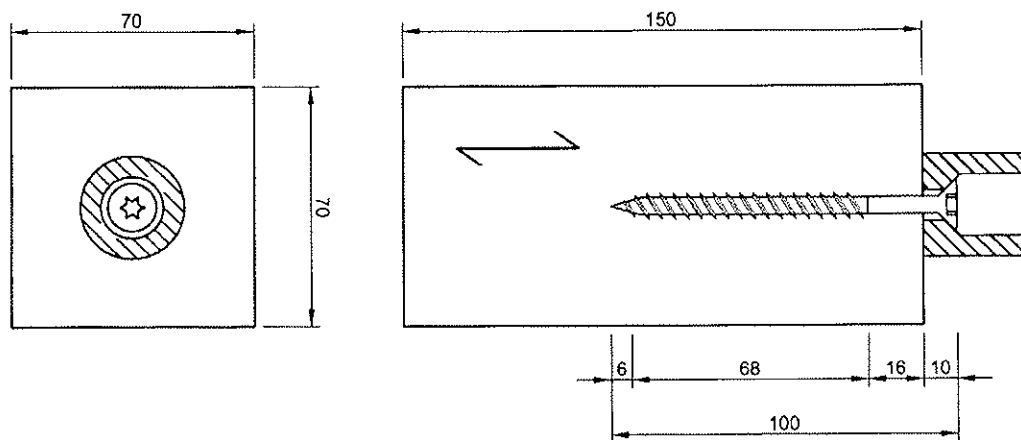


Figure 9: Test specimen

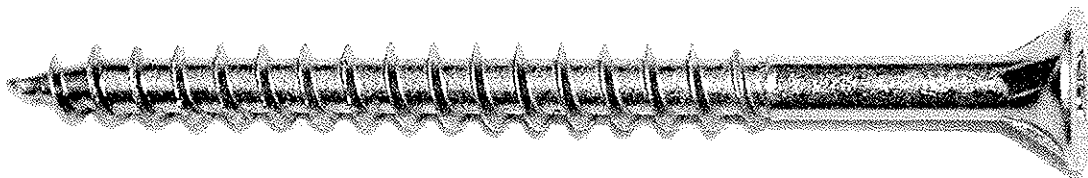


Figure 10: Screw diameter 8.0 mm

Table 2: Results of pull out tests at different temperatures with screws (10 tests per temperature, moisture content after heating)

| Test temperature | Density [kg/m ³] | COV [%] | Withdrawal shear strength [N/mm ²] | COV [%] | Moisture content [%] |
|------------------|------------------------------|---------|--|---------|----------------------|
| 20°C | 464 | 4.42 | 5.66 | 9.6 | 12.1 |
| 50°C | 460 | 4.61 | 4.58 | 11.5 | 9.8 |
| 80°C | 466 | 3.34 | 3.84 | 12.1 | 6.2 |
| 100°C | 466 | 3.73 | 3.61 | 12.9 | 2.6 |
| 120°C | 475 | 6.18 | 3.68 | 14.5 | 2.1 |
| 150°C | 471 | 4.97 | 3.32 | 16.1 | 1.2 |
| 180°C | 470 | 4.58 | 2.63 | 13.7 | 0.3 |

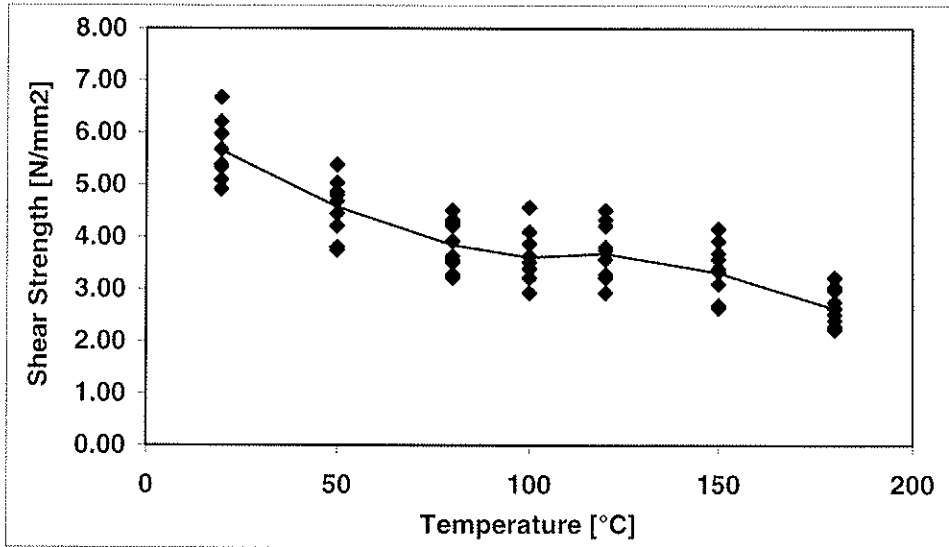


Figure 11: Withdrawal shear strength of the screws versus test temperature.

3.2 Epoxy adhesive

The shear strength of the epoxy adhesive is given in the product specification of the producer ASTORit [3]. The tests were carried out according to the German standard DIN 53283. Figure 12 shows the influence of the temperature on the shear strength of the applied epoxy adhesive.

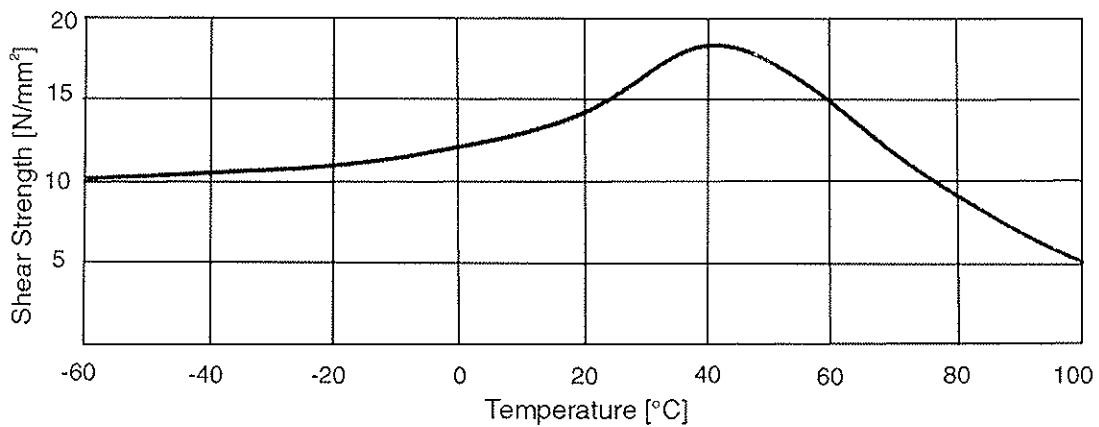


Figure 12: Shear strength of the epoxy adhesive in a tension test versus test temperature [3].

4 Discussion of the results

4.1 Tests at 20°C

First, the shear strength in the bond line at room temperature was compared with values from the literature: Aicher, Gustafsson and Wolf [4] obtained the following mean shear strengths $f_{v,mean}$ for adhesives based on epoxies from tests of the GIROD-Program:

$$f_{v,mean} = \min \left\{ \begin{array}{l} 8.0 \text{ N / mm}^2 \\ 129 d_h^{-0.52} \lambda^{-0.62} (\rho / 480)^{0.45} \end{array} \right. \quad (2)$$

- Where: d_h Diameter of the hole in the timber in mm
 λ Rod slenderness $\lambda = \ell_a / d_h$, with ℓ_a = anchorage length
 ρ Timber density at 12% moisture content

For $d_h = 16$ mm, $\lambda = 160/16 = 10$ and $\rho = 414 \text{ kg/m}^3$ formula (2) gives: $f_{v,mean} = 6.8 \text{ N/mm}^2$. This matches very good with the tests results ($f_v = 7.0 \text{ N/mm}^2$, see table 1).

4.2 Tests at higher temperatures

The shear resistance of the adhesive at room temperatures is higher than that of the timber. The ultimate resistance of the connection is therefore governed by the timber resistance. The strength of the epoxy increases with an increasing temperature up to 40°C, then it decreases (see figure 12). The connection strength is governed by the timber strength up to a temperature of approximately 90°C. Above that temperature the strength of the epoxy decreases very fast, therefore the resistance of the connection is governed by the epoxy adhesive. This behaviour can be explained when the relative strength of the glued-in rods is compared with that of the screws (figure 13).

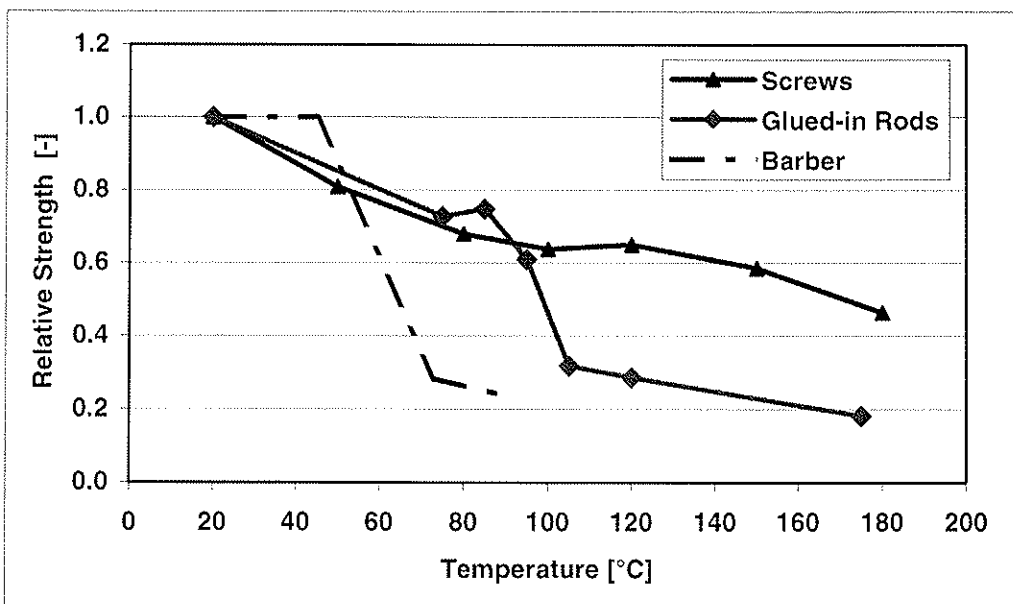


Figure 13: Relative strength of the glued-in bars compared with the screws

From 20°C to 80°C, the decrease of strength is the same for the glued-in rods and for the screws. Between 75°C and 85°C, there is a little increase of the strength for the glued-in-rods probably because of a smoother shear strength distribution along the bond line. Above 90°C, the decrease of the resistance is much more pronounced with the glued-in rods than with the screws.

4.3 Comparison with the tests of Barber

In 1994, Barber [5] carried out similar test at the University of Canterbury, New Zealand. In his tests he used two different epoxy adhesives. The glued-in steel bars of 20 mm diameter had an embedment length of 200 mm. The results of Barber and the trend line he found are given in figure 14.

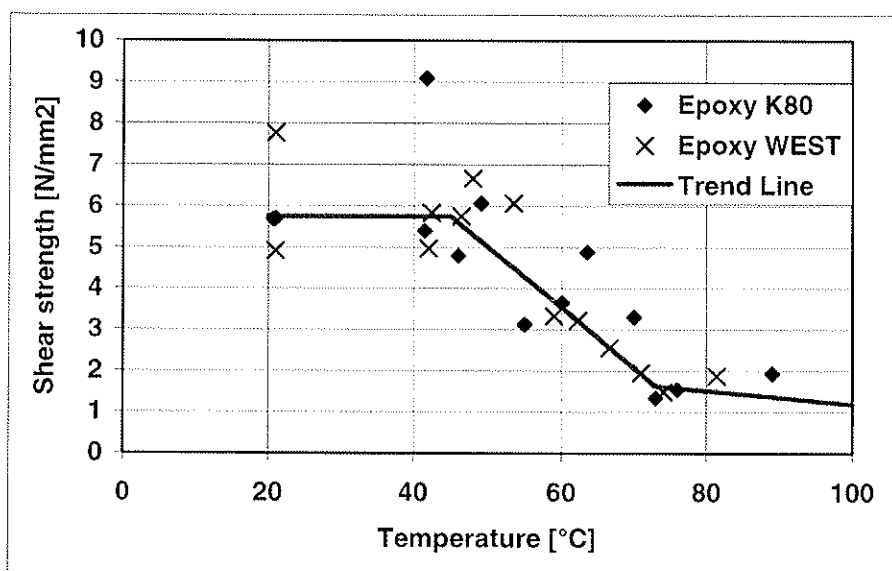


Figure 14: Shear strength versus temperature of the tests carried out by Barber [5]

The failure was caused by splitting of the timber for most specimen. Therefore, it is difficult to compare Barber's results with the tests of the ETH where no splitting failure occurred. Barber found no reduction of the strength up to a Temperature of 45°C. The loss in strength of the epoxy begins at around 45°C compared to 90° in the tests of the ETH. This shows that different epoxy adhesives has a very different temperature behaviour.

5 Comparison of tests with oven heated specimen and fire tests

No fire tests were carried out with screws loaded parallel to the grain direction of the timber. Therefore, the difference between tests with oven heated specimens and fire tests is discussed in the following using tests on screws loaded perpendicular to the grain direction. The tests were carried out at the ETH in a research project with the aim to enlarge the experimental background of design models for the fire resistance of timber-concrete composite floors [6, 7].

The shear resistance of screwed connections between timber and concrete is mainly governed by the withdrawal capacity of the screws. Pull out tests were carried out with oven heated specimens and with specimens subjected to ISO-fire as well. A connection which was experimentally analysed consisted of a self-drilling screw with a collar to limit the screwing depth and a head for connection to the concrete. The threaded part of the screw has an outer diameter of 7.3 mm and a net section of 4.3 mm. The threaded length is 95 mm. The screw dimensions are shown in figure 15.

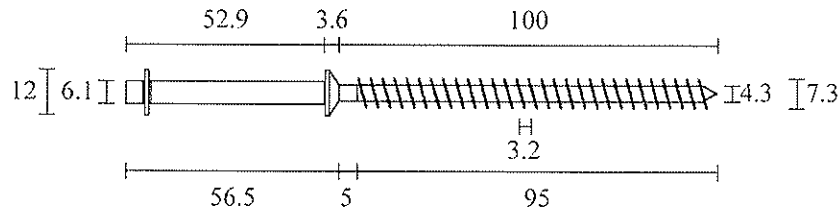


Figure 15: Self-drilling screw for timber-concrete composite elements

When the connector is subjected to tension, the screw fails when the tensile strength of the steel screw or the shear resistance between timber and screw is exceeded. The tests results reported in this paper consider only the shear failure between timber and screw. The fire behaviour of the screws subjected to tension was experimentally analysed with the test arrangement shown in figure 16.

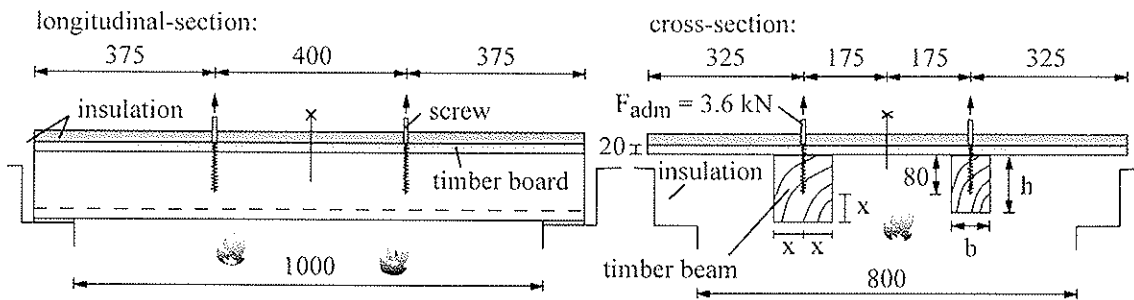


Figure 16: Test arrangement for the pull out tests with the screws subjected to the ISO-fire

All fire tests were performed at the Swiss Federal Laboratories for Materials Testing and Research (EMPA) in EMPA's small furnace (1.2x1.0 m) using ISO-fire exposure. For each fire test, two timber beams were placed in the small furnace and on each beam two connectors were tested. The connectors were screwed 80 mm into the timber. In the fire tests the temperature in selected locations, the deformation of the connectors and the tensile force were measured. The fire tests were performed using two different procedures:

- The specimen was exposed to the ISO-fire for 20, 30 or 40 minutes with the permissible load applied to the connectors. If no failure occurred in this time, the load was increased until failure occurred.
- The specimen was loaded with the permissible load and then exposed to the ISO-fire until failure.

The specimens consisted of squared timber beams with a moisture content of about 13%. The mean wood density of the 11 squared timber beams was 383 kg/m^3 with a coefficient of variation of 3.7%. Three squared timber beams were used to perform 19 pull out tests at room temperature. The mean value of the withdrawal shear strength measured at room temperature was 6.3 N/mm^2 with a coefficient of variation of 4.8%.

Further pull out tests with oven heated specimens were carried out at the ETH in Zürich. The specimen dimensions are shown in figure 17 and consisted of glued laminated timber with a moisture content of about 11%. The mean wood density of the 12 specimen was 442 kg/m^3 with a coefficient of variation of 4.4%. The mean value of the withdrawal shear strength measured at room temperature was 7.0 N/mm^2 with a coefficient of variation of 5.7%.

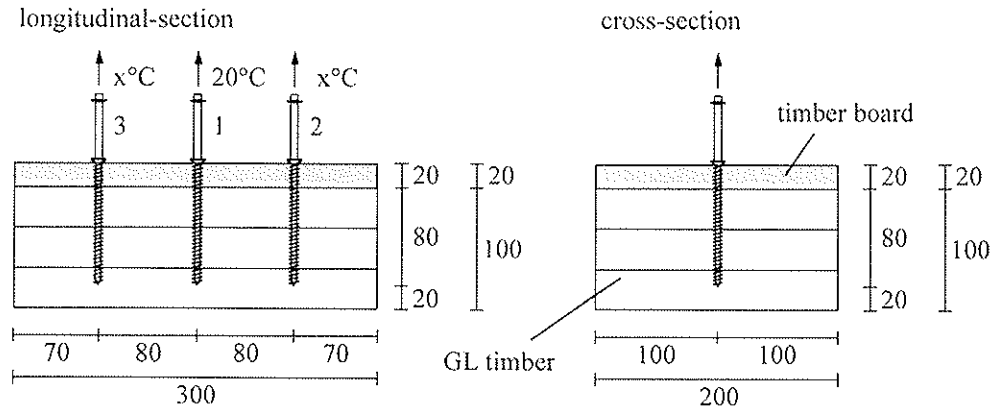


Figure 17: Test arrangement for the pull out tests with oven heated specimen

For each specimen, three connectors were screwed 80 or 70 mm into the timber. One screw of each specimen was tested at room temperature. After heating the timber in an oven to the corresponding temperature, the other screws were tested. The temperature in the timber was continuously measured during the heating process and the loading of the specimen.

The relative withdrawal shear strength is given in figure 18 as a function of the wood temperature. For the fire tests, the average temperature of the wood along the screw was considered.

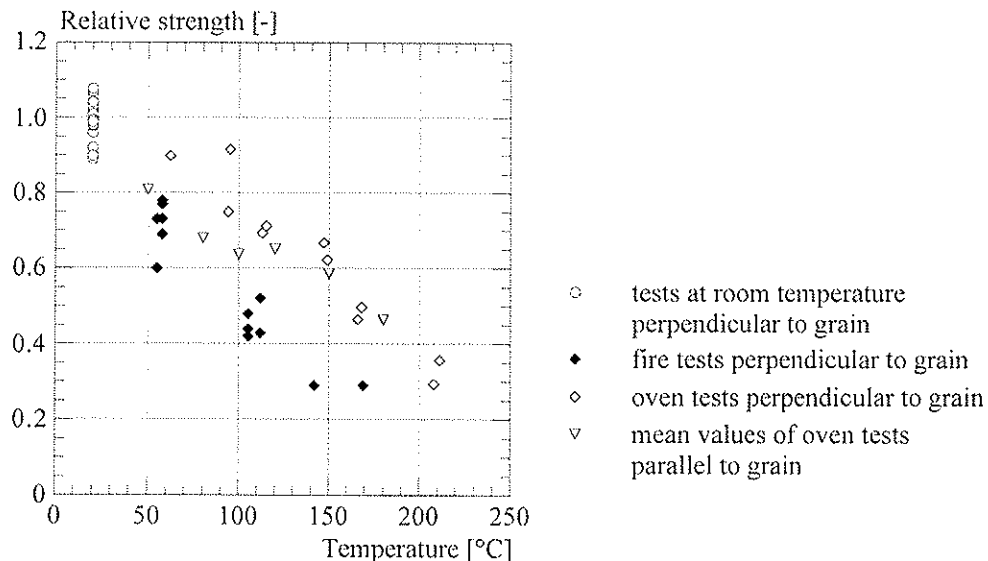


Figure 18: Relative withdrawal shear strength versus wood temperature

Figure 18 shows that the reduction of the withdrawal shear strength in function of the wood temperature for the fire tests is considerably greater than for the oven tests. The average withdrawal shear strength for the oven tests at 110°C is 70% of the average strength at room temperature, while the average strength for the fire tests at 105°C is only 45% of the strength at room temperature.

The observed different reduction of the withdrawal shear strength for the fire tests and the oven tests in function of the wood temperature can be explained with several reasons.

The first reason is the influence of moisture content. For the oven heated tests the specimens were heated for several hours to the corresponding temperature. After heating the moisture content was measured and a high drying rate of the timber was observed (see table 2). The test specimens heated up to 100°C showed a moisture content of only 2-3%. During the fire test on the other hand, the timber cross-section is subjected to a great time dependent temperature and moisture gradient. In the timber part of the cross-section with temperatures near 100°C the moisture content even increased up to 14-15%. Therefore different level of moisture contents have to be considered for the fire tests and the oven tests.

Kollmann [8] investigated the influence of a changing moisture content. He measured the effect of temperature on the bending modulus of elasticity of heated specimens. The tests were performed at room temperature and at constant temperature of 40, 60, 80 and 100°C respectively. The specimen were repeatedly loaded and unloaded at time intervals of 1.5 minutes or more during a total test duration of 60 minutes. The lowest moduli of elasticity were recorded at the second or third loading cycle when the target temperature in the timber was reached but the moisture content was not yet decreased. During the following loading cycles the modulus of elasticity increased again (see figure 19), due to the drying of the timber beginning on the surface and then continuing to the middle of the specimens,.

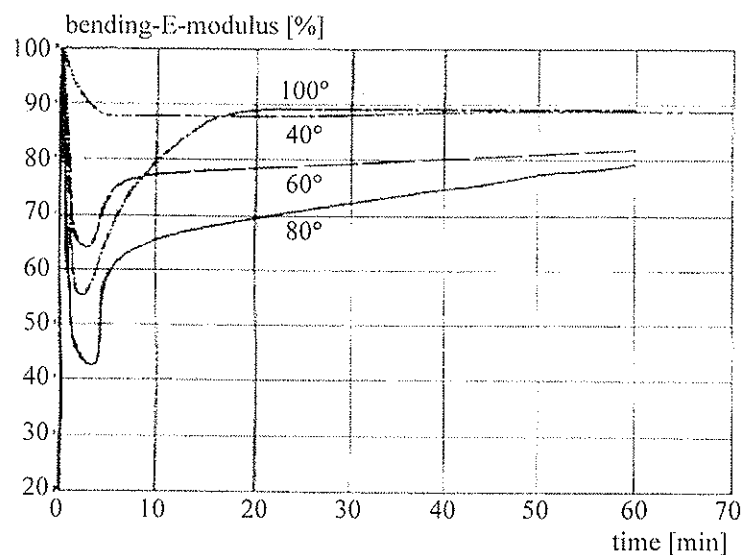


Figure 19: Time dependent reduction of the bending E-modulus versus wood temperature

Another reason for the observed different reduction of the withdrawal shear strength for the fire tests and the oven tests is the effect of loading rate. The effect of the loading rate is already considerable at room temperature. This effect could be much greater at elevated temperature and sensitive to moisture changes.

Figure 20 compares typical load-deformation curves of the two different test methods. It clearly shows that not only the strength but also the stiffness is considerably greater in the fire tests than in the oven tests.

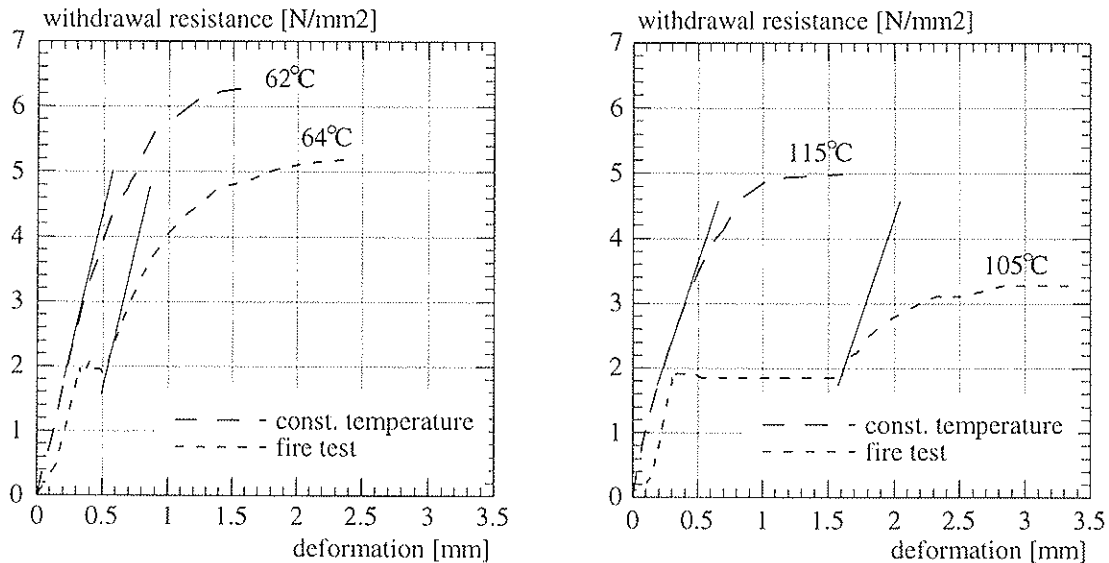


Figure 20: Typical load-deformation diagrams of for the fire tests and the oven tests

Considerable creep deformations were observed in all fire tests. When the connectors were pulled out at the end of the fire tests, a time dependent reduction of the withdrawal shear stiffness and strength was measured.

In the oven tests on the other hand, the connectors were not loaded during the heating to the corresponding temperature. The connection was loaded only during a short time period in the pull-out test after drying of the timber. Therefore no creep effect in the oven test occurred.

6 Conclusions

Tests on screws and glued-in rods with oven heated specimen showed the influence of the temperature on the properties of the timber and the adhesive. Comparative tests with specimen subjected to ISO-fire and oven heated specimen showed, that the strength and stiffness values obtained in fire tests are smaller than the values measured on oven heated specimen.

7 References

- [1] Hilty, P., *Auszieh widerstand von eingeklebten Stahlstäben bei hohen Temperaturen*. Diplomarbeit, Institut für Baustatik und Konstruktion, ETH Zürich, 2001.
- [2] Gehri, E., *Ductile behaviour and group effect of glued-in steel rods*. In Proc. RILEM Symposium on Joints in Timber Structures, Stuttgart, Germany, 2001.
- [3] ASTORit, *GSA-Ankersystem*, Technische Erläuterungen – Zweikomponentenklebstoff auf Epoxidbasis, 1996.

- [4] Aicher, S., Gustafsson, P.J., Wolf, M., *Load displacement and bond strength of glued-in rods in timber influenced by adhesive, wood density, rod slenderness and diameter*. In Proc. of 1st RILEM Symposium on Timber Engineering, Stockholm, 1999, pp. 369–378.
- [5] Barber, D.J., *Fire Resistance of Epoxied Steel Rods in Glulam Timber*. Research report 94/1, Department of Civil Engineering, University of Canterbury, Christchurch, New Zealand, 1994.
- [6] Frangi, A., Fontana, M., *Versuche zum Tragverhalten von Holz-Beton-Verbunddecken bei Raumtemperatur und Normbrandbedingungen*. Institut für Baustatik und Konstruktion (IBK). ETH Zürich. IBK Bericht Nr. 249. Birkhäuser Verlag Basel. Juli 2000.
- [7] Frangi, A., *Brandverhalten von Holz-Beton-Verbunddecken*. Institut für Baustatik und Konstruktion (IBK). ETH Zürich. IBK Bericht Nr. 269. Birkhäuser Verlag Basel. September 2001.
- [8] Kollmann, F., *Über das mechanische Verhalten von Kiefernholz bei Biegung und Temperaturen zwischen 20° und 100°*. Svenska Träforskningsintitutet, Trätekniska Avdelningen, Meddelande 22, Stockholm, 1951.

**INTERNATIONAL COUNCIL FOR RESEARCH AND INNOVATION
IN BUILDING AND CONSTRUCTION**

WORKING COMMISSION W18 - TIMBER STRUCTURES

**PERFORMANCE BASED CLASSIFICATION OF ADHESIVES
FOR STRUCTURAL TIMBER APPLICATIONS**

R J Bainbridge
C J Mettem
TRADA Technology

J G Broughton
A R Hutchinson
Oxford Brookes University

UNITED KINGDOM

Presented by: R J Bainbridge

- W Bakens stated that in development of performance based concepts in other communities different terminologies were used with different groups and asked if there was linkage with some of these groups.
- R J Bainbridge responded that links have been established through CEN mandates.

Performance Based Classification of Adhesives For Structural Timber Applications

Bainbridge, R.J., Principal Engineer, TRADA Technology, UK
Mettem, C.J., Chief Research Engineer, TRADA Technology, UK
Broughton, J.G. Joining Technology Research Centre, Oxford Brookes University, UK
Hutchinson, A.R. Joining Technology Research Centre, Oxford Brookes University, UK

Abstract

Many of the recently developed and emerging technologies aimed at enhancing the opportunities for structural timber require the use of adhesives. Examples of innovative developments include timber composite materials, structural connections, localised reinforcement and improved repair and renovation work. These offer substantial benefit, but are reliant upon use of non-traditional timber adhesives, often with thick bond line or 'gap-filling' capabilities.

It is vital that users can specify an adhesive with the correct properties for the intended application, but currently no performance classification system is available. Whilst, under laboratory conditions, innovations employing adhesive bonding methods and materials can achieve connections demonstrated to be significantly more efficient than those used at present, these are specific to controlled conditions and a single adhesive brand formulation. However, in industry there remain perceptual barriers coupled with a lack of practical information that has prevented the technology from realising its considerable potential.

A provisional basis for the formulation of a performance-based classification of structural timber adhesives is proposed in this paper, drafted in the context of the Eurocode 5 structural design approach. This includes review of CEN mandates on structural adhesives, polymeric sealant performance classification standards and existing structural timber adhesive guidance. Recommendations are also made concerning the development of the proposed classification basis.

1. Introduction

Many of the recently developed and emerging technologies aimed at enhancing the opportunities for structural timber require the use of adhesives. Examples of innovative product and technique developments include timber composite materials, structural connections, localised reinforcement and improved repair and renovation work:

- Glued laminated timber members with small volumes of bonded-in glass fibre reinforced composite (GFRP) are reported to lead to substantial savings (24% on real case study bridges [1]).
- Local Reinforcement in highly stressed areas such as notches and connector locations can also be very beneficial – for example adhesive bonded glass fibre can increase bolt type shear joint strength by more than 50% for additional costs of less than 10% [2].
- Connection solutions reliant upon bonded-in rods are found to be extremely efficient – for example, full size tests on moment resistant column-foundation joints have demonstrated joint efficiencies of 75% compared to the moment capacity of the column itself [3]. Research on small scale joints has highlighted the advantage of thick bondlines to transfer load efficiently [4].

All of these techniques are reliant upon use of non-traditional timber adhesives, commonly with thick bond line or 'gap-filling' capabilities. Considering the potential benefit achieved through use of low volumes of adhesives in these applications, the efforts to realise the advantages must be focused upon establishment of commonly recognised performance criteria. Experts and industrial specialists involved in other engineering fields (mechanical and civil) have much to offer timber construction in such technology transfer.

Users need to specify an adhesive with the correct properties for the intended application, but currently no performance classification system is available. Whilst, under laboratory conditions, innovations employing adhesive bonding methods and materials can achieve connections demonstrated to be significantly more efficient than those used at present, these are specific to controlled conditions and a limited number of

single adhesive brand formulation. However, in industry and amongst construction professionals there remain perceptual barriers, coupled with a lack of practical information.

Advice for actual structural engineering designs needs to take into account whether the intention is to use either close-gap or gap-filling adhesives. Most well established timber adhesives are of the former type, and there is a considerable lack of user knowledge and design information for timber adhesives other than those for factory manufacture of glued laminated timber and finger joints. At present, where practitioners are considering innovative developments employing adhesives for timber, they are tempted to extrapolate information related to close gap timber-timber bonded joints. Research results [3] show that such extrapolation is highly inappropriate and in some cases unsafe.

The *solution* is, therefore, to pay particular attention to the development of a framework for a *performance classification* of adhesives for timber structures. This will also provide a method by which low-environmental-impact adhesive types can be assessed, and subsequently introduced to replace less environmentally acceptable materials. Such an approach is available for construction sealants within the ISO 11600 classification scheme, and it is now being taken up strongly by that industry. The grouped classification approach is also compatible with the developments underway through CEN Mandate 127 on Construction Adhesives [5].

2. Adhesive Classification

A review has been made of CEN mandate M127 '*Construction Adhesives (Draft)*' [6] and the answer from CEN TC193 [7]. This is of relevance to the subject of structural adhesive performance classification. In addition, the following documents were also reviewed, due to their shared commonality of scope with certain aspects of the research:

- CEN Mandate M128, Products Related To Concrete, Mortar and Grout (Draft) [8] and the answer from CEN TC104 [9].
- prEN 1504-4, '*Products and Systems For The Protection and Repair of Concrete Structures - Definitions, requirements, quality control and evaluation of Conformity - Part 4: Structural Bonding*' [10]
- EN 301, '*Adhesives, phenolic and aminoplastic, for load-bearing timber structures: Classification and Performance Requirements*' [11]

Through this review, a number of key areas for reference emerged, which will be of use in defining the performance classification methodology:

- scope: end use and field of application
- performance characteristics
- performance requirements
- attestation of conformity
- dangerous substances
- product identification

3. Polymeric Sealant Performance Classification

An international standard, *ISO 11600:1993 Building construction- Sealants - Classification and Requirements* [12], is available as a basis for performance classification and selection guidance of those products. Sealants are in many ways broadly similar to adhesives, and so there is potential for adoption and incorporation of some attributes of the classification into draft timber adhesive performance specifications. However, requirements of adhesives are more complex and structurally demanding, necessitating a more involved system.

The key aspects identified as useful are:

- the outline performance classification methodology
- classification matrix identification
- performance classification system
- designation system approach to product description

4. Target Application Linked Design Considerations & Adhesive Performance Parameters

Key target construction applications in which adhesive materials may be used with timber, are identified in Table I. In order to integrate these with a performance based classification system, it is necessary to identify:

- the overall product type aimed at the application (whether thin bond lines, thicker gap filling bond lines or adhesive resin based grouts or mortars are indicated)
- the substrates onto which bonding will be required (one of which will be wood, the other may be wood, 'W', or a non-wood based material, 'X', following the classification ethos of CEN M127)

On this basis, a provisional application related classification could be developed, as shown in Table 1.

| Application | Product Type* | Substrates | | | | | | |
|------------------------------|---------------|-------------------|------------------------|-----------------------|-----------------|-----|--------------------|--------------------|
| | | Classification ** | Non-wood substrate (X) | | | | | |
| | | | Mild Steel*** | High Tensile Steel*** | Stainless Steel | FRP | Epoxy Coated Rebar | Glass Fibre Fabric |
| Bonded-in rods | GF | W-X | • | • | • | • | • | |
| Bonded-in plates | GF | W-X | • | • | • | • | • | |
| Surface bonded reinforcement | GF | W-W, W-X | | | | • | | • |
| | TB | W-W, W-X | | | | • | | • |
| Timber lap joints | GF | W-W | | | | | | |
| | TB | W-W | | | | | | |
| Crack/fissure filling | GF | W-W | | | | | | |
| | MG | W-W | | | | | | |
| Thin webbed box / I beams | GF | W-W | | | | | | |
| | TB | W-W | | | | | | |
| Replacement section repairs | MG | • **** | | | | • | • | |
| Laminated timber products | TB | W-W | | | | | | |

Notes:
 * TB = Thin Bondline, GF = Gap Filling, MG = Adhesive resin based mortar or grout
 ** W-W = wood-wood, W-X = Wood to other substrate
 *** including galvanised/theradised steel rods
 **** acts as a bulk grout material, normally taken that adhesion to substrates not generally critical

Table 1 Structural Application Related Reference Substrates

The performance characteristics for consideration in relation to these applications can be drawn from those recommendations made in CEN mandates M127 (Structural Adhesives) and M128 (Concrete Protection and Repair Products) and viewed in relation to those products that have a history of use. This may have emerged through common usage, and through research findings in relation to the specific applications. Such information is compiled in Table 2. Internationally, this may be incomplete.

| Product Type * | Applications | Performance Characteristics | Common Target Adhesive Products | | | | |
|----------------|--|---|---------------------------------|------|----|----|----|
| | | | EP | PRF | AC | PU | MF |
| TB | Surface bonded reinforcement Timber lap joints Laminated timber products Thin webbed box / I beams | As for M127 'Structural Adhesives' | • | • | • | • | • |
| GF | Bonded-in rods Bonded-in plates Surface bonded reinforcement Timber lap joints Narrow Crack/fissure filling Thin webbed box / I beams | | • | •*** | • | • | |
| MG | Replacement section repairs Crack/fissure filling | As for M128 'Concrete Protection and Repair Products' | • | | | | |
| TB / GF / MG | Non-Structural | As for M127 'Adhesives For Tiles' | • | • | • | • | • |

Key:
 * TB = Thin Bondline, GF = Gap Filling, MG = Adhesive resin based mortar or grout
 ** EP = Epoxy, PRF = Phenol Resorcinol Formaldehyde, AC = Acrylic, PU = Polyurethane, MF = Melamine Formaldehyde
 *** Specially filled formulations only

Table 2 Timber Adhesive Performance Requirements

5 Link Between Performance Parameters & Structural Design Codes

Considering both BS5268 and Eurocode 5, the latter presents the more realistic arena for these developments. BS5268: Part 2 tends to be very prescriptive. This would not be in the spirit of a performance classification, thus this section will focus upon potential development in conjunction with EC5 limit states design of timber structures.

In structural timber design, amongst the most important issues in determining actual performance, are service conditions and duration of load. Service conditions are considered with respect to temperature and relative humidity, treated through design according to target service class. Common service classes are described in both BS5268: Part2 and DDENV1995-1-1 (Eurocode 5: Part 1.1).

The classification and performance requirements for traditional phenolic and aminoplastic adhesives covered in EN301 identify climatic conditions and 'adhesive type' classifications, as in Table 3. These classifications are also identified in EC5 (cl. 3.5 (2) and cl. 3.5.(3)) and so there is sense in maintaining this within the performance classification system.

| Temperature | Climatic Equivalent* | Examples | Adhesive Type |
|-------------|----------------------|---|---------------|
| > 50 °C | Not specified | Prolonged exposure to high temperature | I |
| ≤ 50 °C | > 85% rh at 20 °C | Full exposure to the weather Heated and ventilated building | I |
| | ≤ 85% rh at 20 °C | Exterior protected from the weather Short periods of exposure to the weather | II |

* 85% rh at 20°C will result in a moisture content of approximately 20% in softwoods and most hardwoods, and a somewhat lower moisture content in wood based panels

Table 3 Adhesive Types for Use in Different Climatic Conditions, as Defined in EN 301 [11]

A basic classification compatible with this scheme can be directly linked to the service classes, as shown in Table 4. Since SC3 is a more demanding environment than SC1 or SC2, it follows that type I adhesives may be used in all service classes.

| Service Class | Adhesive Type |
|---------------|---------------|
| 1 | II |
| 2 | |
| 3 | |

Table 4 Linkage of Service Class to EN 301 Adhesive Type Definitions

As an alternative classification route worthy of consideration, the adhesive type classification might be extended to include a 'Type III', specifically for Service Class I applications.

In the wider context of structural design and the scope of design codes, the essential design information to be established, independent of specific code is summarised in Figure 1 [13,14].

The treatment of such items in Eurocode 5 Part 1.1 is summarised in Table 5. Eurocode 5: Part 2, Bridges, also contains additional information on design of bonded-in rods and fatigue performance verification. It is important to bear in mind that items not specifically covered in sections of the code are not necessarily prohibited and that the reference codes are themselves the subject of development.

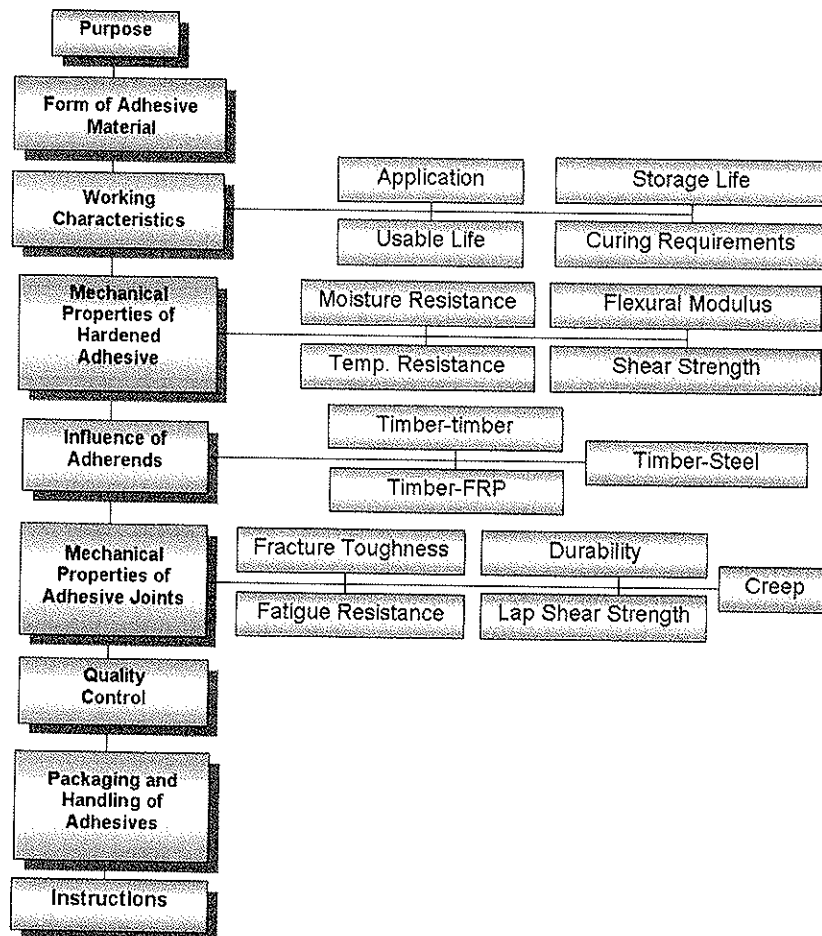


Figure 1 Essential Design Information Elements to be Established Through Performance Classification [13,14]

| Item | Reference | Comments |
|---|--|--|
| Purpose | EC5-1-1 3.2 SOLID TIMBER 3.2.5 Finger Joints 3.3 GLUED LAMINATED TIMBER Large Finger Joints 5.3 COMPONENTS 5.3.1 Glued Thin-Webbed Beams 5.3.2 Glued Thin-Flanged Beams 5.3.4 Mechanically Jointed and Glued Columns | Only thin bond line applications covered specifically as means of forming member/components or as part of controlled manufacturing (glulam large finger joints) process. |
| Form of Adhesive Material | EC5-1-1 3.5 ADHESIVES | EN 301 Type I and Type II adhesives identified, but others not excluded. |
| Working Characteristics Application Storage Life Usable Life Curing Requirements | EC5-1-1 GLUED JOINTS (2) GLUED JOINTS (2) GLUED JOINTS (2) GLUED JOINTS (2) | Adhesive manufacturer's recommendations should be followed |
| Mechanical Properties of Hardened Adhesive Flexural Modulus Moisture Resistance Temperature Resistance Shear Strength | EC5-1-1 - Through reference to adhesive joints via EN301 only Through reference to adhesive joints via EN301 only Through reference to adhesive joints via EN301 only | By test to EN 302 By test to EN 302 By test to EN 302 |
| Influence of Adherends Timber - Timber Timber - Steel Timber - FRP | EC5-1-1 - - - | Limited coverage concerns timber-timber only |
| Mechanical Properties of Adhesive Joints Fracture Toughness Durability Fatigue Resistance Lap Shear Strength | EC5-1-1 - 3.5 ADHESIVES P(1) - Through reference to EN301 only | See description in text of this report By test to EN 302: Part 1 |
| Quality Control | EC5-1-1 GLUED JOINTS, (1) 7.7.2 PRODUCTION & WORKMANSHIP CONTROL (1) | Manufacturer quality control Adhesive type, production process and glue-line quality |
| Packaging and Handling of Adhesives | EC5-1-1 7.3 GLUED JOINTS (2) | Adhesive manufacturer's recommendations should be followed |
| Instructions | EC5-1-1 7.3 GLUED JOINTS (2) | Adhesive manufacturer's recommendations should be followed |

Table 5 Coverage by Eurocode 5: Part 1.1 With Respect To Essential Design Information Requirements

6. Formulation Of Provisional Performance Classification Methodology

From the review of the methodology for performance classification of sealants, an approach to an appropriate performance classification methodology has been identified, as in Figure 2.

A provisional classification methodology has been developed on this basis, as described in the following sections.

This methodology has been consolidated in the form of a draft provisional classification methodology document.

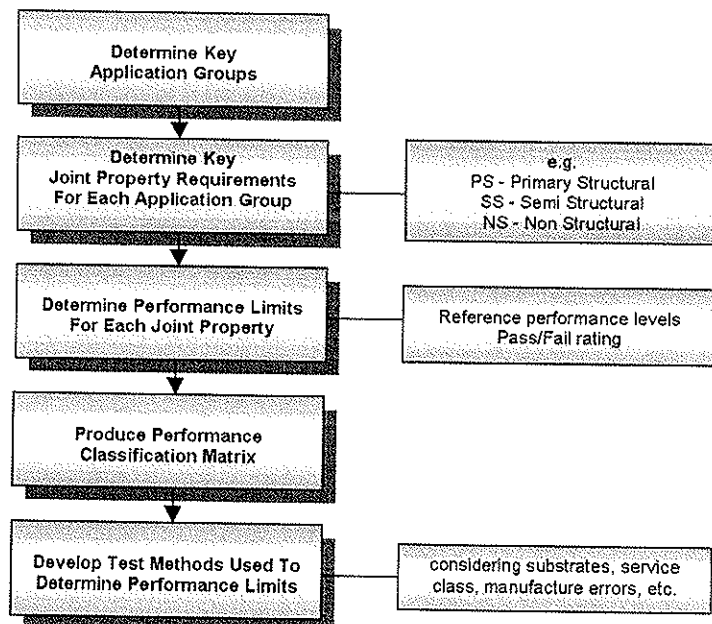


Figure 2 Provisional Performance Classification Development Methodology

6.1 Key Application Groups

Through the review process described above, key application groups have been identified, as shown in Table 6. This is expanded in the form of a classification structure in Figure 3 and a provisional designation system in Figure 4.

| Use | Application | Service Class | Structural Performance Requirement | Substrates* |
|----------------|----------------|---------------|------------------------------------|-------------|
| Structural | Thin Bondline | 1 2 3 | High Medium Semi-Structural | W-W W-X |
| | Gap Filling | | | |
| | Mortar / Grout | | | |
| Non-Structural | Thin Bondline | 1 2 3 | Non-Structural | W-W W-X |
| | Gap Filling | | | |
| | Mortar / Grout | | | |

Notes:
* W-W = wood-wood, W-X = Wood to other substrate

Table 6 Proposed Construction Timber Adhesive Application Groups

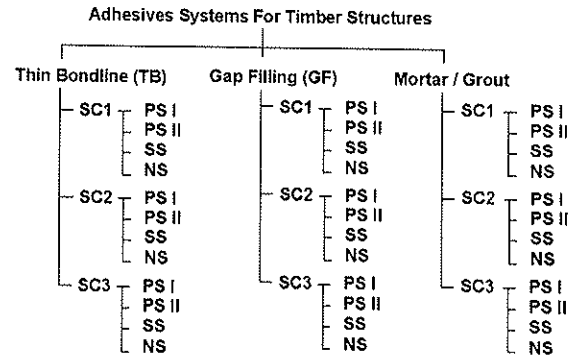


Figure 3 Provisional Timber Adhesive Performance Classification System

| Timber Adhesive | Application Type | Service Class Type | Structural Sub-class | Test Substrates | Surface preparation |
|-----------------|------------------|--------------------|----------------------|-----------------|---------------------|
|-----------------|------------------|--------------------|----------------------|-----------------|---------------------|

Figure 4 Provisional Designation System for Timber Adhesives

6.2 Key Joint Property Requirements For Each Application Group

Performance characteristics for each application group can be compiled with respect to the guidance established in CEN M127 and M128, as shown in Table 7, and prEN1504, as shown in Table 8.

| Family/ Subfamily | Durability | |
|--------------------------------------|---|--|
| Structural - Thin Bond / Gap filling | Y (Against water, UV, ozone, temperature, oil, biological attack, alkali, humidity, freeze-thaw, moisture, shrinkage, ... as relevant) | <ul style="list-style-type: none"> Bond Strength (e.g. shear, tensile, peel, cleavage, delamination) Tensile Strength Fatigue Strength Impact resistance Heat Resistance (including behaviour in elevated temperatures from fire) Creep Reaction to fire Release of dangerous substances* |
| Structural - MG | Y (Against alkali, corrosion, abrasion, frost, de-icing salt, temperature change, ... as relevant) | <ul style="list-style-type: none"> As relevant to the type of product: Bond / adhesion strength, Shear strength, Compressive strength, Tensile strength, Bending strength, Shrinkage/expansion, Workability, Sensitivity to water, Pull-out behaviour, Crack-bridging, Diffusion resistance, Filling share, Penetration behaviour, Composition, Corrosion protection/inhibition, Water repellence, Modulus of elasticity, Coefficient of thermal expansion, Glass transition temperature Reaction to fire Water vapour permeability Water permeability Release of dangerous substances* Thermal Conductivity |
| Non-Structural | Y (Against water, moisture, temperature, chemicals, freeze-thaw, ... as relevant) | <ul style="list-style-type: none"> Reaction to fire Release of dangerous substances* Bond Strength (e.g. shear adhesion, tensile adhesion) Creep Impact resistance |

Notes: * in particular, those dangerous substances defined in Council Directive 76/769/EEC, as amended.

Table 7 Performance Characteristics For Timber Construction Adhesives on CEN M127/M128 Basis

| Performance Characteristic | Product Type | | |
|---|---|---|---|
| | Thin Bondline | Gap Filling | Mortar / Grout |
| Suitability for application to vertical surfaces to top horizontal surfaces by injection | <input type="checkbox"/> <input type="checkbox"/> <input type="checkbox"/> | <input type="checkbox"/> <input type="checkbox"/> <input type="checkbox"/> | <input type="checkbox"/> <input type="checkbox"/> <input type="checkbox"/> |
| Suitability for application and curing under the following special environmental conditions: low or high temperature ¹ wet substrate | <input type="checkbox"/> | <input type="checkbox"/> | <input type="checkbox"/> <input checked="" type="checkbox"/> |
| Adhesion timber to timber steel to timber FRP to timber corrosion protected steel to timber ² hardened grout/mortar to timber | <input checked="" type="checkbox"/> <input checked="" type="checkbox"/> <input type="checkbox"/> <input type="checkbox"/> <input type="checkbox"/> | <input checked="" type="checkbox"/> <input checked="" type="checkbox"/> <input type="checkbox"/> <input type="checkbox"/> <input type="checkbox"/> | <input checked="" type="checkbox"/> |
| Durability of system thermal cycling moisture cycling | <input checked="" type="checkbox"/> <input checked="" type="checkbox"/> | <input checked="" type="checkbox"/> <input checked="" type="checkbox"/> | <input checked="" type="checkbox"/> <input checked="" type="checkbox"/> |
| Material characteristics for the designer open time at minimum, standard and maximum application temperatures workable life at minimum, standard and maximum application temperatures modulus of elasticity in compression modulus of elasticity in flexure compressive strength shear strength glass transition temperature coefficient of thermal expansion shrinkage | <input checked="" type="checkbox"/> <input checked="" type="checkbox"/> <input checked="" type="checkbox"/> <input type="checkbox"/> <input checked="" type="checkbox"/> <input checked="" type="checkbox"/> <input checked="" type="checkbox"/> <input checked="" type="checkbox"/> <input checked="" type="checkbox"/> <input checked="" type="checkbox"/> | <input checked="" type="checkbox"/> <input checked="" type="checkbox"/> <input checked="" type="checkbox"/> <input type="checkbox"/> <input checked="" type="checkbox"/> <input checked="" type="checkbox"/> <input checked="" type="checkbox"/> <input checked="" type="checkbox"/> <input checked="" type="checkbox"/> <input checked="" type="checkbox"/> | <input checked="" type="checkbox"/> <input checked="" type="checkbox"/> <input checked="" type="checkbox"/> <input type="checkbox"/> <input checked="" type="checkbox"/> <input checked="" type="checkbox"/> <input checked="" type="checkbox"/> <input checked="" type="checkbox"/> <input checked="" type="checkbox"/> <input checked="" type="checkbox"/> |
| NOTES: 1. Temperatures may be nominated by the producer for the intended use. 2. In this context corrosion protection implies the application of a corrosion inhibiting priming coat to a mild steel <input checked="" type="checkbox"/> = a material characteristic which shall be considered for all intended uses <input type="checkbox"/> = a material characteristic which shall be considered for certain intended uses | | | |

Table 8 Performance Characteristics for Intended Uses Based Upon prEN1504

7. Forward Look

A provisional outline proposal for timber adhesive performance classification has been drafted, based on the format and content of EN301, prEN 1504-4 and ISO11600. This now requires identification of provisional performance as a starting point for development of a Provisional Performance Classification Matrix. This will emerge as the appropriate test methods for timber applications are identified through future work tasks in this research. Existing methods and previous experimental research methods will be considered with regard to the identified property requirements in order to establish methods and performance levels.

8. Conclusions

Conclusions drawn from the review work and other research to date:

- CEN mandates M127 and M128 provide a useful starting point in combination with EN 301 and prEN1504-4 for development of a performance classification methodology for adhesive systems for use in timber structures.
- The performance classification of polymeric sealant materials for construction purposes presented in ISO 11600 demonstrates a model for development of a broadly similar performance classification methodology for adhesive systems for use in timber structures
- Through identification of applications, it is apparent that there are three types of adhesive applications, (thin bond, gap filling and adhesive based mortars/grouts). These can be linked to actual applications, by way of consideration of the substrate materials. The choice of adhesive is a function of the substrates and the process by which the adhesive is incorporated in the final product, component or assembly.
- The key factors to be considered in order to establish a link between adhesive performance and timber design codes are duration of load effects and service class effects, which act in combination to define the design behaviour model for both serviceability and ultimate limit states.
- A limited range of experimental evidence for this is already available, with certain confirmatory of practical importance, and with certain adhesive classes.

Acknowledgements



This project is co-sponsored under a UK Government construction research programme and by the Timber Research and Development Association (TRADA). The project is also supported by contributions in kind provided by Oxford Brookes University, Anthony Hunt Associates, Rotafix, Permabond, Sika, Cranfield University and Andrews Kent & Stone (on behalf of The Thames Valley Branch of IStructE). TRADA Technology gratefully acknowledges their sponsorship and thanks them for their support.

References

- [1] TINGLEY, D.A. and GAI, C. (1998). FRP Reinforced Glulam Performance: Case Study of The Lighthouse Bridge. Volume 2, 5th World Conference on Timber Engineering, Montreaux, Switzerland.
- [2] JODIN, P., ADJANOHOUN, G. and NIANDOU, H. (1999). Local Reinforcement of Timber Structures By Composite Materials. COST C1 Final Report of Working Group 'Timber Joints' – Semi-rigid Timber Joints: Structural Behaviour, Modelling and New Technologies.
- [3] RIBERHOLT, H. (1986). Glued Bolts in Glulam. Report R210, Department of Structural Engineering, Technical University of Denmark.
- [4] BROUGHTON JG and HUTCHINSON AR (2001). Pull-out behaviour of steel rods bonded into timber. Materials and Structures - RILEM, Vol.34, March, pp100-109
- [5] CEN/TC193 (1999). MCG N 4 Adhesives – Answer To Mandate M127 On Construction Adhesives (Draft 1).
- [6] CEN/TC193 (1998). Construction Adhesives (Draft). CEN Mandate M127, CONSTRUCT 98/294 rev 1.
- [7] CEN/TC193 (2000). Answer To Mandate M127 - Construction Adhesives (Draft).
- [8] CEN/TC104 (1999). Products Related To Concrete, Mortar and Grout (Draft). CEN Mandate M128.
- [9] CEN/TC104 (2000). Answer To Mandate M128 - Products Related To Concrete, Mortar and Grout (Draft).
- [10] CEN (2000). prEN 1504-4 (Draft) - Products and Systems For The Protection and Repair of Concrete Structures - Definitions , requirements, quality control and evaluation of Conformity - Part 4: Structural Bonding. CEN, Brussels.
- [11] CEN (1992). EN 301 - Adhesives, Phenolic And Aminoplastic, For Load-Bearing Timber Structures: Classification And Performance Requirements. CEN, Brussels.
- [12] BSI (1993). BS ISO 11600:1993, Implementation of ISO11600: 1993, Building construction - Sealants - Classification and requirements. BSI, London.
- [13] MAYS, G.C. and HUTCHINSON, A.R. (1992). Adhesives in Civil Engineering. Cambridge University Press, UK.
- [14] INSTITUTION OF STRUCTURAL ENGINEERS. The Structural Use of Adhesives, 1999, IStructE, London.